INTERSCIENCE MONOGRAPHS AND TEXTS IN PHYSICS AND ASTRONOMY

Edited by R. E. MARSHAK

Volume I: E. R. Cohen, K. M. Crowe, and J. W. M. DuMond
THE FUNDAMENTAL CONSTANTS OF PHYSICS

Volume II: G. J. Dienes and G. H. Vineyard
RADIATION EFFECTS IN SOLIDS

Volume III: N. N. Bogoliubov and D. V. Shirkov
INTRODUCTION TO THE THEORY OF QUANTIZED FIELDS

Volume IV: J. B. Marion and J. L. Fowler, *Editors*
FAST NEUTRON PHYSICS In two parts
  Part I: Techniques
  Part II: Experiments and Theory

Volume V: D. M. Ritson, *Editor*
TECHNIQUES OF HIGH ENERGY PHYSICS

Volume VI: R. N. Thomas and R. G. Athay
PHYSICS OF THE SOLAR CHROMOSPHERE

Additional volumes in preparation

INTERSCIENCE MONOGRAPHS AND TEXTS IN PHYSICS AND ASTRONOMY

Edited by R. E. MARSHAK

University of Rochester, Rochester, New York

VOLUME VI

Editorial Advisory Board

H. ALFVEN, *Royal Institute of Technology, Stockholm, Sweden*
L. V. BERKNER, *Associated Universities, New York, New York*
H. J. BHABHA, *Tata Institute, Bombay, India*
N. N. BOGOLIUBOV, *Academy of Sciences, Moscow, U. S. S. R.*
S. CHANDRASEKHAR, *Yerkes Observatory, Williams Bay, Wisconsin*
J. W. DuMOND, *California Institute of Technology, Pasadena, California*
L. GOLDBERG, *University of Michigan, Ann Arbor, Michigan*
M. GOLDHABER, *Brookhaven National Laboratory, Upton, New York*
C. HERRING, *Bell Telephone Laboratories, Murray Hill, New Jersey*
J. KAPLAN, *University of California, Los Angeles, California*
C. MØLLER, *Institute for Theoretical Physics, Copenhagen, Denmark*
L. NÉEL, *University of Grenoble, Grenoble, France*
W. K. H. PANOFSKY, *Stanford University, Stanford, California*
R. E. PEIERLS, *University of Birmingham, Birmingham, England*
F. PRESS, *California Institute of Technology, Pasadena, California*
B. ROSSI, *Massachusetts Institute of Technology, Cambridge, Massachusetts*
L. SPITZER, Jr., *Princeton Observatory, Princeton, New Jersey*
B. STROMGREN, *Institute for Advanced Study, Princeton, New Jersey*
G. TORALDO di FRANCIA, *University of Florence, Florence, Italy*
G. E. UHLENBECK, *University of Michigan, Ann Arbor, Michigan*
V. F. WEISSKOPF, *Massachusetts Institute of Technology, Cambridge, Massachusetts*
H. YUKAWA, *Kyoto University, Kyoto, Japan*

PHYSICS OF THE SOLAR CHROMOSPHERE

RICHARD N. THOMAS
Boulder Laboratories, National Bureau of Standards,
Boulder, Colorado
R. GRANT ATHAY
High Altitude Observatory, University of Colorado,
Boulder, Colorado

INTERSCIENCE PUBLISHERS, INC., NEW YORK
Interscience Publishers Ltd., London 1961

IIA Lib.

Copyright © 1961 by Interscience Publishers, Inc.

ALL RIGHTS RESERVED

Library of Congress Catalog Card Number 61–6547

INTERSCIENCE PUBLISHERS, INC., 250 Fifth Avenue, New York 1, N. Y.

For Great Britain and Northern Ireland:

INTERSCIENCE PUBLISHERS LTD., 88/90 Chancery Lane, London, W. C. 2

PRINTED IN THE UNITED STATES OF AMERICA

Dedication and Acknowledgement

Much of the inspiration for the theoretical development and most of the material upon which the analytical results depend comes from data obtained at the 1952 Khartoum eclipse. For the planning, support, and execution of a successful eclipse expedition at Khartoum we gratefully dedicate this monograph to John W. Evans, John P. Hagen, and Walter O. Roberts.

The entire support for the Khartoum eclipse expedition of the High Altitude Observatory of the University of Colorado, and for much of the analysis of the data, was provided by the Office of Naval Research. Partial support for various phases of the theoretical developments and analysis of the data has been provided by the Boulder Laboratories of the National Bureau of Standards and the Sacramento Peak Observatory of the Air Force (Research and Development Command). Most of the developments reported in the monograph represent a joint research program of the Boulder Laboratories of the National Bureau of Standards, the High Altitude Observatory, and the Sacramento Peak Observatory.

For their kind permission to reproduce figures from the journals indicated, we are indebted to:

L'académie des sciences de France, *Comptes rendus;* Centre national de la recherche scientifique de France, *Annales d'astrophysique;* Smithsonian Institution, *Contributions from the Smithsonian Astrophysical Observatory;* University of Chicago, *The Astrophysical Journal.*

Preface

Although we are the formal authors of this monograph, the ideas in it and their application represent so much the fusion of the thinking—agreement and disagreement—of several close colleagues and ourselves, that to call the monograph "ours" is almost fatuous. Indeed, we have split the preparation of the several chapters between us, not to indicate sole authorship of the work summarized therein—as will be clear from the references to the work upon which the summary is based—but to ensure as complete and current coverage of this rapidly evolving field as possible.

C. W. Pecker and J-C. Pecker have been involved in virtually every phase of the work, from the early arguments on the importance of the non-LTE methodology, through the measurement and analysis of the Khartoum data, to the present diffusion of the application of the methodology downward to the photosphere and upward to the corona. J. T. Jefferies came, supposedly, for a brief visit, but its length, and the breadth of his influence have become a benign Hydra in the evolution of the non-LTE methodology and the analysis of chromospheric structure. The results of R. B. Dunn's meticulous and stimulating work on chromospheric structure continue to be published mainly by others; we can only emphasize our debt for the material and advice he has provided us. The efforts of J. B. Zirker and S. R. Pottasch have focused attention on an extension of the methodology to clarify the structure of the lowest chromosphere and on application of the methodology to the novae and diffuse nebulae. Our hopes that the approach may be extended to include more explicit treatment of velocity fields have been largely reflected in the work of C. A. Whitney on cepheids, and in his preliminary work on granulation. Although we have not considered the solar prominances in this monograph, the work on them by F. Q. Orrall and H. B. Zirin emphasizes the short-sighted nature of this omission in the over-all scheme of the non-LTE configuration of a gaseous ensemble. The careful observations of line profiles at the limb and over plages by E. v. P. Smith, and in flares by E. v. P. Smith and H. J. Smith, have been responsible for much thought and analysis, only a part of which has been summarized here. H. R. Johnson and S. Matsushima have carried through detailed numerical explorations of HeI and H, respectively, to lay the basis for much of our physical "feel" for these problems.

While they have not been directly involved in the details of these non-LTE investigations, we are indebted to several colleagues for much discussion on a number of problems considered here: J. W. Warwick, on our attempts at reformulation of the source-function problem; E. N. Parker, on problems of radiative stability; B. E. J. Pagel, on the problems of the solar limb and non-LTE in H^-; L. M. Branscomb, S. N. Milford, and M. J. Seaton, on problems of cross sections; and especially R. O. Redman and J. Houtgast, on eclipse spectra, results, and analysis.

R. N. Thomas and R. Grant Athay

Contents

1 The Problem of the Solar Chromosphere and Its Bearing on the General Problem of Stellar Atomspheric Structure, by *R. N. Thomas* 1
- I. Definitions and Statement of the Problem of the Solar Chromosphere 1
- II. The Significance of the Outer Solar Atmosphere in the General Study of the Structure of Stellar Atmospheres 4
- III. High-Energy Aerodynamics and Stellar Atmospheres 6
- IV. The General Stellar Atmosphere 9
- V. The Solar Chromosphere 14
- VI. Explicit Statement of the Kind of Non-LTE Effects Treated in This Monograph, and Their Relation to the Transport Problems of Interest 18

2 Chromospheric Data, by *R. Grant Athay* 25
- I. Introduction 25
- II. Eclipse Observations of the Chromosphere 27

3 Variations in Chromospheric Structure and Mass Motions, by *R. Grant Athay* 45
- I. Introduction 45
- II. Positional Variations 45
- III. Temporal Variations 51
- IV. Data on Mass Motions—Spicules 57

4 The Spectroscopic State of a Gas in a Statistically Steady State, by *R. N. Thomas* 78
- I. The Equations of Statistically Steady State 78
- II. Solutions of the Equations of Statistical Equilibrium 92
- III. The Problem of Specifying $\int \bar{I}_\nu \varphi_\nu \, d\nu$ in an Arbitrary Gas Mass and Results on the Associated Source Function 106

5 Thermal Stability of a Gas with a Non-Radiative Energy Input and Radiative Efflux, by *R. Grant Athay* 142
- I. Steady-State Energy Transfer 142
- II. Dominant Sources of Radiation Loss 148
- III. Details of the Model 155
- IV. Comments on the Model 168

6 **The Analysis of Emission in the Optical Continuum to Obtain $n_e(h)$ and $T_e(h)$ Under the Assumption of a Spherically Symmetric Lower Chromosphere,** by *R. N. Thomas* 170

I. Introduction 170
II. Critical Summary of Interpretation of Non-Eclipse Observations in the Optical Continuum 173
III. Interpretation of Eclipse Observations in the Optical Continuum 193

7 **Extension of the Model to Include Helium Emission,** by *R. Grant Athay* 229
I. Estimate of Helium Free-Bound Emission 229
II. Helium Excitation 231
III. High-Temperature Excitation of Helium 234
IV. General Formulation of Model 242
V. Calculation of Model 246
VI. Active Regions 254

8 **An Extension of the Model to Include Radio Noise Data,** by *R. Grant Athay* 261
I. Radio Noise Emission 261
II. A Model From Radio Data 264
III. Discussion of the Model 268

9 **Data in Whose Analysis the Effects of Both Self-Absorption and of Departures from a State of Local Thermodynamic Equilibrium Must Be Included,** by *R. N. Thomas* 272

I. General Principles Underlying the Analysis of the Line Spectrum 273
II. Analysis of the Hydrogen Lines 280
III. Summary of Analysis of the Metallic Spectrum of the Chromosphere 352

10 **Summary Comments on the Chromospheric Model,** by *R. N. Thomas* and *R. Grant Athay* 376

Appendix I, by *R. Grant Athay* 388

Appendix II 405

Bibliography 411

Index 419

CHAPTER 1

The Problem of the Solar Chromosphere and Its Bearing on the General Problem of Stellar Atmospheric Structure

R. N. THOMAS

I. Definitions and Statement of the Problem of the Solar Chromosphere

At the extreme solar limb the intensity of the continuous emission in the optical spectrum drops by a factor e over a region some 100 km in extent, thereby giving rise to the appearance of a sharp boundary. Immediately following this rapid drop, two marked changes occur in the character of the optical spectrum: (1) The spectrum changes from a strong continuum emission, broken by absorption lines, to a spectrum dominated by emission lines of neutral and singly ionized atoms superposed upon a weaker continuum. (2) For both lines and continuum, the emission scale height, which is the distance required for a decrease in intensity by a factor e, becomes much greater than the 100 km characterizing the continuum at the limb. These two characteristics of the emission persist for some 10,000 km, with only the strongest lines remaining visible throughout the entire region. This region, in which emission lines of neutral and singly ionized atoms are observed, is called the *chromosphere.* The first 5000 km, which presents a quasi-uniform appearance, is called the *lower chromosphere.* The upper 5000 km, where the emission is concentrated in small spike-like columns, is called the *upper chromosphere.* The columns are called *spicules.* The *classical chromospheric problem* is to find an explanation of the large scale heights of the chromospheric emission.

Above the chromosphere is the *corona,* in which the emission scale heights have values much larger than the chromospheric emission scale heights, and whose spectrum is of a still different type.

The continuum is fainter than in the chromosphere, and the emission lines in the visible part of the spectrum consist of a few lines arising from forbidden transitions in metal atoms nine or more times ionized. The intensities of the lines, and, to a lesser extent, of the continuum, vary with both time and position on the sun (cf. Chapter 3). The coronal emission lines are observed out to a distance of about one solar radius beyond the limb, and the continuum is observed out to several radii. For about the first one-half of the radius above the limb, there are no absorption lines in the coronal spectrum. However, at greater distances from the limb, the Fraunhofer lines of the solar disk spectrum gradually reappear. In this monograph our interest in the corona is restricted to those layers lying immediately above the chromosphere.

The chromosphere and corona together comprise the *outer solar atmosphere.* It is customary to distinguish the outer atmosphere, whose properties are inferred from limb spectra, from the *lower* or *normal solar atmosphere*, whose properties are inferred from disk spectra. Customarily, those regions of the lower atmosphere wherein arises the continuous spectrum are called the *photosphere.* The regions producing the absorption lines have often been called the *reversing layer.* This concept of "reversing layer" is, however, a misleading one, as we shall see in discussing line production, and is best forgotten. The distinction between *lower* or *normal* parts of the solar atmosphere and the outer solar atmosphere has arisen from two conceptual standpoints.

First, most astronomers feel that they understand the character of the lower atmosphere in terms of what may be called the "classical" theory of stellar atmospheres, which assumes the local applicability of thermodynamic and hydrostatic equilibria and does not take into account the existence of the outer atmosphere. This theory predicts a monotonic outward decrease of material density and of excitation, thus of emission scale height.

Second, from considerations based partly upon the predictions from the classical theory and partly upon interpretations of observational data, some astronomers feel that the outer atmosphere has no influence upon the observed disk spectrum (cf. van de Hulst, 1953).

In opposition to the foregoing viewpoint, there are some who maintain that the cores of the strong Fraunhofer lines are formed in the chromosphere. On the basis of eclipse observations of the chromosphere, we believe that many of the intermediate strength lines, as well as the strong lines, are of chromospheric origin.

Thus, in entering a discussion of the outer solar atmosphere, we recognize four main problems: (1) What is the significance of the observed increase in emission scale heights just above the solar limb, in terms of the thermodynamic structure of the outer solar atmosphere? Particularly, we ask the relation between emission gradients and density gradients. (2) What alteration in the physical assumptions underlying the classical models of the solar atmosphere are required in order to produce this outer atmosphere? (3) What changes must be introduced into conventional methodology underlying the interpretation of solar (and ultimately stellar) spectra, required by these derived characteristics of the outer solar atmosphere? (4) To what extent must any current empirical characteristics of the lower solar atmosphere be modified by such a change in analytical methodology?

The initial approach to the problems above must be an empirical one. However, much of the analytical methodology applied to the early observational material has been based upon concepts that are valid only under the assumptions defining the framework of the classical theory. Thus, the most important aspect of any study of the solar chromosphere must be a re-examination of this analytical methodology. Considerable controversy has arisen over widely divergent answers to the problems above, derived from the same observational data, but subjected to different kinds of analytical treatment. Thus, this monograph is an inquiry into a methodology of analysis of the solar chromosphere, as well as an analysis of the solar chromosphere itself.

For many years the 1932 eclipse data of Cillié and Menzel (1935) served as the focal point for discussions of chromospheric problems. A re-discussion of these data based on a strong change in analytical methodology (Thomas, 1948b, 1949a, 1950a), showed considerably higher values for the amount of absorbing material in the chromosphere than previous estimates had given, and wide departures from results which would be required by the classical methodology of analysis of stellar atmospheric spectra. A program was planned for the 1952 eclipse which would greatly increase the scope of the observational data and provide a firmer basis on which to attack the chromospheric problems. The data from this eclipse have substantiated the notions that the chromosphere has a strong effect on the disk spectrum, and that significant departures from a state of local thermodynamic equilibrium exist, and their analysis has yielded a wealth of new information on the thermodynamic structure of the chromosphere.

In this monograph we concentrate our discussion on the 1952 eclipse data obtained by the High Altitude Observatory expedition to Khartoum, Sudan, with the aim of exploring the above enumerated problems. We supplement these data with certain disk observations, spicule observations made outside of eclipse with coronagraphs, and with radio noise data. Such an approach, with the principal emphasis simply on determining empirically the structure of the outer solar atmosphere, fails to put the problem of the *existence* of the outer solar atmosphere in its full perspective. Therefore, in the remainder of this introductory chapter we discuss the outer solar atmosphere in relation to its general role in clarifying the problems of the structure of the solar and stellar atmospheres.

II. The Significance of the Outer Solar Atmosphere in the General Study of the Structure of Stellar Atmospheres

The existence of the outer solar atmosphere with its unexpectedly large emission scale heights relative to the photospheric scale height must be regarded as anomalous in terms of the classical model of a stellar atmosphere. The classical model predicts a monotonically decreasing scale height with increasing distance from the sun. In order to account for the observed outward increase in emission scale heights, one usually postulates either an energy source other than that carried by the radiation field, or a source of mechanical momentum capable of supporting the atmosphere. In the first alternative, the anomalous scale heights are attributed to the thermal structure of the atmosphere, which departs from the structure of the classical atmosphere. In the latter alternative, the thermal structure of the classical atmosphere in radiative equilibrium is preserved.

Associated with the gross, over-all anomally of large scale heights are other aspects of the outer atmosphere which stand in a priori contradiction to the assumptions underlying the conventional theoretical model. Outstanding among these other aspects is the existence of large differences in emission scale heights between lines of different ions and between different lines from the same ion, the presence of ionized helium in the chromosphere and highly ionized metals in the corona, and the existence of material velocities exceeding the thermal velocity at the temperatures given by the conventional theoretical model.

The solar chromosphere-corona is not the only example of a stellar atmosphere whose extent is anomalous relative to conventional models. Indeed, in some stars the "abnormal" component represents the entire visible atmosphere. In most cases of such extended atmospheres, rather sizable velocity fields appear to be present and some non-radiative source of thermal energy seems to be required. We now ask whether the macroscopic velocity fields are coupled with the thermodynamic state of the atmosphere? If so, how does this coupling modify the conventional atmospheric model? Although the departures from the predictions of the conventional model of a stellar atmosphere occur most obviously only in the *outer* solar atmosphere, the proximity of the sun and the consequent wealth of observational detail make the solar chromosphere a natural starting point for such an investigation.

If there is a coupling between the macroscopic velocity field and the thermodynamic state of the gas, the local kinetic temperature is no longer fixed solely by the radiation field. Under such conditions, it cannot safely be assumed that the atomic energy levels are populated as they would be under conditions of thermodynamic equilibrium at either the local kinetic temperature or the local radiation temperature. Instead, the detailed excitation and de-excitation processes must be carefully examined.

The depth in a star where departures from thermodynamic equilibrium become relevant is a question that has always worried astronomers. In the lower atmospheric regions, whence originates the continuous spectrum, surprisingly great success has been had with the application of the various distribution functions that are rigorously valid only under conditions of thermodynamic equilibrium. In the outer atmospheric region, where there is the possibility of a non-radiative energy source and a radiation sink, conditions are most favorable for the onset of non-thermodynamic-equilibrium effects. Again, the detailed information made possible by the proximity of the sun presents the chromosphere as a natural source of empirical information.

From a more "solar" viewpoint, the chromosphere is an extremely interesting component of the atmosphere. The central components of the strongest Fraunhofer lines originate here. The ultraviolet emission lines observed in rocket spectra of the solar disk appear also to originate in the chromosphere. In addition, many phenomena of solar activity arise in or near the chromosphere.

In a broad sense, our ultimate aim in this monograph is a revision, or extension, of the conceptual basis underlying the classical model of a stellar atmosphere, along the direction set by the problems just posed. In a specific sense, we seek a detailed knowledge of one such non-classical atmosphere as a guide to our change in concepts. Consequently, we try to exhibit the conceptual evolution that has resulted, in part, from the introduction of new observational data, and in part from a re-analysis of existing data.

III. High-Energy Aerodynamics and Stellar Atmospheres

The properties ascribed to the gaseous ensembles studied in stellar astrophysics and those studied in laboratory gas dynamics have traditionally differed in the degree of excitation of internal degrees of freedom in the gas, and the energy of the macroscopic velocity fields relative to the internal energy of the gas. In the astronomical situation, ambient temperatures correspond to more than 10^3°K. The conventional models of a stellar atmosphere assume negligibly small velocity fields, and the radiation field provides both energy source and sink. In the laboratory situation, ambient temperatures correspond to about 10^2°K. The velocity field provides the local energy source, and viscosity and heat conduction provide the energy sink. Or, such was the situation prior to about 1947.

Since 1947, studies of both stellar atmosphere and laboratory gas dynamics have converged on the problem of how to describe a gaseous ensemble when there is appreciable coupling between the macroscopic velocity field and the radiation field. In both cases, the concern with this problem results from an awakened interest in very high gas velocities. The high velocity in the stellar atmosphere case serves to introduce the possibility of a local source of mechanical energy in addition to radiative energy. In the laboratory case, the high velocity serves to provide highly excited atoms, which, in turn, provide a radiative sink of energy. Thus, in both cases, the local mechanical dissipation of energy and radiative efflux of energy occur as a cyclic process.

Such a cyclic process introduces the possibility of a departure from thermodynamic equilibrium. In the conventional approach to stellar atmospheres, a "local thermodynamic equilibrium" assumption is introduced, which couples the internal degrees of freedom to the radiation field by forcing the relation between local emission and absorption of radiation to follow Kirchoff's law for thermodynamic equilibrium. In the conventional gas dynamics, a "local thermodynamic equilibrium" assumption couples the internal degrees of freedom of the gas to the macroscopic velocity field by forcing the temperature to follow velocity via a constant value of the specific heat ratio.

In each of these two types of "local thermodynamic equilibrium" assumptions, the goal is to represent the distribution functions of the atoms over the various internal energy states by one or two parameters, and thus to avoid the necessity of discussing the detailed mechanism of atomic interactions. In the presence of cyclic processes, the question of a non-thermodynamic-equilibrium configuration for the gaseous ensemble arises and the details of all atomic processes must be considered. Thus, in essence, the over-all problem reduces to that of describing the general configuration of a gaseous ensemble.

The problem of a general approach to the description of a gaseous ensemble with possible departures from thermodynamic equilibrium is not a trivial one. If the distribution of electron density n_e, electron temperature T_e, velocity field v, and chemical composition of a gaseous ensemble is known, it is possible, in principle, to predict the emergent radiation field—or, on the other hand, to infer n_e, T_e, v, and chemical composition from the emergent radiation field.

On the purely theoretical side, an a priori prediction of the configuration the gas will assume can be attempted from a knowledge of the energy sources. In general, observations are neither sufficiently precise nor detailed to proceed wholly empirically, and our physical insight has not matured sufficiently to guard against unwarranted simplification in the assumptions defining the theoretical model. Thus, in practice, a composite of the two approaches must be adopted. The chief guide is the physical consistency between the theoretical approach and the observational data. The major hope for advancement lies in obtaining detailed observations on such non-thermodynamic-equilibrium configurations, both astronomically and in the laboratory, which will allow development of our physical insight and testing of analytical investigations.

Interests in astrophysical and laboratory studies of gaseous ensembles in which the velocity and radiation fields are coupled differ in three essential aspects.

First, the laboratory interest in coupling between the radiation and velocity fields has arisen fairly recently, accompanying the development of methods to obtain such high gas velocities. The extent to which these effects can be induced is limited to the magnitude of the velocities that can be produced. In the astronomical case, velocities of wide range in amplitude have always existed; only recently have their implications been investigated.

Second, the composition of the gas and the character of the impressed velocity field are a priori known in the laboratory case. The primary problem is the development of an analytic description of the configuration of the gas and of the radiation field. In the astronomical case, the problem is to ascertain the character and origin of the velocity field as much as its effect upon the atmospheric structure.

Third, the stellar atmosphere itself has such a slow time scale of change that at any given time it seems safe to treat the gas, as a whole, as being in a statistically steady state. In the laboratory, however, it is difficult to maintain a high-energy configuration other than transiently. In partial compensation, laboratory gas densities are much higher, thus speeding up all relaxation processes.

In consequence of the comparison just made, the stellar atmosphere and laboratory studies are strongly complimentary in an investigation of this field of ultra-speed gas dynamics. Laboratory investigations provide information on relaxation rates, verify the accuracy of computations on atomic cross sections, and clarify the physical validity of new concepts such as those involved in attempts to provide a generalized theory of turbulence. Astronomical observations of stellar atmospheres provide detailed information on a gaseous ensemble in a steady state, but not necessarily in thermodynamic equilibrium.

In the past there have been several joint aerodynamical-astronomical discussions of problems arising in the interstellar medium.

For the first time, in the summer of 1960, there will be a similar symposium for aerodynamicists and astronomers on the problems of the stellar atmosphere. A major requirement underlying such a discussion is an observational and analytical investigation of stellar atmospheres aimed principally at clarifying the physical conditions in those "extended" stellar atmospheres whose properties seem associated in a major way with aerodynamic motions. Let us turn, then, to a brief recapitulation of the problems of a general stellar atmosphere.

IV. The General Stellar Atmosphere

Prior to about 1947 the approach to the structure of stellar atmospheres was based completely on the notion of a gaseous ensemble whose properties were fixed by the assumptions of radiative equilibrium, local thermodynamic equilibrium, and negligible velocity fields. The analysis of stellar atmospheres via this "classical" model was just emerging from a period in which an approximation to the model, the gray-body approach with continuous absorption coefficient independent of frequency, had seemed adequate to predict the distribution of temperature in the atmosphere. In essence, the earlier analysis of the line spectrum for purposes of abundance determination had dealt with one "mean level" in the atmosphere; and a precise knowledge of the temperature distribution over the whole atmosphere was not critical. However, Wildt's (1939) identification of the H^- ion as the source of the continuous opacity in stars later than about AO and Chandrasekhar's (1945, 1946) detailed determination of its properties, had simultaneously explained the high degree of success of the gray-body approximation for the sun and other intermediate type stars and spurred investigations of the non-gray case. These investigations were supplemented by more extended and precise empirical determinations of temperature distribution in the solar atmosphere from limb-darkening measures in the continuum. At the same time, more detailed investigations of models of line formation were underway, including specifically the detailed dependence upon the temperature structure of the atmosphere. Of particular interest was the influence of the more detailed models upon abundance determination.

In consequence, what seemed to be the two outstanding theoretical problems on the atmospheric structure at this epoch, prior to about 1947, were both concerned with an improved calculation of the temperature distribution. One problem, formulated directly under the framework of the assumptions defining the classical model of the atmosphere, sought to provide an adequate treatment of the "blanketing effect" resulting from the addition of line absorption to the continuous opacity. The other problem sought a correction to the temperature distribution in the lower atmosphere, by providing an adequate treatment of the convection zone associated with the ionization of hydrogen and possibly helium. In this convective zone, the strict application of radiative equilibrium must be dropped, and so the problem represents a first departure from the strictly "classical" atmosphere.

From an observational and conceptual standpoint the ultimate adequacy of the "classical" atmospheric model defined above seems less certain. Such doubts center primarily on the rather widespread indication of appreciable velocity fields, with speeds exceeding the thermal velocity of the classical atmospheric model; and an equally widespread indication of atmospheres that are anomalously extended relative to the predictions of the classical model. The two phenomena are often linked, in that an atmosphere exhibiting one characteristic is prone to exhibit the other. Four main categories of stars appear to exhibit one and/or the other of these effects: (1) shell stars, consisting of a central star surrounded by a semi-detached envelope; (2) practically all, if not all, the variable stars; (3) a number of nonvariable giants and supergiants in the early spectral classes; (4) the outer atmosphere of the sun, and, by implication, the outer atmospheres of a good portion of the main-sequence stars.

The usual inferences on the extent of an atmosphere refer to the distribution of a particular stage of excitation of a particular ion. To turn such observations into density variation with height requires a knowledge of the spectroscopic state as a function of height, which requires some atmospheric model. In general, observations are so limited that one can only conclude that the results are anomalous on the basis of the classical model, but he is not able to say what the actual density variation is in the atmosphere. For a long time, the semi-intuitive expedient was adopted of treating the inferred macroscopic velocity fields as a simple extension of molecular motion, which gave a "turbulent" pressure, thus an atmospheric extension.

But no coupling was allowed between the macroscopic velocity field and internal degrees of freedom of the gas. Therefore, of the assumptions defining the classical atmosphere, just one was dropped, that of negligible velocity fields. Under this picture, the temperature distribution fixed by the assumptions of radiative equilibrium and local thermodynamic equilibrium remains, and an observed distribution of emission can be converted to a distribution of density. This approach seems to have developed following a suggestion by Rosseland (1929) that the Reynold's numbers occurring in astronomy, based on stellar rotation, were large enough that some turbulent motion should be expected. The concept of such "turbulence" was invoked by McCrea (1929) to support the solar chromosphere and by Struve and Elvey (1934) in their discussion of observations of some 10 F-type supergiants. The primary difficulty in such a concept of "turbulence" is that it by-passes the important question of how to avoid the local dissipation of mechanical energy and thus the rejection of all the assumptions defining the classical atmosphere. Chandrasekhar (1934) raised this objection to McCrea's original discussion, on the basis that the Gaussian distribution of "turbulent" velocities adopted by McCrea implied collisions, hence energy dissipation. The "turbulence" theory was propped up by removing the specification of the velocity distribution, and postulating an unknown mechanism which inhibited energy dissipation. Thomas (1947, 1948a) reopened the question by objecting per se to the whole concept of superthermic turbulent, or random, motion without local dissipation of energy, and suggested that the supposed velocity fields were more likely a blend of systematic macroscopic motions and high kinetic temperatures generated by this motion. It would seem that the proper approach is that which drops all a priori concepts on the nature of the velocity fields and attempts to relate the velocity field and optical spectrum in order to infer the properties of such a gaseous ensemble.

The origin of velocity fields is, of course, a relevant aspect from the standpoint of a model of the stellar atmosphere. Moreover, a really adequate description of the velocity field cannot be developed unless it embodies the origin of the field. If the question of origin is by-passed, the choice of the most physically coherent description is weakened, and some method of introducing the velocity field as an empirical parameter must be developed. Nevertheless, knowledge of this originic question is so insecure that its solution must be regarded as one of the desired results rather than a physically clear parameter of the investigation. It does seem that the velocity field must arise from an instability of one sort or another. The original suggestion by Rosseland (1929) of turbulence arising from stellar rotation offers one possibility. The pulsation associated with variable stars is another possible source. An amplification of the small velocity fields arising in low-lying zones of convective instability by the atmospheric density gradient, as suggested by Biermann (1946) and by Schwarzschild (1948) offers a natural extension of the classical atmospheric model. The problem is to provide, from these or other sources, velocity fields ranging from those in the sun through those in the Wolf-Rayet stars to the outbursts of the novae. Thus, it seems reasonable to conduct our inquiry into velocity fields through a kind of kinematic study in which we inquire into the details and consequences of their existence rather than their cause.

A study of the velocity fields in a stellar atmosphere is usually carried out by indirect means. A major requirement is a separation of atomic thermal velocity from macroscopic gas velocity. If the thermodynamic state of the gas is not to be prejudged, it is necessary to recognize the difficulty of this apparently simple problem. Even studies of solar spicules and prominences on the limb offer complications, for the distinction must be made between material velocity and the motion of excitation fronts. Thus, in general, an empirical inference of a macroscopic velocity field is closely linked with an assumption on the spectroscopic state of the atmosphere.

It has not proved to be feasible as yet to cope in detail with many of the dynamical problems which occur in stellar atmospheres, even without the complications of magnetic fields. Thus, we attempt idealizations of certain outstanding features of such motion, to gain insight. For the case of the pulsating variables, we have attempted to idealize the problem to a piston oscillating at the base of an atmosphere (Thomas and Whitney, 1953; Whitney 1955 et seq.). For application to the solar spicule, we have investigated (Thomas, 1948a, 1950c) the behavior of a supersonic jet in a gravitational field, the effect of the jet on the atmosphere, and we should particularly like to ask the effect of radiation on the temperature of the jet. For the Wolf-Rayet stars, we have considered (Thomas, 1949b) the problem of inter-penetrating systems of jets. In each of these problems, the spectroscopic state of the resulting ensemble is desired. Conversely, we have attempted to interpret the spectroscopic state of the atmosphere in terms of the physical conditions prevalent in the atmosphere. All these attempts represent but first approximations—to which hydromagnetic effects, questions of radiative stability, etc., must be applied.

The analysis of the spectroscopic data in terms of the electron temperature T_e, electron density n_e, and occupation numbers of the various energetic states is more complicated than usual because of the necessity to allow for departures from thermodynamic equilibrium. In some cases, the analysis yields the occupation numbers themselves; in other cases, it yields only the ratio of occupation numbers. Thus, one must be able to calculate the occupation numbers for any given gaseous ensemble. The existing knowledge of inelastic collision cross sections for thermal electrons, and, in most cases, optical transition probabilities, is inadequate for such calculations. Because of the inadequacy, the limited calculations of occupation numbers that have been made are considerably uncertain. These calculations are mainly of interest in indicating the kind of effects to be expected.

In order to circumvent the lack of physical parameters, as extensive a set of data as possible is required to develop a methodology as well as to investigate the atmosphere. Although the chromosphere and corona represent but a small part of the total mass of the atmosphere, the sun is a natural focal point of investigation. Most of the data referring to the outer atmosphere have heretofore come from a few isolated eclipse observations, but the details of these results are quite extensive. Moreover, the large aperature coronagraph and high-resolution spectrographs at Sacramento Peak and McMath-Hulbert Observatories in the United States, and similar instruments abroad, are now in operation. Since the central parts of many lines of the solar Fraunhofer spectrum apparently originate in the chromosphere, the high-resolution disk instruments are capable of providing considerable data relevant to the chromosphere.

For these reasons, we summarize in this monograph the results of our investigation of the solar chromosphere, and the development of the analytical methodology underlying the investigation, as it has thus far progressed. The impetus for this investigation commenced from the assumption that the solar chromosphere provides the most readily studied example of a stellar atmosphere whose state is fixed by a local dissipation of mechanical energy and a radiative efflux.

V. The Solar Chromosphere

We have stated the problem of the solar chromosphere as the existence of the large emission scale heights relative to that scale height which gives rise to the solar limb and which would be predicted by the "classical" theory of stellar atmospheres based on a neglect of large-scale velocity fields and non-radiative energy transfer. We have mentioned the apparent evidence for superthermic, macroscopic velocity fields and asserted that such evidence suggests values of T_e much in excess of those predicted by the classical model of stellar atmospheres. The kind of observational effects, and evolution of thinking, cited in the preceding section for the general stellar atmosphere is duplicated exactly when we consider the specific question of the outer solar atmosphere. To bring this specific problem into sharper focus, we summarize the chromospheric problem as it appeared at about 1930, at about 1947, and at present, within the framework of the discussion of the last section. The epoch of 1930 marks a dividing line between the period of uncalibrated observations of gross structure and the detailed spectrophotometric eclipse observations. Serious investigations into the energetic effect of velocity fields in stellar atmospheres began in about 1947.

In the early 1930's, the "chromosphere anomaly" was simply the existence of large emission scale heights, and, less often, of the variation of scale height from one ion to another. Attempts were made to correlate the variation of scale height with ionization potential of the particular ion and thus with excitation effects resulting from a temperature gradient. Such a temperature gradient was difficult to fit in with the classical model atmosphere, which was essentially isothermal at these levels. Other attempts involved gravitational or charge stratification, until it was realized that practically infinitesimal macroscopic motions of any kind suffice to keep the atmosphere well mixed. Thus attention was directed mostly toward simply explaining the existence of large emission scale heights and the details were ignored.

Efforts fell into two broad categories. In each, only the assumption of negligible velocity fields was dropped. One type of proposal, McCrea's (1929) "turbulence" model already mentioned, simply postulated the existence of a random velocity field within a uniform atmosphere. The second type of proposal dropped the assumption of a uniform atmosphere, and considered the chromosphere to be a composite of gas streams. Two alternatives were discussed. One, a quantitative treatment by Chandrasekhar (1934), consisted of a system of streams associated with a checkerboard of hot and cold regions over the solar surface, which produced a pattern of differential radiation pressure. The other, a qualitative suggestion by Menzel (1931), consisted of a statistical array of prominences or filaments.

All these proposed models were capable of a superficial representation of an increased scale height in the chromosphere. The basic question explicitly posed was the extent to which the chromosphere might be treated as a quasi-continuous gaseous medium. The extent to which the energy residing in the velocity field would couple with the thermal state of the gas was left undiscussed.

By 1947 the formulation of the chromospheric problem was beginning to change radically, largely because of a conceptual change in the problem of the coupling between macroscopic and thermal velocity fields. The physical model of the chromosphere was that of a quasi-uniform gas, in which an appreciable dissipation of mechanical energy occurred, and on which the formalism of local thermodynamic equilibrium was no longer forced. The idea of an "anomalous extent to the atmosphere" was replaced by the idea of a nonradiative energy source which heated the atmosphere, thereby accounting for its extent. This idea had already been applied to the corona as a result of Edlen's (1939) identification of the coronal lines with highly ionized atoms whose presence required $T_e \sim 10^{6}$°K. Redman's (1942) observation of chromospheric line profiles at the 1941 eclipse apparently supported the notion as applied to the chromosphere. Several possibilities were discussed for the energy source: by Biermann (1946), by Schwarzschild (1948), by Schirmer (1950), and by Schatzman (1949) from the standpoint of the solar granulation as a source of acoustic noise which propagated into the outer atmosphere, where it dissipated; and by Thomas (1948a) from the standpoint of the solar spicules as superthermic streams of matter which heated the gas in the enveloping atmosphere.

These discussions of a chromosphere having a kinetic temperature higher than the boundary temperature were rudimentary, largely because of lack of sufficient observational data. Both the non-radiative energy required to sustain the chromosphere and the energy actually residing in the various proposed energetic sources were highly uncertain.

Since 1947, attempts have been made to obtain additional data on the system of mechanical energy input, to advance the understanding of the thermodynamic structure of the chromosphere, and to develop the analytical methodology needed to discuss such an atmosphere. In terms of actual numerical results the greatest progress has been made in the structural direction, largely from the observations at the 1952 eclipse. Considerable progress has been made in the development of the analytical methodology; the greatest handicap in detailed numerical application lies in the lack of atomic cross sections. Over this same period, however, there has been a slight shift back to the chromospheric problem as stated in 1930. The chromosphere has assumed a symbiotic appearance, with high- and low-temperature properties at the same heights. Arguments have appeared attempting to explain away the high temperature properties in favor of a low temperature configuration, and conversely. Following a suggestion advanced by Giovanelli (1949), the idea of a two-component chromosphere consisting of hot and cold vertical columns has grown in favor. Along with this development, the question of whether the chromosphere is not simply a composite of gas streams has reappeared. Thus, the chromosphere problem as it appears today might be stated as:

Over-all: Is the chromosphere wholly a collection of gas streams, superposed on a negligible uniform gaseous substratum, or is the chromosphere a quasi-uniform gaseous atmosphere into which a system of mass motions discharges?

Detailed: What is the thermodynamic state of the material comprising the chromosphere? Is the chromospheric structure random in space and in time, or is it statistically regular?

Originic: What is the physical source or cause of the mass motions?

Any attempt to bring into focus the chromospheric problem as it appears at present would be incomplete without a brief summary of recent thinking on the structure of the upper photosphere. In essence, this thinking revolves around the concept of a spherically symmetric solar atmosphere. The two outstanding theoretical problems of the classical atmosphere, as stated in the foregoing section, are that of the boundary temperature T_0, and that of the description of the convection zone. On the basis of a spherically symmetric atmosphere, the problem of the boundary temperature as it relates to the chromosphere is physically clear, even if there is not yet a satisfactory theoretical or empirical specification of T_0. For, once T_e begins to rise above T_0, there must be a non-radiative dissipation of energy. Consequently, the first major goal in presenting a chromospheric model is that of specifying the height at which T_e exceeds T_0. As a broad generalization of current empirical evidences from various sources, it appears that 4500 ± 300° is a reasonable estimate for T_0, on the basis of an assumed spherically symmetric atmosphere. We summarize this material in Chapter 6. Thus, in analyzing the height distribution of T_e in the chromosphere, particular attention must be paid to the height h_0, where $T_e \gtrsim 4200°$. At least here, if not at lower heights, the assumption of radiative equilibrium becomes invalid.

On the other hand, attempts to describe the convection zone lead to departure from a strict spherical symmetry. Some sort of convective pattern exists, with ascending and descending currents carrying non-zero energy, and the temperature distribution must, in consequence, vary across a given horizontal surface. Even though these fluctuations average out in a large enough scale, there is non-uniformity on a small scale. The question becomes the size of the non-uniformity and of the scale. In addition, there exists the possibility that such non-uniformity in the convection zone produces disturbances which propagate upward from the convection zone proper and induce a non-uniformity in the overlying layers.

Such considerations, coupled with the observed phenomenon of granulation, have led to two kinds of discussion of this convection-zone-induced non-uniformity. On the one hand, there are attempts to link the granulation to the convection zone and thence to the energy source for the chromosphere-corona. It is not yet clear whether the granulation itself represents the convective elements, the picture first suggested by Unsöld (1930); a kind of turbulence associated with the convection, as suggested by Biermann (1946) and by M. Schwarzschild (1948); or a system of acoustic waves produced by the convection and propagating upward as suggested by

Schatzman (1953) and by Thomas (1954). Estimates as to the actual temperature fluctuations across a granule depend very strongly upon the size ascribed to the "bright" granular regions. We summarize existing data and inferences from them in Chapter 6.

On the other hand, de Jager (1954), Böhm (1954), and Vogt (1956) have proposed a multi-component structure for those parts of the atmosphere in which the Fraunhofer lines are produced. These discussions have, to all practical purposes, been carried out neglecting departures from the local thermodynamic equilibrium assumption. It is not the purpose of this monograph to present much consideration of the general Fraunhofer line spectrum—we discuss only certain lines having strong bearing on the chromospheric model. However, we present in Chapter 6 a few brief comments on the above analyses, as they bear on the question of the existence of large-scale inhomogeneities in T_e near the photosphere-chromosphere boundary.

VI. Explicit Statement of the Kind of Non-LTE Effects Treated in This Monograph, and Their Relation to the Transport Problems of Interest

We have emphasized, in this introductory chapter, that the primary problem confronting a re-examination of the analytical approach to stellar atmospheres lies in a proper treatment of the coupling between macroscopic velocity field, microscopic degrees of freedom of the gas, and electromagnetic radiation field. What we have called the classical aerodynamical approach concentrates on the macroscopic mechanical transport problem. What we have called the classical stellar atmospheric approach concentrates on a mixture of macroscopic and microscopic radiative transport problems. Each obviates the necessity of a simultaneous inquiry into distribution functions over the microscopic degrees of freedom of the gas by some kind of local thermodynamic equilibrium (LTE) assumption, which couples microscopic distribution functions to macroscopic parameters of the transport problem. When either has had occasion to go beyond the most frequently treated aspect of a complete neglect of the other, the treatment has usually been considerably oversimplified by some ad hoc assumption; the concept of "astronomical turbulence" having no energetic coupling to the thermal state of the atmosphere is an example. Thus, the interesting *kind* of ex-

tension beyond the wholly classical viewpoint—astronomical or aerodynamical—is one introducing some energetic coupling between radiative and mechanical transport problems.

The analytical developments in this monograph starting in Chapter 4, introduce such an extension by considering an energetic coupling involving negligible monentum transport. Thus, the viewpoint is almost diametrically opposite to that underlying the introduction of "astronomical turbulence," which is based on momentum coupling but neglects energy coupling. Consider a quick summary of the usual successive stages of approximation to the two transport problems, and the associated local thermodynamic equilibrium assumptions on the coupling with the microscopic distribution functions, in order to place in focus our approach in this monograph.

A. Mechanical Transport via the Boltzmann Equation

Write the Boltzmann equation in terms of the distribution function $f_{i\alpha}$ for the number of ions i in energy level α with velocity components v_j and acceleration a_j at position x_j, representing a process of type A carrying the ion from state (α,v_j) to (β,v'_j) by $\mathcal{P}_A(\alpha,v_j;\beta,v'_j)$ and its inverse by $\mathcal{R}_A(\beta,v'_j;\alpha,v_j)$. Then we have

$$\frac{\partial f_{i\alpha}}{\partial t} + v_j \frac{\partial f_{i\alpha}}{\partial x_j} + a_j \frac{\partial f_{i\alpha}}{\partial v_j} = - \mathop{\mathrm{S}}_{A,\beta,v'_j} [\mathcal{P}_A(\alpha,v_j;\beta,v'_j) - \mathcal{R}_A(\beta,v'_j;\alpha,v_j)] \qquad (1\text{-}1)$$

Alternatively, introducing the distribution function $F_{i\alpha}$ measured relative to the mean flow velocity, ${}_{i\alpha}q_j$, of atoms in the (i,α) state, we have

$$\frac{\partial F_{i\alpha}}{\partial t} + V_j \left[\frac{\partial F_{i\alpha}}{\partial x_j} - \frac{\partial F_{i\alpha}}{\partial V_k} \frac{\partial\, {}_{i\alpha}q_k}{\partial x_j} \right] + \frac{\partial F_{i\alpha}}{\partial V_j} \left[a_j - \frac{d\, {}_{i\alpha}q_j}{dt} \right] = - \mathop{\mathrm{S}}_{A,\beta,v'_j} (\mathcal{P} - \mathcal{R}) \qquad (1\text{-}2)$$

with

$$V_j = v_j - {}_{i\alpha}q_j; \qquad \frac{d}{dt} = \frac{\partial}{\partial t} + {}_{i\alpha}q_j \frac{\partial}{\partial x_j} \qquad (1\text{-}3)$$

V_j and d/dt should carry subscripts $i\alpha$, but their omission should cause no confusion in the following.

B. Radiative Transport

Write the radiative transfer equation in its usual form in terms of specific intensity I_ν (energy in the range $\nu \pm d\nu/2$ per unit solid angle crossing unit area normal to the beam per unit time), rather than a photon distribution function $I_\nu(c_j,x_j)/h\nu$. We use c_j for the components of light velocity c. Then we have

$$\begin{aligned} \frac{\partial I_\nu}{\partial t} + c_j \frac{\partial I_\nu}{\partial x_j} &= - \mathop{\mathrm{S}}_{A,\nu'} [\mathcal{P}_A(\nu;\nu') - \mathcal{R}_A(\nu';\nu)] \\ &= - (\kappa_\nu I_\nu - \epsilon_\nu)c \qquad (1\text{-}4) \end{aligned}$$

where κ_ν and ϵ_ν are absorption coefficient and emissivity.

Consider now the various degrees of local thermodynamic equilibrium assumptions conventionally introduced when treating the transport problems individually; we are interested in trying to identify a rough parallellism between mechanical and radiative aspects. To investigate the parallellism completely consistently, we should compare the analysis of mean flow velocity with that of integrated (over frequency) radiative flux, or we should compare a spectral analysis of the velocity field with that of the monochromatic radiative transfer problem. Indeed, for a proper treatment of the effects of a velocity field on the optical spectrum we should have to adopt the latter viewpoint. Here, however, we are attempting to ask how to introduce a first-approximation coupling of velocity field and radiation field in terms of an observable effect in the line spectrum. So, we mix the approaches—which is, when one asks what is usually done in practice, the usual approach.

1. Zero Order. Complete thermodynamic equilibrium: No gradient appears in thermodynamic variables of zero order. ${}_{i\alpha}q = 0$; $I_\nu = B_\nu(T)$, the Planck function; and $F_{i\alpha} = F_0(T)$, the compound of Maxwellian velocity distribution, Boltzmann distribution over internal energy levels, Saha distribution over ionization states.

2. First Order. Distribution function for transfer quantities given locally by the thermodynamic-equilibrium value at the local value of a temperature parameter.

a. Mechanical. $F_{i\alpha} = F_0(T_k)$ everywhere locally, but a gradient in T_k and ${}_{i\alpha}q \neq 0$ permitted. T_k is the kinetic temperature, defined by the Maxwellian velocity distribution. The usual treatment of a one-component gas—either (i, α) the same for all atoms or the distribution over internal energy states assumed to have no explicit dependence upon the V_j—then gives the three equations expressing conservation of mass, momentum, and energy through multiplication of the Boltzmann equation (1-2) by m, mV_j, and $mV_jV_j + U = E$ and integrating over V_j and α, viz,

$$\frac{d\rho}{dt} + \rho \frac{\partial q_j}{\partial x_j} = 0 \tag{1-5}$$

$$\rho \left[\frac{dc_j}{dt} - a_j \right] + \frac{\partial p}{\partial x_j} = 0 \tag{1-6}$$

$$\frac{d}{dt} n\bar{E} + (p + n\bar{E}) \frac{\partial c_j}{\partial x_j} = 0 \tag{1-7}$$

n is the particle density and m the mass; p, ρ are gas pressure and gas density. If we introduce the coupling-assumption

$$n\bar{E} = p/(\gamma - 1) \tag{1-8}$$

the energy equation integrates to the polytropic relation

$$p = K\rho^\gamma \tag{1-9}$$

and the microscopic distribution function has been completely coupled to the macroscopic velocity field. The essential physical approximation is the assumption of complete predominance of atomic collisional rates, elastic and inelastic, over any other rate; so that distribution functions always adjust instantaneously to the local value of T_k, which is coupled to q through Eqs. (1-5) through (1-9).

b. Radiative. The analogue to the mechanical case would be $I_\nu = B_\nu(T_r)$, with T_r fixed wholly by the local radiation density. The essential physical approximation is the assumption of complete predominance of radiative rates, so that distribution functions always adjust to the local radiation density. Because the microscopic distribution functions over the internal energy levels will in consequence be the Boltzmann and Saha relations at T_r, we shall also have

$$\epsilon_\nu/\kappa_\nu = B_\nu(T_r) \tag{1-10}$$

so that Eq. (1-4) becomes

$$\frac{\partial B_\nu(T_r)}{\partial t} + c_i \frac{\partial B_\nu(T_r)}{\partial x_i} = 0 \tag{1-11}$$

This configuration is uninteresting astrophysically, because of the required isotropy of radiation field, which does not let us examine a radiating gas mass, having a free—or non-reflecting—boundary. Actually, this case is in more direct correspondance with the mechanical case for $q = 0$, corresponding to zero flux, mechanical or radiative.

If we introduce the less-restrictive assumption $\bar{I}_\nu = B_\nu(T_r)$, where the bar indicates average over angular distribution, we retain the assumed predominance of radiative rates, and T_r remains fixed wholly by the radiation density. Also, Boltzmann and Saha relations remain valid at T_r, thus also Eq. (1-10). Equation (1-11) gives way to

$$\frac{\partial B_\nu(T_r)}{\partial t} + \int c_i \frac{\partial I_\nu}{\partial x_i} \frac{d\omega}{4\pi} = 0 \qquad (1\text{-}12)$$

In the steady-state configuration of a plane-parallel atmosphere, the configuration usually treated in discussing stellar atmospheres, the monochromatic flux gradients are zero; but I_ν need not be istropic, so that the case of a free-boundary with no incident radiation field may be treated.

3. Second Order. Deviation from thermodynamic-equilibrium value permitted in distribution function for transfer quantities, but size of deviation small

a. Mechanical. Distinguish between distribution function in atomic velocities, F', and the remainder of $F_{i\alpha}$, that covering the distribution over internal molecular and atomic degrees of freedom. Then $F' = F'_0(T_k)(1 + \psi)$, and ψ is determined by a perturbation treatment of the Boltzmann equation. Equations (1-6) and (1-7) become

$$\rho\left[\frac{dc_j}{dt} - a_j\right] + \frac{\partial p}{\partial x_j} + \frac{\partial p_{jk}}{\partial x_k} = 0 \qquad (1\text{-}13)$$

$$\frac{d}{dt} n\bar{E} + \frac{\partial h_k}{\partial x_k} + [\delta_{jk}(n\bar{E} + p) + p_{jk}] \frac{\partial c_j}{\partial x_k} = 0 \qquad (1\text{-}14)$$

and p_{jk}, h_k are specified, respectively, by the average of mV_jV_k and mV^2V_k over the perturbation distribution function $F'_0\psi$. The internal degrees of freedom may or may not be assumed directly coupled to the velocity field through the assumption of Eq. (1-8). The usual practice, however, is to assume the validity of the Boltzmann and

Saha distributions at T_k to compute the energy partition over internal degrees of freedom. Because elastic collisional rates generally exceed inelastic, the introduction of a departure of F' from the Maxwellian value while simultaneously forcing the validity of Boltzmann and Saha relations is hardly consistent. The justification in the usual application is the relatively low mechanical energies involved, so that excitation of other than molecular internal degrees of freedom is rare. In more modern work, however, dealing with hypersonic (or hyperthermal!) velocities the problem becomes of importance. We emphasize it here, both for comparison with the radiative situation and for orientation in formulating a reasonable approach to a non-LTE calculation of occupation numbers for atomic energy levels.

b. Radiative. Rather than seeking a solution as a perturbation on $\bar{I}_\nu = B_\nu(T_r)$, one usually turns directly to make some assumption on the interaction process between the local material and the radiation field, thus on the value of $S_\nu = \epsilon_\nu/\kappa_\nu$, then proceeds to evaluate I_ν. The classical assumption is that S_ν lies somewhere intermediate to $B_\nu(T_e)$ and $\bar{I}_\nu$, where T_e is the local kinetic temperature of the electrons. The accompanying assumption on the distribution function for internal atomic degrees of freedom is the local applicability of the Boltzmann and Saha relations at T_e. These assumptions represent a curious compound of assumptions that radiative rates, chiefly ionization, are rapid enough to determine T_e by the local radiation density; and that inelastic collisional rates are rapid enough to fix occupation numbers of atomic energy levels.

4. **Further Approximation.** To proceed beyond the second-order approach, there are several possible directions, the essence of each of which is the introduction of a multi-component gas. In a rough sort of way, we can divide these into two main directions: one, a principal concern with the effect of physical differences between components on the transport problem, e.g., the introduction of differential diffusion and hydromagnetic effects by having one component charged, or the introduction of differential diffusion by components of different masses; the other, a principal concern with the problem of energetic coupling, where we ask explicitly into the problem of distribution functions over atomic energy levels and their coupling with velocity and radiation fields. Our main concern is the latter, in this monograph.

We have already noted that the second-order mechanical approximation is likely inconsistent, at higher energies, in the sense of introducing a departure in F' from F'_0 while retaining Boltzmann and Saha distribution functions. We also note that the second-order approximation is usually of importance over the first-order only in regions of strong gradients, such as in shock waves, in boundary layers, etc. Finally, we note that in any circumstance in which inelastic collisional excitation becomes of comparable importance to radiative, the assumptions of both first and second order on I_ν are completely open to question. These considerations suggest that as a first attempt to consider coupling between radiation and velocity fields, including a proper treatment of internal degrees of freedom, we investigate an atmosphere in which we do not have strong gradients in either time or space. Then, we may assume the first-order approximation for F'—$F' = F'_0$—adopt a microscopic viewpoint to compute distribution functions for internal degrees of freedom, then evaluate I_ν directly from the radiation transfer equation. We can then ask from an a posteriori viewpoint what processes couple most strongly to the kinetic temperature entering F_0.

The one complication in an otherwise-straightforward approach comes if we write, as we must, the equivalent of Eq. (1-5) for each energy level. We obtain

$$\frac{dn_{i\alpha}}{dt} + n_{i\alpha}\frac{\partial_{i\alpha}q_j}{\partial x_j} = -\mathbf{S}\,[\mathcal{P}_A(\alpha;\beta) - \mathcal{R}_A(\beta;\alpha)] \tag{1-15}$$

and note that even the assumption of a spectroscopically steady state—$dn_{i\alpha}/dt = 0$—does not reduce the problem to the set of algebraic equations usually considered, Eq. (1-15) with left side zero. We have remaining the divergence of ${}_{i\alpha}q$. In our considerations of Chapter 4 et seq. we set this term equal to zero. This assumption is stronger than the neglect of gradients large enough to require a departure of F' from F'_0. We must bear this point in mind when asking how widely the analytical methodology developed in this monograph may be applied. The next step in improvement would be to include the divergence term in a solution of the equations of spectroscopically steady state. The third step would introduce the perturbation on F' associated with the presence of the viscosity and heat-conduction terms in the usual second-order mechanical transport solution.

CHAPTER 2

Chromospheric Data

R. GRANT ATHAY

I. Introduction

The first observations of the chromosphere were made visually at the total solar eclipse of 1870 by C. A. Young. Although the corona had been photographed in 1860, photography of the chromospheric spectrum was not accomplished until the eclipse of 1893. Thereafter, photographs of chromospheric spectra became a regular feature of eclipse observations. Not until 1926, however, did Davidson and Stratton (1927) successfully attempt photometric standardization. Subsequent eclipse expeditions have furnished much valuable data, but, even collectively, these data still leave much to be desired.

Limitations on the use of chromospheric data obtained at eclipse are imposed primarily by the incompleteness of the data rather than the inaccuracy of a given observation. The data usually do not have sufficient resolution in position on the limb and height above the photosphere or they cover too narrow a spectral region. Thus, in summarizing the data we shall attempt to indicate the inherent limitations characterizing a given set of data, and the direction of improvement desired in future observations, rather than discuss in detail the instrumental problems and observing techniques. We adopt this attitude to emphasize the need for more adequate data and to point out the major uncertainties in interpreting chromospheric phenomena. We recognize, however, that limitations are usually deliberately imposed in order that we may concentrate on specific problems.

Chromospheric observations made outside of eclipse may be placed in two categories: spectral and structural. Until fairly recently, spectral observations at the solar limb outside of eclipse have concentrated largely on the corona and prominences. However, as early as 1909, Hale and Adams succeeded in photographing the chromospheric spectrum with the 60-foot-tower telescope at Mt. Wilson, and somewhat later Adams and Burwell (1915) published a list of chromospheric lines observed outside of eclipse. More recent observers have concentrated on determining the profiles of chromospheric lines. For example, we cite the studies of Hα, Hβ, and Hγ by Keenan (1932), of Hα by de Jager (1952) and E. v. p. Smith (1957), and of rare earth and metal lines by H. Smith (1957) and Parker (1957). In addition, Athay (1958a and 1959a) and Michard (1959) have studied profiles of spectral lines for individual spicules (cf. Chapter 3). All these extra-eclipse observations suffer large errors in both the zero point of the height scale and in relative heights, so that it is impossible to specify the height to which a given observation applies to within about 1000 km. A further disadvantage of these data arises from the fact that the chromospheric emission-line spectrum is superposed upon a scattered light spectrum containing the Fraunhofer absorption lines. Thus, in quality and height resolution these data do not compare with eclipse data.

Structural observations of the chromosphere can be made on the solar disk by isolating the light in the cores of the strong Fraunhofer lines and at the limb by isolating any particular line that is strong enough to show above the background of scattered light. Observations at the limb, made primarily in Hα using coronagraphs and Lyot filters, have yielded rather extensive data on the structure and velocity fields of spicules, which are summarized in Chapter 3. Because of the short observing period, these data are quite impossible to get at eclipse.

Spectroheliograms of the solar disk made in the Hα line of hydrogen and the K line of CaII reveal many of the structural details of the chromosphere. Unfortunately, however, practically no interpretations of these data have been made. We shall use some of these data in our discussion of the chromosphere without making any attempt to summarize them here.

A further source of data not mentioned in the foregoing comes from radio noise observations of the sun at mm and cm wavelengths. We discuss the radio data that apply to the chromosphere in Chapter 8 where it is used as a check on the model derived from optical data.

II. Eclipse Observations of the Chromosphere

A. Single Spectrogram (Slitless)

Because the chromosphere appears as a thin crescent at eclipse, a spectrograph can be used without a slit. This eliminates the necessity for accurate guiding as well as the need for additional focusing optics. However, the data obtained from slitless spectrographs yield only total line intensities rather than line profiles.

Early eclipse observers concentrated primarily on determining the gross spectral characteristics of the chromosphere. Mitchell's (1947) observations provide an extensive series of records covering five eclipses between 1901 and 1937; the data for each eclipse are derived from a single spectrogram taken during each flash. Observations of this type were not standardized. Line intensities were estimated visually, and the thicknesses of the emitting layers were determined from the lengths of the crescents and the geometry of the eclipse.

Campbell's "moving-plate" technique was an improvement over the single stationary spectrograms. In his spectrograph a long, narrow slit, set parallel to the direction of dispersion just in front of the photographic plate, permitted only the central portion of the crescent to reach the film. The plate moved at right angles to the direction of dispersion, accomplishing the effect of observing a greatly magnified solar image. Since the relative positions of sun and moon changed continuously during the exposure, the intensity of the spectral line changed along the direction of motion of the plate. The lengths of the lines were used as a measure of the thickness of the emitting layer just as were the lengths of the crescents in Mitchell's method. The chief disadvantage in the moving-plate observations was that only a small sector of the chromosphere could be observed and this sector had to be pre-selected. This led to the possibility that the region selected might include prominences and other phenomena of solar activity that could seriously alter the character of the observed emission and make it unrepresentative of the average chromosphere.

Several discussions of the data from moving-plate and crescent spectrograms have been published. Menzel's (1931) analysis of moving-plate data and Wildt's (1947) treatment of crescent data represent the outstanding summaries of this epoch of unstandardized eclipse observations. Their data give rough numerical values for the scale heights of the emission. The roughness results primarily from the lack of photometric standardization, which necessitates the use of indirect methods for determining scale heights.

B. Multiple Spectrograms (Slitless)

To overcome the disadvantages of the single spectrogram observations, Pannekoek and Minnaert (1928) and Menzel (Cillié and Menzel, 1935) used a "jumping-film" technique to obtain several slitless spectrograms during each flash. This method of observing incorporates the advantages of both the moving-plate and the crescent spectrograms. The spectrograms can be used to obtain intensity as a function of height at as many points on the limb as desired. A more elaborate camera is necessary, but the increase in data more than compensates for the added complexity of the equipment.

At the 1932 eclipse, Menzel obtained spectrograms each 2.4 sec, corresponding to a height resolution of 833 km. From these data he found emission scale heights ranging from ~1000 km for helium to ~300 km for metals. Thus, the height resolution was of the same order as the larger scale heights. At the 1936 eclipse, Menzel reduced the exposure interval to 2.0 sec with a 700-km height resolution, again of the same order as the scale height of emission. For many years, the data from the 1932 eclipse served as the standard reference for chromospheric work. However, the inadequacy of these data may be illustrated in the following way.

To formalize the problem of specifying the physical conditions in the chromosphere, $\mathcal{E}_\lambda$, is defined as the emission per unit volume at wavelength λ and E as the intensity of radiation in the spectral line that reaches the earth from the volume contained between the planes defined by $Z = -1/2$ and $Z = +1/2$ in the coordinate system depicted in Fig. 2-1. Hence,

$$E = \int_h^\infty \int_{-\infty}^\infty \int_0^\infty \mathcal{E}_\lambda e^{-\tau_\lambda} \, d\lambda \, dy \, dx \tag{2-1}$$

where h is the height of the moon's limb above the solar limb and the optical depth τ_λ is

$$\tau_\lambda = \int_{-\infty}^{\infty} n_j \alpha_\lambda \, dy \tag{2-2}$$

n_j is the number of absorbing atoms, i.e., those in the lower state of the transition producing the line, and α_λ is the atomic absorption coefficient. Before the data from slitless spectrograms are used to infer the thermodynamic structure of the chromosphere, it is necessary to solve Eq. (2-1) for

$$\mathcal{E} = \int_0^{\infty} \mathcal{E}_\lambda \, d\lambda$$

This solution corresponds to a double differentiation of the data. Unless $E(h)$ is known with considerable accuracy, the solution for $\mathcal{E}$ may contain large errors. It is therefore essential that observations of integrated emission give reliable intensities at height intervals considerably less than a scale height, if they are to be used for detailed discussions of emission per unit volume. The data for the 1932 and 1936 eclipses do not satisfy these requirements.

At the 1945 eclipse, Lindblad succeeded in obtaining spectrograms at intervals of 0.05 sec with a height resolution of ~21 km. However, in order to get the required light intensity, the dispersion

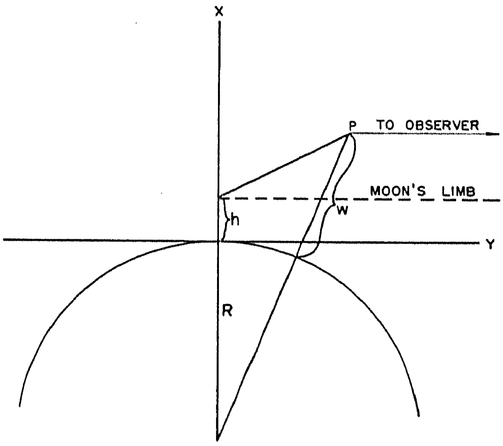

Fig. 2-1. The coordinate system used for discussions of eclipse data.

was reduced to 100 A per mm. This limited the data to the strongest lines only. Kristensen (1955) published scale heights obtained from Lindblad's spectrograms, but absolute intensities were not given.

At the 1952 eclipse, the High Altitude Observatory expedition succeeded in obtaining spectrograms at intervals of 0.4 sec, giving a height resolution of 110 km. These observations cover the spectrum from 8800 to 3400 A with ~10 A per mm dispersion. Figure 2-2 exhibits prints of two of the spectrograms.

Several other expeditions have successfully observed the flash spectrum. The data obtained from these expeditions are summarized in Table 2-1.

C. Slit Spectrograms

Despite the relative simplicity of observing with a slitless spectrograph, the use of the slit introduces several advantages, the most important of which is greatly improved line profiles. In addition to making possible the determination of line profiles, the slit spectrograph increases the contrast of the lines over the continuum. This increased contrast is especially valuable for studying the metal lines with relatively small scale heights, since it increases the range of heights over which the lines may be observed.

Redman (1942, 1955) published line profiles for hydrogen, helium, and metal lines at a few heights for the 1941 and 1952 eclipses. His discussion of the line profiles at the 1941 eclipse provided much of the stimulus for our re-examination of the chromospheric problem.

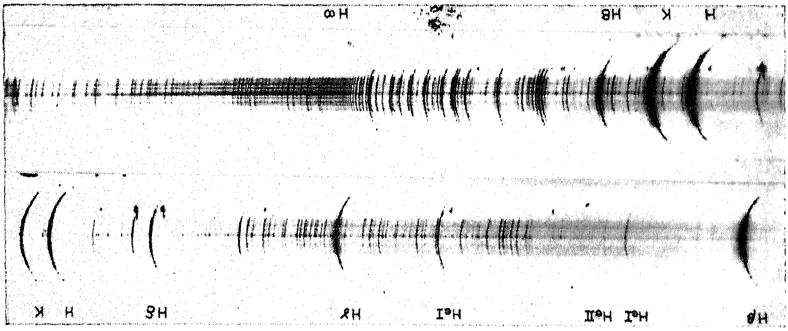

Fig. 2-2. The blue, violet, and ultraviolet regions of the chromospheric spectrum photographed at the 1952 eclipse.

The fact that our discussion centers around the data from slitless spectrograms should not be taken to imply that we consider the data from slit spectrograms less important. Past observations with slit spectrographs, however, have been designed to give line profiles at a few heights in the chromosphere, and they have not proved to be sufficient for a detailed discussion of its thermodynamic structure.

D. Future Observations

In our opinion, the advantages to be gained by using slit spectrographs have not been fully exploited. It is hoped that planners

Table 2-1. Photometric Data from Eclipses[a]

Eclipse date	Observing method	Published data	Height range, km	Height resolution, km	References
1927	WS-MM	E_R all lines λλ4154–4768; E_A and β'Hγ and He4472	One ht.; low ch. 0–3000	— 700	Pannekoek and Minnaert, 1928
1932	SS-MS	E_A and β' hydrogen lines Hβ-H31, and continuum; helium and selected metal lines λλ3330–5876	670–4000	833	Cillié and Menzel, 1935
1936	SS-MS	E_A and β' hydrogen, Hα-H28; helium and selected metal lines, λλ3664-7100	290–10,000	700	Hemmendinger, 1939; Athay, Menzel, & Orrall, 1957
	NS-SM	Profiles and E_R hydrogen lines, Hδ-H26, and metal lines λλ4077-5896	One ht.; low ch.	—	Thackery, 1937
1940	NS-SS	Profiles Hβ, Hγ, Hδ, He4472 and metal lines λλ4200-4600	One ht. 1500	—	Redman, 1942
1941	SS-MM	E_A and β' hydrogen lines Hα-H18; helium and metal lines λλ3692-6563	500–9000	1000	Vyazanitsyn, 1951

(continued)

Table 2-1. Photometric Data from Eclipses[a] (*continued*)

Eclipse date	Observing method	Published data	Height range, km	Height resolution, km	References
1945	SS-MM	E_A and β' hydrogen lines, Hβ-H12; few helium and metal lines, $\lambda\lambda$3680-5876	650–6200	1100	Vyazanitsyn, 1952
	SS-MS	E_R and β' hydrogen lines, Hβ-H16; few helium and metal lines and continuum	200–9000	65	Kristensen, 1955
1952	NS-MS	Profiles hydrogen lines H7-H31; helium 5876, 4026, and 3820 and metal lines $\lambda\lambda$3430-6040	200–2600	600	Redman and Suemoto, 1954; Redman, 1955
	SS-MM	E_A and β' hydrogen lines Hβ-H11; helium and metal $\lambda\lambda$3770-4900	200–5000	430	Houtgast, 1957
	SS-MS SS-MM	E_A and β' hydrogen lines, Hα-H31, and continuum; helium and metal lines, $\lambda\lambda$3440-8700	100–6300	108	This monograph and references

---

[a] Code to observing method 12-34.

12 WS = wide slit, NS = narrow slit, SS = slitless.

3 S = single spectrogram, M = multiple spectrogram.

4 S = β' determined by using single region on limb,
M = β' determined by using multiple regions on limb.

Height resolutions refer to successive exposures; where multiple regions on the limb were used the height resolution is effectively improved.

E_A, absolute intensity; E_R, relative intensity.

of future eclipse expeditions will consider seriously the advantages of combining the slit and slitless spectrographs. The greatest single need in optical data is a complete set of data from one eclipse. These data should include line profiles, total line intensities, and continuum intensities in absolute units at several points on the limb. The height resolution should be small compared with the scale heights. In order to get the data required for an adequate discussion of the thermodynamic conditions in the chromosphere, it is important to observe the spectrum from as far as possible in the ultraviolet to the red of the Paschen series limit. We do not yet have usable observations of the Paschen lines, except in a single abnormal region of the chromosphere. Paschen series data would be of great value when combined with Balmer series data for a study of the excitation conditions in hydrogen. This point will be brought into better perspective in Chapter 9.

III. Data for Normal Chromospheric Regions

We have noted in the preceding discussion that observations of the slitless type must give intensities as functions of height if we are to solve Eq. (2-1) for the emission per unit volume. It is convenient to represent the height dependence of the observed emission in the form

$$E = \sum B_i e^{-\beta_i h} \tag{2-3}$$

From the geometry in Fig. 2-1, and the condition $w \ll R$ we obtain, to a good approximation.

$$h = x + y^2/2R \tag{2-4}$$

In the case of small optical depth, Eqs. (2-1), (2-3), and (2-4) reduce to

$$\mathcal{E} = (1/2\pi R)^{1/2} \sum_i B_i \beta_i^{3/2} e^{-\beta_i h} \tag{2-5}$$

If the optical depth is not small, Eq. (2-5) must be multiplied by a factor less than unity to account for the fraction of the emission reabsorbed in the chromosphere. Since this factor depends upon the absorption coefficient and the distribution of absorbing atoms through the chromosphere, it will differ from one line to another (cf. Chapter 9).

We define the local emission gradient β', and the surface brightness of the chromosphere F, by

$$\beta' = -d \ln E/dh = -(1/E)(dE/dh) = -F/E \tag{2-6}$$

One term in Eq. (2-3) is adequate to represent the data for many of the lines, in which case, $\beta' = \beta$ and is independent of height. For some lines and the Balmer continuum, however, β' changes with height, and additional terms are required.

Table 2-1 contains a description of data obtained at eclipses where the observations gave line profiles or β'. Figure 2-3 exhibits the epoch of these observations, as well as that of less complete observations, relative to the sunspot cycle.

A complete tabulation and discussion of all data from the various eclipse expeditions would be very useful. Unfortunately, the instances in which complete photometric results have been published are rare. In general the literature contains a preliminary description of results, occasionally a table of comparative values of β', but rarely an extensive set of data. By restricting our discussion to the High Altitude Observatory's data for the 1952 eclipse we do not mean to imply either that these data are characteristic of the chromosphere at all times, or that their accuracy, per single observation, exceeds that of all other such data. We believe only that they are somewhat more complete and extensive than any yet tabulated and are therefore more suitable for analytical and expository purposes.

In the following presentation of the 1952 observations, the intensities refer to the emission in all directions from a 1-cm slice of atmosphere contained between two parallel planes defined by $Z = 1/2$ and $Z = -1/2$. The data referred to in Sections A through F are averaged over a strip 12,000 km wide centered at 23° North latitude

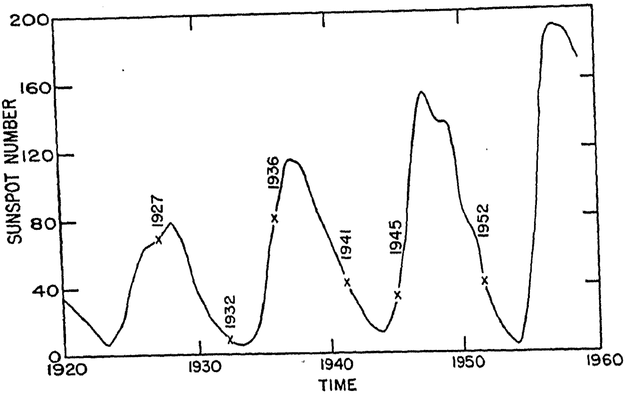

Fig. 2-3. The location of eclipses for which chromospheric data are available relative to the sunspot cycle.

on the east solar limb. This region was free from prominences and other activity on eclipse day and during the days immediately before and after the eclipse. In Chapter 3 we discuss a region, centered at 11° South latitude on the west limb, which was located directly over an active sunspot area. Both the chromospheric and coronal emissions were abnormally intense in this region. It is of special interest both because of its peculiar characteristics and as a basis for checking the consistency of the conclusions arrived at from analysis of the data for the normal region. All numerical data are tabulated in the Appendix.

A. Continuum at λ4700

The continuum on the long wavelength side of the Balmer series limit is produced primarily by scattering of photospheric light by free electrons, by emission from the negative hydrogen ion, and by the Paschen continuum (Athay, Menzel, Pecker, and Thomas, 1955; Athay, 1959b; Chapter 6). It is, therefore, of considerable value in determining the chromospheric model (Thomas, 1950; Zanstra, 1950). There are three main reasons for selecting a wavelength near λ4700: (1) relatively few spectral lines are in the region, (2) the relative importance of the contribution from scattering by free electrons is at maximum, and (3) the intensity varies slowly with wavelength.

The continuum intensity at λ4700 is plotted against height in Figure 2-4. We define the zero point of the height scale as the height where $\tau_{4700} = 1$ for a tangential ray. Equation (2-1) may then be rewritten in the form

$$E_{4700} = \int_h^\infty \int_0^\tau S_\lambda e^{-\tau_\lambda} \, d\tau_\lambda \, dx \tag{2-7}$$

where S is the source function.

If we assume T_e to be constant with height and local thermodynamic equilibrium to hold for the continuum, $S_\lambda = B_\lambda \neq f(\tau)$ and

$$\begin{aligned} \mathbf{F}_{4700} = -\frac{dE_{4700}}{dh} &= \int_0^\tau B_{4700}(T_e) e^{-\tau} \, d\tau \\ &= B_{4700}(T_e)(1 - e^{-\tau}) \end{aligned} \tag{2-8}$$

If we further assume τ to decrease exponentially with increasing height, $\tau = 1$ where $d^3E/dh^3 = 0$, i.e., at the point of inflection on a plot of E versus h. An inspection of Fig. 2-4 shows that $h = 0$, determined in this way, occurs near $h = 100$ on the adopted height scale, which

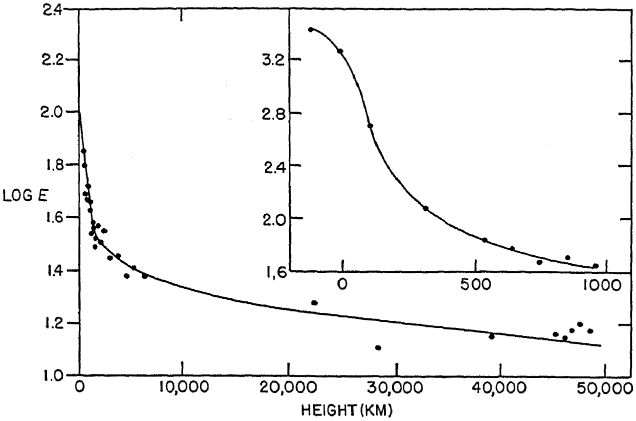

Fig. 2-4. The continuum at λ4700 in the chromosphere and corona. The inset shows the continuum very near the solar limb. (From R. G. Athay et al., 1955, *Astrophys. J.*, suppl., **1**, 510.)

we determined from preliminary data. However, it would be premature to correct the height scale by this amount until there is a better understanding of the behavior of τ_λ and T_e in this region.

In the original discussion of the continuum data (Athay et al., 1954) we tried six representations in the form of Eq. (2-3). We repeat here only the most accurate of the representations, viz.,

$$\begin{aligned} E_{4700} = {} & 385 \exp(-7 \times 10^{-8} h) + 67.5 \exp(-2.2 \times 10^{-8} h) \\ & + 10 \exp(-6 \times 10^{-9} h) + 12.1 \exp(-4 \times 10^{-9} h) \\ & + 8.5 \exp(-7 \times 10^{-10} h) + 17.4 \exp(-5 \times 10^{-11} h) \end{aligned} \quad (2\text{-}9)$$

For $h > 100$ km, τ is small for the continuum, and Eq. (2-5) applies. Equations (2-5) and (2-9) yield

$$\begin{aligned} \mathcal{E}_{4700} = {} & 1.07 \times 10^{-14} \exp(-7 \times 10^{-8} h) \\ & + 3.3 \times 10^{-16} \exp(-2.2 \times 10^{-8} h) \\ & + 7.0 \times 10^{-18} \exp(-6 \times 10^{-9} h) \\ & + 4.6 \times 10^{-18} \exp(-4 \times 10^{-9} h) \\ & + 2.4 \times 10^{-19} \exp(-7 \times 10^{-10} h) \\ & + 9.2 \times 10^{-21} \exp(-5 \times 10^{-11} h) \end{aligned} \quad (2\text{-}10)$$

for the emission per cm³.

B. Balmer Continuum

The Balmer free-bound emission is superimposed on a background continuum arising from other sources. The intensity of this background continuum can be measured for $\lambda \geq 3700$. Data obtained from our spectrograms indicate that for heights where $\tau_c \ll 1$, over the range λλ8600 to 3700 the background continuum follows the photospheric curve quite closely, and it appears safe to extrapolate to wavelengths shorter than λ3700 by using the photospheric curve. Doing this, we readily separate the Balmer free-bound continuum from the background continuum (Athay et al., 1954).

Data at four wavelengths in the Balmer continuum are given in Table A-2 of the Appendix. To extend the λ3640 data to heights below 500 km we combined data from three points on the limb.

Above 500 km the data can be represented, to within the allowed accuracy, by single exponential terms. Least-squares fits to the data at λ3640, λ3600, λ3550, and λ3500 give the following equations:

$$\log E_{3640} = 2.89 \pm 0.04 - (0.95 \pm 0.03) \times 10^{-8}h \qquad \text{(2-11a)}$$

$$\log E_{3600} = 2.83 \pm 0.04 - (0.91 \pm 0.03) \times 10^{-8}h \qquad \text{(2-11b)}$$

$$\log E_{3500} = 2.79 \pm 0.04 - (0.91 \pm 0.03) \times 10^{-8}h \qquad \text{(2-11c)}$$

$$\log E_{3500} = 2.73 \pm 0.04 - (0.89 \pm 0.03) \times 10^{-8}h \qquad \text{(2-11d)}$$

Figure 2-5 is a plot of $\log E_{3640}$ versus height. Three curves are drawn through the data; one corresponding to Eq. (2-11a); one labeled "best fit," which corrects the curve from (2-11a) to fit the data below 500 km; and one corresponding to the equation

$$E_{3640} = 3000 \exp(-5 \times 10^{-8}h) + 360 \exp(-1.8 \times 10^{-8}h) \qquad \text{(2-12)}$$

Figure 2-5 also contains a curve of F versus height, which is derived from the curve labeled "best fit," and displaced from its true position on the intensity scale in order to include it in the figure.

The curve of F versus height shows a sharp maximum near 500 km. Similar maxima appear in the data for most of the Balmer lines although, for the most part, these maxima result from a single observation below 500 km. Our purpose in combining data at λ3640 from three regions on the limb is to check the reality of this maximum in F. Any reasonable curve through the data results in a similar maximum, and we conclude that it is a real effect. The exist-

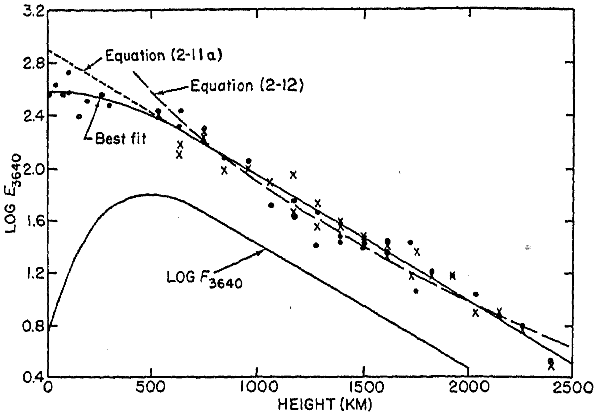

Fig. 2-5. The head of the Balmer continuum in the low chromosphere. The curve of surface brightness F is derived from the "best-fit" curve for E. (From R. G. Athay, et al., **1955**, *Astrophys. J.*, suppl., **1**, 506.)

ence of this maximum serves as an important check on the chromospheric model.

C. *Balmer and Paschen Lines*

The measurement of line intensities, though more laborious, does not entail the difficulties associated with the reduction of the continuum data. The reduction process becomes simply that of integrating the area under the line profiles. In general, the intensities of the strong lines are more accurately determined because of the increased contrast between the line and the background continuum. However, a serious problem arises because the range of intensities, $\simeq 10^4$, exceeds the range of sensitivity of photographic films. The High Altitude Observatory program at Khartoum avoided this difficulty by using an image divider to give two images of the spectrum, with an intensity ratio of about 100 : 1.

The Balmer line intensities are tabulated in Table A-3 of the Appendix. These data represent a combination of two regions on the limb about 25,000 km apart (Athay et al., 1954), one of which corresponds to the region where the continuum data were measured. Figure 2-6 is a plot of the data for one line at both regions of the limb. It is evident that there is no significant difference between the two regions. In the process of reducing the line data, some of the lines

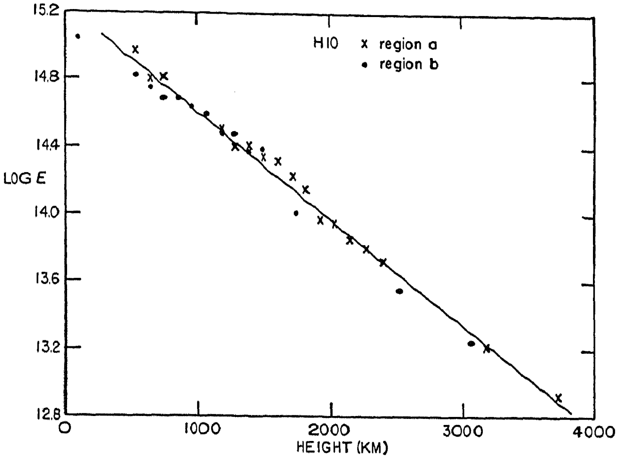

Fig. 2-6. H10 at two different regions of the solar limb.

were measured twice. The probable error of a given measurement from 56 such cases is ±0.04 in log E. More serious errors undoubtedly arise from local irregularities in the film grains.

In the last two columns of Table A-3 in the Appendix we give values of β' at 2000 km and at the height where the line fades into the background continuum. These values of β' are estimates obtained from plots of log E versus height, as in Figure 2-6. Values are given to three figures, but the last figure is not significant. For most of the lines the error in β' is estimated to be about $\pm 0.05 \times 10^{-8}$.

For $12 \leq k \leq 28$, a single exponential term provides a good representation of the data for each line. We have tried least-squares representation of log E versus height for both linear and quadratic representations. In each case, the probable error of the coefficient of the quadratic term is about the same size as the coefficient itself; so we conclude that the linear representation is satisfactory. However, the sign of the quadratic term is the same for all lines, indicating a very slight upward curvature at the greatest height observed. It is of interest to note that the same kind of effect is present in the data on the Balmer free-bound continuum. The marginal nature of the effect precludes too great attention, but we shall return to this point when we discuss the model of the chromosphere. For $k \geq 29$, there are departures from a single exponential which apparently arise from a strong blend in H30, which also overlaps with the wings of H29 and H31.

For $k \leq 12$, there is a steady trend toward a decrease in β' with decreasing height in the low chromosphere. It should also be noted that there is a monotonic increase in β' with increasing h. At λ3640, corresponding to $k = \infty$, $\beta' = 2.19 \times 10^{-8}$, in good agreement with the limiting β' for the higher-order lines.

The meager data available for the Paschen lines is given in Table 4 of the Appendix. It is not possible to estimate reliable values of β' from these data.

D. Helium Lines

The 1952 eclipse spectrograms show several helium lines with sufficient intensity to permit reliable photometric measurement. Lines of the 2^1s-k^1p, 2^1p-k^1d, 2^3p-k^3s, and 2^3p-k^3d series of neutral helium and the Paschen-α line of ionized helium are present. In addition, there is a weak line from the transition 2^1p-3^1s which cannot be accurately measured; a line from the transition 2^3p-3^3s is blended with H8. The intensity of this latter helium line can be separated from H8 by interpolating between H6 and H9 to obtain the intensity of H8.

Intensities of the helium lines (Athay and Menzel, 1956) are given in Table A-5 of the Appendix. Figure 2-7 is a plot of log E versus height, with the corresponding curve of log F versus height for the neutral helium line λ7065. Most of the other neutral helium lines exhibit essentially the same variation of log E and log F with height. In contrast to the data for hydrogen, there is no evidence for systematic changes in β' from line to line in the helium data. The only notable departures from the curves in Fig. 2-7 occur for some of the lines which appear to be blended in the low chromosphere. These lines show a larger β' at low heights. However, because β' for helium is considerably smaller than for the metal lines, the effects of blends decrease rapidly with height. The maximum in the curve of log F versus height near 1100 km is evident in all the neutral helium lines. In order to represent the neutral helium data with an analytical expression, we smooth the data by averaging the intensities of the unblended lines, and then fit the smoothed data with a series as given in Eq. (2-3). We obtain, for $h > 1000$ km (Athay and Menzel, 1956),

$$E_{kj} = (10^{16}/\delta_{kj})[1.26 \exp(-1.27 \times 10^{-8}h) - 40 \exp(-3.7 \times 10^{-8}h) + 100 \exp(-4.6 \times 10^{-8}h) - 1600 \exp(-9.2 \times 10^{-8}h)] \quad (2\text{-}13)$$

The δ_{kj}'s measure the relative intensities of the lines, and have the values given in column 2 of Table A-5 in the Appendix. Equation (2-13) *does not fit the data below 1000 km and should not be used below this height.*

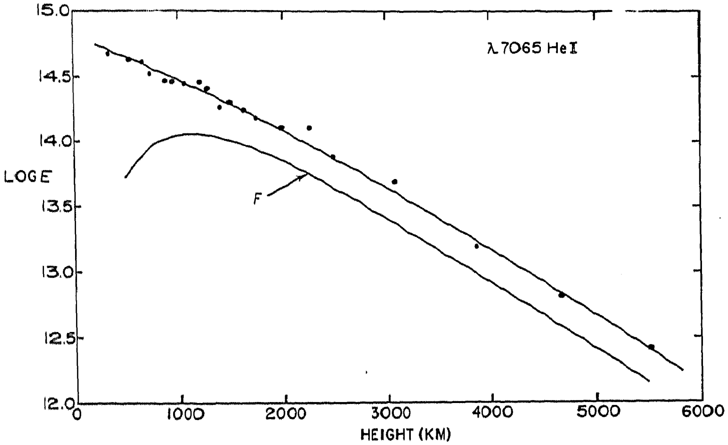

Fig. 2-7. The triplet line 3^3s-2^3p of HeI showing integrated intensity E and surface brightness F.

The ionized helium line λ4686 shows discernible differences from the neutral helium lines. Curves of log E and log F versus height for this line are shown in Fig. 2-8. β' is somewhat smaller than for neutral helium, especially in the low chromosphere, and the maximum in the log F curve seems to lie near 1500 km. These differences may be real or they may be due to errors in the data. Unfortunately, this line is weak and the data are not quite as reliable as they are for the stronger neutral helium lines.

The maxima in the log F curves for helium are analogous to the maximum in the log F curve for the Balmer continuum emission at λ3640.

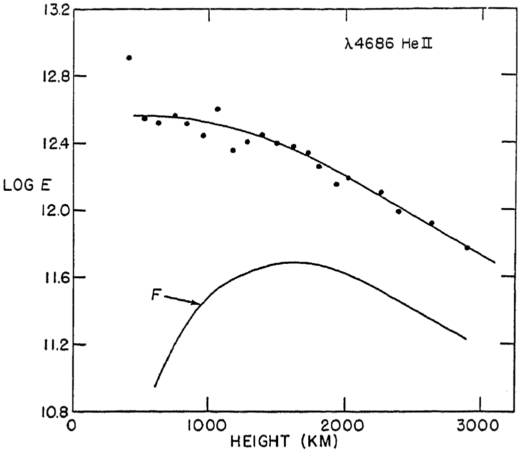

Fig. 2-8. The Paschen-α line of HeII showing integrated intensity E, and surface brightness F.

E. Metal Lines

The metal lines show more diversity than either the hydrogen or helium lines. The intensity variation with height for each of the metal lines seems to be adequately represented by a single exponential term. However, β' varies through a range from $\sim 4.6 \times 10^{-8}$ to 0.7×10^{-8}. Line intensities and values of β' are tabulated in Table 6 of the Appendix (Zirker, 1956, 1958).

Figure 2-9 is a plot of log E versus height for several of the metal lines. It is evident from this figure that the differences in β' do not arise from errors in the data. The most significant correlation with β' seems to come from the absolute intensities of the lines (Zirker, 1956, 1958). No systematic dependence of β' on either excitation or on ionization potential is indicated by the data. Previous suggestions that such correlations existed apparently resulted from generalization drawn from insufficient data.

F. Other Data

In addition to the data tabulated in the preceding sections, data exist for the CN band at λ3883 (Pecker and Athay, 1955; D. V. Thomas, 1958) and for the coronal lines (Athay and Roberts,

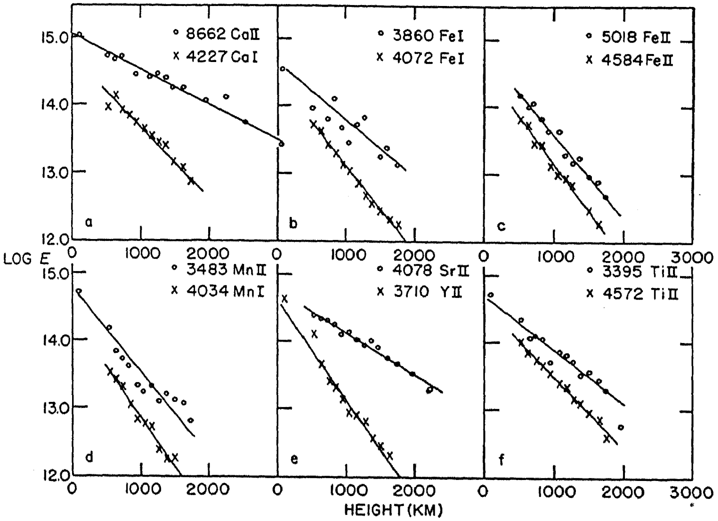

Fig. 2-9. Representative lines of neutral and ionized metals.

1955). The CN emission is observed only in the lower 750 km of the chromosphere. For the intensity at the band head, β' is 4.7×10^{-8}. Houtgast (1953) found a similar value of β' for the emission gradient of the total band intensity.

Our interest in the coronal-line data lies not so much in determining the coronal model as in fixing a boundary condition on the chromospheric model. The FeXI line at λ7892 was measured over a height range from 2000 km to 46,000 km at two regions on the limb, one of which coincided with the region where the chromospheric measurements were made. In both regions the Climax and Sacramento Peak coronal isophotes for λ5303 of FeXIV and λ6374 of FeX showed that the emission at the limb at the time of eclipse was as strong as, or stronger than, the emission in adjacent longitudes. Furthermore, there were no signs of local condensations of increased brightness near these regions. Thus it seemed safe to assume that the observed emission was actually representative of the region over the limb. The data for the two regions (Athay and Roberts, 1955) are plotted in Fig. 2-10.

We are interested in determining the lowest height at which the emission from FeXI is present in measurable quantity, which re-

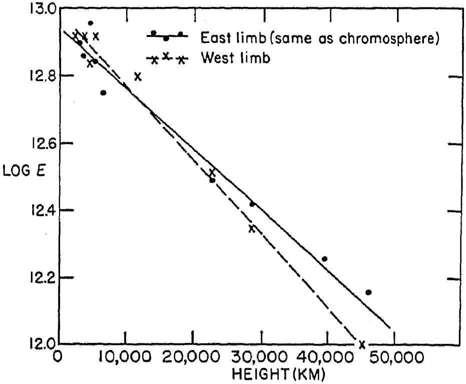

Fig. 2-10. The coronal line λ7892 of FeXI.

quires that we have the curve of log F versus height. The data in Fig. 2-10 are not numerous enough to give the detailed shapes of the curves of log E versus height near the extremities of the data, and the straight lines shown appear to be as good a representation as the data justify. If F has a maximum at some height above 2000 km, as we expect, there should be a marked decrease of β' at heights below the maximum. It is quite evident from Fig. 2-10 that any marked decrease in β' must occur below 8000 km. Therefore, we have a strong boundary condition on the upper chromosphere, viz., we require our chromospheric model to account for emission from FeXI at height as low as 8000 km, and possibly much lower.

CHAPTER 3

Variations in Chromospheric Structure and Mass Motions

R. GRANT ATHAY

I. Introduction

In any detailed discussion of chromospheric structure, its regularity, in both the spatial and the temporal senses, raises important questions. In the spatial sense, to what extent does the chromosphere depart from spherical symmetry? In the temporal sense, does the chromospheric spectrum show a variability over the solar activity cycle, or possibly exhibit a more local variation in time? Another closely allied question is whether the chromospheric structure shows any association with the various types of mass motion occurring in the outer solar atmosphere.

We shall discuss the evidence bearing on these three facets to the question in this chapter.

II. Positional Variations

The most direct evidence for chromospheric irregularity comes from eclipse and extra-eclipse observations of the solar limb made monochromatically in the stronger spectral lines. The top of what we have called the lower chromosphere in Chapter 1 appears to be quite irregular in height, and the upper chromosphere appears to consist entirely of spicules. Further evidence that the chromospheric structure departs markedly from spherical symmetry comes from disk observations that were made in the centers of the strong Fraunhofer lines.

Spatial irregularities in chromospheric structure seem to be of two main types, which differ in both size and spectra. The large-scale structure has a characteristic size lying in the range 10^4 to 10^5

km and spectral features which differ considerably from those of the "average" chromospheric spectrum. The small-scale structure has a characteristic size of some 10^3 km, and a spectrum very similar to that of the average chromosphere.

Plages, flares, and sunspots appear in extra-eclipse observations as such large-scale structures. At eclipse the so-called, but poorly named, "hot spots" fall into the class of this large-scale structure. The fine mottling in spectroheliograms provides evidence of the small-scale structure in disk observations. Spicules provide the evidence for the small-scale structure at the limb, in both eclipse and extra-eclipse observations. The correspondence between the structure seen on the disk and at the limb is, however, very poorly understood.

Leighton (1959) reports that CaII plages show a close association with regions of increased magnetic field strength, and Howard (1959) notes the same effect in Hα plages. There can be little doubt, then, that spatial and temporal irregularities in chromosphere structure result in many instances from a more or less direct coupling with magnetic fields. The coupling most probably arises through an energy transfer from the magnetic fields to the chromospheric gases. Therefore, we shall treat the spectroscopic data independently of the magnetic field data.

A. Large-Scale Structure

Eclipse observers have variously referred to abnormal regions of the chromosphere as: "hot spots" (Cillié and Menzel, 1935); "excited regions" (Hemmendinger, 1939); and "active regions" (Athay, Evans, and Roberts, 1953; Athay and Thomas, 1957a). In all cases the regions referred to were located over plages and under regions of bright coronal emission in the λ5303 line. However, the pronounced anomalies in the chromospheric spectrum extended for only 1 to 2° along the limb, which was considerably less extensive than either the associated plage or coronal regions.

In this section we summarize the data for active regions at the 1932, 1936, and 1952 eclipses. We shall, however, center our discussion of active regions around the 1952 eclipse data, which are tabulated in the Appendix, since they are far more extensive than the earlier data.

The 1952 active region first appeared as a new sunspot group near the east solar limb. During disk passage the sunspots and plages developed in size, and flares were reported on three separate occasions. On the day of the eclipse the region was centered on the west limb. The yellow coronal line λ5694, arising from CaXV (Edlén, 1942, 1954; Rohrlich, 1956; C. Pecker, Billings, and Roberts, 1954; Layzer, 1954, 1956) was observed, for the first time at eclipse, in this region (Athay et al., 1953; Lyot and Dollfus, 1953; Athay and Roberts, 1955). Chromospheric emission extended to unusually great heights. Lines of high excitation potential were abnormally strong at all heights, whereas lines of low excitation potential were relatively weak at low heights and strong at greater heights. A region apparently devoid of chromospheric-type emission lay immediately adjacent to this region of enhanced emission. Here even the very strongest lines showed emission too faint to measure reliably. Moon profile pictures revealed no lunar features of sufficient size to obscure the chromospheric emission.

In some respects this region of reduced emission is just as interesting, if not more so, than the region of increased emission. However, since there are no quantitative data we can only speculate about its nature. There are, however, considerable data for the region of increased emission. The Paschen lines are bright in this region and suitably exposed for photometric studies. Unfortunately,

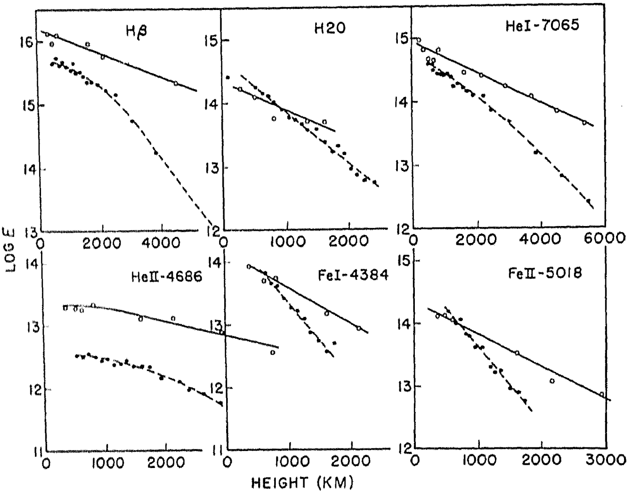

Fig. 3-1. Comparisons of 1952 active region and normal region for selected lines: ●, normal; ○, active. (From R. G. Athay and R. N. Thomas, 1957, *Astrophys. J.*, 125, 794–795.)

the ultraviolet spectrograph did not operate properly during the time this region appeared, so the Balmer line data are very limited.

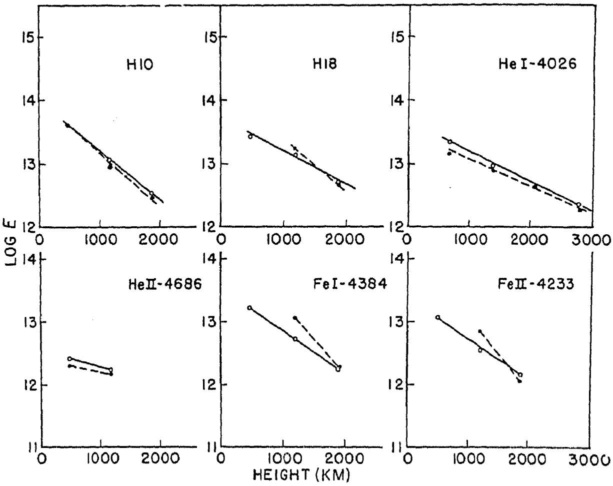

Fig. 3-2. Comparisons of 1936 active region and normal region for selected lines: •, normal; ○, active. (From R. G. Athay and R. N. Thomas, 1957, *Astrophys. J.*, 125, 794–795.)

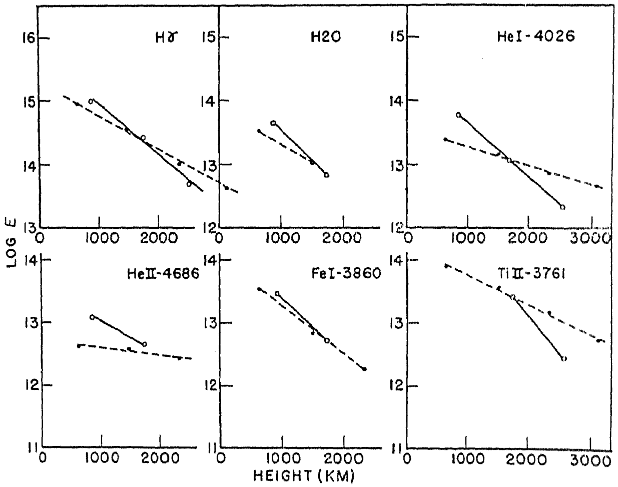

Fig. 3-3. Comparisons of 1932 active region and normal region for selected lines: •, normal; ○, active. (From R. G. Athay and R. N. Thomas, 1957, *Astrophys. J.*, 125, 794–795.)

Because of an instrumental failure, none of the spectrographs continued to operate until third contact. Thus, the zero point of the height scale had to be estimated by extrapolation from second contact. Irregularities in the moon profile and errors in the time assumed for the duration of totality could lead to as much as 1000 km error in the zero point of the height scale determined in this way. The relative heights, however, are accurately known.

Comparisons between the emission in normal chromospheric regions and in the active regions are exhibited in Figs. 3-1, 3-2, and 3-3. Neither the 1932 nor the 1936 active regions represent as strong a departure from the normal chromosphere as the 1952 region. It is evident from the data that the 1936 region is similar in nature to the 1952 region, whereas the 1932 region is apparently of a different nature.

B. Small-Scale Structure

Although we have stated that the small-scale structures in the chromosphere have spectral features similar to those of a large portion of the chromosphere, we do not mean to imply that these features are necessarily difficult to recognize. When observed at the limb, the spicules in the upper chromosphere stand out prominently in projection against a relatively dark background as illustrated in Figs. 3-4 and 3-5. When observed against the bright solar disk, however, they are much more difficult to distinguish, if, indeed, they can be distinguished at all. Spicule observations made outside of eclipse contribute heavily to our understanding of chromospheric structure. These observations are summarized in Section 4-IV.

Because of the irregular appearance given to the chromosphere by spicules, many observers have asked whether the chromosphere

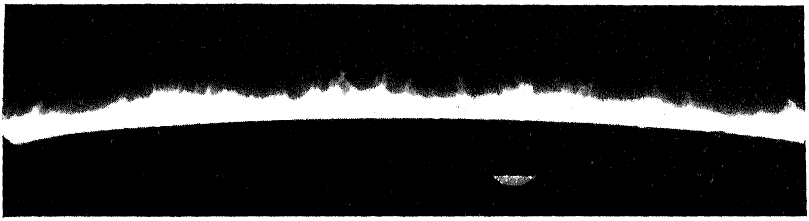

Fig. 3-4. A monochromatic Hα photograph of the polar chromosphere and spicules taken with the Sacramento Peak chromosphere camera. (Courtesy R. B. Dunn.)

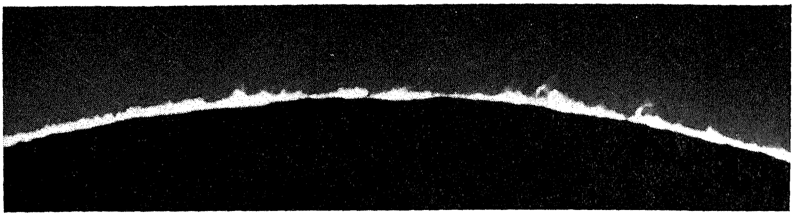

Fig. 3-5. A white-light photograph of the chromosphere and spicules taken at the 1930 eclipse by the Swarthmore expedition. (Courtesy Sproul Observatory.)

itself is not simply an array of spicules. There are two possible interpretations to such a question. One interpretation might be that virtually all the material in the chromosphere is concentrated in spicules, with interspicular regions essentially "empty." Alternatively, most of the radiation normally classed as chromospheric might arise in the spicules with interspicular material radiating a quite different spectrum even though the mass distribution might be nearly uniform. In our discussions of a chromospheric model, we shall pay particular attention to this question.

At this point it is well to consider whether there is any meaning to the concept of an "average" region of the chromosphere as applied to eclipse data. Eclipse spectra, as a rule, do not resolve the fine details of much of the spicular structure. Thus, we recognize that a particular region of the limb represents an average of the emission from surrounding regions. Of necessity, there is an averaging over all regions lying in the line of sight and because of instrumental and atmospheric effects there is an averaging in the direction perpendicular to the line of sight. Furthermore, in any photometric data reduction, the use of a microdensitometer, or other recording device, introduces an additional averaging. The microdensitometer slit employed in the reduction of the 1936 and 1952 data averaged over a length of arc extending 12,000 km along the solar limb. Spicule statistics indicate that three to four observable spicules normally fall in such a sector of the limb. Thus, eclipse data represent an average over spicular and interspicular regions. If the concept of an "average" region of the chromosphere is meaningful, it is necessary that eclipse data show essentially the same characteristics at different points on the limb.

Hemmendinger (1939) measured line intensities and scale

heights at 14 regions on the solar limb for the 1936 eclipse. Nine of these regions showed very similar line intensities as well as similar scale heights. The five remaining regions all showed prominence features. For the 1952 eclipse, we studied three regions of the limb, two of which showed nearly identical features (cf. Fig. 9-2).

The third region was the active region discussed in the preceding section and was chosen for its outstandingly peculiar characteristics. Houtgast (1958) also determined scale heights for the 1952 eclipse by combining data from several regions on the limb. Generally, his results agree quite well with the results for the two normal regions we studied. However, he found slight evidence that the relative line intensities change by small amounts from one region to another. From extensive studies of the Hα chromosphere outside of eclipse, Dunn (1956) found little evidence for significant changes in either scale height or intensity from one region to another, provided the emission was averaged over an arc length comparable to that used in the reduction of eclipse data.

In summary, it appears that for the emission averaged over a length of arc of about 12,000 km there are only small differences in scale heights and line intensities. Therefore, a particular chromospheric region of this scale may be regarded as being representative of the chromosphere in general.

III. Temporal Variations

Since the solar corona exhibits marked systematic changes in structure throughout the sunspot cycle, it would not be too surprising to find similar changes in chromospheric structure. Such changes might be manifested through changes in scale heights or through changes in absolute and relative line intensities. An inspection of Table 2-1 indicates, however, that few data are available for an investigation of systematic changes in the chromosphere. Furthermore, since the scale heights differ for different lines, both absolute and relative line intensities vary with height above the solar limb. Any differences in the zero points of the height scales will therefore tend either to obscure or enhance the evidence for such systematic changes. For example, a change in the zero point of the height scale by as little as 300 km changes the ratio of intensities of helium lines to faint metal lines by about a factor of two, and changes the absolute intensity of faint metal lines by about a factor of three. Thus,

Table 3-1. Representative Values of $\beta' \times 10^8$

λ	Ident.	1932 CM[a]	1932 AMO	1936 AMO	1941 V	1945 V	1945 K	1952 HAO
4861	Hβ	1.16	—	1.38	1.20	0.95	1.33	1.60
4101	Hδ	1.16	—	1.15	1.32	1.22	1.43	1.70
3835	H9	1.22	—	1.52	1.37	1.12	1.54	1.51
3750	H12	1.22	—	1.82	1.47	1.11	1.70	1.68
3712	H15	1.30	1.6	1.82	1.55	—	1.82	1.73
3692	H18	1.20	1.9	2.0	2.04	—	—	1.85
3679	H21	1.42	2.1	2.4	—	—	—	1.96
3671	H24	1.47	2.3	2.4	—	—	—	2.05
3666	H27	1.61	2.2	1.9	—	—	—	2.08
3661	H31	1.54	—	—	—	—	—	2.12
3640	H∞	1.54	2.3	—	—	—	—	2.19
5876	HeI	1.33	—	0.99	0.88	0.73	1.01	1.25
4713	HeI	0.50	1.30	0.8	1.96	—	—	1.25
4472	HeI	1.03	—	0.99	1.11	0.87	0.95	1.25
4026	HeI	0.67	1.40	0.90	0.75	0.87	—	1.25
4686	HeII	0.30	0.92	0.7	—	—	—	1.00
4227	CaI	2.11	—	2.44	1.33	—	—	2.16
4072	FeI	1.78	2.6	3.7	—	—	—	2.95
4064	FeI	1.78	3.0	3.6	1.28	—	—	2.84
4045	FeI	1.78	2.8	3.0	1.14	—	—	2.58
3860	FeI	2.04	—	2.2	1.36	—	—	1.94
3764	FeI	2.11	3.1	1.9	—	—	—	3.12
3746	FeI	1.69	2.2	2.2	—	—	—	2.92
3720	FeI	1.69	2.1	—	—	—	—	2.31
5018	FeII	—	—	2.9	1.32	—	2.78	2.90
4584	FeII	—	—	4.3	1.23	—	—	3.21
5184	MgI	1.81	—	1.75	1.64	0.66	—	2.16
4078	SrII	1.12	1.7	1.57	1.60	1.31	1.78	1.47
4572	TiII	1.58	—	2.9	2.60	—	—	2.54
3761	TiII	1.13	2.0	1.55	1.46	1.11	1.58	2.31
3759	TiII	1.13	2.0	1.72	1.46	—	—	2.18
3774	YII	—	3.8	—	—	—	—	3.43

[a] CM, Cillié and Menzel, 1935; AMO, Athay, Menzel, and Orrall, 1957; V, Vyazanitsyn, 1951, 1952; K, Kristensen, 1955; HAO, see references in text.

line intensities are not well suited for a study of temporal changes in chromospheric structure.

On the other hand, above 1000 km, the scale heights of all the chromospheric lines appear to be independent of height, and for the majority of lines the same holds true for $h \geq 100$ km. Therefore, scale heights can be compared at different eclipses irrespective of the zero point of the height scale.

Table 3-1 contains values of β' for representative lines observed at five eclipses. The two entries for the 1932 eclipse represent two independent reductions of the same set of spectrograms at the same point on the limb, and the differences in β' arise from differences in the photometric standarization. A comparison of 1932 data with data from other eclipses indicates that the reduction by Cillié and Menzel (1935) probably contains large systematic errors, and that the second reduction of the data by Athay, Menzel, and Orrall (1957) is more reliable. The two entries for the 1945 eclipse are from spectrograms obtained by different expeditions.

The 1932 eclipse occurred within one year of sunspot minimum, and the 1936 eclipse about one year before maximum. The remaining three eclipses all occurred within about two years of sunspot minimum. Thus, we rely heavily on the 1932 and 1936 eclipse data for any evidence of systematic changes through the sunspot cycle.

An estimate of the relative accuracy of the values given for β' can be made from Fig. 3-6, which shows plots of log E versus height for the hydrogen Balmer line originating on the ninth quantum level. The slopes of the curves are proportional to β'. It is evident that the values of β' are well determined for the 1936, 1945, and 1952 eclipses. For the 1932 and 1941 eclipses, β' is subject to relatively large errors. Of the two sets of data for the 1945 eclipse, those given by Kristensen (1955) are apparently more reliable.

With the exceptions of the 1932 data of Cillié and Menzel and the 1945 data of Vyanzanitsyn, Table 3-1 shows little evidence to suggest systematic changes in β' through the sunspot cycle. In an earlier discussion (Athay and Thomas, 1956) we found evidence for marked systematic changes in β'. This discrepancy arose from the fact that we used the 1932 data of Cillié and Menzel and the 1936 data of Hemmendinger. Subsequently, we (Athay et al., 1957) restandardized the 1932 and 1936 data using the same reduction techniques employed in the 1952 data. As noted above, the changes in

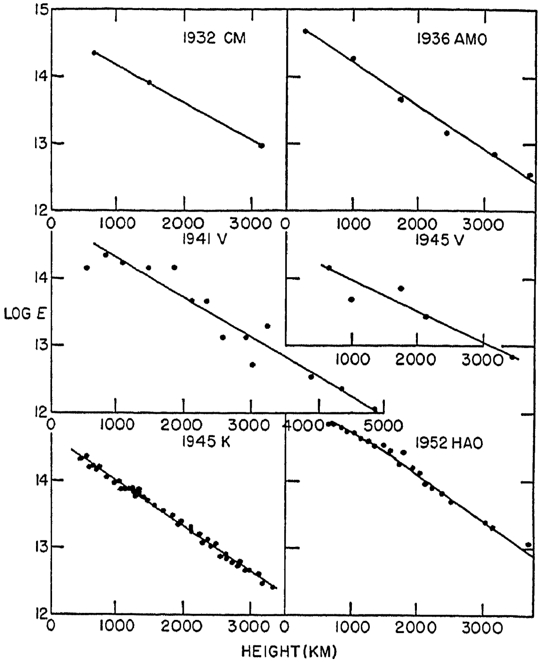

Fig. 3-6. Illustration of the reliability of β for H9.

the 1932 data resulted from changes in photometric standardization. The changes in the 1936 data, however, resulted from extensions of the data to a greater intensity range, and therefore a more accurate determination of β'. Since both the 1932 data of Cillié and Menzel and the 1945 data of Vyanzanitsyn are of questionable accuracy, we must conclude that β' is essentially constant in time as well as in position on the solar limb. We also emphasize, as already indicated by our compilation of data, that many more data are required before any great confidence can be placed in this conclusion. Correlations of β' in 1932 and 1936 with β' in 1952 are illustrated in Figs. 3-7 and 3-8.

Although a comparison of line intensities at different eclipses is subject to systematic errors, such comparisons must be made before it can be determined whether the chromospheric structure changes with time. In an effort to make the comparisons as meaningful as possible, the zero points for the height scales in the 1932 and 1936 data were re-determined (Athay et al., 1957) according to the same

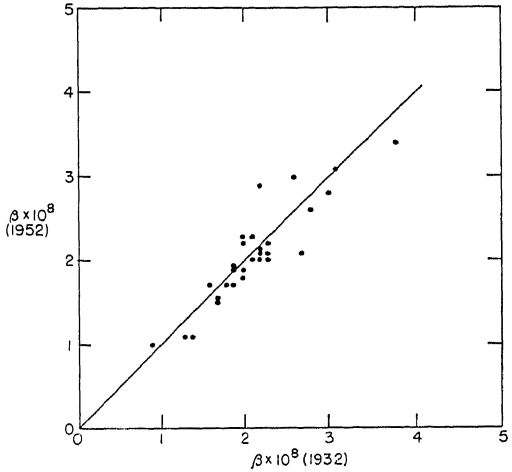

Fig. 3-7. Correlation in β between 1952 and 1932 eclipses. (From R. G. Athay et al., *Smithsonian Contrib. to Astrophys.*, 2, 45-48.)

criterion used in the 1952 data. Systematic errors, resulting from errors in the zero point of the height scale, should now be reduced to a minimum in these three sets of data.

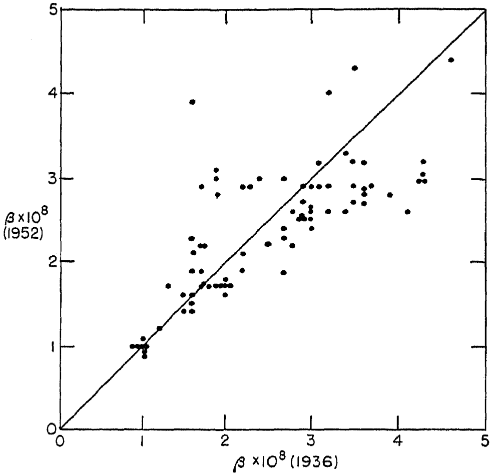

Fig. 3-8. Correlation in β between 1952 and 1936 eclipses. (From R. G. Athay et al., 1957, *Smithsonian Contrib. to Astrophys.*, 2, 45-48.)

Figure 3-9 contains plots of log E versus height for lines of different excitation potential. It is evident from these plots that the relative line intensities in the three sets of data are the same over a wide range in excitation potential. Therefore, on the basis of the data presently available, we conclude that the mean chromospheric excitation is constant in time.

The data in Fig. 3-9 indicate a difference of 0.5 to 0.6 in the logarithm in the absolute intensities between the 1952 eclipse and the other two eclipses. By further comparing the continuum intensities near the photosphere and the coronal continuum intensities in the polar corona, Athay et al. (1957) concluded that these apparent differences in absolute intensities resulted predominantly from photometric errors rather than from real changes in chromospheric emission, and that the errors were divided about equally between the 1952 data and the other two sets of data. Thus, the absolute intensity scale for the 1952 data seems to be too high by about 0.2 to 0.3 in the logarithm.

If the intensity of the continuum emission at λ4700 near the limb is made to agree for the 1932, 1936, and 1952 eclipses, the line

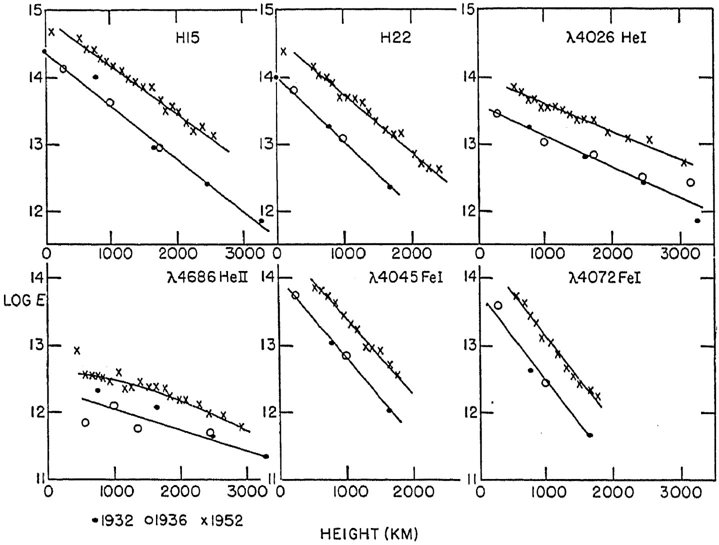

Fig. 3-9. Comparisons of β and E for selected lines at 1932, 1936, and 1952 eclipses. (From R. G. Athay et al., 1957, *Smithsonian Contrib. to Astrophys.*, 2, 45–48.)

intensities from the 1932 and 1952 eclipses agree also, whereas the line intensities at the 1936 eclipse are relatively weak by about 0.3 in the logarithm. This discrepancy between the line and continuum data in 1936 is apparently the only evidence for significant variation in chromospheric emission at the three eclipses. Even this evidence, however, may represent a photometric difficulty rather than a real change in chromospheric emission. More data giving reliable absolute intensities are therefore needed before definite conclusions can be drawn. We can only conclude that we find, as yet, no clear evidence for systematic large-scale changes in chromospheric emission.

IV. Data on Mass Motions—Spicules

The strongest and most direct evidence for the existence of velocity fields in the chromosphere comes from spicule observations. These short-lived jets which surge upward through the chromosphere into the corona lead to the classical description of the chromosphere as a "burning prairie." In recent years, observers using the coronagraphs at Climax, Sacramento Peak, and Pic du Midi have furnished valuable data on the motions, sizes, distributions, and life histories of spicules.

In addition to the spicules, which are imbedded in the chromosphere, the chromosphere is bombarded from above and below by streams of prominence matter. Energetically, one of these streams is probably comparable to several spicules. However, they are far less numerous than spicules and are generally a less important component of the velocity field. Although prominence streamers undoubtedly have a marked local effect on chromospheric structure, in our compilation of chromospheric data we have purposely avoided discussion of such regions until proper data are available.

Finally, the chromosphere overlies a photosphere, covered with fine granulation, which is associated either directly or indirectly with velocity fields. It is not yet known whether granules and spicules represent two aspects of the same general velocity field or single aspects of two separate velocity fields having different origins. Unfortunately, there is much uncertainty about the meaning of granule statistics (e.g., Uberoi, 1955) because of uncertainties in the size, velocity, and spectrum of individual granules, as well as in the interpretation of these data as discussed in Chapter 6. The recent observations made from high altitude balloons, and with the high-resolution spectrographs at McMath-Hulbert and Sacramento Peak Observatories represent promising advances toward obtaining the desired data. We do not feel it is advisable to make use of these data until more complete observations and analysis are available.

A. Characteristics of Spicules

Early solar observers (cf. Secchi, 1877) successfully registered their visual observations of spicule structure in quite detailed freehand drawings. Marriott obtained the first photographs of spicules at the 1930 eclipse, and Mohler (1951) later estimates sizes and numbers of spicules from these eclipse pictures. Bugoslavskaya (1946) studied spicule orientations and numbers at the 1945 eclipse. In 1943 Roberts discovered that, under good observing conditions, spicules could be observed with a Lyot filter and coronagraph. Subsequently he and his co-workers measured lifetimes, velocities, and sizes of numerous spicules (Roberts, 1945; Roberts et al., 1949; Rush and Roberts, 1954). Dizer (1952) made similar studies using Lyot's observations at Pic du Midi. Dunn improved the quality of spicule observations considerably by using improved observing techniques with the large chromosphere camera at Sacramento Peak (Dunn, 1956; Lippincott, 1956, 1957; Athay, 1959a). Figure 3-4 exhibits one of Dunn's spicule photographs.

Some pertinent spicule statistics are given in Table 3-2. The results are consistent for the most part, even though different instruments and different observing techniques are used. The most extensive data are derived from Dunn's observations, which undoubtedly include a higher percentage of small faint spicules than do the other data.

Figure 3-10 exhibits isopleths of the number of identifiable spicules crossing a given height in the chromosphere at different solar latitudes (Athay, 1959a). The mean heights and the number of spicules are seen to increase from equator to pole. Also the height where the maximum number of spicules occurs increases from 5000 km at the equator to 6500 km at the poles. In general, the polar spicules are oriented more nearly along a radial direction than those in equatorial regions, and according to van de Hulst (1953) they tend to align with coronal features.

Rush and Roberts (1954) found that spicules of a given lifetime are more numerous for the shorter lifetimes. They also found that there is a marked linear correlation between the maximum

Table 3-2. Spicule Statistics[a]

Observer	No. per radian	Diameter, km	Height, km	Max. height, km	Velocity, km/sec	Lifetime, min	References
Mohler-Marriott	171	1300	—	—	—	—	Mohler (1951)
Roberts	—	2500	—	11,000	30	4–5	Roberts (1945)
Dizer	—	—	7000	—	20–40	2	Dizer (1952)
Rush-Roberts	42	2000	7000	15,000	30	3.5	Rush and Roberts (1954)
Lippincott-Dunn	200 poles, 150 equator	1000	9500 poles, 7300 equator	12,000	26	5	Lippincott (1957)

[a] All values are means.

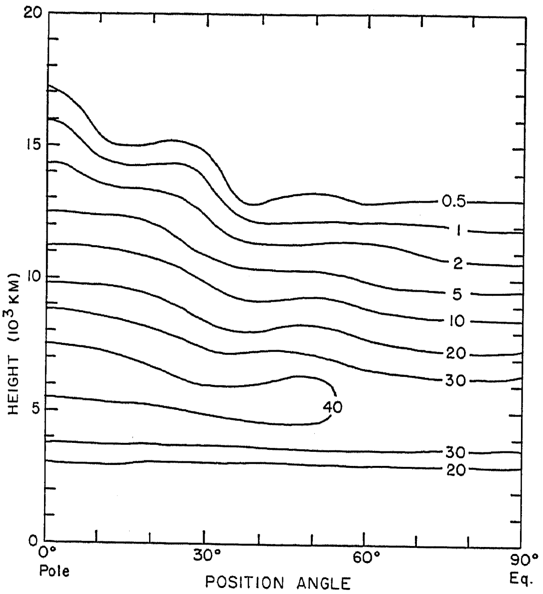

Fig. 3-10. Isopleths of spicule numbers as a function of height and latitude. (From R. G. Athay, 1959, *Astrophys. J.*, 129, 167.)

height attained by a spicule and its velocity of ascent. Lippincott (1957) found a small but significant correlation between maximum height and total lifetime of a spicule.

One of the more important spicule observations is that of spicule motions. The apparent life history of a typical spicule has been described as a rise at uniform velocity to maximum height, where the spicule pauses for about one-third of its lifetime, then either fades in brightness or falls back along its original path at the speed of ascension. Roughly, half of the spicules fade from view while still at maximum height. The foregoing description of spicule motions must be evaluated in terms of the accuracy to which spicule velocities have been measured. Velocities are determined by plotting the apparent heights of the spicules against time. The apparent heights contain errors from seeing excursions which, at best, are of the order of 1″ of arc, and from lack of a well-defined reference point. Thus, the height of a spicule at any one time is uncertain by about ±500 km in terms of the heights measured at other times in the spicule history.

Figure 3-11 shows the locus of height versus time for a typical spicule, represented alternatively by the assumption of constant velocity of ascent and descent with one-third of the lifetime at maximum height and by the assumption of motion under the sole force of the solar gravitational field (Thomas, 1948; Athay and Thomas, 1957b). In order to distinguish between these two rather contradictory assumptions the velocity must be accurately determined during the time the spicule is near its maximum height. Until this can be done, either of these assumptions, or any intermediate combination, is acceptable on the basis of the observations. A constant upward and downward velocity implies that there are upward forces just counteracting the downward force of gravity, and that there are discontinuities in velocity when maximum height is attained. Motion under the sole force of the gravitational field, on the other hand, implies that whatever force accelerates the spicule in its upward motion ceases to act before the spicule becomes visible. Either of these alternatives is very likely an oversimplification of the actual forces acting. It is of interest to note, however, that if the spicule motions are assumed to be governed primarily by the gravitational field, then the observed correlations between velocity and maximum height and lifetime and maximum height are easily understood. On the other hand, if constant velocity is assumed, there is no a priori reason for either correlation.

Miss Lippincott (1957) found large regions of the solar limb of the order of 10^5 km in length over which the spicules show syste-

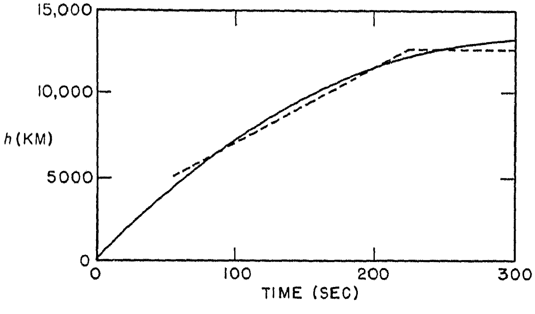

Fig. 3-11. Two alternative models for spicule motions. The dashed line represents a constant velocity with one-third of lifetime at maximum height. The solid curve represents motion in a gravitational field. (From R. G. Athay and R. N. Thomas, 1957, *Astrophys. J.*, **125**, 806.)

matic orientations and similar life histories. These regions have lifetimes of the same order as the mean lifetimes of individual spicules, and may represent a fundamental association between spicules and large-scale velocity fields or magnetic fields. Until more data are available, however, such an association can be only speculative.

B. The Total Number of Spicules on the Sun

A problem of prime importance in consideration of spicule structure and its effect on the chromosphere is the determination of the total number of spicules on the sun at a given time. Such a determination is complicated by the fact that spicules are observed at the limb of the sun, which means that the line of sight is tangential to the spherical surface of the sun. Therefore, spicules are inevitably seen lying both fore and aft of the true solar limb.

For a spicule located at an angle θ from the limb, the apparent height h is related to the true height h^* by

$$h = h^* - 105\theta^2 \tag{3-1}$$

where h^* and h are measured in km and θ is measured in degrees. Thus, spicules that have a true height of 15,000 km will have apparent heights of 14,000 km if located 3.1° from the limb, 10,000 km if located 6.9° from the limb, and 5000 km if located 9.7° from the limb.

For each degree away from the limb, the tangential distance from the limb increases by about 12,000 km. Since the average spicule diameter is of the order of 1000 km, spicule counts at the limb are averaged over a path length many times the mean spicule diameter. If there are a large number of spicules on the sun, a given line-of-sight path will very likely intersect more than one spicule, and the counted number of spicules may be far less than the actual number. The apparent decrease in spicule numbers below the maxima in Fig. 3-10 is most likely due, in part, to this effect of obscuration resulting from unresolved spicules. We consider first the problem of converting the observed spicule number to the actual number along the line-of-sight path and second, the problem of correcting for line-of-sight effects.

If the number of spicules that can be counted at a given apparent height and the mean apparent diameter of a spicule are known, it is possible to compute the number of spicules actually present in the line of sight at that height (Athay, 1959a). However, since the problem involves line-of-sight projections and obscuration by overlapping, it is necessary to know the spatial distribution, relative surface brightness and optical thickness of spicules. In the following it is assumed that spicules are randomly distributed over the solar surface, that they all have the same surface brightness and that they are optically thick in Hα. These latter two assumptions are equivalent to the assumption that if three or more spicules overlap when projected against the plane of the sky only one brightness maximum will be observed. It is necessary to make such assumptions at the outset, but, following the computations, it will be shown that these assumptions do not have any great influence on the results.

The problem of relating the observed brightness maxima to the true spicule number is analagous to dropping objects, say spicules, at random, into a series of boxes and then determining the relationship between the number of spicules dropped and the number of boxes containing one or more spicules.

Divide a 12° sector of the solar circumference into m boxes defined by

$$m = (2\pi R_0/d)(12/360) \tag{3-2}$$

where d is the mean *apparent* diameter of a spicule. Then consider that N spicules are dropped at random into these boxes, and determine S, the number of spicule-like features that can be counted. S differs from the number of boxes containing spicules because each box is the width of one spicule. If two adjacent boxes each contain one or more spicules, the spicules will blend together so that a total of only one spicule will be counted in the two boxes. Similarly, any series of j boxes each containing one or more spicules will contribute only one count in the spicule statistics. Designate $0j0$ as a configuration of j adjacent boxes, all of which contain one or more spicules and are bounded at either end by empty boxes, and S_{0j0} as the number of these configurations. Then, the number of spicule-like features counted is

$$\sum_{j=1}^{m-2} S_{0j0}$$

If P_0 is the probability of a given box being empty, $1 - P_0$ is the probability that a given box contains one or more spicules. Hence, the probability for a single occurrence of a configuration $0j0$ is $P_0^2(1 -$

$P_0)^j$. The number of such occurrences is $(m/j)P_0^2(1 - P_0)^j$, and therefore, the total number of features counted is

$$S = mP_0^2 \sum_{j=1}^{m-2} (1 - P_0)^j/j = -mP_0^2 \ln P_0 \qquad (3\text{-}3)$$

since $m \gg 1$. For, a random distribution of spicules

$$P_0 = [1 - (1/m)]^N \simeq e^{-N/m} \qquad (3\text{-}4)$$

again since $m \gg 1$. Therefore,

$$S = Ne^{-2N/m} \qquad (3\text{-}5)$$

In Dunn's films, from which the data in Fig. 3-10 were taken, the mean apparent spicule diameter in the upper chromosphere is about 1″ of arc, or some 700 km. If the spicule diameter is constant with height, S has a maximum value of $S_m = m/2e$. The data plotted in Fig. 3-10 show $S_m = 37$ at the equator and 42 at the poles. $S_m = 37$ corresponds to $m = 200$ or $d = 730$ km, and $S_m = 42$ corresponds to $m = 230$ or $d = 640$ km. Thus, the observed values of S_m are consistent with Eq. (3-5) and the observed mean spicule diameter.

Using Eq. (3-5) and the observed S and S_m, we compute N at each height and for each latitude. Once this is done, it is a straightforward matter to extend the computations to obtain N^*, the number of spicules in a 6.2 by 12° area of the solar surface, (cf. Rush and Roberts, 1954; Athay and Thomas, 1957).

Table 3-3 contains values of S, N, and N^* for the average number of spicules in a 12° sector of solar latitude. Having determined N, we can now estimate the effects of the assumptions of optical thickness and equal surface brightness. The greatest danger in these assumptions is at low heights where an overestimate of S, as it is defined by Eq. (3-2), leads to an underestimate of N. At 3000 km, $S \simeq 20$ and $N \simeq 300$. In order to increase N by a factor of two, S must be reduced by a factor of 10. The number of spicule configurations in this case would be two, and almost all the observed brightness maxima should result from overlapping of a few optically thin spicules or from a few spicules of above average brightness. If this were the case, the average diameter of the brightness maxima would be of the same order as the spicule diameter. Hence, the total width of the 20 maxima in a 12° sector would be about 14,000

Table 3-3. Computed Values of N and N^*

	6°			30°			54°			78°			Av
h, 10^3 km	S	N	N^*	S	N	N^*	S	N	N^*	S	N	N^*	N^*
3	17.8	340	181	20.1	300	166	19.3	290	172	21.4	240	150	167
4	34.2	210	134	34.6	190	135	36.0	170	122	35.3	135	100	123
5	38.9	170	130	40.0	130	101	39.6	120	96	36.5	90	74	100
6	41.5	120	99	40.0	90	77	38.9	85	76	32.6	58	52	76
7	41.0	90	78	35.2	64	57	30.0	47	42	23.9	34	31	52
8	36.1	63	57	24.7	35	30	19.4	25	23	15.2	19	18	32
9	28.5	41	38	17.9	23	21	11.5	14	13	8.0	9	8.7	20
10	18.7	24	22	9.9	11	10	5.8	6	5.5	3.9	3.9	3.7	10
11	11.6	14	13	5.8	5.8	5.4	2.8	2.8	2.7	1.7	1.7	1.7	5.7
12	6.1	6.1	5.8	2.8	2.8	2.8	1.2	1.2	1.2	1.0	1.0	1.0	2.7
13	3.5	3.5	3.4	1.3	1.3	1.3	0.6	0.6	0.6	0.5	0.5	0.5	1.4
14	1.7	1.7	1.7	0.7	0.7	0.7	0.3	0.3	0.3	0.4	0.4	0.4	0.8
15	0.9	0.9	0.9	0.3	0.3	0.3	0.1	0.1	0.1	0.2	0.2	0.2	0.4
16	0.6	0.6	0.6	0.1	0.1	0.1	—	—	—	0.1	0.1	0.1	0.2
17	0.3	0.3	0.3	—	—	—	—	—	—	—	—	—	0.1

km, which corresponds to a fraction f of the arc length of approximately 0.1.

According to the assumptions used in this paper, all the spicules enter into the statistics on the average diameter of the brightness maxima, and we should have

$$f = 1 - P_0 = 1 - e^{-N/m} \tag{3-6}$$

From Eq. (3-6) and Table 3-3 with $m = 200, f = 0.8$ at 3000 km. Therefore, observed values of f should provide a good check on the reliability of the computed values of N.

Visual estimates of f were made for 109 frames in the four surveys used in this analysis. The estimated values at 3000 km ranged from 0.5 to 0.9 with an average of 0.7. Clearly, then, the computed values of N do not seem to be in error by as much as a factor of two.

Possible errors in N^* are more difficult to estimate. However, since the tendency is to underestimate N at both 3000 and 4000 km, the maximum numerical error in N^* at 3000 km is the same as the numerical error in N at 3000 km. An error of a factor of two in N corresponds to a maximum error of a factor of three in N^*. Since the error in N appears to be considerably less than a factor of two, it is probably safe to assume that the error in N^* from this source is also less than a factor of two.

We have assumed in the discussion above that spicules are obscured by other spicules only, whereas there may be other obscuring matter such as a continuous substratum of chromospheric gases, particularly at low heights. In such a case, we would underestimate S, as defined by Eq. (3-2), and overestimate N at low heights. Hence, this effect works in the opposite direction to those discussed in the preceding paragraph.

The total number of spicules on the sun extending to height h or above is $555N^*$. Hence, there are about 9.3×10^4 spicules extending to 3000 km or higher and about 5.6×10^4 extending to 5000 km or higher. For a mean diameter of 700 km, the spicules extending to 3000 km or higher cover a fraction 0.006 of the solar surface.

A previous estimate (Athay and Thomas, 1957b) of spicule numbers gave somewhat smaller values for N and N^* at low heights. Our earlier analysis started with Lippincott's (1957) data giving $S_h - S_{h+1}$ as a function of height. By assuming the two alternative laws of motion stated in the preceding section and further assuming that $S = N$ for heights above 10,000 km, we derived the probability

P_m, of a spicule reaching maximum height h_m. From P_m we then derived N for heights below 10,000 km. Our estimate of the total spicule number was close to 10^4. However, the uncertainties in this method of estimating N and N^* are likely to be considerably larger than those in the analysis presented here.

Figure 3-12 shows plots of log $(N_h - N_{h+1})$ versus height from the data in Table 3-3 and our earlier computations. For illustration, we also show Lippincott's values of $S_h - S_{h+1}$. Above 10,000 km, the plots in Figure 3-12 decrease exponentially with height. Some authors (cf. Rush and Roberts, 1954; Evans, 1955; Coates, 1958) have attempted to obtain N in the low chromosphere by extrapolating this exponential curve as illustrated in Fig. 3-12. Such an extrapolation leads to something like 10^6 spicules over the solar surface, rather than the much smaller values obtained from an analytical interpreta-

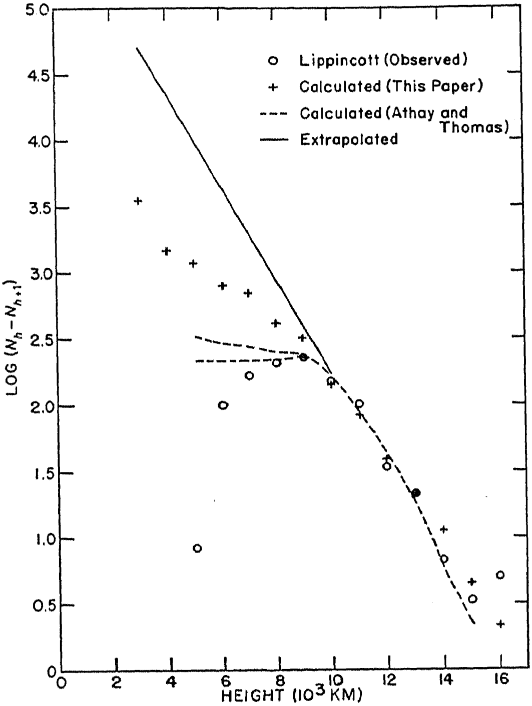

Fig. 3-12. The number of spicules terminating in height intervals of 1000 km as observed at the solar limb in projection against the sky. (From R. G. Athay, 1959, *Astrophys. J.*, 129, 170.)

tion of the data. It is our considered opinion that the use of this extrapolation technique has no justification and that the results are in consequence unreliable. We return to this problem of spicule numbers in connection with our discussion of the chromospheric model.

C. *Profiles of Spectral Lines in the Emission from Spicules*

In addition to studies of spicule motions and numbers, extra-eclipse observations provide valuable information on the thermodynamic state of spicules through studies of line profiles. Michard (1956 and 1959) and Smith (1957) studied Hα profiles in spicules and Athay (1958a and 1960a) studied profiles of Hα, Hβ, and Hγ as well as the K line of CaII and the D_3 line of helium. Spectrograms of these lines are shown in Fig. 3-13.

The emission lines in the spectra of spicules observed outside of eclipse are superimposed on the spectrum of photospheric and chromospheric light arising from seeing excursions of the solar image on the spectrographic slit and from additional photospheric light scattered in the instruments and in the earth's atmosphere. This background spectrum must be subtracted from the composite spectrum in order to obtain the true profiles of the spicule line. The D_3 line presents

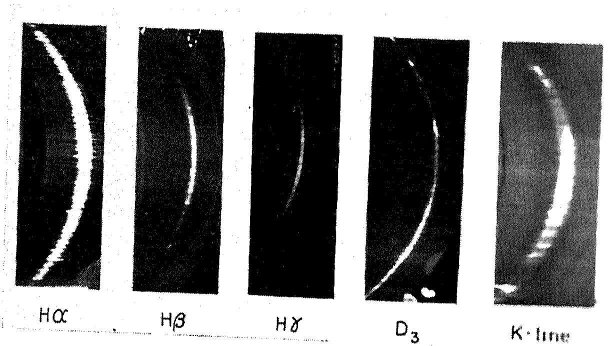

Fig. 3-13. Spicule structure in the brightest spectral lines. Dispersion is perpendicular to the central portion of the arc, which roughly follows a line of constant height in the chromosphere. The background absorption lines are from photospheric light scattered in the earth's atmosphere and coronagraph. The K line is observed in the second-order spectrum, and the remaining lines are observed in the first-order spectrum. (Courtesy G. W. Curtis and K. W. Watson, High Altitude Observatory.)

no particular problem since there is no corresponding Fraunhofer line in the photospheric spectrum. The other lines, however, are superposed on strong Fraunhofer lines, and corrections for scattered light must be made.

Michard corrected the $H\alpha$ profiles for scattered light in his earlier work by subtracting the observed spectrum adjacent to a spicule from the composite spectrum of the spicule plus scattered light. However, both Smith (1957) and Athay (1958a) subtracted the Fraunhofer spectrum, observed near the edge of the photospheric disk, from the composite spectrum, after normalizing the continua in the two spectra as illustrated in Fig. 3-14. In Michard's initial observations made with a tower telescope the corrections to the profile for scattered light were large. However, both Smith and Athay used coronagraphs at high altitudes for observing the profiles, which reduced the scattered light to a point where the average corrections to the profile at the center of the line were about 10 percent. Under these conditions, it makes little difference how the corrections are made in detail.

Michard's early observations, in which he was forced to make large corrections, gave $H\alpha$ profiles much narrower than those obtained by Smith and Athay. In later observations, however, he obtained profiles that were in good agreement with those obtained by the latter authors (Michard, 1959).

The D_3 profiles, which require no correction for an underlying absorption line, are slightly asymmetric due to multiplet structure.

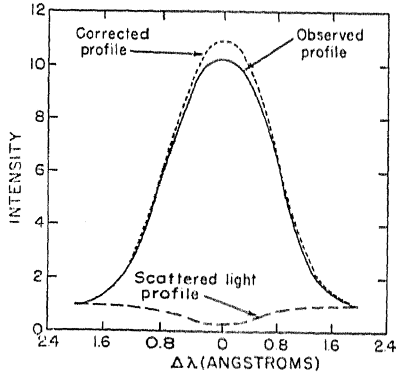

Fig. 3-14. Illustration of correction to observed profiles for scattered light.

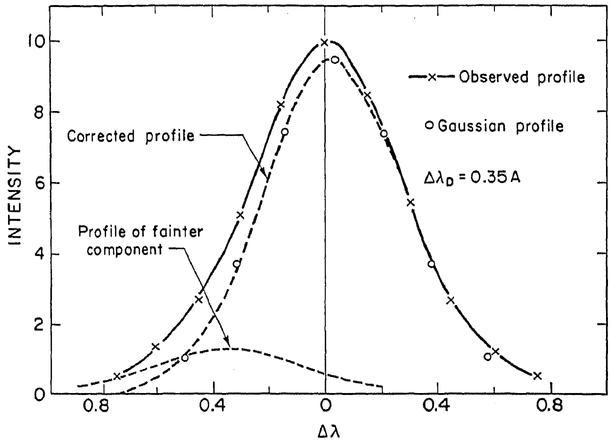

Fig. 3-15. Illustration of correction to d_3 profile for multiplet structure. (From R. G. Athay, 1958, *Annals d'Astrophysique*, 21, 10.)

The corrections for multiplet structure, assuming an equivalent doublet with intensity ratio 8 : 1 and separation of 0.35 A, is illustrated in Fig. 3-15. After this correction is made the D_3 profiles are Gaussian in shape.

The distributions of corrected half-widths, defined as the total width of the profile at the half intensity points, are shown in Fig.

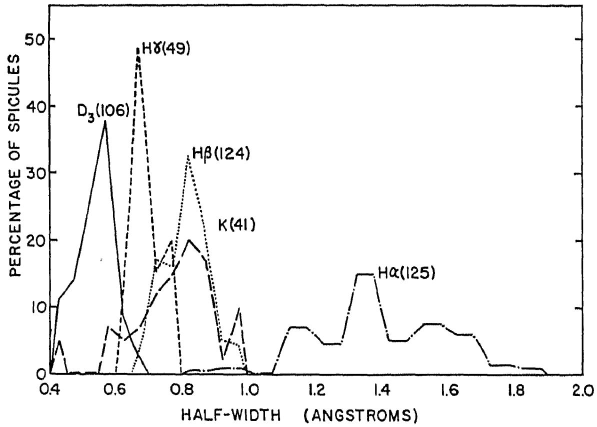

Fig. 3-16. Distributions in observed half-widths of spectral lines for spicules. The numbers in parentheses indicate the number of profiles studied. (From R. G. Athay, 1960, *Annals d'Astrophysique*, 23, 7.)

3-16 for the five lines observed. For three of the lines, Hβ, Hγ, and D$_3$, the dispersion about the mean is rather small. For all these lines, over half of the spicules have half-widths within ± 0.05 A of the mean value. The accuracy to which the half-widths are determined is also about ± 0.05 A. It therefore, appears that the intrinsic half-widths for each of the lines Hβ, Hγ, and D$_3$ are very nearly the same from spicule to spicule. Furthermore, for each of these lines, the profiles tend to be Gaussian in shape suggesting that the spicules are optically thin.

The profiles of both Hα and the K line show considerably more dispersion in half-widths than do the profiles of the other lines. In addition, the K-line profiles and the wider Hα profiles, as illustrated in Figures 3-17 and 3-18, tend to be flat-topped, which is characteristic of saturation due to self-absorption. The narrower Hα profiles with half-widths of less than 1.2 A are Gaussian, however.

In the central regions of the lines observed the broadening must either be from the Doppler effect or from saturation due to non-negligible opacity. The Hβ, Hγ, and D$_3$ profiles and the narrower Hα profiles are clearly broadened by thermal or microscopic non-thermal velocity fields with a Gaussian distribution because the profiles are Gaussian. The wider Hα profiles and the K-line profiles are obviously broadened by something other than velocity fields with a Gaussian distribution, however.

The mean half-widths of the lines are Hα = 1.43 A, Hβ = 0.82 A, Hγ = 0.69 A, D$_3$ = 0.54 A, and K = 0.77 A (Athay, 1958a, 1960a). When corrected by a factor $(6563/\lambda)\sqrt{(m/m_{\text{H}})}$, which should give the

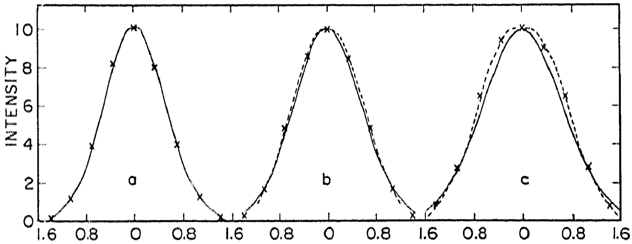

Fig. 3-17. The mean Hα profile (crosses) for spicules whose individual profiles have half-widths between: (a) 1.1 to 1.2 A; (b) 1.3 to 1.5 A; (c) 1.6 to 1.7 A. The solid curves are Gaussian profiles through the center and e^{-1} points on the observed profiles. The dashed curves are computed for a constant source function and $\tau_0 = 1$ (b) and $\tau_0 = 2$ (c). (From R. G. Athay, 1958, *Annals d'Astrophysique*, 21, 8.)

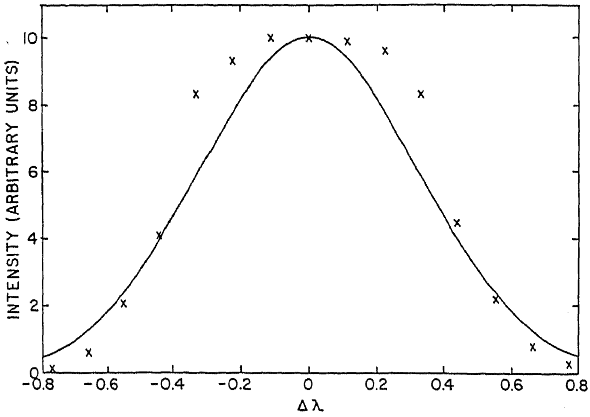

Fig. 3-18. The mean K-line profile (crosses) for spicules whose individual profiles have half-widths between 0.77 and 0.81 A. The solid curve is a Gaussian profile through the center and e^{-1} points. (From R. G. Athay, 1960, *Annals d'Astrophysique*, 23, 6.)

same half-width for each line if the broadening is purely thermal, the means are: Hα = 1.43 A, Hβ = 1.11 A, Hγ = 1.05 A, D_3 = 1.22 A, and K = 8.15 A. The difference between the half-widths for Hβ and Hγ is probably not significant, and the values are in good agreement with the narrower, unsaturated Hα profiles. The slightly greater half-width for D_3 could be due to non-thermal motions.

If the broadening were due entirely to non-thermal motions, the D_3 and K-line half-widths should be corrected by a factor 6563/λ, which gives D_3 = 0.61 A and K = 1.31 A. Since the D_3 half-width is now less than those for the hydrogen lines, this alternative is unlikely. One might envision a spicule model in which the helium emission arises from different volume elements than the hydrogen and CaII emission. However, there is good evidence from eclipse data that this is not the case (cf. Chapter 7), and all spicules apparently emit both Hα and D_3 (Athay, 1958a) in about the same proportions. Furthermore, the shape of the K-line profile clearly indicates that the broadening is not due solely to a velocity field with a Gaussian distribution.

The mean Hβ and D_3 half-widths correspond to a combination of thermal and non-thermal broadening characterized by a kinetic temperature of 54,000° and a random, non-thermal velocity field of 6.5 km/sec. The mean Hγ and D_3 profiles correspond to 45,000° and

8.6 km/sec. It seems, therefore, that the kinetic temperature within spicules is of the order of 50,000°. Before accepting this conclusion, however, we must explain the anomalous broadening of the Hα- and K-line profiles.

The Gaussian form of the narrower Hα profiles together with the systematic tendency of the wider profiles to show the effects of saturation suggests that the optical thickness in the Hα line is non-negligible in most spicules. If the source function is assumed to be constant throughout the spicule, the observed profiles can be fitted in almost all cases with equivalent Gaussian profiles broadened by self-absorption. The values of τ at the line center range from 0 to 2, and the half-widths of the Gaussian profiles range from 1.15 to 1.25 A. Since, these half-widths are somewhat greater than the mean half-widths observed for Hβ and Hγ after they are corrected to the wavelength of Hα, we have probably underestimated τ_0. Similar corrections and comparisons of the profiles of the early Balmer lines in prominences (Jefferies and Orrall, 1958) and in the lower chromosphere (Athay and Smith, 1956) lead to the same discrepancies between Hα and the later lines. Thus, the mean optical thickness in the center of Hα in spicules is probably somewhat greater than unity, and the broadening is undoubtedly due to a combination of Doppler broadening and saturation.

The unexpectedly large half-width of the K line in spicules presents an interesting problem. Because of the systematic rectangular shape of the profile, the broadening cannot be due entirely to random motions with a Gaussian distribution. Furthermore, it seems improbable that it could be broadened to such an extent by self-absorption. The accepted abundance of calcium relative to hydrogen in the sun is about 2.5×10^{-6}. The hydrogen density in spicules is about 10^{11} (cf. Chapter 7), and the diameter is of the order 10^8 cm or less. Therefore, the number of calcium atoms in a square-cm column running along a spicule diameter is about 2.5×10^{13}. The absorption coefficient at the center of the K line is $2.9 \times 10^{-12} (T_e \times 10^{-4})^{-1/2}$, and if all calcium is singly ionized the optical thickness at the center of the line would be about 70. This could produce the observed broadening. However, since the ionization potential of CaII is only 11.87 volts it seems unlikely that CaII would be the most abundant calcium ion for $T_e \simeq 50{,}000°$. Although detailed calculations have not been carried out, we would expect the opacity in the K line to be much less than 70, and probably less than unity.

If we were to adopt a spicule model in which the broadening of the K line were due to high opacity, we would be forced to adopt, at the same time, a random "turbulence" with a most probable velocity of at least 25 km/sec in order to explain the widths of the Hβ and Hγ lines. Since this would produce too much broadening for the D_3 line, we would be forced to attribute the D_3 emission to entirely different volume elements where the "turbulence" was very much smaller, but where T_e was much higher in order to accomplish the separation of hydrogen and helium emissions.

Such a picture is implausible from several standpoints. In the first place, the observational data suggest, as we noted earlier, that the hydrogen and helium emissions come from the same regions. Also, we should expect to observe the lines of such ions as SrII and TiII, which have not been observed even though spectra have been taken.

The best criteria as to whether the hydrogen and helium emissions arise in the same volume elements are the relative line intensities. The theoretical intensity ratio of Hα to D_3 for an optically thin gas is given by

$$\mathrm{H}\alpha/\mathrm{D}_3 = (h\nu_{23}A_{32}n_3)\mathrm{H}\alpha/(h\nu_{23}A_{32}n_3)\mathrm{D}_3 \tag{3-7}$$

where n_3 is the population of the upper level of the transition and A is the transition probability. Since the optical thickness is not large in either of these lines, this equation should hold quite accurately for spicules. The n_3 ratios may be computed from the Boltzmann-Saha equation modified by a b_k factor to account for departures from thermodynamic equilibrium. If we use a subscript i to designate the ions of hydrogen and helium, we have

$$n_k = (h/2\pi mk)^{3/2} n_e n_i T_e^{-3/2} (b_k \tilde{\omega}_k / 2\mathrm{u}_i) e^{\chi_k/T_e} \tag{3-8}$$

For hydrogen and helium, the ionization energies, x_k, are the same for $k \geq 3$, and the constants $\tilde{\omega}_k$, u_i, and A_{kj} are well known. Thus from Eqs. (3-8) and (3-7) we find

$$\mathrm{H}\alpha/\mathrm{D}_3 = 1.3\ (n_p/n_{\mathrm{II}})[b_3(\mathrm{H})/b_{33_d}(\mathrm{He})] \tag{3-9}$$

The b'_ks have been calculated for a range of chromospheric models (cf. Chapters 4 and 7). The calculated values give $b_3(\mathrm{H})/b_{33_d}(\mathrm{He}) \approx 2$. The ratio of proton density n_p to HeII density n_{II} has a minimum value that is constant throughout the range of temperature where helium is predominantly singly ionized, since hydrogen will also be predominantly ionized. Under these conditions, n_p/n_{II} is given by the relative abundance of hydrogen to helium, which, for the sun, is about 10. Thus, the theoretical ratio of Hα/D$_3$ has a minimum value of about 20. A region that emits in D$_3$ must, therefore, emit in Hα with at least 20 times the intensity of the D$_3$ emssion. If there is a separate region that emits in Hα, but not in D$_3$, and contributes more than half to the total Hα emission, the observed Hα/D$_3$ ratio must exceed 40. In the upper chromosphere and in idividual spicules the observed ratio is about 15, which strongly suggests that Hα and D$_3$ arise in the same volume elements.

There are several good reasons, therefore, for assuming that hydrogen and helium emissions originate in the same volume elements within the spicule, and no apparent reasons for assuming the opposite other than the anomalous width of the K line.

If we dismiss self-absorption as the broadening mechanism for the K line, we must, of course, attribute the broadening to a velocity field. Clearly, the velocity field cannot be thermal, and, in view of the arguments above we must suppose that the hydrogen and helium do not share in the same velocity field with CaII.

Leighton (1959) suggests a similar picture for the relative velocity fields of CaII and neutral atoms in the chromospheric regions where the emission features in the K line are formed. This suggestion follows an earlier suggestion by Piddington (1956) that under certain conditions perturbations in the magnetic fields in the solar atmosphere may cause the ions to move systematically with respect to the neutral atoms. Leighton calls upon the increased kinetic energy of the CaII ions to explain the K_2 emission features via atom-atom collisions. While this explanation of the K_2 emission features seems both unlikely and unnecessary (cf. Jefferies and Thomas, 1959), the suggestion of a possible differential motion of CaII with respect to the neutral atoms merits further attention as a broadening mechanism in the lines of ionized elements.

If we suppose that the spicules either follow magnetic lines of force in their upward motion or carry their own internal magnetic fields, it seems likely that the magnetic field will be perturbed and at least possible that these perturbations could produce systematic motions of the ions with respect to the neutral particles. Piddington's (1956) calculations suggest that if the magnetic field is of the order of 10 gauss and the ion density is of the same order as the neutral atom density the neutral atoms will not be forced to move with the ions. In spicules the neutral atom density is probably a few orders of magnitude less than the ion density, which would tend to force the neutral atoms to move with the ions. However, if the perturbations in the field have a short period or if their amplitude is less than a mean free path for a neutral atom-ion collision (about 1 km), the same result may be obtained with a smaller ratio of neutral atom to ion density.

An alternative and perhaps more probable mechanism for giving the ions a velocity component not shared by neutral atoms is the forced gyrations of the ions about the lines of force in a magnetic field oriented at some angle to the spicule motion. A proton with a velocity of 30 km sec^{-1} has a radius of gyration of 30 cm in a magnetic field of 10 gauss. It is reasonable to expect, therefore, that the gyrations of the ions will be on a much smaller scale than the spicule diameter so that the spicule will not tend to rotate as a whole and the neutral atoms will not be forced to rotate with the ions even though collisions may be frequent. The mean free path of a CaII ion in a spicule is of the order of 1 km, and the collision frequency of the order 10 sec^{-1}. Thus, a CaII ion could gyrate in a field as small as 1 gauss. On the other hand, the average hydrogen atom that emits Hα must first have a recombination to the ground state followed by a double absorption of Lyman-α and Balmer-α photons. This process requires about 15 sec, during which time the atom undergoes several encounters with protons. Similarly a HeI atom requires about 0.1 sec before emitting a D_3 quantum and undergoes about 10 collisions with protons during this time. Thus, such a mechanism might explain the anomalous broadening of the CaII profile without affecting the hydrogen and HeI profiles. It also offers attractive possibilities as an energy mechanism for heating the spicule.

Admittedly, such a suggestion is highly speculative. On the other hand, the alternative suggestion of a velocity field that is shared by hydrogen and CaII, but not by helium seems even more speculative and somewhat less probable. Also, it seems evident that spicules are closely related to magnetic field phenomena. The systematic orientations of spicules over regions of the sun with diameters of the order 150,000 km (Lippincott, 1957), and the tendency of polar spicules to align themselves with coronal features (van de Hulst, 1953), suggest such an association.

The close association between magnetic fields and CaII (Leighton, 1959) and Hα (Howard, 1959) plages further illustrates the role of magnetic fields in chromospheric phenomena. However, one should not immediately jump to the conclusion that the spectroscopic features of the chromosphere are to be explained through the interaction of charged particles and magnetic fields independently of the thermodynamic properties of the chromosphere. Thus, even though there is considerable evidence of the role of magnetic fields in chromospheric phenomena, our suggestion that the broadening of the K line in spicules results from a direct coupling of CaII with magnetic fields is indeed speculative.

CHAPTER 4

The Spectroscopic State of a Gas in a Statistically Steady State

R. N. THOMAS

I. The Equations of Statistically Steady State

A. Some Comments on Formalism

For convenience, we develop all relations between occupation numbers and thermodynamic parameters in such a form that their similarity with, and departure from, the corresponding relations of thermodynamic equilibrium are emphasized. We write the expression for the rate of change of the occupation number n_k of the kth energy level of a particular ion in the symbolic form

$$\partial n_k/\partial t = \mathbf{S}_{\alpha,j} \left\{ \mathcal{P}(\alpha;k,j) - \mathcal{R}(\alpha;k,j) \right\} \tag{4-1}$$

where $\mathcal{P}(\alpha;k,j)$ denotes a process of type α which carries an atom from energy level k to energy level j; and $\mathcal{R}$ denotes the inverse process. As customary, the symbol S denotes either a sum or an integral, depending upon whether the sum ranges over a discrete or a continuous set. The atomic transition processes are radiative excitation and ionization, and collisional excitation and ionization by atoms and by electrons.

The various assumptions on the configuration of the ensemble are represented by special cases of Eq. (4-1). Thermodynamic equilibrium is defined as the detailed balancing of each process by its inverse, so each brace on the right side of Eq. (4-1) vanishes individually. The most general alternative which keeps the left side of the equation zero is for the double summation on the right side to vanish as a whole. This is the case of the statistically steady state. Intermediate cases consist of the assumption that one or the other of the single sums vanishes. If, for each j, the sum over α vanishes,

we assume a complete coupling between the states k and j. It is hard to see how such a situation can exist; but the problem has, on occasion, been discussed, although usually by neglecting all states save k and one other. A more common assumption requires that the sum over j vanish for each α. Again, the most frequent form of this assumption in the astronomical literature is that in which all processes save one or two are neglected. Usually the processes retained are radiative excitation and ionization. That is, one discusses what he calls the statistically steady state of an atmosphere where the density is so low that collisional processes may be neglected and only radiative processes assume significance. In practice, this assumption frequently is abused in that its results are applied under conditions where a neglect of collisional processes is hard to justify.

Each of the assumptions above leads to a set of algebraic equations whose simultaneous solution gives the occupation numbers of the energy levels. Among the alternative assumptions, only that of a statistically steady state avoids some degree of degeneracy; for in this state we have one equation for the occupation number of each energy level, each equation involving the occupation numbers of the other energy levels. In the other cases, one has several equations for each energy level, all reducing to the same result. If a steady state does not exist, then the set of equations (4-1) describes the time history of the occupation numbers, and a complete set of occupation numbers at some epoch is required to solve the problem. The same set of atomic parameters, no more and no less, is required to describe the various interaction processes in the time-dependent and steady-state cases. Only for thermodynamic equilibrium are the distribution functions independent of the details of the interaction processes. Hereafter, unless otherwise specified, we discuss the assumption of statistically steady state. Thus, we set the left side of Eq. (4-1) equal to zero.

To develop the statistically steady state in such a way as to exhibit its relation to the thermodynamic equilibrium state, we rewrite Eq. (4-1) as

$$0 = \mathop{\mathbf{S}}_{\alpha,j}\mathcal{P}(\alpha;k,j)\{1 - [\mathcal{R}(\alpha;k,j)/\mathcal{P}(\alpha;k,j)]\} \tag{4-2}$$

Under thermodynamic equilibrium, the condition of detailed balancing is both necessary and sufficient to determine the distribution functions, and these must not depend upon the details of the atomic interaction processes. Then, since the condition of detailed balancing is given by the vanishing of each term in the double sum in Eq. (4-2), and $\mathcal{P}(\alpha;k,j)$ does not vanish in thermodynamic equilibrium, the braces $\{\ \}$ must vanish and contain no details of the atomic interaction processes. In the statistically steady state, the braces $\{\ \}$ do not vanish, and may contain explicit or implicit dependence upon the parameters describing the atomic interactions. Since these atomic interaction parameters depend only upon the interaction processes and not the state of the ensemble as a whole, the change in $\{\ \}$ from the steady-state value to the thermodynamic equilibrium value cannot come about through a change in value of the atomic interaction parameters. The change must, therefore, be associated directly with the change in occupation numbers of the energy levels, with the onset of the degeneracy mentioned earlier, in such a way that any explicit or implicit dependence of the $\{\ \}$ upon atomic interaction parameters vanishes. It would seem advisable, therefore, to introduce a set of parameters, isomorphic to the occupation numbers, whose behavior exhibits explicitly this dependence of the $\{\ \}$ on the occupation numbers.

For this purpose, we follow the procedure originally devised in a form appropriate to a gas at very low density by Menzel and coworkers (1937 et seq.) in discussing the planetary nebulae, and developed more completely by Thomas (1948 et seq.) in discussing solar and stellar atmospheres. That is, we express the occupation number of the kth energy level in terms of its value in a thermodynamic equilibrium configuration characterized by the same values of n_e, T_e, and the number n_i of ions of one stage higher ionization than the state containing n_k. We emphasize that n_i is the actual concentration present; not that which would be present in thermodynamic equilibrium at n_e, T_e, and a given relative abundance of atoms.

$$n_k = [(h^2/2\pi m_e \mathbf{k} T_e)^{3/2}\, n_e n_i (\bar{\omega}_k/2U_i)\, e^{\chi_k/\mathbf{k}T_e}] b_k \qquad (4\text{-}3)$$

The quantity in brackets is the Boltzmann-Saha expression for the occupation number in thermodynamic equilibrium, $\mathbf{k}$ is the Boltzmann constant, U_i is the partition function of this ion; and $\bar{\omega}_k$ is the statistical weight of state k. The quantity b_k is a pure number, representing the departure of n_k from its value given by the thermodynamic equilibrium relations, thus of arbitrary numerical range.

This introduction of b_k provides a proper exhibition of the degeneracy of the thermodynamic equilibrium state; for Eq. (4-3) with $b_k \neq 1$ gives the general distribution function for the occupation numbers and replaces the set of equations (4-2). Moreover, the braces $\{\ \}$ in Eq. (4-2) now depend explicitly upon the non-equilibrium parameters b_k, and their vanishing accompanies $b_k = 1$. Thus, using the b_k as the parameters describing the population of the energy level, rather than the occupation numbers themselves, we have always before us a direct comparison of the occupation numbers to those obtained in thermodynamic equilibrium, and a direct measure of the degree to which the various terms in the equations contribute to the departure from thermodynamic equilibrium. We proceed now to set up the equations explicitly in terms of the b_k, from the standpoint of the detailed processes involved.

B. Consideration of the Detailed Processes Entering the Equations

We consider the individual terms entering Eq. (4-2), which involve radiative and collisional transitions between level k and level j.

1. Radiative Processes. In a state of thermodynamic equilibrium, the transition rates due to radiative processes between level k and level j of lower energy are:

Spontaneous transitions from k to j:

$$A_{kj}n_k \tag{4-4a}$$

Induced emissions from k to j:

$$B_{kj}n_kB_\nu(T_e) \tag{4-4b}$$

Absorptions from j to k:

$$B_{jk}n_jB_\nu(T_e) \tag{4-4c}$$

$B_\nu(T_e)$ is the Planck function and A_{kj}, B_{kj}, B_{jk} are the Einstein coefficients defined in terms of the mean radiation intensity rather than energy density. We write the condition of detailed balancing

$$[A_{kj} + B_{kj}B_\nu(T_e)]n_k - B_{jk}B_\nu(T_e)n_j = 0 \tag{4-5}$$

Use Eq. (4-3) with $b_k = 1$, and introduce the expression for the Planck function

$$B_\nu(T_e) = (2h\nu^3/c^2)[e^{h\nu/kT_e} - 1]^{-1} \tag{4-6}$$

to obtain the usual relation between the A's and B's:

$$B_{kj}\tilde{\omega}_k = B_{jk}\tilde{\omega}_j \tag{4-7a}$$

$$A_{kj} = B_{kj}(2h\nu^3/c^2) \tag{4-7b}$$

Consider now the statistically steady state. Introduce two functions ϕ_ν and ψ_ν which are, respectively, the profiles of the absorption and induced emission processes, and which are normalized to unity, viz.,

$$\int \phi_\nu \, d\nu = 1 = \int \psi_\nu \, d\nu \tag{4-8}$$

Also introduce I_ν, the specific intensity of the radiation field at the point considered, and denote by $\bar{I}_\nu$ the value of I_ν averaged over solid angle. Then in place of the transition rates given by the expressions (4-4) we have the following for this non-equilibrium state:

Spontaneous: $$A_{kj}n_k \tag{4-9a}$$

Induced: $$B_{kj}n_k \int \bar{I}_\nu \psi_\nu \, d\nu \tag{4-9b}$$

Absorption: $$B_{jk}n_j \int \bar{I}_\nu \phi_\nu \, d\nu \tag{4-9c}$$

In practical application, the profile ψ_ν is identical with the profile ϕ_ν, and hereafter we do not distinguish between them. Further, we define a quantity W_{jk} by

$$\bar{I}_{\nu_0} W_{jk} = \int \bar{I}_\nu \phi_\nu \, d\nu \tag{4-10}$$

where $\bar{I}_{\nu 0}$ is the value of $\bar{I}_\nu$ at the center of the line. Again in thermodynamic equilibrium, $W_{jk} = 1$, so it plays a role in the radiation field similar to that of the b_k in the occupation numbers of the atomic energy levels. For convenience, since one often discusses radiation intensity in terms of the temperature of an equivalent black body, we define the radiation temperature T_r at ν_0 by

$$B_{\nu_0}(T_r) = \bar{I}_{\nu_0} \tag{4-11}$$

Also to simplify the equations, we introduce

$$\frac{\chi_k}{\mathrm{k}T_e} = \frac{h\nu_k}{\mathrm{k}T_e} = X_k, \qquad X_j - X_k = X_{jk}$$
$$\frac{\chi_k}{\mathrm{k}T_r} = \frac{h\nu_k}{\mathrm{k}T_r} = Y_k, \qquad Y_j - Y_k = Y_{jk} \tag{4-12}$$

where χ_k is the ionization energy from level k. Then, using Eq. (4-3), (4-9), and (4-10) we write the typical radiative term, for transitions between discrete levels, in the form

$$\mathcal{P}\{1 - (\mathcal{R}/\mathcal{P})\} = A_{kj}n_k\{1 - W_{jk}[(b_j/b_k)e^{X_{jk}} - 1]/(e^{Y_{jk}} - 1)\} \tag{4-13}$$

From Eq. (4-13) for the discrete states, we obtain immediately the expression for the free-bound radiative transitions, according to the purely formal process of replacing the upper discrete level by a continuous range of energy levels. Following Menzel and Pekeris (1935), we specify these energy levels of the free electron by simple extension of the expression for the energy levels of a hydrogenic configuration. That is, we introduce the variable κ, having a continuous range of values, by:

$$h\nu_\kappa = hRZ^2/\kappa^2 = m_e v^2/2 \tag{4-14}$$

where R is the Rydberg constant and Z is the charge on the ion. These relations follow from the expression for the bound levels in the hydrogenic configuration, expressed in terms of the principal quantum number n, by the substitution $n \rightarrow i\kappa$. The total energy then changes from negative to positive, corresponding to the change from bound to free levels. Since the analogue of the spontaneous transition from the upper level is an electron capture from the continuous range of energy levels, a two-body process, we replace n_k in equation (4-4a) by the product of n_i and $n_{e\kappa}$, the number of electrons per unit range in κ. We also replace A_{kj} by $A_{\kappa j}$, which we interpret as the transition probability, per ion, for $n_{e\kappa}$ to be captured on level j. Thus, the radiative term linking discrete and continuum levels in Eq. (4-2), the analogue of the expression (4-13), is

$$\int_{\nu_j}^{\infty} A_{\kappa j}n_i n_{e\kappa}\{1 - W_{\kappa j}[(b_j/b_\kappa)e^{X_{j\kappa}} - 1]/(e^{Y_{j\kappa}} - 1)\}\, d\kappa \tag{4-15}$$

For the continuum levels, the analogue of the modified Boltzmann-Saha equation (4-3) is the Maxwell-Boltzmann equation written in the proper form, viz.,

$$n_i n_{e\kappa}\, d\kappa = \left[4\pi\left(\frac{m_e}{2\pi \mathbf{k} T_e}\right)^{3/2} n_e n_i v^2 \exp\left(-\frac{m_e v^2}{2\mathbf{k}T_e}\right)dv\right] b_\kappa$$

$$= \left(\frac{h^2}{2\pi m_e \mathbf{k} T_e}\right)^{3/2} n_e n_i \frac{\tilde{\omega}_\kappa}{\tilde{\omega}_e U_i} \exp\left[\frac{-h\nu_\kappa}{\mathbf{k}T_e}\right] b_\kappa \; d\kappa \qquad (4\text{-}16)$$

where

$$\tilde{\omega}_\kappa = 4\pi(m_e^2/h^2)(2RZ^2/\kappa^3)v\cdot\tilde{\omega}_e\cdot U_i \qquad (4\text{-}17)$$

From the manner in which we have defined W_{jk} by Eq. (4-10) and from our definition of $n_{e\kappa}$, we see that a value $W_{\kappa j} \neq 1$ has practical utility only in the event that we wish to define T_r once and for all in a given free-bound continuum, and to allow the variation of W with κ to preserve a correct representation of $\bar{I}_\nu$. We shall, indeed, follow this approach.

In actually introducing the terms (4-13) and (4-15) into Eq. (4-2), and entering into numerical computations, it is usually more convenient to use the oscillator strength rather than the transition probability. The relation

$$A_{kj} = (\tilde{\omega}_j/\tilde{\omega}_k)(8\pi^2\epsilon^2\nu^2{}_{kj}/mc^3)f_{jk} \qquad (4\text{-}18)$$

is valid for transitions from both discrete and, as Menzel and Pekeris demonstrated, continuum levels. It is also often convenient to write the expression for f_{jk} in the form

$$f_{jk} = (2^6R^3/3\pi\sqrt{3})j^{-3}k^{-3}\nu^{-3}\tilde{\omega}_j{}^{-1}g_{jk}Z^6 \qquad (4\text{-}18a)$$

where g_{jk} has been computed by Menzel and Pekeris (1935) for both discrete and continuous transitions. It is also convenient to replace the integral over κ in the expression (4-15) by one over ν, using the relation

$$d\kappa = -\kappa^3\, d\nu/2RZ^2 \qquad (4\text{-}19)$$

2. Inelastic Collisional Processes. It seems quite valid to neglect collisional excitation and ionization by atoms relative to that by electrons in the situations of interest to our investigations, for we are interested in thermal collisions, with energies corresponding to less than about 10$10^6$°K, or a few hundred volts mean energy. Indeed, over most of the chromosphere we shall be concerned with temperatures below 10^5°K, and thus mean energies less than 10 ev. Since, for comparable excitation and ionization, an incident electron and atom must have roughly the same velocity—not energy—the influences of inelastic collisions by atoms can usually be ignored.

Define $\pi a_0^2 Q_{jk}$ as the inelastic collision cross section for excitation from level j to k, where a_0 is the Bohr radius. Then the rate of collisional excitation is

$$C_{jk} = 4\pi(m_e/2\pi \mathbf{k} T_e)^{3/2} n_e n_j \pi a_0^2 \int_{\nu_0}^{\infty} Q_{jk}(\nu,j,k) v^3 e^{-m_e v^2/2\mathbf{k}T_e}\, dv$$

$$= n_j \Omega_{jk}(n_e, T_e) \qquad (4\text{-}20)$$

Similarly, the rate of collisional de-excitation is

$$\mathrm{C}_{kj} = \mathrm{n}_k \Omega_{kj}(n_e, T_e) \qquad (4\text{-}21)$$

If n'_k and n'_j denote the occupation numbers in a state of thermodynamic equilibrium at the same values of n_e, T_e, then detailed balancing requires

$$n'_k \Omega_{kj} = n'_j \Omega_{jk} \qquad (4\text{-}22)$$

By combining Eq. (4-22) with Eq. (4-3), we find, for the collisional term involving discrete levels in Eq. (4-2),

$$\mathcal{P}\{1 - (\mathcal{R}/\mathcal{P})\} = n_j \Omega_{jk}(1 - (b_k/b_j)\} \qquad (4\text{-}23)$$

By the same arguments, but considering individual levels in the continuum, we obtain, for the net collisional ionization rate,

$$4\pi(m_e/2\pi \mathbf{k} T_e)^{3/2} n_e n_j \pi a_0^2 \int_{\nu_0}^{\infty} Q_{j\kappa}(\nu,j,\kappa)[1 - (b_\kappa/b_j)] v^3 e^{-m_e v^2/2\mathbf{k}T_e}\, dv \qquad (4\text{-}24)$$

These results permit us to write each term in the set of equations (4-2), but the terms involve the unspecified collision cross sections and oscillator strengths. We summarize, then, the available data on the atomic parameters.

C. Considerations of the Cross Sections Entering the Detailed Processes

1. Radiative Processes. The computations of Menzel and Pekeris (1935) provide reliable f values for hydrogen. These same f values hold for HeII.

f values for HeI have been computed by a number of authors (cf. Goldberg, 1939; Hylleraas, 1937; Trefftz, Schluter, Dettmar, and Jorgens, 1957). Although the numerical values given by the different authors vary, the diferences are generally less than 20 percent. Thus, these values seem to be generally reliable.

For neutral and ionized atoms other than these, only a limited number of *f* values are available, and these are subject to considerable uncertainty, especially in absolute value. Allen (1955) presents a compendium of those values which have appeared in the literature. A recent survey article by Garstang (1955) provides a summary of computed values. An article by Allen and Asaad (1955) provides a rather pessimistic view of the reliability of *f* values for the iron group (T_i to N_i) of complex atoms in terms of the agreement between experimental and theoretical values. However, because these theoretical values result from applying theoretical methods developed by Bates and Damgaard (1949) to situations for which they were not intended, the situation is possibly better than the article implies. Rohrlich has recently proposed a method for an accurate evaluation of *f* values for configurations involving *s* and *p* electrons, which may also give reasonably accurate values for higher electron systems. In any event, the set of reliable *f* values for, say, the metals is, at present, not sufficiently extensive to allow a systematic attack on the data relating to the metallic chromosphere.

In Chapter 9, we shall see that the f_k values for the individual Stark components of hydrogen should enter a completely satisfactory discussion of chromospheric emission in the hydrogen lines. Machine computations of these f_k values for the first 20 members of the Lyman, Balmer, Paschen, and Brackett series of hydrogen are in progress by Underhill and Waddell, and will soon be available. These f_k values are not particularly critical; however, in the solution of the equations of statistical equilibrium, they are of interest chiefly in the discussion of line profiles.

2. Collisional Processes. The problem of thermal collisional cross sections, even for electron-atom collisions involving hydrogen and helium is, indeed, a serious one. In recent years there has been a gratifying upsurge of interest in the problem, but, unfortunately, little in the way of detailed results as yet. The classical approximation procedures such as Born first-order approximation are satisfactory only when the energy of the electron considerably exceeds that of the particular transition. As we have already noted, we are especially interested in those chromospheric regions where T_e rises from the photospheric value of 4000°—6000° to 20,000°—50,000°, and never interested where T_e exceeds $\sim 10^{6\circ}$K. Thus, particularly for transitions involving the lower states of H, He, and the ionized metals, one must have serious concern over a simple use of the Born approximation in evaluating cross sections.

In our first work on hydrogen (Thomas, 1948) we attempted to correct somewhat for the overestimate of cross sections that the Born approximation gives at these low energies, by arbitrarily adopting a somewhat lower value for the cross section Q_{12} for the transition from the ground level to the first excited level, and then using the Born first-order approximation to fix relative cross sections for other transitions. For the relative cross sections in the *jk* transition, we took Q proportional to the electric dipole moment $Q \propto k^7(k-1)^{2k-5}(k+1)^{-2k-5}$. The value adopted for the lowest transition represented an attempt to improve upon the Born approximation by using calculations by Massey and Mohr (1931), which introduced exchange, to estimate the correction. The Born value gives $Q_{12} = 4.1$ at the excitation energy of the 1–2 transition and the Massey and Mohr value gives about 2 at this same energy (dropping to 1 between 20 and 30 ev). Judging by a comparison of calculated ionization cross sections to observations on H_2 molecules, where the theoretical cross sections still seem high by about 70 percent, we decreased the excitation cross sections to $Q_{12} = 1$. Because of the uncertainty in the precise value of Q, the slow change in theoretical value with energy, and the exponential decrease of thermal electrons having energies higher than the excitation energy, we have assumed that Q is independent of energy. In our initial computations (Thomas, 1948) on ionization, we actually introduced an energy dependence into the cross section, which carried along in later computations (Matsushima, 1952), but it is questionable whether a single average value would not be equally representative of our state of knowledge.

In treating the same problem, Giovanelli (1948) initially assumed Q to vary inversely as the square root of the electron energy. Relative values of Q were taken proportional to the optical (absorption) transition probability. Later computations by Jefferies (1953) and Jefferies and Giovanelli (1954) used the energy dependence given by calculations of Bates, Leech, Fundaminsky, and Massey (1950) based on the Born approximation. The collision rates computed from these results lie within a factor 2 or 3 of the rates obtained by choosing constant Q and relative values proportional to the optical (absorption) transition probability.

Recent work (Fite, 1958) leads to values of the integrated cross section which are lower, by about a factor of 5 to 10 for both Q_{12} and the ionization cross sections relative to the values we used. The chief effect seems to come from the more precise determinations of the behavior of the cross sections near the threshold energy. It has not seemed worthwhile to re-compute our solutions of the equations of statistical equilibrium with these new values, because of the uncertainty in the cross sections not yet experimentally investigated. Thus, we present explicit results on occupation numbers only as illustration of the direction of the departure from LTE. This result should be borne in mind in any large-scale program for computing occupation numbers. Since, as we shall show, the occupation number of the ground state is roughly inversely proportional to the collision cross section, these new values of cross sections mean *that the values we tabulate underestimate the occupation numbers.*

Our own computations ignore the term structure of the quantum states specified by the principal quantum number; we have assumed that collisions are sufficiently frequent to establish a Boltzman distribution over the different terms of a given level. Giovanelli has treated the lowest three levels, including the term structure, plus the continuum. The inclusion of the term structure does not seem to make too much difference in the final solution, however, so the term structure is no longer included in a later paper (Jefferies and Giovanelli, 1954). Since we have good photometric observations out to H_{31} in the Balmer series, and can actually detect lines to H_{35}, we are very much interested in the b_k for the large k. Thus, we do not wish to consider only the lowest few quantum levels in our solution of the equations for the statistically steady state, and so we require cross sections for these higher levels.

Thus, we face two distinct problems in our discussion of collision cross sections. First, we consider the accuracy with which we can specify the rate of collisional excitation from the lowest levels, which in essence depends upon the cross sections for excitation to the next higher one or two levels only. Judging from the variety of assumptions used by our group, by Giovanelli and by Giovanelli and Jefferies, the resultant occupation numbers do not depend drastically upon the particular assumption. Second, we consider the collision rates involving transitions between the higher levels, $10 < k < 30$. For the collisional interchange between levels k and $k + \Delta$, which become large terms in the equations of statistical equilibrium, we have little guide other than the Born approximation coupled with a realization that the exchange terms must be very large. Thus, we can only point to this second problem—$Q(k, k + \Delta)$ as a function of k and Δ—as probably the outstanding need for further knowledge in the inelastic collision rates for hydrogen. S. N. Milford and a group at St. John's University are investigating this problem.

Data on the collision cross sections for helium are given by Bates et al. (1950), Massey and Burhop (1952), and by Massey and Moiseiwitsch (1954). Again, these data refer only to collisional excitation from the ground state, and not between excited states. Jefferies (1955) proceeds to introduce cross sections between several of the higher states by comparison with corresponding data from hydrogen. Again, we emphasize the necessity to develop methods to obtain cross sections between these upper states.

The information for various collisional cross sections for atoms other than hydrogen and helium is sketchy and sparse. Summary articles by Massey (1955, 1956) and Seaton (1958) may be consulted. In brief, essentially no systematic set of data is available by which any group of metallic lines may be investigated from the standpoint of a solution of the equations for statistical equilibrium.

3. Summary. In view of these limitations on the cross sections presently available, the main thing one may hope to do in the way of investigating the spectroscopically steady state in a configuration departing from LTE is to see how far he can go in some wholly algebraic computations and in some illustrative computations for hydrogen and helium. The latter approach we illustrate in Section 4-II, the former in Section 4-III.

Because of the above uncertainty, we adopt constant mean cross sections in calculating collisional rates, unless otherwise specified. For constant Q, Eq. (4-20) and (4-23) give for the *net* rate of collisional excitation:

$$\Delta C_{jk} = 2\sqrt{\pi}(2\mathbf{k}T_e/m_e)^{1/2}\, a_0^2 n_e n_j Q_{jk}[1 - (b_k/b_j)](X_{jk} + 1)e^{-X_{jk}} \tag{4-25}$$

We also note that the electron velocity distribution is essentially Maxwellian under all conditions. (By essentially we mean that we have not yet been able to find a mechanism which permits, in the statistically steady state, a non-trivial departure from the Maxwellian distribution.) Thus, $b_\kappa = 1$. Then Eq. (4-24), with constant $Q_{j\kappa}$, gives

$$2\sqrt{\pi}\, a_0^2(2\mathbf{k}T_e/m_e)^{1/2}\, n_e n_j Q_{j\kappa}[1 - (1/b_j)](X_j + 1)e^{-X_j} \tag{4-26}$$

for the net rate of collisional ionization.

D. *Explicit Form for the Equations of Statistical Equilibrium*

From Eqs (4-2), (4-3), (4-13), (4-17), (4-25), and (4-26) we obtain the set of algebraic equations characterizing the statistically steady state:

$$\begin{aligned} b_k \Bigg\{ C_1 T_e^{1/2} n_e \tilde{\omega}_k \Bigg[\sum_{k+1}^{\infty} Q_{kj} \left(1 - \frac{b_j}{b_k}\right) e^{X_j} (X_{kj} + 1) \\ + Q_{k\kappa}\left(1 - \frac{1}{b_k}\right)(X_k + 1)\Bigg] + \sum_{1}^{k-1} \tilde{\omega}_j f_{jk} \nu_{jk}^2 e^{X_k} \\ \times \left[1 - W_{jk} \frac{(b_j/b_k)e^{X_{jk}} - 1}{e^{Y_{jk}} - 1}\right]\Bigg\} \\ = C_1 T_e^{1/2} n_e \sum_{1}^{k-1} Q_{jk}\left(1 - \frac{b_k}{b_j}\right) \tilde{\omega}_j e^{X_k}(X_{jk} + 1) b_j \\ + \sum_{k+1}^{\infty} b_j \tilde{\omega}_k f_{kj} \nu_{kj}^2 e^{X_j} \left[1 - W_{kj} \frac{(b_k/b_j)e^{X_{kj}} - 1}{e^{Y_{kj}} - 1}\right] \\ + \frac{1}{2RZ^2} \int_{\nu_k}^{\infty} \tilde{\omega}_k f_{k\kappa} \nu^2 \kappa^3 e^{-h\nu/\mathbf{k}T_e} e^{X_k} \\ \times \left[1 - W_\kappa \frac{b_k e^{X_{k\kappa}} - 1}{e^{Y_{kj}} - 1}\right] d\nu \end{aligned} \tag{4-27}$$

where

$$C_1 = (2\pi\mathbf{k}/m_e)^{1/2}\, a_0^2\, (m_e c^3/4\pi^2 e^2) = 0.74 \times 10^{11}$$

one sets

$$b_i = \lim_{k\to\infty} b_k = 1$$

and correspondingly,

$$X_i = \lim_{k\to\infty} X_k = 0$$

Aside from the uncertainties introduced by our incomplete knowledge of the atomic cross sections, there are two major difficulties in the solution of the set of equations (4-27): first, the specification of the local radiation field through values for W_{jk} and T_r; second, the fact that the set of equations is, formally, an infinite set.

The second difficulty is the less serious. In the first place, because of the excluded volume principle, we have in practice only a finite set of discrete energy levels. For example, in the chromosphere we observe only out to about H_{35} in the hydrogen Balmer series, and slightly higher in the Paschen. In the second place, the asymptotic condition that $b_k \xrightarrow[k \to \infty]{} 1$ reduces greatly the problem of the solution. One simply proceeds by iteration, recognizing that after a few iterations, the values of b_k for the lower k are reasonably well settled. As we have already mentioned, we are greatly interested in the b_k for $k > 10$, so we hope that some kind of asymptotic expressions may ultimately be found; for this we require a knowledge of $Q(k, k + \Delta)$ as $\Delta \to 0$.

The other difficulty, the specification of the local radiation field, presents a serious problem which, in general, one can solve only by attacking the radiation transfer problem in all the lines and continua covered by the discussion. Since we require a knowledge of the occupation numbers of the energy levels in order to specify the source-function entering the transfer problem, we must solve equations (4-27) and the transfer equations simultaneously. Such a comprehensive treatment, including all lines, has not yet been attempted. Because of the physical nature of the situations where interest in the statistically steady state arises, one can sometimes gain considerable insight by treatments of less generality. In particular, our interest lies in such gaseous configurations as the chromosphere, where the atmosphere has high optical opacity only in limited spectral regions. Over most of the visible spectrum, particularly in the continuum, the atmosphere has little or no influence on the radiation field, and we can consider the intensity to be well specified. In the central regions of some lines, however, the local opacity of the atmosphere is so high that the radiative intensity is essentially fixed by local conditions alone. In these two cases, where we can consider the local radiative intensity as either fixed independently of conditions in the chromosphere or specified essentially by local conditions alone, we can obtain solutions of the equations (4-27) without further approximation. In intermediate cases, we require accompanying solutions of the transfer equation for one or several lines and continua. Only fairly restricted treatments of special cases have as yet been carried out. We proceed to discuss these solutions.

II. Solutions of the Equations of Statistical Equilibrium

A. Computations for Hydrogen as Illustrating the Solution

1. Thin-Atmosphere Solution: *radiation field specified a priori.* A thin atmosphere is defined to be a gas mass whose contribution to the local radiation field is negligible; the parameters T_r and W_{jk} in Eq. (4-27) are fixed by external conditions which do not depend upon the state of the gas mass considered. If the chromosphere satisfied the thin-atmosphere criterion, the radiation field in it would be fixed by the photosphere. A necessary corollary would be the absence of any chromospheric effect upon the Fraunhofer disk spectrum. In terms of the classical, and, unfortunately, often still current, notion of the chromosphere, it would, indeed, satisfy the thin-atmosphere criterion throughout the ordinary optical spectrum. From our standpoint, we view the solution under this approximation simply as representing a limiting case.

A given point in the chromosphere is exposed to photospheric radiation from essentially one hemisphere. The effect of averaging over the solid angle in the chromosphere is approximately equivalent to averaging over the solar disk as viewed from the earth. For the majority of the visible radiation, the energy distribution in the integrated disk spectrum is approximated reasonably well by a 6000° black body. In the violet and ultraviolet, and in the strong Fraunhofer lines, the observed radiation intensity falls significantly below a 6000° black body. Thus as a first approximation, we represent the photospheric radiation field by setting $T_r = 6000°$ and allowing W_{jk} to vary between 0 and 1. We shall see when we consider a thick atmosphere that this range in W_{jk} does not cover the complete range of possibilities. The obvious exception is a situation where the local opacity in the transition considered is so high that $b_j \sim b_k$ and $T_r \rightarrow T_e$. This approach with $T_r = 6000°$ and $0 < W_{jk} < 1$ is a good one for the classical notion of a transparent chromosphere; for under it the net radiative transitions

$$1 - W_{jk}[(b_j/b_k)\, e^{X_{jk}} - 1]/(e^{Y_{jk}} - 1)$$

are easy to evaluate. The solution of equations (4-27) by iteration is clearest and most straightforward when formulated in terms of these net rates. We shall see that the approach to the thick atmosphere terms can also be expressed in terms of the net rates; indeed, that the expression is the most natural way to incorporate the transfer problem into the equation of statistical equilibrium. Thus, we adopt this approach in terms of net rates from the start.

The set of equations (4-27) can be solved numerically for b_k if T_r, W_{jk}, T_e, and n_e are specified. Table 4-1 contains values of b_k for $1 \leq k \leq 10$, $T_r = 6000°$, $T_e = 35{,}000°$, $n_e = 2 \times 10^{11}$, and $W_{jk} = 1$ and 0.

For the calculations in Table 4-1A, we assumed that Q_{1k} varied as

$$Q_{1k} = Q_{12} \frac{k^7 (k-1)^{2k-5}}{(k+1)^{2k+5}}; \qquad Q_{12} = 1 \tag{4-28}$$

and that the ionization cross section is:

$$Q_{1i} = (E - 13.52)/36.5, \qquad \mathrm{E} \leq 50 \text{ ev} \tag{4-29}$$

For the calculations in Table 4-1B, we included collisional excitations from all levels, using the values

$$Q_{kj} = Q_{12}(B_{kj}/B_{12}); \qquad k < j, \qquad Q_{12} = 1 \tag{4-30}$$

$$Q_{ki} = Q_{1i}(B_{ki}/B_{1i}) \tag{4-31}$$

and

$$Q_{1i} = 0.096 \tag{4-32}$$

Table 4-1. b_k for No Chromospheric Radiation; $n_e = 2.10^{11}$; $T_e = 35{,}000°$; $T_r = 6000°$; $W_{jk} = W$

W	b_1	b_2	b_3	b_4	b_5	b_6	b_7	b_8	b_9	b_{10}
A. Collisional excitations from ground level only[a]										
1	2.1×10^6	11	4.7	3.4	2.9	2.6	2.4	2.3	2.2	2.1
0	2.3×10^6	12	5.3	3.9	3.3	3.0	2.8	2.6	2.5	2.4
B. Collisional excitations from all levels[b]										
1	1.6×10^6	9.1	3.8	2.8	2.3	2.0	1.8	1.5	1.4	1.2
0	1.9×10^6	10	4.4	3.2	2.7	2.4	2.2	1.9	1.6	1.4

[a] Thomas (1948).

[b] Matsushima (1952).

The differences between the two sets of solutions in Table 4-1 are hardly negligible, but they are not as large as a factor of two. (See further note on this point in Appendix II.)

Table 4-1 was computed at a time when our attention was focused on a region of the chromosphere, located roughly 500 to 2000 km above the solar limb, and characterized, we believed, by $n_e \sim 2 \times 10^{11}$ and $T_e \sim 35{,}000°$. The validity of these computations rests primarily on the validity of the assumption of no chromospheric contributions to the radiation field present. To test this assumption, we compute n_1 for $T_e = 35{,}000°$, $n_e = 2 \times 10^{11}$ and the b_1 values given in Table 4-1. We obtain $n_1 \sim 10^9$. The absorption coefficient at the center of Ly-α is $0.55 \times 10^{-13}(T_e \times 10^{-4})^{-1/2}$; so in less than 1 km of chromospheric material, we reach optical depth unity at the center of Ly-α. For values of T_e below 35,000°, the opacity in Ly-α increases. Thus, solutions for b_k based on no chromospheric contribution to the radiation field in any part of the spectrum cannot be of interest in those chromospheric regions where n_e is as great as 10^{11}. In consequence, we must turn to an alternative solution that considers a chromosphere which is opaque to the early Lyman lines.

While discussing the present approximation, we should, however, pay particular attention to Giovanelli's (1948b) computations based on the same assumption of negligible chromospheric radiation. Giovanelli treated only levels having principal quantum number 1, 2, 3 and the continuum, but he also included the term structure. He used the assumption expressed by Eq. (4-30) to fix the relative collision cross sections, but used an absolute cross section Q_{12} that differed slightly from the one we used, in that an energy dependence is introduced. The collisional excitation from a term of state j to a term of state k is assumed to be proportional to the statistical weight of the term. Collisional excitation between terms of a given principal state is neglected. This neglect assumes major significance only for the (assumed) metastable $2s$ term, where a very substantial overpopulation occurs. In later computations, both the neglect of collisional interchange between terms of a given principal state and the breaking down of a principal state into terms are replaced (Jefferies, 1953; Jefferies and Giovanelli, 1955) by the assumption of sufficient collisional interaction between terms of a given principal state to bring about equipartition between the terms. Thus, only the principal states are considered.

Giovanelli tabulated (1948b) occupation numbers for the range of values; $T_r = 5000°$; $W_\nu = 1, 0.5, 0$; $n_e = 10^{13}, 10^{12}, 10^{11}, 10^{10}, 10^{9}, 10^{8}$; $T_e = 7500°, 1 \times 10^4, 1.5 \times 10^4, 2.5 \times 10^4, 5 \times 10^4, 1 \times 10^4$. The general characteristics of the results of these computations are the same as those of Table 4-1; viz., for $T_e > T_r$ the total occupation numbers of the states exceed their value for thermodynamic equilibrium at the same T_e and n_e, that is, $b_k > 1$. Moreover, b_k is greater for the lower principal quantum numbers.

For a more detailed comparison of Giovanelli's results with ours, we combine the occupation numbers for the terms of a given state, convert his occupation numbers to b_k, and tabulate his results for $n_e = 10^{11}$ and $T_e = 2.5 \times 10^4$ in Table 4-2.

Table 4-2. Computations by Giovanelli (1948)

W	b_1	b_2	b_3
1	2.3×10^5	0.50×10^3	6.6
0.5	1.9×10^5	0.90×10^3	6.3
0	0.65×10^5	3.2×10^3	3.5

The major difference between our values and his lies in b_1 and b_2 which are, respectively, smaller and greater than our values. This result is a direct consequence of ignoring collisional interchange between $2s$ and $2p$ terms; for the $2s$ term has no "downward exit" and increases in population at the expense of the ground level. Thus, since this collisional interchange between terms cannot be ignored, b_1 is too low and b_2 is too high. However, we shall see in the next section that including the chromospheric radiation acts to decrease b_1 and increase b_2 in the direction of the results in Table 4-3 over those in Tables 4-1 and 4-2. We turn then to this next approximation.

2. Thick-Atmosphere Solution: *radiation field specified locally.* A locally opaque atmosphere is defined to be a gas mass in which the radiation field at a point within the gas mass is fixed only by the local value of the source-function. That is, the change of the source-function is negligible through a sphere, surrounding the point, whose radius corresponds to an optical thickness $\sim$1. This criterion must, of course, be checked for every wavelength. The case where it is satisfied at each wavelength reduces to LTE. Thus, we are interested in those cases where the atmosphere is locally thick at a limited number of frequencies.

We introduce j_ν as the normalized profile of the emission function; then, using equations (4-9) we write the equation of radiative transfer in the form

$$4\pi(\mu/h\nu)(dI_\nu/dx)$$
$$= -B_{jk}n_jI_\nu[1 - (B_{kj}/B_{jk})(n_k/n_j)]\phi_\nu + A_{kj}n_kj_\nu \qquad (4\text{-}33)$$

with

$$\int j_\nu \, d\nu(d\omega/4\pi) = 1 \qquad (4\text{-}34)$$

We assume that if we treat only strong lines we can ignore the contribution of the continuous absorption coefficient to the opacity in the line. Then, defining

$$d\tau_\nu = -(h\nu/4\pi)B_{jk}n_j[1 - (B_{kj}/B_{jk})(n_k/n_j)]\phi_\nu \, dx \qquad (4\text{-}35)$$

Eq. (4-33) becomes, using Eq. (4-7),

$$\mu(dI_\nu/d\tau_\nu) = I_\nu - S_\nu \qquad (4\text{-}36)$$

where the source-function is

$$S_\nu = \frac{2h\nu^3}{c^2}\left(\frac{\tilde{\omega}_j}{\tilde{\omega}_k}\frac{n_k}{n_j} - 1\right)^{-1}\frac{j_\nu}{\varphi_\nu} \qquad (4\text{-}37)$$

or, introducing n_k from Eq. (4-3),

$$S_\nu = \frac{2h\nu^3}{c^2}\left(\frac{b_k}{b_j}\,e^{h\nu/\mathrm{k}T_e} - 1\right)^{-1}\frac{j_\nu}{\varphi_\nu} = B_\nu(T_{\mathrm{ex}})\,\frac{j_\nu}{\varphi_\nu} \qquad (4\text{-}38)$$

We obtain the radiation intensity at some point in the atmosphere by integrating Eq. (4-36) over depth and direction, viz.,

$$\bar{I}_\nu(t_\nu) = \int (d\omega/4\pi)\int (d\tau_\nu/\mu)S_\nu e^{-(\tau_\nu - t_\nu)/\mu} \qquad (4\text{-}39)$$

We have already remarked that $\Delta t_\nu = 1$ at the center of Ly-α corresponds to only a kilometer or so for the case $n_e = 10^{11}$, $T_e = 3.5 \times 10^4$ and the approximation which ignores any perturbation by the chromosphere on the radiation field. Thus, we may treat the extreme case of a chromospheric perturbation on the Lyman radiation field by assuming S_ν for the Lyman lines to have negligible variation over a distance in which $\exp\left[-(\tau_\nu - t_\nu)/\mu\right]$ drops from unity to essentially zero. In this case $\bar{I}_\nu(t_\nu)$ becomes just $S_\nu(t_\nu)$. Then, from Eq. (4-38), (4-10), (4-34), and (4-11) we see that the radiative transitions in the Lyman lines, as expressed by Eq. (4-13), vanish in the equations of statistical equilibrium (4-27). That is, we have detailed balancing in the Lyman lines, but not necessarily in any other region of the spectrum.

Table 4-3 contains solutions of b_k for the case $n_e = 2 \times 10^{11}$ and $T_e = 3.5 \times 10^{4}$°K in the situation where we assume a chromosphere that is locally opaque in the Lyman lines. Again, the two sets of b_k correspond to neglecting and including collisional excitation from levels other than the ground state.

Table 4-3. b_k for Detailed Balancing in the Lyman Lines

	b_1	b_2	b_3	b_4	b_5	b_6	b_7	b_8	b_9	b_{10}
	Collisional excitations from ground level only[a]									
$W = 1$, $k > 1$	4.6×10^4	1.0×10^3	52	18	11	7.8	6.5	5.6	5.1	4.8
$W = 0$, $k > 2$, $W_{2k} = 0.0049$	3.4×10^6	5.5×10^5	150	30	14	9.4	7.3	6.1	5.3	4.8
	Collisional excitations from all levels[b]									
$W = 1$, $k > 1$	4.2×10^4	1.2×10^3	57	19	11	8.1	6.5	5.6	4.9	4.4
$W_{2k} = 0$, $W = 1$, $k > 2$	2.4×10^5	2.4×10^5	72	27	16	11	8.6	6.8	5.5	4.6

[a] Thomas (1949); induced emissions have been improperly treated in this paper, so solution is not conceptually satisfactory although actual numerical change is probably small.

[b] Matsushima (1952).

The major differences between the results in Tables 4-1 and 4-3 lie in the increase of b_2, and to a very much lesser extent the b_k for $k > 2$, at the expense of b_1. The reason for such changes is apparent when we compare Eq. (4-27) with and without the radiative terms connecting levels 1 and k. In the equation for the ground state, the coefficient of b_1 on the left side of the equation remains constant while the right side of the equation decreases because the second term vanishes. By contrast, for $k \geq 2$, the coefficient of b_k on the left side of the equation decreases while the right side remains the same. The effect is the greatest for the first excited level, $k = 2$, because only the Lyman radiative term occurs in the coefficient on the left side of the equation.

Because of the small size of the term for 2-k collisional excitation relative to that for photoexcitation, the value of W_{23} for the 2–3 transition becomes very important. The results in Table 4-3 demonstrate this effect. Thus, the height in the atmosphere where $H\alpha$ is formed becomes a critical question. Using the values for b_2 in Table 4-3, we compute $n_2\alpha_{23} = \Delta\tau_{23}$ at the line center to be $\sim 10^{-7}$. Hence, optical depth unity corresponds to a chromospheric column, having $n_e = 2 \times 10^{11}$ and $T_e = 3.5 \times 10^4$, which is $\sim$ 100 km in length. On this basis, we concluded early in our investigations (Thomas, 1949) that the chromosphere must be opaque in at least the central part of Hα and the centers of the early Balmer lines, although not necessarily "locally opaque" as in the case of the Lyman lines. Note that this conclusion is essentially independent of the particular value of T_e used in the computations, because of the predominance of the W_{23} term in the equation for b_2. Indeed, the quantity $b_2T_e^{-3/2} \exp(X_2)$ is essentially independent of T_e, varying strongly with W_{23}. For example, a set of calculations we have made for the case $W_{23} = 0.1$, negligible optical depth in the Lyman continuum, and $n_e = 10^{10}$ to 10^{12} (Athay and Thomas, 1955) gives

T_e	1×10^4	2×10^4	3.5×10^4
$10^3 b_2 T_e^{-3/2} \exp(X_2)$	4	3	5

In order to fix the correct value of W_{23} to be used in the solution, therefore, we require a detailed treatment of the chromospheric emission and absorption in the Balmer series. We formulate an approach to this problem in Section 4-III. In Chapters 6 and 9 we apply the approach to the analysis of chromospheric absorption. Here, in Table 4-3, we only exhibit results corresponding to the range in values for W_{23}.

If we examine the equation of statistical equilibrium for the ground level in the case of local opacity in the Lyman lines, we find a situation somewhat analogous to that found for the first excited level. The value of b_1 is extremely sensitive to the radiation field in the Lyman continuum. The situation is *not*, however, that which one usually finds in the literature; viz, one usually sees the statement that the Saha (LTE) ionization equation is applicable whenever the opacity in the Lyman continuum is high (van de Hulst, 1953; Böhm-Vitense, 1955; Kononovitch and Shklovsky, 1957). The question, of course, is "how high"; the usual statements seem to imply minimal values somewhere in the range 2 to 10 for τ_ν at the head of the Lyman continuum. By considering the simplified case where we represent the hydrogen atom by its three lowest discrete levels plus a continuum, we can demonstrate the incorrect nature of this "usual" statement.

We restrict our attention to atmospheric regions satisfying the condition of local opacity in the Lyman lines (a necessary condition for large Lyman continuous opacity), and to values of T not so high as to invalidate the approximation

$$\int_{Z_k}^{\infty} e^{-Z}dZ/Z \sim e^{-Z_k}/Z_k; \qquad Z_k = X_k, Y_k; \qquad k = 1 - 3 \quad (4\text{-}40)$$

Then, equations (4-27) may be written as follows, for an atom with three discrete levels plus a continuum:

$$b_1\left(1 - \frac{b_2}{b_1}\right)C_{12} + b_1\left(1 - \frac{b_3}{b_1}\right)C_{13} + b_1\left(1 - \frac{1}{b_1}\right)C_1 = F_{11} - b_1F_{12} \quad (4\text{-}41\text{a})$$

$$-b_1\left(1 - \frac{b_2}{b_1}\right)C_{12} + b_2\left(1 - \frac{b_3}{b_2}\right)C_{23} + b_2\left(1 - \frac{1}{b_2}\right)C_2 - b_3e^{X_3}K_{32}\{\text{H}\alpha\} = F_{21} - b_2F_{22} \quad (4\text{-}41\text{b})$$

$$-b_1\left(1 - \frac{b_3}{b_1}\right)C_{13} - b_2\left(1 - \frac{b_3}{b_2}\right)C_{23} + b_3\left(1 - \frac{1}{b_3}\right)C_3 + b_3e^{X_3}K_{32}\{\text{H}\alpha\} = F_{31} - b_3F_{32} \quad (4\text{-}41\text{c})$$

where

$$K_j = \frac{2^5R^2j^{-3}}{3\pi\sqrt{3}} = 2.11 \times 10^{31}j^{-3}; \qquad K_{32} = \tilde{\omega}_2 f_{23}\nu_{23}{}^2 = 1.06 \times 10^{30}$$

$$F_{j1} = K_jX_j^{-1}; \qquad F_{j2} = K_jX_j^{-1}\,(X_je^{X_j})W_j/(Y_je^{Y_j})$$

$$C_{12} = \frac{3.8 \times 10^6 n_e T_e^{3/2}(X_{12} + 1)e^{X_2}}{1 + 0.34(10^{-4}T_e)};$$

$$C_1 = 1.0 \times 10^6\, n_e T_e^{3/2}(X_1 + 2)$$

$$C_{jk} = C_{12}\,[f_{jk}\nu_{jk}^{-1}\tilde{\omega}_j/f_{12}\nu_{12}^{-1}\tilde{\omega}_1]\,\frac{X_{jk} + 1}{X_{12} + 1}\,e^{-X_{2k}};$$

$$C_j = jC_1\frac{\tilde{\omega}_j}{\tilde{\omega}_1}\frac{X_j + 2}{X_1 + 2}; \qquad \{\mathrm{H}\alpha\} = \left\{1 - \int \bar{I}_\nu \varphi_\nu\, d\nu/S_{23}\right\}$$

and we use Fite's most recent values for the cross section, Q_{12}. S_{23} is the source function for Hα.*

If the Saha equation is to be valid, the solutions to these equations must be $b_1 = b_2 = b_3$. Just as we have discussed for the lines, we may under conditions of sufficiently high opacity in the continuum have detailed balance there. Thus, for sufficiently high Lyman continuous opacity, we have detailed balance in it; the right side of Eq. (4-41a) vanishes, and the left side is indeed satisfied by $b_1 = b_2 = b_3$. However, with this solution the left sides of Eqs. (4-41b) and (4-41c) also vanish, requiring the right sides to be zero and thus also detailed balance in the Balmer and Paschen continua. However, a sufficient condition for detailed balance in these continua is *not* simply detailed balance in the Lyman continuum; so we must conclude that $b_1 = b_2 = b_3$ is not, after all, a solution to all three equations. This illustrates the gist of the reason that so many of the pseudo-arguments on departures from LTE lack validity; they rest on a consideration of only a part of the equations of statistical equilibrium, failing to keep always in sharp focus that LTE implies detailed balance in *each* transition, not just the particular one considered. Under conditions of high enough T_e and n_e, one might expect to drive an arbitrary system to LTE. If, however, the optical opacity is not high everywhere in the spectrum, one must consider the departure from LTE induced by the radiative leaks.

The case of the atom having two discrete levels plus a continuum provides a particularly straightforward illustration of the

---

* We prove in Section 4-III that S_{23} is frequency-independent over the line, and thus can be written as

$$S_{23} = 2h\nu_{23}^3/c^2[(b_2/b_3)e^{X_{23}} - 1]^{-1}$$

leading to the above expression for $\{H\alpha\}$ from Eq. (4-13).

physical points involved in looking for a solution other than $b_j = b_k = 1$. Consider the situation of high local opacity in the Lyman continuum, but negligible opacity in the overlying atmosphere to the Balmer continuum. Thus, the Balmer continuous radiation field is treated as known; the Lyman, as unknown. With $F_{2k} > C_{12} \gg C_1$, Eqs. (4-41a) and (4-41b) give the following for this two-level atom:

$$\begin{aligned} b_2/b_1 &\sim 1 + \omega, \qquad 0 < \omega \ll 1 \\ b_2 &\sim F_{21}/F_{22} + \text{very small} \\ F_{12} &\sim F_{11}/b_1 \end{aligned} \tag{4-42}$$

That is, physically: (1) because of detailed balance in the Lyman continuum, the local values of b_1 and b_2 are essentially equal, but they are *not* necessarily both equal to one, their values being determined by the local value of T_e plus the (constant) Balmer continuous radiation field; (2) the radiation field in the Lyman region "adjusts" to the local T_e through these b_1,b_2 values—Ly-α has essentially the LTE value $B_\nu(T_e)$, while the Lyman continuum has the LTE value divided by b_1.

Each additional discrete level added to the atom modifies the result slightly, chiefly in the value of b_k for the highest level. Thus, turning to the atom with three discrete levels, and introducing the quantities

$$\Delta = b_3 e^{X_3} K_{32}\{\mathrm{H}\alpha\}/F_{21}, \qquad M = C_{13}/C_{12}, \qquad N = C_{23}/C_{12},$$

$$P = F_{12}/C_{12}, \qquad U = F_{21}/C_{12} = F_{11}/2C_{12}, \qquad R = F_{22}/C_{12}$$

we solve Eqs. (4-41a) and (4-41b) simultaneously to obtain

$$b_1 = \frac{2U + M + (U[1 + \Delta] + N)(R + 1 + N)^{-1}}{P + M + (R + N)\,(R + 1 + N)^{-1}}$$

$$\sim 2U\,\frac{1 + (1 + \Delta)/2R}{P + 1 + M} \tag{4-43}$$

$$b_2 = \frac{(P + 1 + M)(U[1 + \Delta] + N) + 2U + M}{(P + M)\,(R + 1 + N) + R + N}$$

$$\sim \frac{2U}{R}\,\frac{(P + 1 + M)\,(1 + \Delta)/2 + 1}{(P + 1 + M) + (P + M)/R} \tag{4-44}$$

noting U, $R \gg 1$. As in the preceding paragraph, we are interested in atmospheric regions where the Balmer continuous opacity is small; we consider, however, the whole range of Lyman continuous opacity, subject to this restriction on the Balmer opacity.

We recognize three regions of behavior of b_1, in order of decreasing Lyman opacity of the overlying atmosphere—thus, in order of increasing atmospheric height of the region considered.

a. Region 1. High local opacity in the Lyman continuum; detailed balance valid. This condition of detailed balance in the Lyman continuum is equivalent to the relation

$$b_1 = F_{11}/F_{12} = 2U/P$$

which, substituted in Eq. (4-43), gives

$$\begin{aligned} b_1 &= (U/R)(1 + \Delta)/(1 + M) \\ &= W_{2i}^{-1} Y_2 e^{Y_2}(1 + \Delta)/(1 + M)e^{-X_2}/X_2 \qquad (4\text{-}45) \end{aligned}$$

$$b_2 = b_1(1 + M) \qquad (4\text{-}46)$$

With the exception of the term in Δ, the results are those already obtained above for the two-level atom. $\Delta \propto b_3\{\mathrm{H}\alpha\}$; $\{\mathrm{H}\alpha\}$ varies between limits of zero—under conditions of detailed balance in Hα—and some value less than unity, which we comment on in the last section of this chapter. In Section 4-III we develop a method for computing $S_{23}(\tau_\alpha)$, where τ_α is the optical depth at the center of H_α, and show that apart from the radiation field in the Balmer continum—whose value is constant by the conditions of the problem—S_{23} does indeed depend only upon τ_α. Thus, adding more levels to the atom will not change the value of $\{\mathrm{H}\alpha\}$; such a change will come about only through the change in the value of b_3, echoing our general statement made above.

b_1, b_2 show no direct dependence upon the local value of n_e in this region 1. Since, however, τ_α depends upon n_e at all heights above that considered, there is an indirect, second-order, dependence of the solution upon n_e.

Region 2. Intermediate Lyman continuous opacity; too small for detailed balance, too large for $\bar{I}$(LyC) *to be independent of* τ(LyC). In this region, a solution of the transfer problem in the Lyman continuum is critical. We use Eqs. (4-43) and (4-44); the value of P comes from the solution of the transfer problem; we can say nothing further at this point on the character of the solution. We discuss a detailed solution in Chapter 6, where we analyze observations of the optical continuum to infer n_e, T_e, and b_1.

c. Region 3. Negligible Lyman continuous opacity. As the height of the region considered increases, I_{LyC} approaches its emergent value. If T_e increases outward in the atmosphere sufficiently rapidly, P ultimately becomes very small relative to 1. That is, collisional excitation from the first to the second level predominates over photoionization as the depopulating influence on the first level. If the condition $P \lesssim 1$ occurs at low enough heights that the condition of local opacity in the Lyman lines is still valid, then Eq. (4-43) becomes

$$b_1 \sim 2U[1 + (1 + \Delta)/2\mathrm{R}]/(1 + M) \sim 2U$$
$$= K_1/X_1C_{12} = f(T_e)/n_e \qquad (4\text{-}47)$$

The essential point here is $b_1 \sim n_e^{-1}$. The corresponding expression for b_2 is independent of n_e, except through the indirect effect of the dependence of the quantity Δ upon τ_α. Thus, in this third region, the increase of b_1 with height in the atmosphere becomes much more rapid than that of b_2.

Figures 4-1 and 4-2 illustrate these algebraic results. In these computations, we have made use of developments in the following sections of this chapter; so we do not go here into the details underlying the computations. We wish only to illustrate by Figs. 4-1 and 4-2 the error introduced by accepting as valid the "usual" statements on the regions of applicability of the Saha equation.

Finally, we note that the algebraic results derived above illustrate our earlier remarks on the quantities upon which b_2 and n_2 depend. From Eq. (4-44) we have

$$b_2 = (2U/R)(P, R, \Delta) = Y_2e^{Y_2}[1 + \Delta]/(X_2e^{X_2}W_2) \qquad (4\text{-}48)$$

a slow-varying function of P and R. Thus, since $X_2 \propto T_e^{-1}$, we see that $[b_2T_e^{-1} \exp{(X_2)}]$ depends only slightly on T_e, through the factor $b_3e^{X_3}$, but strongly depends upon the Balmer Hα radiation field through the dependence $\Delta(\tau_\alpha)$.

3. Cases Intermediate to Those of Thin and Thick Atmospheres. When the gas mass considered is neither so diffuse as to make negligible contribution to the radiation field present, nor so concentrated that only the locally produced radiation field is of

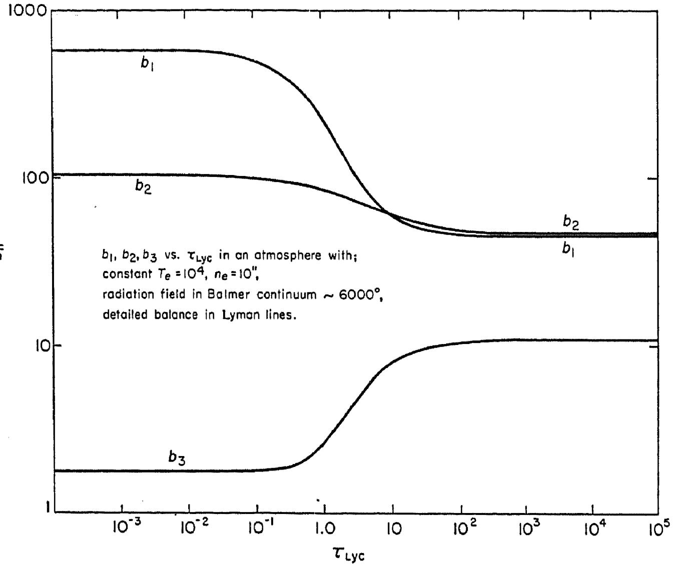

Fig. 4-1. Computation of Pottasch and Thomas (1959) showing b_1 and b^2 in a bounded atmosphere having constant T_e and n_e. (From S. R. Pottasch and R. N. Thomas, 1959, *Astrophys. J.*, **130**, 941.)

importance, there is no recourse but to consider simultaneously the solution of the radiative transfer equation and the equations of statistical equilibrium. Because, however, it is the term $\int \bar{I}_\nu \varphi_\nu \, d\nu$ which enters the equations of statistical equilibrium, and because the b_k enter the value of $\bar{I}_\nu$ only as ratios through S_ν, the situation is somewhat more amendable than, for example, in the discussion of line profiles.

For example, if we suppose that the absorption coefficient has a purely Doppler profile, then we see that the value of $\int \bar{I} \varphi_\nu \, d\nu$ is fixed by the central few Doppler widths of the line alone, unless $\bar{I}_\nu$ increases exponentially outward from the line center, for a Doppler-φ_ν varies as exp $[-(\Delta\nu/\Delta\nu_D)^2]$. Thus, apart from the variation of $\bar{I}_\nu$ with ν, the integrand has dropped to about 10^{-2} its central value at two Doppler widths from the line center, and 10^{-4} its central value at three Doppler widths. For a non-exponentially increasing line

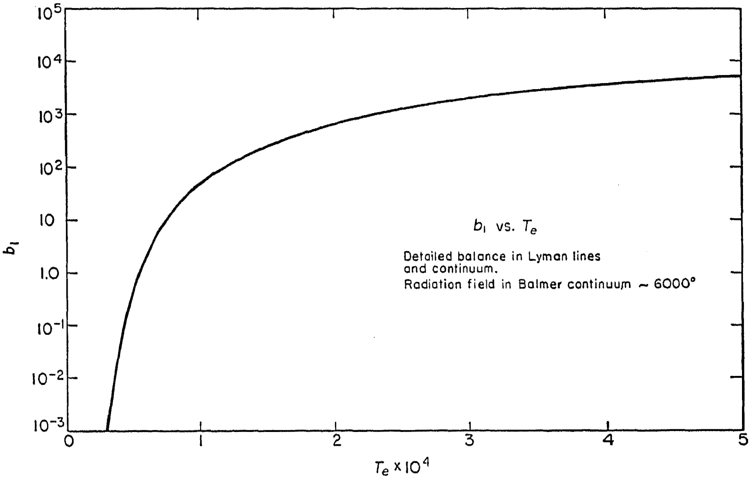

Fig. 4-2. Computation of Pottasch and Thomas (1959) showing $b_1(T_e)$ in part of an atmosphere satisfying the criterion of region 1. (From S. R. Pottasch and R. N. Thomas, 1959, *Astrophys. J.*, **130**, 941.)

profile, we make an error of only a few per cent in $\int \bar{I}\varphi_\nu \, d\nu$ by ignoring that part of the line beyond two Doppler widths from the center. In consequence, we need concern ourselves only with some small central region of the line, the size of the region being fixed by the accuracy with which we need the value of the radiative term.

As a consequence of this result, we must proceed to answer two questions: (1) What is the form of the absorption coefficient, in the particular gas mass investigated? That is, given the actual absorption coefficient, not just an assumed Doppler profile, what portion of the line need we consider to specify $\int \bar{I}_\nu\varphi_\nu \, d\nu$ to a given accuracy? (2) What can we say about the profile of $\bar{I}_\nu$ over the central region specified by the answer to the first question?

A second point of simplification arises because we need not know each of the b_k individually in order to solve the transfer equation. We need only the b_L/b_U ratio for the transition giving the radiation considered, where U and L refer to upper and lower levels of the transition. This ratio suffices to determine the factor $B_\nu(T_{ex})$ in Eq. (4-38). Moreover, the result of the preceding two paragraphs makes easier the determination of the second factor in Eq. (4-38), the ratio j_ν/φ_ν, for we need investigate this factor only over a small core of the line, not in the wings.

In Section III we proceed to investigate the points just enumerated, which must form the basis for a systematic study of the solutions of the equations of statistical equilibrium. This investigation has thus far proceeded to rudimentary stages only, and has resulted in no such sets of values of b_k as those coming from the thin- and thick-atmosphere limiting cases. Indeed, only fairly qualitative results have thus far been forthcoming. We shall show, however, that these results do provide a sufficient basis for guiding the direction of our analysis of certain of the eclipse data, and for allowing us to interpret the results of this analysis and of the analysis of some data on the Fraunhofer lines in terms of chromospheric mass distribution and structure. We follow the general pattern of the development by Thomas (1957) and Jefferies and Thomas (1958, 1959).

III. The Problem of Specifying $\int \bar{I}_\nu\varphi_\nu\,d\nu$ in an Arbitrary Gas Mass and Results on the Associated Source Function

A. The Profile of the Absorption Coefficient in the Chromosphere

The chromosphere has two primary characteristics: its opacity in the ordinary optical continuum is negligible, and T_e increases outward. Thus, we have a low density, relatively high temperature atmosphere. As we shall see in Chapter 6, an analysis of data from the continuum gives $n_e \sim 5 \times 10^{11}$ and $T_e \sim 6000°$ at a chromospheric height of 500 km. Thereafter n_e decreases and T_e increases upward, so that these values of n_e and T_e form upper and lower limits, respectively, for the chromosphere above this height. We shall use these values as limits in the following discussion.

For hydrogen, the major sources of line broadening are Stark and Doppler. Following the treatment by Underhill (1950), we have for the atomic absorption coefficient

$$\alpha_\nu\,d\nu = \frac{\pi\epsilon^2}{m_e c}\left\{\sum_q \frac{f_q}{n'^2\pi^{1/2}\,\Delta\nu_D}\int_{-\infty}^{\infty} H\left[a, \left(\frac{\Delta\nu}{\Delta\nu_D} - \frac{\beta}{y}\right)\right] W(\beta)\,d\beta + f_0\,\frac{H(\alpha, \Delta\nu/\Delta\nu_D)}{\pi^{1/2}\,\Delta\nu_D}\right\} d\nu \qquad (4\text{-}49)$$

where

$$Y = 2.24 \times 10^{-3} X_q^{-1}\lambda^{-1}F_0^{-1}(10^{-4}T_e)^{1/2};$$

$$\Delta\lambda_q = \frac{3h\lambda^2 F}{8\pi^2 m_e \epsilon c} X_q;$$

$$F = F_0\beta = F_0 \times 1.25 \times 10^{-9} n_p^{2/3};$$

$$\int_{-\infty}^{\infty} W(\beta)\, d\beta = 1; \qquad (4\text{-}50)$$

$$\beta = Y \frac{\Delta\nu'}{\Delta\nu_D}; \qquad X_q = n(n_2 - n_1) - n'(n'_2 - n'_1);$$

$$f_q = (8\pi^2 m_e \nu / 3h) \mid x_q \mid^2$$

x_q is the matrix element of the dipole moment of the transition for the particular Stark components: the subscript q refers to the Stark component displaced from the central component by $\Delta\lambda_q$; n, n' are the principal quantum numbers of the upper and lower levels of the transition; and n_1, n_2, $n'_1 n'_2$ are four of the usual six quantum numbers characterizing the problem in parabolic coordinates; and $W(\beta)$ is the Holtzmark distribution function. The function $H(a,\nu)$ is the usual relation between natural and Doppler broadening, cf Harris tables (1948).

For sufficiently large y, $\mathrm{H}(a, [(\Delta\nu/\Delta\nu_D) - (\beta/y)])$ does not vary appreciably in the interval where $W(\beta)$ makes its major contribution to the integral. For example, at $\beta = 3$, the integral over $W(\beta)$ alone has reached 75 percent of its total value; at $\beta = 2$, 55 percent. Thus, if $\mathrm{H}(a, [(\Delta\nu/\Delta\nu_D) - (\beta/y)])$ does not change appreciably from $\mathrm{H}(a, \Delta\nu/\Delta\nu_D)$ by the time $\beta \sim 3$, we may neglect the Stark effect without introducing more than 25 percent error in the particular qth component; and 50 percent error for $\beta \sim 2$. We note that for small a, $\mathrm{H}(a,v)$ is essentially $\exp(-v^2)$; and for the early lines of the hydrogen Paschen and Balmer series with transition probability 10^8 to 10^7, a is small enough that $H(a,v)$ is indeed essentially Gaussian out to ~ 3 Doppler widths. Thus, the total change in α_ν over the Doppler core is e^9 or 10^4 for these hydrogen lines. As we cross the Doppler core for a line formed in a thick atmosphere, we traverse an atmospheric region where τ_0, the optical depth at the line center, varies by $\sim 10^4$. Underestimate of α by a factor of 2, although serious for fixing a precise value of τ_0 and a particular location in the atmosphere, is not so serious in the attempt to fix an over-all pattern to the place of origin of the lines.

For the solar chromosphere, and for most other extended atmospheres, $n_p < 10^{12}$, so $F_0 < 0.12$. Also X_q varies from 0 to $n(n-1) + n'$. Thus

$$y > 1.9.10^2(10^{-4}T_e)^{1/2}\{[n(n-1) + n']\,\lambda(\text{microns})\}^{-1}$$

For $T_e \gtrsim 10^4$, $y > 3$ for Lyman lines earlier than Ly-8 and for Balmer lines earlier than Hβ. For later Balmer lines, $y > 3$ for those components for which $X \lesssim 16$. Such components comprise an appreciable portion of the absorption coefficient; for example, 65 percent at Hγ. Furthermore, when $n_p < 10^{11}$, X_q need only be less than 50, and all Stark components of Balmer lines out to Hϵ produce negligible departure from the Doppler profile. Thus, so long as we restrict our attention to Hα to H_6 and the corresponding early Lyman lines, we may ignore broadening, other than Doppler, over a core some three Doppler widths in extent.

For the higher Balmer lines we must evaluate the profile of the absorption coefficient in detail. However, we have seen that the solution of the equations of statistical equilibrium is much less sensitive to $\int \bar{I}\varphi_\nu \, d\nu$ for the higher hydrogen lines than for the lower. Only when we discuss self-absorption in considering line profiles and total emission in individual lines does the question of the profile of the absorption coefficient for the later lines become important.

For the metallic lines, the damping coefficient is the sum of natural and collisional broadening; Van der Waals' encounters with neutral hydrogen atoms provide the collisional damping. From Aller (1953) we obtain

$$\Gamma_{\text{coll}} \sim 2\pi n_{\text{H}} \left(\frac{8kT_e}{\pi m_{\text{H}}}\right)^{0.3} \left(0.8 \times 10^{-32}\frac{R_k}{a_0^2}\right)^{0.4} \qquad (4\text{-}51)$$

where we neglect the reciprocal mass of the metal relative to that of hydrogen in computing the mean relative speed. n_{H} is the number of neutral hydrogen atoms and R_k^2 is the mean-square radius corresponding to the upper level of the transition. We take $R_k^2/a_0^2 = 100$, noting that we must be in error by $10^{2.5}$ before we introduce an order of magnitude error in Γ. We then obtain $\Gamma_{\text{coll}} \sim 3 \times 10^{-8}$

$(10^{-4}T_e)^{0.3}n_{\mathrm{H}}$. For $n_{\mathrm{H}} < 10^{16}$ to 10^{15}, which is representative of the upper photosphere, $\Gamma_{\mathrm{coll}} \leq \Gamma_{\mathrm{nat}}$ for lines with transition probabilities of order 10^8 to 10^7, and in this case

$$\begin{aligned} a &= \frac{\Gamma}{4\pi\,\Delta\nu_D} \\ &= 0.64 \times 10^{-3}(10^{-8}\Gamma)(10^{-4}T_e)^{-1/2}\left(\frac{m_m}{m_{\mathrm{H}}}\right)^{1/2} \lambda(\text{microns}) \end{aligned} \tag{4-52}$$

Harris' tables show the Doppler core to be three Doppler widths in extent for $a = 0.64 \times 10^{-3}$, 2.7 Doppler widths for $a = 0.64 \times 10^{-2}$, and 3.5 Doppler widths for $a = 0.64 \times 10^{-4}$. Thus we may safely assume that for lines with transition probabilities of 10^8 to 10^7 the absorption coefficient over a region three Doppler widths from the line center has a Doppler profile in the chromosphere and upper photosphere.

B. *The Value of j_ν/φ_ν*

To evaluate the ratio j_ν/φ_ν we must consider the details of the emission processes. In a broad sense, the processes are of two kinds. The first kind is coherent scattering, viz, absorption followed immediately by remission at the same frequency in the *frame of reference of the atom.* The second is any other process—collisional excitation followed by radiative emission, absorption in the j to k transition and re-emission in the k to s transition, etc. In this second variety of processes, there is essentially no correlation between the excitation process and the emission process. If the correlation is, indeed, zero, and if we ignore all sources of line broadening save Doppler, the profile of j_ν is the same as that of φ_ν—Doppler—and j_ν/φ_ν is unity. What correlation exists is very much less than for the case of coherent scattering, and we now proceed to show that even for coherent scattering j_ν/φ_ν is effectively unity. Once we have shown this, we are quite sure that for both types of emission processes mentioned, we may safely take $j_\nu/\varphi_\nu = 1$.

Consider now the case of coherent scattering in the reference frame of the atom. Since only Doppler broadening is of importance, the frequency dependence of the emission in a given direction is fixed uniquely by the velocity distribution function of the atoms in that direction. We consider only a thermal velocity field. If, then, all atoms in a given volume element absorbed simultaneously, and emitted simultaneously, both j_ν and φ_ν would have a frequency dependence corresponding to a Maxwellian velocity distribution, and their ratio would be unity. If, as is the actual case, only a fraction absorb simultaneously, then the velocity distribution function for this fraction of atoms is not, in general, the same along the direction of the incoming radiation, which they absorb, and along an arbitrary direction in which the radiation is scattered. The difference represents the frequency dependence of j_ν/φ_ν—taking into account that radiation is incident from all directions. This problem was studied by Henyey (1940); we use a different approach which permits a somewhat more direct solution.

In the reference frame of the atom, emission and absorption occur at frequency ν_0. Consider incident radiation—frequency ν_1 in the stationary coordinate system—of intensity $I\nu_1$, scattered through an angle θ, thus contributing Δj_ν to the source function in that direction. Choose the Z axis of a rectangular coordinate system along the direction of the scattered radiation. In the plane defined by $[I_{\nu_1}, \Delta j_\nu]$, θ is the polar angle of I_{ν_1}. Take w as the Z component of velocity, and q and V, respectively, as velocity components along the radial and tangential directions in the X,Y plane, with the radial direction defined by the intersection of the $[I_{\nu_1}, \Delta j_\nu]$ and $[X, Y]$ planes. Then we have the relations between ν_0, ν_1, and ν—where ν is the frequency of the scattered radiation:

$$\nu = \nu_0[1 - w/c] \tag{4-53}$$

$$\nu_0 = \nu_1[1 + (w/c)\cos\theta + (q/c)\sin\theta] \tag{4-54}$$

Thus the distribution in ν is fixed by the distribution in w; and we ask the relation of the distribution over w for the absorbing atoms to the distribution over w in the general ensemble, which is Maxwellian. Thus we wish to hold ν, or w, and the z-axis fixed and integrate over all scattering processes producing ν in the given direction. That is, we integrate over ν_1 and θ; or, since the distribution function is given in terms of q, over q and θ. If $\Phi(\theta)$ is the function giving the angular dependence of the scattering and α_{ν_0} is the atomic absorption coefficient at the center of the line, we have

$$j'_\nu \text{ (scat) } \frac{d\omega}{\sigma\pi^{1/2}} = \int_\omega \Phi \, d\omega \int_{q,V} I_{\nu_1}(iz,\theta)\alpha_{\nu_0}(\sigma\pi^{1/2})^{-3} \exp\left(\frac{-[q^2 + w^2 + V^2]}{\sigma^2}\right) \times dw \, dq \, dV \tag{4-55}$$

with

$$\alpha_{\nu_0} = (\pi\epsilon^2/m_e c) \, f_{Lu}(\lambda_0/\sigma\pi^{1/2}) \tag{4-56}$$

and

$$j'_\nu n_L = j_\nu A_{uL} h\nu n_u \tag{4-57}$$

for pure scattering. Transforming variables $dw \to d\nu$ and $dq \to d\nu_1$ and introducing the relations

$$\begin{aligned} \frac{q^2}{\sigma^2} = \frac{c^2}{\sigma^2}\left[\frac{\nu_0 - \nu_1}{\nu_0} - \frac{\nu_0 - \nu}{\nu_0}\cos\theta\right]^2 \csc^2\theta \\ = (x - y\cos\theta)^2 \csc^2\theta, \end{aligned} \tag{4-58}$$

$$x = \Delta\nu_1/\Delta\nu_D, \qquad y = \Delta\nu/\Delta\nu_D, \qquad \Delta\nu_D = \sigma\nu_0/c$$

we obtain, for Eq. (4-55)

$$\begin{aligned} j'_\nu \text{ (scat) } d\nu = [e^{-y^2}\alpha_{\nu_0} \, d\nu]\left[(\sigma\sqrt{\pi})^{-1}\int_{-\infty}^{\infty} dV \exp\left(-\frac{V^2}{\sigma^2}\right)\right] \\ \times\left\{\int_\pi^0 \Phi \, d\theta \int_0^{2\pi} d\varphi \int_{-\infty}^{\infty} \frac{I_{\nu_1} \, dx}{\pi^{1/2}} \exp[-(x - y\cos\theta)^2 \csc^2\theta]\right\} \end{aligned} \tag{4-59}$$

The first bracket on the right of Eq. (4-59) is the absorption coefficient α_ν; the remainder, therefore, represents the correction factor by which the profile of the emission coefficient j'_ν departs from that of α_ν or φ_ν. If I_{ν_1} shows negligible variation with ν_1 over the line, then, and only then, does the profile of j'_ν or of j_ν follow trivially that of α_ν. We may demonstrate the situation by computing several simple cases:

(i) $\qquad I_{\nu_1} = I_{\nu_0} \qquad$ and $\qquad \Phi(\theta) = 1/4\pi$

The substitution $z = [x - y\cos\theta]\csc\theta$ leads to the result

$$j'_\nu \, d\nu = I_{\nu_0}\,(e^{-y^2}\alpha_{\nu_0} \, d\nu) \tag{4-60}$$

so that

$$j'_\nu/\alpha_\nu = I_{\nu_0}$$

(ii) $I_{\nu_1} = I_{\nu_0} \exp[-(\Delta\nu_1/\Delta\nu_D)^2]$ and $\Phi = 1/4\pi$

The substitutions

$$z = x\sqrt{(1 + \csc^2\theta)} - y\,\frac{\cos\theta\csc^2\theta}{(1+\csc^2\theta)^{1/2}};$$

$$p = \cos\theta; \qquad s^2 = \frac{p^2}{2-p^2}$$

lead to the result

$$j'_\nu/\alpha_\nu = I_{\nu 0}\int_0^1 e^{-y^2s^2}/(1+s^2)\,ds \tag{4-61}$$

The coefficient of I_{ν_0} shows a variation of a factor of 4 over the range $y = 0 \rightarrow 3$, by contrast with the range of 10^4 shown by I_ν itself. Thus the approximation of a frequency-independent source function is far better than that of coherent scattering, where S_ν would follow the ν variation of I_ν.

(iii) $I_{\nu_1} = I_{\nu_0} \exp[-(\Delta\nu_1/\Delta)^2]$ and $\Phi = 1/4\pi$

Set

$$r = \Delta\nu_D/\Delta, \qquad z = x\sqrt{(r^2+\csc^2\theta)} - y\cos\theta\csc^2\theta/\sqrt{(r^2+\csc^2\theta)}$$

$$p = \cos\theta, \qquad t^2 = 1 + r^{-2}, \qquad s^2 = p^2/(t^2 - p^2)$$

Then

$$j'_\nu/\alpha_\nu = I_{\nu_0}r^{-1}\int_0^{(t^2-1)^{-1/2}} e^{-s^2y^2}/(1+s^2)\,ds \tag{4-62}$$

(iv) I_ν as in case (iii); $\Phi = (3\pi/16)\,(1+\cos^2\theta)$

Use the same substitutions as in case (iii). Then

$$\frac{j'_\nu}{\alpha_\nu} = I_{\nu_0}\frac{3}{4r}\int_0^{(t^2-1)^{-1/2}} \frac{1+(1+t^2)s^2}{1+s^2}\,\frac{e^{-s^2y^2}}{1+s^2}\,ds \tag{4-63}$$

In each of these cases the coefficient of I_{ν_0} shows a very much smaller range than I_ν itself, except for the case of I_ν essentially constant (large r). Table 4-4 exhibits the numerical results in the four cases;

we combine cases (ii) and (iii) by setting $\Delta = \Delta\nu_D$. The "pure absorption" or "completely non-coherent" approximations are not strictly accurate to describe the variation of the source-function j_ν/α_ν over the line profile, for there is a variation by about a factor of 4 over the first three Doppler widths. On the other hand, the approximation is better than the "pure scattering" assumption by more than three orders of magnitude.

We have, thus far, neglected the angular dependence of j_ν/α_ν by ignoring an angular dependence of I_ν. If we introduce this in an approximate way by setting

$$I_\nu = I_{\nu 0}[1 + a \cos \psi] \exp [-(\Delta\nu/\Delta)^2] \qquad (4\text{-}64)$$

where ψ is the angle with the outgoing radius, we see immediately that there is no difference in j_ν/α_ν for radial in-going and out-going beams. For, $\cos \psi = \pm \cos \theta$ in the case of the radial beams; the integral in each of cases (i) to (iv) is an even function of $\cos \theta = p$;

Table 4-4. Dependence of $f(y) = j'_\nu[\alpha_\nu I_{\nu 0}]^{-1}$ upon ν for $\Delta = \Delta\nu_D$

Tabular values of $\log [f(y = 0)/f(y)]$					
$\Delta\nu/\Delta\nu_D$	0	0.5	1.0	2.0	3.0
(i)	0	0	0	0	0
(ii)	0	0.03	0.10	0.29	0.45
(iv)	0	0.04	0.13	0.36	0.54

thus the angularly dependent, linear term in $\cos \theta$ drops out in the integration over θ. Therefore, we neglect the angular dependence of j_ν/α_ν in this discussion.

C. *The Determination of* $\bar{I}_\nu(\tau_\nu)$, $I_\nu(0)$, and $S_\nu(\tau_\nu)$

From the preceding section, we see that, up to a maximum possible error of a factor 4 at three Doppler widths from the line center, we may take j_ν/α_ν equal to unity. Thus from Eq. (4-42), S_ν does not vary with ν over that part of the line which contributes significantly to terms entering the equations of statistical equilibrium. In consequence, from Eq. (4-44), the variation of $\bar{I}_\nu[\tau_\nu]$ and of I_ν [0] with ν comes only from the variation of $S_{\nu 0}$ with $\tau_{\nu 0}$. Thus to solve the equations of statistical equilibrium at a given point in the atmosphere, we need to know the values of T_e and n_e at *this* point *and* the value of a *single* numerical quantity, S_{ν_0}, for each transition entering the equations, at *each* point in a certain neighborhood of the given point. The size of the neighborhood is fixed by our concern with only the central two or three Doppler widths of the line, or a range in τ_{ν_0} of a factor e^4 to e^9, i.e., 50 to 10^4, about the point in question. Likewise, to compute the emergent intensity I_ν [0] in this central Doppler core, we require S_{ν_0} for $1 \lesssim \tau_{\nu_0} < 50$ to 10^4. Using the relation $S_{\nu_0} = B_{\nu_0}[T_{ex}]$, we can refer to this quantity to be specified at each point, for each transition, in terms of T_{ex}.

Clearly, we cannot a priori investigate model atmospheres in which we specify T_{ex} as, for example, we might specify a distribution of T_e and n_e and seek the energetic flux which will maintain this. The T_{ex} must be consistent with the equations of statistical equilibrium for whose solution such a specification of $T_{ex}[\nu_0, \tau_{\nu_0}]$ would suffice. The only two cases in which something about T_{ex} can be specified a priori are the two extreme cases which we have already treated: (1), the locally opaque atmosphere, in which we simply assume a constant (but unspecified) value of S_{ν_0} over the whole range of τ_ν which effectively contributes to $\bar{I}_\nu$ at a given point—hence, a constant value of $\bar{I}_\nu$ over ν; and (2), the thin atmosphere, where the only radiation arises externally and suffers no appreciable absorption, thus giving a specified constant value of $\int \bar{I}_\nu \phi_\nu \, d\nu$.

It is thus clear that a precise solution of the equations of statistical equilibrium at a given point requires, in essence, their solution over the whole atmosphere in order to obtain a self-consistent set of T_{ex}. We can, however, ask whether approximate solutions are possible, which will permit T_{ex} to be determined sufficiently well to serve as the basis of the next approximation to the solution of equations at a given point. We should expect the answer to be yes, at least to the extent to which we require rigor here; for we are mainly trying to see what kind of analytical framework is permitted in our discussion of the eclipse data. Thus, we will be satisfied if we can obtain the general behavior of the solutions to be expected in that kind of an atmosphere which we believe the chromosphere to be.

We proceed in several stages, in order to make clear the physical picture. First, we consider the line originating from the first excited state. To make clear the departure of the result from the usual statement that the process of line formation lies intermediate to the

cases of local thermodynamic equilibrium and pure coherent scattering, we consider an atom having just two discrete energy levels plus a continuum. Then we pass to the general case, showing that it differs very little from that of the two-level atom in the expression for $B_\nu(T_{ex})$ for the lowest lying resonance line. We consider a rough approximation to the radiation field associated with this expression for the source-function in order to exhibit the variation in value of the source-function as we pass from a thin atmosphere to a locally opaque atmosphere. With these results, we proceed to a less detailed computation of $B_\nu(T_{ex})$ for the second resonance line and the first subordinate line. We treat an atom with three discrete energy levels plus a continuum, this model being sufficient to demonstrate the difference in behavior between resonance and subordinate lines. We cast the approach to the three-level atom in a form which permits an immediate generalization to the multi-level atom. We then consider the transfer problem in certain simplified atmospheres, in order to demonstrate the run of $S_{\nu_0}(\tau_{\nu_0})$. Finally, we summarize the discussion by emphasizing once again the utility of an approach in terms of net rates.

1. Detailed Treatment of the Lowest-Lying Resonance Line. From Eq. (4-27), we have the equation of statistical equilibrium for the ground state of an atom having only two discrete levels plus a continuum:

$$\begin{aligned} b_1 C_1 T_e^{1/2} n_e \bigg[Q_{12}\left(1-\frac{b_2}{b_1}\right) e^{X_2}(1+X_{12}) \\ + Q_{1\kappa}\left(1-\frac{1}{b_1}\right)(1+X_1)\bigg] \\ = b_2 f_{12}\nu^2 e^{X_2}\left[1 - W_{1-2}\,\frac{(b_1/b_2)e^{X_{12}}-1}{e^{Y_{12}}-1}\right] \\ + \frac{e^{X_1}}{2RZ^2}\int_{\nu_1}^{\infty} f_{1\kappa}\nu^2\kappa^3 e^{-h\nu/kT_e}\left[1 - W_\kappa\,\frac{b_1 e^{X_{1\kappa}}}{e^{Y_{1\kappa}}-1}\right] d\nu \end{aligned} \tag{4-65}$$

Introduce the quantities

$$L_{11} = \int_{\nu_1}^{\infty} \frac{\kappa^3\nu^2 f_{1\kappa}}{\nu_{12}^2 f_{12}}\,\frac{W_\kappa}{e^{Y_{1\kappa}}-1}\,\frac{d\nu}{2RZ^2} \tag{4-66}$$

$$L_{21} = \int_{\nu_1}^{\infty} \frac{\kappa^3\nu^2 f_{1\kappa}}{\nu_{12}^2 f_{12}}\left(1 + \frac{W_\kappa}{e^{Y_{1\kappa}}-1}\right)\frac{d\nu}{2RZ^2}\,e^{-X_{1\kappa}} \tag{4-67}$$

$$\epsilon = \frac{0.74 \times 10^{11} Q_{12} n_e T_e^{1/2}(1 + X_{12})(1 - e^{-X_{12}})}{\nu^2 f_{12}} \tag{4-68}$$

$$\eta = \epsilon \frac{Q_{1\kappa}}{Q_{12}} \frac{1 + X_1}{1 + X_{12}} e^{-X_2} \frac{(b_2{}^{-1}e^{X_{12}} - 1)}{e^{X_{12}} - 1} + L_{11}\left(b_2{}^{-1}e^{X_{12}} \frac{L_{21} - 1}{L_{11}}\right) \tag{4-69}$$

Then Eq. (4-68) gives, after some algebra,

$$B_\nu(T_{\text{ex}}) = \frac{W_{1-2}\bar{I}_{\nu 0}}{1 + \epsilon + \eta} + \frac{\epsilon[1 + (Q_{1\kappa}/Q_{12})(1 + X_1)/(1 + X_{12})e^{-X_2}]}{1 + \epsilon + \eta} B_\nu(T_e) + \frac{2h\nu^3}{c^2} \frac{L_{11}}{1 + \epsilon + \eta} \tag{4-70}$$

for the source function. We note that, had we neglected the continuum, we would have obtained only the first two terms on the right.

It is of interest to comment here on the formal resemblance of Eq. (4-70) to the Milne treatment (1930) of the two-level atom, and the Stromgren treatment (1935) of the two-level plus continuum model. In each of these cases the quantity $\bar{I}_\nu$, rather than $\bar{I}_{\nu 0}$, appears in the first term on the right. The presence of $\bar{I}_\nu$ provides the basis for the oft-quoted remark that the source-function generally lies intermediate to the case of pure coherent scattering, $S_\nu = \bar{I}_\nu$, and the case of local thermodynamic equilibrium, or pure absorption at the electron temperature, $S_\nu = B_\nu(T_e)$. In fact, of course, two assumptions underlie this remark: first, that the left side of Eq. (4-70) is indeed the source-function, which requires $j_\nu/\varphi_\nu = 1$; and second, that $\bar{I}_\nu$ can be removed from all the integrals in which it occurs. Milne and Stromgren by-pass this second assumption by writing the equations of statistical equilibrium not for the energy state as a whole but for an element of the state. Thus, the essential physical assumption is that the interchange between substates may be neglected. The assumption is clearly unjustified for the region of the Doppler core, where we are most concerned for the value of the source function. In the general case, the assumption must be justified in detail; this has not been done. Thus we must conclude that Eq. (4-70) is the proper expression, in which case the source-function has no term depending upon coherent scattering. Rather, the source-function has three terms competing for the major role, none of which varies with frequency across the Doppler core.

We can see immediately that the second term, that depending upon collisional excitation, is much smaller than the other terms if $B_\nu(T_e)$ has a value anywhere near that of $\bar{I}_{\nu_0}$. For, since we consider resonance lines, $Q_{12} \sim 1, f_{L2} \sim 1, \nu \sim 10^{15}, n_e < 10^{12}, 5000 < T_e < 10^6$. Thus $\epsilon \lesssim 10^{-4}$. This is essentially the result found by Pannekoek (1930), and interpreted by him to imply the predominance of coherent scattering as the mechanism of line formation. We note, of course, the non-validity of this conclusion by the preceding arguments.

To evaluate the relative importance of the last term in Eq. (4-70), we must compute the L's. For this purpose we consider the special case W_κ = constant, and $X_{1\kappa}, Y_{1\kappa} \gg 1$. W_κ = constant implies a Planck distribution of the radiation near the head of the free-bound continuum of the ground state. The other condition simply assumes a sufficiently great ionization energy relative to $\mathbf{k}T_e$ and $\mathbf{k}T_r$, which is hardly a restriction. With these two assumptions, we obtain

$$L_{11} = \frac{32 g_{\mathrm{II}}}{3\pi\sqrt{3}} \frac{R^2}{f_{12}\nu_{12}{}^2} \frac{W_\kappa}{Z^2\tilde{\omega}_1} \frac{e^{-Y_1}}{n_1{}^3 Y_1} \tag{4-71}$$

$$\frac{L_{21}}{L_{11}} = W_\kappa{}^{-1} Y_1 e^{-X_1} \left[\frac{e^{Y_1}}{X_1} + \frac{W_\kappa}{X_1 + Y_1}\right] \tag{4-72}$$

We see that η, like ϵ, is considerably less than unity. The last term then lies essentially in the ratio exp $(-Y_2)$ to the term in $\bar{I}_{\nu_0}$. χ_2 is about 8 ev for Ca$^+$ and Sr$^+$, and about 3 ev for K, Na, Ca, Al, and Mg; thus for T_r about 6000°, the corresponding values of Y_2 are about 15 and 6. Thus for Ca$^+$ and Sr$^+$ the term in L_{11} is about the same size as that in ϵ, and considerably smaller than that in $\bar{I}_\nu$.

If T_r lies near T_e, the photo-ionizations exceed the collisional excitations, and the term in L_{11} dominates in fixing the central intensity of the lines. This is the essence of the argument on the central intensity of resonance lines presented by Stromgren (1935). On the other hand, in the chromosphere we expect T_e to lie considerably above T_r, and we introduce the possibility of a reversal in importance of terms. Consider the situation.

As T_e increases over T_r, the relative importance of the photoelectric term to the collisional decreases as $n_e \exp(Y_1 - X_{12})$. Thus, we may divide the resonance lines into three groups, with parameters χ_{12} and χ_1. One group, typified by H and the non-metals, has both χ_{12} and χ_1 large, about 10 and 14 ev, respectively; the resonance lines and series head lie in the far ultraviolet. A second group, the singly ionized metals typified by Ca^+, has small χ_{12} and large χ_1, about 3 and 12 ev respectively, resonance lines in the visible and series heads in the far ultraviolet. The third group, the neutral metals typified by Na, has both χ_{12} and χ_1 small, some 3 and 5 ev, respectively, resonance lines in the visible, and series heads in the ultraviolet. Taking $n_e = 10^{11}$ as a representative value for the low chromosphere, we see that for $T_r = 6000°$, the collisional term predominantes over the photoelectric for T_e above 7500° for the H group; for T_e above 3500° for the Ca^+ group; and we require a drop of T_r to about 4000° before T_e of 10,000° raises the collisional term to dominance in the Na group. While the particular value of n_e fixes the detailed numerical results, the exponential terms in T_e and T_r play such a dominating role that these results do not change significantly as regards which term dominates for a variation by an order of magnitude in n_e, in either direction.

These results give us an immediate approach to interpreting $I_\nu(0)$ in terms of the distribution of T_e and n_e. For roughly, $I_\nu(0) \sim \frac{1}{2}\bar{I}_\nu(\tau_\nu = 1)$. Thus, we may compute $\bar{I}_{\nu 0}$ from $I_\nu(0)$, evaluate T_r, and see whether $\epsilon B_\nu(T_e)$ should predominate in the expression for the source-function according to the criterion just obtained. If $\epsilon B_\nu(T_e)$ does predominate, we may obtain a good estimate of T_e from the roughest kind of estimate of n_e, because of the exponential dependence upon T_e. If, on the other hand, the term in $I_{\nu 0}$, or in L_{11} predominates, we must consider the radiation field in more detail. Because of the small size of ϵ already mentioned, the term in $\bar{I}_{\nu 0}$ usually predominates, and we must solve the detailed transfer problem to establish the relation between $\bar{I}_\nu(0)$ and ϵ, T_e. We return to this point below.

We may readily show that replacing the atom having just two discrete levels by the actual atom does not change these results. Indeed, writing Eq. (4-27) for the actual atom, we obtain just Eq. (4-70), provided we make the substitution $\eta \rightarrow \eta_1$ and replace the numerator of the second term on the right side of the equation by $\epsilon(1 + \psi)$, where

$$\eta_1 = \eta + \epsilon \sum_3^\infty \frac{Q_{1k}}{Q_{12}} \frac{1 + X_{1k}}{1 + X_{12}} e^{-X_{2k}} \frac{(b_k/b_2)e^{X_{12}} - 1}{e^{Y_{12}} - 1}$$

$$+ \sum \frac{A_{k1}}{A_{21}} \frac{b_k}{b_2} \frac{\tilde{\omega}_k}{\tilde{\omega}_1} e^{-X_{2k}} \left[1 - W_{k1} \frac{(b_1/b_k)e^{X_{k1}} - 1}{e^{Y_{1k}} - 1} \right] \qquad (4\text{-}73)$$

$$\psi = \frac{Q_{1k}}{Q_{12}} \frac{1 + X_1}{1 + X_{12}} e^{-X_2} + \sum_3^\infty \frac{Q_{1k}}{Q_{12}} \frac{1 + X_{1k}}{1 + X_{12}} e^{-X_{2k}} \qquad (4\text{-}74)$$

These quantities are all small in the chromosphere where $b_k > b_{k+j}$. Thus, our conclusions on the relation between $B_\nu(T_{ex})$ and the local values of n_e, T_e, and $\bar{I}_\nu$ hold for the general case as well as for the atom having just two discrete levels.

Consider a schematic approach to the relation between $S_\nu(=B_\nu[T_{ex}])$ and the local value of the radiation field. In particular, we wish to exhibit the transition between the cases of a thin atmosphere and of a locally opaque atmosphere, which were discussed in preceding sections. We have the general relation

$$\bar{I}_\nu(t_\nu) = \int d\omega/4\pi \int S_\nu(t_\nu) e^{-(\tau_\nu - t_\nu)/\mu}\, dt_\nu/\mu \qquad (4\text{-}75)$$

for the radiation field at the point t_ν, with the value of S_ν given by the preceding discussion as

$$S_\nu = \frac{W_{1-2}\bar{I}_{\nu 0}}{1 + \eta + \epsilon} + \frac{\epsilon}{1 + \eta + \epsilon} B_\nu(T_e) + \frac{2h\nu^3}{c^2} \frac{L_{11}}{1 + \eta + \epsilon} \qquad (4\text{-}76)$$

If we consider points where the atmosphere is locally opaque, then by definition S_ν is constant in those regions of the integrand of Eq. (4-75) where the exp $(-\tau)$ term is not so small as to provide negligible contribution. Thus Eq. (4-75) gives, for local opacity, $\bar{I}(t_\nu) = S_\nu(t_\nu)$. According to our discussion at the opening of this section, S_ν is to be taken as frequency-independent over the line profile, at a particular point in the atmosphere, in evaluating the integral: $\int S_\nu \varphi_\nu \, d_\nu$. Thus,

$$\bar{I}_{\nu 0} W_{1-2} = \int \bar{I}_\nu \varphi_\nu \, d\nu = \int S_\nu \varphi_\nu \, d\nu = S_\nu \qquad (4\text{-}77)$$

Then combining Eqs. (4-77) and 4-76), we obtain for local opacity

$$S_\nu = B_\nu(T_{\text{ex}}) = \frac{\epsilon B_\nu(T_e)}{\eta + \epsilon} + \frac{2h\nu^3}{c^2} \frac{L_{11}}{\eta + \epsilon} \qquad (4\text{-}78)$$

On the other hand, consider the case where the atmosphere is *not* locally opaque. Then we may expand $S_\nu(t_\nu)$ and obtain, from Eq. (4-75),

$$\bar{I}_\nu(t_\nu) = S_\nu(t_\nu)[1 - a_\nu] \tag{4-79}$$

where a_ν depends upon grad S_ν and t_ν.

$$\bar{I}_{\nu 0} W_{1-2} = S_\nu \int (1 - a_\nu)\varphi_\nu \, d\nu = S_\nu(1 - \bar{a}_{12}) \tag{4-80}$$

and from Eqs. (4-80) and (4-76),

$$B_\nu(T_{\text{ex}}) = \frac{\epsilon B_\nu(T_e)}{\bar{a}_{12} + \eta + \epsilon} + \frac{2h\nu^3}{c^2} \frac{L_{11}}{\bar{a}_{12} + \eta + \epsilon} \tag{4-81}$$

Because ϵ and η_1 have values $\sim 10^{-2} - 10^{-6}$, $\bar{a}$ need not be large in order to decrease $B_\nu(T_{ex})$ very considerably over the value computed for the case of local opacity. In essence, the positive value of $\bar{a}$ comes from the asymmetry in opacity of the atmosphere in the inward and outward directions. The gradient of S_ν increases or decreases the effect, depending upon whether it is positive or negative outward. The easiest way to see the result is simply to solve the transfer problem for several atmospheres. We do this after considering the form of S_ν for the higher resonance lines.

2. Simplified Treatment of the Higher Resonance Lines and of the Lowest Subordinate Line, Together with an Approach to Generalization. For this purpose, we consider an atom having just three discrete levels plus a continuum. The situation differs from that covered by equations (4-41) in that we do not make the assumption of detailed balance in the resonance lines initially, but consider the general case. Then the equations of statistical equilibrium for this atom, written in the form of equations (4-41), are

$$b_1(1 - b_2/b_1)C_{12} + b_1(1 - b_3/b_1)C_{13} + b_1(1 - b_1^{-1})C_1 - b_2\delta_{21} - b_3\delta_{31} = F_{11} - b_1F_{12} \cdot \tag{4-82a}$$

$$-b_1(1 - b_2/b_1)C_{12} + b_2(1 - b_3/b_2)C_{23} + b_2(1 - b_2^{-1})C_2 + b_2\delta_{21} - b_3\delta_{32} = F_{21} - b_2F_{22} \tag{4-82b}$$

$$-b_1(1 - b_3/b_1)C_{13} - b_2(1 - b_3/b_2)C_{23} + b_3(1 - b_3^{-1})C_3 + b_3\delta_{31} + b_3\delta_{32} = F_{31} - b_3F_{32} \tag{4-82c}$$

where

$$\delta_{21} = e^{X_2}K_{21}\{\text{Ly-}\alpha\}; \qquad \delta_{31} = e^{X_3}K_{31}\{\text{Ly-}\beta\}; \qquad \delta_{32} = e^{X_3}K_{32}\{\text{H}\alpha\} \tag{4-83}$$

and the numerical coefficients are as defined following equations (4-41) for hydrogen, with the corresponding change in numerical values of cross sections or nuclear charge for other atoms. Also, in case the values of T are too high for the approximation of Eq. (4-40) to be valid, the F_{jk} should be expressed in terms of the exponential integrals.

We wish to obtain an expression for the source-function for each of the lines Ly-α, Ly-β, and Hα from equations (4-82), and compare it with the simple expression of equation (4-70) for an atom having two discrete levels plus a continuum. From what has already been demonstrated, we do not expect S_{12} to differ significantly; we ask about S_{13} and S_{23}. If we solve the three equations simultaneously for the b_k, and then construct the expression for S_{jk}, we obtain quite elaborate expressions involving the various rate coefficients. If we hope to use this passage to the three-level from the two-level atom as a guide toward generalization to multi-level atoms, such elaborate expressions are not particularly useful. It is preferable, then, to attempt to find algebraically simpler solutions based on the essential physics of the configuration studied.

We emphasize the motivation of this inquiry into the form of the source function: to specify the local radiation field in those cases where the non-LTE atmosphere considered is optically thick enough to contribute significantly to the radiation field present. We are particularly interested in the factor in Eq. (4-2) giving the net rate of radiative transitions, the factor we have denoted as, e.g.,

$$\{\text{Ly-}\alpha\} = \left[1 - \int \frac{\bar{I}_\nu \varphi_\nu \, d\nu}{S_{12}}\right] \tag{4-84}$$

and hereafter call the net radiative bracket, NRB. Our proof of the frequency independence of S_{jk} over the core of the line permits us to write the NRB in this form. To evaluate NRB we must solve a transfer equation in the line; we proceed to this problem in the next section. Here, we note only that because we consider an atmosphere with a non-radiative energy supply, NRB ≥ 0 — detailed balance in the line corresponds to NRB $= 0$; the upper limit of NRB is obviously 1, and actually will be appreciably less than 1. Noting that the source-function is a ratio of absolute rates, we develop the following simplified approach to a solution.

We investigate the equations pair-wise—the kth and the jth equations to get S_{jk}—in terms of the net radiative rates for all line transitions save the one whose source-function is sought, which we express in terms of absolute rates; thus our solution will involve the δ_{jk}. For lower lying lines than the one considered, the opacity will be greater, NRB will be non-trivially less than unity, and the term in δ will consequently be smaller than the term giving the absolute rate in the line considered. For higher lying lines, the coefficient of NRB will be less than that for the line considered; so even if NRB $\sim$ 1 (which we will show it is not in the last section of this chapter), the term giving the absolute rate in the line considered will again exceed the net rate in the higher lying line. Because the net rate is positive, we combine the δ_{jk} terms with the absolute capture rate from the continuum, the F_{k1}. Because the opacity in the continuum is considerably smaller than in the lines, the value of F_{k2} will be fixed in the region where we investigate the line transition, and an NRB computed for the continuum will have reached a constant value (cf. the last section of this chapter). Since the chromosphere will not generally be opaque for the various continua, we do not generally evaluate the NRB by our approach in the following sections, and it is more convenient to treat ionizations and recaptures separately. (Such continua are treated by the thin-atmosphere approximation.) Thus, for the radiative transitions we have reduced a consideration of the line to an *equivalent two-level atom.* We proceed in a similar way to treat the collisional terms, comparing net rates in other transitions to absolute rates in the line considered.

If we consider the equations pair-wise, and group terms in the manner outlined, we see that the general pair of equations can be written in the form—denoting the upper and lower levels of the transition by subscripts U and L, respectively, and other levels above and below these levels by a and l, respectively

$$b_L(C_{LU}[1 + \rho] + \delta_{Ll} + F_{L2}) + b_U(-C_{LU} - \delta_{UL}) = \mathfrak{F}_{L1} \qquad (4\text{-}85a)$$

$$b_L(-C_{LU}) + b_U(C_{LU} + \delta_{UL} + \mathfrak{R}) = \mathfrak{F}_{U1} \qquad (4\text{-}85b)$$

where

$$
\begin{aligned}
&\rho = (C'_L + C'_{La})C_{LU}{}^{-1}; \qquad \mathfrak{F}_{L1} = F_{L1} + b_a\delta_{aL} + b_l C'_{lL} \\
&\mathfrak{R} = C'_U + F_{U2} + C'_{Ua} + \delta_{Ul}; \qquad \mathfrak{F}_{U1} = \mathrm{F}_{U1} + b_a\delta_{aU} + b_l C'_{lU} \\
&C'_{jk} = C_{jk}(1 - b_k/b_j); \qquad C'_k = C_k(1 - 1/b_k)
\end{aligned} \tag{4-86}
$$

Equations (4-85) assume the simplified form for the two-level atom, in the case $\rho = \delta_{Ll} = \mathfrak{R} = 0$ and $\mathfrak{F}_{L1} = F_{L1}$, $\mathfrak{F}_{U1} = F_{U1}$; they lead in this case to Eq. (4-70). Solving these equations for b_L and b_U (using the definition of δ_{UL} in terms of S_{LU} and $\int \bar{I}_\nu \varphi_\nu \, d\nu$), and constructing the expression for $B_\nu(T_{ex}) = S_{LU}$, Eq. (4-38), we obtain

$$
S_{LU} = \frac{\begin{aligned}\frac{2h\nu^3}{c^2}\frac{\mathfrak{F}_{U1}}{\mathfrak{F}_{U1} + \mathfrak{F}_{L1}}\frac{\delta_{Ll}e^{-X_L}}{K_{UL}} + \int \bar{I}_\nu\varphi_\nu \, d\nu \\ + \epsilon\left[1 + \frac{\rho\mathfrak{F}_{U1}}{\mathfrak{F}_{U1} + \mathfrak{F}_{L1}}\right]B_{\nu_0}(T_e) + \frac{2h\nu^3}{c^2} \\ \cdot \frac{\mathfrak{F}_{U1}}{\mathfrak{F}_{U1} + \mathfrak{F}_{L1}}\frac{F_{L2}e^{-X_L}}{K_{UL}}\end{aligned}}{\begin{aligned}1 - \frac{\mathfrak{F}_{U1}}{\mathfrak{F}_{U1} + \mathfrak{F}_{L1}}\frac{\delta_{Ll}e^{-X_L}}{K_{UL}} \\ + \epsilon\left[\frac{1 - e^{-X_{LU}}\left(1 + \dfrac{\rho\mathfrak{F}_{U1}}{\mathfrak{F}_{U1} + \mathfrak{F}_{L1}}\right)}{1 - e^{-X_{LU}}}\right] \\ + \frac{\mathfrak{F}_{U1}}{\mathfrak{F}_{U1} + \mathfrak{F}_{L1}}\frac{F_{L2}e^{-X_L}}{K_{LU}}\left[\frac{\mathfrak{F}_{L1}}{\mathfrak{F}_{U1}}\frac{\mathfrak{R}}{F_{L2}}e^{X_{LU}} - 1\right]\end{aligned}} \tag{4-87}
$$

where ϵ is as defined in Eq. (4-68).

Consider the resonance lines, $L = 1$. Then there is no term l so the terms in δ_{kl} and the collision terms in the $\mathfrak{F}$ drop out. Thus, the *form* of S_{LU} is that of Eq. (4-70), the only possible change lying in the numerical values of η, L_{11}, and the correction factor multiplying ϵ. Since $C_{12} > C_{13}$, C_2, the correction factor on the coefficient of ϵ is less than unity for Lyα. For Lyβ, $\rho > 1$ provided $(1 - b_2/b_1) > C_{13}/C_{12}$. Then the size of the correction coefficient on ϵ, as well as any change in η and L_{11}, depends upon the values of δ_{aL} and δ_{aU}, which must await an evaluation of NRB to give numerical values. We note the ratios $\mathfrak{F}_{U1}(\mathfrak{F}_{U1} + \mathfrak{F}_{L1})^{-1}$ and $\mathfrak{F}_{L1}(\mathfrak{F}_{U1} + \mathfrak{F}_{L1})^{-1}$ have values $(1 + U/L)^{-1}$ and $(1 + L/U)^{-1}$ if the approximation (4-40) is valid and the δ terms are negligible relative to the F_{k1}; while if the δ terms are very large, these ratios cannot exceed unity. Thus, η and L_{11} may show a significant *decrease* arising from $\mathcal{F}_{k1} \neq F_{k1}$, but any increase can only be a small factor, $(1 + U/L)$. η may *increase* by the ratio $(C'_L + C'_{Ua})/F_{L2}$ if the radiation field in the Balmer continuum is small, but L_{11} remains constant under a change in the quantities dominating $\mathcal{R}$. For hydrogen, this last effect is negligible.

Consider the subordinate line. The remarks above again apply to the terms other than the first in the numerator and the second in the denominator, whose presence gives a marked change in form to S_{LU} over that of Eq. (4-70). The effect is to increase S_{LU}—that is, a decrease of b_2 relative to b_3—so long as δ_{21} does not vanish. This is, of course, the direction of the change between the thick and thin atmosphere solutions; compare the solutions in Tables 4-3 and 4-1, respectively. If now we pass to the case of local opacity in the Lyman lines, $\delta_{Ll} = 0 = \delta_{Ul}$ and the expression for S_{LU} takes on the form of Eq. (4-70). For the three-level atom, terms with subscript a do not exist for this subordinate transition and S_{LU} becomes indeed essentially identical with Eq. (4-70), noting that $b_1C'_{1k}$ becomes small compared with F_{k1}.

These results are readily generalized beyond the 3-level atom to a multilevel atom. Indeed our algebraic expressions have essentially done the generalization already; we need only sum over l and a. Since the major coefficients are always those where U and a, and L and l, are separated by one, these added terms will be small compared with those already carried. To investigate the *numerical* behavior of the various coefficients, we must proceed to evaluate NRB, for which purpose we require $S_{LU}(\tau)$ and $\bar{I}_\nu(\tau)$.

3. The Predicted Behavior of $S_L(\tau_\nu)$ and of $\bar{I}_\nu(\tau_\nu)$. Because the general form of Eq. (4-70) involves two radiative transfer problems, that in the line and that in the free-bound continuum, we consider first only the restricted problem where the free-bound continuum contribution is constant. That is, we confine our attention to atmospheric regions where the optical depth in the free-bound continuum is small. Further, we consider separately the cases when the collisional and when the photo-ionization terms predominate, ignoring the situation when the two terms must be included simultaneously. We adopt this procedure simply for expository clarity, treatment of the general case offering no added difficulty.

In Eq. (4-70) we drop the [1 + small] terms, so that our expression for the source function in the line becomes

$$S_L = \left[\int \bar{I}_\nu \, \varphi_\nu \, d\nu + \epsilon B_{\nu_0}(T_e) + \mathcal{L} \right] / (1 + \epsilon + \eta) \qquad (4\text{-}88)$$

Also, we use the explicit solution, Eq. (4-87), to cast the expression for η in a form not involving any b_k.

$$\epsilon = 0.7 \times 10^{11} Q_{12} n_e T_e^{1/2} [1 + X_{12}][1 - e^{-X_{12}}] \nu_{12}^{-2} f_{12}^{-1} \qquad (4\text{-}89)$$

$$\eta = \frac{2^5}{3\pi\sqrt{3}} \frac{n_1}{n_1 + n_2} \frac{R^2}{\tilde{\omega}_1 f_{12} \nu_{12}^2} \frac{W_{\kappa 1}}{n_1^3 Z^2} \frac{e^{-Y_1}}{Y_1} [e^{Y_1 - Y_2} - 1] \qquad (4\text{-}90)$$

where the n_i in this equation are the principal quantum numbers, and

$$\mathcal{L} = \eta (2h\nu^3/c^2) \, [e^{Y_1 - Y_2} - 1]^{-1} \equiv \eta B^*_{1,2} \qquad (4\text{-}91)$$

We use the Eddington approximation

$$\tfrac{1}{3}(d^2 \bar{I}_\nu / d\tau_\nu^2) = \bar{I}_\nu - (S_L + r_\nu S_c)/(1 + r_\nu) \qquad (4\text{-}92)$$

to investigate $S_L[\tau_\nu]$. r_ν is the ratio of opacity in the continuum to that in the line, $d\tau_C/d\tau_L$. S_C is the source function in the continuum, for which we assume LTE, choosing a distribution of T_e which contains the essential feature of the chromosphere, a rise following the photospheric drop to a minimum,

$$S_C = S_1[1 + \beta\tau_0 + A \exp(-c\tau_0)] \qquad (4\text{-}93)$$

τ_0 is the optical depth at the line center and $\beta = 1.5 r_0$. As we shall see in later chapters, we do not expect such a simple distribution of T_e to actually be the case, but it will suffice to demonstrate the general behavior of S_L to be expected over much of the observed region. In the same spirit, we adopt constant values over the atmosphere for r_ν, ϵ, η, and $\mathcal{L}$ in the solution; we expect the use of constant r_ν and ϵ to be particularly unrealistic. We follow the lines of the treatment by Jefferies and Thomas (1958, 1959).

Equation (4-93) has been solved by the method of discrete ordinates, replacing the integral entering the expression for S_L by a sum. Since the weighting function ϕ_ν is Gaussian, the division points for the quadrature are based on the zeros of the Hermite polynomials; the division points and weights are given in Trumpler and Weaver (1953). Equation (4-92) then reduces to a set of simultaneous equations, from which the solution follows in the standard way.

Collisional S_L, i.e., $\eta = 0$:

$$S_L = S_1(1 - \gamma) \cdot \left\{ (1 + \beta\tau_0)(1 + \epsilon) + A(q + \epsilon)[e^{-c\tau_0} + \sum L_j e^{-k_j\tau_0}] \right\} \qquad (4\text{-}94)$$

with the L_j determined by the boundary condition

$$A(q + \epsilon)\left[\sum \frac{L_j}{1 - k_j/\chi_i} + 1\right]\tilde{\omega}_i = -\left\{(1 - \beta/\chi_i) + A\left[\frac{\tilde{\omega}_i(q - 1) + 1}{1 - c/\chi_i} - (q + \epsilon)\tilde{\omega}_i\right]\right\} \qquad (4\text{-}95)$$

Photoelectric S_L, i.e., $\epsilon = 0$:

$$S_L = S_1(1 - U)\left\{(1 + \beta\tau_0)\Big(1 - \frac{\eta\Sigma\alpha_j V_j)}{1 - \Sigma\alpha_j V_j} + \frac{\mathfrak{L}/S_1}{1 - \Sigma\alpha_j V_j} \cdot [1 + \Sigma L_j e^{-k_j\tau_0}] + Ap[e^{-c\tau_0} + \Sigma L_j e^{-k_j\tau_0}]\right\} \qquad (4\text{-}96)$$

with boundary conditions for the L_j

$$\left[\frac{\mathfrak{L}/S_1}{1 - \Sigma V_j\alpha_j} + Ap\right]\left[\sum \frac{L_j}{1 - k_j/\chi_i} + 1\right] = -\left\{(1 - \beta/\chi_i)\left[V_i^{-1} - \frac{\eta}{1 - \Sigma V_j\alpha_j}\right] + A\left[\frac{p + W_i/V_i}{1 - c/\chi_i} - p\right]\right\} \qquad (4\text{-}97)$$

where the k_j are determined by

$$\sum_i \frac{y_i\alpha_i}{1 - k^2/\chi_i^2} = 1 \qquad \begin{array}{l} y_i = \tilde{\omega}_i \text{ (collisional)} \\ y_i = V_i \text{ (photoelectric} \end{array} \qquad (4\text{-}98)$$

and the symbols are defined by

$$\begin{aligned}
&\int \bar{I}_\nu \varphi_\nu \, d\nu = \sum_1^n \bar{I}_i \alpha_i \\
&\qquad \chi_i^2 = 3\phi_i^2(1 + r_i)^2; \qquad \phi_i = \varphi_i \pi^{1/2} \Delta\nu_D; \qquad r_0 = r_i \phi_i \\
&\qquad \gamma = \frac{\epsilon}{1 + \epsilon}; \qquad U = \frac{\eta}{1 + \eta}; \qquad \tilde{\omega}_i = \frac{1 - \gamma}{1 + r_i}; \\
&\qquad\qquad V_i = \frac{1 - U}{1 + r_i}; \qquad W_i = \frac{r_i}{1 + r_i} \\
&\qquad q = \left[\sum \frac{\alpha_i(1 - \tilde{\omega}_i)}{1 - c^2/\chi_i^2}\right]\left[1 - \sum \frac{\alpha_i \tilde{\omega}_i}{1 - c^2/\chi_i^2}\right]^{-1}; \\
&\qquad b = \left[\sum \frac{\alpha_i W_i}{1 - c^2/\chi_i^2}\right]\left[1 - \sum \frac{\alpha_i V_i}{1 - c^2/\chi_i^2}\right]^{-1}
\end{aligned} \tag{4-99}$$

To fix A, S_1 and c, we specify the temperature of the upper solar atmosphere, T_e[max]; the minimum temperature, T_e[min]; and the location of the latter in terms of optical depth in the continuum, τ_{Cm}. We have the relations

$$\begin{aligned}
&A \sim R[1 + 1.5\, \tau_{Cm}]; \qquad R = B_\nu(T_e \max)/B_\nu(T_e \min); \\
&c/r_0 = \tau_{Cm}^{-1}\{\ln[R(\tau_{Cm} + 2/3)] + \ln(c/r_0)\}; S_1 \sim B_\nu(T_e \min)
\end{aligned} \tag{4-100}$$

For the sun, T_e[min] $\sim$ 4500° ± 500°. Using the value 4000°, we obtain the (Table 4-5) values of A and c/r_0 corresponding, respectively, to a range of values for T_e[max] and τ_{Cm} of current solar interest. The numerical relation between A and T_e corresponds to the wave length of Hα.

Table 4-5. Parameters of Eq. (4-93)

T_e(max)	A	τ_{Cm}	c/r_0
1×10^4	25	0.001	1.5×10^4
2×10^4	120	0.01	1.28×10^3
5×10^4	430	0.03	4.0×10^2
1×10^5	1000	—	—

Figures (4-3) and (4-4) illustrate $S_L(\tau_C)$ and $I_\nu(0)$ for the cases $\epsilon = 10^{-4}$, $r_0 = 10^{-4}$, $\tau_{Cm} = 0.01$ and a range in A.

The behavior of S_L for the photoelectric case in which η and

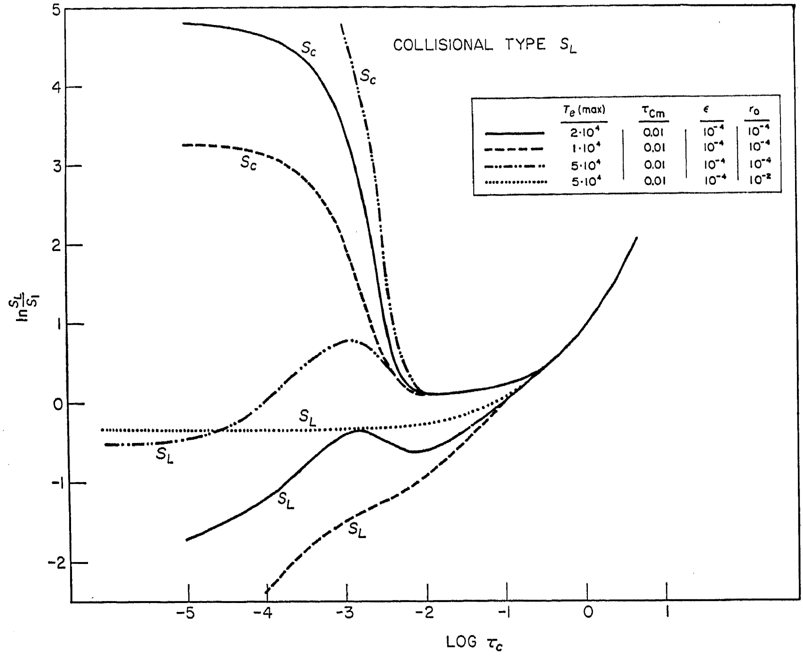

Fig. 4-3. Collisional-type S_L for differing distributions of T_e. (From J. T. Jefferies and R. N. Thomas, 1959, *Astrophys. J.*, 129, 401.)

B^* are constant is similar to that for the collisional case with constant T_e, for we have

$$S_L = \left[\int \bar{I}_\nu \varphi_\nu \, d\nu + \eta B^*\right] / (1 + \eta) \qquad (4\text{-}101)$$

The difference in the two cases comes about because B^* is not in general the same as $B_\nu[T_e]$; thus, S_L does not couple directly to S_C. The coupling comes about only in the regions deeper than those where our approximation of constant B^* is valid; in the deeper regions B^* approaches $B_\nu[T_e]$.

In the extreme case $r_0 = 0$, we obtain directly from Eq. (4-96),

$$S_L = B^*[1 + \sum_j \bar{L}_j e^{-k_j \tau_0}] \qquad (4\text{-}102)$$

and S_L asymptotically approaches B^* from below. Our approxi-

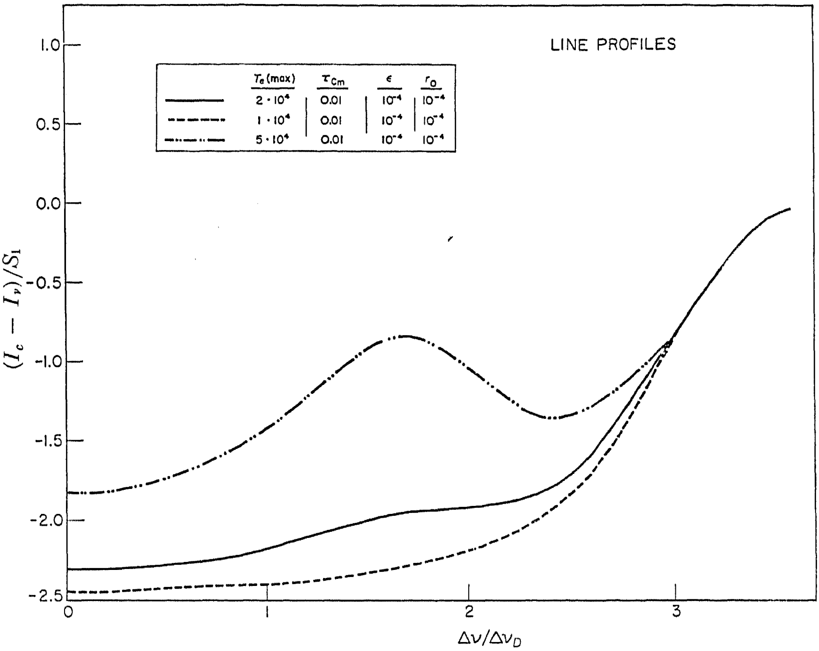

Fig. 4-4. Line profiles corresponding to S_L in Fig. 4-3. (From J. T. Jefferies and R. N. Thomas, 1959, *Astrophys. J.*, **129**, 401.)

mation of constant B^* is valid only in those atmospheric regions having low free-bound opacity. Provided that such regions occur in that part of the atmosphere where T_e is decreasing outward, we see that in the lower part of the atmosphere $S_L > B_\nu[T_e]$. In the upper regions, of course, the inequality reverses.

One may show that the same relative behavior of S_L versus $S_C = B_\nu\,(T_e)$ holds for the case $r_0 > 0$, by considering the signs of the terms in Eq. (4-97). One can show by numerical computation that the result holds for all $A \lessapprox 600$ (T_e(max) $\lessapprox 7 \times 10^4$). Simply for illustration, we present the solution for $\mathcal{L}/S_1 = 0.05$, $\eta = 0.01$, and $r_0 = 10^{-4}$ in Fig. 4-5.

From these results we draw several conclusions. For a sufficiently weak line (large r_0), or for a sufficiently small value of τ_{Cm}, or for a small value of A, S_L decreases monotonically outward for a collision-dominated S_L. For a photo-ionization dominated S_L, S_L

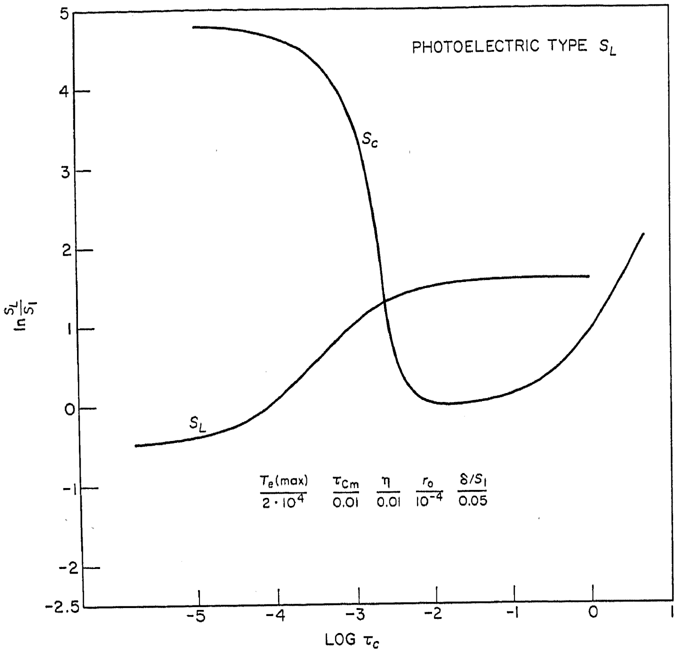

Fig. 4-5. Photoelectric-type S_L for a particular photospheric radiation field. (From J. T. Jefferies and R. N. Thomas, 1959, *Astrophys. J.* **129**, 401.)

decreases monotonically outward for all cases—at least so long as we are in a region transparent in the free-bound continuum. On the other hand, given a stronger line (small r_0), larger A or larger τ_{Cm}, one may for a collision-dominated S_L obtain an $S_L[\tau_\nu]$ which exhibits an initial rise to a maximum and then an eventual decrease. Thus, given a chromosphere, we have the possibility of observing a Fraunhofer line having a self-reversed, emission core. Conversely, an observed self-reversed emission core in a line which would be expected to have a collision-dominated S_L is good evidence for a nontrivial rise in T_e over an atmospheric region where τ_0 in the line is still reasonably large. The absence of such a core for such a line must be interpreted with caution—the choice lying between an unresolved or washed out core and a set of characteristic parameters which would give only a monotonic outward decrease in S_L.

An a priori decision as to the type behavior expected for S_L for a given line requires knowledge of ϵ, r_0, η, and $\mathcal{L}$. The two latter may be estimated from the observed intensity in the free-bound continuum. The uncertainty in ϵ lies mainly in the cross section. The greatest difficulty lies in the choice of r_0, and particularly in the effect of its variation, which we have ignored. The uncertainty lies largely in the H^- concentration in the upper photospheric layers, arising from uncertainty as to the ionization of hydrogen, which in turn arises from uncertainty in the non-equilibrium ionization conditions. We have already commented on these in an earlier section. In some cases the alternative on the behavior of S_L is clear-cut, such as for those lines expected to be photo-ionization dominated—the neutral metals and the Balmer lines—and for those lines where r_0 is clearly very large, such as the Ca^+ H and K. The uncertainty in r_0 for these last lines is reflected in an uncertainty as to where the large T_e required by the self-reversed emission cores must occur.

As a final comment, noting that we have hoped in the above to lay general guides to be used in the analysis of chromospheric data, we may ask whether our results lie in an obvious contradiction with solar observation. Or, do their predictions agree with the salient solar facts of life on line profiles? We quickly see that the agreement is satisfactory, as follows.

In a broad way, we observe four types of line-profiles: two types at the limb and two types in the Fraunhofer disk spectrum (see Fig. 4–6).

a. Profile A. Because profile A represents the upper regions,

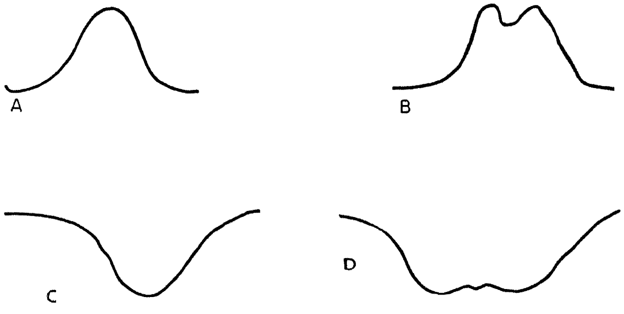

Fig. 4-6. Profile A, all lines at great heights; B, all strong lines in low chromosphere; C, H Balmer and NaD prototype; D, Ca^+ H and K prototype. A and B, limb; C and D, disk.

where it is not a priori clear that high optical depth is reached anywhere in the line, we can say nothing about the change in S_L with depth in the atmosphere and thus the variation in I_ν resulting from a variation of S_L. The profile of the line may simply reflect the change in opacity across the line. (Simply because we have no a priori knowledge, however, is not sufficient justification for the often-adopted expedient of assuming constant S_L in analyzing the profile.)

b. Profile B. In profile B the self-reversed line center would imply, at least in the central core of the line where S_L is frequency-independent, that S_L decreases outward monotonically over the region of observation. Our results in Figs. 4-3 and 4-5 predict such behavior at sufficiently great heights. We note that the tangential optical depth to a given point is some 50 times that measured radially. Consequently, even for a collision-dominated S_L, it is not clear that we should see, at the limb, the region in which S_L increases outward. Figure 4-3 shows that if $r_0 \sim 10^{-4}$, the outward rise in S_L stops at $\tau_0 \sim 10$, measured radially, thus about 500, measured tangentially. Thus we should just begin to pick up an emission core at about 2.5 Doppler widths from the line center, which is just about at the limit of the Doppler core bounding our discussion of a frequency-independent S_L. Thus, any conclusions become precarious.

We note one possible exception. Our discussion of the subordinate lines, e.g., the Balmer lines, holds only for the regions of local opacity in the resonance lines. If, looking tangentially, we were able to observe a region where the tangential Balmer opacity exceeded unity but the radial Lyman opacity became less than that required for local opacity, we would again be looking outside the limits of our discussion. Since S_L rises for the Balmer lines under these conditions (i.e., b_2 drops, for a given T_e), our conclusions above might change. Since we have not computed the problem, further discussion here is unwarranted. We note the problem, however.

c. Profile C. Profile C is precisely the profile predicted, at least qualitatively. Thus, in subsequent analysis, it seems very safe to assume S_L to decrease monotonically outward.

d. Profile D. Again, we should expect this type of profile for these lines. Because of the observation of a type B profile at the limb during eclipse observations, it would appear that in analysis of eclipse observations we may with safety deal with an S_L which is assumed to decrease monotonically outward. If discrepancies occur, we should, however, be prepared to admit in the region 2–3 Doppler widths from the line center an S_L which increases outward. A second conclusion from this profile would be that already mentioned, a requirement of a non-trivial increase in T_e in the low chromosphere. Because the actual results on height and separation of emission maxima depend so critically upon A, ϵ, r_0, and τ_{Cm} it is impossible to draw detailed quantitative conclusions as to the value of T_e required in the chromosphere from such broad considerations as those presented here. We defer more detailed discussion to Chapter 9. Here, we wish only to emphasize that the observed emission core of the H and K lines is the most obviously direct evidence of a non-trivial rise in T_e in the low chromosphere. The point does not appear to have been emphasized—indeed, it seems in general to have been overlooked or ignored.

Finally, we should comment that if we are correct in our assessment of the parameters upon which S_L depends for the Balmer lines, an inference of S_L from the Balmer lines gives T_e only as a second-order effect. Indeed, we should be able to predict the rough behavior of T_{ex} for the Balmer lines from the observed T_r in the free-bound continuum. Although we defer discussion until the analysis of the Balmer data in Chapter 9, we do note here that the overall run of $T_{ex}(\tau_\alpha)$ is remarkably close to the inferred results coming from center-limb observations of the Balmer lines.

Thus, we conclude that we have laid a reasonably good foundation for an understanding of the general kind of behavior of $S_L(\tau_0)$ of the type we require in analyzing the eclipse observations and supplementary data.

4. Summary on Computing Net Radiative Transitions, with Particular Application to the Methodology of Solution of the Equations of Statistical Equilibrium and to the Computation of the Local Energy Balance. We have continually emphasized the utility of formulating solutions to the equations of statistical equilibrium in terms of *net* rates of transitions. For collisional transitions, these net rates are proportional to $(1 - b_j/b_k)$. For radiative transitions, the net rates are proportional to

$$\text{NRB} = \left[1 - \left(\int \bar{I}_{\nu_{jk}} \varphi_{\nu_{jk}}\, d\nu / S_{jk}\right)\right] \qquad (4\text{-}103)$$

For detailed balance in the transitions, each of these quantities vanishes, without necessarily implying $b_j = 1$. By formulating the solution in terms of these net rates one obtains, in addition to a solution for the b_k, a direct measure of the net importance of each kind of transition in preserving the non-LTE character of the atmosphere, viz, how much the net process differs from zero. Thus, in viewing the spectroscopic state of the chromosphere as the result of the cyclic process,

$$\text{Mechanical energy in} \rightarrow \text{local increase in } T_e \rightarrow$$
$$\rightarrow \text{collisional excitation} \rightarrow \text{radiative efflux}$$

one has a measure of the importance of each contributor to each step of the cycle. The reader must not take this caution, and tool, lightly; the literature presents many examples where the equations of statistical equilibrium have been written and simplified by retaining only those terms showing the largest *absolute* rates. When the difference of two of these absolute rates becomes comparable to the "small" terms neglected, the results of the solution become valueless.

In discussing the thin-atmosphere case, we wrote the expression (4-103) for the net radiative transitions as

$$1 - W_{jk}[(b_j/b_k)e^{X_{jk}} - 1]/(e^{Y_{jk}} - 1) \tag{4-104}$$

set T_r equal to the "temperature" characteristic of the continuum in the visual spectrum, and sought solutions as functions of the parameter W_{jk} in the range $0 \leq W_{jk} < 1$. In the thick-atmosphere case, we set the net radiative transitions equal to zero in the Lyman lines, and adopted the thin-atmosphere approach to T_r and W_{jk} in the remaining transitions. From the results of the preceding section (3), we see that a solution of the transfer equation gives us immediately the numerical value of the bracket (4-103) and thus provides us with the approach to the general situation. That is, the expression (4-88) for S_{jk} gives, when substituted in the expression (4-103),

$$\left\{1 - \frac{\int \bar{I}_\nu \varphi_\nu \, d\nu}{S_{jk}}\right\} = \left\{\frac{\epsilon B_{\nu 0}(T_e) + \eta B^*{}_{j,k}(Y_k)}{S_{jk}(\tau_0)} - [\epsilon + \eta]\right\} \tag{4-105}$$

A solution of the transfer equation gives $S_{jk}(\tau_0)$, and thus the value of the bracket as a function of τ_0. Parameters of the solution are η and $B^*{}_{j,k}(Y_k)$, and a model of the distribution of T_e and n_e, which gives r_0, ϵ, and $B_{\nu 0}(T_e)$.

We are particularly interested in the possible range of values for the NRB. Specific numerical results depend upon the solution of the transfer equation under the conditions imposed by a particular set of values for the parameters of the solution. We ask, however, whether it is possible to reach at least certain general physical results, characterized by certain broad classes of values for the parameters, much as we found in the preceding section (3) certain broad classes of line profiles characterized by the predominance of either $\epsilon B_{\nu_0}(T_e)$ or $\eta B^*_{j,k}(Y_k)$.

First, we note in the case of hydrogen an immediate contrast in the range of values of the NRB compared with that for the factor $(1 - b_U/b_L)$, to which the net rate of collisional excitation is proportional. At great depths, LTE holds and $b_U/b_L \to 1$. High in the atmosphere, $b_1 \propto n_e^{-1}$, while $b_U \to 1$ for large U; thus $b_U/b_1 \to 0$. Thus, this factor for the collisions ranges between 0 at great depths, and 1, at great-enough heights. (For the Lyman lines, b_2 is large enough in the region of formation of the Balmer lines that the limits are effectively the same.) On the other hand, the NRB has the lower limit 0, but the upper limit departs from unity because the value of $\int \bar{I}_\nu \varphi_\nu \, d\nu$ is not at all negligible relative to S_{jk}, even near $\tau \sim 0$, as we saw in the preceding section (3).

Indeed, returning to the qualitative discussion on the behavior of S_L in section (1), Eqs. (4-76) through (4-81), we can get a quick physical picture of the behavior of the NRB. Under conditions of local opacity in the line, Eq. (4-78) gives $S_L = (\epsilon B_{\nu_0} + \eta B^*_{j,k})/(\epsilon + \eta)$, so that the expression (4-105) for the NRB vanishes identically. If, on the other hand, there is some effect which vitiates the condition of local opacity, then we obtain equation (4-81) for S_L, and NRB does not vanish. We recognize two physically different sources for such behavior. One occurs if the region considered is simply sufficiently near the surface that an asymmetry in $\bar{I}_\nu$ (direction) arises because of this opacity effect even apart from any effect arising from a gradient in S_L. A second occurs if in some region of the atmosphere there exists a very steep gradient in $\epsilon B_{\nu_0}(T_e)$. (We have constrained our thinking to those situations where $B^*_{j,k}$ is constant. If we remove this restriction, we should need to consider the transfer problem in the continuum, and should still require a gradient in T_e to obtain one in $B^*_{j,k}$; so our present treatment does not sacrifice generality.) The first of these sources provides a monotonic increase in the value of NRB toward the surface. The second source introduces the possibility of a local extremal in NRB at some non-negligible τ_0. We shall see in the next chapter that regions of steep gradient in T_e are to be expected, from considerations of radiative stability. Thus, in discussing the question of the energy balance of the chromosphere, the possibilities of such local extrema must be carefully considered.

We can make the physical conditions of the preceding paragraph more explicit in terms of a specific solution of the transfer equation, if we again consider the approximation in which r_0 and ϵ are held constant and in which $S_C[= B_{\nu 0}(T_e)]$ is given by Eq. (4-93). Following the same procedure as in section 3, only retaining the complete form of Eq. (4-88) for S_L rather than considering separately the two cases $\{\epsilon B_{\nu_0} \gtrless \eta B^*_{j,k};\ \epsilon \gtrless \eta\}$ we obtain

$$S_L = S_1\delta\{(1 + \beta\tau_0)(\epsilon + s_0) + Q\,[1 + \Sigma L_j e^{-k_j\tau_0}] + A(\epsilon + s)[e^{-c\tau_0} + \Sigma L_j e^{-k_j\tau_0}]\} \tag{4-106}$$

where

$$\delta = (1 + \epsilon + \eta)^{-1}; \qquad \Lambda_i = \frac{\epsilon\delta + r_i}{1 + r_i};$$

$$\pi_i = \delta(1 + r_i)^{-1}; \qquad Q = \frac{\eta B^*/S_1}{1 - \Sigma\alpha_j\pi_j},$$

$$s = \left[\sum \frac{\alpha_j\Lambda_j}{1 - c^2/\chi_j^2}\right]\left[1 - \sum \frac{\alpha_j\pi_j}{1 - c^2/\chi_j^2}\right]^{-1};$$

$$s_0 = [\Sigma\alpha_j\Lambda_j][1 - \Sigma\alpha_j\pi_j]^{-1}$$

subject to the boundary conditions, which determine k_j, L_j:

$$\sum[\pi_i\alpha_i/(1 - k^2/\chi_i^2)] = 1 \tag{4-107}$$

$$[A(\epsilon + s) + Q]\left[\sum \frac{L_j}{1 - k_j/\chi_i} + 1\right] = -\left\{(1 - \beta/\chi_i)(\Lambda_i/\pi_i + s_0) + A\left[\frac{\Lambda_i/\pi_i + s}{1 - c/\chi_i} - (\epsilon + s)\right]\right\} \tag{4-108}$$

Thus, substituting S_L from Eq. (4-106) into Eq. (4-105),

$$\mathrm{NRB} = \left\{ \frac{\epsilon\,[1 + \beta\tau_0 + Ae^{-c\tau_0}] + \eta B^*_{j,k}/S_1}{\begin{array}{l}\{A(\epsilon + s)[e^{-c\tau_0} + \Sigma L_j e^{-k_j\tau_0}] \\ \qquad + Q[1 + \Sigma L_j e^{-k_j\tau_0}] \\ \qquad\qquad + (1 + \beta\tau_0)(\epsilon + s_0)\}\delta\end{array}} - (\epsilon + \eta) \right\} \tag{4-109}$$

For strong lines like Lyα, Hα, Ca$^+$ H and K, the low-lying lines of HeI, and many metallic lines r_0 is very small in the low chromosphere, generally less than 10^{-4} and usually very much smaller. For $r_0 \lesssim 10^{-4}$, the values of the k_j are essentially independent of r_0. So long as $r_0 \lesssim 10^{-3}\epsilon$, the values of Λ_i and π_i are also effectively independent of r_0. Thus, we again turn to the case $r_0 = 0$ to obtain some insight into the behavior of the NRB, with the expectation that this limiting case will be valid for some of the very strong lines. Then we obtain

$$\Lambda_i = \epsilon\delta;\ \pi_i = \delta;\ s_0 = \epsilon/(\epsilon + \eta);\ Q = \eta B^*/\delta(\epsilon + \eta)S_1$$

$$s = s_0 \left[\sum \frac{\alpha_i}{1 - c^2/\chi_i^2}\right]\left[\sum \frac{\alpha_i(1 - c^2/\chi_i^2[\epsilon + \eta])}{1 - c^2/\chi_j^2}\right]^{-1} \tag{4-110}$$

Set $\sigma = (\epsilon + s)/(\epsilon + s_0)$. Then Eq. (4-109) becomes

$$\mathrm{NRB} = (\epsilon + \eta) \left\{ \frac{\epsilon[1 + \beta\tau_0 + Ae^{-c\tau_0}] + \eta B^*/S_1}{\begin{array}{l}\epsilon[1 + \beta\tau_0 + A\sigma(e^{-c\tau_0} + \Sigma L_j e^{-k_j\tau_0})] \\ \qquad + [1 + \Sigma L_j e^{-k_j\tau_0}]\eta B^*/S_1\end{array}} - 1 \right\} \tag{4-111}$$

When the right-hand side of Eq. (4-108) is negligible compared with unity, we have $\Sigma L_j = -[1 - \sqrt{(\epsilon + \eta)}]$. Then the value of NRB at $\tau_0 = 0$ for either of the two cases that $\sigma = 1$ or the photoionization terms dominate becomes

$$\begin{aligned}\mathrm{NRB}(\tau_0 = 0) &= [\sqrt{(\epsilon + \eta)}][1 - (\epsilon + \eta)] \\ &\quad \times \{1 + \epsilon(\epsilon + \eta)^{-1/2}(\epsilon A + \eta B^*/S_1)^{-1}\}^{-1}\end{aligned} \tag{4-112}$$

In either of these two cases, the variation of NRB is monotonic between the value given by Eq. (4-112) at $\tau_0 = 0$ and the value 0 at large τ_0. These conditions require large A and/or Q, and in addition $c^2 < \chi_i^2(\epsilon + \eta)$. If they are satisfied, the variation of NRB is particularly easy to compute between the two extremes given, for the k_j and L_j depend only upon $(\epsilon + \eta)$, and can be computed once and for all.

If these conditions are not satisfied, then both the value of $\mathrm{NRB}(\tau_0 = 0)$ and the result on its monotonic variation may change from the results above. The conditions of the last paragraph essentially characterize an isothermal atmosphere, by the restriction on the value of c. In looking at special cases for particular application, we have found in some cases a non-monotonic variation of NRB for the collision-dominated case. Thus, caution must be exercised in considering only the values $\mathrm{NRB}(\tau_0 = 0)$ and $\mathrm{NRB}(\tau_0 \text{ large})$ to establish limits on NRB.

More detailed discussion is best deferred to specific applications which we make in the following chapters. Here, we wish only to emphasize the necessity, and utility, of applying some such approach as the above to a discussion of the value of the NRB. We have already seen in the discussion attending Eqs. (4-85) and (4-87) how an approach to solution of the equations of statistical equilibrium is simplified and clarified when expressed in terms of the NRB. By considering limits on the value of the NRB for the various transitions, we are often able to further simplify such expressions as that of Eq. (4-87). By performing such simplification via the expressions for the net rates, we do not run the risk of the error mentioned earlier, viz, neglecting terms involving small absolute rates relative to those involving large absolute rates, whereas the relative sizes of net rates may make such a procedure quite unjustified.

We also note that the NRB explicitly enters any attempt to construct a theoretical model of the chromosphere by balancing some source of mechanical energy input against a radiative dissipation. Indeed, if we integrate the equation of transfer over angle and frequency, we have

$$\frac{1}{4\pi}\frac{d}{d\tau_1}\int F_\nu\,d\nu = \sum_j -\frac{d\tau_{0j}}{d\tau_1}(S_L)_j(\mathrm{NRB})_j - \int (S_C - \bar{I}_\nu)\frac{d\tau_c}{d\tau_1}\,d\nu \tag{4-113}$$

where j denotes a particular line and τ_1 is the optical depth at some arbitrary frequency. Thus, we see that the local flux gradient is simply the sum of source-function times the respective NRB. And of course, the local flux gradient is simply the excess radiative energy produced locally, which equals the mechanical energy dissipated locally. Therefore, in computing a theoretical model of a chromosphere-type atmosphere by balancing mechanical energy in against radiative energy out, we must use Eq. (4-113) and the value of NRB becomes critical.

The usual discussions in the literature vary between treating the problem by the thin-atmosphere approximation with $W_{jk} = 0$, thus assuming that all emitted radiation escapes, and treating the net transition rate to be zero in the stronger lines, thus assuming no radiation to escape in these transitions. A better estimate would result from applying the above-derived limits on the value of the bracket; the extra labor involved is not great. Further reference, and numerical details on the limits established above and on some special cases, may be found in the discussions by Thomas (1960) and by Zirker (1960). Application, in addition to those in the following chapters, is illustrated in the discussion of Hα and hydrogen free-bound emission by Pottasch and Thomas (1959) and the discussion of Ca$^+$ H and K by Jefferies and Thomas (1960).

Finally, we should return to the questions of the net radiative processes and energy flux for the continuum, that were raised in section 2 when we outlined our general approach to the equivalent two-level atom. In the continuum, the source function is frequency-dependent, so that we do not have exactly the same form for the NRB as in the case of the lines. Referring to Eqs. (4-41) or (4-82), we see that the quantity corresponding to the NRB is

$$\text{Net-Rate-Bracket-Continuum} \equiv (\text{NRBC})_j = (1 - b_j F_{j2}/F_{j1}) \qquad (4\text{-}114)$$

Also, from Eq. (4-113), we see that what enters the expression for the flux gradient is not the product of NRBC and (integrated) source function, but quite different quantities, which are computed by integrating emissions and absorptions of energy, rather than transition rates, over frequency.

In the simple case treated in our analysis of b_1 and b_2 for hydrogen under conditions of detailed balance in the Lyman lines, a three-level atom, and the approximation of the exponential integral by $\exp(-Z)/Z$, we would obtain

$$\begin{aligned} \text{Net transition rate} &= F_{j1}(\text{NRBC})_j \\ \text{Local flux gradient} &= h\nu_j F_{j1}(\text{NRBC})_j \end{aligned} \qquad (4\text{-}115)$$

From the values of the quantities entering equations (4-41), and the values of b_1, b_2 in the various cases covered by Eqs. (4-43) through (4-48), we readily find for the two extreme cases covered by the analysis below.

Bracket case	Detailed balance-Ly-C, transparent in $B_\alpha C$:	$F_{12}/C_{12} \ll 1$
$(NBRC)_1$	0	1
$(NRBC)_2$	$-\Delta$	$-(2 + \Delta)$

The negative value for $(NRBC)_2$ corresponds, of course, to the predominance of photo-ionizations over collisional excitations in the source function for Hα.

The interesting cases are those lying intermediate to these two extremes, where we must solve the transfer problem in the Lyman continuum. We shall see in Chapter 6 that our treatment of this transfer problem is as yet extremely simple-minded, in essence a one-point quadrature in integrating the radiation field over the absorption coefficient. Also, for a more precise treatment near the region of detailed balance in the Lyman continuum and small values of Δ, we should retain all the terms for b_1, b_2 in Eqs. (4-43) and (4-44), since the NRBC represent the small difference of large quantities and we have different orders of approximation to zero. Finally, in the region where departures from detailed balance in the Lyman lines occur, b_2 drops and NRBC changes its behavior (as does NRB for Hα). Here, however, we wish only to emphasize the necessity of treating carefully the questions of net transitions and net radiative balance in the continuum, and distinguishing their behavior from that of the lines.

All these considerations result from working with a source function in the lines of the form of Eq. (4-88) and using simplified atomic models to evaluate the parameters. By comparing the actual atom to the two and three-level approximations, we have, however, seen that this is an excellent first approximation for resonance lines and low-lying subordinate lines. For higher subordinate lines, the problem must be further investigated. The *general* form of Eq. (4-87) would seem to incorporate most of the possibilities. What we really require is a detailed study of each atomic line, to infer what kind of a representation is most suited for this line. Such a study requires both enlarging the kind of developments reported in this chapter, and obtaining the necessary atomic parameters to compute the numerical size of the various rate-processes occurring. We have embarked on such a study in a joint program involving staff members of the Boulder and Washington Laboratories of the National Bureau of Standards, the Sacramento Peak Observatory of the Air Force, the High Altitude Observatory of the University of Colorado and colleagues abroad, particularly those to whom we have already expressed our indebtness in the foreword. In this chapter, we hope only that we have presented a sketch of the evolution, to date, of our thinking on these problems, and the direction and requirements of a really satisfactory approach to the non-LTE problem in the configuration whose prototype is the stellar atmosphere, whether it appears in astrophysical or laboratory investigations.

CHAPTER 5

Thermal Stability of a Gas with a Non-Radiative Energy Input and Radiative Efflux

R. GRANT ATHAY

I. Steady-State Energy Transfer

The preceding chapter deals with the problems of specifying the populations of atomic energy levels and the emission of radiation under the general conditions of a spectroscopically steady-state configuration with arbitrarily specified values of T_e, n_e, and incident radiation field. In application of the results of this analysis, one hopes to invert the process in order to infer T_e and n_e from the spectroscopic data. Before attempting this, however, we consider a more general approach based upon rather broad, unrestrictive assumptions concerning the energy balance in the chromosphere.

The existence of a steady state in the spectrum of a gaseous atmosphere implies the existence of steady-state energy transfer through the atmosphere. As long as the energy input and output mechanisms are not specified, T_e may take on arbitrary values. However, as soon as the energy mechanisms are specified and are of known magnitude, then, in general, T_e is determinable.

In this chapter, we follow our earlier assumptions that the energy input is by some non-radiative mechanism, which we leave further unspecified, and that the energy output is by radiative processes. In this way, we can determine, to some extent, the temperature structure of the atmosphere (Athay and Thomas, 1956a). By later comparing this structure with empirical models, we gain some additional insight to the energy-transfer problem.

Two conditions must be satisfied in a steady-state energy transfer: The energy input must balance the energy output, and this equilibrium must be stable against small perturbations. If the energy input is E_{in} and the energy output is E_{out}, the first condition is expressed symbolically by

$$E_{\text{in}} = E_{\text{out}} \tag{5-1}$$

For the configuration to be stable, it is sufficient to add the condition

$$\frac{dE_{\text{in}}}{d\mathrm{T}_e} < \frac{dE_{\text{out}}}{d\mathrm{T}_e} \tag{5-2}$$

For, as long as this condition is satisfied changes in T_e by $+\Delta T_e$ result in a net energy outflow with a subsequent cooling and changes by $-\Delta T_e$ result in a net energy inflow with a subsequent heating. Hence, perturbations in T_e will be resisted by the overcompensating changes in E_{out}, and T_e will reach an equilibrium value. On the other hand, if $dE_{\text{out}}/dT_e < dE_{\text{in}}/dT_e$, any small perturbation in the temperature field will amplify, and no stable value of T_e will exist.

We proceed, then, to investigate the temperature structure of the chromosphere permitted by the stability criterion expressed by Eq. (5-2). We assert that T_e can have only those values that satisfy this condition.

A. Consideration of E_{out}

The energy loss from the chromosphere is presumably dominated by radiative processes. Some additional energy may be lost through mass motions and thermal conduction. However, thermal conduction is likely to be important only in regions of unusually strong temperature gradient, as illustrated by the calculations of Giovanelli (1949) and Woolley and Allen (1950). Since $dT_e/dh \geq 0$, the chromosphere is stable against ordinary convection currents. Therefore, we do not expect large energy losses through this process. There are, to be sure, velocity fields as evidenced by spicule motions and Doppler shifts in the spectral lines. These velocity fields undoubtedly play a role in the energy equilibrium, but no adequate quantitative discussion of this problem exists. We conjecture, however, that the net effect of these velocity fields is to transfer energy to the chromosphere through some mechanism as, for example, the generation of acoustic waves as suggested by Schwarzschild (1948) and Biermann (1948).

The net radiative output is the energy radiated minus that absorbed, viz.,

$$E_{\mathrm{rad}} = \sum_{\alpha,k} A_{kj}{}^{\alpha} n_k{}^{\alpha} h\nu \left[1 - \left(\int \bar{I}_\nu \phi_\nu \, d\nu / S_\nu \right) \right] \tag{5-3}$$

where the superscript denotes an atom of type α. In general, the sum in Eq. (5-3) may be positive, negative or zero, depending upon the details of the energy balance. In the case of radiative equilibrium, the sum vanishes and T_e in the upper chromosphere takes on the value T_0, the theoretical boundary temperature for radiative equilibrium. On the other hand, if the chromosphere loses energy by some non-radiative process, the sum becomes negative so that there is a net gain of energy by radiative processes. Similarly, if there is a net gain of mechanical energy, the sum must be positive. In this latter case, T_e will lie above T_0. Essentially all estimates of T_e based upon observational data place it above T_0 (cf. Chapter 6). Hence, as suggested earlier, the evidence indicates a net radiative outflow and a non-radiative inflow of energy.

The foregoing comments on the sum in Eq. (5-3) apply only to the net result of all processes. In considering individual processes, we must evaluate the brackets for the particular transitions in question.

In discussing the radiative energy output of the chromosphere in the present context, it is more convenient to define the energy in terms of unit mass rather than unit volume. If we denote the bracket in Eq. (5-3) as NRB, the emission per unit mass of chromospheric matter from atoms in the $(i - 1)$ stage of ionization is of the form

$$E_{kj} = K_{kj} n_e n_i (n_{\mathrm{H}} + n_p)^{-1} b_k T_e{}^{-3/2} \exp(\chi_k / T_e) \mathrm{NRB}_{kj} \tag{5-4}$$

in bound-bound transition,

$$E_{\infty j} = K_{\infty j} n_e n_i (n_{\mathrm{H}} + n_p)^{-1} T_e{}^{-1/2} \mathrm{NRB}_{\infty j} \tag{5-5}$$

in free-bound transition, and

$$E_{ff} = 1.4 \times 10^{-27} n_e n_i (n_{\mathrm{H}} + n_p)^{-1} T_e{}^{1/2} \mathrm{NRB}_{ff} \tag{5-6}$$

in free-free transitions.

For those resonance and subordinate lines for which the approximations $r_0 = 0$, $\epsilon B_\nu(T_e) \gg \eta B^*$ and $A(\epsilon + \eta)^{1/2} \gg 1$ are valid, Eq. (4-109) reduces to

$$\mathrm{NRB}_{kj} = (\epsilon + \eta)[-\Sigma L_i e^{-k_i \tau_0} / (e^{-c\tau_0} + \Sigma L_i e^{-k_i \tau_0})] \tag{5-7}$$

for values of τ_0 such that $c\tau_0 \lesssim 1$ and $k_i \tau_0 \lesssim 1$ for some i. When τ_0 approaches infinity NRB approaches zero, and when τ_0 approaches zero NRB approaches $(\epsilon + \eta)^{1/2}$, provided ϵ and η are small compared to unity. In Chapter 4 we indicated that an extremum in NRB may occur for $\tau > 0$. In the present context we are concerned mainly with the two extremes, $\tau \approx 0$ and τ very large. The extremal values of NRB are, in all cases evaluated, less than the values at $\tau = 0$. Since our main interest in this chapter is in identifying the major sources of energy output, and we are mainly concerned with the condition $\tau = 0$ or τ very large, we shall not consider these possible extremal values further.

For the strong subordinate lines for which ηB^* exceeds $\epsilon B_\nu(T_e)$ Eq. (4-109) reduces to

$$\mathrm{NRB}_{kj} = \eta[-\Sigma L_i e^{-k_i\tau_0}/(1 + \Sigma L_i e^{-k_i\tau_0})] \tag{5-7a}$$

for intermediate values of τ_0. As τ_0 approaches zero NRB approaches $\eta^{1/2}$ provided $\eta \ll 1$. For all of the subordinate lines except Hα of hydrogen, we shall have occasion to use NRB for small values of τ_0 only. Under these conditions, NRB $\approx (\epsilon + \eta)^{1/2}$ which is a slow function of T_e if $\epsilon > \eta$ and independent of T_e if $\eta > \epsilon$.

For the resonance free-bound continuum, the approximation $r = 0$ is no longer valid. r is here defined as the ratio of continuum opacity from all sources other than the free-bound transition in question to the opacity in the particular free-bound transition. However, in this case NRB near the continuum limit is equal to the difference in the recombination and photoionization rates divided by the recombination rate. When T_e appreciably exceeds T_{rad}, as it does in the chromosphere and when τ_0 is not large, the recombination rate generally exceeds the photoionization rate by a significant factor. Therefore, NRB is essentially unity, and is again a relatively slow function of T_e. This same conclusion can be reached by considering the behavior of Eqs. (5-7) and (5-7a) for the higher series members. For the higher lines, η increases and as the series limit is approached NRB approaches unity.

In the free-free continuum, the opacity of the chromosphere is essentially zero, and radiative absorptions are much less frequent than emissions. Thus, we set NRB = 1.

Consider first the cases of low opacity where the bracket is a slow function of T_e. As T_e increases, E_{kj} and E_k for a particular ion rise sharply to maxima, then decrease somewhat more slowly. E_{ff} behaves similarly if an $(i + 1)$ stage of ionization is possible. However, if an $(i + 1)$ stage of ionization is not possible—for example, H and HeII—E_{ff} rises rapidly at first, then continues to rise more slowly for higher values of T_e.

The absolute intensity of the maximum emission from a particular ion increases with increasing density and decreases with increasing T_e. Since density decreases outward and T_e apparently either increases outward or is constant, $E_{\max}$ for a particular ion must also decrease outward.

In the case of high opacity, the net radiative leak approaches zero, and may be a strong function of T_e. But, as T_e increases, the opacity must decrease to smaller and smaller values so that the foregoing arguments still apply. Thus, the radiative leak from a particular transition increases to a maximum then decreases as T_e increases. It is this property of radiative energy losses that determines, to a large extent, the temperature structure of the chromosphere and corona.

B. *Consideration of* E_{in}

If we knew the precise form of $E_{\text{in}}(h)$, we could, in principle determine $T_e(h)$ by equating E_{out} to E_{in}. Unfortunately, we do not yet know either the mechanism of energy input or the amount needed to maintain equilibrium. Indeed, the most promising solution to the problem of specifying E_{in} seems to lie in an empirical determination of $E_{\text{out}}(n_e,T_e)$ with sufficient precision to determine the nature of the source. Without a knowledge of chromospheric structure and of source functions and opacities in the various spectral lines, such an attempt to determine E_{out} is fruitless. Thus, we cannot expect to know the detailed characteristics of E_{in} until we first have a fairly complete understanding of the chromospheric model.

The anomalous extent of the chromosphere and the apparent increase in T_e with height relative to that predicted for a stellar atmosphere in radiative and hydrostatic equilibrium suggests a nonradiative supply of energy. Furthermore, the existence of macroscopic velocity fields in the chromosphere implies a mechanical dissipation of energy and, in consequence, a coupling of the energy in the velocity field with the energies in the internal degrees of freedom of the atoms. We proceed on the basis that E_{in} is certainly nonradiative and most likely mechanical in nature. Quantitative details are lacking, and, in particular, we do not know how E_{in} varies with T_e. We note, however, that it is characteristic of mechanical systems to transmit energy to a medium at a rate that varies directly with the difference between the kinetic energy of the source and the thermal energy of the medium. Thus, we expect that $dE_{\text{in}}/dT_e < 0$.

For the present, we must be satisfied with the most plausible assumptions we can make regarding E_{in}, which will allow us to discuss the stability criterion (5-2). We note first of all that in general E_{out} is a strong function of T_e, and unless E_{in} is also a strong function of T_e the stability criterion will be violated near the maximum in E_{out}. In this case, the stability criterion becomes $dE_{\text{out}}/dT_e = 0$.

A further justification for using this criterion can be made in the following way: Empirically, we know that there is a large change in the degree of ionization between the lower chromosphere and the corona. Thus, the condition (5-2) on the energy balance must be such as to require transitions to successively higher states of ionization with increasing height. Such transitions will occur if E_{in} decreases more slowly with height than $E_{\text{max}}(\alpha)$, E_{max} for ion α, for those ions that contribute most to E_{out}. For, in this case, E_{in} will eventually exceed $E_{\text{max}}(\alpha)$ and the energy balance must shift to another ion. Hence, we may assume that $dE_{\text{in}}/dh > dE_{\text{max}}(\alpha)/dh$.

Consider, now, the radiation from a particular ion. If $dE_{\text{in}}/dT_e < 0$ the stability criterion (5-2) will be violated for a T_e that is greater than the T_e where $E_{\text{out}} = E_{\text{max}}(\alpha)$, and as height increases the condition $E_{\text{in}} = E_{\text{out}} = E_{\text{max}}(\alpha)$ will be reached before the stability criterion is violated. Since $dE_{\text{in}}/dh > dE_{\text{max}}(\alpha)/dh$, immediately above the height where $E_{\text{in}} = E_{\text{max}}(\alpha)$ we must have $E_{\text{in}} > E_{\text{max}}(\alpha)$. The energy balance requires, therefore, that the atmosphere adjust to such conditions that a new ion can supply the necessary energy output. Hence, the stability criterion of interest in the chromospheric problem is

$$dE_{\text{out}}/dT_e \geq 0 \tag{5-8}$$

C. The T_e Model

The detailed T_e model of the chromosphere depends, of course, upon the detailed form of E_{in}. However, the general characteristics of the model are determined by the stability criterion (5-8). The outstanding features of the model are the transitions from one dominant source of emission to another. Since these transitions represent an increase in ionization, they must be accompanied by an increase in T_e. Were it not for the effects of thermal conduction, these increases in T_e would occur as discontinuities. The calculations of Giovanelli (1949) and Woolley and Allen (1950) indicate that a transition from 5000 to 100,000° would occur in about 100 km if thermal conduction were the only method of energy transfer. Although radiation transfer will modify their results to some extent, we may still regard these increases in T_e in the transitions from one dominant source of radiation loss to another as being essentially discontinuous when considering the over-all model.

Between the sharp rises in T_e, we expect plateaus of relatively low temperature gradient. Each dominant source of radiation loss will form one of these plateaus and the subsequent sharp jump in T_e to the next plateau. Within the plateaus, the gradient in T_e will be determined, in part, by the gradient in E_{in}. However, in view of the foregoing discussion the ends of the plateaus are properties of the chromospheric radiation field only. Because of this, we may specify the properties at the ends of the plateaus in much more detail. In considering the end points of the plateaus and in identifying the dominant sources of radiation loss, we shall assume that E_{out}, hence E_{in}, is constant across the transition from one dominant source to another. This contradicts our conclusion that $dE_{\text{in}}/dT_e < 0$. However, without knowing the explicit form of E_{in}, we cannot proceed in any other way.

Parker (1953) has previously interpreted the onset of thermal instability in terms of a collapse of the atmosphere into a configuration of higher density, which is manifested in the form of transient phenomena of solar activity. Our interpretation in terms of a rise in T_e and a steady-state configuration should be more representative of the general solar atmosphere. We also note that Kiepenheuer (1953) suggested that the principal source of emission from the corona was free-free emission, and that the thermal instability of this emission gave rise to coronal condensations and prominences. However, once hydrogen is ionized the free-free emission is proportional to $T_e^{1/2}$ and is consequently stable against changes in T_e. The error in Kiepenheuer's argument apparently arises from the use of the free-free emission per unit frequency rather than that integrated over frequency.

II. Dominant Sources of Radiation Loss

In the foregoing, we have stated the stability criterion for the chromospheric temperature field and indicated the type of model to be expected. Before proceeding with the details of the model, we must first identify the likely dominant sources of radiation loss.

Ideally, we should investigate the terms in Eq. (5-3) for each transition of each ion as a function of T_e and n_e. To do this, we would require a detailed solution of the transfer equation for each transition in order to evaluate the bracket terms. Such a treatment is beyond the scope of this work, and until we have better knowledge of atomic cross sections it is, in fact, an insurmountable problem. We must therefore proceed along somewhat less rigorous lines. Such an approach is possible because the opacities for the different spectral lines and continua whose radiations are strongest change by large factors from one transition to another. Thus, the problem often reduces to cases where the opacity is either very large or very small. In these two extreme cases, at least, we can make reasonable estimates of the effect of the bracket terms in Eq. (5-3).

We begin this less quantitative discussion by first considering the observed spectrum of the chromosphere and the known relative abundances of the elements. Table 5-1 contains Allen's (1955) summary of relative abundances for the 16 most abundant elements.

If the temperature in the chromosphere and corona increased smoothly with height to the value $\sim 10^6$ in the lower corona, all ions up to those with ionization potentials of the order of 300 volts should be present at some height and they should all radiate. We could not expect to observe the radiation from all these ions, since some would emit in unobserved regions in the ultraviolet spectrum only. However, we might expect to observe the majority of the ions observed in

Table 5-1. Relative Abundances

Element	Log abundance (no. of atoms)	Element	Log abundance (no. of atoms)
H	10.0	Si	5.5
He	9.0	S	5.1
O	6.8	Ni	4.5
N	6.5	Na	4.5
C	6.3	Al	4.5
Ne	6.1	Ca	4.4
Fe	5.8	A	4.3
Mg	5.6	Cl	3.8

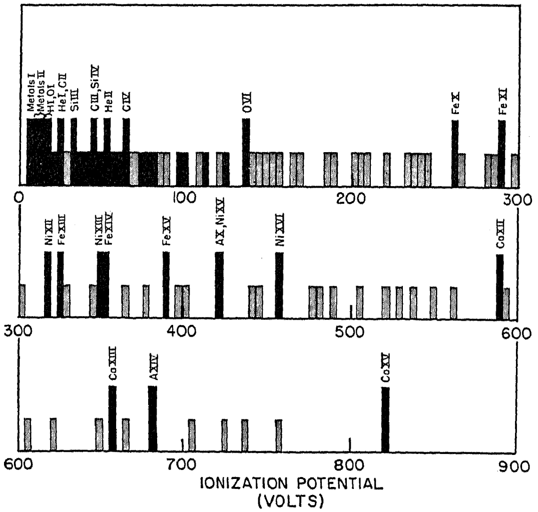

Fig. 5-1. Ionization potentials of ions whose lines are observed in the solar spectrum (long, solid bars) and in stars or nebulae (short, solid bars). The short cross-hatched bars show possible ions of abundant elements.

stellar and nebular spectra. In Fig. 5-1, we plot both the observed and possible ions of the elements in Table 5-1 against ionization potential. The longer shaded areas represent ions observed in the chromospheric and coronal spectra. The shorter shaded areas represent ions observed in stellar and nebular spectra, and cross-hatched areas represent unobserved ions. We note that between HeII and FeX, a range of 207 volts in ionization potential, only 2* of the possible 33 ions are observed, whereas 11 of the 33 are observed in stellar and nebular spectra. We conclude, therefore, that the temperature structure of the chromosphere is such that most of the observable ions in this range of ionization energies do not produce measurable radiation. By implication, then, most of these ions are not present in appreciable abundance.

We now ask which of the ions identifiable in the solar spectrum are likely to be the dominant sources of emission? In the photosphere the H$^-$ continuum provides the dominant radiation, and this must certainly be considered as a likely dominant source in the lowest layers of the chromosphere. The spectrum of the low chromosphere is characterized by strong emission from hydrogen, helium and neutral and singly ionized metals. Hydrogen emission, however, greatly exceeds the emission from any other single ion, and we suspect neutral hydrogen as a possible dominant source of emission. Because of the relatively large abundance of helium, it is immediately a suspect also. This suggestion is strengthened by the fact that HeI emission is strong in the visual regions of the chromospheric spectrum. The HeII line at λ4686 is faint in comparison with the observed HeI lines in the visual part of the spectrum. However, the resonance line of HeII at λ304 is considerably stronger than the resonance line of HeI at λ584 (Rense, 1958), and HeII must be considered also as a possible dominant source of radiation.

---

* Since this compilation was made, Violett and Rense (1959) have reported lines in the solar "rocket" spectrum of two additional ions within this range of energies, OIV (77 volts) and OV (114 volts). One or two other tentative identifications have also been reported.

Between 60 and 260 volts ionization energy only the ions of CIV and OVI are identified. In both cases the resonance lines are observed as faint emission lines in the ultraviolet rocket spectra (Johnson, Malitson, Purcell, and Tousey, 1958). Since these lines are faint in comparison with both the resonance and subordinate lines of hydrogen and helium, these ions probably need not be considered as dominant sources of emission. Above 260 volts, several ions are observed. However, since all of these ions are identified with the corona it appears that the major suspects for dominant sources of emission in the chromosphere are H$^-$, H, HeI, and HeII. A further possible suspect is free-free emission, which we could not expect to identify in the above way.

Having selected the possibilities for the dominant sources of radiation loss, we now consider them somewhat more quantitatively. The constants in Eqs. (5-5) and (5-6) for hydrogen and helium, apart from the b_k factors, are tabulated in Table 5-2 for the continua, the strongest resonance line, and, the strongest subordinate line. One of these transitions should dominate the energy loss for each ion. For the H$^-$ emission, which will be of importance at the very lowest heights only, we assume local thermodynamic equilibrium, so that

$$E_{\mathrm{H}^-} = 4\pi[n_{\mathrm{H}^-}/(n_{\mathrm{H}} + n_p)] \int_0^\infty \alpha_\nu B_\nu(T_e)\, d\nu \qquad (5\text{-}9)$$

where α_ν is the H$^-$ absorption coefficient. After numerical integration, using the absorption coefficient tabulated by Chandrasekhar and Breen (1946), we obtain

$$E_{\mathrm{H}^-} = 1.6 \times 10^{-21} n_{\mathrm{H}^-} (n_{\mathrm{H}} + n_p)^{-1} T_e^4$$

and from the ionization equation we obtain

$$E_{\mathrm{H}^-} = 6.6 \times 10^{-37} n_e n_{\mathrm{H}} (n_{\mathrm{H}} + n_p)^{-1} T_e^{5/2} \exp(8.6 \times 10^3/T_e) \tag{5-10}$$

Since the low chromosphere is opaque to the Lyman lines and early Balmer lines of hydrogen (cf. Chapter 9), we cannot estimate a priori the energy flux in these emissions. However, the chromosphere is certainly transparent to the Balmer continuum of hydrogen and the H^- emission, and, for illustration, we may compare these two sources of energy loss by setting the brackets in Eq. (5-5) equal to unity. In Fig. 5-2, we plot the emission from H^- and the Balmer free-bound emission for $n_{\mathrm{H}} + n_p = 10^{14}$. The H^- emission exceeds the Balmer free-bound emission for $T_e \leq 5300°$. However, it does not violate the stability criterion established by Eq. (5-8) until $T_e \sim 10^4$ where the Balmer free-bound emission greatly predominates. Since the NRB for the Balmer continuum is negative, the plot in Fig. 5-2 is not directly relevant. However, for $T_e \approx 10^4$, τ in the Lyman continuum is not large and NRB is approaching unity (cf. Chapter 6). The energy loss in the Lyman continuum exceeds the total energy radiated in the Balmer continuum and, therefore, certainly exceeds that due to H^-. Thus, even though

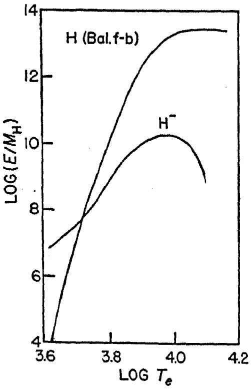

Fig. 5-2. Illustration of the relative radiative energy losses in various processes assuming thermodynamic equilibrium and no absorptions. The emission from H^- and the Balmer free-bound emission for $n_{\mathrm{H}} + n_p = 10^{14}$. (From R. G. Athay and R. N. Thomas, 1956, *Astrophys. J.*, **123**, 302.)

H^- emission may dominate at some heights it will not enter into the stability criterion for the radiation field.

It seems evident, then, that neutral hydrogen will form the first dominant source of radiation in the chromosphere so far as the stability criterion is concerned. We note from Table 5-2 that, because the abundance of helium is less than that for hydrogen by about a factor of 10, hydrogen emission will exceed HeI emission for the corresponding transition for all values of T_e unless the b_k's and brackets for HeI appreciably exceed those for hydrogen. The computations by Zirin (1956), Jefferies (1955), and Athay and Johnson (1960) indicate that the b_k's for the HeI triplets are of the same order of magnitude as those for hydrogen, whereas for the singlets they are smaller than for hydrogen (cf. Chapter 7). For the subordinate transitions, NRB is essentially the same for the two atoms. Thus, in these transitions the radiation loss from hydrogen exceeds that for HeI. We cannot be certain, however, that the radiation loss in the resonance lines of HeI does not exceed the radiation loss in the subordinate transitions in hydrogen for some value of T_e.

We note from Table 5-2 that if the b_k's and brackets for the HeII transitions are not considerably smaller than those for hydrogen the radiation loss from HeII may exceed that for hydrogen for high values of T_e. Zirker's (1959) calculations indicate that the b_k's for HeII are indeed comparable to those for hydrogen. The calculations on the excitation of HeI (Athay and Johnson, 1960; cf. Chapter 7) and HeII (Zirker 1959) in the chromosphere show conclusively that the observed HeI radiation as well as the HeII radiation originates in regions in which HeI is much less abundant than HeII. On this basis, we conclude that HeII radiation is the most likely dominant energy loss following H radiation.

Following HeII, the most likely dominant source of emission is either a coronal ion, OVI, or free-free transitions of electrons in the fields of protons. The ratio of intensities of free-free emission to the free-bound continua of HeII is

$$E_{ff}/\Sigma E_{k\infty} = 1.6 \times 10^{-7}(n_p/n_{\mathrm{III}})T_e \tag{5-11}$$

Because n_p/n_{III} has a value of approximately 10, the free-free emission will not dominate over the HeII free-bound emission until T_e exceeds 6×10^5. In reality, of course, we should compare the HeII emission at the top of the HeII plateau with the free-free emission at the base of the next plateau. There is presumably a large

Table 5-2. Coefficients for Equations (5-5) and (5-6)

	Hydrogen			HeI			HeII		
	E_{21}	E_{32}	$\sum_{1}^{\infty} E_{k\infty}$	E_{21}	$E_{2^3S-2^3P}$	$\sum_{1}^{\infty} E_{k\infty}$	E_{21}	E_{32}	$\sum_{1}^{\infty} E_{k\infty}$
K_{kj}	1.3×10^{-17}	4.9×10^{-19}	5.4×10^{-22}	2.4×10^{-17}	1.8×10^{-20}	1.8×10^{-21}	8.3×10^{-16}	3.1×10^{-17}	8.6×10^{-21}
$X_k \times 10^{-4}$	3.92	1.75	—	3.68	4.20	—	15.7	6.95	—

increase in T_e between these plateaus, and there must be a correspondingly large decrease in n_e, which greatly reduces the free-free emission. Under these conditions, the free-free emission will not balance the free-bound emission of HeII for any value of T_e. Therefore, following HeII, the next dominant source of emission apparently arises from a coronal ion.

For purposes of illustration, we show in Fig. 5-3 the hydrogen and helium emission for $n_H + n_p = 10^{11}$ and the brackets and the b_k's equal to unity.

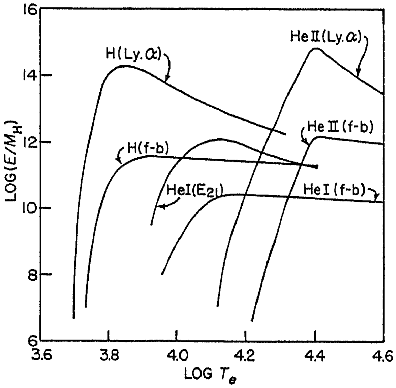

Fig. 5-3. Illustration of the relative radiative energy losses in various processes assuming thermodynamic equilibrium and no absorptions. The hydrogen and helium emission for $n_H + n_p = 10^{11}$. (From R. G. Athay and R. N. Thomas, **1956**, *Astrophys. J.*, **123**, 302.)

III. Details of the Model

In the foregoing, we have indicated that the chromosphere is characterized by two major sources of emission, and that these sources form temperature plateaus followed by sharp increases in temperature. The conclusion that there are only two sources is based largely upon the assumption that E_{in} is constant across the transition from one temperature plateau to another. If this assumption is relaxed, it may be necessary to consider other dominant sources of emission and their associated temperature plateaus such as, for example, HeI, OVI, and free-free transitions. From the empirical evidence, there is no good indication that this is actually the case, however, and we shall proceed under the assumption that only the hydrogen and HeII plateaus are present.

The significance of these conclusions regarding the dominant sources of emission go somewhat beyond their use in the present context. When we turn to a consideration of chromospheric models as inferred empirically, we shall find that a non-spherically symmetric model must be considered. Once spherical symmetry is abandoned there are an infinite number of possible variations in the model, and we must have some logical basis on which to proceed. On the basis of two temperature plateaus in the chromosphere and one in the corona, the model should involve a maximum of three different temperature regimes along a surface of constant height. If the departures from spherical symmetry are not of large amplitude, then only two temperature regimes will occur at any one height and a two-component model has some physical basis. Fortunately, this is the simplest alternative to the spherically symmetric model.

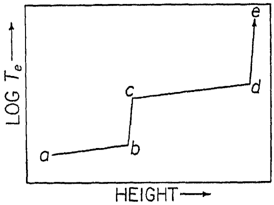

Fig. 5-4. A schematic T_e model for the chromosphere showing the hydrogen and HeII plateaus.

Along any given radius, we expect the chromospheric model to be of the form exhibited schematically in Fig. 5-4. Point *a* represents the height where the energy input from non-radiative sources begins to dominate over the energy input from radiative sources. At this point T_e, begins to increase outward. The detailed behaviour of T_e as a function of height depends upon the nature of E_{in}. However, at some height, E_{out} must transfer from hydrogen to HeII as the dominant source. This transition begins at point *b* and ends at point *c*. From *c* to *d*, HeII is the dominant source of E_{out}, and the transition *d* to *e* represents the transition from HeII to the next major plateau.

One of the most serious difficulties encountered in trying to evaluate the thermodynamic conditions at the extremes of the temperature plateaus arises from the uncertainties in the bracket terms in Eq. (5-3). Rather than attempting to evaluate the bracket for each transition considered, we shall proceed by assuming that the opacities are small at the point considered and that the bracket has a constant value.

Following the calculations based upon the assumption of low opacities, we shall attempt to estimate the actual opacities and to evaluate the effect of the brackets on the results.

A. General Equations

In order to determine T_e at points b and d where the instabilities of the hydrogen and HeII emissions set in, we must specify the conditions under which fluctuations in T_e occur. If perturbations are introduced that cause fluctuations in T_e with a time scale that is less than the time scale for pressure readjustments, the fluctuations in T_e will occur essentially at constant density. On the other hand, if the time scale of the fluctuations in T_e is longer than the time scale for pressure readjustments the fluctuations will occur at constant pressure. A priori we cannot choose between these two extreme conditions without detailed knowledge of the model and its perturbations. Thus, we shall compute the instabilities for both cases.

For fluctuations at constant density,

$$n_{\mathrm{H}} + n_p = \text{constant} \tag{5-12}$$

and for fluctuations at constant pressure,

$$(n_{\mathrm{H}} + n_p + n_e)T_e = \text{constant} \tag{5-13}$$

Since the instability of the hydrogen emission will not occur until hydrogen is appreciably ionized, we may set $n_p = n_e$. Hence Eqs. (5-12) and (5-13) become

$$n_{\mathrm{H}} + n_e = \text{constant} \tag{5-14}$$

and

$$(n_{\mathrm{H}} + 2n_e)T_e = \text{constant} \tag{5-15}$$

We also need the ionization equation for hydrogen and HeII, which may be written

$$n_{i-1} = 4.14 \times 10^{-16} n_e n_i b_1 T_e^{-3/2} \exp(\chi_1/T_e) \tag{5-16}$$

The instability condition expressed by Eq. (5-8) will involve terms of the form $\partial \ln b_k/\partial T_e$ and $\partial \ln b_k/\partial n_e$. For $k \geq 2$ these terms arise from Eq. (5-4) for the line emission, and for $k = 1$ the terms arise from the ionization equation (5-16). We will assume that $\partial b_k/\partial T_e = \partial b_k/\partial n_e = 0$ for $k \geq 2$. The computations on the b_k in the preceding chapter indicate that we need question this assumption only for b_2. It will become clear, however, in the course of our computations of the degree of ionization at the instability points that even for b_1 the assumption above does not seriously affect the results. On the other hand, the numerical value of b_1 is of importance in determining T_e corresponding to the degree of ionization where the instability sets in. Thus, we shall drop the b_k terms from Eq. (5-5) but retain the b_1 in Eq. (5-16).

In Chapter 4, we developed an expression for b_1 for the case of detailed balancing in the early Lyman lines. As we noted above, we shall find that b_1 has little effect on the value of n_{i-1}/n_i at the point where instability sets in. For both hydrogen and HeII, the maximum emission occurs where $n_{i-1}/n_i \sim 10^{-1}$–10^{-2} (Tables 5-3 and 5-5). In the chromosphere n_i is of the order 10^{11} to 10^{10} for hydrogen and helium. Thus, n_{i-1} is of the order 10^{10} to 10^{8} when the instability sets in. The absorption coefficients are of the order 10^{-14} to 10^{-13} in the early Lyman lines and of the order 10^{-17} at the head of the Lyman continuum. With these limits, the path length required to give unit optical depth is less than 10 km in the early Lyman lines and over 100 km in the Lyman continuum. As we indicated above, we expect the transitions between temperature plateaus to occur in less than 100 km. At the beginning of the transition, then, we expect conditions such that the atmosphere is opaque in the early Lyman lines, but not in the continuum. In this case Eq. (4-47) for b_1 is appropriate for hydrogen.

For convenience, we repeat here a somewhat simplified equation for b_1 for hydrogen, which is obtained from Eq. (4-47):

$$b_1(H) \approx 1.5 \times 10^{14} T_e^{1/2} n_e^{-1} \exp(-\chi_2/T_e) \qquad (5\text{-}17)$$

For HeII, the situation is somewhat different since radiative ionizations from the second quantum level are much less effective than for hydrogen. Thus, ionizations occur mainly from the ground state. For detailed balancing in the resonance lines, and for a radiation temperature $\leq 7000°$ in the Lyman continuum of hydrogen,

$$n_1(\mathrm{HeII})/n_{\mathrm{III}} = \Sigma A_{\infty j} C_{21}/C_{2\infty} C_{12}$$

or

$$b_1(\mathrm{HeII}) \approx 2 \times 10^{10} n_e^{-1} T_e^{3/2} \qquad T_e \lesssim 30{,}000^\circ \qquad (5\text{-}18)$$

and

$$b_1(\mathrm{HeII}) \approx 1.3 \times 10^{15} n_e^{-1} T_e^{1/2}, \qquad T_e \gtrsim 30{,}000^\circ \qquad (5\text{-}18a)$$

For the thin-atmosphere approximation,

$$n_1(\mathrm{HeII})/n_{\mathrm{III}} = \Sigma A_{\infty j}/C_{1\infty}$$

which increases b_1 by a factor of 30 in Eq. (5-18) and a factor of 20 in Eq. (5-18a). The dependence upon n_e and T_e remains the same.

B. Beginning of the Hydrogen Plateau

Without a detailed knowledge of the energy-input mechanism and its importance relative to radiative energy transfer, little can be said about point *a*. However, the location of this point both in terms of T_e and in terms of h is a problem of great significance in the understanding of the solar atmosphere.

The plot in Fig. 5-2 indicates that H^- emission is a much slower function of T_e than is neutral hydrogen emission. This being the case, if E_{in} is relatively constant with height the rise in T_e at the beginning of the hydrogen plateau is very likely to exhibit an initial steep rise through the region where H^- dominates and a subsequent slower rise after neutral hydrogen takes over.

C. Instability of Hydrogen Emission, Point b

Through the instability criterion given by Eq. (5-8) and the equations for E_{out} with the brackets set equal to a constant, we may solve for n_{II}/n_e as a function of T_e at the point of instability. By combining this relationship with Eqs. (5-16) and (5-17) we may then determine T_e uniquely.

For the following cases of constant pressure and constant density perturbations, we give expressions for n_{H}/n_e including the b_1 terms, then with the b_1 terms evaluated from Eq. (5-17), and, finally, in an approximate numerical form. For constant pressure, we have used the additional assumption that $n_{\mathrm{H}}/n_e \leq 1$, which is shown to be true for constant density.

(*i*) *Constant Density:*

α lines:

$$\frac{n_{\mathrm{H}}}{n_e} = \frac{3/2 + \chi_k/T_e}{2(\chi_1/T_e - \chi_k/T_e) - 2T_e(\partial \ln b_1/\partial T_e) - (3/2 + \chi_k/T_e)n_e(\partial \ln b_1/\partial n_e)}$$

$$= (3/2 + \chi_k/T_e)/[3/2(\chi_1/T_e + 1/3) - \chi_k/T_e]$$

$$\simeq 6.3 \times 10^{-6}\, T_e + (0.67/k^2) \tag{5-19}$$

β continuum:

$$\frac{n_{\mathrm{H}}}{n_e} = \frac{1}{4[1 + \chi_1/T_e - T_e(\partial \ln b_1/\partial T_e)] - n_e(\partial \ln b_1/\partial n_e)}$$

$$= \frac{1}{3(\chi_1/T_e + 1)}$$

$$\simeq 2.1 \times 10^{-6} T_e \tag{5-20}$$

(*ii*) *Constant Pressure:*

α lines:

$$\frac{n_{\mathrm{H}}}{n_e} = \frac{2\chi_k/T_e + 5}{5/2 + (3\chi_1/T_e) - (2\chi_k/T_e) - 3T_e(\partial \ln b_1/\partial T_e) - [(\chi_k/T_e) - \tfrac{1}{2}]n_e(\partial \ln b_1/\partial n_e)}$$

$$= (2\chi_k/T_e + 5)/[9/4(\chi_1/T_e) - (\chi_k/T_e) + 1/2]$$

$$\simeq 1.4 \times 10^{-5} T_e + (0.89/k^2) \tag{5-21}$$

β continuum:

$$n_{\mathrm{H}}/n_e = 1/[3/2 + (\chi_1/T_e) - T_e(\partial \ln b_1/\partial T_e) + 1/2\, n_e(\partial \ln b_1/\partial n_e)]$$

$$= 1/[3/4(\chi_1/T_e) + 1/2]$$

$$\simeq 8.5 \times 10^{-6} T_e \tag{5-22}$$

If we assume b_1 = constant rather than the values given by Eq. (5-17), all the final numerical forms for n_{H}/n_e are multiplied by a factor of about 3/4. Since $(\epsilon + \eta)^{1/2}$ varies more slowly with T_e and n_e than does b_1, the effect of neglecting the brackets in determining n_{H}/n_e is negligible, provided that the opacity is small.

We may now solve Eqs. (5-16), (5-17), and (5-19) to (5-22) for explicit values of n_{H}/n_e and T_e at the points of instability. Table

5-3 exhibits the results for emission arising from level k for the two conditions of constant pressure and constant density.

According to the results in Table 5-3, the values of n_H/n_e and T_e at the points of instability are nearly the same for perturbations at constant pressure as they are for perturbations at constant density. Also, as we have noted, the value of n_H/n_e is not affected to an appreciable extent by the b_1 factor. For example, in thermodynamic equilibrium and constant pressure, $n_H/n_e = 0.05$ at the point of instability for the free-bound transitions. On the other hand, $T_e = 7500°$ in this case, as compared with the much higher value obtained when b_1 is included.

Table 5-3. Hydrogen Instability, Point b

	Constant density		Constant pressure	
	n_H/n_e	T_e	n_H/n_e	T_e
2	0.23	11,000	0.35	10,600
3	0.14	11,400	0.24	11,000
4	0.11	11,600	0.20	11,200
5	0.095	11,800	0.18	11,400
f-b	0.025	13,600	0.090	11,800

Before accepting any of the results in Table 5-3, we must estimate the NRB terms in Eqs. (5-4) and (5-5). Since the bracket is presumably zero at large optical depth and positive at small optical depth it must increase outward. The only effect it can have on the results in Table 5-3, therefore, is to delay the instability for a given transition to lower values of n_H/n_e and higher values of T_e.

Since the value of NRB is a function of τ, we must estimate τ_0 for the various transitions considered. For the free-bound continuum, $n_H/n_e \leq 0.1$ and $T_e = 13,000°$. In the regions of strong hydrogen emission, n_e is of the order 10^{11} (cf. Chapter 6), and n_H is therefore of the order 10^{10} when the instability sets in. These values will serve as a reference point for estimating opacities.

Following the onset of instability, T_e rises abruptly and n_H must decrease abruptly. Since we have assumed that the transition between plateaus occurs in less than 100 km, we must also assume that the scale height for n_H is of this same order. Hence, there should be about 10^{17} hydrogen atoms above the instability point for the free-bound continuum. The absorption coefficient at the head of the Lyman continuum is 6×10^{-18} at 11,000°, and the optical depth is therefore about 0.6. Since the opacity decreases as ν^{-3}, the "average" opacity for the continuum is small. On the other hand, the absorption coefficient at the center of Lyman-α is about 6×10^{-14}, and the optical depth is about 6×10^3. For the opacities in the Balmer transitions, we must estimate the population of the $k = 2$ level. From Eq. (4-48) for b_2, we obtain

$$n_2 \approx 3.2 \times 10^{-16} n_e^2 T_e^{-3/2} \approx 10^4$$

The empirical scale height for n_2 in the chromosphere is about 600 km (cf. Chapter 6), which leads to about 10^{12} for the total number of absorbing atoms. The absorption coefficient in the center of Balmer-α is about 5×10^{-13}. Hence the optical depth is of order unity.

Since the opacity is not large in the free-bound transitions, NRB for the Lyman continuum should be near unity. For Lyman-α, on the other hand, NRB should be of the order $(\epsilon + \eta)$. For Balmer-α, the bracket should be of the order of $\eta^{1/2}$.

The ratio of radiation loss in Balmer-α to that in the continuum, at the point of instability in the continuum, is

$$E(\text{Bal-}\alpha)/E_{\text{Cm}} = 9 \times 10^2 T_e^{-1} b_3 e^{\chi_3/T_e} \text{NRB}(\text{Bal-}\alpha) \qquad (5\text{-}23)$$

where NRB (Bal-α) denotes the bracket for Balmer-α. For detailed balancing in the Lyman lines, the observed radiation filed in Hα and $T_e = 13{,}000°$, $b_3 \approx 10$ (cf. Athay and Thomas, 1955). Hence, the ratio given by Eq. (5-23) is about 3 NRB (Bal-α). For Balmer-α under conditions of detailed balancing in the Lyman lines, $\eta \approx 0.0036$ (cf. Chapter 9) and $\text{NRB}_{32} \approx 0.06$ for $\tau_{32} \leq 1$. Evidently, then, the radiation loss in Balmer-α never exceeds the maximum radiation loss in the free-bound continuum.

There remains the question of the radiation loss in Lyman-α relative to that in the continuum. For intermediate values of τ_0, the relative radiation loss given by Eqs. (5-4) and (5-5) is

$$E(\text{Ly-}\alpha)/E_{\text{Cm}} = 2.4 \times 10^4 T_e^{-1} b_2 e^{\chi_2/T_e} \text{NRB}(\text{Ly-}\alpha) \qquad (5\text{-}24)$$

From Eq. 4-48 we adopt

$$b_2 e^{\chi_2/T_e} = (Y_2/X_2) e^{Y_2} \qquad (5\text{-}25)$$

which gives

$$E(\text{Ly-}\alpha)/E_{\text{Cm}} = 4.8 \times 10^3 \,\text{NRB}(\text{Ly-}\alpha) \tag{5-26}$$

For Lyman-α, $\epsilon \approx 10^{-7}$ and $\eta \approx 10^{-4}$. Thus, for intermediate values of τ_0 and $T_e = 10^4$ the energy loss in Lyman-α is comparable to that in the continuum. At higher values of T_e, τ_0 will decrease and NRB(Ly-α) will approach $\eta^{1/2}$. However, this must be associated with a decrease in n_e, and the energy loss may or may not exceed its value for lower values of T_e. Therefore, in the region of maximum continuum emission, where we estimate $\tau_0 = 6 \times 10^3$ in Lyman-α, NRB $\approx 10^{-4}$ and the energy loss in the continuum apparently exceeds that in Lyman-α. At some subsequent height where τ_0 has decreased to a small value, the radiation loss in Lyman-α may exceed the maximum loss in the continuum. In order to estimate the value of T_e where this occurs, we assume that n_eT_e is constant at the value it has at the point where the free-bound continuum has its maximum energy loss, viz., $\approx 10^{15}$. We find (Athay, 1960b), $\tau_0 = 1$ for $T_e \approx 80{,}000°$ and $n_e \approx 10^{10}$. However, before these conditions are attained, the HeII free-bound continuum (and possibly other HeII radiations) will dominate the energy output.

In view of the foregoing discussion, it therefore appears that the radiation loss in the hydrogen plateau is dominated by the free-bound continuum. Empirical evidence that this is the case comes from the fact that the energy emitted by the chromosphere in the Balmer continuum alone exceeds the energy emitted in Lyman-α and Balmer-α. From the results inTable 5-3, we conclude, then, that the hydrogen plateau terminates for $n_{\text{H}}/n_e \simeq 0.02$ to 0.09 and $T_e \simeq$ 12,000 to 14,000°.

At point *b*, T_e begins to rise sharply. How far it will rise depends upon the next source of emission, which we have tentatively identified with HeII.

D. Transition to the HeII Plateau, Point c

The energy loss from HeII radiation at point *c* depends, of course, on the values of the brackets in Eq. (5-3) as well as the b_k's. The b_k's for HeII are comparable to those for hydrogen (cf. Zirker, 1959). The opacities and the brackets, however, are considerably different. In order to decide which transitions are likely to be important in the energy loss, we must first estimate the opacities.

Since the transition from b to c occurs in a shallow layer of the chromosphere, the transition must occur at nearly constant pressure. From Table 5-3 we see that $n_{\mathrm{H}} \ll n_e$ and $n_e = n_p$ at heights above point b. Thus, the condition of constant pressure is

$$n_e T_e = \text{constant} \tag{5-27}$$

Also, if helium is ionized sufficiently for HeII emission to be strong we may assume that $n_{\mathrm{II}} \gg n_{\mathrm{I}}$. In this case, the total helium density is

$$n_{\mathrm{II}} + n_{\mathrm{III}} = 0.1 n_e \tag{5-28}$$

Since we must have $n_{\mathrm{II}} \leq 0.1 n_e$, for $n_e \leq 10^{11}$ the number of atoms in the ground state of HeII is $\leq 10^{10}$. The scale height for helium is about 10^8 cm, so the total number of absorbing atoms for the Lyman series is $\leq 10^{18}$. The absorption coefficients are comparable to those for hydrogen. Therefore, at the base of the HeII plateau there should be high opacity in the early Lyman lines, but not in the continuum. This being the case, the dominant energy loss is either from Balmer-α or the free-bound continuum.

Our problem, then, is to balance either Balmer-α or the free-bound continuum emission of HeII against the maximum free-bound emission from hydrogen. With the brackets equal to unity and the b_3 for HeII obtained from Zirker's (1959) calculations, it is not possible to obtain such a balance. However, the Balmer-α radiation loss from HeII comes within a factor of 3 of the balance, and the free-bound continuum radiation from HeII comes within a factor of 10. Thus, if we relax somewhat the assumption that E_{in} is constant across the transition and allow $dE_{\mathrm{in}}/dT_e < 0$, as we concluded it should, HeII radiation may still form a temperature plateau. We assume that this is the case, and show in Chapter 7 that there is strong empirical evidence to support it.

In the case of hydrogen Balmer-α, the chromosphere is opaque and there is a strong radiation field. Radiative excitations therefore play a major role in the equilibrium, and the bracket is always small compared to unity. However, this is not the case for the Balmer-α line of HeII, since the chromospheric opacity is very low (Athay, 1958 and 1960b), and the radiation field is very weak in comparison with the source function in the line. Thus, radiative excitations are slow compared with the downward transitions, and the bracket should approximate to unity. The dominant energy loss in the HeII plateau is, therefore most likely in the Balmer-α transition. We shall comment further on the conditions at the base of the plateau following our calculations for the top of the plateau.

E. Instability of HeII Emission, Point d

Because perturbations in the temperature field at constant density and constant pressure lead to very similar results we will consider only the perturbations at constant density. Throughout the region where HeII emission is stable $n_{\text{I}} \ll n_{\text{II}}$. Hence, the condition of constant density may be written

$$n_{\text{II}} + n_{\text{III}} = \text{constant} \tag{5-29}$$

The procedure for computing the point of instability for HeII is exactly the same as the procedure followed for hydrogen and the same considerations apply. We again take b_k constant for $k \geq 2$. The instability sets in for:

$$\begin{aligned} \textit{Lines}: n_{\text{II}}/n_{\text{III}} &= [3/2 + (\chi_k/T_e)]/\{(\chi_1/T_e) - (\chi_k/T_e) \\ &\quad - [T_e(\partial \ln b_1/\partial T_e)] - 3/2\} \\ &= [3/2 + (\chi_k/T_e)]/[(\chi_1/T_e) - (\chi_k/T_e) - 2] \\ &\simeq 2.4 \times 10^{-6}T_e + (1.00/k^2) \end{aligned} \tag{5-30}$$

$$\begin{aligned} \textit{Continuum}: n_{\text{II}}/n_{\text{III}} &= 1/2/[1 + (\chi_1/T_e) - T_e(\partial \ln b_1/\partial T_e)] \\ &= 1/[(2\chi_1/T_e) + 1] \\ &\simeq 8 \times 10^{-7}T_e \end{aligned} \tag{5-31}$$

As was the case for hydrogen, the instability conditions when $b_1 = 1$ are very near those obtained by multiplying Eqs. (5-30) and (5-31) by 3/4. From Eqs. (5-16), (5-18), (5-20), and (5-31), we can obtain T_e at point *d*. Table 5-4 exhibits the results for the first three excited energy levels and the continuum. Again we note that the results on T_e depend rather critically on the numerical value of b_1.

We emphasize that the results in Table 5-4 apply only when the brackets are constant. Since n_{II} is of the order $0.03n_e$ when the instability in Balmer-α sets in, and since n_e is probably about 10^{10}, about 10^{16} to 10^{15} HeII atoms are above the instability point. Hence,

Table 5-4. HeII Instability, Point *d*

k	n_{II}/n_{III}	T_e
2	0.39	59,000
3	0.26	61,000
4	0.21	64,000
f-b	0.05	71,000

the early Lyman lines still have high opacity. Since we have concluded that the bracket is near unity for Balmer-α and the continuum, the end of the HeII plateau should come within the limits 60,000 to 70,000°. We note that these limits are much different from those given in our earlier work (Athay and Thomas, 1956a), where we made an erroneous assumption on the value on b_1 for HeII.

The condition $\tau_0 = 1$ in Lyman-α of HeII occurs for $T_e \approx 1.2\text{–}1.6 \times 10^5$ (Athay, 1960b). If the electron pressure is constant, the ratio of Lyman-α energy loss near $\tau_0 = 1$ to the maximum continuum energy loss is about b_2 NRB. For HeII, $\epsilon = 10^{-8}$ and $\eta \approx 10^{-11}$, and for small τ_0 NRB $\approx 10^{-4}$. Quite possibly then b_2 NRB could exceed unity, or if $dE_{1n}/dT_e < 0$ as we have suggested, the energy output in Lyman-α could balance E_{1n}. This would result in a *second* plateau for HeII. However, we can do little more than speculate about the existence or non-existence of such a plateau just as in the case of OVI, free-free emissions, and Lyman-α of hydrogen.

Empirically, the chromospheric radiation in the Lyman-α line of HeII exceeds that in the Balmer-α line of HeII by at least an order of magnitude and the radiation in the Lyman-α line of hydrogen exceeds or is comparable to that in Lyman-α of HeII. The radiation temperature in the Lyman-α line of HeII is of the order of 20000° (Athay, 1958), and in the Lyman-α line of hydrogen it is of the order of 7000° (Athay and Thomas, 1956b). Therefore essentially all of the energy in these lines must arise from an energy source other than photospheric radiation. Thus, the empirical evidence suggests that there are indeed regions of the atmosphere where the radiation losses in Lyman-α of hydrogen and HeII exceed the radiation loss in Balmer-α of HeII. As we noted above, the plateau due to Lyman-α of HeII should occur at $T_e \approx 1.2\text{–}1.6 \times 10^5$ and that due to hydrogen at $T_e \approx 8 \times 10^4$. However, these estimates of T_e are highly uncertain due to uncertainties in collision cross sections. In view of the uncertain nature of these plateaus, we shall not consider them in more detail. Their presence or absence does not affect the two lower plateaus due to subordinate transitions of hydrogen and HeII.

The empirical evidence on the strength of the resonance line of HeI at λ584 leaves some doubt as to whether or not the energy loss in this line exceeds the energy loss in the Balmer-α line of HeII. Thus, we must still consider the possibility of a plateau being formed by this line. If there is such a plateau, it must occur for a T_e such that $\tau_0 \lesssim 1$. Since τ_0 depends upon the density and the scale height as well as upon T_e, we cannot determine a unique value of T_e that corresponds to $\tau_0 = 1$. However, for $10^{10} \leq n_e \leq 10^{11}$ and a scale height of 1000 km, we obtain $45{,}000° \leq T_e \leq 55{,}000°$ (cf. Chapter 7). Thus, the HeI plateau, if such exists, would be essentially the same as the HeII plateau due to the subordinate transitions.

Returning now to the conditions at the base of the HeII plateau, we note that the Balmer-α flux of HeII decreases by about a factor of 10 from its maximum value if we decrease T_e to 40,000° holding the pressure and b_3 constant, and by about a factor of 1000 if we decrease T_e to 30,000°. Hence, unless E_{in} is a strong function of T_e, T_e at the base of the HeII plateau will not be much below 40,000°. In this case, there should be a sharp demarkation between the top of the hydrogen plateau and the base of the HeII plateau.

If the plateau is formed by the resonance line of HeI, we should not expect τ_0 to exceed about 10. For $n_e = 10^{10}$ and a scale height of 1000 km, $\tau_0 = 6$ at $T_e = 40{,}000°$ and $\tau_0 = 70$ at $T_e = 30{,}000°$ (cf. Chapter 7). Thus, we again conclude that T_e would not fall much below 40,000° and that the HeI plateau would be essentially the same as the HeII plateau.

The top of the HeII plateau should be marked by the upper boundary of the chromosphere as it would be observed in the Balmer-α line of HeII. Since there is still considerable hydrogen emission for $T_e = 60{,}000°$, the upper boundary of hydrogen Balmer-α probably is a good indicator of the end of this plateau.

F. The Transition to the Corona, Point e

Since it is beyond the scope of this monograph to consider the details of coronal problems, we shall not attempt to evaluate T_e at point e. However, it is of interest to note the large jump in ionization between the upper chromosphere and corona, which, we believe, arises quite naturally from the large drop in relative abundances in the elements heavier than helium.

The free-bound radiation from a hydrogen-like ion of nuclear charge Z and relative abundance Q is proportional to

$$QZ^4/k^3$$

where k is the principal quantum number of the bound level. For both hydrogen and HeII, this quantity if of order unity. For elements of greater atomic weight and whose ionization potential is less than about 800 volts, which is the highest ionization potential of any known coronal ion (CaXV), the greatest value of QZ^4/k^3 is about 0.2. This value occurs for both OVI and FeXVI whose relative abundances are about 10^{-3} and 10^{-4}, respectively. Woolley and Allen (1948) and Elwert (1954) estimate the coronal line radiation to be about one order of magnitude more intense than the free-bound radiation. It appears therefore that the high degree of ionization in the corona is required in order to raise the coronal radiation to the necessary value.

It is also of interest to note that the chromosphere requires at least as much, if not more, energy input than the much hotter corona. It is not clear whether one should compare energy input per unit volume, per ion or per unit mass. The energy radiated in the Lyman series of H and HeII considerably exceeds the total radiation from the corona (Violett and Rense, 1959; Elwert, 1954; and Woolley and Allen, 1948). Thus, the average energy loss by radiation from a unit volume of the chromosphere greatly exceeds the corresponding quantity from the corona. The average energy losses per ion and per unit mass are of the same order of magnitude in the two regions. It appears, therefore, that the chromosphere requires somewhat more non-radiative energy input than the corona.

IV. Comments on the Model

We have suggested that the chromospheric model is of the type shown schematically in Fig. 5-3, and we have formed estimates of T_e at the beginning and end of the temperature plateaus. The uncertainty in T_e increases markedly from point b, where it is of the order $\pm 10^3$, to point d, where it is of the order $\pm 10^4$. Above point d, we are uncertain as to the existence and extent of additional plateaus with $T_e \approx 1 \times 10^5$ and $T_e \approx 2 \times 10^5$ before the final transition to the corona at $T_e \approx 10^6$. However, these plateaus presumably radiate a spectrum that is considerably different from the chromospheric spectrum observed in the visual and photographic regions, and they are not necessarily of major importance in the interpretation of the observed spectrum.

Despite the uncertainties in the higher plateaus, the results obtained on the basis of the energy-balance arguments are of great value. In particular, we now understand just why the chromosphere has a sharp upper boundary, and we understand why certain lines observed in nebular and stellar spectra are absent from the chromospheric and coronal spectrum. In general we expect two temperature plateaus that are relatively isothermal in the sense that T_e does not change by large factors across the plateaus. Since we have postulated a non-radiative energy source, it seems only logical that this energy source will vary over the solar surface. If the energy source varies, we expect the model to change by changing the heights at which the plateaus occur. We do not expect the temperatures at the extremities of the plateaus to change appreciably. Thus, at a given height in the chromosphere we may find both plateaus, and the chromosphere will have a non-spherically symmetric structure. We expect that all long-lived phenomena of solar activity in the chromosphere such as plages and faculae will change the model only by changing the relative proportions of the two components.

Above point *d*, we have indicated that T_e rises either to about 1×10^5, 2×10^5, or to a coronal value. Thus, in the upper levels of the chromosphere we may expect to have components on the HeII plateau mixed with components at higher temperatures. In extreme cases, all of the plateaus may occur at the same height, although we do not expect this as a general rule.

One crucial test of these arguments can be obtained by studying the lowest heights at which coronal line emission occurs. On the basis of the arguments above, we should start to see coronal line emission in the upper levels of the chromosphere where we begin to distinguish spicular detail. Eclipse and coronagraph data (Athay and Roberts, 1955; Lippincott, 1955) indicate that spicular detail is pronounced above about 5000 km. Thus, we expect coronal line emission to be observed down to about 5000 km. There is evidence from eclipse data as we noted in Chapter 2, that this is indeed the case (Athay and Roberts, 1955).

The Analysis of Emission in the Optical Continuum to Obtain $n_e(h)$ and $T_e(h)$ Under the Assumption of a Spherically Symmetric Lower Chromosphere

R. N. THOMAS

I. Introduction

In Chapter 1, we emphasized that the primary observational characteristic directing attention to the outer solar atmosphere is the existence of emission gradients whose values (1) lie much below the values we would expect on the basis of the classical model of a stellar atmosphere applied to the sun, and (2) range very considerably from one line to another. In the corona, the apparent anomaly of such low emission gradients has been removed by the general acceptance of T_e values so high that the corresponding isothermal density gradients lie very close to the observed emission gradients. In the lower chromosphere, by contrast, there is no such general agreement on the resolution of the apparently anomalously low emission gradients. At one extreme is the viewpoint we have advocated (Thomas, 1948, et seq.): The "anomaly" in the observed emission gradients results from a significant rise in T_e in the lowest chromosphere, accompanying a non-radiative energy input with associated differential excitation effects that must be computed free from preconception as to the applicability of the usual LTE relations. At the opposite extreme lie models which hold the value of T_e constant at the "boundary-value" of the photosphere and explain the decreased emission gradients in terms of a "turbulent" pressure, but permit no energetic coupling between "turbulent" motion and internal kinetic degrees of freedom of the chromospheric atoms. A prototype of such a model is that by Woolley and Allen (1950). Thus, the first question to resolve in a study of the structure of the outer solar atmosphere is the extent to which observational data require a significant rise in T_e in the lower chromosphere, over whatever minimum value T_e reaches in its general outward decrease through the photosphere. We ask where T_e(min) occurs, the value of T_e(min), and what is the lowest height where T_e significantly exceeds T_e(min).

In analyzing the chromospheric data for information on T_e(min) it is natural to begin with the continuum, for two reasons. First, in attempting to compare the behavior of T_e in the lower chromosphere with that in the photosphere, it is advantageous to base such comparative results on the same kind of data whenever possible. The distribution of T_e in the photosphere comes primarily from limb-darkening measures made in the continuum, outside eclipse. Eclipse observations provide a means of carrying these disk observations across the limb and into the chromosphere. Second, non-LTE effects enter an interpretation of continuum data to a much lesser degree, and in a less sensitive way, than they enter an interpretation of the line spectrum. In certain cases, particularly that of He and Ca^+, *general* conclusions on the presence of values of T_e exceeding those in the upper photosphere may be more directly obvious from the presence of a line, or the form of a line profile. However, *detailed* information on the variation of T_e through the lowest chromosphere follows most directly from an analysis of the continuous spectrum.

We order our discussion of the continuous spectrum about the realization that a good, *direct* determination of T_e(min) from the observed continuous intensity is not feasible unless T_e(min) occurs: (1) either within the range covered well by disk limb-darkening data, which for presently existing data corresponds to $\tau_{5000} \gtrsim 0.05$ (τ_{5000} is the optical depth in the continuum at 5000 A); or (2) at heights above those defining the solar limb. This realization follows directly from the expression for the emergent intensity along an arbitrary direction in which the total optical depth is τ_t; viz.,

$$I_\nu(0) = \int_0^{\tau_t} S_C e^{-\tau_C} \, d\tau_C$$

which equals *either*

$$\left[S_C + \frac{dS_C}{d\tau_C}\right]_{\tau_C=0} - \left[S_C + \frac{dS_C}{d\tau_C}\right]_{\tau_C=\tau_t} e^{-\tau_t} + \int_0^{\tau_t} \frac{d^2S_C}{d\tau_C{}^2} e^{-\tau_C}\, d\tau_C \qquad (6\text{-}1)$$

or

$$\bar{S}_C(1 - e^{-\tau_t}) + \int_0^{\tau_t} (dS_C/d\tau_C)e^{-\tau_C}\, d\tau_C$$

where $\bar{S}_c$ represents a mean of S_c at the two integration limits. For very large τ_t, such as occur in disk observations, the first of the relations (6-1) shows that $I_\nu(0)$ lies very close to $S_C(\tau_C \sim 1)$ unless $d^2S_C/d\tau_C{}^2$ is large. For depths below S_C(min), the variation of S_C with τ_C is essentially that of radiative equilibrium or less, and the approximation just stated is good to 10 to 20 percent in $I_\nu(0)$. Thus, the variation of $I_\nu(0)$ as the observed direction approaches the limb is essentially that of S_C with height; and the inference of S_C(min), if it exists, is unambiguous. For very small τ_t, the second of the relations (6-1) shows that $I_\nu(0)$ represents a simple average of emissivity, i.e., $S_C\, d\tau_C$, along the line of sight. Particularly near S_C(min), where $dS_C/d\tau_C$ vanishes, the change in $I_\nu(0)$ with distance from the limb reflects the height gradient of the emissivity unambiguously. Provided we can relate both S_C and emissivity to T_e, we have then a good measure of the height gradient of T_e.

When, however, τ_t is neither so large that $\exp(-\tau_t)$ is negligible, nor so small that $\exp(-\tau_t) \sim 1 - \tau_t$, then the value of $I_\nu(0)$ measures τ_t as much as it does S_C or emissivity. The height gradient of I_ν is more sensitive to the height gradient of τ_t than to that of S_C or emissivity. Indeed, because τ_t varies roughly exponentially with height in an atmosphere having small gradient in kinetic temperature, and because τ_t enters the expression for I_ν exponentially, even an exponential dependence of S_C on T_e does not suffice to remove the predominance of τ_t. At those heights spanning the limb, any inference of T_e can come only indirectly, from its effect on the scale of variation of τ_t.

Thus, we order our discussion of the continuous spectrum according to these observations on the nature of the determination of $T_e(h)$ in the lowest chromosphere. First, we summarize critically the results of existing analyses of limb-darkening observations made on the disk, to obtain an idea of $S_C(\tau_C)$ in the range $\tau_C \gtrsim 0.1$. To these results we append a summary of Dunn's recent narrow-band-filter observations in the vicinity of $H\alpha$, which appear to offer a method to extend the usual limb-darkening range of observations. We thus extend $S_C(\tau_C)$ to $\tau_C \sim 0.05$, and possibly to 0.02–0.01. Second, we proceed to analyze eclipse observations made in the continuum, at heights above the steep drop in I_ν at the limb. Third, we return to look at the transition region of the limb, asking what can be said about $T_e(h)$ from attempts to infer the opacity gradient. Our considerations in this third aspect must be heavily influenced by what we infer on the dynamical structure of this transition region by interpolating between the results on the adjoining regions.

II. Critical Summary of Interpretation of Non-Eclipse Observations in the Optical Continuum

A. *Limb-Darkening Observations on the Disk*

First, we wish to obtain a summary of the results from limb-darkening measures made on the solar disk, outside eclipse, as they lead to a distribution $T_e(\tau_\lambda)$, within limits $\tau_\lambda(\min) < \tau_\lambda < \tau_\lambda(\max)$. τ_λ(min and max) refers to the limits within which $T_e(\tau_\lambda)$ is determined to some specified accuracy by the measured values of $I_\lambda(\tau_\lambda = 0,\mu)$. To obtain such information, one must first assume spherical symmetry to invert $I_\lambda(0,\mu)$ and obtain $S_C(\tau_\lambda)$; then he must assume $S_C = B_\lambda(T_e)$ to obtain $T_e(\tau_\lambda)$. We ask into the validity of these assumptions in Section C. First, however, we simply try to summarize the results in the literature, not questioning the assumptions.

One finds two main difficulties in trying to abstract from the literature a model $T_e(\tau_\lambda)$ which is in good accord with the various investigations that have been reported. First, there is the very real physical problem of uncertainty on the absolute standardization at the center of the disk, $I_\lambda(0, 1)$. Second, there is the artificially introduced problem encountered when one tries to abstract from a summary article, which has collected and combined various sets of observations, an actual mean empirical model based on an empirical consideration of the limb-darkening data alone, in contrast to what the author of the article presents as an empirical model.

Two investigations, in good accord with respect to limb-darkening measures of $I_\lambda(0,\mu)/I_\lambda(0, 1)$, may present quite different models

$T_e(\tau_\lambda)$ because of differing choices for $I_\lambda(0, 1)$. In the main, the values for $I_\lambda(0, 1)$ come from the classic Smithsonian program carried out by Abbot and collaborators, corrected for the presence of Fraunhofer lines and reduced to the center of the disk, and spot-checked by higher dispersion measures. (cf. Minnaert's summary, 1953.) The results of Minnaert's exhaustive rediscussion of these data have generally been adopted for $I_\lambda(0, 1)$. The only systematic corrections, until the last few years, lay in the infrared (cf. Peyturaux, 1952; Pierce, 1954). Recent measures in the visual spectral region (Labs, 1957; Makarova, 1957) show appreciable deviation from the Minnaert $I_\lambda(0, 1)$; the deviation lies in the direction of raising T_e at given τ_λ in this region of λ.

We note that an internal consistency check exists, if we are willing to assume the validity of LTE in the continuum, spherical symmetry, and the accuracy of theoretical values for the absorption coefficient of H^-; for the several $T_e(\tau_\lambda)$ models corresponding to different λ must give the same T_e at a given physical depth. We comment later on the condition of LTE and spherical symmetry, but departures from them will not introduce difficulty over the whole range of atmospheric regions considered. In earlier years, the intercomparison of the $T_e(\tau_\lambda)$ for different λ was mainly used to infer or check the continuous absorption coefficient. Recent theoretical (Chandrasekhar, 1958) and experimental (Branscomb and Smith, 1955; Smith and Burch, 1959) work lends considerable confidence to the numerical values of the H^- free-bound absorption coefficient. (See further notes on this point in Appendix II.) There seems little doubt that in the visual region, H^- furnishes the opacity. On the basis that any remaining discrepancy in the $T_e(h[\tau_\lambda])$ results in the visual region must come from discrepancies in the $I_\lambda(0, 1)$ determination, Pierce and Waddell (1959) conclude that the Minnaert values for $I_\lambda(0, 1)$ are preferable to the results based on the more recent measures in the visual region cited above. We adopt this conclusion of Pierce and Waddell in this monograph, noting, however, that any change in $I_\lambda(0, 1)$ in the direction of these newer results will increase $T_e(\tau_\lambda)$ for λ in the visual region (see Fig. 6-1).

Turn now to the second problem, abstracting from existing work a model $T_e(\tau_{5000})$ which is in good accord with limb-darkening measures, given the Minnaert $I_\lambda(0, 1)$ as absolute intensity standard. (Unless it is otherwise specified, we shall hereafter use optical depth

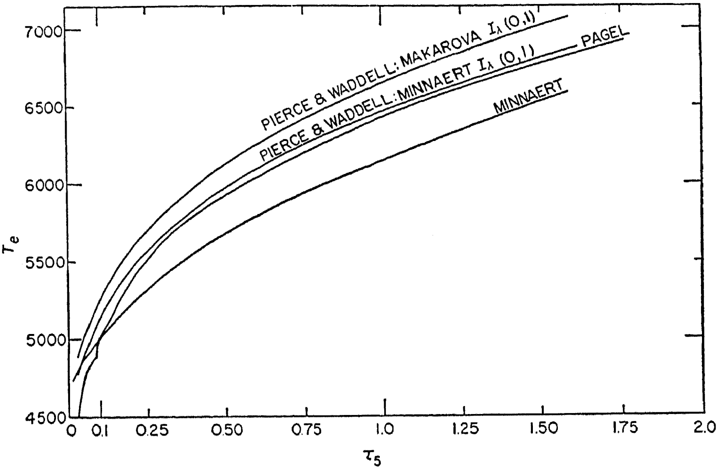

Fig. 6-1. A comparison by Pierce and Waddell of $T_e(\tau_{5000})$ determined from the same set of $I_\lambda(0, \mu)/I_\lambda(0, 1)$ but using the Minnaert $I_\lambda(0, 1)$ on the one hand and the Makarova $I_\lambda(0, 1)$ on the other.

in the continuum at 5000 A, and designate it as τ_5.) If we consider, as an example, Minnaert's detailed and comprehensive survey (1953) of the solar photosphere, the difficulties in locating a truly empirical mean model $T_e(\tau_5)$ to use as reference become clear.

In presenting his finally adopted photospheric model, Minnaert divides $T_e(\tau_5)$ into three regions of τ_5, according to the information upon which $T_e(\tau_5)$ is based:

(1) $\tau_5 > 1$: results based on consideration of line profiles, Minnaert stating that the structure of the deep photosphere is derived with more certainty from line profiles than from the continuum.

(2) $1 > \tau_5 > 0.01$: results derived observationally from limb darkening in the continuum.

(3) $0.01 > \tau_5 > 0$: results based on theoretical boundary temperature, with calculations including blanketing effect of lines.

From this description of the basis of the photospheric model, one would assume that the distribution $T_e(\tau_5)$ would be reasonably sensitive to the limb-darkening measures within the interval $0.01 < \tau_5 < 1$, but not outside the interval; and also, that the model would give a reasonable representation of the measures. Neither of these expectations is satisfied, and an inquiry into them is illuminating on this question of empirical models.

Consider first the direct question of the agreement of the model with the absolute intensity measures at the center of the disk, $I_\lambda(0, 1)$. A numerical integration, using the model, of

$$I_\lambda(0, \mu) = \int_0^\infty B_\lambda(T_e[\tau_\lambda])e^{-\tau_\lambda/\mu}\, d\tau_\lambda/\mu \tag{6-2}$$

is not necessary; an indirect approach suffices. Consider a representation of B_λ often used in inverting limb-darkening measures

$$B_\lambda(\tau_\lambda) = a_\lambda + b_\lambda\tau_\lambda + c_\lambda\tau_\lambda^2 \qquad \text{(6-3)}\dagger$$

Using (6-3) and (6-2) gives

$$I_\lambda(0,\mu) = a_\lambda + b_\lambda\mu + 2c_\lambda\mu^2 = B_\lambda(\tau_\lambda = \mu) + c_\lambda\mu^2 \tag{6-4}$$

Observationally, $c_\lambda < 0$ (limb-darkening greater than linear in μ). Thus, any satisfactory model $T_e(\tau_\lambda)$ must give

$$I_\lambda(0,\mu) < B_\lambda(T_e[\tau_\lambda = \mu]) \tag{6-5}$$

In Fig. 6-1 we have reproduced Minnaert's model, those by Pierce and Waddell already quoted, and simply for later reference a model by Pagel (1956). Table 6-1 exhibits $B_\lambda(T_e[\tau_\lambda = 1])$ computed from these models together with Minnaert's standard $I_\lambda(0, 1)$, for several values of λ. We compute τ_λ from τ_5 simply by taking the ratio of H^- absorption coefficients, using the values given by Chandrasekhar and Breen (1946). It is clear that Minnaert's model does not satisfy the criterion (6-5), but the other two models both do.

The source of the difficulty with Minnaert's model is readily located. After an initial comparison of several empirical models obtained from limb-darkening measures (cf. his Table 7), all of which show much closer agreement than the above-discussed discrepancy between Minnaert and Pierce-Waddell model, Minnaert converts

---

† The representation

$$B_\lambda(\tau_\lambda) = a_\lambda + b_\lambda\tau_\lambda + E_2(\tau_\lambda) \tag{6-3a}$$

is more often used in practice, because of its more satisfactory behavior for $\tau_\lambda = 0$ and ∞; but for our present purposes (6-3) is completely adequate and is better for exposition. Were we to use the equation in this footnote, we would reach the same conclusion as in the following.

Table 6-1. $I_\lambda(0, 1)$ Compared with $B_\lambda(T_e[\tau_\lambda = 1])$

λ	$I_\lambda(0, 1) \times 10^{-14}$	$10^{-14}B_\lambda(T_e[\tau_\lambda = 1])$ for various models Minnaert	 Pierce-Waddell	 Pagel
3700+	4.52	4.26	5.56	5.36
4000	4.60	4.17	5.42	5.27
4400	4.53	4.03	5.19	5.08
5000	4.16	3.68	4.65	4.51
5400	3.80	3.41	4.25	4.13
6000	3.31	2.96	3.61	3.52
6400	3.00	2.72	3.28	3.19
7000	2.56	2.40	2.86	2.79
8000	1.95	1.88	2.20	2.15
9000	1.52	1.49	1.72	1.69

these models from $T_e(\tau_5)$ to the form $T_e(\log P)$, apparently for facility of comparison with theoretical models. He has then formed his mean model from the $T_e(\log P)$ model (cf. his Table 10). The difficulty with such a procedure lies in the insensitivity of the $T_e(\log P)$ form of a model to considerable changes in the $T_e(\tau_\lambda)$ form [even assuming that the same chemical composition has been used in the conversion from $T_e(\tau_\lambda)$ to $T_e(\log P)$] (see Fig. 6-2). (The models are plotted as tabulated by the authors; note the slight shift in Pagel's model along the log P axis necessary to place it on the same

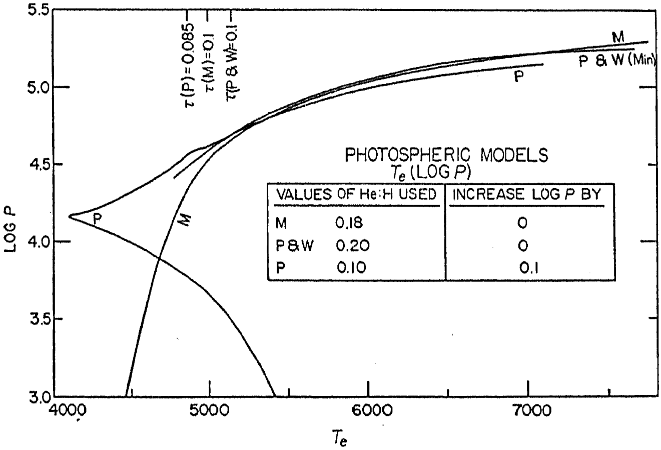

Fig. 6-2. $T_e(\log P)$ for the three models of Fig. 6-1.

basis as the others coming from the different helium abundance assumed.) It is very difficult to distinguish between the models in the region $\tau \gtrsim 0.1$, whereas the difference is marked in the $T_e(\tau_\lambda)$ plane. Thus, we can only caution against this procedure followed by Minnaert if one wishes to construct an *empirical* model in accord with the limb-darkening measures.

Turn to the second point, the region over which a model based on limb-darkening measures should have reasonable validity. To specify this region, we ask what variations in $T_e(\tau_\lambda)$ are compatible with the estimated accuracy of $I_\lambda(0,\mu)$, in the limiting regions of large and small τ_λ. We replace Eq. (6-2) by the system of equations

$$I_\lambda(0, \mu_i) = \sum_j B_\lambda(T_e[\tau_\lambda])(\tau_{\lambda j}/\mu_i)e^{-\tau_{\lambda j}/\mu_i} \,\Delta \ln \tau_\lambda \tag{6-6}$$

with

$$1 > \mu_i > \mu_{\min} \qquad \text{and} \qquad \tau_\lambda(\max) > \tau_{\lambda j} > \tau_\lambda(\min)$$

where we divide the range in $\ln \tau_\lambda$ into equal intervals according to the size of the region over which we permit the fluctuation in T_e to occur, and $\mu_{\min}$ represents the limiting region toward the limb to which the measures may be trusted. Then we may estimate the amount by which T_e may be changed throughout the given interval in $\ln \tau_\lambda$, without changing the observed $I_\lambda(0,\mu_i)$ by more than its accuracy $\Delta I_\lambda/I_\lambda$, as

$$\frac{\Delta T_e(\tau_j)}{T_e(\tau_j)} = \frac{\Delta I_\lambda(\mu_i)}{I_\lambda(\mu_i)} \left\{ \sum_k B_\lambda(\tau_k) \frac{\tau_k}{\mu_i} e^{-\tau_k/\mu_i} \right\} \times \left\{ B_\lambda(\tau_j) \frac{\tau_j}{\mu_i} e^{-\tau_j/\mu_i} \frac{e^{C_{2\lambda}/T_e}}{e^{C_{2\lambda}/T_e} - 1} \frac{C_{2\lambda}}{T_e} \right\}^{-1} \tag{6-7}$$

with

$$B_\lambda(T_e) = C_{1\lambda}(e^{C_{2\lambda}/T_e} - 1)^{-1}$$

We pick $\Delta \log \tau = 0.33$ as giving the steps in τ which are of interest here. By considering large $\tau_{\lambda j}$ for $\mu_i = 1$, and small $\tau_{\lambda j}$ at $\mu_i = \mu_{\min}$, we set, respectively, the limits of validity $\tau_\lambda(\max)$ and $\tau_\lambda(\min)$ between which the limb-darkening data give a reasonable determination of $T_e(\tau_\lambda)$. From Pierce (1954), we take $\mu_{\min} = 0.2$ for $\Delta I_\lambda/I_\lambda \lesssim 0.01$. Minnaert gives no estimate for these quantities, nor does he attempt to justify his limits 1 and 0.01 for $\tau_\lambda(\max)$ and $\tau_\lambda(\min)$, respectively. Table 6-2 contains values of the summand in Eq. (6-6), which measures the contribution of each interval in ln τ_5 to $I_\lambda(0,\mu)$, and of the ΔT_e computed from Eq. (6-7).

From these results in Table 6-2, we conclude that a model based on limb-darkening data of the extent and accuracy adopted above can be specified only within the following limits:

In the range:

$$2 \gtrsim \tau_5 \gtrsim 0.1 \qquad \Delta T_e \lesssim \pm 50^\circ \text{ over an interval 0.33 in } \log \tau_5$$

$$\left\{\begin{array}{l} 3 \gtrsim \tau_5 \gtrsim 2 \\ 0.1 \gtrsim \tau_5 \gtrsim 0.05 \end{array}\right\} \Delta T_e \lesssim \pm 100^\circ$$

$$\left\{\begin{array}{l} \tau_5 \gtrsim 4 \\ 0.05 \gtrsim \tau_5 \end{array}\right\} \Delta T_e \gtrsim \pm 200^\circ$$

Thus, we can reasonably expect to extend the model based on continuum measures alone somewhat deeper than Minnaert suggests. Indeed, it seems much more reasonable to us to rely on these measures

Table 6-2. Quantities Determining Change in $I_\lambda(0, \mu)$ Associated with $\Delta T_e(\tau_\lambda)$ for $\Delta \log \tau = 0.33$ [$T_e(\tau_5)$ from Pierce-Waddell Model]

		$B_5(T_e)[\tau_5/\mu_i]\, e^{-\tau_5/\mu_i}$				$\Delta T_e(\tau_5)$ over $\Delta \log \tau = 0.33$		
	μ_i	1	0.6	0.2	0.1	1	0.6	0.2
τ_5	T_e							
10.00	10,000	0.11	0.00	0.00	0.00	Large		
4.64	8,270	5.56	0.42	0.00	0.00	220°	Large	
2.15	7,190	$18.1\underline{5}$	7.24	0.02	0.00	50°	100°	
1.00	6,470	$17.1\underline{0}$	$14.6\underline{2}$	1.57	1.27	40°	40°	215°
0.464	5,930	8.31	10.17	6.50	5.24	80°	50°	45°
0.215	5,490	1.63	5.24	7.68	5.38	340°	80°	30°
0.100	5,140	1.33	2.07	4.44	3.18		180°	50°
0.0464	4,880	0.48	0.78	2.00	1.47			100°
0.0215	4,680	0.18	0.29	0.82	0.58			220°
0.01	4,590	0.07	0.12	0.36	0.07			480°
0.001	4,500							
	Σ	52.92	40.95	23.39	17.19			

in the continuum for estimates of T_e at $\tau_5 \gtrsim 1$ than on Minnaert's suggested use of line profiles. In the outer layers, which are our concern in this monograph, we must be prepared to admit uncertainties of about ±500° if we wish to extrapolate the model to $\tau_5 \sim 0.01$ as Minnaert suggests. By considering limb-darkening observations at wavelengths where the absorption coefficient of H^- reaches its maximum, about λ8500, we can decrease the values of τ_5 (min), for given ΔT_e, about 35 percent. We must, however, conclude that the greatest height in the atmosphere to which we can push these limb-darkening observations is about 1 to 2 scale heights, in τ_5, *below* the $\tau_5 \sim 0.01$ level.

This last conclusion is of particular interest to us in considering Pagel's model, which proposes $\tau_5 = 0.015$ for T_e(min). The actual basis for this proposal lies in Pagel's analysis (1955) of a group of weak FeI lines under the assumption that $S_L = B_{\nu_0}(T_e)$. In the present chapter, we ask only whether there may be evidence for the continuum supporting a minimum at such relatively low heights, or possibly simply supporting the trend of the Pagel model in these regions. We can only conclude that such evidence cannot be expected from limb-darkening measures out to $\mu = 0.2$. At greater optical depths, Pagel's model lies systematically below that of Pierce and Waddell, by about 50° for $\tau_5 \gtrsim 0.25$ and by about 100° for $0.1 \lesssim \tau_5 \lesssim 0.25$. Random differences of this size would be indistinguishable, according to the criteria above; the actual systematic difference should result in the Pagel model producing about 5 percent lesser values of $I_\lambda(0,\mu)$ than the observed values underlying the Pierce-Waddell model. We return to this question in asking into non-eclipse methods of extending this range of limb-darkening measures, in the following section. (See further notes on this point in Appendix II.)

Considering the results from Table 6-2, the representations of the Pierce-Waddell models in terms of the Minnaert and Makarova $I_\lambda(0, 1)$, and the comparison of the Pierce-Waddell and Pagel models, we conclude that the following is about all that can be said about conditions near the limb on the basis of limb-darkening measures on the disk out to $\mu = 0.2$:

τ_5	0.1	0.05	0.01
T_e	5150 ± 100°	4900 ± 100°	4500 ± 500°

B. Narrow-Band Interference Filter Observations Near the Limb

As a part of the calibration procedure in his study of the low chromosphere by narrow-band, interference-filter observations in Hα, Dunn (1959) also obtains observations near the limb, in the continuum near Hα. This technique enables him to solve the scattered light problem somewhat better than the more conventional types of limb-darkening studies, and he is consequently able to extend his observations considerably closer to the limb (see Fig. 6-3).

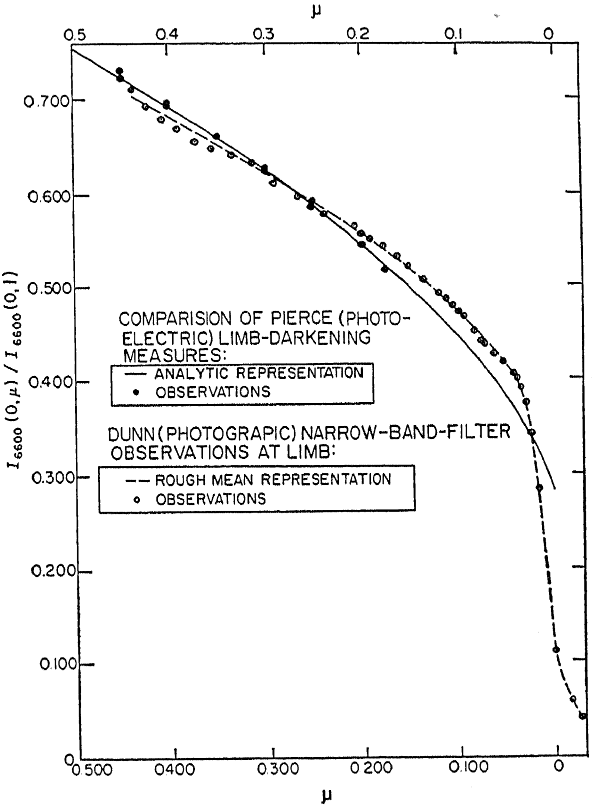

Fig. 6-3. A comparison of Dunn's observations with those underlying the Pierce-Waddell model. The solid curve through the Pierce-Waddell model is their representation by the expression $I_\lambda(0, \mu)/I_\lambda(0, 1) = 0.837 + 0.333\mu - 0.554 \{1 - \mu \ln [1 + 1/\mu]\}$, which corresponds to Eq. (6-3a) for $B_\lambda(\tau_\lambda)$ at λ6600 A.

From a conservative standpoint, there is the temptation to simply regard these two sets of data, obtained quite independently by quite different methods, as agreeing remarkably well in absolute value and variation with μ. The differences between the two curves can be reconciled by slight changes in T_e, lying within the bounds established above. In the region $\mu > 0.2$ covered by the actual Pierce-Waddell data, the difference between the two sets of measures is less than about 1.5 percent. Thus, we cannot interpret these results for $\mu > 0.2$ as suggesting any change from the Pierce-Waddell model, to within the limits $\Delta T_e = \pm 50°$ for $2 \gtrsim \tau_5 \gtrsim 0.1$ set above. In the region $\mu < 0.2$, Dunn's data lie less than 5 percent higher than the Pierce-Waddell analytic extrapolation up to $\mu \sim 0.02$, where they cross this extrapolation, thereafter dropping off rapidly relative to the Pierce-Waddell extrapolation. Increases in the Pierce-Waddell model of 50 to 75° over the interval $0.2 \gtrsim \tau_{6600} \gtrsim 0.1$ suffice to modify the predicted emission to agree with Dunn's results. At the point where the two curves cross, equating $I_\lambda(0,\mu)$ to $B_\lambda(T_e)$ gives 4750° for the corresponding value of T_e.

From a less conservative standpoint, we might try to interpret the drop-off in Dunn's curve for $\mu < 0.02$. Unfortunately, we recognize that this part of the curve is badly determined, particularly its position relative to the limb. The position of the crossover point lies just 200 km inside the limb, $\sim 0''.25$; Dunn estimates his data are reliable for heights below 500 km below the limb, and are becoming marginal near the 200-km point. Indeed, he has tried to determine this section of the curve by forcing agreement with the eclipse observations made above the limb. Thus, in discussing this section of Dunn's curve—essentially that above the crossover, but probably also that above 500 km inside the limb, $\mu \sim 0.04$—we enter the domain in which eclipse data begin to contribute. If indeed the drop in I_λ is as rapid as indicated by Dunn's results, in the region where they are marginal, then we must carefully investigate opacity effects to see whether the drop should be primarily associated with them or with an actual further drop in T_e. Thus, we defer further consideration of $I_\lambda(0, \mu \text{ or } h)$ to Section 6-IIIB. (See further notes on this point in Appendix II.)

On the basis of this intercomparison of Dunn's results with the predictions of the Pierce-Waddell model, we conclude that the model near the limb should be

τ_5	0.1	0.05	~0.02
T_e	5200 ± 50°	4900 ± 100°	~4750°

We include the last point as an *estimate* of the region farthest to the limb actually covered by data, thus the lowest value of T_e actually observed.

C. Consideration of the Assumptions Underlying Sections 6-IIA and B

1. LTE in the Continuum—$S_C = B_\nu(T_e)$. To our knowledge, the only published quantitative assessment of the departure of S_C from $B_\nu(T_e)$ (in the H^- continuum) is that by Pagel (1956, 1957, 1959), which is mainly concerned with the region $\tau_5 \lesssim 0.01$. In the following, we draw heavily upon Pagel's suggestions, but recast the approach in the structure of Chapter 4, and introduce for expository clarity several approximations in computing transition rates.

The effective contributors to the continuous emission, and opacity, in the disk spectrum are H^- and neutral hydrogen, with free-bound and free-free transitions from both. Thus, we can write S_C, using subscripts ϵ and a to denote emission and absorption, as

$$S_C = \frac{\Sigma j_{\nu i} n_{\epsilon i}}{\Sigma \alpha_{\nu i} n_{a i}} = \frac{n_e n_H K(T_e,\nu) + n_e n_H F(T_e,\nu) + n_e n_p G(T_e,\nu) + n_e n_p \mathrm{H}(T_e,\nu)}{n_{H^-}\alpha_{H^- fb} + n_e n_H \alpha_{H^- ff} + n_3 \alpha_{3,fb} + n_e n_p \alpha_{H,ff}} \tag{6-8}$$

n_H, n_{H^-}, n_e, n_p denote the concentration of neutral hydrogen, H^-, electrons, and protons, respectively; we confine our attention to 3640 A < λ < 8100° so that only the Paschen continuum of neutral hydrogen counts, denoting by n_3 the occupation number of the Paschen ground state. As in Chapter 4, we define the non-LTE factors b_k in terms of an LTE configuration having the same T_e, n_e, and concentration of ions of the energy state considered.

Denote the LTE value for a concentration by an asterisk. Then, since in LTE we have the relation (including the induced emissions as negative absorptions)

$$j_{\nu i} n^*_{\epsilon i} = a_{\nu i} n^*_{a i} B_\nu(T_e) \tag{6-9}$$

we can use it to evaluate the quantities in the numerator of Eq.

(6-8) in terms of those in the denominator, $B_\nu(T_e)$, and the appropriate b_k factors. We obtain

$$S_C = B_\nu(T_e) \times \frac{n^*_{\mathrm{H}^-}\alpha^*_{\mathrm{H}^-\mathrm{fb}} + n_{\mathrm{H}} n_e \alpha_{\mathrm{H}^-\mathrm{ff}} + n^*_3 \alpha^*_{3,\mathrm{fb}} + n_e n_p \alpha_{\mathrm{H},\mathrm{ff}}}{n_{\mathrm{H}^-}\alpha_{\mathrm{H}^-\mathrm{fb}} + n_{\mathrm{H}} n_e \alpha_{\mathrm{H}^-\mathrm{ff}} + n_3 \alpha_{3,\mathrm{fb}} + n_e n_p \alpha_{\mathrm{H},\mathrm{ff}}} \tag{6-8a}$$

Denote the ratio of each of the last three terms in the numerator to the first term by the symbols, respectively: $R_{\mathrm{H}^-\mathrm{ff}}$, $R_{3,\mathrm{fb}}$, $R_{\mathrm{H},\mathrm{ff}}$. The R's represent the ratios of the opacities in a situation where n_e, n_p, n_{H}, T_e are specified and n_{H^-} has its LTE value in terms of the specified quantities. Since we look for small departures from LTE in the present context, the difference between α^* and α, coming from non-LTE effects in the stimulated emissions, may be neglected. Then S_C may be written

$$S_C = B_\nu(T_e) \frac{1 + R_{\mathrm{H}^-\mathrm{ff}} + R_{3,\mathrm{fb}} + R_{\mathrm{H},\mathrm{ff}}}{b_{\mathrm{H}^-} + R_{\mathrm{H}^-\mathrm{ff}} + b_3 R_{3,\mathrm{fb}} + R_{\mathrm{H},\mathrm{ff}}} \tag{6-8b}$$

Making reference to the radiative cross sections collected in Chapter 4, and to the computations on H^- cross sections by Chandrasekhar and Breen (1946), we can evaluate the R's. We find, for λ5000 A, the results given in Table 6-3. It remains to evaluate b_{H^-} and b_3.

We note that the result is not sensitive to the precise value of b_3. From the Pierce-Waddell model, we find: at $T_e \sim 6000°$, $n_e \sim 3 \times 10^{13}$; at $T_e \sim 5000°$, $n_e \sim 5 \times 10^{12}$. Thus, an uncertainty of a factor of two in b_3, for b_3 near unity, amounts to less than a 1 percent uncertainty in the denominator (6-8b), thus in S_C, so long as b_{H^-} is not less than order-of-magnitude unity. Below, we find that this

Table 6-3. Numerical Values for the R's in Eq. (6-8b)

		T_e	
	4000°	5000°	6000°
$R_{\mathrm{H},\mathrm{ff}}/R_{3,\mathrm{fb}} \sim 3 \times 10^{-5} T_e \exp(-X_3)$	0.001	0.004	0.006
$R_{3,\mathrm{fb}}/R_{\mathrm{H}^-\mathrm{fb}} \sim 4 \times 10^{15} T_e^{3/2} n_e^{-1} \times \exp(-X_{13} - X_{\mathrm{H}^-})$	$7 \times 10^4/n_e$	$2 \times 10^8/n_e$	$3 \times 10^{11}/n_e$
$R_{\mathrm{H}^-\mathrm{ff}}/R_{\mathrm{H}^-\mathrm{fb}} \to$ (Chandrasekhar and Breen)	0.02	0.04	0.07

last condition on b_{H^-} is satisfied. In Section 6-III, we consider the numerical value of b_3 in the vicinity of the limb, remarking here only that it lies within this factor two of unity. Thus, any effect of b_3—indeed, of the whole term $R_{3,\mathrm{fb}}$—lies at the level of the accurracy of determination of S_C as discussed in Section 6-IIA.

For the determination of b_{H^-}, we have the simplest case of the equations of statistically steady state to solve, viz, an atom with but one bound state. Were our assumptions underlying (4-27) adequate, we should have only one non-LTE parameter to compute, b_{H^-}. These equations rest on the assumption of only photoexcitation, inelastic excitation by free electrons, and the corresponding inverse process. However, Pagel (1959) has cited recent estimates by Dalgarno to suggest that the rates of the associative detachment reaction

$$\mathrm{H} + \mathrm{H}^- \rightleftharpoons \mathrm{H}_2 + e \tag{6-9}$$

are sufficiently great to require its inclusion in the equations of statistical equilibrium for H^-. Thus, from Eq. (4-3), (4-24), and the rates corresponding to Eq. (6-9) treated as in Chapter 4, we have the equation of statistical equilibrium for the bound state of H^-:

$$\begin{aligned} n_e n_{\mathrm{H}^-}(1 - b_{\mathrm{H}^-}{}^{-1})D_{e,\mathrm{H}^-} &+ n_{\mathrm{H}} n_{\mathrm{H}^-}[1 - (b_{\mathrm{H}_2}/b_{\mathrm{H}^-})]D_{\mathrm{H},\mathrm{H}^-} \\ &= 4\pi \left\{ n^*_{\mathrm{H}^-} \int_{\chi_{\mathrm{H}^-}}^{\infty} \alpha^*_{\mathrm{H}^-} B_\nu(T_e)\, d\nu/h\nu \right. \\ &\qquad \left. - n_{\mathrm{H}^-} \int_{\chi_{\mathrm{H}^-}}^{\infty} \alpha_{\mathrm{H}^-} \bar{I}_\nu \, d\nu/h\nu \right\} \end{aligned} \tag{6-10}$$

As in the preceding, we have combined stimulated emissions into the absorption coefficient. D_{e,H^-} and $D_{\mathrm{H},\mathrm{H}^-}$ denote rates of collisional ionization and associative detachment, per unit concentration of interacting particles, respectively. Solving Eq. (6-10) for $b_{\mathrm{H}^-} = n_{\mathrm{H}^-}/n^*_{\mathrm{H}^-}$, we find

$$b_{\mathrm{H}^-} = \frac{n_e D_{e,\mathrm{H}^-} + n_{\mathrm{H}} D_{\mathrm{H},\mathrm{H}^-} b_{\mathrm{H}_2} + 4\pi \int_{\chi_{\mathrm{H}^-}}^{\infty} \alpha^*_{\mathrm{H}^-} B_\nu(T_e)\, d\nu/h\nu}{n_e D_{e,\mathrm{H}^-} + n_{\mathrm{H}} D_{\mathrm{H},\mathrm{H}^-} + 4\pi \int_{\chi_{\mathrm{H}^-}}^{\infty} \alpha_{\mathrm{H}^-} \bar{I}_\nu \, d\nu/h\nu} \tag{6-11}$$

We want to form a first estimate of the relative sizes of these terms. We can write [cf. Eq. (4-24)]

$$D_{e,\mathrm{H}} = (2/\sqrt{\pi})\,\pi a_0^2\,\bar{Q}_{e,\mathrm{H}^-}\,(2kT_e/m)^{1/2}\,[X_{\mathrm{H}^-} + 1]\,e^{-X_{\mathrm{H}^-}} \tag{6-12}$$

Geltman's recent computations (1959) give $\bar{Q}_{e,\mathrm{H}^-}$ about unity; so we set $\bar{Q}_{e,\mathrm{H}^-} = 1$. Also, any reasonable kind of representation of Chandrasekhar's values for $\alpha_{\mathrm{H}^-}(\nu)$ gives

$$4\pi \int_{X_{\mathrm{H}^-}}^{\infty} \alpha^*_{\mathrm{H}^-} B_\nu(T_e)\,d\nu/\nu \sim 1 - 2 \times 10^3 T_e e^{-X_{\mathrm{H}^-}} \tag{6-13}$$

(use 1.5 as coefficient)

For the integral over $\bar{I}_\nu$, we note that the observed emission from the whole solar disk mimics $B_\nu(T_e \sim 5800°)$ over the interval $3700 < \lambda < 16000$. Thus, we use $\bar{I}_\nu \sim 0.5B_\nu(5800°)$ to evaluate the integral over $\bar{I}_\nu$ in regions of very small τ_5, where there is the greatest likelihood of a difference between S_C and $B_\nu(T_e)$. At greater τ_5, we use $\bar{I}_\nu \sim 0.5\,(1 + 1.5\tau_5)\,B_\nu(5800°)$. For $D_{\mathrm{H},\mathrm{H}^-}$, Pagel quotes an estimate of Dalgarno that the value lies within a factor 4 of $10^{-9.5}$ cm^3 sec^{-1} over the range of T_e of interest. To evaluate b_{H_2}, we should have to investigate the problem of the statistically steady state for H_2. To our knowledge, no investigations of the possible non-LTE configurations of molecules in the solar atmosphere have been attempted, or even considered; the problems of lack of cross sections discussed in Chapter 4 apply with equal force to these molecular reactions. If the contribution of $D_{\mathrm{H},\mathrm{H}^-}$ is small, the problem is not critical; if the contribution from $D_{\mathrm{H},\mathrm{H}^-}$ predominates overwhelmingly, the value of b_{H^-} is extremely sensitive to the net rate

$$(1 - b_{\mathrm{H}_2}/b_{\mathrm{H}^-})D_{\mathrm{H},\mathrm{H}^-}.$$

Here, we simply proceed under the pious hope that the principal rates characterizing the H_2 equilibrium are sufficient to maintain an LTE concentration.

With these values, we use our results from Sections 6-IIA and B, together with the estimates of n_H and n_e taken from the Pierce-Waddell model, to obtain the values in Table 6-4 for the quantities in Eq. (6-11). We have computed two sets of values for b_{H^-}; those following directly from the above value of $D_{\mathrm{H},\mathrm{H}^-}$, and a set corresponding to a decrease in $D_{\mathrm{H},\mathrm{H}^-}$ by a factor 4. From the values in Table 6-4, we draw several conclusions:

First, if the value of $D_{\mathrm{H},\mathrm{H}^-}$ lies close to Dalgarno's numerical estimate, then the b_{H^-} in the next-to-last line of Table 6-4 shows, when applied to Eq. (6-8b), that S_C differs from $B_\nu(T_e)$ by a maximum of 1 to 2 percent in the range covered by disk observations. This amounts to 10 to 20° in T_e, so is negligible in comparison with the accuracy of determination discussed in Section 6-IIA.

Second, if $D_{\mathrm{H},\mathrm{H}^-}$ has been overestimated by no more than the factor four used in the last line of Table 6-4, the difference between S_C and $B_\nu(T_e)$ still does not exceed about 5 percent, which is about 50°. Because the difference is systematic for $\tau \gtrsim 0.05$, the effect is an overestimate of T_e of this amount from the observations, in the region $0.05 \lesssim \tau < 0.4$. Again, since this uncertainty is the same size as that coming from the one percent observational accuracy discussed in Section 6-IIA, its neglect is not serious.

Table 6-4. Estimate of b_{H^-} from Eq. (6-11)

τ_5	0.01	0.05	0.1	0.2	0.375	1.0
T_e	4400°	4900°	5200°	5450°	5800°	6470°
$\log n_e$	12.32	12.57	12.84	12.99	13.28	13.87
$\log n_{\mathrm{H}}$	16.24	16.61	16.75	16.89	17.01	17.11
$n_e D_{e,\mathrm{H}^-}$	3.2×10^3	6.8×10^3	1.4×10^4	2.1×10^4	4.5×10^4	2.0×10^5
$n_{\mathrm{H}} D_{\mathrm{H},\mathrm{H}^-}$	0.6×10^7	1.3×10^7	1.8×10^7	2.5×10^7	3.3×10^7	4.1×10^7
$4\pi \int \alpha^*_{\mathrm{H}^-} \times B_\nu(T_e)d\nu/h\nu$	0.9×10^6	1.2×10^6	1.5×10^6	1.7×10^6	1.9×10^6	2.5×10^6
b_{H^-}	0.99	1.02	1.02	1.02	1.01	1.00
b_{H^-}(with $D_{\mathrm{H},\mathrm{H}^-}/4$)	0.98	1.04	1.07	1.06	1.04	1.01

Third, our approximations in evaluating the rates other than $D_{\mathrm{H},\mathrm{H}^-}$ are clearly quite adequate, so long as $D_{\mathrm{H},\mathrm{H}^-}$ does not drop much below the limit set on its uncertainty.

Fourth, if b_{H_2} departs from unity by as much as 10 percent, its effect predominates on b_{H^-}; and the resulting uncertainty exceeds that due to observational inaccuracy. It is, therefore, clear that the uncertainty on b_{H_2} is the major one in accepting the conclusion reached here, that deviation of S_C from $B_\nu(T_e)$ may be neglected in the interpretation of disk observations carried out at the one percent level of accuracy.

2. Spherical Symmetry of the Solar Photosphere. *a. Considerations Based on White-Light Granulation.* On the disk, the white-light granulation provides the direct evidence of a general departure from a strict condition of spherical symmetry. In passing from the qualitative observation that brightness fluctuations called granules exist, to a quantitative interpretation of the fluctuation as $\Delta T_e(\mathbf{r})$, there are two problems: what is the actual quantitative value of the brightness fluctuation; how does one translate this value into $\Delta T_e(\mathbf{r})$.

Published values of the observed brightness fluctuation range from about 5 to about 35 percent; the size of the structure associated with these fluctuations ranges from about $0''.4$ to $15''$ or about 300 to 11,000 km. There is general agreement that the largest sizes represent unresolved groups of individual granules. There is general disagreement on the size to be attached to an individual granule—or, better, the frequency distribution of granule sizes. The point is critical in attaching physical meaning to the observed brightness fluctuation; for it is frequently argued that the smaller brightness fluctuation actually represents a greater fluctuation from an individual granule smeared out over several granules and their surroundings.

The best of Janssen's original observations (1896) showed a size range for individual features of about 350 to 2000 km with the average $\sim$ 1000 km. By arguments based on a comparison of "turbulent" velocities in the solar atmosphere as inferred from line profiles on the one hand and from total line absorption on the other, Richardson and Schwarzschild (1950) suggested that even features of a 1600-km dimension represented statistical blends of smaller, unresolved, elements. They concluded that the diameter of the "turbulent" elements of maximum average velocity was 100 to 200 km; in a later paper, Frenkiel and Schwarzschild (1952) revised the size to 300 km. In accordance with these sizes, they suggested that random fluctuations in T_e should exist which would correspond to 30 to 35 percent in brightness. On the other hand, Thiessen (1955) contends that visual observations show the characteristic sizes of individual granules to be 750 to 1500 km, with associated brightness fluctuations 30 to 35 percent.

In the last few years, observers have essentially reconfirmed Janssen's original observations as the true features of solar granulation. Rösch's work at the Pic du Midi (1955, et seq.) shows the same features near the center of the disk, and demonstrates that individual granules are still visible up to $\sim$ $5''$ from the limb, with the geometrical contour of the 1 to 2″ feature changing from center to limb as one would expect if it were a single entity, not a statistical ensemble of much smaller entities. Balloon observations have essentially reproduced Janssen's best observations (Blackwell and Dolfus, 1957; Schwarzschild, 1958) Schwarzschild's results have at this time not been completely analyzed, but he and Mrs. Schwarzschild find (1959) that the size range appears to be 300 to 3000 km. Even these balloon observations give no evidence of the very small granules with the very high brightness contrast suggested in the preceding paragraph.

With these results on the size distribution, and the results of three detailed photographic investigations of brightness fluctuations showing excellent agreement—ten Bruggencate, Grotrian, von der Pahlen (1938) at λ 3900, 4.3 per cent; ten Bruggencate and Muller (1942) at λ 4350, 8 percent; Richardson and Schwarzschild (1950) at λ5800, 5.0 percent—we believe that granulation may be best characterized as a brightness fluctuation of about 5 percent across an individual element whose average diameter is about 1000 km. There is a measurable contrast up to at least 5″ from the solar limb, or to $\mu \sim 0.1$; but there is as yet no published material available on the quantitative change in contrast to the limb. (It is to be hoped that Rösch's and Schwarzschild's investigations will provide this important information in the near future.)

We turn now to the second question, how to translate this brightness fluctuation into $\Delta T_e(\mathbf{r})$. Too often, one finds in discussions of granulation simply the statement that a certain contrast corresponds to a certain ΔT_e value, with no comment on where in the atmosphere this ΔT_e occurs. Recalling our computation of the ΔT_e associated with a given error in observed intensity, and looking at Table 6-2, it is clear that the value of ΔT_e associated with a given contrast is a strong function of where ΔT_e occurs. The point has been stressed by de Jager and Pecker (1955). Historically, the granulation has been associated with the solar convection zone, and the granules interpreted as the actual convective elements. On this basis, the elements should not exist at heights much above the top of the convective zone, which occurs near $\tau_5 \sim 1$ according to current thinking (Minnaert, 1953). Böhm-Vitense (1953) computes, from a model based on such a picture of granulation, that the granules should extend up to $\tau \sim 0.3$. Making reference to Table 6-2, we note that $\Delta T_e \sim 50°$ at depths everywhere below $\tau \sim 0.3$ suffices to produce this 5 percent contrast at the center of the disk. The same is essentially true at $\mu = 0.6$. At $\mu \sim 0.2$, the contrast would drop to $\sim$1.5 percent for the same ΔT_e, or require ΔT_e to extend upward to $\mu \sim 0.1$ to give the same contrast; at $\mu \sim 0.1$, the contrast would be undetectable. If we wish to confine ΔT_e to regions below the $\tau = 0.3$ level, and to detect a granule at $\mu = 0.1$ (assuming a contrast of 1 to 2 percent is necessary for detection), then we require $\Delta T_e \sim 100$ to 200° at $\tau \sim 0.3$. To hold the contrast to 5 percent at the center of the disk, we require, however, ΔT_e to decrease rapidly downward. For example, if we set $\Delta T_e = 200°$ over the interval 0.33 in $\log \tau$ centered at $\tau = 0.46$, $\Delta T_e = 50°$ over the same interval centered at $\tau = 1.00$, and $\Delta T_e = 0$ elsewhere, we find contrasts: 5 percent at $\mu = 1$, 8 percent at $\mu = 0.6$ and 0.2, and 2 percent at $\mu = 0.1$. Changing ΔT_e to 150° in the interval centered at $\tau = 0.46$, keeping it at 50° around $\tau = 1$ and zero elsewhere, we find contrasts: 4 percent at $\mu = 1$, 6 percent at $\mu = 0.6$ and 0.2, and 1.5 percent at $\mu = 0.1$.

Clearly, neither the data presently available on granule-contrast as a function of position on the disk, nor the theory of granulation interpreted as actual convection elements, are adequate to distinguish between these last two alternatives, nor between these and other alternatives based on a finer mesh in $\Delta \log \tau$ and more continuity in the variation of ΔT_e. (Indeed, Böhm-Vitense's actual theory predicts extreme ΔT_e values $\lesssim 3500°$ at given geometric position, extreme $\Delta T_e \lesssim 1000°$ at given τ, and a mean $\Delta T_e \sim 300$ to 400° at given τ. Here, however, we are interested in the theory only as giving a rough value for the smallest τ which the elements might reach.) We wish only to emphasize that *if* we interpret the individual granules as convective elements not extending above some $\tau \sim 0.3$, and *if* we can detect individual granules out to $\mu \sim 0.1$ with a contrast 1 to 2 percent, then we require $\Delta T_e \sim 100$ to 200° near $\tau \sim 0.3$ and ΔT_e dropping off sharply on either side of $\tau \sim 0.3$. This requirement on ΔT_e predicts a center-limb variation in granule contrast which may show a maximum between $\mu = 0.6$ and 0.2. Any modification in the picture which acts to extend upward the region of emission from the granules acts to make more uniform in depth, and smaller, the ΔT_e; and, conversely.

A means to extend upward the influence on $\Delta T_e(\mathbf{r})$ of the convective elements lies in the suggestion (Biermann, 1946; Schwarzschild, 1948) that the convection may become unstable and produce turbulence, with the corresponding pressure fluctuations producing acoustic waves, which propagate upward. However, to accomplish the purpose for which they were suggested, viz., to provide the energy supply to maintain the corona and chromosphere, the amplitude of these progressive waves must be so small in the photospheric regions as to cause negligible ΔT_e; otherwise, the waves must dissipate in the upper photosphere or lowest chromosphere. (cf. van de Hulst, 1953).

Alternatively, there is the suggestion (Schatzman, 1953, 1954; Thomas, 1954) that the observed features of granulation are not the convective elements but are the progressive waves generated by the convection. The wave amplitude is then by definition much greater; no attempt is made to require the waves to penetrate above the lowest chromosphere, so the ΔT_e associated with the wave in the photospheric regions must be significant. Radiative cooling will, however, hold ΔT_e in such a wave below 150 to 200° in those regions where the local continuous opacity is not too high. For reference, we note that a "granule" of dimension 1″ will have the following (horizontal) optical thickness:

τ	0.01	0.05	0.1	0.2	0.375	0.1
$\Delta\tau$	1	3	6	10	21	73

Thus, for $\tau \lesssim 0.05$ the granules are effectively completely transparent to radiation from surrounding regions, and radiative cooling is highly effective; at $\tau \sim 0.1$, the center of the granule begins to be seen by its neighborhood (cf. Table 6-2). If we can produce a combination of convective element and progressive wave which maintains a $\Delta T_e \sim 50°$ over the whole region $0.1 \lesssim \tau \lesssim 2$, we can match the observations without producing a granule contrast which first rises, then falls toward the limb.

Summarizing, the evidence is strong that we must admit fluctuations $\Delta T_e \sim 50°$ near $\tau \sim 1$, $50° \lesssim \Delta T_e \lesssim 150°$ near $\tau \sim 0.3$, and $\Delta T_e \lesssim 150°$ for $0.1 \gtrsim \tau \gtrsim 0.01$. Any more precise narrowing of these limits, or a more detailed specification of the variation of ΔT_e must await more detailed studies of the center-limb variation of granule contrast.

b. Considerations Based on the Fraunhofer Lines. Although we restrict ourselves to the continuum in this chapter, models of an inhomogeneous lower solar atmosphere have been based so heavily upon discussions of absorption lines (Böhm, 1954; de Jager, 1954a, 1954b, 1957a; Voigt, 1956) that a comment on this approach is in order here. In brief, we give small weight to the conclusions based on these analyses, for two reasons: (1) From a consistency standpoint, the models are incompatible with each other and with the results just discussed on white-light granulation; (2) from a theoretical standpoint, the analyses have to all practical purposes ignored non-LTE effects.

Consider first the consistency argument. Böhm attempts to tie his model to Böhm-Vitense's treatment of the convection-zone mentioned above. In consequence, his ΔT_e *increase* monontonically with decreasing τ, with values $\sim \pm 500^\circ$ at $\tau = 1$ and $\pm 700^\circ$ at $\tau = 0.1$. He concludes that such a model is necessary to provide an adequate representation of the center-limb variation of the NaD and FeI a^3F–y^3F° lines. On the other hand, Voigt adopts a model with ΔT_e *decreasing* monotonically with decreasing τ, with values $\sim \pm 500^\circ$ at $\tau = 1$, $\pm 100^\circ$ at $\tau = 0.1$, and $\Delta T_e = 0$ for $\tau \lesssim 0.03$. Voigt concludes that such a model is necessary to represent the profiles and center-limb variations of OI λ7772/74/75. Thus, there are two alternatives: either the behavior of the two sets of lines studied by Böhm and Voigt are determined wholly by conditions at τ (*continuum*) $\gtrsim 1$, or it is impossible to satisfy the behavior of both sets in the same kind of atmosphere. The first alternative would vitiate any conclusions on a model above $\tau \sim 1$, and is, moreover, not realistic physically. Thus, there remains only the second alternative, which simply states that one must look elsewhere than to temperature inhomogeneities to explain the material considered by these authors. We note further that fluctuations $\Delta T_e \sim 500^\circ$ near $\tau = 1$ will stand in strong disagreement with the picture based on white-light granulation.

Our objections from a theoretical standpoint come under this category of looking elsewhere for a key to the interpretation of the behavior of the Fraunhofer lines. In each of these discussions—by Böhm, de Jager, and Voigt—it is taken as self-evident that $S_L = S_C = B_\nu(T_e)$. Yet, in Chapter 4 we have shown that the resonance lines of the neutral metals—and the early Balmer lines of hydrogen—have a photoelectric type S_L, which at least to a first approximation has no term directly dependent upon $B_\nu(T_e)$. Thus, for the NaD lines we certainly cannot accept an analysis based upon $S_L = S_C$. The FeI a^3F–y^3F° lines should be analysed individually before a reliable general conclusion can be reached; but because the lines as so deep-lying relative to the ground state, one would be tempted to consider the photoelectric—S_L as a better first approximation than $B_\nu(T_e)$. Indeed, Böhm finds it necessary to introduce departures from the LTE occupation numbers in the ground state, by assuming an increased "ionization temperature" over the local value of T_e in the upper photosphere ($\tau \lesssim 0.1$). *Particularly* for such low-lying FeI levels, however, it is obvious that any significant departure from LTE in the ionization will reflect to similar degree in the occupation number of these levels and thus in S_L; so we consider Böhm's approach to be internally inconsistent. Finally, we note that Voigt follows essentially the same procedure in the OI lines—$S_L = S_C = B_\nu(T_e)$ and a correction in the higher photospheric layers for a non-LTE occupation number in the ground state. Because the energy-level configuration from which these lines arise resembles so closely that of the Balmer lines, we again would consider a photoelectric type S_L as a far more reliable approximation than $S_L = B_\nu(T_e)$.

We should emphasize that we hardly wish to be understood as arguing against the existence of inhomogeneities in T_e, or their possible utility in interpreting the behavior of the Fraunhofer lines on the disk. We urge only that investigations into the possible occurrence of such inhomogeneities be conducted with a proper skepticism for the applicability of LTE concepts, and with a critical attempt to evaluate non-LTE effects.

III. Interpretation of Eclipse Observations in the Optical Continuum

In the introduction to this chapter, we stressed the importance of determining where in the upper photosphere or lowest chromosphere T_e reaches its minimum value, and the rate of its rise thereafter. In summarizing the results of analysis of the continuum observed on the disk, we concluded in the preceding section that T_e is still decreasing monotonically outward at $\tau_5 \sim 0.02$, where it has a value about 4700°. Analysis of granulation observations suggests fluctuations in T_e of size about 50° near $\tau_5 = 1$, and $\gtrsim 50°$—possibly reaching about 150°—near $\tau_5 = 0.1$. No empirical conclusion can be drawn on the presence, or size, of such fluctuations in the region $\tau_5 \lesssim 0.1$, where they become of most interest in this question of behavior of T_e near minimum.

In the first part of the present section, we attempt to set an unambiguous upper limit to the height of occurrence of $T_e(\mathrm{min})$ by passing over the region of the sharp solar limb, where the height variation of the emission is a strong function of the total optical thickness of the atmospheric region observed, and investigating those regions where the emission is simply the integral of the emissivity along the line of sight. There, properly taking account of non-LTE effects, we can relate emissivity directly to T_e, and obtain $T_e(h)$. In the second part, we return to the intermediate boundary regions, to attempt to narrow the limits on the position and magnitude of $T_e(\mathrm{min})$.

A. Regions Where the Emission Is Simply the Integral of the Emissivity

As summarized in Chapter 2, we consider emission from the continuum at the 1952 eclipse in two spectral regions: λ4700, where we have data covering the height range $-120 < h < 48, 500$ km; and at the head of the Balmer series, where we have data covering the height range $0 \lesssim h < 2400$ km. In our preliminary discussion of these data (Athay, Menzel, Pecker, Thomas, 1955), we considered the effective source of the emission at λ4700 to lie in free-bound and free-free emission from H^-, and scattering of photospheric radiation by free electrons, with negligible contribution from free-bound and free-free transitions of neutral hydrogen. The neglect of the Paschen free-bound emission is not warranted, and we include it here. de Jager (1957b) and Thompson (1958) argue that Thompson scattering from neutral hydrogen is important; de Jager asserts that it dominates the emission at λ4700 for $500 < h < 1000$ km. We have disputed this conclusion (Athay, 1959), but it is as easy to carry the Rayleigh term along in the analysis as it is to enter an a priori justification of its neglect. Because we have extrapolated the emission in the continuum above the Balmer series head to λ3640 and subtracted it from the observed emission there, the residual intensity at λ3640 should result from Balmer free-bound transitions only.

Following the procedure of Section 6-IIC1, using α'_ν as the absorption coefficient α_ν modified to include induced emissions and a superscript* to denote the LTE configuration, we obtain the contribution to the emissivity from each of these sources (ergs cm^{-3} in all directions per unit frequency):

Scattering of photospheric radiation, $\bar{I}_{\nu p}$:

Electrons: $$j_\nu = 2\pi\, \bar{I}_{\nu p} n_e \sigma_T \tag{6-14a}$$

Neutral hydrogen: $j_\nu = 2\pi \bar{I}_{\nu p} n_{\mathrm{H}} (1026\ \text{Å}/\lambda)^4 \sigma_T$ (Unsold, 1955) (6-14b)

$\sigma_T = 8\pi\epsilon^4/3m^2c^4 = 6.65 \times 10^{-25}$; $\bar{I}_{\nu p}(\lambda 4700) = 2.28 \times 10^{-5}$ (Minnaert, 1953, Table 1)

H$^-$ *emission:*

fb: $$\begin{aligned} j_\nu &= 4\pi n^*_{\mathrm{H}^-}\, \alpha'^*_{\mathrm{H}^-\mathrm{fb}} B_\nu(T_e) \\ &= 4.14 \times 10^{-16} (2\pi h\nu^3/c^2) n_e T_e^{-3/2} e^{-X_\nu} e^{X_{\mathrm{H}^-}} n_{\mathrm{H}} \alpha_{\mathrm{H}^-\mathrm{fb}} \end{aligned} \tag{6-14c}$$

$$\alpha_{\mathrm{H}^-\mathrm{fb}} = 3.14 \times 10^{-17} \text{ at } \lambda 4700 \text{ (Chandrasekhar 1958)}$$

ff: $$\begin{aligned} j_\nu &= 4\pi n_e n_{\mathrm{H}} \alpha'^*_{\mathrm{H}^-\mathrm{ff}} B_\nu(T_e) \\ &= 4.14 \times 10^{-16} (8\pi h\nu^3/3c^2) n_e T_e e^{-X_\nu} n_{\mathrm{H}} a_{\mathrm{H}^-\mathrm{ff}} \end{aligned} \tag{6-14d}$$

where $a_{\mathrm{H}^-\mathrm{ff}}$ is the absorption coefficient per neutral hydrogen atom and per unit electron pressure tabulated by Chandrasekhar and Breen (1946).

T_e	3600	4200	5040	5600	6300	7200
$a_{\mathrm{H}^-\mathrm{ff}} \times 10^{27}$	4.82	3.86	2.97	2.55	2.15	1.79

H *emission:*

fb: $$j_\nu = 2.15 \times 10^{-32} g_{\mathrm{fb}} n^{-3} n_p n_e T_e^{-3/2} e^{X_n} e^{-X_\nu} \tag{6-14e}$$

where g_{fb} is the Gaunt factor tabulated by Menzel and Pekeris (1935) and n is the quantum number of the level. Thus,

Balmer fb at λ3646:

$$j_\nu = 2.35 \times 10^{-33} n_p n_e T_e^{-3/2} \tag{6-14f}$$

Paschen fb at λ4700:

$$j_\nu = 7.75 \times 10^{-34} n_p n_e T_e^{-3/2} e^{X_3} e^{-X_\nu} \tag{6-14g}$$

where we have used 0.876 and 0.975 for the g factors for the Balmer emission at λ3646 and Paschen at λ4700, respectively. A g factor of 0.986 at λ4700 for the free-free transitions gives ff: $$j_\nu = 6.72 \times 10^{-38} n_p n_e T_e^{-1/2} e^{-X_\nu} \qquad \text{(6-14h)}$$

The sum of the j_ν at the particular wavelength equals $\mathcal{E}$ (in the notation of Chapter 2). From Chapter 2, we have $\mathcal{E}_{4700}$ given by Eq. (2-10). To obtain $\mathcal{E}_{3646}$, we invert Eq. (2-1) with $\tau_\lambda = 0$, using Eq. (2-11a) for E_{3646}. Thus,

$$\mathcal{E}_{3646} = 0.49 \times 10^{-17} E_{3646} = 3.8 \times 10^{-15} \exp(-2.2l) \qquad \text{(6-15)}$$

where l is h measured in units of 10^8 cm. *This relation* (6-15) *is valid only in the height range* $500 < h < 2400$ *km.* For heights above 2400 km, we have no data; for heights below 500 km, we must proceed numerically because of the maximum in F_{3646} near 500 km, which was discussed in Chapter 2.

From the preceding theoretical expressions for j_ν, and the observational results leading to $\mathcal{E}_\nu$, we see that we have two relations between the four quantities n_e, n_p, T_e, n_H. (Under the assumption of a spherically symmetric atmosphere, which we have already implicitly used in the manner of our converting E_ν to $\mathcal{E}_\nu$.) As Zirker has emphasized (1956), these three observational relations serve to fix n_H with very little uncertainty in the region in which emission from H^- dominates, because of the sensitivity of the H^- emission to T_e through the value of n_H. In our preliminary discussion of these data, we assumed that in these atmospheric regions the departure of n_H from ionization equilibrium would be small enough that this sensitivity of n_H to T_e would serve to fix T_e reasonably closely. Zirker's calculations showed that with these data, an uncertainty of a factor 2 in n_H corresponded to an uncertainty of ±1500° in T_e and an uncertainty of a factor 10^2 to 10^3 in b_1, at 500 km. (That is, a total range of a factor 4 in n_H at 500 km is accompanied by a range of about 3000° in T_e and about 10^5 in b_1.) In consequence, we have developed (Pottasch and Thomas, 1959) the simplified approach to b_1 outlined in Section 4-IIA2, and we use this method for obtaining $b_1(T_e, n_e)$ as a third relation to adjoin to the two observational relations in analysing the data. An assumed hydrogen: metal ratio would complete the set of relations required for determinacy of solution; however, above the 500 km level a preliminary computation shows hydrogen, rather than the metals, to supply the electrons, so $n_e = n_p$ and no assumption on hydrogen:metal abundance is required. We proceed under the assumption $n_e = n_p$, justifying it by self-consistency from the results; below 500 km we introduce a hydrogen:metal abundance where necessary.

1. The Region $500 < h < 2400$ **km.** *Wholly empirical model.* From Eqs. (6-14f) and (6-15) we obtain

$$n_e n_p T_e^{-3/2} = 1.62 \times 10^{18} e^{-2.2l} = f(h) \tag{6-16}$$

From Eqs. (6-14) through (6-14d), (6-14g), and (2-10) we have, replacing the number of neutral hydrogen atoms n_{H} by the number n_1 in the ground state, expressing n_1 by Eq. (4-3), and substituting $f(h)$ for $n_e n_p T_e^{-3/2}$,

$$\begin{aligned} n_e + 6.78 \times 10^{-22} f(h) b_1 e^{X_1} \{ 1.39 \times 10^3 + f n_e^{-1} e^{-X_\Delta}(1 + \psi) \} & \\ + 8.13 \times 10^{-6} f e^{-X_\delta}(1 + \theta) = g(h) & \end{aligned} \tag{6-17}$$

where

$$\begin{aligned} X_\Delta &= X_\nu - X_{\mathrm{H}^-} = 2.18/10^{-4} T_e; \qquad X_\delta = X_\nu - X_3 = 1.31/10^{-4} T_e \\ \psi &= 1.28 \times 10^{-10} T_e^{5/2} e^{-X_{\mathrm{H}^-}} (a_{\mathrm{H}^-\mathrm{ff}}/3.10^{-27}) \\ \theta &= 0.87 \times 10^{-4} T_e e^{-X_3} \end{aligned} \tag{6-18}$$

$$\begin{aligned} g(h) = {} & 1.14 \times 10^{14} e^{-7l} + 3.51 \times 10^{12} e^{-2.2l} + 7.38 \times 10^{10} e^{-0.6l} \\ & + 4.87 \times 10^{10} e^{-0.4l} + 2.5 \times 10^9 e^{-0.07l} + 1.0 \times 10^8 e^{-0.005l} \end{aligned} \tag{6-19}$$

In section 4-IIA2 we found three regions of behavior of b_1; and Fig. 4-1, computed for an atmosphere having constant n_e and T_e, provides a rough guide to these regions in terms of τ_{LyC}, the optical depth at the head of the Lyman continuum. Region 1, $\tau_{\mathrm{LyC}} \gtrsim 10^2$, has high-enough opacity for detailed balancing in the Lyman continuum, but transparency in the Balmer continuum, and here $b_1 = b_1(T_e)$. In region 2, $0.1 \lesssim \tau_{\mathrm{LyC}} \lesssim 10^2$, b_1 depends upon T_e, n_e, and the radiation field in the Lyman continuum. Region 3 has negligible opacity in the Lyman continuum, and $b_1 = F(T_e)/n_e$. We can make a tentative estimate of τ_{LyC} from our preliminary analysis, where we found $n_{\mathrm{H}} \sim 10^{14}$ at 500 km. The scale height of $g(h)$, Eq. (6-19), provides a rough estimate of that of n_{H}, in the region where H^- emission predominates, and varies from ~250 km at 500 km height to ~1000 km. at 2400-km height. With $\alpha_{\mathrm{LyC}} \sim 6 \times 10^{-18}$, we estimate $\tau_{\mathrm{LyC}} \sim 10^4$ at 500 km. and $\sim 10^2$ at 2400 km. Thus, we estimate that the height range $500 \text{ km} < h < 2400$ km falls mainly in region 1 of the b_1 variation; but because we are likely to be seriously in error with the assumptions underlying these estimates at the upper end of the interval, the solution may enter region 2 there. Therefore, we approach, by approximation, the solution for $T_e(h)$ and $n_e(h)$ from Eqs. (6-16), (6-17), and that giving $b_1(T_e, n_e)$. In the first approximation, we use Eq. (4-45), which characterizes $b_1(T_e, n_e)$ in region 1, to compute n_e, T_e, n_{H} for 500 km $< h <$ 2400 km. With these values, we obtain better values for τ_{LyC} and ask whether we need modify these first-approximation results by solving a transfer equation in the Lyman continuum, thus entering region 2.

Equation (4-45) gives $b_1(T_e,\Delta;Y_2)$. Y_2 is defined by $\bar{I}'_\lambda(\tau = 0) = B_\lambda(T_r)$, where $\bar{I}'_\lambda$ is $\bar{I}_\lambda$ computed over one hemisphere, thus giving $W_{2\kappa} = \frac{1}{2}$ in Eq. (4-45). From Minnaert's values (1953) for $I_\lambda(\tau = 0, \mu = 1)$ and $\bar{I}'_\lambda/I_\lambda(\mu = 1)$, we find $Y_2 = 6.62$ (corresponding to $T_r =$ 5940°). Substituting numerical values for the various quantities, we obtain from Eq. (4-45)

$$b_1 = 0.994 \times 10^4(e^{-X_2}/X_2)[1 + 0.904 b_3 X_3 e^{X_3}\{\text{H}\alpha\}]/(1 + M) \qquad (6\text{-}20)$$

$$b_2 = b_1(1 + M) \qquad (6\text{-}21)$$

$$M = 0.26[(X_1 + 1)/(X_{12} + 1)][1 + 0.34(10^{-4}T_e)]e^{-X_2} \qquad (6\text{-}22)$$

It remains to compute the factor involving b_3 and $\{\text{H}\alpha\}$ in Eq. (6-20).

In Section 4-IIIC3, we formulated an approach to the solution of the transfer problem for resonance and strong subordinate lines; and in Section IIIC4, we discussed the associated value of the NRB, which we have here denoted by $\{\text{H}\alpha\}$ for Hα. The solution is characterized by values of the parameters η and B^*, given, respectively, by Eqs. (4-90) and (4-91); by the value of r_0; and by the particular chromospheric model chosen, although the latter enters as a second-order effect for strong lines of the photoionization dominated type, such as Hα. We write

$$S_{23} = (2h\nu^3/c^2)\{(b_2/b_3)e^{X_{23}} - 1\}^{-1} = C_\nu\{(b_2/b_3)e^{X_{23}} - 1\}^{-1} \qquad (6\text{-}23)$$

and use Eqs. (4-105), (6-20), and (6-21) to obtain for this photoionization dominated case (ϵ and ϵB_{ν_0} are neglected)

$$\Delta_{\text{H}\alpha} = 0.904 b_3 e^{X_3} X_3\{\text{H}\alpha\}$$

$$= \frac{0.399 \times 10^4\,\eta(1 + C_\nu/S_{23})^{-1}(B^*/S_{23} - 1)}{1 - 0.399 \times 10^4\eta(1 + C_\nu/S_{23})^{-1}(B^*/S_{23} - 1)} \qquad (6\text{-}24)$$

A word is in order on our use of Eq. (6-23) to determine b_3 rather than Eq. (4-41c). In essence, we recognize what we have already emphasized in Chapter 4; that in any k-level approximation to the actual atom, the most serious error occurs in the value of b_k. Thus, in determining the value of b_1 under conditions of detailed balance in the Lyman continuum so that $b_1 \sim b_2$, we have carried the third level as a perturbation, obtaining from it the correction term, $\Delta_{\mathrm{H}\alpha}$, to the value of b_2 and thus of b_1. (Note that in regions 2 and especially 3, where b_1 and b_2 diverge, Δ becomes trivial for b_1, but remains in the same force as a correction for b_2.) Thus, were we to compute b_3 from Eq. (4-41c), we should recognize the possibility of an error introduced by the neglect of the NRB for Paschen-α, i.e., of $\{\mathrm{P}\alpha\}$. (The radiative term between two adjacent levels predominates over the collisional up to $k \sim 10$, based on our quite bad knowledge of the collisional cross section between adjacent levels for large k.) For example, carrying through a sample calculation of b_3 from Eq. (4-41c) with a term in Paschen-α added, we find that the two leading terms in the numerator of an expression for b_3 are $7.8 \times 10^{29} X_3^{-1} + 3.8 \times 10^{29} b_4 e^{X_4}\{\mathrm{P}\alpha\}$; the $\{\mathrm{P}\alpha\}$ term is not involved in the denominator. The uncertainty is, in consequence, not trivial.

On the other hand, the determination of the source function is not as sensitive to these difficulties. In essence, we have determined S_{23} from Eqs. (4-41b) and (4-41c), neglecting the C_{1j} terms. If, now, one includes a Paschen-α term and computes S_{23}, he shows readily that he obtains just the expression used in Chapter 4 with the exception that η becomes

$$\eta_{23} = \frac{2^5}{3\pi\sqrt{3}} \frac{R^2}{\tilde{\omega}_2 f_{23} \nu_{23}{}^2} \frac{W_{\kappa 2}}{2^3} \frac{e^{-Y_2}}{Y_2} \times [e^{Y_2 - Y_3}(1 + \Delta_{\mathrm{P}})^{-1} - 1] \left[1 + \frac{3/2}{1 + \Delta_{\mathrm{P}}}\right]^{-1} \qquad (6\text{-}25)$$

rather than the expression (4-90). The correction term

$$\Delta_{\mathrm{P}} = 0.35\, b_4 X_4 e^{X_4}\{\mathrm{P}\alpha\}$$

amounts to something less than ~ 0.2 in the range $6000° < T_e < 8000°$, with $\eta \sim 0.005$; so η_{23} does not differ appreciably from the value predicted by Eq. (4-90). Thus, S_{23} computed as in Chapter

4 is very good; the value of b_2 determined from Eq. (6-21) already includes the second approximation to b_2; so a value of b_3 computed from these two results gives a consistency with these two good results which would not result from the use of Eq. (4-41c) and an attempt to correct for the effect of Paschen-α.

Return now to the value of $\Delta_{\mathrm{H}\alpha}$ given by Eq. (6-24). Because $C_\nu/S_{23} \gg 1$, while $B^*/S_{23} \to 1$ at great depths and $\gg 1$ at small τ_α and varies monotonically between these limits (cf. Section 4-IIIC4), we have the limits on $\Delta_{\mathrm{H}\alpha}$

$$0 \leq \Delta_{\mathrm{H}\alpha} \leq \frac{0.399 \times 10^4\, \eta_{23} B^* C_\nu^{-1}}{1 - 0.399 \times 10^4\, \eta_{23} B^* C_\nu^{-1}} \tag{6-26}$$

Again, from Minnaert's data we obtain $Y_3 = 3.00$; then Eqs. (4-90) and (4-91) give $\eta_{23} = 0.0036$ and $B^* = 0.0274 C_\nu$. The corresponding upper limit on $\Delta_{\mathrm{H}\alpha}$ from Eq. (6-26) is 0.65. Thus, if we use Eq. (6-20) with $\Delta_{\mathrm{H}\alpha} = 0$ or 0.65, we span the range in b_1 and the two values differ by a maximum of a factor 1.65. The iteration procedure is in consequence rapidly convergent. We have from Eqs. (6-27) and (6-20)

$$0.994 \times 10^4 (e^{-X_2}/X_2) \leq b_1 \leq 1.64 \times 10^4 (e^{-X_2}/X_2) \tag{6-27}$$

We use either of the limits in Eq. (6-27) with Eqs. (6-16) and (6-17) to compute T_e, n_e, b_1, n_2, τ_α at each height. Then, from the solution $S_{23}(\tau_\alpha)$ we compute $(1 - S_{23}/B^*)$ which, multiplied into the right side of Eq. (6-26), gives the correct value of b_1. In general, one or two iterations suffice to obtain a self-consistent solution.

We should comment on the particular solution used for $S_{23}(\tau_\alpha)$. Table 6-5 exhibits $(1 - S_{23}/B^*)$ for various values of the parameters η, r_0, τ_{Cm}, A. We have

$$\begin{aligned} r_0 &= [(n_{\mathrm{H}^-}\alpha_{\mathrm{H}^-} + n_3\alpha_{\mathrm{fb}3})/n_2\alpha_{\mathrm{H}\alpha}] \\ &= 3.68 \times 10^{-22} n_e T_e^{-1} (b_1/b_2)(\exp{[X_{12} + X_{\mathrm{H}^-}]}) \\ &\times [1 + 2.66 \times 10^{15} n_e^{-1} T_e^{3/2} (b_3/b_1) \exp{(-[X_{13} + X_{\mathrm{H}^-}])} \end{aligned} \tag{6-28}$$

Values of the H$^-$ contribution, which is the first term on the left in Eq. (6-28), and of the relative Paschen opacity, which is the second term in the bracket for the T_e of interest at $500 < h < 2400$ and for $n_e = 10^{12}$ are:

T_e	4000	4500	5000	5500	6000	7000	8000
H^-	5.1	0.13	7×10^{-3}	6.5×10^{-3}	9×10^{-5}	2×10^{-6}	3×10^{-7}
Paschen	5×10^{-8}	—	—	0.002	0.022	0.96	17

These values correspond to b_1/b_2 and b_3/b_1 equal unity, so overestimate the Paschen contribution. We shall also see that $n_e < 10^{12}$ for $h > 500$ km, so r_0 is less than the values tabulated. Preliminary computation with the limits set by Eq. (6-27) gives $T_e \gtrsim 6000°$ for $h \gtrsim 500$ km, so we are interested only in $r_0 < 10^{-4}$. Table 6-5 shows, then, that the difference in solution between those for $r_0 = 0$ and those for $r_0 = 10^{-4}$ is essentially trivial for our present application; so the question of the decrease with increasing height of r_0 is not important and we simply use the solution for $r_0 = 0$.

The foregoing provides a straightforward procedure for computing n_e, T_e, n_1, etc., at each height from the empirical functions $f(h)$ and $g(h)$ *provided* that these functions represent the data sufficiently well and that the data are sufficiently accurate. Within the region where the H^- emission dominates, we have an accurate determination of both T_e and n_e. The accuracy of determination of n_H is essentially the accuracy to which $f(h)$ and $g(h)$ are specified; because of the exponential dependence of n_H on T_e, the relative accuracy of T_e is consequently high. The accuracy of determination of n_e is essentially twice that of $f(h)$. Outside the region where the H^- emission dominates, we have a reasonably accurate determina-

Table 6-5. *Values of* $\{1 - S_{23}/B^*\}$ for Various Values of the Parameters η, r_0, τ_{Cm}, A

				τ_0									
η	r_0	τ_{Cm}	A	0	0.1	0.5	1	2	5	10	20	50	100
0.01	0	—	—	0.90	0.89	0.85	0.81	0.75	0.62	0.48	0.32	0.17	0.11
0.005	0	—	—	0.93	0.92	0.90	0.87	0.82	0.72	0.60	0.45	0.28	0.20
0.0036	0	—	—	0.94	0.93	0.91	0.89	0.85	0.76	0.65	0.51	0.34	0.25
0.001	0	—	—	0.97	0.97	0.96	0.94	0.92	0.87	0.81	0.71	0.58	0.50
0.01	10^{-4}	0.01	120	0.89	0.88	0.84	0.79	0.73	0.59	0.44	0.29	0.17	0.13
0.001	10^{-4}	0.01	120	0.95	0.95	0.93	0.91	0.87	0.82	0.75	0.67	0.58	0.52
0.01	10^{-4}	0.001	120	0.90	0.89	0.85	0.82	0.76	0.63	0.49	0.33	0.18	0.13
0.001	10^{-4}	0.001	120	0.97	—	—	0.94	—	0.88	0.82	0.74	0.62	0.54

tion of n_e but a poor determination—by comparison with the situation at lower heights—of T_e. In essence, the accuracy of each of T_e and n_e is that of $f(h)$ and $g(h)$. We turn to the results of the solution for quantitative detail.

Table 6-6 presents the solution. The numerical values given by the functions $f(h)$ and $g(h)$ do not permit a solution for $h \gtrsim 1000$ km with T_e increasing monotonically with height. The numerical reason is a too-rapid decrease of $g(h)$ with increasing height relative to that of $f(h)$; the physical reason is the passage from a region where H^- dominates to one where it is negligible, so that small errors in f and g strongly influence the derived values of T_e. Table 6-7 illustrates the situation by giving the relative contribution of the various terms entering $g(h)$, together with the *minimum* amounts by which f and g must be changed to permit a solution with $dT_e/dh \geq 0$. Because n_2 is very insensitive to the derived value of T_e (varying as $T^{-1/2}$ or as $f(h)T_e$), we give in Table 6-6, in brackets at each height, the computed value of n_2 for $T_e = 7500°$, and the corresponding value of τ_α. We also give a value of 7500° for T_e at each $h > 1000$ km, together with an estimate of ΔT_e from the following paragraph.

Consider the reliability of the quantities in Table 6-6:

(1) For $h \sim 500$ to 750 km where H^- emission dominates: Trying various representations for the integrated emission $E(h)$, which are compatible with the scatter in the observed data at λ4700, we find a resulting scatter of about 50 percent in $g(h)$. Such a variation in $g(h)$, or one of the same size in $\{f(h)\}^2$, leads to about 50 percent variation in n_H, thus about 250° in T_e. The corresponding variation in n_e is about 10 percent.

(2) For $h > 1000$ km where H^- emission is negligible: The scatter in the observed $\log E(h)$ at λ4700 is about ±0.1, or about 25 percent in $E(h)$, for these heights. Because $g(h)$ is the second derivative of $E(h)$, the uncertainty will be magnified. Again, an uncertainty of about 50 percent would not seem unduly pessimistic. Thus, a 25 percent uncertainty in n_e would seem a reasonable estimate. We note that at these heights the maximum contribution from the Paschen continuum, estimated for large T_e, thus $X_\delta \sim 0$, definitely lies under the electron-scattering contribution. Thus, a limit of 50 percent to a factor 2 on the uncertainty in n_e from all these sources would seem a fair estimate. Even if we set a very small uncertainty on $f(h)$, the uncertainty in T_e associated with that in

Table 6-5. Solution for Atmospheric Parameters Under Assumption of Detailed Balance in Lyman Continuum of Hydrogen

h	T_e	n_e	n_2	τ_d	$b_1 = b_2$	n_1	τ_{LyC}	$1 + \Delta$
500	6250 ± 250	$5.2 \times 10^{11} \pm 10\%$	$1.63 \times 10^{6} \pm 20\%$	61	3.4	$6.2 \times 10^{13} \pm 50\%$	0.53×10^{4}	1.14
750	6750 ± 500	$4.2 \times 10^{11} \pm 10\%$	1.06×10^{6}	38	6.1	9.9×10^{12}	0.73×10^{3}	1.18
1000	7500 ± 500	$3.4 \times 10^{11} \pm 25\text{–}50\%$	7.1×10^{5}	24	12.6	1.15×10^{12}	92	1.23
1500	(>7500)	1.25×10^{11}	(2.6×10^{5})	(8)	—	—	—	(1.38)
	← 25–50% →							
2000	(>7500)	0.75×10^{11}	(9×10^{4})	(3)	—	—	—	(1.48)
	← 25–50% →							
2400	(>7500)	0.50×10^{11}	(4×10^{4})	(1)	—	—	—	(1.54)
	← 25–50% →							

Table 6-7. Relative Importance of Various Terms Entering $g(h)$, and Change in $f(h)$ and $g(h)$ Required to Give Solution with $dT_e/dh \geq 0$

h	n_e	n_{H} (Rayleigh)	H⁻fb	H⁻ff	Paschen	f-f
500	10	3	72	5	10	0.3
750	30	2	37	3	27	1
1000	50	0.5	8	1	38	2
	Require 20 percent rise in $g(h)$ or 30 percent drop in $f(h)$					
1500	65	0.5	4	0.5	28	2
	Require 50 percent rise in $g(h)$ or factor 2 drop in $f(h)$					
2000	85	—	—	—	15	—
	Require 50 percent rise in $g(h)$ or factor 2 drop in $f(h)$					
2400	85	—	—	—	15	—
	Require 50 percent rise in $g(h)$ or factor 2 drop in $f(h)$					

n_e leaves the value of T_e in the range $h \gtrsim 1000$ km essentially unspecified within a factor 2 or so, except that it must exceed about 7500° if we require the gradient of T_e to be monotonic.

(3) One of us has suggested (Athay, Menzel, Orrall, 1957) that all intensities derived from the High Altitude Observatory 1952 eclipse observations (Athay, Billings, Evans, and Roberts, 1954) should be reduced by about a factor 2, in order to bring the absolute intensities into accord with those observed at the 1932 and 1936 eclipses, after all data from the three eclipses have been reduced on a common scheme having standards based on the coronal scattered-light continuum observed in the solar polar region. Such a change would enhance the difficulties encountered in our present analysis—these difficulties require an increase in the empirical intensities, not a decrease. We note that this suggested change in absolute intensities does not arise in any way from a consideration of the absolute calibration standards for the original 1952 data by themselves: Thus, I prefer in the light of our present knowledge and internal consistency of the 1952 data, to consider the suggested correction by a factor of two to be unjustified, and to ascribe its origin to a difference in physical state of the chromosphere-corona from one eclipse to another. This is hardly a satisfactory situation; only data from further eclipses can clarify the point.

(4) We do not consider in this chapter the effect of departure from spherical symmetry on either the solution or the computation

of the representations $f(h)$ and $g(h)$. Here, we note only that the helium emission—upon whose occurrence the first-order discussion of the departure from spherical symmetry is based—appears to originate at $h \gtrsim 1100$ km. Consequently, the results in Table 6-6 suggest that T_e for the great mass of chromospheric material (along the line of sight at a given height) has increased beyond values where H^- dominates the visual spectrum well before a significant fraction of the chromosphere has been heated sufficiently to produce helium emission. We return to this point in Section 6-IIIA3 below.

(5) We have used Eq. (6-20) for b_1; this procedure is strictly applicable only under conditions of detailed balance in the Lyman continuum. From Fig. 4-1, we estimate such a condition to hold for $\tau_{\mathrm{LyC}} \gtrsim 100$; thus from Table 6-6, we expect the results for $h \lesssim 1000$ km to be satisfactory. But, above 1000 km, the contribution to the solution from terms involving n_{H} is essentially negligible. Thus, the values of T_e and n_e in Table 6-6 will not be modified by any change required from the expression of Eq. (6-20) for b_1. On the other hand, the n_1 and n_2 computed from values of T_e and n_e at $h \gtrsim 1000$ km may require modification.

From Eq. (4-44), we see that if $R \gg 1$, the value of b_2 is still given by Eq. (6-20) for any behavior of the Lyman continuous radiation field—thus at all chromospheric heights, up to a correction $(1 + 1/R)$. At 1000 km, $R = 25$, and increases upward. Thus, the b_2 values in Table 6-6 are reliable, up to the uncertainty in T_e.

From Eq. (4-43) et seq. we see that b_1 (hence n_1) increases over the values given in Table 6-7 for $h \gtrsim 1500$ km. Ultimately, at small τ_{LyC}, we see from Eq. (4-47) that it approaches the value (region 3)

$$b_1 = [1.40 \times 10^{24} e^{-X_2} n_e^{-1} T_e^{-3/2} (1 + 0.34 \times 10^{-4} T_e)]/X_2(X_{12} + 1) \tag{6-29}$$

Above 1000 km, Table 6-6 suggests $T_e \geq 7500°$; the value of b_1 from Eq. (6-29) for $T_e = 7500°$ is $1.6 \times 10^{14}/n_e$. Thus, the values of b_1 and n_1 estimated from Eq. (6-29) would be about a factor 100 higher than those estimated from Eq. (6-20), at these heights above 1000 km. However, such values would increase τ_{LyC} by essentially the same factor, and throw the solution back into region 1. Thus, to provide a proper set of values in the region $h \gtrsim 1000$ km, *once we have a reliable set of values* $T_e(h)$, we must actually solve the transfer problem in the Lyman continuum. We defer consideration of this solution of the transfer problem until Section 3 below, for in the present section we have concern only with the distribution of T_e and n_e that we can infer from the values of $f(h)$ and $g(h)$ alone.

We may then summarize the results on the region $500 \text{ km} < h < 2400 \text{ km}$ that can be derived from the values of $f(h)$ and $g(h)$ as follows:

(1) At 500 km, T_e has risen 1300 to 2000° over the minimum value reached in the upper photosphere. Hydrogen has reached the 1 percent ionization level, and the degree of ionization is rapidly increasing further with height. Thus, we must categorically reject all chromospheric models of the Wolley-Allen (1950) prototype, which regard the temperature of the low chromosphere as constant at the minimum value reached in the upper photosphere, with no significant rise until the top of the low chromosphere, around 5000 km. The ionization of hydrogen is negligible in the low chromosphere in such models. The essential physical difference between such models and those—such as we have found here—showing a significant rise in T_e below 1000 km lies in the requirement that there occurs a very significant non-radiative energy input in these lowest chromospheric regions, as we have emphasized in Chapter 1. Thus, the difference between these two classes of models is not simply 25 percent difference in T_e in the region 500 to 1000 km, it is a basic physical difference in the energetic balance; consequently in the kind of description (LTE versus non-LTE) of the energetic distribution functions characterizing the atmosphere, thus ultimately in the whole way one analyzes and discusses the physical state of the atmosphere. We cannot overemphasize this point; it is often lost sight of in discussions of the low chromosphere, the upper photosphere, and mechanisms of spectral line formation.

We also must reject an intermediate category of models which show at most a very slight increase in T_e in the lowest chromosphere, $T_e \lesssim 5000°$ up to heights greater than 2500 km for most of the chromospheric material. Such a model for a spherically symmetric chromosphere is that by Böhm-Vitense (1954). The Woltjer model (1954) is essentially the Woolley-Allen model modified by introducing hot spicules, which occupy negligible volume, so that most of the chromospheric mass lies at the boundary value of T_e. de Jager's most recent model (1957b) is similar to Woltjer's, as regards T_e for most of the chromospheric material—$T_e < 5000°$ up to 2500 km for the interspicular material.

T_e in the low chromosphere in van de Hulst's model (1953) lies just slightly above those in the last paragraph, reaching 5850° at 2000 km and hydrogen being only 10 percent ionized there. Again, such a model as this is incompatible with the data.

(2) Although the density of hydrogen is well determined in the range 500 to 1000 km, its gradient begins to become badly determined at the upper end of the range because of the decrease in H^- emission. Thus, we cannot answer with complete certainty the question of the relative importance of energy and momentum input from the non-radiative energy source, throughout this range. If, however, we compute an effective gravity from the results given in Table 6-6, we find the following values for its ratio to the actual solar value:

	He:H		
Height interval, km	0.05	0.10	0.20 (by number)
500–750	1.18	1.06	0.90
750–1000	1.40	1.26	1.06

These values lie remarkably close to unity, relative to the uncertainty in the values of $T_e(h)$. For the most likely value of He:H, about 0.10, a decrease in T_e of about 200° at 1000 km over the Table 6-6 model, and a much smaller change at 500 km, suffice to give exactly the solar values for the effective gravity. These changes in T_e lie well within the uncertainty limits given in Table 6-6. Moreover, these departures from the solar gravity lie nowhere near the factor 10 or so associated with the classical chromospheric anomaly, and underlying the hypothesis of a "turbulence" having superthermic velocities to explain the structure of the chromosphere. From these results, we find no anomaly at all in the density gradient of the chromosphere in this region 500 km $< h <$ 1000 km. A distribution of material under hydrostatic equilibrium represents quite adequately the observations made in the continuum.

This result suggests that we attempt to obtain a better model for $T_e(h)$ above 1000 km by using the condition of hydrostatic equilibrium together with the observed functions $f(h)$ and $g(h)$. We construct such a model in Section 3 below. In the present section, we wish to confine our results entirely to what can be learned from a wholly empirical analysis, under the assumption of spherical symmetry.

(3) Because of the small sensitivity of the value of n_2 to the value of T_e, the results in Table 6-6 give considerable information on the Balmer opacity and source-function for the Balmer lines. We return to this point in Chapter 9.

2. The Region Below 500 km but with τ_{4700} and $\tau_{\mathrm{BaC}} \ll 1$. From the results in Table 6-6, we find for the tangential optical thickness of the chromosphere (since we are interested for $T_e \lesssim 6000°$, we compute only the H$^-$ opacity at λ4700; cf. Table 6-3):

$$\begin{aligned} \tau_{4700} &\sim 1.8 \times 10^{-3} \exp(10[0.5 - l]) \\ \tau_{3646} &\sim 0.12 \exp(1.67[0.5 - l]) \end{aligned} \qquad (6\text{-}30)$$

Thus, if we again neglect the optical depth term in computing E from $\mathcal{E}$ in the region $0 < h < 500$ km, we will underestimate the emissivity by factors not to exceed about 30 percent at 0 km. Although syste-

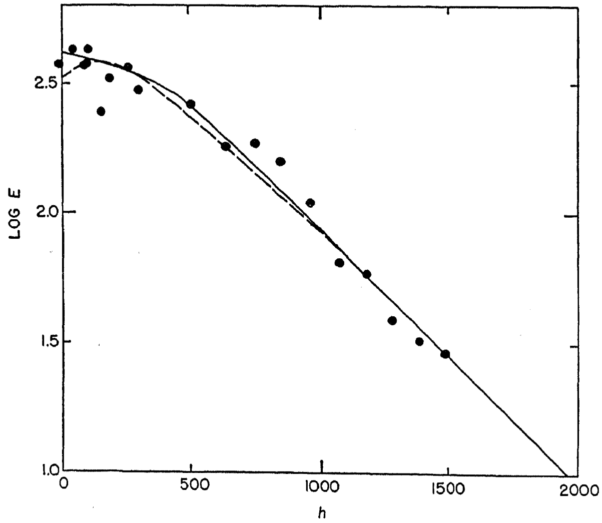

Fig. 6-4. Integrated emission at head of Balmer continuum. Solid curve, first two terms of Eq. (6-31); dashed curve, Eq. (6-32). ●, observed points, $h \leq 1500$ km.

matic, the correction is not large compared with the uncertainty in the functions $f(h)$ and $g(h)$; so as a first approximation we adopt the procedure of the preceding Section 6-IIA1 in relating E to $\mathcal{E}$. We return to the question, when we check the derived results for consistency.

Numerical values for $f(h)$ and $g(h)$ must come from the same procedure as that adopted above 500 km., viz., numerical differentiation of the $E(h)$ data. We consider f and g in turn.

a. $f(h < 500$ *km*). Numerical values for $f(h < 500$ km) present great difficulties because of the apparent maximum in f implied by the trend of the data below 500 km, combined with the severe observational scatter. If $f(h)$ drops off rapidly below 500 km, then the scatter of the data makes its precise value essentially indeterminate. We illustrate the situation by two examples.

First, write

$$
\begin{aligned}
E(h < 500) = E(500) + K \int_h^{500} dl \\
\times \left\{ \int_{-\infty}^{y_m} f(h > 500)\, dy + \int_{y_m}^{\infty} f(h > 500)\, dy \right\} \\
+ \int_h^{500} dl \int_{-y_m}^{y_m} f(h < 500)\, dy \\
= E(500) + E(\text{shell, radius} \geq 500) \\
+ \Delta(\text{contribution, radius} \leq 500) \qquad (6\text{-}31)
\end{aligned}
$$

K is the ratio, (2.35×10^{-33}), between $\mathcal{E}$ and f. y_m is the value of y corresponding to the shell at 500 km. The contribution of the first two terms on the right represents the E which would be observed if there were no Balmer free-bound emission below 500 km, i.e., if $n_e n_p T_e^{-3/2}$ were zero for $h < 500$ km. We can compute these first two terms from Eq. (6-16); the result is the solid curve in Fig. 6-4.

Second, assume for $E(h)$ the form

$$E(h) = 776 e^{-2.21}(1 - Ae^{-al}) \qquad (6\text{-}32)$$

Such an equation will give a behavior similar to that observed, and show a maximum in $f(h)$. A reasonably wide variety of values for A and a will represent a mean curve through the observations below 500 km; the values all show maxima in E near $l = 0.1$, maxima in

$f(h)$ near 0.55 to 0.50 for l, and $f(h) \leq 0$ for $l \leq 0.25$ to 0.30. One of the better fitting of these representations, with $A = 0.57$ and $a = 4$, is the dashed curve in Fig. 6-4; we have $f = 0$ for all l below that where f reaches zero. The observed values of E are plotted for $h < 1500$ km.

Clearly, the observational data do not suffice to distinguish between the two alternatives (6-31) or (6-32), nor between them and a number of similar representations. In such a situation, any attempt to estimate $f(h < 500 \text{ km})$ by using the various representations would only lead to results which reflected the details of the particular assumed representations rather than the true physical situation, and thus be essentially numerology rather than physics. All we can really conclude, is that none of the alternative representations changes much the value of $f(h)$ near 500 km (within the 50 percent, factor 2 uncertainty discussed already), and all give a sharp drop in $f(h)$ within a few hundred kilometers below 500 km.

b. $g(h < 500 \text{ km})$. The data underlying the specification of $g(h)$ suggest almost as bad a situation for $g(h < 500 \text{ km})$ as for $f(h < 500 \text{ km.})$. The function E_{4700} is determined by just four observed points below 500 km., and $g(h)$ is essentially the second derivative of E. The situation is better than in the case of $f(h)$ only in that E_{4700} is clearly increasing rapidly, in value and derivative, as compared with the essentially constant value of E_{3640}.

The particular form used for $g(h)$ above 500 km leads to values of $E(h)$ lying considerably below the observed values for $h \lesssim 300$ km. However, a modification in the representation of Eq. (6-19), consisting of a change in only the first two terms, suffices to remedy the situation below 300 km without changing $g(h)$ above 500 km beyond the limits already set. This change is

$$1.14 \times 10^{14}e^{-7l} + 3.51 \times 10^{12}e^{-2.2l} \rightarrow 7.22 \times 10^{14}e^{-9.66l} + 1.30 \times 10^{12}e^{-1.65l} \quad (6\text{-}33)$$

Figure 6-5 compares the predictions of $g(h)$, and this modification which we call $g'(h)$, to the observed values of $E(h)$. We also draw a free-hand curve, which is an equally satisfactory representation of the observed $E(h)$, which does not differ appreciably from $g(h \gtrsim 600$ km), yet which differs considerably in its predictions on $g(h < 500$ km). Thus, the observed E_{4700}, in the range $-110 \text{ km} < h \lesssim 500$

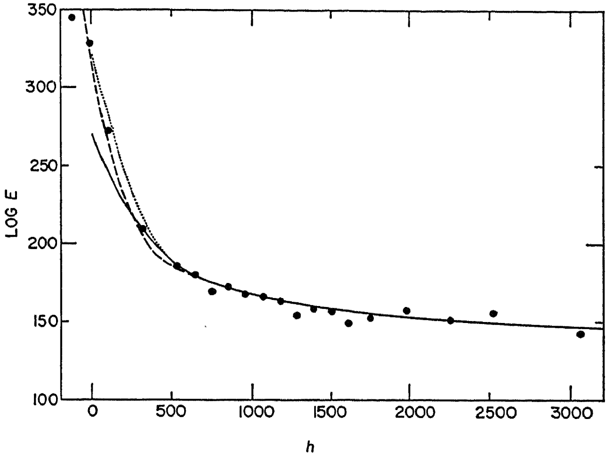

Fig. 6-5. ——, representation of Eq. (2-10). ····, representation of Eq. (2-10) modified by relation (6-49). – – –, free-hand curve. ●, observed points.

km, do not give a determinate function $g(h)$. We can obtain reasonable values for E, rough values for dE/dh, and probably order-of-magnitude estimates for the second derivative, which measures $g(h)$. In our initial analysis (Athay, Menzel, Pecker, and Thomas, 1955) we attempted to set a rough lower limit on $T_e(h \sim 0)$ by using the relation

$$-dE_\lambda/dh = \int_0^\tau S_C e^{-\tau}\, d\tau \sim \bar{B}_\lambda(T_e)(1 - e^{-\tau}) \qquad (6\text{-}34)$$

and assuming $\exp(-\tau) \ll 1$. We consider the situation for non-negligible τ in Section B; in the present section, we ask whether we can say anything at all about that part of the region below 500 km where the opacity is negligible.

c. Rough Estimate of a Model for 750 km $> h > h(\tau_{4700} \sim 1)$. With the results above on $f(h < 500 \text{ km})$ and $g(h < 500 \text{ km})$ a wholly empirical model for $h \lesssim 500$ km. constructed from data presently available would have little reliability. Essentially, our information on the region $h < 500$ km consists of the following:

(1) A rough value of dE_{4700}/dh, and an order-of-magnitude value for g.

(2) the knowledge that $d \ln f(h)/dh \geq 0$, with the zero value holding near 500 km.

(3) the empirical results for 500 km $< h <$ 1000 km. satisfy the condition of hydrostatic equilibrium.

Although the numerical values of $f(h < 500)$ are observationally indeterminate from our present data, the conclusion that $f(h)$ drops sharply below 500 km suggests an alternative physical relation to replace the empirical $f(h)$ and thus permit a determination of T_e, n_e, etc., for $h <$ 500 km. That is, the occurrence of a maximum in $f(h) = n_e n_p T_e^{-3/2}$ in this region near 500 km. can only reflect the balance between the outward decrease in density and increase in ionization of hydrogen. We have, using equations (4-3) and the left-hand equality for b_1 in Eq. (6-27),

$$(d/dh)\ln(n_e n_p T_e^{-3/2}) = (d/dh)\ln\{ n_1 T_e(1.05 \times 10^{-16} T_e^2 e^{X_{12}})^{-1}\}$$

$$= (d/dh)\ln(n_1 T_e) + (X_{12} - 2)(d/dh)\ln T_e \quad (6\text{-}35)$$

In regions where $n_1 \gg n_p$, which is true for $h \lesssim 750$ km from Table 6-6, the first term on the right is the pressure gradient, and measures the density gradient. The second term measures the temperature-dependence of the ionization. Just as we have earlier introduced the theoretical relation on the behavior of b_1 as a measure of the ionization of hydrogen in the non-LTE situation, so now we might seek to introduce the condition of hydrostatic equilibrium as a measure of the density gradient, to replace the observationally indeterminate relation $f(h)$.

Alternatively to the results in Section 6-IIA1, we can check the suggestion empirically in the region above 500 km by comparing the derived results on $T_e(h)$ with the empirical ones from Table 6-6. The equation of hydrostatic equilibrium is, denoting by r the He:H abundance by number,

$$(d/dh)\{[(n_1 + n_p)(1 + r) + n_e]\mathrm{k}T_e\} = -gm_{\mathrm{H}}(n_1 + n_p)(1 + 4r) \quad (6\text{-}36)$$

which, for $n_1 \gg n_p$, becomes

$$(d/dh)\ln(n_1 T_e) = -3.32 \times 10^{-4} T_e^{-1}(1 + 4r)/(1 + r) \quad (6\text{-}36\mathrm{a})$$

Since for $h >$ 500 km the left side of Eq. (6-35) is constant and equals -2.2×10^{-8} cm^{-1}, Eq. (6-35) and (6-36a) combine to give an ordinary differential equation in T_e; so that we need neither of the observational functions $f(h)$ and $g(h)$, only T_e at some height. With $r = 0.1$ we have the solution

$$(Z/Z_0)[(1 - 0.52Z_0)/(1 - 0.52Z)]^{0.674} = \exp[0.358(l - l_0)]$$
$$Z = 10^{-4}T_e \qquad (6\text{-}37)$$

If we take $T_e = 6250°$ at 500 km—the value from Table 6-6 at 500 km—Eq. (6-37) predicts $T_e = 6680°$ at 750 km as compared with 6725 from Table 6-6, 7150 versus 7500° at 1000 km, and 7600° versus an indeterminate solution at 1250 km. The solutions at the greater heights violate the condition $n_1 \gg n_p$, which underlies Eq. (6-37). There is, however, no basic difficulty; we must simply integrate (6-35) and (6-36) numerically rather than algebraically. We return to the point below; the values above simply give a good approximation to the result coming from hydrostatic equilibrium.

Application of the condition of hydrostatic equilibrium provides, if it is valid, a straightforward approach to T_e, particularly in those regions where the observational conditions become indeterminate. We require, therefore, a reliable starting value for the integration, somewhere in the height range $500 < h < 1000$ km. Thus, we ask into the degree of variation of T_e at various heights arising from choosing one or the other of the alternatives on the empirical representations.

We have already set limits of uncertainty in the solution underlying Table 6-6. The major source of uncertainty in applying Eq. (6-36) and (6-35) as we have done lies in the possibility that we cannot take a constant value for the left side of Eq. (6-35) down to 500 km, but must replace it with something like an expression of the form given by Eq. (6-32). In this event, there are two effects: (1) The left side of Eq. (6-35) decreases (numerically) strongly near 500 km; (2) the value of $f(h)$ used to determine T_e at 500 km decreases. With the parameters already used, $A = 0.57$ and $a = 4$, we can estimate the effect numerically. The left side of Eq. (6-35) becomes

$$-2.2 \times 10^{-8} + 10.8 \times 10^{-8}e^{-4l}(1 - 2.7e^{-4l})^{-1} \qquad (6\text{-}38)$$

and the value of $f(h)$ at 500 km becomes 3.40×10^{17} rather than the value 5.38×10^{17} used in the solutions in Table 6-6. To set extreme limits for the effect, we set the expression above equal to zero, and integrate Eq. (6-36a) plus Eq. (6-35) with left side equal to zero, obtaining

$$(Z/Z_0) \exp(-0.170[Z - Z_0]) = \exp(0.358[l - l_0]) \qquad (6\text{-}39)$$

The new value of $f(h)$ at 500 km gives a starting value there of $T_e = 5940°$, following the procedure underlying Table 6-6. Then, Eq. (6-39) gives $T_e = 6570°$, 7270°, and 8050° at 750, 1000, and 1250 km, respectively.

The interesting result from these several solutions—wholly empirical, and theoretical from hydrostatic equilibrium—is the small fluctuation in the value of T_e at 750 km, about ±75°. The fluctuation near 500 km reflects the uncertainty in the behavior of $f(h)$ near its maximum; the uncertainty for $h \gtrsim 1000$ km is largely that in the empirical value coming from the very rapidly dwindling importance of H^-. Thus, for an adopted starting value for T_e, we believe that we should choose a value at 750 km as the most stable and reliable. We take $T_e = 6650°$ at 750 km, estimating $\Delta T_e \sim \pm 75°$. To fix a density, we note that $f(h)$ at 750 km also shows small variation between the different representations: 3.11×10^{17} from our original representation based on a constant slope for the logarithmic emission at λ3646; and $\sim 2.7 \times 10^{17}$ for the several representations of Eq. (6-32), which give a maximum in the emission. We adopt $f(h) = 3.0 \times 10^{17}$ at 750 km, leading to $n_e = n_p = 4.04 \times 10^{11}$, $n_1 = 1.21 \times 10^{13}$.

We give in Table 6-8 the results for three solutions at 500 km, each starting from the value at 750 km, and the assumption of hydrostatic equilibrium, but differing in the assumed behavior of $f(h)$.

"Numerical" signifies that we have used the expression (6-38) for $d \ln f(h)/dh$ in a step-by-step integration. The "observed" value of g(500 km) from the representation by Eq. (2-10) is 4.71×10^{12}. The "observed" f(500 km) from Eq. (6-16) is 5.38×10^{17}; that corresponding to Eq. (6-32) with the A, a values used before is 3.40×10^{17}.

Table 6-8. Varying Solution at 500 km for Varying grad $f(h)$

$-d \ln f(h)/dh$	Z	$n_1 \times 10^{-13}$	$n_e \times 10^{-11}$	$f \times 10^{-17}$	$g \times 10^{-12}$
2.2×10^{-8}	0.622	6.65	5.25	5.54	5.13
Numerical	0.611	6.95	4.38	3.95	4.09
0	0.602	7.05	3.83	3.09	3.45

The "best" solution would seem to lie between the first two cases; we adopt $T_e = 6150°$ at 500 km.

We cannot hope to obtain a definitive model $T_e(h)$ for $h \lesssim 500$ km. We can, however, place limits on the model, by the following procedure. From Eqs. (6-35) and (6-36a), we see that $d \ln f(h)/dh = 0$ gives a lower bound for the sets of values of $d \ln T_e/dh$ satisfying the condition $d \ln f(h)/dh \geq 0$. Thus, a solution $T_e(h)$ computed from Eq. (6-39) will provide an upper bound on $T_e(h \leq 500 \text{ km})$. We give such a solution in Table 6-9, together with the corresponding values of n_1, n_e, n_{H^-}, and optical depths in the various spectral regions. We compute n_1 by integrating Eq. (6-36). Since we overestimate T_e, we shall underestimate n_1; thus, we will underestimate the optical depth. Since we have adopted $d \ln f(h)/dh = 0$, $f(h)$ remains constant at its value at 500 km; n_e and n_p then follow from $f(h = 500)$ and the equation

Table 6-9. Model Corresponding to an Upper Bound on $T_e(h < 500 \text{ km})$

h, km	$10^{-4}T_e$	$10^{-14}n_1$	$10^{-11}n_e$	$10^{-5}n_{\mathrm{H}^-}$	tang $\tau_{\lambda 4700}$	rad $\tau_{\lambda 5000}$	$10^{-13}g(h)$
500	0.615	0.695	4.72	0.290	0.0023	1×10^{-5}	0.460
400	0.591	1.46	4.63	0.670	0.0051	3×10^{-5}	0.769
300	0.568	3.15	4.58	1.62	0.012	6×10^{-5}	1.42
200	0.546	6.99	4.65	4.10	0.029	2×10^{-4}	2.81
100	0.525	16.0	5.04	11.5	0.078	4×10^{-4}	5.93
0	0.505	37.8	6.36	38.8	0.24	1×10^{-3}	15.6

$$n_e = n_p + 10^{-4}n_1 \tag{6-40}$$

in which we have adopted an H : metal abundance of 10^4. Because $f(h)$ should actually decrease, with decreasing height, we shall overestimate n_e until the metals take over from hydrogen as the main source of free electrons, after which we shall underestimate n_e because of the underestimate of $10^{-4}n_1$. Note that in using Eq. (6-39) we ignore the variation of the term $(1 + \Delta)$. In the region $h \lesssim 500$ km, the values of Δ given in Table 6-7 suggest that the neglect is not important in the present context. We also present computed $g(h)$ in Table 6-9, corresponding to the values given for n_1, T_e, n_e. These computed values of $g(h)$ lie intermediate to the values given by the earlier representations $g(h)$ and $g'(h)$, but much closer to the former, so are probably too small.

Two rough checks can be applied to the results in Table 6-9. First, we can integrate $g(h)$ to compute $E(h)$; second, we can estimate dE/dh at the lowest heights from the data, and use Eq. (6-34) to obtain T_e. Integrating $g(h)$ gives values for E lying within about a factor 2 of the observed, but systematically lower. The direction of the discrepancy corresponds to our underestimate of n_1. A value for T_e determined from Eq. (6-34) and the observed data near 0 km gives $\sim$5000° if τ_C be assumed large, and $\tilde{<}$ 6000° if $\tau_C \sim 0.5$.

From the value of τ(tangential) given in Table 6-9 at the lowest heights, and noting that this is an underestimate because of the underestimate on n_1, we see that at these lowest heights we enter the region where the emission ceases to be the integral of the emissivity. Thus, we defer further consideration of the solution at these lowest heights until Section 6-IIIB, where we try to join this solution to that obtained in Section 6-IIB from narrow-band filter observations at the limb.

3. A Model for $h > 750$ km Based on Hydrostatic Equilibrium. Our empirical solution in Section 6-IIIA1 suggests that the condition of hydrostatic equilibrium is satisfied by the observations in the continuum up to about 1000 km, when these data cease to give a reliable estimate of $T_e(h)$. Thus, we now ask what kind of a distribution $T_e(h)$ would result if we assume hydrostatic equilibrium and the *slope* of the function $f(h)$, tying the results to values of T_e, n_e, n_1, etc., at 750 km. Observationally, the appearance of HeI at $h \sim 1100$ km has been taken to imply that a significant departure from spherical symmetry appears at these heights, thus that an extrapolation of results below this height to greater heights may be unjustified. In the following, however, we attempt to push the analysis in terms of a spherically symmetric model to the limit, asking what $T_e(h)$ would result from the conditions above. Then, we offer a few comments on the meaning of the results, and their link to the He emission and the question of non-spherically symmetric models, deferring major consideration of the latter to Chapters 7 and 8.

We restore the factor $(1 + \Delta)$ entering the complete expression for b_1 in Eq. (6-27). Then, Eqs. (6-35) and (6-36) give the following convenient set of equations for the upward integration from 750 km. We have set H : He = 10, by number; and $Z = 10^{-4}T_e$.

$$\begin{aligned}[11.78/Z - 2 - 3.34 n_e/n_1](d/dh)\ln Z \\ = (1 + n_e/n_1)[4.22 \times 10^{-8}/Z - 2.2 \times 10^{-8}] \\ + 0.10 \times 10^{-8}(n_e/n_1) + (d/dh)\ln(1+\Delta)\end{aligned} \qquad (6\text{-}41)$$

$$n_e^2 = 10^6 Z^{3/2} f(h) \qquad (6\text{-}42)$$

$$n_1 = 1.05 \times 10^{-12}(1+\Delta) Z e^{X_{12}} f(h) \qquad (6\text{-}43)$$

$$n_2 = 4.20 \times 10^{-12}(1+\Delta) Z f(h) \qquad (6\text{-}44)$$

Δ follows from Eq. (6-26) as before. We obtain the results in Table 6-10, as our revised model for $h \geq 750$ km. Note that $\tau_{\text{LyC}} \lesssim 100$ for $h \gtrsim 1100$ km; so that our criterion for the validity of Eq. (6-20) for b_1 fails at greater heights. Thus, at these heights, we must consider the transfer problem in the Lyman continuum.

We can abstract in a manner convenient for application here, an approach to this transfer problem developed by Pottasch and Thomas (1960). We have the source function in the Lyman continuum given by

Table 6-10. Model of the Chromosphere for 750 km $< h \lesssim$ 1320 km Assuming Hydrostatic Equilibrium

h, km	$Z = 10^{-4}T_e$	$10^8 \dfrac{d\ln Z}{dh}$	$10^{-11}n_e$	$10^{-11}n_1$	$10^{-5}n_2$	τ_{LyC}	$\tau_{\text{Ly}\alpha}$	$\tau_{\text{H}\alpha}$
750	0.665	0.284	4.04	121	9.98	1×10^3	1×10^7	34.5
850	0.684	0.291	3.69	62.8	8.38	—	—	28.5
950	0.704	0.303	3.38	31.9	7.02	—	—	23.4
1000	0.715	0.314	3.24	22.7	6.44	2×10^2	2×10^6	21.7
1050	0.727	0.329	3.10	16.0	5.92	140	—	20.5
1100	0.740	0.356	2.97	11.0	5.42	96	—	18.7
1150	0.754	0.390	2.86	7.79	4.98	58	—	17.7
1200	0.770	0.464	2.75	5.05	4.61	35	3×10^5	17.0
1225	0.779	0.519	2.70	4.08	4.44	28.0	—	—
1250	0.7901	0.633	2.65	3.19	4.28	19.8	2×10^5	—
1260	0.7954	0.714	2.64	2.87	4.22	16.0	—	—
1270	0.8016	0.836	2.62	2.55	4.16	13.5	—	—
1280	0.8090	1.008	2.61	2.26	4.11	11.2	1×10^5	—
1290	0.8183	1.285	2.60	1.98	4.06	9.0	—	—
1300	0.8310	1.820	2.60	1.71	—	6.6	7×10^4	—
1310	0.8504	2.84	2.62	1.42	—	4.7	—	—
1320	0.897	8.11	2.69	1.1	—	2.5	—	—

$$S_{\mathrm{LyC}} = (2h\nu^3/c^2)(b_1 e^{X_\nu} - 1)^{-1} = (2h\nu^3/c^2)S'_{\mathrm{LyC}} \qquad (6\text{-}45)$$

and using b_1 from Eq. (4-43),

$$\begin{aligned}(S'_{\mathrm{LyC}} e^{X_\nu})(X_1 e^{X_1})^{-1} &\cong (b_1 X_1 e^{X_1})^{-1} \\ &= [P/2U + (M+1)/2U]/[1 + M/2U + (1+\Delta)/2R](e^{-X_1}/X_1) \\ &= \mathcal{Y}/(1+\Gamma) + \psi \qquad (6\text{-}46)\end{aligned}$$

where

$$\begin{aligned}\mathcal{Y} &= (e^{-Y_1}/Y_1); \qquad \Gamma = [(1+\Delta)/2R]; \\ \psi &= [(M+1)(2UX_1 e^{X_1})^{-1}]/(1+\Gamma)\end{aligned} \qquad (6\text{-}47)$$

Then we multiply the Eddington-approximation form of the transfer equation, Eq. (4-92), by $d\nu/\nu$ and integrate over ν to obtain

$$\begin{array}{ccccc} \frac{1}{3}\frac{d^2}{d\tau_1{}^2}\int_{\nu_1}^{\infty} e^{-Y_\nu}\frac{d\nu}{\nu} = & \nu_1{}^6\int_{\nu_1}^{\infty}\frac{e^{-Y_\nu}}{\nu^6}\frac{d\nu}{\nu} & - & \nu_1{}^6\,[S'_{\mathrm{LyC}}e^{X_\nu}] & \int_{\nu_1}^{\infty}\frac{e^{-X_\nu}}{\nu^6}\frac{d\nu}{\nu} \\ \downarrow & \downarrow & & & \downarrow \\ \frac{1}{3}\frac{d^2}{d\tau_1{}^2}\left[\frac{e^{-Y_1}}{Y_1}\right] = & \left[\frac{e^{-Y_1}}{Y_1} + kr_1\right] & - & [S'_{\mathrm{LyC}}e^{X_\nu}] & \left[\frac{e^{-X_1}}{X_1} + kr_2\right] \end{array} \qquad (6\text{-}48)$$

$$\begin{aligned}\frac{1}{3}\frac{d^2}{d\tau_1{}^2}\mathcal{Y} = \mathcal{Y} - \left[\frac{\mathcal{Y}}{1+\Gamma} + \psi\right] &= \Lambda\mathcal{Y} - \psi \\ \Lambda &= \Gamma\,[1+\Gamma]^{-1}\end{aligned} \qquad (6\text{-}49)$$

The approximation consists in neglecting the terms kr_1 and kr_2 in Eq. (6-48) relative to the other terms in the respective bracket, and in adopting this "one-point" quadrature representation of the Lyman continuum by its value at the series head. The net effect of the first part of the approximation is to overestimate the variation of $\mathcal{Y}$; if the approximation is not correct, we should in essence replace Γ in Eq. (6-49) by $(kr_1\mathcal{Y}^{-1})$. The net effect of the "one-point" quadrature will be an underestimate of the scale over which the radiative leak will occur; viz., an increase in b_1 over that given by Eq. (6-27) will not come until higher in the atmosphere, at a lower τ_{LyC}. (Compare our developments in the last part of Chapter 4, on the 3-point versus the 1-point quadrature.)

In the reference cited, we have investigated the solution of Eq. (6-49) under various representations of the variation of ψ/Λ with τ_1. To an accuracy commensurate with our use of the "one-point" quadrature, we may simply use the solution $\mathcal{Y} = \psi/\Lambda$ out to such values of τ_1 that the radiative leak gives a significant gradient in $\mathcal{Y}$. That is, we use the solution of Eq. (6-48) valid for constant ψ/Λ, *viz.*,

$$\mathcal{Y} = \frac{\psi}{\Lambda}\left[1 - \frac{\exp(-\sqrt{(3\Lambda)}\tau_1)}{1+\sqrt{\Lambda}}\right] \equiv \frac{\psi}{\Lambda} F(\tau_1) \tag{6-50}$$

The use of this equation assumes that in the region of strong variation of $F(\tau_1)$, the variation of ψ/Λ is small in comparison. Set

$$\text{ш} = \frac{2R(1+\Delta)^{-1}+1}{2R(1+\Delta)^{-1}F(\tau_1)+1}; \qquad \frac{d\ln \text{ш}}{dh} \sim 0.158 \times 10^{-18} n_1(\text{ш} - 1) \tag{6-51}$$

Then we modify Eqs. (6-41)–(6-44) by adding to the right side of Eq. (6-41) the term $(d \ln \text{ш}/dh)$, and by increasing the value of n_1 as given by Eq. (6-43) by the factor ш. These modifications have been applied to give the solution above 1100 km, in Table 6-10. In the solution we have assumed that we could approximate τ_{LyC}, which requires the integral $\int n_1 dh$, by using

$$\int_h^\infty n_1 dh \sim n_1(d\ln n_1/dh)^{-1} \tag{6-52}$$

Because $d \ln n_1/dh$ increases with height, we shall overestimate τ_{LyC} and so understimate $d \ln Z/dh$.

We have carried the solution self-consistently only to $h \sim 1300$ km. Above this height, $d \ln Z/dh$ is rising so rapidly that considerable iteration is required to obtain complete consistency among all quantities. Too-detailed work is not justified, because in regions of such steep gradient in T_e other effects, such as thermal conduction, which we have neglected, must be included. Our aim here is simply to explore the kind of behavior of T_e if we apply hydrostatic equilibrium. The values given for 1310 and 1320 km have sufficient internal consistency to indicate that the discontinuity in T_e comes at about 1320 km, subject to the influence of these neglected terms, which will smooth the gradient somewhat.

To carry the solution above the abrupt rise in T_e, three general problems must be resolved.

a. The Value of T_e at the Top of the Rise. A minimum value for

T_e is fixed by the requirement that $d \ln Z/dh \geq 0$. Above the discontinuity, $n_e \gg n_1$, so that Eqs. (6-36) and (6-35) give

$$(d \ln Z)/dh = 2/7(\beta_\infty - 4.42 \times 10^{-8}/Z)$$

$$= 0.63 \times 10^{-8}(1 - 2.01/Z) \quad \text{(6-53)}$$

A value larger than this minimum $T_e = 2.01 \times 10^4$ would follow from our results in Chapter 5 on the beginning point of the He plateau. To obtain the results in Chapter 5, it was necessary to introduce an assumption about the relative non-radiative energy input above and below the jump in T_e. Here, we have held constant β_∞. Any definitive physical model of the chromosphere must rest upon a careful examination of this question of the variation with height of the non-radiative energy input.

b. A Recomputation of the Results in Table 6-10, *Introducing the Effect of a Discontinuity in* T_e. Primarily, since such a discontinuity will drop n_1, the effect will be to drop the Lyman continuous opacity, thus force downward the position of the rapid rise in T_e. We can estimate the effect by summarizing the behavior of b_1 and n_1:

For high opacity in the Lyman continuum, we have detailed balance in it, and in the notation used earlier,

$$b_1 = U(1 + \Delta)/R, \qquad \tau_{\text{LyC}} \gtrsim 10^2 \quad \text{(6-54)}$$

For lesser Lyman continuous opacity, we have the transition from this case of b_1 independent of n_e to the case where it depends upon n_e as a function of τ_{LyC}; viz., for $10^2 \lesssim \tau_{\text{LyC}} \lesssim 1$,

$$b_1 = 2U\left(1 + \frac{[1 + \Delta]}{2R}\right)\left[1 + \frac{2R}{1 + \Delta}\, \mathrm{F}(\tau_{\text{LyC}})\right]^{-1}$$

$$\sim \frac{U}{R}(1 + \Delta)F^{-1} \quad \text{(6-55)}$$

For $\tau_{\text{LyC}} \lesssim 1$, we take that radiation field in the Lyman continuum to be constant and equal to its value at $\tau_{\text{LyC}} \sim 1$, and obtain

$$b_1 = 2U\{1 + [(1 + \Delta)/2R]\} \sim 2U \quad \text{(6-56)}$$

As τ_{LyC} drops, so also does $\tau_{\text{Ly}\alpha}$. Across the jump in T_e, there is the possibility that we leave the condition of detailed balance in the Lyman lines. By solving the equations of statistical equilibrium for a three-level atom without assuming detailed balancing (cf. Chapter 4), we obtain

$$b_1 = 2U \times$$

$$\left\{\frac{1 + 0.5\,[(\mathrm{R}^{-1} + \delta_{21}/F_{22})/(1 + \delta_{21}/F_{22})]}{(1 + \delta_{21}/F_{22})^{-1} + F_{12}/C_{12} + 0.127[(X_{13} + 1)/(X_{12} + 1)]e^{-X_{23}}}\right\} \tag{6-57}$$

in the notation of Chapter 4, Eqs. (4-40) et seq., and using

$$\delta_{21} = K_{21}e^{X_2}(\mathrm{NRB})_{1,2} \tag{6-58}$$

where NRB is defined in Eq. (4-103). Using Eq. (6-56) to represent the situation of detailed balance in the Lyman lines, Eq. (6-57) to represent the situation of non-detailed balance, and Eq. (6-53) to estimate $d \ln Z/dh$, and setting $d \ln n_e/dh \sim 1 \times 10^{-8}$, above the jump in T_e, for $n_e \sim 2.5 \times 10^{11}$, we obtain the quantities given in Table 6-11 (db and ndb refer to detailed balance and non-detailed balance):

Table 6-11. Quantities above Jump in T_e

	n_1		$n_1(d \ln n_1/dh)^{-1}$		$\tau_{\mathrm{Ly}\alpha}$	
Z	db	ndb	db	ndb	db	ndb
2	10^9	10^{10}	10^{17}	10^{18}	10^4	10^5
3	10^8	10^9	10^{16}	10^{17}	10^2	10^3

We recognize that the applicability of detailed balance requires the net rate of radiative transitions to fall below the captures from the continuum. We apply the methodology of Chapter 4, and the expression for the NRB for Lyα of hydrogen, to compute that $\tau_{\mathrm{Ly}\alpha} \sim 10^3$–$10^4$ satisfies the criterion for ignoring the Lyα radiative transitions (k_3 for Lyα is about 0.7×10^{-3}; and $\epsilon B_\nu \gg \eta B^*$ for Lyα; then use Eq. (4-111) for NRB). Thus, the region above the jump probably satisfies detailed balance if Z is as low as 2, but not if it is as high as 3. In any event, the Lyman continuous opacity of the region can be ignored. Thus, since the scale height for n_1 from the model of Table 6-10 is about 50 km at 1300 km, and about 100 km at 1200 km, we must expect a completely consistent model, which includes the effect of the abrupt rise in T_e to something in excess of 2×10^4°K, to give lower values of τ_{LyC} than those in Table 6-10.

c. Consistency of Results Above and Below the Jump with the Conditions of Hydrostatic Equilibrium and β_∞ = Constant. The two requirements are

$$(n_1 + 1.9n_e)T_e\Big)_{\text{below}} = 1.9n_eT_e\Big)_{\text{above}} \tag{6-59}$$

and

$$n_e^2T_e^{-3/2}\Big)_{\text{below}} = n_e^2T_e^{-3/2}\Big)_{\text{above}} \tag{6-60}$$

If now the jump in T_e occurs at a point where $n_e \gtrless n_1$, conditions (6-59) and (6-60) cannot be satisfied simultaneously; for the first requires a decrease in n_e, and the second, an increase. Thus, we must either require the jump to occur where $n_1 > n_e$—by about a factor of five for $Z = 2$ or a factor of ten for $Z = 3$—or drop one of the two conditions (6-59) or (6-60) above the jump.

The first alternative would force the jump back to $h \sim 1100$ km (cf. Table 6-10). It is of considerable interest that this is the height which has been assigned as the beginning of HeI emission (cf. Chapter 7).

To vitiate the assumption of hydrostatic equilibrium, we must have some change in physical conditions in the vicinity of the jump—e.g., the decrease in density above the jump might make significant the momentum input accompanying the non-radiative energy input. To vitiate the constancy of β_∞, we must show that it is only *apparently* constant. That is, that introducing a variation of the type required in $n_e^2T_e^{-3/2}$ will still permit an apparent variation of E_{3640} mimicing a constant exponential.

Until we consider the effect of a departure from spherical symmetry, it is not worthwhile to investigate these three alternatives further. For example, we might consider a model where E_{3640} came from only a part of the atmosphere along the line of sight, and this part formed a fraction varying as $\exp(-\beta_\infty h)$ with height. We would obtain essentially the same values for T_e, n_e, n_1, etc., near 500 km, but above 500 km we would have a steeper gradient in T_e. Thus, we defer further consideration to Chapters 7 and 10. Here, we have wished only to explore the consequences of continuing above 1000 km. the same physical conditions existing below it. We find that the gradient in T_e would be considerably steeper than suggested in our earlier analysis (Athay, Menzel, Pecker, Thomas, 1955), reaching, indeed, such values below 1500 km as to make not quite so surprising the appearance there of He emission. Whether the actual conditions suggested by this incomplete analysis are quantitatively adequate must be deferred, pending the results of the next chapter.

4. Estimate of T_e from the Emission at Several Wavelengths in the Balmer Continuum. In Chapter 2, Eqs. (2-11a) through (2-11d), we have given results of measures made at λλ3600, 3550, and 3500 in addition to those already used at λ3648. There is a systematic trend between the several sets of measures although the scatter is very strong (e.g., the β value is the same for λ3600 and λ3550). We ask whether we can make any estimate at all of T_e from such measures, and the wavelength dependence of the Balmer free-bound emission as given in Eq. (6-14e). From Menzel and Pekeris (1935), we compute values of $g_{\mathrm{fb}} = 0.887$, 0.889, and 0.910 at λλ3600, 3550, and 3500, respectively. With these values, and the parameters of Eqs. (2-11a) through (2-11d), we evaluate the terms entering the equation

$$(hc/kT_e\lambda_2)[(\lambda_2 - \lambda)/\lambda] = \ln L_{\lambda_2}/L_\lambda - (\beta_2 - \beta) \qquad (6\text{-}61)$$

where

$$L_\lambda = (\beta/g_{\lambda\mathrm{fb}})A_\lambda\sqrt{(\beta/2\pi R)}$$

a subscript 2 denotes λ3648, and log A_λ is the constant term in Eq. (2-11). We obtain the values of T_e that are given below in Table 6-12.

From these results, we can probably conclude that $dT_e/dh > 0$, but no more. Such T_e values as those indicated at 500 to 1000 km would require impossibly high emission at λ4700, relative to the observations. The systematic decrease of T_e with decreasing λ suggests that the extrapolation of the background continuum to the

Table 6-12. T_e from λ-Variation of Balmer Continuum

h	500	1,000	1,500	2,000
λ3600	3,100	4,400	7,700	29,000
λ3550	4,000	4,800	6,200	8,800
λ3500	3,800	4,600	5,600	7,400

short-wavelength side of λ3648 has probably not been sufficiently well done to permit the analysis above in terms of small differences. We include these results only because the method has been used several times in the literature.

B. Regions of Significant Opacity, Where the Emission Is the Integral of the Source Function

In Section 6-IIIA3 we have constructed a model that represents an upper boundary for the values of $T_e(h)$ in the region $0 < h < 500$ km. Because of this limitation, the estimate of τ(tangential, λ4700) made from this model is an underestimate; even so, at height 0, τ_{tang} lies near unity. An increase in τ_{tang} over the value in Table 6-9 by a factor 10 would make the atmosphere (effectively) completely opaque. Even on the basis of the model of Table 6-9, such an increase would occur within 200 km. below the 0 km level; because the model provides an underestimate, (effective) complete opacity must occur closer to the 0-km level. We now discuss the relationship between Dunn's observations, the observations E_{4700} from the 1952 eclipse, and this upper limit model from Table 6-9 in an attempt to improve the Table 6-9 model and say something about the value and position of T_e(min); for comparison with other work on this region of the atmosphere, we use Pagel's model (1956) already referred to (cf. Figs. 6-1 and 6-2).

Although Dunn believes his data to be quite reliable only for heights below about 500 km inside the limb, and to be marginal near the crossover with the Pierce-Waddell extrapolation at 200 km inside the limb, he informs us that the steep drop thereafter must be taken quite literally, even though its details may be uncertain. Using Minnaert's value (1953) for $I_{\lambda 6600}$ (0, 1) of 2.85×10^{14} erg sec^{-1} cm^{-2}, we obtain from Dunn's data:

h, km (Dunn's scale)	−500	−200	−100	0
$I_{\lambda 6600} \times 10^{-14}$	1.15	0.98	0.82	0.32
$I_\lambda = \overline{B_\lambda(T_e)} \rightarrow T_e$	4940°	4760°	4600°	3830°

The last line is based on the assumption that the atmosphere is opaque along the line of sight. The problem is to decide how much of the apparent drop in T_e represents an opacity effect.

As discussed in Section 6-IIIA3, the data on emission at λ4700 are few in this region of the atmosphere. As a rough check on our model, we estimate a value for $I_{\lambda 4700} = (d \ln E/dh)(E/4\pi)$ from the empirical data plotted in Fig. 6-5, obtaining a value $\sim 1.1 \times 10^{14}$ erg sec^{-1} cm^{-2} near 0 km on our scale. We have the relationship between $B_\lambda(T_e)$ at λ4700 and λ6600:

T_e	4000°	4500°	4750°	5000°
$B_{\lambda 6600}/B_{4700}$	1.65	1.30	1.17	1.06

This estimate gives excellent agreement with Dunn's results on $I_{\lambda 6600}$ if we take the position corresponding to our estimate to lie between -200 and -500 km on Dunn's scale—a position on the disk below the steep drop in I_λ at the limb—and if we take $T_e \sim 4750$ to 5000° in computing the ratio $B_{\lambda 6600}/B_{\lambda 4700}$. We note that the values in Table 6-9 predict a value for $I_{\lambda 4700}$ at 0 km within 10 to 20 percent of the above empirical estimate, although they underestimate the value of E by a factor of two or so.

If our value of $I_{\lambda 4700}$ from the empirical data is an underestimate, we obtain agreement with Dunn's data by assigning our 0 km to correspond to a point even farther on the disk on Dunn's scale, and requiring T_e to rise above 5000°. If our value of $I_{\lambda 4700}$ is an overestimate, our 0 km must lie between about 0 and -200 km on Dunn's scale. The rate of decrease in Dunn's values is so great in this atmospheric region that the conversion from $I_{\lambda 4700}$ to $I_{\lambda 6600}$ places no particular restriction on T_e for the range under consideration.

Noting that the model of Table 6-9 must represent an upper limit to $T_e(h)$, we conclude that a value of T_e near 4750 to 5000° at 0 km on our scale is the most likely alternative. The reasoning is as follows:

Consider first the result if we take our empirical estimate of $I_{\lambda 4700}$ literally. If T_e is to lie in the range 4750 to 5000° at height 0 km on our scale, then the values of T_e computed from Dunn's data under the assumption of an opaque atmosphere require τ_{6600} to be high enough that the atmosphere is indeed effectively opaque near height 0 km on our scale, or about -200 km on Dunn's scale; that is, $\tau_{6600} \gtrsim 2$. Since the ratio of absorption coefficients at λ_{6600} and λ_{4700} is about 2, we require $\tau_{4700} \gtrsim 1$, while the model of Table 6-9 gives about 0.25. The required change in this model is in the correct direction, the question is the size of the change required. We have two alternative ways to introduce the change.

On the one hand, we can arbitrarily drop T_e to 4750° at 0 km, holding n_e fixed; we increase n_1 and τ by a factor ~ 4.5. So long as we hold $d \ln (n_e n_p T_e^{-3/2})/dh = 0$, we cannot reconcile this new value of n_1 at 0 km with the value at 500 km and maintain hydrostatic equilibrium. To preserve hydrostatic equilibrium, we should have to drop T_e at 500 km by about 200°; the change would carry upward in the model of Table 6-10.

On the other hand, we can arbitrarily drop T_e to 4750° at 0 km, but allow n_e to change, and $d \ln (n_e n_p T_e^{-3/2})/dh \neq 0$, with a positive value for this last somewhere in the interval $0 < h < 500$ km. If we take $d \ln (n_e n_p T_e^{-3/2})/dh > 0$ across the whole interval, we require a value about 2×10^{-8} to lower T_e to 4750° from 6150° at 500 km. But, such a value would decrease $(n_e n_p T_e^{-3/2})$ by almost the amount n_1 increased from the drop in T_e; the net rise in n_1 becomes about a factor 2. If we take $d \ln (n_e n_p T_e^{-3/2})/dh > 0$ across some upper part of the interval, and less than zero across the lower, we can increase somewhat the rise in n_1 at 0 km. The extreme of such a procedure would result if we introduced a minimum in T_e in the interval 0 to 500 km.

If our empirical value of $I_{\lambda 4700}$ is an underestimate, the difficulties discussed above increase without a corresponding gain anywhere. If the empirical value is an overestimate, and our height zero agrees with Dunn's scale closer to his 0 km, we again have two alternatives. Either we drop T_e below about 4750° and retain the requirement $\tau_{6600} \gtrsim 2$ at 0 km on our scale; or we hold T_e at about 4750 to 5000° and allow the atmosphere to depart from being effectively opaque at λ6600. The first alternative makes more pronounced any of the difficulties encountered above when we took literally our estimated $I_{\lambda 4700}$. The second alternative is permissible so long as the change in $I_{\lambda 4700}$ lies well within a factor 2; for otherwise the predicted value of $I_{\lambda 4700}$ from the (adjusted) model of Table 6-9 will considerably exceed the empirical value.

Thus, we conclude that T_e lies near 4750 to 5000° at our height 0 km, with τ_{6600}(tang) ~ 2 or possibly a little less. A decision between these alternatives cannot be made on the basis of presently available data, nor can we draw conclusions on the position or size of T_e(min). We can only conjecture, from this discussion, that *if* T_e(min) does *not* occur in the interval $10^{-5} \gtrsim \tau_{4700} \lesssim 0.02$, then T_e(min) $\sim$ 4750°. Such a value is considerably higher than that in current general usage. We should therefore compare our values with a typical model having T_e(min) $\sim$ 4000° near $\tau_5 \gtrsim 0.01$; for this purpose, we consider Pagel's model, where the behavior of T_e near minimum has been inferred from the behavior of weak Fe lines.

In Table 6-13 we reproduce Pagel's model in the range $0.1 < \tau_5 < 10^{-5}$. From Fig. 6-1, it is already clear that T_e from Pagel's model falls everywhere below that from the Pierce-Waddell model, and thus considerably below the predictions of Dunn's data near the limb. The present observations in the continuum provide no real check on Pagel's suggestions of a minimum at $\tau_5 \sim 0.01$; they can only suggest that the drop in T_e given by this model for $\tau_5 \gtrsim 0.05$ is too great for good agreement with the Pierce-Waddell and Dunn limb-darkening observations. Thus, if we are to preserve a value T_e(min) $\sim$ 4000° near $\tau_5 \sim 0.01$, we require this minimum to be reached essentially as a continuation of the drop from Dunn's values of $I_{\lambda 6600}$.

This last result comes into conflict with the analysis of the infrared FeI lines (Pagel, 1955) underlying Pagel's model. Because this analysis was carried out under the LTE assumption, one can only raise the question of the relation between Pecker's recent work (1957) on equally weak lines—which suggest non-LTE effects—and a possible resolution of the discrepant values of the gradient of T_e sug-

Table 6-13. Pagel's Model of the Low Chromosphere[a]

rad τ_{5000}	T_e	$10^{-14}n_1$	$10^{-11}n_e$	h, km, arbitrary zero
1×10^{-5}	5800	0.417	2.76	500
1×10^{-4}	5600	3.10	4.64	202
2×10^{-4}	5525	5.70	5.34	122
4×10^{-4}	5430	10.8	5.35	42
8×10^{-4}	5315	20.1	6.38	−36
3.2×10^{-3}	4900	72	7.76	−183
8×10^{-3}	4430	135	10.6	−252
1.5×10^{-2}	4100	232	13.7	−274
3×10^{-2}	4500	305	20.5	−312
1×10^{-1}	5010	550	46.8	−391

[a] MN **116**, 608 (1956).

gested here. No results on this monograph on the non-LTE effects have been unambiguously shown to be applicable to weak subordinate lines; this problem must be investigated. It is extremely suggestive that Pecker's results show the same *direction* of effect as would result if we assumed that we could take over the formalism developed for the resonance lines. This result provides an impetus to the needed theoretical investigation.

We note that the values of the various quantities in the model of Table 6-9 and Pagel's, reproduced in Table 6-13, lie very close. Since Pagel's model in this region is essentially based on our 1952 observations, the result is not surprising. It does suggest again, however, that T_e(min) most probably occurs in the interval $10^{-3} \lesssim \tau_5 \lesssim 10^{-2}$, with a value as low as 10^{-4} possibly not excluded, if T_e(min) is to have a value significantly below about 4750°.

The chief difference between Pagel's model in the region $0 \lesssim h < 500$ km. and ours lies (1) in our model being an upper limit on $T_e(h)$ from our use of $d \ln (n_e n_p T_e^{-3/2})/dh = 0$, and (2) Pagel's neglect of departures of b_1 and b_2 from unity. Pagel comments on the value of b_2, stating that the results at λ_{3640} prohibit b_2 departing by more than a small factor from unity in this atmospheric region, and raising the question whether this result and the large values obtained by Pecker and Pecker (1956, cf. Chapter 9) in the region $h \gtrsim 1000$ km can be reconciled. Our formula,

$$b_2 = 0.994 \times 10^4 (e^{-X_2}/X_2)(1 + \Delta)$$

gives values about 0.5 at 5000° and about 2 at 6000°; at heights > 1000 km, b_2 can reach about 10^3 at $T_e = 2 \times 10^4$ if in these regions the condition of detailed balance in the Lyman lines remains valid.

To resolve more completely the model in this region—500 km $\lesssim h \lesssim 500$ km, or $0.05 \lesssim \tau_5(\text{rad}) \lesssim 10^{-5}$, we must await more detailed observations in the continuum from the 1959 eclipse on the one hand, and a treatment of the source function for weak metallic lines on the other. (See further notes on this point in Appendix II.)

CHAPTER 7

Extension of the Model to Include Helium Emission

R. Grant Athay

The model in the preceding chapter is based upon the Balmer free-bound continuum of hydrogen and the continuum at λ4700 only. Since there are no direct observations of other free-bound continua, the model can be extended to include emission from other elements only by making use of line data. The line data introduce the additional complications of possible departures from thermodynamic equilibrium and non-negligible opacity. In the case of helium, however, several lines of the singlet and triplet series are observed, which makes it possible to obtain a good estimate of the free-bound continuum intensity from the observed line intensities. Also, as we noted in Chapters 2 and 3, the helium lines show no evidence of self-absorption either in the relative emission gradients for different lines or in the line profiles. We may therefore obtain indications of departures from thermodynamic equilibrium without the ambiguity introduced by self-absorption. Furthermore, we expect the emission from helium to play a strong role in determining the thermodynamic state of the chromosphere. For these reasons we turn next to the helium data.

I. Estimate of Helium Free-Bound Emission

Since the helium lines are apparently unaffected by the effects of self-absorption, the term $\{\text{abs}\}$ in Eq. (2-5) may be set equal to unity, in which case,

$$\mathcal{E}_{kj} = [\beta^{3/2}/(2\pi R)^{1/2}]E_{kj} \tag{7-1}$$

and from Eq. (2-17),

$$\begin{aligned}\mathcal{E}_{kj} = {} & [1/\delta_{kj}][0.027 \exp(-1.27 \times 10^{-8} h) \\ & - 4.3 \exp(-3.7 \times 10^{-8} h) + 15 \exp(-4.6 \times 10^{-8} h) \\ & - 680 \exp(-9.2 \times 10^{-8} h)] \qquad (7\text{-}2)\end{aligned}$$

This latter equation is valid, of course, for $h \geq 1100$ km only, as was the case for Eq. (2-13). The emission per unit volume $\mathcal{E}_{kj}$ is also given by

$$\mathcal{E}_{kj} = h\nu A_{kj} n_k \qquad (7\text{-}3)$$

The transition probabilities A_{kj} are known from the matrix elements computed by Hylleraas (1937) and others (cf. Allen, 1955), and the δ_{kj}'s are tabulated in the Appendix. The populations of the excited energy levels n_k may therefore be obtained directly from Eqs. (7-2) and (7-3).

The modified Boltzmann-Saha equation for n_k is

$$n_k = 4.14 \times 10^{-16} n_e n_{\mathrm{II}} T_e^{-3/2} b_k (\tilde{\omega}_k/4) e^{\chi_k/T_e} \qquad (7\text{-}4)$$

which may be rewritten in the form

$$\log (10^{16} n_k/1.04\tilde{\omega}_k) = \log n_e n_{\mathrm{II}} T_e^{-3/2} + \log b_k + (0.434\chi_k/T_e) \qquad (7\text{-}5)$$

Then, since $b_k \rightarrow 1$ as $k \rightarrow \infty$, a plot of the quantity on the left side of Eq. (7-5) against χ_k must have an intercept at $\chi_k = 0$ equal to $\log n_e n_{\mathrm{II}} T_e^{-3/2}$. Also, the difference between this intercept and the left side of Eq. (7-5) for a given k is $\log b_k + (0.434\chi_k/T_e)$.

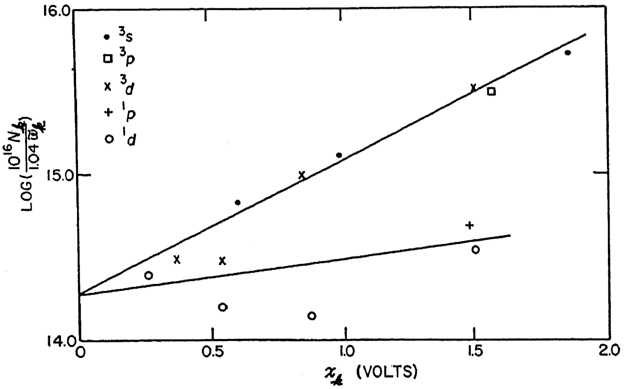

Fig. 7-1. Illustration of the estimate of $n_e n_{\mathrm{II}} T_e^{-3/2}$ and T_{ex} for the HeI lines in the normal chromosphere at h = 1500 km. (From R. G. Athay and D. H. Menzel, 1956, *Astrophys. J.*, **123**, 289.)

Figure 7-1 exhibits such a plot for the data at 1500 km. The lines were drawn to give most weight to the strongest spectral lines, whose intensities are more accurately known, and to give a common intercept at $\chi_k = 0$. The intercept is well defined, and gives

$$n_e n_{\text{II}} T_e^{-3/2} = 1.7 \times 10^{14} \tag{7-6}$$

at 1500 km. Since the relative intensities of the helium lines do not change with height,

$$n_e n_{\text{II}} T_e^{-3/2} = 1.7 \times 10^{14}\{\varphi^*(h)/[\varphi^*(1.5 \times 10^8)]\} = 1 \times 10^{17}\varphi^*(h) \tag{7-7}$$

where $\varphi^*(h)$ is the quantity in brackets in Eq. (7-2). Again, we note that Eq. (7-7) is valid for $h \geq 1100$ km only.

There are a few additional points of interest in connection with Fig. 7-1 that should be discussed before examining the model further.

II. Helium Excitation

A. T_{ion} *and* T_{ex} *for Helium*

The b_k's were introduced in the Boltzmann-Saha equation to allow for departures from thermodynamic equilibrium. Alternatively, they could be absorbed in the exponential terms by defining an equivalent set of ionization temperatures, $T_{\text{ion}}(k)$, for each energy level. Or, in the same sense, a set of excitation temperatures, $T_{\text{ex}}(jk)$ relating the populations of levels k and j could be defined. In general, these alternative procedures require just as many parameters as the b_k's, and do not offer any particular advantages. However, in some cases the populations of several energy levels are all related by a single $T_{\text{ex}}(jk)$ or $T_{\text{ion}}(k)$, and it is useful to identify these cases wherever possible. The b_k's are defined such that

$$b_k e^{\chi_k/T_e} = e^{k/\chi T_{\text{ion}}(k)} \tag{7-8}$$

and

$$(b_j/b_k)e^{\chi_{jk}/T_e} = e^{\chi_{jk}/T_{\text{ex}}(jk)} \tag{7-9}$$

where

$$\chi_{jk} = \chi_j - \chi_k \tag{7-10}$$

Hence, in a plot such as Fig. 7-1 the slope of the line connecting levels k and j is a measure of $T_{\text{ex}}(jk)$ and the slope of the line connecting level k to the continuum is a measure of $T_{\text{ion}}(k)$.

The triplet levels in Fig. 7-1 seem to define a straight line, which requires that $T_{\text{ex}}(jk) = T_{\text{ion}}(k)$ for all combinations of k and j. Thus, a single T_{ex} or T_{ion} serves to specify the populations of all the triplet energy levels in terms of the continuum or any of the bound levels. For the triplets in Fig. 7-1, we find $T_{\text{ex}} = 6300°$ with an estimated uncertainty of $\pm 700°$, which agrees rather well with the value $5300° \pm 300$ found by Goldberg (1939) from 1932 eclipse data. For the singlets, we cannot really tell whether a single value of T_{ex} is adequate. The lower line in Fig. 7-1 was drawn on the assumption of a single T_{ex} for the singlets, and we find $T_{\text{ex}} \simeq 23000°$ with an estimated uncertainty of $\pm$ 10,000°.

The marked difference between T_{ex} for singlet and triplet levels is a striking and unambiguous example of departure from thermodynamic equilibrium in the chromosphere. For example, the 3^3s, 3^3p, and 3^3d levels are over-populated by about a factor of ten relative to the corresponding singlet levels.

Since only one HeII line is observed in the chromospheric spectrum, we have no direct determination of T_{ex} for HeII. However, the observed line, λ4686, gives us n_4 and we can set an upper limit to n_1 from the total helium density. The model in Chapter 6 suggests a total hydrogen density of 1×10^{11} at 1500 km. Thus, the total helium density should be near 1×10^{10}, which serves as an upper limit for n_1. From the intensity of λ4686, we find $n_4 = 4 \times 10^{-3}$ at 1500 km, and from the Boltzmann equation we find $T_{\text{ex}}(1\text{-}4) \geq$ 18,000° for HeII.

B. The Source of Helium Excitation

The presence of strong emission from HeI and HeII in the low chromosphere requires an energetic excitation mechanism. Either we must permit regions with kinetic temperature of at least 18,000° as low as 1100 km or we must assume that helium is excited by an external radiation field. Miyamoto (1947) and others have suggested that ultraviolet radiation from the corona is responsible for the high state of excitation of helium, and Wurm (1948) has argued against excitation by collisional mechanisms. On the other hand, non-spherically symmetric models with alternate "hot" and "cold" columns have

been proposed by Giovanelli (1949), Hoyle (1949), Hagen (1954), Woltjer (1954), Athay and Menzel (1956), and Thomas and Athay (1956).

If external radiation is assumed to produce the excitation of helium in the chromosphere, two conditions must be met: (1) The optical depths at λ500 must be small down to at least 1100 km, where the maximum helium emission occurs, and (2) the external radiation must provide at least as many quanta as are emitted by recombinations to HeI and HeII. Since the excitation temperatures in the HeI singlets and in HeII are considerably greater than the photospheric radiation temperature, whereas the radiation field is essentially the photospheric radiation, the brackets in Eq. (5-3) must be very near unity. Therefore, to be consistent with the assumption of an external radiative excitation we must assume that these lines arise from recombinations and cascades back to the ground state. Consider first the question of chromospheric opacity.

The hydrogen density at 1100 km, obtained from the model in the preceding chapter is about 1×10^{12}; and if the relative hydrogen: helium abundances are in the ratio 10:1, the helium density is 1×10^{11}. The scale heights of the helium emission are about 10^8 cm for both HeI and HeII. Hence, the total number of helium atoms in a radial column of 1 cm^2 cross section is 1×10^{19}.

If we assume spherical symmetry, Eq. (7-6), together with the n_e and T_e in the model of Chapter 6 gives $n_{\text{II}} = 4 \times 10^8$ at 1100 km. Since n_{H} is about 5×10^{12}, most of the helium is presumably neutral. The continuous absorption coefficient of helium at λ500 is 7.5×10^{-18} (Huang, 1948). Hence, the radial optical depth down to 1100 km is

$$\tau_{500} = N_{\text{I}}\alpha_{500} \simeq 100 \qquad (7\text{-}11)$$

Similarly, we may argue that the total number of hydrogen atoms above 1100 km is about 10^{20} and since the Lyman continuum absorption coefficient at λ500 is about 10^{-18}, the optical depth is about 10^2. At λ230, corresponding to the ionization of HeII, the optical depth due to HeI absorption is about 25. In view of these large optical depths at wavelengths where ionization may occur, coronal radiation could scarcely play a role in the excitation of helium if the chromosphere is spherically symmetric.

Turning now to the second point, we note that the number of quanta emitted in the singlet line λ6678 in a radial column of 1 cm² cross section above 1500 km is

$$Q_{6678} = (1/h\nu) \int_{h = 1500\text{ km}}^{\infty} \mathcal{E}_{6678}(h)\, dh \tag{7-12}$$

From Eq. (7-3), we obtain $Q_{6678} = 2.6 \times 10^{15}$ quanta sec⁻¹ cm⁻². The coronal radiation at wavelengths shorter than λ500 is estimated at about 2×10^{13} quanta $\text{sec}^{-1}\ \text{cm}^{-2}$ (Elwert, 1954; Woolley and Allen, 1950). Thus, even if we drop the assumption of spherical symmetry and allow the coronal radiation to penetrate the chromosphere, the number of ultraviolet quanta emitted by the corona is over 100 times too small to account for the observed excitation of helium.

One final argument may be advanced against the assumption that coronal radiation produces the observed excitation of helium in the chromosphere. The strongest coronal radiations are highly localized in centers of activity associated with sunspot zones. On the other hand, the emission from chromospheric helium is rather uniformly distributed over the entire sun and shows no recognized tendency to concentrate systematically below active coronal regions.

III. High-Temperature Excitation of Helium

In view of the strongly compelling arguments against excitation of helium emission in the chromosphere by an external radiation field, we shall adopt the alternative viewpoint that it is excited by the thermal properties of the chromosphere. In adopting this alternative, we must also adopt a non-spherically symmetric model for the chromosphere, as the following analysis of HeI demonstrates. Thus, we must consider a model in which only a fraction of the chromosphere gives rise to the observed HeI emission. Our immediate interest is in the value of T_e in the helium regions. The observed line intensities lead to an evaluation of $\log b_k e^{\chi_k/T_e}$ from Eq. (7-5). Therefore, our problem is to compute the populations of the singlet and triplet levels for prescribed values of T_e and n_e following the procedures outlined in Chapter 4.

Fortunately, the problem is somewhat simpler in the case of HeI than it is for hydrogen, because the chromosphere has small opacity in all the subordinate lines and the radiation field is just the photospheric radiation field. Hence, the problem can be solved without solving simultaneously the transfer equations for the subordinate lines. Also, collision cross sections from the ground state are known more accurately for HeI than for hydrogen.

Populations of the singlet and triplet levels of HeI have been computed by Jefferies (1955), Zirin (1956 and 1957), de Jager and de Groot (1957), and Athay and Johnson (1960). A semi-empirical analysis of the HeI lines has been carried out by Shklovsky and Kononovitch (1958).

In the analysis carried out by Shklovsky and Kononovitch, the authors attempt to determine T_e from the observed occupation number n_{3^3d} by an iterative procedure in which they assume that $b_1 = b_{3^3d} = \tau^{-1}(\lambda 504)$ whenever $\tau(\lambda 504) < 1$ and $b_1 = b_{3^3d} = 1$ whenever $\tau(\lambda 504) > 1$. Such a procedure has no physical basis, and, with the exception of de Jager and de Groot, who assume $b_1 = 1$, all other authors find $b_1 \gg b_{3^3d} \gg 1$. Furthermore, b_1 may exceed unity by a large factor even when $\tau(\lambda 504) > 1$ (cf. Chapter 4).

The calculations by Jefferies lump the $2s$ and $2p$ terms together, and they do not include enough of the excited states to allow an adequate comparison with observations. Zirin assumes in his calculations that there are no transitions between the terms of a given level for $k \geq 3$, and because of this there are strong departures from thermodynamic equilibrium in the populations of the various terms of a given level. For example, he assumes that electrons leave the 3^1d level mainly by spontaneous transitions to 2^1p. However, if there is a strong coupling between 3^1d and 3^1p, the strongest transition is to 1^1s via 3^1p. Since these transition rates differ in order of magnitude, this question is a critical one. From the intensities of the lines arising from the transitions 3^3d-2^3p, 3^3p-2^3s, 3^3s-2^3p, 3^1d-2^1p, 3^1p-2^1s, and 3^1s-2^1p it appears that terms of the same parity for the third principal levels are populated in direct proportion to their statistical weights, which implies strong coupling between terms. Therefore, we cannot accept Zirin's calculations for applications to the chromosphere.

De Jager and de Groot consider two cases: One in which ionization occurs only by electron collisions, and one in which ionization occurs only by absorptions of photons from an *external* radiation field. Neither of these cases can possibly lead to thermodynamic equilibrium for the ionization of helium. Despite this obvious conclusion, however, de Jager and de Groot unaccountably set

$b_1 = 1$. Furthermore, they claim to have too much HeII emission relative to HeI at a value of $T_e \simeq 8600°$. This claim is not to be taken seriously, however, since their own numerical results actually give the HeII emission too faint by at least thirteen orders of magnitude.

The calculations by Athay and Johnson (1960) are for a 12-level atom as illustrated in Fig. 7-2. The $2s$ and $2p$ terms are considered

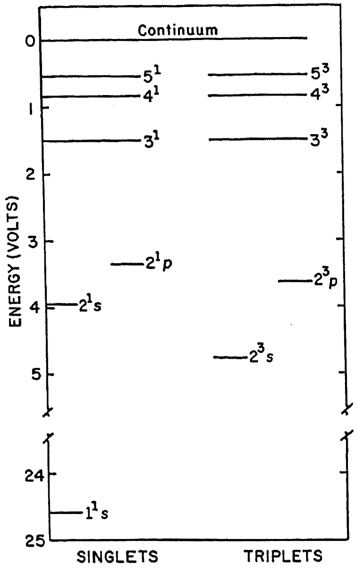

Fig. 7-2. The idealized helium atom for which b_k's are calculated. (From R. G. Athay and H. E. Johnson, 1960, *Astrophys. J.*, 131, 416.)

separately, and the terms of the 3, 4, and 5 principal levels are assumed to be populated as they would be in thermodynamic equilibrium. It is assumed that the only coupling between the triplets and singlets is via collisions to and from the ground state and via the continuum. Otherwise, all transitions are included. Under these assumptions, the populations of the triplet levels are independent of the populations of the excited singlets, and, to a close approximation, independent of the opacities in the resonance lines of the singlets. Furthermore, the population of the ground state is independent of the population of the excited bound states. Hence, the singlets and the triplets plus the 1^1s level may be treated as two independent atoms with six bound levels plus a continuum.

Because there are permitted radiative transitions from the excited singlets to the ground state, the populations of the excited singlets depend critically upon the degree of detailed balancing in the resonance lines. The degree of detailed balancing in a line is given directly by the value of the bracket

$$\left[1 - \left(\int \bar{I}_\nu \varphi_\nu \, d\nu / S_\nu\right)\right]$$

which we denote in the following by NRB. Even though the NRB may be carried as a parameter of the calculations, the relative values of the NRB must be known for the different lines of the resonance series. Two extreme cases were considered by Athay and Johnson: one in which NRB $\propto e^{-a\tau_0}$, where a is the same for all lines, and one in which NRB $\propto e^{-\sqrt{3(\epsilon+\eta)}\tau_0}$. In the former case, the NRB increases rapidly from its value at the first line of the resonance series to a value near unity for the third and higher lines. In the latter case, however, the NRB is much smaller for the second and third lines than for the first line, but it increases again for higher lines. The effect of these approximations, then, is to vary the NRB for the second and third lines of the resonance series from values much smaller to values much greater than the NRB for the first resonance line. Extended calculations for determining NRB explicitly have since been carried out by Johnson (1960).

Representative values of b_k for HeI and the ratio $n_{\mathrm{I}}/n_{\mathrm{II}}$ are given in Table 7-1. To a first approximation, the b_k for $k \geq 2$ are independent of n_e, and b_1 is inversely proportional to n_e, as was the case for hydrogen also. However, in contrast with the results for hydrogen, $b_k < 1$ for some of the singlets when NRB $= 1$. For detailed balancing in the resonance line, NRB $= 0$, the b_k's for the singlets are comparable to those for the triplets.

Empirical and computed values of the quantity $\log b_k e^{\chi_k/T_e}$ are given in Table 7-2. The value of NRB for the first resonance line is chosen to give agreement between the computed and empirical values of $\log b_k e^{\chi_k/T_e}$ for $k = 3$ in the singlets. Since the intensities of all the HeI lines decrease with height at the same rate, the empirical values of $b_k e^{\chi_k/T_e}$ are independent of height.

Table 7-1. Computed Values of b_k and n_I/n_{II} for $n_e = 10^{11}$

			Triplets					Singlets									
								NRB = 0 detailed balance					NRB = 1 no absorptions				
T_e	n_I/n_{II}	b_1	b_{2^3s}	b_{2^3p}	b_{3^3}	b_{4^3}	b_{5^3}	b_{2^1s}	b_{2^1p}	b_{3^1}	b_{4^1}	b_{5^1}	b_{2^1s}	b_{2^1p}	b_{3^1}	b_{4^1}	b_{5^1}
1×10^4	2.2×10^5	9×10^3	240	53	4.8	1.6	1.3	190	70	7.9	2.7	1.6	1.5	0.00075	0.021	0.051	0.071
2×10^4	1.6	3×10^5	2,600	310	9.8	2.3	1.7	2,300	610	25	4.7	3.0	46	0.032	0.11	0.14	0.20
3×10^4	0.026	1×10^6	5,000	490	12	2.8	1.8	6,900	1,600	47	7.9	4.4	110	0.080	0.22	0.20	0.24
4×10^4	0.0025	2×10^6	7,800	680	13	2.8	2.0	12,000	2,600	64	10	5.9	310	0.18	0.33	0.27	0.34
5×10^4	0.00067	3×10^6	8,300	690	12	2.8	1.9	16,000	3,300	75	11	6.2	390	0.25	0.46	0.34	0.39

Table 7-2. Computed and Empirical Values of $\log b_k + 0.434\,\chi_k/T_e$

	Triplets					Singlets: NRB $\propto e^{-\alpha\tau_0}$				Singlets: NRB $\propto e^{-\sqrt{3(\epsilon+\eta)}\,\tau_0}$			
k	2^3s	2^3p	3	4	5		3	4	5		3	4	5
Empirical	—	—	1.30	0.82	0.42	—	0.43	—0.09	—0.03	—	0.43	—0.09	—0.03
T_e:						NRB Lyman-α				NRB Lyman-α			
1×10^4	4.78	3.55	1.44	0.63	0.38	5×10^{-5}	—	—0.33	—0.57	1×10^{-3}	—	—0.18	—0.37
2×10^4	4.61	3.40	1.37	0.58	0.37	3×10^{-4}	—	—0.28	—0.39	3×10^{-3}	—	—0.14	—0.19
3×10^4	4.50	3.30	1.33	0.59	0.35	7×10^{-4}	—	—0.23	—0.37	1×10^{-2}	—	—0.14	—0.18
4×10^4	4.50	3.28	1.30	0.56	0.37	1×10^{-3}	—	—0.21	—0.32	3×10^{-2}	—	—0.04	—0.06
5×10^4	4.40	3.20	1.23	0.54	0.33	2×10^{-3}	—	—0.17	—0.28	2×10^{-1}	—	—0.01	—0.10

Surprisingly good agreement between the computed and empirical values of b_k is found for the triplets for all values of T_e. The fundamental reason for the insensitivity to T_e is that the populations of the triplet levels are determined primarily by the radiation field, and because of the low opacity this does not vary with ambient T_e.

For the singlets, the agreement between computed and empirical values of b_k is satisfactory for either choice of the relative weights of the NRB for the resonance lines, and again a satisfactory representation can be obtained for any value of T_e. However, the value of the NRB is specified by the values of n_e, T_e, and b_1, which imposes an additional condition on the equilibrium populations for the singlets.

For the HeI resonance line, $\eta \approx 5 \times 10^{-5}$, $\epsilon \approx 10^{-8}$ and $r_0 \approx 10^{-6}$ to 10^{-4} for the ranges of T_e considered in Table 7-1. However, the continuous opacity is due mainly to the Lyman continuum of hydrogen and the source function for the continuum is $b_1^{-1}(H) \times B_\nu(T_e)$ rather than $B_\nu(T_e)$. Thus, the factor $b_1^{-1}(H)r_\nu B_\nu(T_e)$ enters the transfer equation in place of the $r_\nu B_\nu(T_e)$ considered in chapter 4. Since $b_1(H)$ is of the order of 10^3 when $r_0 = 10^{-6}$ and of the order 10^4 when $r_0 = 10^{-4}$, $b_1^{-1}(H)r_0 \lesssim \epsilon$, and the approximation $r_0 = 0$, as used in Chapter 4, is justified. We may therefore use Eq. (5-7) to estimate values for the NRB factor. The dominant term in $\sum L_j e^{-k_j \tau_0}$ in the third-order approximation is the term with $j = 3$ for which $L_3 \approx -1$ and $k_3 \approx 8 \times 10^{-4}$. We estimate c $\lesssim \tau_0^{-1}$, in which case Eq. (5-7) reduces to NRB $= \eta e^{-8\times 10^{-4}\tau_0}$ for intermediate values of τ_0 and to NRB $= \eta^{1/2}$ for small τ_0. η increases from 5×10^{-5} for Lyman-α of HeI to about 5×10^{-2} for Lyman-β and about unity at the series limit. Thus, when $8 \times 10^{-4}\tau_0 \lesssim 1$, the proper weighting resembles the case $e^{-a\tau_0}$ more than it does the case $e^{-\sqrt{3\eta\tau_0}}$. For $8 \times 10^{-4}\ \tau_0 \gg 1$, a more detailed solution for NRB is necessary (Johnson, 1960).

To estimate the value of the NRB for the first resonance line, we must have some idea of the density in the regions responsible for the helium emission. To obtain an estimate of the density at 1500 km we consider the value of $n_e n_{\text{II}} T_e^{-3/2}$ as given by Eq. (7-6). In all subsequent calculations we assume that the abundance of helium relative to hydrogen is 0.1. However, we recognize that this abundance is uncertain by a factor of 2. If, then, we replace n_{II} by

$$0.1n_e[1 + (n_{\text{I}}/n_{\text{II}}) + (n_{\text{III}}/n_{\text{II}})]^{-1}$$

and consider that only a fraction a_1 of the chromosphere may be producing helium emission, we have

$$a_1 n_e^2 = 1.7 \times 10^{15} T_e^{3/2}(1 + n_{\text{I}}/n_{\text{II}} + n_{\text{III}}/n_{\text{II}}) \qquad (7\text{-}13)$$

From the values of $n_{\text{I}}/n_{\text{II}}$ in Table 7-1 and Zirker's value of $n_{\text{III}}/n_{\text{II}} = 0.68$ at 50,000°, we find the values of $a_1 n_e^2$ given in Table 7-3. Since $a_1 \leq 1$, we must have $10^{11} \leq n_e$.

Table 7-3. Estimates of n_e, τ_0 in λ10,830, and τ_0 and NRB in the Resonance Line

T_e	$a_1 n_e^2$	τ_0(λ10,830)	τ_0(λ584)	$k_3\tau_0$	NRB
1×10^4	3.8×10^{26}	1.2×10^{-5}	4.7×10^4	38	$\sim 10^{-4}$†
2×10^4	1.2×10^{22}	0.17	2.1×10^4	17	$\sim 10^{-5}$
3×10^4	9×10^{21}	0.16	7.1×10^2	0.70	$\sim 10^{-4}$
4×10^4	1.4×10^{22}	0.09	59	0.047	$\sim 10^{-3}$
5×10^4	3.2×10^{22}	0.02	8	0.0064	$\sim 10^{-2}$

An independent estimate of n_e may be obtained from the disk observations of the λ10,830 line (Mohler, Pierce, McMath, and Goldberg, 1950). The mean central intensity in this line is about 0.95 of the continuum intensity. Since helium is not found in excited levels in the lowest layers of the chromosphere, we may write to a good approximation

$$I_0 = I_{\text{ph}} e^{-\tau_0} + S_0(1 - e^{-\tau_0}) \qquad (7\text{-}14)$$

From the calculated values of b_{2^3s} and b_{2^3p}, $S_0 \sim I_{\text{ph}}/2$ and we find from Eq. (7-14) $\tau_0 \sim 0.1$. Column 3 in Table 7-3 contains calculated values of τ_0 for λ10,830 for $n_e = 10^{11}$ and a scale height of 10^8 cm. Since τ_0 in λ10,830 is proportional essentially to n_e^2, the proper value of n_e must be near 10^{11} in the regions where the maximum density of excited HeI is found. This argument alone is sufficient to exclude $T_e \approx 10{,}000°$ as a possible solution since $n_e > 2 \times 10^{13}$.

Using a value of $n_e = 10^{11}$, we may now estimate τ_0 in the first resonance line at λ584. Column 4 of Table 7-3 contains the estimated values. Column 5 of Table 7-3 contains estimated values of

---

† See footnote on p. 241.

$k_{3\tau_0}$. For $T_e < 30{,}000°$, $k_{3\tau_0}$ is large and the NRB is considerably smaller than the empirical values in Table 7-2. These estimates of the numerical values of the NRB together with the empirical values in Table 7-2 suggest that $T_e \gtrsim 40{,}000°$. Because of uncertainties in the NRB, collision rates, helium abundance, n_e, etc., we might admit values of T_e as low as 30,000°. However, under no reasonable circumstances could we admit T_e as low as 20,000°. Furthermore, these results are not invalidated by our neglect of intersystem transitions between excited singlets and triplets. Since the triplets are overpopulated with respect to the singlets, the net exchange must be from triplets to singlets; in which case the empirical values of the NRB in Table 7-2 represent lower limits and the inferred value of T_e is also a lower limit. The good agreement between the computed and empirical values of b_k for the triplets suggests that the intersystem transitions are indeed of little importance. If we attempt to raise T_e to much higher values, say 80,000°, HeII becomes much less abundant than HeIII and we again run into unreasonable values for n_e. Therefore, T_e seems to be limited to the range 40,000 to 80,000°.†

At first impression, this seems like a surprisingly high value for T_e in the regions emitting HeI radiation. However, there are several independent indications of similar values of T_e in the regions of the chromosphere that are known to emit strongly in HeI and or HeII. These may be listed as follows: (1) Mohler and Goldberg's (1956) observations of the λ10,830 profile indicate a Doppler broadening corresponding to an equivalent T_e of about 50,000°. (2) $H\alpha$, $H\beta$, $H\gamma$, and D_3 line profiles for individual spicules indicate $T_e \simeq 45{,}000$ to 55,000° (cf. Chapter 3). (3) The theoretical model in Chapter 5 suggests that T_e should jump to a value $\gtrsim 40{,}000°$ at the base of the HeII plateau. (4) Zirker's (1959) calculations of the excitation of λ4686 in the chromosphere indicate $T_e = 40{,}000°$ if the coupling with Lyman-α of hydrogen is not of major importance. All of these indications of T_e are uncertain to some extent. Nevertheless, they are consistently in the range 40,000 to 50,000°.

---

† Since completion of this manuscript, Johnson (1960) has carried out a self-consistent solution of the transfer equation and statistical equilibrium equations to evaluate the NRB and b_k's for the helium singlets. His detailed calculations confirm the preliminary conclusions stated here. The relatively large value of NRB at $T_e = 10{,}000°$ is a mathematical peculiarity resulting from a particular choice of numbers, and is probably not physically realistic.

The constant ratio of intensities for singlets and triplets at different heights in the chromosphere implies that the NRB is a slow function of τ_0 in the λ584 line, since τ_0 must change with height. This will be the case if $k_3\tau_0$ is small and the NRB $\propto \eta$. On the other hand, if $k_3\tau_0$ is large, the NRB $\propto e^{-k_3\tau_0}$, which varies rapidly with τ_0. Thus, the constancy of the singlet:triplet ratio also indicates that $T_e \gtrsim 40{,}000°$.

In subsequent considerations of the model, we shall consider the regions producing HeI radiation to be isothermal at some mean value of T_e. In view of the calculations above we expect $T_e \gtrsim 40{,}000°$ at the base of the regions producing HeI radiation, which agrees with the predicted values of T_e at the base of the HeII plateau in the theoretical model of Chapter 5. Since the top of the HeII plateau is predicted at $T_e \gtrsim 60{,}000°$, we shall adopt a mean value of T_e of 50,000°. This value of T_e is sufficient to explain both the HeI and HeII radiations, and we need not consider a more complicated model for the HeII data.

IV. General Formulation of Model

A. *Defining Equations*

We have indicated in the discussion above that we must turn to a model which departs from spherical symmetry. Actually, of course, this is not a surprising development. Limb observations of the upper chromosphere show hydrogen, helium, and other chromospheric-type emissions concentrated in spicules covering but a small fraction of the solar surface. Also, disk observations of the chromosphere and photosphere, in both white light and in the cores of the Fraunhofer lines, show surfaces that are mottled by relatively light and dark features. These light and dark features are often associated with Doppler displacements of the spectral lines (McMath, Mohler, Pierce, and Goldberg, 1956). Thus, we have many indications of departures from spherical symmetry, and any extended discussion, which includes enough data, must inevitably lead to a non-spherically symmetric model.

As a first step toward a new model beyond evaluating T_e in the helium regions we make the simplest possible assumption, viz., that the chromosphere, at any fixed height above the photosphere, consists of two types of regions with fractional areas a_1 and a_2

($= 1 - a_1$), so defined that all the helium emission arises from regions of type 1. We further assume that the emission per unit volume obtained by assuming spherical symmetry can be represented by

$$\mathcal{E} = a_1\mathcal{E}_1 + a_2\mathcal{E}_2 \tag{7-15}$$

This latter assumption implies that the individual structures are (1) randomly distributed over the solar surface, and (2) homogeneous within themselves at a fixed height. Note that we do not require that the hydrogen and helium emissions arise from separate volume elements and we do not specify that either type of region is cold or hot relative to the other. Also, we do not assume any particular geometrical shape for the individual regions. Later on we shall identify the two components in the upper chromosphere with spicules and the interspicular regions. However, we have specifically avoided this association at this stage.

The emission from helium is restricted to region 1. By virtue of the assumptions above, Eq. (7-7) becomes

$$a_1 n_{e1} n_{\text{II}} T_{e1}^{-3/2} = 1 \times 10^{17}\ \varphi^*(h) \tag{7-16}$$

Eq. (6-16) becomes

$$a_1 n_{e1}^2 T_{e1}^{-3/2} + a_2 n_{e2}^2 T_{e2}^{-3/2} = f(h) \tag{7-17}$$

and Eq. (6-77) becomes

$$\begin{aligned} a_1[n_{e1} &+ 8.3 \times 10^{-6} n_{e1}^2 T_{e1}^{-3/2} \exp(-1.31 \times 10^4/T_{e1})] \\ &+ a_2[n_{e2} + 8.3 \times 10^{-6} n_{e2}^2 T_{e2}^{-3/2} \exp(-1.31 \times 10^4/T_{e2}) \\ &+ 2.9 \times 10^{-5} n_{e2}^3 b_1 \alpha_\nu T_{e2}^{-1/2} \exp(1.26 \times 10^5/T_{e2})] = g(h) \end{aligned} \tag{7-18}$$

where the term containing n_e^2 arises from the Paschen continuum and the term containing n_e^3 arises from the H$^-$ emission. Since, with increasing height, n_e decreases and T_e increases, the H$^-$ and Paschen terms decrease relative to the electron scattering term. Above the height where both the H$^-$ and Paschen terms become negligible relative to electron scattering, Eq. (7-18) reduces to the simple form

$$a_1 n_{e1} + a_2 n_{e2} = g(h) \tag{7-19}$$

The spherically symmetric model in Chapter 6 suggests that Eq. (7-19) should hold for $h \geq 2000$ km.

Below the maxima in the helium emission, the observational data are not adequate to determine the emission per unit volume with a reasonable degree of precision. The data suggest that the emission drops very rapidly at lower heights, and we have no compelling reason to indicate a pronounced non-uniformity in chromospheric structure for $h \leq 1000$ km. So far as our data are concerned, the model in Chapter 6 is adequate at these heights. Hence, we need consider the model for $h \geq 1000$ km only.

The Equations (7-16) to (7-19) contain six unknowns: a_1, n_{e1}, T_{e1}, n_{e2}, T_{e2}, and n_{II}. Hence, in order to solve for these unknowns we must either find additional relationships between them or we must make additional assumptions. On the basis of the calculations in the preceding section we may set $T_{e1} = 50{,}000°$ with reasonable assurance that it is not in error by a large percentage. From Zirker's calculations, $n_{\text{III}}/n_{\text{II}} = 0.7$ at $T_e = 50{,}000°$, and from Table 7-1 $n_{\text{I}}/n_{\text{II}} \ll 1$. We may therefore set $n_{\text{I}} + n_{\text{II}} + n_{\text{III}} = 1.7 n_{\text{II}} = 0.1 n_e$. Equation (7-6) then becomes

$$a_1 n_{e1}^2 T_{e1}^{-3/2} = 1.7 \times 10^{18} \varphi^*(h) = \varphi(h) \qquad (7\text{-}20)$$

and the problem is reduced to four unknowns.

Before considering a fourth relationship between these unknowns it is instructive to consider the gross features of the model in somewhat more detail.

B. Comments on General Structure

The assumptions under which we are working in this chapter say nothing about the detailed form of the model either from a thermodynamical or geometrical standpoint. We could, of course, deduce some of these details from numerical computations based on the quantities $f(h)$, $g(h)$, and $\varphi(h)$, which are derived from the observational data. However, it is helpful to consider the general conclusions that can be arrived at independently of the detailed model.

Consider the relative importance of regions 1 and 2 in producing the hydrogen emission. From Eqs. (7-17) and (7-20), we can determine both $a_1 n_{e1}^2 T_{e1}^{-3/2}$ and $a_2 n_{e2}^2 T_{e2}^{-3/2}$ independently of the model. Table 7-4 contains the percentage of the Balmer continuum emission arising in region 1 according to the two approximations to $f(h)$ given by Eqs. (2-11a) and (2-12). Below 3000 km,

Table 7-4. Percentage of Hydrogen Balmer Continuum Emission in Region 1

h	1500	2000	3000	4000	5000	6000
%	5-6	9-12	40-46	76-100	100	100

the hydrogen Balmer continuum emission originates mostly in region 2, whereas above 4000 km it originates almost entirely in region 1. Hence, in the low chromosphere the hydrogen and helium emissions are separated, and in the high chromosphere they are merged.

In the low chromosphere where hydrogen emission is in region 2 and helium emission in region 1, region 1 must be hotter than region 2. However, in the high chromosphere, where both hydrogen and helium emissions are concentrated in region 1, we have two possibilities. We have defined a_1 as the fractional area of the sun giving rise to helium emission. On eclipse spectrograms exposed above 5000 km, spicule structure is clearly evident in the early Balmer lines of hydrogen as well as in the helium lines. The detailed structure is the same in both the hydrogen and helium lines (Athay and Roberts, 1955; Athay, 1958a), which is also suggested by the results in Table 7–4. Thus, by definition, region 1 is to be identified with the spicules above 5000 km. From our analysis of spicule statistics in Chapter 3, we estimate $a_1 \simeq 0.003$ and $a_2 \simeq 1$ at 5000 km. Therefore,, the emission in region 2 may be weak either because n_{e2} is low or T_{e2} is high. We noted in Chapter 2 that there is evidence for strong emission from FeXI in the upper reaches of the chromosphere. This observation, if correct, strongly implies that T_{e2} is much higher than T_{e1} in the upper chromosphere. Also, since the spicules, which constitute region 1 in the upper chromosphere, are observed as jets shooting into region 2, it seems necessary that the density in the spicules exceeds the density in region 2. Thus, we conclude that $T_{e2} > T_{e1}$ and $n_{e2} < n_{e1}$ in the high chromosphere.

Up to this point, we have made no assumption about the geometrical form of the chromospheric elements other than to identify region 1 with spicules in the upper chromosphere. The simplest assumption for the low chromosphere seems to be that of vertical columns, which we now consider. We note from Table 7-4 that the hydrogen and helium emissions cannot both be in vertical columns, since these emissions are separated in the low chromosphere and merged in the high chromosphere. Thus we consider the following two possibilities: (1) helium emission is in vertical columns, and (2) hydrogen emission is in vertical columns. These two alternatives are illustrated schematically in Fig. 7-3. In the first alternative [Fig. 3(a)] regions 1 and 2 consist of vertical columns. Since $T_{e1} > T_{e2}$ in the low chromosphere and $T_{e1} < T_{e2}$ in the high chromosphere, this first alternative requires a reversal in the direction of the horizontal gradient in T_e between adjacent columns in the middle layers of the chromosphere. In the second alternative [Figure 3(b)], neither region 1 nor region 2 forms vertical columns, and the horizontal gradient in T_e between adjacent atmospheric columns may have the same direction at all heights.

Our considerations of the chromospheric energy balance in Chapter 5 indicate that in a vertical column of the solar chromosphere the predominant energy loss by radiation should shift first from hydrogen to HeII then from HeII to some coronal ion. This sequence is followed in Fig. 3(b), but not in Fig. 3(a). Thus, we favor the assumption that the hydrogen emission is in vertical columns. One must realize, that the non-uniform structure of the chromosphere may consist of hot or cold cloudlike features, as suggested by McMath et al. (1956), rather than vertical columns. However, the spicules observed in the upper chromosphere suggest a columnar structure, and the introduction of cloudlike features is an unwarranted complication at this point.

V. Calculation of Model

A. *Evaluation of a_1*

Since we still have four unspecified parameters and only three relationships between them from observational data, we cannot derive a detailed model without either adding more observational data or making further assumptions. We proceed by considering the parameter a_1.

For heights of 5000 km and greater, we have direct evidence that region 1 is to be identified with spicules; and from the analysis of spicule statistics in Chapter 3, we obtain an estimate of $a_1 \simeq 0.003$ at 5000 km. There is, of course, uncertainty in such an estimate; however, there is little chance that a_1 is in error by as much as a factor of 3, and we may safely limit a_1 to the range 0.01 to 0.001. These limits on a_1 serve as the desired fourth relationship for h = 5000 km, and they apply equally well at 6000 km.

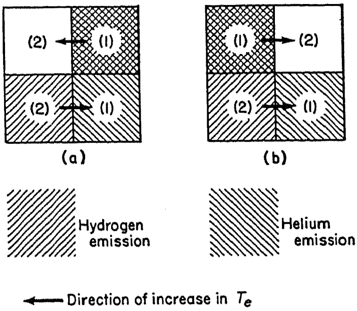

Fig. 7-3. Two alternative geometrical models of the chromosphere.

At lower heights, we also have estimates of the surface area covered by spicules. However, we cannot be certain that region 1 is to be identified with spicules for heights below about 5000 km. In fact, we cannot be certain even that spicules are the only manifestation of non-spherical symmetry at these heights. The absence of pronounced structure in either the hydrogen or helium emission at heights below 3000 km requires that a_1 be greater than about 0.01 and less than about 0.99. We expect therefore that a_1 will increase above the limits given for $h = 5000$ km.

For $h \leq 1000$ km, as we have noted earlier, there is no compelling evidence from the hydrogen and helium data to consider departures from spherical symmetry. The model in Chapter 6 is therefore adequate at these heights, and, by definition, a_1 must again decrease to a value near zero.

In adopting Fig. 3(b) as the most plausible geometrical model, we adopted implicitly a model in which T_e and n_e are inversely related between regions 1 and 2 in the upper chromosphere. Thus, we have a tendency towards pressure equilibrium with the high-temperature regions associated with low density and vice versa. In order to evaluate a_1 in the middle layers of the chromosphere, we assume that the pressure in region 1 is of the same order of magnitude as the pressure in region 2 at the same physical depth. This assumption may be expressed in the form

$$n_{e1}T_{e1} = Wn_{e2}T_{e2}[1 + (n_{\mathrm{H}2}/2n_{e2})] \qquad (7\text{-}21)$$

where $n_{\mathrm{H}2}/2n_{e2}$ may be expressed as a function of T_{e2} and n_{e2} using the expressions for b_1 given in Chapter 4 and W is of order unity.

This equation together with Eqs. (7-16) and (7-17) serves to specify a_1 as a function of T_{e2} and T_{e1}.

The observed dynamic phenomena in the chromosphere suggest that there are probably differences in gas pressure from one region to another at the same depth. Ideally, our model should yield the gas pressure in the two regions of the atmosphere, but this is not possible with the limited data available. For the present, we can derive a detailed model only by assuming some such relationship as expressed by Eq. (7-21).

B. *Calculations of the Model*

Even though we now have four equations in four unknowns the model is still not uniquely defined. We have endeavored to keep the geometrical and physical model as simple as possible. Nevertheless, the model places severe requirements on the observational data. In order to derive the equations defining the model, we have been forced to differentiate the data. In addition, we have introduced an approximate value for T_{e1}, n_{II} and the hydrogen:helium ratio. All these steps introduce uncertainties in the final equations, the most serious of which arises from the differentiation of the data.

Unfortunately, we have no reliable means for estimating the probable errors involved. Some idea of the relative errors can be obtained from alternative analytical representations of the data, which we differentiate to obtain the emission per unit volume. As an example, we consider six alternative representations of the data from which we derive the function g (Athay et al., 1955). The six representations yield values of log g between the limits 11.01 to 10.84 at 2000 km and 9.63 to 9.91 at 6000 km. This suggests that the errors introduced from the differentiations of the data are of the order of a factor of two.

In addition to the errors resulting from the derivation of f, φ, and g, there is a possibility of absolute errors in the photometric calibration, which also affect the model to some extent. In Chapter 3, we indicated that our absolute intensities may be too high by about a factor of two. However, we have no conclusive evidence that this is actually the case, and we shall use the intensities as given. Fortunately, the absolute errors are of less importance than relative errors of the same magnitude.

Because of the aforesaid errors there are a range of values for each of the four parameters of the model that will satisfy the equations. In solving the equations, we arbitrarily vary f, φ, and g by factors of two in either sense, i.e., we allow each function to change from its prescribed value by factors of 2 and ½ independently of the values of the other two functions. Since $a_2 n_{e2}{}^2 T_{e2}{}^{-3/2} = f - \varphi$, changes in f and φ have much more effect on the results than changes in the parameter W. Hence, there is no point in varying W independently of f and φ. In order to set limits on a_1, we take $W = 1$. However, the permitted ranges in the remaining parameters of the model permit values of W considerably different from unity.

For some of the permitted values of the f, φ, and g functions the equations defining the model have no formal solutions. However, for a prescribed value of T_{e2} Eqs. (7-16) and (7-17) together with either Eq. (7-18) or (7-20) may yield a solution. If so, we adopt this solution as a possible one. On the other hand, if it turns out that neither of these two sets of equations has a solution for a given T_{e2} and the permitted ranges in f, φ, and g, we reject this value of T_{e2} from the set of possible solutions.

Since the spherically symmetric model in Chapter 6 gives $T_e = 7500° \pm 500$ at 1000 km and T_e increasing outward at the rate of about 1000° per 500 km, we place a lower limit of 7000° on T_{e2} at 1500 km and higher. At 1500 and 1000 km, the f, φ, and g functions place an upper limit on T_{e2} and both upper and lower limits on a_1, n_{e2}, and n_{e1}. At 3000 and 4000 km, however, the permitted ranges in the f and φ functions allow $a_2 n_{e2}{}^2 T_{e2}{}^{-3/2} = 0$ or $a_1 = 1$. From Eqs. (7-16), (7-17), and (7-21) with $n_H/2n_{e2} < 1$, we have

$$\varphi/(f - \varphi) = (a_1/1 - a_1)(T_{e2}/T_{e1})^{7/2} \tag{7-22}$$

and as a_1 approaches unity

$$f_{\min} - \varphi_{\max} \rightarrow \varphi_{\max}(1 - a_1)(T_{e1}/T_{e2})^{7/2} \tag{7-23}$$

or

$$n_{e2}{}^2 \rightarrow \varphi_{\max} T_{e1}{}^{7/2} T_{e2}{}^{-2} \tag{7-24}$$

Thus, for a given value of T_{e2} we may place an upper limit on n_{e2}.

Equations (7-22) and (7-19) may be used to place lower limits on a_1 and n_{e2}. By letting φ have its minimum value and f its maximum value, we have, from Eq. (7-22),

$$n_{e2}^2 \geq (\varphi_{\min}/a_1) T_{e1}^{7/2} T_{e2}^{-2} \tag{7-25}$$

Also, from Eq. (7-19) we have

$$n_{e2} \leq g_{\max}/(1 - a_1) \tag{7-26}$$

which leads to

$$a_1/(1 - a_1)^2 \geq (\varphi_{\min}/g^2_{\max}) T_{e1}^{7/2} T_{e2}^{-2} \tag{7-27}$$

Unfortunately, we cannot set an upper limit on T_{e2} for $h \geq 4000$ km due to the permitted range of uncertainty in f, φ, and g.

We proceed with the calculations for $h \leq 4000$ km by choosing a value for T_{e2}, then finding the limits on the remaining free parameters. For $h \geq 5000$ km, T_{e2} is too high to be determined by the data we are using, so we evaluate n_{e1} and n_{e2} from the limits on a_1 placed earlier. Table 7-5 exhibits the results. At first glance, the model seems poorly defined indeed. However, a closer inspection of the results in Table 7-5 reveals features that can be used to refine the model considerably. In discussing Table 7-5, we must remember that the columns in the table do not necessarily represent vertical columns in the chromosphere for $h \leq 5000$ km.

At 4000 km, region 1 may be an extension of either region 1 or region 2 at 5000 km. For stability, we require that n_e does not increase outward. If region 1 is continuous from 5000 to 4000 km, then $\log n_{e1} \geq 11.3$ at 4000 km, which requires that $T_{e2} \geq 50{,}000°$. On the other hand, if region 1 at 5000 km joins with region 2 at 4000 km, then $\log n_{e2} \geq 11.3$ at 4000 km, which requires that $T_{e2} \leq 20{,}000°$. At 3000 km, the same two alternatives place essentially the same restrictions on T_{e2}. Furthermore, since $T_{e2} \leq 30{,}000°$ at 2000 km and $\leq 15{,}000°$ at 1500 km, we have a clear indication of two distinct temperature regimes in conformity with the predictions of Chapter 5.

Since we observe spicular structure at 4000 km, which is an extension of the spicular structure at greater heights, it is very probable that a_1 is continuous in this height range. At 3000 km, however, the continuity in a_1 is open to question. At 2000 km, the restriction of T_{e2} to less than 30,000° clearly indicates that a_1 is not continuous down to this height. Furthermore, the results in Table 7-4 suggest that the transition height indicated in Fig. 3(b) lies between 2000 and 4000 km. Inasmuch as several of the neutral

Table 7-5. The Initial Model

h	T_{e2}	a_1	$\log n_{e1}$	$\log n_{e2}$
1500	7,000	0.80–0.55	11.4–11.2	11.4–11.6
	7,500	0.96–0.80	11.4–11.1	11.8–11.7
	8,000	0.98–0.85	11.4–11.1	11.9–11.8
	9,000	0.99–0.80	11.4–11.1	12.4–11.9
	10,000	0.98–0.73	11.4–11.2	12.2–11.7
	12,000	0.97–0.65	11.4–11.2	12.2–11.7
	15,000	0.93–0.40	11.4–11.3	12.3–11.8
2000	7,000	0.995–0.98	11.0–11.3	12.2–11.8
	8,000	0.997–0.95	11.0–11.3	12.4–11.5
	9,000	0.996–0.92	11.0–11.3	12.4–11.4
	10,000	0.995–0.89	11.0–11.3	12.4–11.4
	15,000	0.98–0.67	11.0–11.4	12.2–11.3
	20,000	0.94–0.43	11.0–11.5	12.0–11.3
	25,000	0.85–0.26	11.0–11.6	11.9–11.3
	30,000	0.78–0.15	11.0–11.6	11.8–11.3
3000	7,000	1–0.99	10.8–10.8	12.0–11.7
	8,000	1–0.98	10.8–10.8	11.9–11.6
	10,000	1–0.96	10.8–10.8	11.9–11.6
	15,000	1–0.87	10.8–10.9	11.6–11.1
	20,000	1–0.72	10.8–11.0	11.5–10.8
	30,000	1–0.58	10.8–11.2	11.4–10.6
	50,000	1–0.40	10.8–11.3	11.2–10.4
	100,000	1–0.20	10.8–11.5	10.9–10.3
4000	7,000	1–0.996	10.6–10.6	11.8–11.5
	10,000	1–0.99	10.6–10.6	11.7–11.3
	15,000	1–0.95	10.6–10.6	11.4–11.2
	20,000	1–0.86	10.6–10.6	11.3–10.9
	30,000	1–0.60	10.6–10.9	11.2–10.4
	50,000	1–0.40	10.6–11.3	11.0–10.2
	100,000	1–0.20	10.6–11.8	10.7–10.1
5000	—	0.01–0.001	11.3–12.1	9.7–10.3
6000	—	0.01–0.001	11.3–11.8	9.6–10.2

metal lines are observed up to heights of about 3000 km, we assume that the transition height where region 1 joins with region 2 lies between 3000 and 4000 km.

At 1500 km, the model in Table 7-5 permits continuity with the spherically symmetric model in Chapter 6, viz., $T_{e2} \approx 7500$ to 9000°, and we adopt these limits. Assuming that T_{e2} does not decrease outward, we adopt $T_{e2} \geq 7500°$ for $h \geq 1500$ km. Aside from these limits, any $T_{e2} \leq 30{,}000°$ is possible at 2000 and 3000 km. However, since we have definite indications for two distinct temperature regimes, we limit T_{e2} to less than 11,000° in accordance with the considerations in Chapter 5. For $h \leq 1000$ km, we adopt the model of Chapter 6.

Before proceeding further with our discussion of the model, it is advantageous to consider an alternate designation of components. The separation into regions 1 and 2 was convenient for computation, but it is not convenient for further discussion. The vertical structure resulting from our discussion of Table 7-4 and Fig. 3(b) suggests "hot" and "cold" columns. In the following we will use subscript c to designate "cold" columns, and subscript h to designate "hot" columns. With this notation and the above restrictions, the allowed solutions in Table 7-5 reduce to those in Table 7-6.

Table 7-6. Adopted Model

h	T_{ec}	$\log n_{ec}$	T_{eh}	$\log n_{eh}$	a_c
500	6,250	11.7	—	—	—
1,000	7,500	11.5	—	—	—
1,500	7,500	11.8-11.7	50,000	11.4-11.1	0.04-0.20
	8,000	11.9-11.8		11.4-11.1	0.02-0.15
	9,000	12.4-11.9		11.4-11.1	0.01-0.20
2,000	7,500	12.5-11.8	50,000	11.0-11.3	0.002-0.02
	8,000	12.4-11.5		11.0-11.3	0.003-0.05
	9,000	12.4-11.4		11.0-11.3	0.004-0.08
	10,000	12.4-11.4		11.0-11.3	0.005-0.11
3,000	8,000	11.9-11.6	50,000	10.8-10.8	0-0.02
	9,000	11.9-11.6	50,000	10.8-10.8	0-0.03
	10,000	11.9-11.6		10.8-10.8	0-0.04
4,000	50,000	10.6-11.3	>50,000	<11.0	<0.6
5,000	50,000	11.3-12.1	>50,000	9.7-11.3	0.01-0.001
6,000	50,000	11.0-11.8	>50,000	9.6-10.2	0.01-0.001

The adopted model in Table 7-6 shows an initial rapid decrease in a_c from ~ 1 at 1000 km to ≤ 0.11 at 2000 km, and thereafter a rather slow decrease. In Chapter 3, we estimated that a fraction of about 0.01 of the solar surface was covered by spicules at 3000 km. Thus, the model suggests that for $h \geq 3000$ km, the cold components of the chromosphere are to be identified with spicules. Indeed, this seems to be a reasonable explanation at 2000 and 1500 km as well.

Below 1500 km, where the cold component fills the entire chromosphere, such an association has no meaning.

Within the cold component there seems to be little, if any, change in n_e with height except in the interval 3000 to 4000 km where the jump in T_e occurs. Since spicules are observed as an upward ejection of matter, it is entirely reasonable that the density should remain relatively constant with height. Also, we note that for hydrostatic equilibrium at $T_e = 50{,}000°$, log n_e should decrease by about 0.2 each 1000 km. The hot components of the chromosphere may therefore be in approximate hydrostatic equilibrium. Thus, the model in Table 7-6 is close to a hydrostatic equilibrium model everywhere except in the spicules above 1500 km.

Since log n_{eh} may be as low as 9.7 at 5000 km and equally as low at 4000 km, T_{eh} may rise to a value near 10^6 at 4000 km before the electron pressure exceeds that at 3000 km. The indications of FeXI emission in the upper reaches of the chromosphere are therefore consistent with the model.

The model in Table 7-6 must be regarded as an average working model only. The jump in T_{ec} from the hydrogen plateau to the HeII plateau between 3000 and 4000 km could not be expected to hold for all spicules. Indeed, there may be some spicules that have $T_e \simeq 50{,}000°$ much below 3000 km, and there may be spicules with $T_e \leq 11{,}000°$ above 4000 km. The consistently wide line profiles observed for spicules at $h \simeq 5000$ km indicates, however, that spicules with T_e much less than 50,000° are rare at this height.

We note that the model above gives relatively cold, dense spicules imbedded in a relatively hot, tenuous medium. Models in which the spicules are hotter than the surrounding medium as suggested by Woltjer (1954) and more recently by Michard (1959) are not compatible with the data used in deriving the above model. Also, we note that since the observed spicules are imbedded in a medium in which T_e may be as high as 10^6, in which case the velocity of sound is about 200 km $\sec^{-1}$, we do not require that the observed spicule velocity of 30 km $\sec^{-1}$ be supersonic. Finally, we note that since the line profiles in the upper chromosphere indicate a Doppler broadening corresponding to a T_e of about 50,000°, there is no basis for the often-quoted "turbulent" velocities of about 15 km $\sec^{-1}$ in the upper chromosphere (cf. de Jager, 1959).

VI. Active Regions

It is of interest at this point to consider the data for the active regions discussed in Chapter 3. Unfortunately, these data are not adequate to carry our discussion of models to the same degree of refinement that we have for the normal regions of the chromosphere. For the 1932 and 1936 regions there are no continuum data and only restricted line data. For the 1952 region, there are no data for the Balmer continuum. However, by extrapolating the Balmer line data to the series limit by the same method employed in Fig. 7-1 for extrapolating the helium line data, we can estimate the intensity of the Balmer continuum for heights below 1600 km. We can then proceed to discuss the model for this region in much the same way that we discussed the model for the normal chromosphere. Our discussion of the 1932 and 1936 regions will necessarily be somewhat more qualitative, however.

A. *The Functions $g(h)$, $f(h)$, and $\varphi(h)$ in the 1952 Active Region*

We begin our discussion of the model for the 1952 active region by deriving the functions $g'(h)$, $f'(h)$, and $\varphi(h)$ for this region. We use the prime notation to distinguish these functions for the active regions from the corresponding functions in the normal chromosphere. The function $g'(h)$ follows immediately from the empirical representation of the data for E_{4700}, and Eq. (2-5)

$$\begin{aligned} g'(h) = {} & 1.6 \times 10^{13} \exp(-4.6 \times 10^{-8}) \\ & + 5.7 \times 10^{10} \exp(-3.5 \times 10^{-9} h) \\ & + 1.6 \times 10^{9} \exp(-1.7 \times 10^{-10} h) \end{aligned} \tag{7-28}$$

We obtain $\varphi'(h)$ just as we did $\varphi(h)$ by extrapolating the data for the helium lines to the series limit. Figure 7.4 exhibits the necessary plot. From the intercept in Fig. 7-4 and the observed scale-height, we find

$$a_1' n_{e1}' n_{\rm II}' T_{e1}^{-3/2} = 1.1 \times 10^{15} \exp(-0.55 \times 10^{-8} h) \tag{7-29}$$

The straight lines drawn in Fig. 7-4 give excitation temperatures of ~7200° for the triplets and ~18,000° for the singlets. The probable errors in the excitation temperatures are about the same as they were in the normal chromosphere, and within these probable errors the excitation temperatures in the two regions are consistent. Hence,

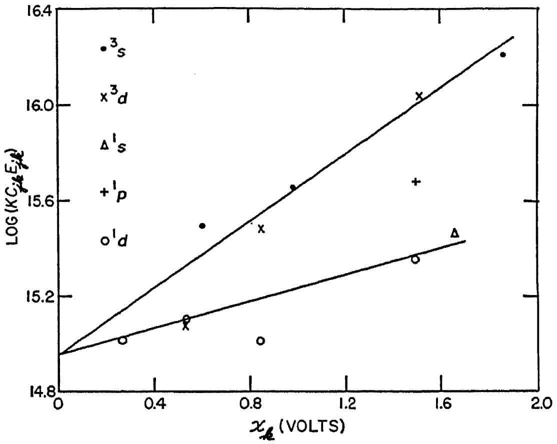

Fig. 7-4. Illustration of the estimate of $n_e n_{\text{II}} T_e^{-3/2}$ from the HeI lines in the active region at $h = 400$ km. (From R. G. Athay and R. N. Thomas, 1957, *Astrophys. J.*, **125**, 798.)

the singlet:triplet ratio is about the same as it is in the normal chromosphere. The HeII line λ4686 is enhanced relative to the nearby HeI line λ4713 by about a factor of two over their normal values. This relative increase in HeII radiation corresponds to an increase in $n_{\text{III}}/n_{\text{II}}$ by a corresponding factor since any change in $b_k e^{\chi_k/T_e}$ must be small compared to changes in n_i at high temperatures. From Zirker's calculations, an increase in $n_{\text{III}}/n_{\text{II}}$ by a factor of two corresponds to a change in T_{e1} from 50,000 to 53,000° only. We may therefore set $T_{e1} \simeq 50{,}000°$ just as we did for the normal chromosphere. However, we must now set $2.4n_{\text{II}} = 0.1n_e$, and Eq. (7-29) becomes

$$\varphi'(h) = 2.6 \times 10^{16} \exp\,(-0.55 \times 10^{-8}h) \qquad (7\text{-}30)$$

In order to derive $f'(h)$ from the Balmer line data we must allow for the effects of self-absorption. From Eq. (2-5) we obtain

$$\mathcal{E}_{kj} = h\nu A_{kj} n_k = (\gamma_{kj}{}^{3/2}/\{\text{abs}\}_{kj})[E_{kj}/(2\pi R)^{1/2}] \qquad (7\text{-}31)$$

and from the non-equilibrium form of the Boltzmann-Saha equation, we find

$$\log\,(KC_{kj}E_{kj}) = \log n_e^2 T_e^{-3/2} + \log\,(b_k\{\text{abs}\}_{kj}) + (0.434\chi_k/T_e) \qquad (7\text{-}32)$$

where

$$K = [2/h(2\pi R)^{1/2}](2\pi mk/h^2)^{3/2} = 1.1 \times 10^{36}$$

and

$$C_{kj} = \gamma_{kj}{}^{3/2}/\nu_{kj}A_{kj}\tilde{\omega}_k$$

We then plot, in Fig. 7-5, the quantity on the left side of Eq. (7-32) versus χ_k assuming that $\gamma_{kj} = \beta_{kj}$. This assumption is certainly not good for the early Balmer lines since the negative slopes of the plots in Fig. 7-5 show unmistakably that self-absorption is important for these lines. However, for the later lines self-absorption should be small and the assumption above should be good. From the intercepts at $\chi_k = 0$ in Fig. 7-5, we obtain

$$f'(h) = 1.9 \times 10^{17} \exp(-1.3 \times 10^{-8}h) \tag{7-33}$$

Figure 7-5 also contains plots of the Paschen line data for the active region. The Balmer and Paschen lines should give the same

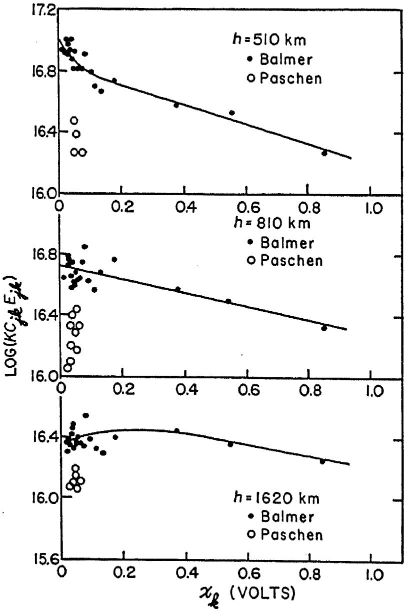

Fig. 7-5. Illustration of the estimate of $n_e n_p T_e{}^{-3/2}$ from the Balmer and Paschen lines in the active region. (From R. G. Athay and R. N. Thomas, 1957, *Astrophys. J.*, **125**, 797.)

intercept at $\chi_k = 0$ since all factors depending upon the quantum numbers are supposedly removed. We note, however, that the Paschen lines appear to be too faint relative to the Balmer lines by factors of about 2 to 3. This discrepancy does not appear to result from photometric errors, since the coronal continuum intensities at the wavelengths of the two series are in same ratio as the photospheric intensities. Furthermore, the infrared CaII triplet lines, which are at the same wavelengths as the Paschen lines, have just the right intensities relative to the H and K lines, which are at about the same wavelength as the Balmer lines. A possible reason for the discrepancy between the Balmer and Paschen line intensities suggested by Athay and Zirin (1957) will be discussed in the concluding chapter. Here, we use the $f'(h)$ derived from the Balmer line data.

B. *The Active-Region Model*

Our primary interest in the active region is to determine how it differs from the normal chromosphere. We could derive a model for the active region by following the same procedure and assumptions employed in the derivation of the model for the normal chromosphere. In the final analysis, however, any indicated changes in the model would be conditioned by the validity of the assumptions made. For this reason, we proceed in a different way.

At 1000 km, $d \ln g'/dh = -3.8 \times 10^{-8}$, whereas $d \ln f/dh = -1.3 \times 10^{-8}$ and $d \ln \varphi'/dh = -0.55 \times 10^{-8}$. Without the H^- term, $g' \propto n_e$. Thus, since $g'(h)$ is a stronger function of height than either $f'(h)$ or $\varphi'(h)$ which is proportional to n_e^2, the H^- term must dominate $g'(h)$. If we express $g'(h)$ in the form

$$g'(h) = a_1 n_{e1} + a_2 n_{e2}[1 + \psi(\mathrm{H}^-)] \qquad (7\text{-}34)$$

We conclude that $\psi(\mathrm{H}^-) > 1$ and $a_2 n_{e2} \psi(\mathrm{H}^-) > a_1 n_{e1}$. These two inequalities together with the functions f' and φ' are useful for placing lower limits on a_1. The first inequality is the more important of the two in limiting a_1, and when combined with Eqs. (7-30) and (7-33) it becomes

$$2.9 \times 10^{-5}[(f' - \varphi')/(1 - a_1)] b_1 \alpha_\nu(T_{e2}) T_{e2} \exp{(1.26 \times 10^5/T_{e2})} > 1 \qquad (7\text{-}35)$$

Since the H^- term is important and the data are for the low chromosphere, the opacity should be sufficiently high to insure detailed balancing in the Lyman continuum. Thus, Eq. (4-45) for b_1 is applicable. As before, f' and φ' are allowed to vary by factors of two in either sense from the explicit values given by Eqs. (7-30) and (7-33). The effective limit on a_1 is then set by $f'_{\max} - \varphi'_{\min}$. The limits on a_1 at 1000 km for selected values of T_{e2} are given in Table 7-7.

Table 7-7. Lower Limits on a_1 at 1000 km

T_{e2}	5500	6000	6500	7000	8000
$a_1 >$	0	0.64	0.90	0.97	0.997

Before discussing the results in Table 7-7, we consider the nature of the changes between the active region and the normal chromosphere. Table 7-8 contains values of $g(h)$, $a_1n_{e1}^2T_{e1}^{-3/2}$ and $a_2n_{e2}^2T_{e2}^{-3/2}$ in the two regions of the chromosphere. In the low chromosphere, the active region is characterized by larger values of $a_1n_{e1}^2T_{e1}^{-3/2}$ and lower values of $g'(h)$ and $a_2n_{e2}^2T_{e2}^{-3/2}$ with the largest effect in $a_1n_{e1}^2T_{e1}^{-3/2}$.

Table 7-8. Comparison of Active Region with Normal Chromosphere

h,	log $g(h)$		log $a_1\, n_{e1}^2\, T_{e1}^{-3/2}$		log $a_2\, n_{e2}^2\, T_{e2}^{-3/2}$	
km	Normal	Active	Normal	Active	Normal	Active
1,000	11.7	11.3	—	16.2	17.2	16.7
2,000	11.0	10.5	15.1	16.0	16.2	16.0
4,000	10.3	10.2	14.4	15.5	13.9	
6,000	9.9	9.9	13.3	15.0	0	
10,000	9.4	9.5				
20,000	8.9	9.0				
50,000	8.2	8.8				

The results in Table 7-7 indicate that a_1 has increased markedly over its value at 1000 km in the normal chromosphere, and this is suggested also by the changes in $a_1n_{e1}^2Te_1^{-3/2}$ and $a_2n_{e2}^2T_{e2}^{-3/2}$. The decrease in $g'(h)$ is consistent with an increase in a_1.

Above 10,000 km, $g(h)$ is greater in the active region than in the normal chromosphere. Since, at these heights in the normal chromosphere, the $\psi(\mathrm{H}^-)$ term is negligible and $n_{e1} > n_{e2}$, the increase in $g'(h)$ could be due to an increase in a_1. However, since the increase in $g'(h)$ persists to heights far above the upper boundary to the observable hydrogen and helium emission, a_1 drops to zero, and there must be a real increase in n_e.

In summary, the 1952 active region suggests a much larger fraction of hot components in the low chromosphere and a density increase at heights above 10,000 km. The density increase together with the greater vertical extent of the chromospheric-type emission suggests a large spicule-like ejection of matter from the low chromosphere or photosphere.

The region of reduced chromospheric-type emission adjacent to the active region is probably due to a still greater increase in the hot components and an invasion of the corona into the layers normally occupied by the low chromosphere.

C. The 1936 and 1932 Active Regions

From considerations of the thermal stability of the radiation field in a steady-state energy balance (Chapter 5), we expect all modifications of the temperature model of the chromosphere to result in a lengthening or shortening of the temperature plateaus rather than changes in the temperatures at which they occur. It is significant that the 1952 active region can be interpreted as such an effect, and it is natural to ask whether similar interpretations are possible for the 1936 and 1932 regions. We must recognize, of course, that changes in density gradients and geometrical structure may overshadow the changes in temperature structure.

The 1936 active region appears to be similar to the 1952 active region in the metal lines and later Balmer lines but more like the normal chromosphere in the helium lines. Thus, we cannot account for the region simply by changing a_1, as we did for the 1952 region. However, we could account for it by increasing a_1 and lowering n_{e1} and n_{e2} slightly. The similar behavior of FeI, FeII, and hydrogen lines argues against a change in T_{e2}, and the similar behaviour of HeI and HeII lines argues against a change in T_{e1}. The greater vertical extent of the hydrogen and metal emission again suggests a spicule-like ejection from the low chromosphere or photosphere.

The 1932 active regions is apparently of a different nature from either the 1936 or the 1952 active region. The main effects in this case are smaller scale heights and greater helium emission relative to hydrogen and metal emission in the low chromosphere. This suggests, as in 1952, that a_1 is larger in the low chromosphere. Since all emissions are larger at low heights in the active region, n_{e1} and n_{e2} must be slightly larger also. Both the continuum and the λ5303 emission in the corona are bright above the active region in the chromosphere. Hence, it seems unlikely that the smaller scale heights result from an increase in the density gradient in this region. This would imply that T_e increases more rapidly to coronal values in this region than in normal regions and would make it difficult to interpret this region as a spicule-like ejection of matter.

The foregoing arguments indicate that we can interpret all the active regions as regions of larger a_1 without resorting to changes in the T_e at which the temperature plateaus occur. These interpretations are consistent with the assumption of steady-state energy balance and thermal stability of the radiation field. Admittedly, however, other interpretations may be possible.

An Extension of the Model to Include Radio Noise Data

R. GRANT ATHAY

I. Radio Noise Emission

Radio frequency radiation at mm and cm wavelengths, where the apparent temperature of the sun is less than 50,000°, originates primarily in the chromosphere. Observational data at these wavelengths, although somewhat limited in scope, contribute further information on the chromospheric model. Two aspects of the radio noise data stand out as particularly useful in deriving or testing empirical models. Firstly, we may use the continuous spectrum of energy versus wavelength at the center of the disk, and secondly, we may use center to limb variations of the emitted energy at a fixed wavelength. The former approach has been used by Hagen (1951) and Piddington (1954), and the latter by Hagen (1954) and Coates (1957).

The radio data alone do not provide sufficient information to derive a detailed chromospheric model independently from optical data. Unfortunately, the models referred to above have either used inadequate optical data or they have used invalid conclusions drawn from optical data. The procedure used here is the same as that used by Athay (1958a), and incorporates optical data with radio data.

Unlike the optical continuum where the primary source of emission in the middle and upper chromosphere is by electron scattering, the radio continuum arises from free-free transitions of electrons in the fields of positive ions, which are mainly protons. Hence, the radio continuum is a thermal property of the chromosphere, whereas the optical continuum is a density property. Since we have assumed a Maxwellian velocity distribution for the free electrons, the radio continuum is presumably formed in thermodynamic equilibrium.

At radio wavelengths, the Planck function reduces to the Rayleigh-Jeans approximation. The source function is, therefore, given by

$$S_\lambda = 2kc\lambda^{-4}T_e \text{ ergs sec}^{-1}\text{ cm}^{-2}\, d\omega^{-1} \tag{8-1}$$

The integral form of the transfer equation gives the observed intensity as

$$I_\lambda = \int_0^{\tau_\lambda} S_\lambda e^{-\tau_\lambda/\mu}\, d\tau_\lambda/\mu \tag{8-2}$$

where τ_λ is the optical depth and $\mu = \cos\theta$. The angle θ is measured from the solar radius intersecting the center of the disk to the radius intersecting the point in question.

The free-free absorption coefficient α_λ at radio wavelengths, including stimulated emissions, is (Martyn, 1949)

$$\alpha_\lambda = 2.5 \times 10^{-23}(\lambda^2 n_e^2/n_f T_e^{3/2})(3.23 + \log T_e - 1/3 \log n_e) \tag{8-3}$$

The term in parenthesis is the Gaunt factor, and n_f is the index of refraction. For the wavelengths and densities of interest in the chromosphere, n_f may be taken as unity. The optical depth is defined by

$$\tau_\lambda = \int_\infty^y \alpha_\lambda\, dy \tag{8-4}$$

where y is the coordinate in the line of sight measured positively outward from the sun.

Since in a spherically symmetric atmosphere the emission at radio wavelengths depends upon n_e and T_e only, in principle a unique model can be determined by varying two independent parameters of the observations. Two such parameters, viz., λ and θ, can be varied. However, in practice, several difficulties arise. On the observational side, the angular resolution of radio telescopes is severely limited because of the mechanical difficulties of constructing large antennas. On the theoretical side, the unknown geometry of the chromosphere adds an additional set of unknowns which complicate the analysis just as they did in the case of optical data. Because of these difficulties, we can use the radio data only as a supplement to optical data.

Central brightness temperatures for the solar disk are available at several wavelengths, but only the shortest wavelengths are of interest in connection with the chromosphere. At wavelengths above about 3 cm, active coronal regions contribute to the observed emission in such a way as to make the sun markedly asymmetric. This asymmetry must be known, as well as any systematic variations across the solar disk, before the observational data can be reduced to central brightness temperature. In the absence of sufficient telescopic resolution, observations made during total eclipse provide the most reliable data for the determination of central brightness and the variation of brightness across the solar disk. Table 8-1 summarizes the central brightness temperatures obtained between wavelengths of 4 mm and 21 cm.

Central brightness temperatures at different wavelengths effectively map the radial temperature structure of the middle and upper chromosphere. However, they tell us nothing concerning the spicule or non-spherical nature of the chromosphere. For this, we must have data on the center-to-limb variations in brightness temperature. The most useful data are those at $\lambda \leq 10$ cm from the "quiet" sun where the emission is almost exclusively chromospheric. Figure 8-1 shows the limiting values of brightness temperature

Table 8-1. Central Brightness Temperatures

λ	Brightness temperature at center of disk, degrees	Method	Reference
4 mm	7,000	1954 eclipse	Coates (1957)
8.6 mm	8,500	1954 eclipse	Coates (1957)
3 cm	19,000	1954 eclipse	Hachenberg, Furstenberg, and Prinzler (1956)
	16,000	1952 eclipse	Blum, Denisse, and Steinberg (1952)
	17,400	Non-eclipse	Minnett and Labrum (1950)
10 cm	23,000	1954 eclipse	Haddock (1957)
		Non-eclipse	Covington and Broten (1954)
21 cm	47,000	Non-eclipse	Christiansen and Warburton (1955)

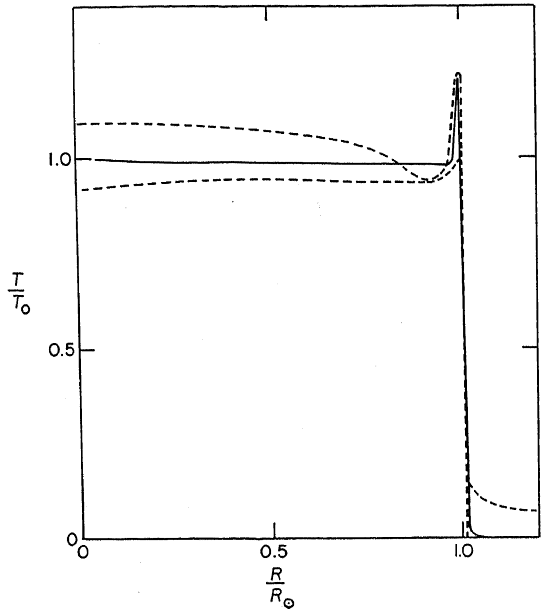

Fig. 8-1. Observed (dashed) and computed (solid) center-to-limb curves of brightness temperature at 8.6 mm. (From R. G. Athay, 1959, *Paris Symposium on Radio Astronomy*, R. N. Bracewell (ed.), p. 99, Stanford University Press.)

across the solar disk at 8.6 mm as derived by Coates (1957) from 1954 eclipse data (dashed lines). We shall use these data in conjunction with the central brightness temperatures.

The most striking features of the center to limb data is the apparent constancy of brightness temperature out to $R/R_\odot \simeq 0.98$. Models derived from central brightness temperatures alone all predict an increase in brightness temperature from center to limb that should be readily observed for $R/R_\odot \gtrsim 0.80$. The absence of limb-brightening out to $R/R_\odot \simeq 0.98$ can be logically explained only by resorting to models which depart from spherical symmetry (Hagen, 1954; Coates, 1957).

II. A Model From Radio Data

Since the radio data are to be used in conjunction with optical data, we shall adopt some of the features from the optical models. Schematically, the optical model including spicular structure can be

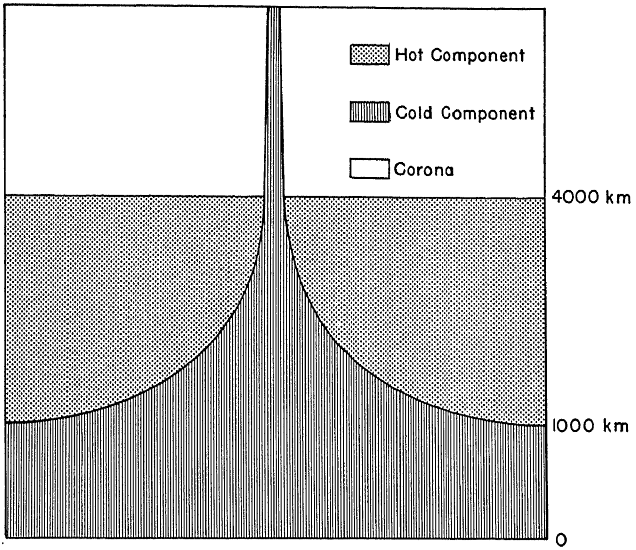

Fig. 8-2. A schematic model of the chromosphere from optical data, with the widths of the hot and cold components proportional to their fractional volumes. This illustration should not be interpreted as a cross section of a chromospheric sample. (From R. G. Athay, 1959, *Paris Symposium on Radio Astronomy*, R. N. Bracewell (ed.), p. 100, Stanford University Press.)

represented as shown in Fig. 8-2. At each height there are five adjustable parameters: n_e and T_e in each component, and the relative proportions of each component. Some of these parameters cannot be determined from existing radio data. For example, if we use the optical model as a guide, the cold component is opaque to the radiation at 4 mm and all higher wavelengths. Hence, we have no way to determine n_e in the cold component. Furthermore, the radio data are insufficient in both quality and quantity to specify the remaining parameters at all heights.

From a practical point of view, we can determine only as many parameters as are required to represent the data. Just how many are required can be determined only by a trial and error method. Because of the small fractional area of the disk covered by spicules for $h \geq 4000$ km, the spicular structure at these heights has a measureable effect on the observed emission at the extreme solar limb only. Below 4000 km, however, the cold components of the atmosphere may become more abundant. In fact, the absence of limb brightening at 8.6 mm for $R/R_\odot \simeq 0.98$ requires that this be so. Since the only information on geometrical structure comes from center-to-limb observations, we must use these data to determine the relative proportions of hot and cold elements. Preliminary calculations indicate that the data can be represented sufficiently well by using a single value for the fractional area of cold components between 1000 km and 4000 km. Thus, we can determine only the average fractional area of cold components in this height interval.

Central brightness temperatures do depend upon the geometry even though they do not help in specifying the geometry. In addition, they depend upon the temperatures and opacities of the different components. Since we have central brightness temperatures at five wavelengths only, we can determine no more than five additional parameters of the model. As we have already noted, the opacity of the cold components is high, so it does not enter the problem directly. Assuming that the hot and cold components can each be characterized by a single value of T_e, and that the hot component can be characterized by a single value of τ, we already have three additional parameters to specify. Furthermore, the corona contributes to the apparent temperature at 21 cm, so we must consider the coronal temperature and opacity. In this case, however, τ must be small, and the contribution to the apparent temperature is $T_e\tau$. Thus, we need only one parameter for the corona. Presumably, we could still add one parameter to the model, but, as we shall see, the data do not really justify it.

Using the optical model as a guide, we adopt the working model given in Table 8-2.

Table 8-2

Cold component	Hot component
$T_e = T_c,\ h \leq 4000$ km	$T_e = T_{\mathrm{H}},\ h \leq 4000$ km
$T_e = T_{\mathrm{H}},\ h > 4000$ km	$\tau = \tau_{\mathrm{H}},\ h \leq 4000$ km
$a_c = 1,\ h < 1000$ km	$T_e\tau = (T_e\tau)_{\mathrm{cor}},\ h > 4000$ km
$a_c = \bar{a}_c,\ 1000 \leq h \leq 4000$ km	
$a_c = a_s,\ h > 4000$ km (a_s = spicular area)	

The values of the parameters T_c, T_{H}, $\bar{a}_c$, and τ_{H} given by the model in the preceding chapter predict too much emission at all wavelengths except 21 cm. Thus, we expect some modification tc the model.

The brightness temperature at wavelength λ and position angle θ may be expressed in the form

$$\begin{aligned} T(\theta, \lambda) = {} & T_c[1 - \bar{a}_c(\theta)]e^{-\tau_{\mathrm{H}}(\theta,\tau)} + T_c\bar{a}_c(\theta)e^{-\xi\tau_{\mathrm{H}}(\theta,\lambda)} \\ & + T_{\mathrm{H}}[1 - \bar{a}_c(\theta)](1 - e^{-\tau_{\mathrm{H}}(\theta,\lambda)}) \\ & + T_{\mathrm{H}}\bar{a}_c(\theta)(1 - e^{-\xi\tau_{\mathrm{H}}(\theta,\lambda)}) + T_{\mathrm{H}}a_s(\theta) + (T_e\tau)_{\mathrm{cor}} \end{aligned} \tag{8-5}$$

where we have set $\tau \ll 1$ for the corona. The factor ξ multiplying τ_{H} in some of the terms accounts for the decrease in τ_{H} from the base of the hot components at 1000 km to the top of the cold components. Assuming that n_e varies expenonentially with height with a reciprocal scale-height of β_e, we have $\xi = e^{-2\beta_e \Delta h}$. In the hot component of the chromosphere $\beta_e \simeq 1 \times 10^{-8}$ cm^{-1}, and, since we are using $\bar{a}_c$ to represent the average area covered by cold elements in the height range 1000 to 4000 km, we pick $\Delta h = 1.5 \times 10^8$. Thus, $\xi \simeq 0.05$.

The line-of-sight optical depth at height h above the base of the hot component is

$$\tau_{\mathrm{H}}(\theta, \lambda) = 2\beta_e\tau_{\mathrm{H}}(0, \lambda) \int_{h/\cos\theta}^{\infty} e^{-2\beta_e h}\, dy \tag{8-6}$$

To a good approximation

$$h = (y^2/2R) + y \cos \theta \tag{8-7}$$

For $R/R_\odot \leq 0.99$, we may use $h = y \cos \theta$, and at the limb $h = y^2/2R$. Hence, on the disk

$$\tau_{\mathrm{H}}(\theta, \lambda) = [\tau_{\mathrm{H}}(0, \lambda)/\cos \theta]e^{-2\beta_e h} \tag{8-8}$$

and at the limb

$$\tau_{\mathrm{H}}(90, \lambda) = 2\tau_{\mathrm{H}}(0, \lambda)(2\pi R\beta_e)^{1/2}e^{-2\beta_e h} \tag{8-9}$$

Since the cold elements are presumed to have a columnar structure $\bar{a}_c(\theta)$ increases toward the limb. The rate at which it increases depends to some extent upon the distribution and dimensions of the cold elements. For simplicity, we assume a random distribution and that the average diameter is of the same order as the average height measured above 1000 km. With these assumptions, the total area covered by cold components, ignoring the fact that one cold element may lie in front of another, is $\bar{a}_c/\cos\theta$. Then, since we have a random distribution,

$$\bar{a}_c(\theta) = 1 - e^{-\bar{a}_c/\cos\theta} \tag{8-10}$$

Since $a_s < 0.01$, $a_s(\theta)$ is important only at the extreme limb.

Solutions for the five unknowns in Eq. (8-5) may readily be obtained through trial and error methods. As is to be expected with a simplified model containing fewer parameters than the number of observational data, the data can not be fitted precisely, and there is a choice to be made as to which data should be fitted best. The data for $\lambda \leq 3$ cm are the most sensitive to the chromospheric model, so we adopt the model that gives the best representation of these data.

The adopted model is given in Table 8-3 and the computed central brightness temperatures are given in Table 8-4. The center to limb variations in brightness temperature at 8.6 mm are shown in Fig. 8-1 as the solid curve. Equally satisfactory representations of the data can be obtained for T_{H} in the range 20,000 to 30,000°.

Table 8-3. Adopted Model

T_e	T_{H}	τ_{H} ($\lambda = 1$ cm)	$(T_e\tau)_{\mathrm{cor}}$ ($\lambda = 1$ cm)	a_c
6500	25,000	0.36	34	0.4

Table 8-4. Computed $T(0,\lambda)$

λ	4 mm	8.6 mm	3 cm	10 cm	21 cm
$T(0,\lambda)$	7100	8500	16,000	26,000	40,000

Similarly, each of the other parameters may be varied to some extent. However, since τ_{H} and $\bar{a}_c$ appear in exponents, these parameters are rather well defined by the model.

III. Discussion of the Model

In comparing the adopted model with the model of the preceding chapter, we note two outstanding differences: (1) $\bar{a}_c$ is much larger than in the preceding model and also much larger than spicule statistics would indicate, and (2) the adopted value of τ_{H} ($\lambda = 1$ cm) corresponds to $n_{e\mathrm{H}} \simeq 2 \times 10^{10}$, which is smaller than in the preceding model by about a factor of ten. Both T_c and T_{H} differ significantly in the two models. However, the values of these parameters inferred from the radio model are rather sensitive to the values of $\bar{a}_c$ and τ_{H}. In broad outline, the two models are, of course, rather similar.

There seems to be little hope of completely reconciling the two models without a basic change in one or the other of the models. This is particularly true of $n_{e\mathrm{H}}$, since both the radio and optical data give $n_{e\mathrm{H}}^2$ rather than $n_{e\mathrm{H}}$. Thus, it seems that some basic revision of the model is necessary. Since the most uncertain aspect of both models lies in the geometry, this is the logical place to question their validity.

The separation of the f and g functions of Chapter 7 in the form

$$a_1 n_{e1}^2 T_{e1}^{-3/2} + a_2 n_{e2}^2 T_{e2}^{-3/2} = f \qquad (8\text{-}11)$$

and

$$a_1 n_{e1} + a_2 n_{e2} = g \qquad (8\text{-}12)$$

is rigorously valid only if $\overline{n_{e1}^2} = \overline{n_{e1}}^2$ and $\overline{n_{e2}^2} = \overline{n_{e2}}^2$. This condition is likely to be obtained only if n_{e1} and n_{e2} are strictly constant at a given height. The model in Chapter 7 suggests that the emission from region 2 is concentrated almost entirely in spicules in the height range 1500 to 4000 km. It is possible that this is also true of the emission from region 1, i.e., there may be some spicules at these heights in which n_e is relatively high and $T_e = T_{\mathrm{H}}$. If so, then we should not insist that $a_1 + a_2 = 1$. In fact, as we have used a_1 and a_2 in Chapter 7, it is quite possible that $a_1 + a_2 \ll 1$. If we adopt this type of model in which some of the spicules below 4000 km have $T_e = T_{\mathrm{H}}$ and some have $T_e = T_c$, but both have relatively high density, we may fill the interspicule regions with relatively low density hot or cold regions in any proportion we wish. If n_e is a factor of 10 below that in the spicules as indicated, these interspicular regions could cover well over 90 percent of the surface area without contributing a large percentage of the optical emission.

Such a model as the above is not entirely unexpected. The spicule phenomenon is an upward surging of matter from regions of high density to regions of lower density. We should expect then, that once the motion starts the spicule is characterized by a higher density than the ambient medium regardless of its temperature. We have no reason for supposing that the spicules originate only in the cold components of the low chromosphere. In fact, the data on line profiles in spicules suggests that they are characteristic of the hot components of the middle chromosphere. Their high density, on the other hand, suggests that they come from the lower, denser, cold components unless they undergo considerable compression in their formative stages. The model in Chapter 7 definitely suggests a spicule-like phenomenon in the cold components of the low chromosphere. Thus, we have indications of spicule structure in both components of the chromosphere, and a model in which there are two temperature regimes each showing spicular structure as illustrated in Fig. 8-3 is not implausible.

The φ and g functions in Chapter 7 lend some support to this picture. For heights of 2000 to 4000 km, where hydrogen and helium emission apparently arise from different volume elements

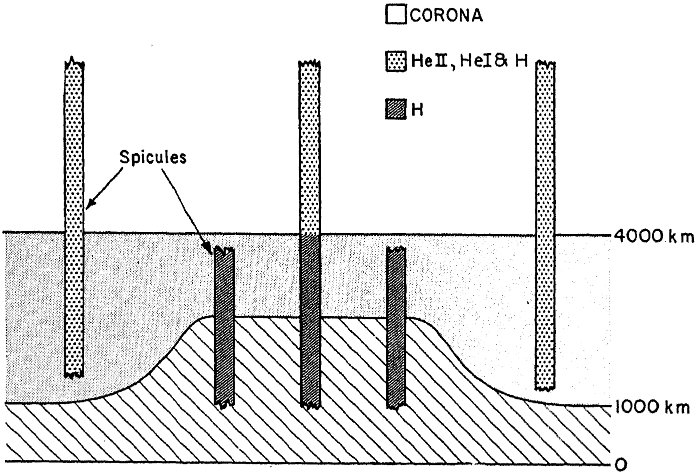

Fig. 8-3. A revised schematic model of the chromosphere from radio and optical data. The columnar features represent spicules of greater density than their ambient medium. This illustration may be interpreted as a schematic cross section of a chromospheric sample. The observed hydrogen and helium spectrum arises mainly in spicules.

and where $a_1 \simeq 1$, the upper limit to $\overline{n}_{e1}$ given by the g function is systematically below the value of $(\overline{n_{e1}^2})^{1/2}$ given by the φ function. This suggests that $\overline{n_{e1}^2} > \overline{n_{e1}}^2$, which is accordant with the suggested revision of the model.

We also note that it is not at all improbable that n_e should drop as low as 10^{10} in some fraction of the middle layers of the chromosphere. For $T_e = 7000°$, the hydrostatic equilibrium scale-height is of the order 200 km. Thus, an extension of the cold elements of the low chromosphere to somewhat greater heights than indicated in the model of Chapter 7 would accomplish the necessary reduction in n_e.

It seems evident that such a model as illustrated by Fig. 8-3 could easily reconcile the optical and radio data. However, we are now considering a model in which there are at least four fractional areas, four densities and two temperature parameters at each height. Therefore, any quantitative attempt to reconcile the models is somewhat meaningless until far more data are available.

Irrespective of the major uncertainties in the geometrical structure, it seems clear that a two-component temperature model is sufficient to represent both the optical and radio data. Even though the adopted radio noise model in Table 8-3 suggests values of T_e that are considerably different from those adopted in Chapter 7, this does not necessarily mean that the former values are wrong. The added geometrical complexity of the model in Fig. 8-3 readily permits a radio noise model with the same values of T_e as in Chapter 7. Furthermore, since the inferred values of T_e are far more precisely determined from optical data than from radio data, there is no good reason from the radio data to suppose that the values of T_e indicated in Chapter 7 are in error by a large percentage. The basic agreement between the values of T_e inferred from optical data and the values predicted from the considerations of thermal stability in Chapter 5 supports this conclusion.

CHAPTER 9

Data in Whose Analysis the Effects of Both Self-Absorption and of Departures from a State of Local Thermodynamic Equilibrium Must Be Included

R. N. THOMAS

Observations of the height variation of the line spectrum permit a direct inference of at most two quantities: the occupation number of the upper energy level of the transition, if self-absorption effects are completely negligible; the distribution in optical depth along the line of sight of the source function for the transition, if self-absorption effects are very large. For intermediate values of self-absorption, we may, under conditions of optimum data, obtain both quantities. By contrast, we obtained in Chapters 6 and 7 direct information on the space distribution of n_e, n_p, n_{H}, n_{HeII}, and T_e from the height-variation of the free-bound emission from H, H^-, and HeI under conditions of negligible self-absorption in the observed emission. It is these latter quantities, plus the other ionic concentrations, which we require to specify the thermodynamic structure of the chromosphere, its energy balance, and its origin. To proceed from the quantities directly inferred from observations of the line spectrum to these other quantities just specified requires an analysis in terms of the non-equilibrium state along the lines of Chapter 4, modified by the effects of self-absorption.

As discussed in Chapter 4, any non-LTE analysis based even upon a perfect set of data must at present admit a considerable degree of inadequacy because of uncertainty on atomic cross sections and incompleteness of theoretical solutions for the variations of source function through an atmosphere of specified structure. Our question, then, is twofold: (1) How much can we infer on the actual chromospheric structure from presently existing data on the line spectrum, making realistic estimates of this a priori inadequacy?

(2) How far can we go in developing general methods of analysis which may be more completely applied to later, more complete data? We proceed by asking first, what would be an ideal set of data for the desired analysis, and second, what can we obtain from the actual data available?

I. General Principles Underlying the Analysis of the Line Spectrum

We may express the specific intensity emergent from the chromosphere in terms of an integral over either geometrical depth or over optical depth, viz.,

$$I_{\nu_{UL}}(h) = (A_{UL}/4\pi)h\nu_{UL}j_{\nu_{UL}} \int_{-\infty}^{\infty} n_U(h,y)e^{-\tau_\nu(h,y)}\,dy \tag{9-1}$$

or

$$I_{\nu_{UL}}(h) = \int_0^{\tau_{\nu\max}(h)} S_\nu(y,h)e^{-\tau_\nu(h,y)}\,d\tau_\nu \tag{9-2}$$

where

$$\tau_\nu = \alpha_{\nu_0}\varphi_\nu \int_y^{\infty} n_L(h,y)[1 - (\tilde{\omega}_L/\tilde{\omega}_U)(n_U/n_L)]\,dy \tag{9-3}$$

The subscripts U and L refer to upper and lower states of the transition, φ_ν and j_ν represent the profiles of absorption and emission coefficients as discussed in Chapter 4, and S_ν is the source function given by Eq. (4-38). The occupation numbers n_k are given by the non-LTE form of the Boltzmann-Saha equation (4-3). The choice of which equation, (9-1) or (9-2), to use in the analysis depends upon the particular circumstance, usually governed by the size of $\tau_{\max}$. For very small τ, the emission essentially measures n_U, and Eq. (9-1) is preferable. For very large τ, we see only a portion of the atmosphere, the emergent I_ν is essentially S_ν near $\tau_\nu \sim 1$, and Eq. (9-2) expresses more directly this opacity effect.

From Eq. (9-1), we see the basic difficulties implicit in an analysis of an observed intensity to infer occupation numbers. Each observed quantity, the emission at a particular wave length in the line, depends upon two parameters, n_U and n_L, together with their distribution through the atmosphere. Thus, we see that the problems fall into two classes: on the one hand, the problems which would arise even if the occupation numbers were individually constant throughout the observed atmospheric region; on the other hand, the problem of the variation of an occupation number through the atmosphere. Consider these two problems in turn.

The case of an atmosphere within which the occupation numbers are individually constant permits, in principle, a unique solution for the occupation numbers from a given set of observed line intensities only in three situations: one, where local thermodynamic equilibrium exists, $b_k = 1$ for all k; a second, where enough lines are observed that some energy level serves as both an upper and a lower level; and the third, where $\tau_{\max}$ is completely negligible for all lines. The first case is obvious, because only three parameters are unknown, n_e, n_i, and T_e, and the observation of at least three lines suffices, in principle, to specify the unknown parameters. In the second case, the observation of a set of m lines having a common lower level involves $m + 1$ unknowns. Adding more lines involving a different lower level does not make the problem determinate, unless we add a line whose upper and lower levels have both occurred as upper or lower levels in lines of the group already considered. If this situation occurs, as, for example, in the Balmer and Paschen lines of hydrogen, we then have at least as many observed quantities as unknown occupation numbers. In the third case, when τ_ν is completely negligible, an observation depends only upon the occupation number of the upper level, and has been illustrated in Chapters 6 and 7.

At the outset, we may state that the present state of observations of the chromosphere is such that none of the three alternatives may be *generally* satisfied. Because the whole chromosphere-corona phenomenon seems to occur as a result of the existence of the cyclic process—mechanical energy in → radiative energy out—we cannot a priori assume local thermodynamic equilibrium. Although essentially all of the work preceding our investigations of the chromosphere from eclipse data (Thomas, 1948, et seq.) was done under the assumption of a negligible τ_ν in any but a very few of the strongest lines, we feel that the full weight of evidence rules against this assumption in most cases other than the material discussed in Chapters 6 and 7. (This evidence is discussed in detail during the final analysis.) Finally, although we made every effort at the 1952 eclipse to obtain data involving the same energy level in several lines, notably through simultaneous observations of the Balmer and Paschen series of hydrogen, we were unsuccessful.

Although the remarks above are correct in so far as determining empirically the occupation number of each energy level, they overstate the difficulty of the situation. In principle, even in the nonequilibrium case, we should require only a finite set of the occupation numbers in order to specify the whole set. Given n_e, T_e, the abundance of the atom relative to hydrogen and the radiation field in those parts of the spectrum to which the chromosphere is opaque, we should be able to compute the occupation numbers. Unfortunately, as discussed in Chapter 4, we do not have complete sets of calculations of the b_k because of uncertainties in the various atomic cross sections entering the calculation and because of the magnitude of the computational task to cover a wide variety of conditions on the value of the local radiation intensity at the frequencies to which the chromosphere may be opaque. One wishes, then, to infer empirically as many occupation numbers as possible. Thus, the analysis must represent an attempt to compromise between the demands of an uncertain theoretical representation and an incomplete set of data.

Consider next the problem of determining the variation of occupation number through the atmosphere. If we do not assume spherical symmetry (and our analysis of the continuum reported in Chapter 7 exhibits the doubtful nature of this assumption) we have two unknown functions to determine, the distribution in h and in τ_ν. Ideally, we have two observable functions, the height variation of the emission and the variation in emission over the line profile. Thus, in principle, we may determine the variation of occupation number through the atmosphere from observation of line profiles at a sequence of heights.

There are several practical difficulties in this scheme. First, the approach presumes observations of profiles for a sufficient variety of lines to meet the conditions for the determination of occupation numbers in a homogeneous atmosphere. Second, the resolution of our observing equipment rarely discriminates below 1″, or some 750 km on the sun, and is usually considerably more gross. For example, the analyzing slit of the microdensitometer used in reducing the 1952 observations corresponded to about 10,000 km on the solar limb. Since the diameter of the chromospheric spicules is < 1000 km and their actual spacing $\sim$ 10,000 km apart, it is not at all obvious that the observed emission can be reduced to the actual emission per cm^2 by simply introducing an area factor into the measured emission. What is actually obtained is an average over the small-scale structure of the chromosphere.

Turning to the vertical resolution, we note from the data in Chapter 2 that 1″ of arc, which is about the limit of resolution of eclipse instruments, corresponds to one or two scale heights for the emission in most lines. Thus, in effect, even a slit system behaves as a slitless system, performing a height integration over the chromosphere.

We shall return to this point at the end of the chapter. Here we wish only to make it clear that the empirical data on height variation consist of an integral relation, even in the most favorable case, and that the observed line profile reflects this height integration. In effect, we obtain information on the line profile at a given height only by differentiating these integral relations, which means, in practice, subtracting observations made at two successive heights.

It is evident that there are two desirable characteristics of a slit system in eclipse observations, once we recognize that it is impractical to have such a sufficiently small slit that the observed slice of the chromosphere is effectively homogeneous. First, we should have a slit which observes the whole effective radiating atmosphere above the moon's limb. For in forming differences between successive observations, either directly, or analytically when curve fitting, such an arrangement ensures that the effective upper limit of the integral over height remains constant and we have a variation introduced by the lower limit only. Second, because the height resolution is fixed entirely by the exposure interval under these conditions, the exposure should be kept as small as possible. In particular, the height resolution should be kept within the scale height of the emission that is measured.

When we now consider our data from the 1952 eclipse, we find that we have satisfied only one of the following three criteria: (1) many lines, overlapping in energy levels of origin; (2) line-profile observations with an effective observation of the whole chromosphere; and (3) high height resolution. Our major effort to satisfy the criteria of many overlapping lines was an attempt to obtain the Balmer and Paschen series of hydrogen, but most of the Paschen data were lost as explained in Chapter 2. We tried only for slitless spectra, wishing to obtain a complete set of data on the later Balmer and Paschen lines, whose intensities are small. We did, however, obtain good height resolution, some 100 km, about a third of even the lowest scale heights. Thus, we expect our analysis to be incomplete on two counts. First, we have no unique empirical solution for the occupation numbers of the energy levels unless we can show either that LTE holds or that self-absorption effects are completely absent. Second, we have no direct approach, from data relating to one ion alone, to inferring departure from spherical symmetry.

The first effect, non-uniqueness in specifying occupation numbers empirically, is the problem of separating non-LTE from self-absorption effects, viz.: observed emission in m lines with the occupation numbers of $m + 1$ energy levels involved as the unknowns. It is possible to at least partially overcome this indeterminacy by supplementing the *observed* height variation of the emission with the *theoretically expected* general form for the variation of occupation numbers and source function through the atmosphere. Such a procedure sacrifices the wholly empirical nature of the result. At the same time, however, if we require only the general form of the height variation of the source function, the form can in certain cases be checked empirically by existing observations of disk and limb profiles. Thus, the approach to occupation numbers becomes again essentially empirical for the case of an assumed spherical symmetry.

The second effect, departures from spherical symmetry, provides a more difficult problem. Zirker (1956) has attempted to investigate the situation by looking for multicomponent models in an approach similar to that adopted for the continuum in Chapter 7. Such an approach rests upon the assumption that spectral emissions corresponding to considerably different levels of excitation may be isolated and ascribed to different gaseous configurations—in this case, to different atmospheric regions—within which the gas differs in thermodynamic state. While it is obvious that this assumption must be true under certain conditions, the problem is to determine these conditions. It is plausible, for example, that a simultaneous observation of the FeI and FeXIV spectra would strongly suggest that we were observing two separate regions along the line of sight, but the situation is not so obvious for excitation levels less widely separated such as in FeI, FeII, and H. The problem lies in our lack

of detailed knowledge of non-LTE effects. Until we can treat, with reasonable completeness, at least one non-LTE configuration for a multicomponent gas which is non-degenerate in the sense that both collisional and radiative processes are included, it is difficult to assess the reliability of any assumptions on the separation of sources of emission. We attempted to investigate this problem in the Wolf-Rayet atmosphere (Thomas, 1949), which offers the classic example of the simultaneous presence of a wide variety of spectral excitation, but the effort is rudimentary. Considerable attention must be paid to Zirker's investigation as representing the only systematic attempt thus far to separate the effects of multi-component structure and non-LTE distribution functions.

Despite the uncertainties and difficulties just summarized, an analysis of the line spectrum, utilizing only presently available data but insisting upon consistency with the non-LTE approach of Chapter 4, does appear to provide considerable information. In particular, such analysis has led to the conclusion that there is much more absorbing material in the chromosphere, and that in consequence the chromosphere has much more influence upon the observed Fraunhofer spectrum, than was previously thought to be the case. From a conceptual standpoint, the result of working with the non-LTE approach has been to also extend an understanding of the mechanism of line formation and to show that the non-LTE approach must be extended to non-chromospheric as well as chromospheric components of the line spectrum. It must, however, be admitted that the great body of astronomers has exhibited considerable reluctance to accept the results of such an analysis, and thus our conclusions upon non-equilibrium effects and the resultant greater influence of the chromosphere upon the Fraunhofer spectrum. (For the most coherent and detailed summary of this opposing viewpoint, see van de Hulst, 1953.)

It must also be emphasized that the outlook in the application of these non-equilibrium concepts to the analysis of chromospheric spectra has evolved very considerably as our awareness of the optical opacity of the chromosphere has grown. Our first studies (Thomas, 1948b, 1949) of non-equilibrium effects in the solar chromosphere were aimed simply at computing the emission to be expected from a chromospheric model differing from the classical one in having a high kinetic temperature but similar in being optically transparent in any but the very strongest lines. We had two purposes: one, to compare this computed emission with the energy input from the system of spicules; the other, to explain certain empirical regularities in the departure of the observed emission from that which would be produced by an optically thin chromosphere in thermodynamic equilibrium. These empirical regularities have been observed since the days of the earliest analyses of eclipse data and have been categorized, but never successfully explained, as "anomalous excitation effects" involving the upper level of the transition. In comparing these initial computations of ours to the empirical regularities in the higher members of the Balmer series of hydrogen, we were greatly surprised to find self-absorption effects, rather than only non-equilibrium effects associated with the upper level, as a major cause (Thomas, 1949, 1950).

The High Altitude Observatory group planned an eclipse program (Khartoum, 1952) to obtain more comprehensive data in order to provide the basis for a more careful study of these notions. Again to our surprise, the self-absorption effects appeared to be much stronger—even among the metals (Zirker, 1956)—than supposed, and to explain even more of the empirical regularities noted. On the basis of these results on chromospheric opacity, at least the central portions of a great many of the Fraunhofer lines of even intermediate strength would be expected to be formed in chromospheric regions.

Thus, we find a shift in the direction of emphasis in these non-equilibrium calculations. We *cannot* consider *only* the case of a gaseous atmosphere upon which is incident a radiation field whose characteristics we know because the atmosphere does not in itself materially alter this incident field. We must, in addition, consider an atmosphere from which may emerge a line spectrum differing very considerably from that incident upon it from the underlying photosphere. The reversing layer, once considered to be the essentially isothermal upper regions of the photosphere, must now be considered to be a composite of upper photosphere and chromosphere.

For these reasons—the reluctance of most astronomers to accept the results of this non-equilibrium approach to the analysis of chromospheric data, and the evolution of the non-equilibrium analytical viewpoint through the course of the chromospheric studies—we adopt an evolution-of-concept approach in this chapter rather than beginning directly with the expectations from Chapter 4. We follow the same procedure in bringing together results obtained from eclipse observations and from the Fraunhofer spectrum. Because of the greater amount of data available, the greater emphasis lies on hydrogen.

II. Analysis of the Hydrogen Lines

The data on the Balmer lines are the most complete, and as already mentioned, the very small amount of data on a very few Paschen lines are essentially useless. In terms of the discussion in Section 9-I and in Chapter 4, we may divide these Balmer-line data into three classes:

(1) Disk observations of the lines up to H10. By combining the several lines, we span a considerable radial optical depth measured, say, in the center of Hα; call this optical depth $\tau_{\alpha r}$.

(2) Eclipse and limb observations of the "early" Balmer lines. Here, we have a reasonable expectation that we may observe regions that are opaque in a tangential direction, but thin in a radial direction Thus, we may extend upward the atmospheric region over which we can study empirically the variation of source function.

(3) Eclipse observations of the "late" Balmer lines, up to about H35. Here, we have a reasonable expectation that the chromosphere will not be wholly opaque in the tangential direction. Comparison of the observed emission to that expected from a thin atmosphere in LTE should provide a direct assessment of non-LTE effects *if* we can remove the self-absorption effects.

From (1) and (2) we may hope to map the variation of $S_L(\tau_{\alpha r})$ empirically. If our analysis in Chapter 4 is correct in assigning the hydrogen Balmer lines to the photoelectric category, then we expect the dependence of S_L to be second order on T_e relative to the first-order dependence on opacity and the radiation field in the Balmer continuum. Thus, an empirical determination of $S_L(\tau_{\alpha r})$ leads primarily to an empirical comparison of the expectation from Chapter 4 on this functional form with that actually observed. In Sections 9-IIA and B, we present the results of such a comparison, in order to gain some idea as to the confidence we may have in the methodology established in Chapter IV. The chief difficulty in comparing the prediction from Chapter 4 with the empirical results, especially as regards the T_e dependence, is to relate $\tau_{\alpha r}$ to the distribution of T_e.

We utilize the results of Chapter 6 to relate $\tau_{\alpha r}$ and τ_{5000} (optical depth in the continuum at λ5000), and $\tau_{\alpha r}$ and linear height scale, as a first estimate of this relation between line and continuous opacity, and linear and optical depth scales. The results of this section make possible some extension of the results from Chapter 6 on the distribution of Balmer opacity.

From (3), we may hope to gain information on both the Balmer opacity and the departure of occupation numbers of energy levels from an LTE distribution. Thus, we obtain further information on the relation between the linear and optical-depth scales, which measure the distribution of absorbing material in the chromosphere. The first question in proceeding to the analysis of the data is how to treat the line data in relation to the results of Chapter 6 obtained from the continuum. Should the line data be treated completely independently, and the results of the analysis compared with that from the continuum? Or, should the line data be analyzed making use of the results from the continuum, to extend the kind of information obtainable? We first summarize existing analyses, which essentially adopt the independent-treatment standpoint; then ask the results of intercomparison. We treat these data in Section 6-IIC.

A. Disk Observations of the Early Balmer Lines, Hα — H10

Our primary concern in this discussion of disk observations of the early Balmer lines is an empirical evaluation and application of the theoretical background developed in Chapter 4 on the form of $S_L(\tau_0)$. Earlier analyses of this material are based on a wide variety of viewpoints as to the thermodynamic quantities upon which S_L most strongly depends. The most extensive treatments have been those by de Jager (1952, 1957) and Böhm-Vitense (1954), aside from our own initial attempt (Athay and Thomas, 1958) to rediscuss their work.

Böhm-Vitense simply assumes $S_L = B_{\nu 0}(T_e)$ as obvious. Both Unsöld (1955), in summarizing Böhm-Vitense's work, and de Jager, in his first analysis, claim to have proved $S_L = B_{\nu 0}(T_e)$ by essentially comparing relative rates for the various transitions from the levels involved but *without* actually computing S_L from the equations of statistical equilibrium. de Jager and Neven proposed (1954) to use the early Balmer lines to infer $T_e(\tau)$ in the outer parts of the general stellar atmosphere, under this assumption $S_L = B_{\nu 0}(T_e)$. In his later work (1957), de Jager drops this position, stating that his proof applied only to photospheric regions and it is now clear that the lines have their origin in the chromosphere. Unfortunately he attempts to evaluate the non-LTE effects by using Giovanelli's first non-LTE computations, which are valid only for an optically thin model of the chromosphere. He later (1959) tries to justify his use of these thin-atmosphere non-LTE values by asserting that even if the absolute values of the b_k are not correct, the relative values probably are. Such an assertion overlooks the point of the large relative change in b_1, b_2, and the higher b_k with the Balmer and Lyman opacity. Although a good part of the rather extensive attempts to investigate the non-LTE configuration in a chromosphere of non-negligible opacity (summarized in Chapter 4) were in the literature prior to these analyses by Böhm-Vitense, Unsöld, and de Jager, these authors seem to have overlooked this material in their investigations.

In our own initial analysis (Athay and Thomas, 1958), we recognized that S_L for the Balmer lines depends mainly upon the local value of the radiation field in Hα and only secondarily upon T_e. Subsequently, our investigations of the source function have produced (Jefferies and Thomas 1959) an algebraic specification of the quantities upon which S_L for Hα depends, as outlined in Chapter 4 and applied in Chapter 6. We wish, then, to recast our initial investigation along lines wholly consistent with these later investigations of the source function.

The most extensive data available for discussion are those of de Jager (1952), with similar, but not so extensive, material coming from Gollnow, ten Bruggencate, Gunther, and Strohmeier (1949). The two sets of data are in fair agreement, as judged on the basis of the internal consistency of each set, although the Göttingen data lie systematically higher than the Utrecht. Figure 9-1 exhibits $I_{\lambda 0}$ versus $\mu = \cos \theta$ for the two sets of data, for the lines Hα — Hδ. In the following, because of its greater completeness, we restrict our attention to de Jager's data.

We consider separately the center of the line, and positions off-center because the latter require an assumption on the profile of the absorption coefficient. In the center of the line, the relative absorption coefficient varies as $\lambda_0 f$, so that we readily establish the relative optical depth from line to line. Thus, we first consider disk observations made in the line center, attempting to combine data from

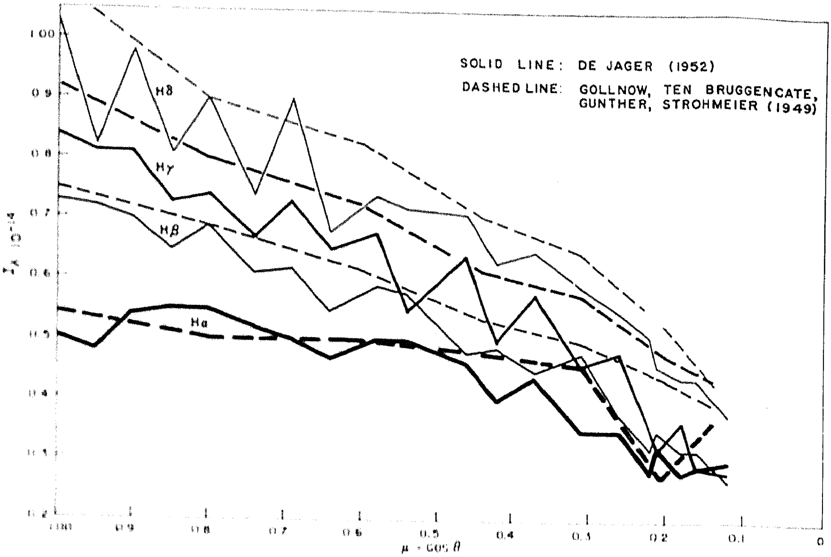

Fig. 9-1. Disk observations of early Balmer lines.

several lines to obtain a greater range in $S_L(\tau_{av})$, then turn to the line profiles.

1. Investigation of $S_L(\tau_{av})$ from Disk Observations Made in the Line Center. *a. The Relation between $S_L(\tau)$ and $I_{\lambda_0}(\mu,\ 0)$ in a Spherically Symmetric Atmosphere.* The first step is to establish the particular form of the correspondence

$$I_\lambda(\mu) \leftrightarrow S_\lambda(\tau_\lambda) \tag{9-4}$$

The empirical data of Fig. 9-1 show sufficient scatter that an attempt to determine the analytic form of $I(\mu)$, thence by inversion that of $S(\tau)$, simply by curve fitting promises only low reliability. Thus, one can succeed only by successive approximation, requiring that the finally determined relation $S(\tau)$ be consistent with the algebraic form of $I(\mu)$ used in analyzing the data.

The usual initial approximation is to assume

$$S_\lambda(\tau_\lambda) = a_\lambda + b_\lambda \tau_\lambda \tag{9-5}$$

which leads to

$$I_\lambda(\mu,\ 0) = a_\lambda + b_\lambda \mu \tag{9-6}$$

or the relation between observed I_λ and inferred S_λ

$$S_\lambda(\tau_\lambda = \mu) = I_\lambda(\mu) \tag{9-7}$$

Böhm-Vitense used this relation throughout her discussion, not asking whether it was consistent with the final $S_\lambda(\tau)$. (As we shall see, it is not.)

On the other hand, de Jager adopted the form

$$S_\lambda(\tau_\lambda) = a_\lambda - b_\lambda \exp(-c_\lambda \tau_\lambda) \tag{9-8}$$

which leads to

$$S_\lambda(\tau_\lambda = c_\lambda^{-1} \ln [c_\lambda \mu + 1]) = I_\lambda(\mu) \tag{9-9}$$

and tabulates the quantities a_λ, b_λ, c_λ determined to give the best fit to the smoothed data of Fig. 9-1. From our discussion in Chapter 4, we would indeed consider a relation of the form of Eq. (9-8) to be more compatible with $S_L(\tau)$ than one of the form of Eq. (9-5); we might expect only that several more exponential terms would be required. Consider this point in more detail.

As in equation (4-92), we recognize that the source function entering the expression for the emergent radiation is

$$S_\lambda = (S_L + r_\lambda S_C)/(1 + r_\lambda) \tag{9-10}$$

We have already discussed the value of r_0 in Chapter 6, Eq. (6-28), and found it to be small for Hα, less than 10^{-4} for $T_e \gtrsim 6000°$. From Tables 6-5 and 6-8, we see that for $T_e \lesssim 6000°$, $\tau_{\alpha r} \gtrsim 10^2$; so we may confine our attention to $T_e > 6000°$ and $r_0(\text{H}\alpha) < 10^{-4}$. From Fig. 9-1, we see that $I_{\lambda_0}(\text{H}\alpha)$ at $\mu = 0.12$ corresponds to $T_{\text{rad}} \sim 3700°$. Thus, if we set a lower bound on S_L by $S_L \gtrsim B_\nu(T_{\text{rad}})$, we see that for H$\alpha$, $S_L \gtrsim 10 r_0 S_C$ for $T_e \lesssim 1.10^5$. Thus, we may use $S_\lambda = S_L$. We have also, in Table 6-5, shown that the solution for $S_L(\tau_0)$, in the case of a photo-ionization-dominated source function, is insensitive to r_0 in such cases, and effectively equal to the solution under the limiting case $r_0 = 0$. This solution is, for constant B^* and η, given by Eq. (4-102)

$$S_L = B^*(1 + \Sigma L_j e^{-k_j \tau_0}) \tag{9-11}$$

and leads to

$$I_{\lambda_0}(\mu, 0) = B^*(1 + \Sigma L_j [1 + k_j \mu]^{-1}) \tag{9-12}$$

Expressions (9-11) and (9-12) resemble expressions (9-8) and (9-9) used by de Jager, except for the several rather than single exponential terms.

The formal solution given by Eq. (9-11) for $S_L(\tau_0)$ has been derived in Chapter 4 on the basis of the definition of B^* and η given by Eqs. (4-90) and (4-91). This derivation also rests upon the use of S_L given by Eq. (4-101). As shown in Section 4-IIIC2, Eq. (4-101) may only be applied to a subordinate line, like Hα, if detailed balance holds in the resonance lines. A priori, we have no guarantee that detailed balance in the Lyman resonance lines does hold in the region where the center of Hα arises. Indeed, from Table 6-10 and the discussion centered around the region of the abrupt rise in T_e, we see that the effective region of formation of the central parts of Hα may lie very near the transition region between detailed balance in Ly-α and its absence. Thus, we ask what modifications we might expect in Eq. (9-11) from such a situation.

We rewrite the expression for the general case, Eq. (4-87), in the form

$$S_L = \left(\int \bar{I}_\nu \varphi_\nu d\nu + \eta B_1{}^* \right) \Big/ (1 + \eta_1) \tag{9-13}$$

where

$$B_1{}^* = B^*(1 + \delta_{Ll}/F_{L2}) \tag{9-14}$$

$$\eta_1 = \frac{F_{U1} F_{L2} e^{-X_L}}{(F_{U1} + F_{L1}) K_{LU}} \left\{ \frac{F_{L1} F_{U2}}{F_{U1} F_{L2}} e^{X_{LU}} - 1 - \frac{\delta_{Ll}}{F_{L2}} \right\} \tag{9-15}$$

We have taken the F to predominate in the expression for the $\mathfrak{F}$ and for R, in conformity with the expression used for Hα when detailed balance has been assumed. (If the reader will compute the various terms entering $\mathfrak{F}$ and R from the data given in Chapters 4 and 6, he will find the procedure correct for Hα.) Thus, the transition between detailed balance and its absence hangs upon the value of (note that τ_0 refers to Ly-α)

$$\frac{\delta_{Ll}}{F_{L2}} \equiv \frac{\delta_{21}}{F_{22}} = \frac{2}{3} \left\{ \frac{-\Sigma L_j e^{-k_j \tau_0}}{e^{-c\tau_0} + \Sigma L_j e^{-k_j \tau_0} + (1 + \beta \tau_0)/A} \right\} \tag{9-16}$$

To evaluate δ_{21}/F_{22}, we have used equations (4-83), the definitions following equations (4-41), Eq. (4-90), and Equations (4-110), the result that $\eta > \epsilon$ and $\epsilon B_{\nu 0}(T_e) > \eta B^*$ for Ly-α, and the numerical values for the Balmer continuum given in Chapter 6, just preceding Eq. (6-20). For Ly-α, we have $\eta = 4 \times 10^{-5}$, thus the values, for the case $c = 0$ [but cf. Section 9-IIIB3]:

k_1	k_2	k_3	L_1	L_2	L_3
0.665	0.0455	0.000601	−0.004	−0.066	−0.924

An upper limit for the right side of Eq. (9-16) is $2/(3\sqrt{\eta_{21}})$ in the case $c = 0$ (cf. Section 4-IIIC4). In the event that we are looking right into the region of a steep rise in T, and must consider $c \neq 0$, this upper limit can increase to $B_{\nu_0}(T_e \text{ max})/B_{\nu_0}(T_e \text{min})$, if this last ratio is larger. From Chapter 6, we see that in the vicinity of that rise which is of interest in discussing the Balmer lines, $T_e(\text{min}) \gtrsim 8000°$ while $T_e(\text{max}) < 10^5$; so this ratio is less than 50. Thus, the last term in the bracket of the numerator in Eq. (9-15) is always very much less than the first term, and $\eta_1(\text{H}\alpha)$ always equals $\eta(\text{H}\alpha)$. However, B_1^* can increase over B^*, by a factor up to about 110. We have the following values for the case $c = 0$:

$\tau_0(\text{Ly-}\alpha)$	10^4	10^3	10^2
δ_{21}/F_{22}	0.002	0.7	5

We may examine the behavior of Hα across the transition region of detailed balance in the Lyman lines in one of two ways. Because the change in B_1^* is small until $\tau_0(\text{Ly-}\alpha) \lesssim 10^3$, we may make an approximate estimate by using Eq. (9-11) with B^* replaced by B_1^*. Alternatively, we may make a more detailed solution by expressing B_1^* as

$$B_1^* = B^*(1 + de^{-\kappa\tau_\alpha}) \tag{9-17}$$

and proceeding to a solution as in Chapter 4. The behavior now mimics that of the collision-dominated case, but we must recognize the difference between $B_{\nu_0}(T_e)$ and B_1^*. We obtain, in place of the expression of Eq. (9-11), the following for the case $r_0 = 0$:

$$S_L = B^*\{1 + \gamma d(1 + \sigma[1 - \gamma])(e^{-\kappa\tau_0} + \Sigma L_j e^{-k_j\tau_0})\} \tag{9-18}$$

$$\left\{\sum_j \frac{L_j}{1 - k_j/x_i} + 1\right\}\{\gamma d(1 + \sigma[1 - \gamma])\}$$

$$= -\left\{1 + \gamma d(1 + \sigma[1 - \gamma])\frac{\kappa/x_i}{1 - \kappa/x_i}\right\} \tag{9-19}$$

$$\sigma = \left[\sum \frac{\alpha_i}{1 - \kappa^2/x_i^2}\right]\left[1 - (1 - \gamma) \sum \frac{\alpha_i}{1 - \kappa^2/x_i^2}\right]^{-1}; \qquad \gamma = \frac{\eta}{1 + \eta} \tag{9-20}$$

The k_j for Hα are the same in Eqs. (9-11) and (9-18); the L_j differ, depending upon the value of κ. As far as fitting the data are concerned, however, the chief difference between Eqs. (9-11) and (9-18) lies in the effective value of the coefficient B^*. If the observed intensity of the line lies above the value predicted by Eq. (9-12), we recognize that the transition from a condition of detailed balance in the Lyman lines is making itself felt. If the observed intensity lies below the value predicted by Eq. (9-11), either something is wrong with the theory we have developed, or possibly departure from spherical symmetry in the atmosphere is at fault. In Section 9-IIA1b we examine the possible influence of this last effect before turning to the data.

First, we ask the behavior of S_L for the other Balmer lines. We may write, from Eq. (4-38),

$$S_L(H_k) \simeq S_L(\mathrm{H}\alpha)(\lambda_{23}/\lambda_{2k})^5 \; (b_k e^{-X_{3k}}/b_3) \tag{9-21}$$

noting that $b_2 e^{X_{2k}}/b_k \gg 1$. We see from Eq. (9-21) or from a generalization of Eq. (4-87) that the principal correction factor describing the transition between detailed balance in the Lyman lines and its absence is the same factor discussed above for Hα. We have already noted that $S_L(\mathrm{H}\alpha)$ has no explicit dependence on T_e, the influence of T_e on its value entering only indirectly through the opacity, where $d\tau_\alpha$ varies as T_e^{-1}. Thus, we also see from Eq. (9-21) that any explicit dependence of $S_L(H_k)$ on T_e enters through the factor $b_k b_3^{-1} \exp(-X_{3k})$.

Consider the generalization to a multi-level atom of Eq. (4-87), which results from summing over a and l in the quantities defined by equations (4-86). So long as F_{U1} dominates $\mathfrak{F}_{U1}$, F_{U2} dominates $\mathfrak{R}$, and the approximation of the value of the exponential integral entering the recombination rate by $X_k \exp(-X_k)$ remains valid, $S_L(H_k)$ has the same form as $S_L(\mathrm{H}\alpha)$ and shows no explicit dependence upon T_e. These conditions already begin to fail for Hβ, however; for example, $Y_4 = 1.40$ and $X_4 \sim (10^{-4}T_e)^{-1}$. Thus we write

$$\eta_{2U} \cong [F_{L1}/(F_{L1} + \mathfrak{F}_{U1})](\mathfrak{R}e^{-X_U}/K_{LU}) \tag{9-22}$$

$$B^* \cong \frac{2h\nu^3}{c^2} e^{-X_{2U}} \frac{F_{L2}}{F_{L1}} \frac{\mathfrak{F}_{U1}}{\mathfrak{R}} = \frac{2h\nu^3}{c^2} \left(\frac{e^{-Y_2}}{2Y_2}\right) X_2 e^{X_U} \frac{\mathfrak{F}_{U1}}{\mathfrak{R}} \qquad (9\text{-}23)$$

and recognize that the essential question is the behavior of $\mathfrak{F}_{U1}/\mathfrak{R}$. The quantities of largest numerical value entering these two terms are $\delta_{j,j-1}$ and $C'_{j,j+1}$. We have not as yet properly explored the behavior of the former; values of the latter are as yet unavailable, although computations on them are in progress by a group at St. John's University under S. N. Milford. Thus a discussion of the behavior of η and B^* for the remainder of the early Balmer lines would not be particularly rewarding at this stage; it would be at most qualitative. We note only that any explicit dependence upon T_e of either η or B^* involves no exponent larger than X_{U-1}, if collision terms dominate; and X_{U+1}, if they do not. Thus, any approximation scheme for the analysis of the Balmer lines that adopts even as a first-order approximation $S_L \sim B_\nu(T_e)$ introduces a fictitious T_e-dependence with error approximating exp $(-X_2)$. A better first-order approximation would be to take $S_L(H_k)$ independent of T_e, introducing the T_e-dependence as the second-order approximation. (We reserve zero-order approximation to refer to that of a constant source function, which has often been used in the literature.) We proceed on this basis, whenever the occasion for such an approximation scheme arises.

b. The Effect of Departures from Spherical Symmetry on an Inference of $S_L(\tau_0)$ *from* $I_{\lambda_0}(\mu,0)$. On the basis of very-high-dispersion studies of line profiles on the solar disk, McMath, Mohler, Pierce, and Goldberg (1956) conclude that the usual direct process of inferring $S_L(\tau_0)$ from $I_{\lambda_0}(\mu,0)$ is invalid. These high-dispersion observations show fluctuations in intensity along the length of the observing slit, at a fixed position, $\Delta\lambda$, on the spectal line. In consequence of these observations, they picture the chromosphere as a broken shell of partially opaque, cloudlike features interwoven with transparent regions. These cloudlike features are "hot," are discrete rather than continuous in form, and are enveloped on all sides by a "cool" medium. Center-limb observations would, in consequence of this model, refer to a mixture of cloud and inter-cloud media, whose relative proportions would change, in general, as the line of sight changed from center to limb. Moreover, a given geometrical thickness corresponds to a considerable difference in optical thickness from one line to another. In consequence, they suggest that an inference of $S_L(\tau_0)$ from $I_{\lambda_0}(\mu,0)$ for a given line is misleading, and a combination of $S_L(\tau_0)$ for several lines into one over-all $S_L(\tau_{\alpha r})$ is invalid.

We believe that this interpretation of the high-dispersion observations is overly simplified, and that the conclusion regarding the use of limb-darkening observations is overly pessimistic. We do not wish to argue against the possible existence and influence of inhomogeneities in the atmosphere; we wish only to place the possibilities of such influence on any particular observationally-inferred parameter into proper focus. We believe that limb-darkening observations of the early Balmer lines, even low-resolution observations, can—when properly interpreted—lead to a reasonable first approximation to an empirical measure of the form of $S_L(\tau_{\alpha r})$. High-resolution observations will, of course, add to the data available and give more information. Consider our reasoning.

First, we do not find this picture of hot clouds in a cold medium convincing, because it is based on an unjustified physical approach to translating observed emission into inferred thermodynamic properties of the emitting region. These authors reach their model by interpreting the self-reversed emission cores of Ca^+ H and K as requiring cooler regions in the highest layers contributing to the line formation, underlain by hot regions, which in turn have cool regions under them. This interpretation forms the basis for their suggestion of hot, discrete clouds enveloped in a cold medium. As we have shown in Chapter 4, a perfectly spherically symmetrical distribution of both thermodynamic parameters and material suffices to produce the self-reversed cores in these Ca^+ lines, with T_e following a simple monotonic increase above its minimum at the photosphere-chromosphere interface.

When considering results inferred from observations of the early Balmer lines in comparison with those inferred from observations of the Ca^+ H and K lines, one must be very cognizant of the results emphasized in Chapter 4, that their S_L depend quite differently upon the atmospheric parameters. Both kinds of line are strong—small r_0; in each, the predominant term in the expression for S_L is the local value of the radiation intensity in the line; they differ, however in the "source" term. For Ca^+, the source term is the local value of $\epsilon B_{\nu_0}(T_e)$; for $H\alpha$, it is a function of the intensities of the Balmer and Paschen continua, which are essentially photospheric radiation fields. We therefore expect the possible influence of atmospheric inhomogeneities on the observed emission to differ considerably between the Balmer and Ca^+ lines. For Ca^+, a variation in T_e may be reflected directly in the term $\epsilon B_{\nu_0}(T_e)$. For the Balmer lines, the effect of any kind of an inhomogeneity must, to first order, be reflected only in a change in opacity. Thus, in addition to challenging the basis upon which physical characteristics of atmospheric inhomogeneities have been inferred by McMath et al., from the Ca^+ observations, we would caution that one cannot even consider their suggested model as having only pseudo-reality, to be used wholly in empirical prediction of the influences acting on some other kind of line. Each kind of line must be considered by itself, properly evaluating the influences determining the behavior of S_L and of the opacity.

An influence of atmospheric inhomogeneities upon the Balmer line emission through their effect upon opacity may enter in two ways, based upon our discussion in Section 9-IIA1a. First, there is the effect of a changed opacity in the Balmer continuum upon the value of B^*. Second, there is the effect of a changed opacity in Ly-α upon the condition of detailed balance in the Lyman lines, thus upon the value of the correction factor, δ_{Ll}/F_{L2}, relating B^* and B_1^*.

A fluctuation in Balmer line-intensity resulting from a fluctuation in Balmer continuous opacity is much more likely to arise from an inhomogeneity in opacity near the level $\tau_\alpha \sim 10^4$ to 10^5 than from a cloud-like inhomogeneity near the level $\tau_\alpha \sim 1$ to 100. B^* is proportional to the integrated, over direction, value of the intensity in the Balmer contiuum. Thus a local cloud can effectively shield the radiation from all directions. However, to induce a fluctuation in B^* of 15 to 30 percent, the value of the local fluctuations in I_{λ_0} reported by McMath et al., one requires at the level $\tau_\alpha \sim 1$ to 100 increases in n_2 by factors of 10^4 to 10^2. From our discussion in Chapters 4 and 6, this change in n_2 must result from the factor $n_e n_p T_e^{-3/2}$, thus requiring increases of 100 to 10 in n_e in the inhomogeneity. In contrast, a fluctuation in B^* of 15 to 30 percent associated with a columnar-type inhomogeneity extending upward from the level $\tau_\alpha \sim 10^5$ would require a homogeneous increase in n_2, thus in $n_e n_p T_e^{-3/2}$, throughout the column of only about this same 15 to 30 percent. Because B^* varies as the integrated intensity over all directions, not just that coming from the base of the column, the actual change in effective B^* at the base of the column must exceed the observed fluctuation in I_{λ_0}. One must investigate the problem of the variation in S_L, and I_{λ_0}, associated with a checkerboard distribution of radial columns for a detailed quantitative answer.

A fluctuation in Balmer line-intensity resulting from a fluctuation in Ly-α opacity, thus a significant increase in B_1^* over B^*, differs from the preceding in that it depends upon the opacity of the overlying, rather than underlying, material. Thus the relevant inhomogeneity must occur at and above the level $\tau_\alpha \sim 1$; it may or may not be associated with an inhomogeneity below this level. As may be seen from the numerical values cited in Section 9-IIA1a, the size of the fluctuation in Ly-α opacity required to produce a fluctuation in B_1^* of 15 to 30 percent depends very strongly upon the Ly-α opacity corresponding to the level $\tau_\alpha \sim 1$ in the "average" atmosphere.

Finally, we note as an over-all effect, that the presence of either type of inhomogeneity will produce a greater center-limb contrast than in the case of a spherically symmetric atmosphere. The low-resolution observations represent a mean of the several regions having variation in Balmer opacity below a given height, and in Lyman opacity above a given height. In either case, as the line of sight shifts toward the limb, the relative contribution of the regions having larger opacity increases, and the larger opacity is, again in either case, associated with a smaller value of B_1^*.

c. Analysis of the Observed $I_{\lambda_0}(\mu,0)$ *to Infer the Behavior of* $S_L(\tau_{\alpha r})$. (*i*) Hα. If we assume the applicability of Eq. (9-12) for Hα—i.e., that Hα is formed in a region satisfying local opacity in the Lyman lines—the values of η, B^*, L_j, and k_j used in Section 6-IIIA1, give

$$\text{H}\alpha\colon\ I_{\lambda_0}(\mu,0) = 2.68 \times 10^{14} \times \left[1 - \frac{0.042}{1+0.668\mu} - \frac{0.513}{1+0.058\mu} - \frac{0.385}{1+0.004\mu}\right] \qquad (9\text{-}24)$$

Thus, Eq. (9-24) predicts 2.87×10^{13} for $I_{\lambda_0}(1,0)$ compared with the observed value $\sim 5.5 \times 10^{13}$; and it predicts a limb-darkening ratio of 0.71 between $\cos\theta = 1$ and 0.12 compared with the observed ratio $\sim$0.5

On the basis of the discussion in Section 9-IIA1a, we would interpret this underprediction of $I_{\lambda_0}(1,0)$ to imply that at the center of the disk, $\tau_{\alpha r} \sim 1$ occurs in a region where significant departure from detailed balance in Ly $-$ α occurs. The numerical value of the under-prediction, coupled with the relations quoted between $\tau_0(\text{Ly} - \alpha)$ and δ_{21}/F_{22}, suggests $\tau_0(\text{Ly} - \alpha) \sim 0.8 \times 10^3$. Although these results do not give any direct measure of T_e, the discussion of Chapter 6 suggests that T_e may be high, $2 \times 10^4 \lesssim T_e$. Thus we ask whether the numerical approximations used in Chapter 6 for the quantities entering η and B^*, replacing the exponential integrals by $X^{-1} \exp(-X)$, are sufficiently accurate to permit these conclusions on the value of δ_{12}/F_{22}. If we replace these values by the actual values of the exponential integrals in evaluating F_{21}, F_{31}, F_{22}, and F_{32}, we introduce the small, second-order dependence of S_{23} on T_e already mentioned. We compute the following:

$10^{-4}T_e$	1	1.5	2	3	4	(Chap. 6)
$10^{-14}B^*$	2.48	2.39	2.32	2.22	2.16	(2.74)
η	0.00312	0.00316	0.00319	0.00324	0.00327	(0.0036)

Thus $B^*\sqrt{\eta}$ shows a maximum departure of about 30 percent below the values used in Chapter 6, for $T_e \lesssim 4 \times 10^4$. The result leaves unchanged the conclusions reached above, except to decrease slightly the inferred value of $\tau_0(\text{Ly-}\alpha)$.

On the basis of Eq. (9-24), the decrease in effective $\tau_{\alpha r}$ between $\mu = 1$ and 0.12 in a spherically symmetric atmosphere would be about a factor 4. Since $|d \ln n_2/dh| < |d \ln n_1/dh|$, the decrease in $\tau_0(\text{Ly-}\alpha)$ is at least this factor. Then the increase in $(1 + \delta_{12}/F_{22})$ by a factor 3 between $\tau_0(\text{Ly-}\alpha) \sim 0.8 \times 10^3$ and 10^2 would imply limb *brightening* by about a factor 2. Because limb *darkening* is observed, we conclude on the basis of Section 9-IIIA1b that inhomogeneities are present. The size of the effect—converting a predicted limb brightening of about a factor 2 for a spherically symmetric atmosphere into a limb darkening of about 50 percent in the actual atmosphere—implies that the opacity effect in these inhomogeneities must lie in largest part in increased Ly-α opacity.

It is of interest that our predicted value for the center of the disk under the assumption of detailed balance in the Lyman lines lies so close to the observed value at $\cos\theta = 0.12$, ~ 2.5 to 3×10^{13}.

If we visualize the inhomogeneities as being of a columnar type, projecting up through the chromosphere as regions denser and cooler than the enveloping atmosphere, thus having higher opacity, then we might expect such a result. That is, our solutions such as that of Eq. (9-11) have been derived for a spherically symmetric atmosphere. On the other hand, we might expect very nearly the same solution for the distribution of S_L in a radial column, near $\tau_\alpha \sim 1$, provided the column was optically thick enough in a transverse direction and that we measured τ perpendicular to the nearest surface. We return to this point in Section 9-IIB. Here, we would only remark that on this basis we might expect fluctuations up to about 50 percent in $I_{\lambda_0}(1,0)$ rather than the 15 to 30 percent reported. Since this difference only corresponds to fluctuations reaching a 10 percent residual intensity in Hα rather than the reported 14 percent, and because any systematic radial motion of the more opaque column would shift the line off-center and raise the observed I_{λ_0}, it is probably best to wait for more detailed investigations following these preliminary reports by McMath et al.

We stress that the preceeding predictions and interpretations of the behavior of $I_{\lambda_0}(\mathrm{H}\alpha)$ rest upon a theoretical S_L that is extremely insensitive to the value of T_e in the region of line formation, except through its dependence upon Ly-α opacity. The explicit T_e dependence enters through the departure of $E_1(-X_U)$ from the value $\exp(-X_U)/X_U$. We emphasize the contrast in behavior of this theoretical S_L and one based either upon the assumption that $S_L = B_{\lambda_0}(T_e)$ or upon the assumption of an S_L derived from non-LTE calculations in a thin atmosphere. Under the assumption $S_L = B_{\lambda_0}(T_e)$, the observed $I_{\lambda_0}(\mu,0)$ would require T_e as low as 3700° in the region of line formation. A result derived under the assumption of a thin atmosphere would require much higher values of δ_{12}/F_{22}, thus predicting a much higher central intensity for Hα. Because the predictions made on the basis of our theoretical S_L agree well with observations when values of Ly-α opacity are adopted that accord with the results of Chapter 6, we consider that we have found strong support for the basic physical treatment underlying our theoretical S_L.

Finally, although a discussion of plages and flares lies outside the scope of this monograph, we note the direction of an investigation of their behavior suggested by the considerations above. Any increase in the central intensity of $H\alpha$ must come from one of three causes: (1) a decrease in effective Ly-α opacity in the region of line formation, (2) an increase in the Balmer continuous intensity, or (3) a sufficiently large increase in T_e and n_e to make $\epsilon B_{\nu 0}(T_e) > \eta B_\nu^*$ for Hα. Of these three alternatives, a little calculation quickly shows that (1) and (3) are the easiest to accomplish. Indeed, even without further calculation, we see from the numerical values already quoted that the central regions of Hα are formed at such values of Ly-α opacity that S_L(Hα) is extremely sensitive to change in τ_0(Ly-α). Having τ_0(Ly-α) near a value $\sim 10^3$ to 10^2 increases S_L(Hα) by a factor about 1.5. Investigations along this line are in progress, and will be reported elsewhere, later.

(*ii*) Hβ – Hδ, Hζ, *and their Relation to* Hα. From the preceding results on Hα, we expect that $I_{\lambda_0}(1,0)$ for Hβ, and $I_{\lambda_0}(\mu > 0.12,0)$ for the other Balmer lines, should effectively originate in regions locally-opaque in Ly-α. Our estimates in Section 9-IIA1c lead to τ_0(Ly-α) slightly less than 0.8×10^3 for the effective place of origin of the center of Hα at the center of the disk. The absorption coefficient drops by a factor 7 from Hα to Hβ, by a factor 20 to Hγ, and by a factor 80 to Hδ. $I_{\lambda_0}(0.12,0)$ for Hβ may admit a measurable increase arising from the decrease in Ly-α opacity. We consider the behavior above the limb in Section 9-IIB. Depending upon the optical thickness of the inhomogeneities at the limb, their effect may or may not be consequential for Hβ-Hδ.

As discussed in Section 9-IIA1a, we have not sufficiently explored the behavior of S_L and the NRB for subordinate lines of multilevel atoms to have confidence in theoretical values for S_L in the cases of Hβ-Hδ. At least at the time this is written, we do not have a sufficiently precise knowledge of the quantities entering $\mathfrak{F}_{U1}$ and $\mathfrak{R}$ to compute reliable numerical values for them. We recognize only that F_{U1} and F_{U2} provide lower limits for $\mathfrak{F}_{U1}$ and $\mathfrak{R}$. An inspection of the other terms entering these quantities suggests that the relative underestimate is probably larger for $\mathfrak{F}_{U1}$ than for $\mathfrak{R}$, thus that B^* is underestimated and η overestimated, but this is a conjecture rather than an established result at this stage of our investigations. If we do use these lower limits to estimate B^* and η, use the approximation $r_0 = 0$, and apply Eq. (9-11), the predicted values of $I_{\lambda_0}(1,0)$ lie below the observed by about 25 percent for Hβ and about a factor 2 for Hγ. Thus the underestimate increases as we go higher in the series, which is the direction of the effect of the neglected terms and opposite in direction to the effect of Ly-α opacity. Since the value of $I_{\lambda 0}$ varies roughly as $B^*\sqrt{\eta}$, we believe that our conjecture is a sound one.

We note that were the above lower limits the correct values, we could immediately judge the size of the second-order explicit dependence of S_L on T_e. They would show about 15 percent decrease in $S_L(\mathrm{H}\alpha)$ from $T_e \sim 7500°$ to $T_e \sim 4 \times 10^4$, about 30 percent for $S_L(\mathrm{H}\beta)$, and about 45 percent for $S_L(\mathrm{H}\gamma)$ over the same range in T_e. Such variation is very small compared to that of $B_{\lambda_0}(T_e)$. The important difference, as already noted, is the disappearance of the term $\exp(X_2)$ from S_L; this term will not reappear when these lower limits on $\mathfrak{F}_{U1}$ and $\mathfrak{R}$ are replaced by the actual values, since none of the terms entering them depend upon it.

Because these numerical uncertainties on the quantities specifying S_L for Hβ and the higher Balmer lines preclude a detailed numerical intercomparison between predicted and observed $I_{\lambda_0}(\mu,0)$, we can only ask whether theory and observation agree on the general form of $S_L(\tau)$. It is useful to distinguish three stages of conceptual evolution in this kind of an inquiry, which has characterized empirical analyses both of hydrogen-Balmer and of other strong solar lines for information on the source function. First, there is the stage defined by the assumption $S_L = B_{\lambda_0}(T_e)$. Rather than inquiring into the form of S_L, the inquiry focuses on the use of $I_{\lambda_0}(\mu,0)$ to extend the empirical $T_e(\tau)$ model constructed at greater depths from limb-darkening observations in the continuum. The cited investigations by the Kiel and Utrecht groups typify this stage. Second, there is the stage characterized by the recognition that $T_{\mathrm{ex}} \neq T_e$—where T_{ex} is defined by $S_L = B_{\lambda_0}(T_{\mathrm{ex}})$—but by the assumption that at a given point in the atmosphere, T_{ex} has the same value for several spectral lines of a given atom, possibly even for lines from several atoms. The methodology based on this assumption has been mainly aimed at intercomparison of line profiles (cf. Section 9-IIA2). In the third stage, one recognizes that T_{ex} must in general differ from one line to another. We may call upon the quantitative theory developed for Hα, and the semi-quantitative theory for the other Balmer lines, as a guide to the most feasible checks on the theory.

The most direct empirical argument against the form $S_L = B_{\lambda_0}(T_e)$, and in favor of the form resulting from our non-LTE theoretical approach, results from a comparison of the signs of $dT_{ex}/d\tau_{\alpha r}$ and $dT_e/d\tau_{\alpha r}$. Böhm-Vitense and de Jager established the empirical relation $T_{ex}(\tau_0)$ for each line by applying, respectively, Eqs. (9-7) and (9-9). A shift along the log τ_0 abscissa by applying the differential logarithm of absorption coefficient, Δ log $\lambda_{2k}f_{2k}$, combines the results on a common log $\tau_{\alpha r}$ scale. Figure 9-2 shows these results for $\mu = 1$. There is an uncertainty in origin for the abscissa corresponding to that in kinetic temperature, of amount log $T_k^{1/2}$; we have used $T_k = 1 \times 10^4$. We have represented the uncertainty in choice between Eq. (9-7) and (9-9) by plotting the results as a line parallel to the log $\tau_{\alpha r}$ axis rather than individual points. We have also added de Jager's values for H8, and for H10, H11, H12, H15. de Jager's analysis does not treat H10 to H15 by Eq. (9-8); so we use Eq. (9-4) and indicate the uncertainty in effective origin by an arrow. So long as the single expontial term in Eq. (9-9) provides a reasonable representation of the data, the addition of more exponential terms, such as in Eq. (9-12), will give a result lying on the line segment linking these two extremes from Eqs. (9-7) and (9-9). Thus the

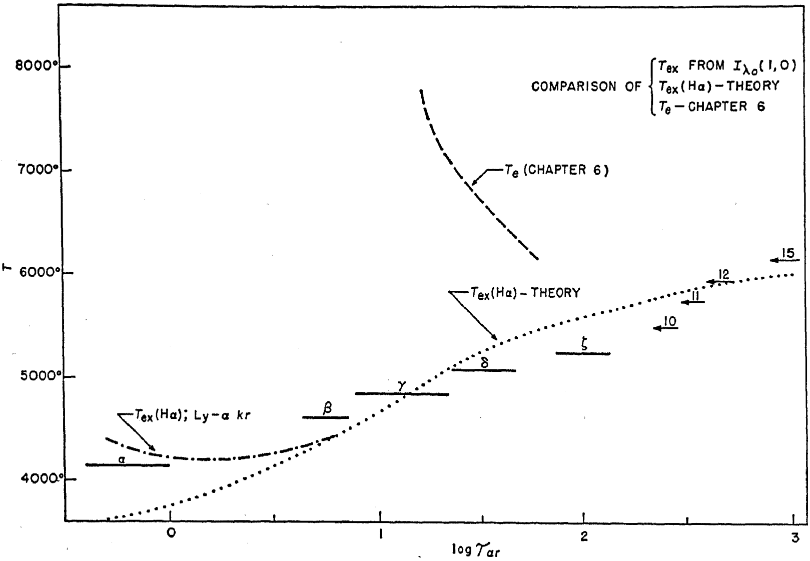

Fig. 9-2. Comparison of T_{ex}[Hα] theoretical with empirical T_{ex} for early Balmer lines.

sign of the slope of $dT_{\mathrm{ex}}/d\tau_{\alpha r}$ is well fixed in Fig. 9-5, even though the precise value of the slope at any point is not. It remains to determine $dT_e/d\tau_{\alpha r}$ at corresponding points.

The essence of the Böhm-Vitense and de Jager arguments lies in the a priori identification of T_{ex} with T_e, thus $T_{\mathrm{ex}}(\tau_{\alpha r})$is assumed to join continuously to $T_e(\tau_C)$. In consequence, they regard the monotonic outward decrease of T_{ex} as reflecting a continued outward decrease of T_e, and the slopes of T_{ex} and T_e agree by assumption. By analysis of eclipse observations of the later Balmer lines, Böhm-Vitense (1956) offers arguments for the validity of the adopted junction point for the two curves, $T_{\mathrm{ex}}(\tau_{\alpha r})$ and $T_e(\tau_C)$. We have attempted to show (Athay and Thomas, 1958a) that such joining of the two curves requires an underestimate by two orders of magnitude in Balmer opacity of the chromosphere, as measured by the results of our own analyses of these later Balmer lines (Thomas, 1949, 1950; Matsushima, 1952; Athay and Thomas, 1955). We treat these late Balmer lines in Section 9-IIC. Here, we need only draw upon our analysis of the continuum in Chapter 6, which provides values of T_e and $\tau_{\alpha r}$ at the same chromospheric heights. The dashed curve in Fig. 9-2 represents these results from Chapter 6. There is no question but that $dT_{\mathrm{ex}}/d\tau_{\alpha r}$ and $dT_e/d\tau_{\alpha r}$ have opposite signs in the region of formation of the centers of Hα-Hγ, and that $T_{\mathrm{ex}} \neq T_e$. Some measure of uncertainty lies in the values of $\tau_{\alpha r}$ above 1000 km because of the abrupt rise in T_e and the resulting uncertainty on the question of detailed balance in the Lyman lines. However, the results in Section 9-IIA1ci suggest only a change by a factor of 2 in b_2 resulting from this effect, at $\tau_{\alpha r} \sim 1$.

The dotted curve in Fig. 9-2 represents the results of our prediction of $T_{\mathrm{ex}}(\mathrm{H}\alpha)$ from Eq. (9-11). The dot-dash increase near $\tau_{\alpha r} \sim 1$ represents a rough measure of the effect of departure from detailed balance in Ly-α, as discussed in Section 9-IIA1ci. We emphasize that the only parameters entering the dotted curve are the observed intensities of Balmer and Paschen continua. The estimate of the dot-dashed curve rests on the observed underprediction of $I_{\lambda_0}(1,0)$ for Hα (Section 9-IIA1ci), and the value of $\tau_0(\mathrm{Ly}\text{-}\alpha)$ required to raise the prediction. To the extent that we might assume a common T_{ex} for all Balmer lines at a given point in the atmosphere, predicted and observed T_{ex} lie in remarkably good agreement. Thus, we might say that the empirical data substantiate through the second stage of empirical analysis our theory for the source function for the Balmer lines. Finally, we recognize that the uncertainty in the value of b_k through uncertainty in the values of $\mathfrak{F}_{k1}$ and $\mathcal{R}$ prohibit an extension to the third stage of analysis and an inquiry into the function $T_{\text{ex}}(k)$. From the definition of T_{ex}, we see that

$$T_{\text{ex}} = T_e[1 + 0.456(10^{-4}T_e)(\lambda/\lambda_{\text{H}\alpha}) \ln b_2/b_k]^{-1} \qquad (9\text{-}25)$$

We may attempt to set an upper limit on T_{ex} by assuming $b_k \geq 1$ and taking its lower limit in Eq. (9-25). The results in Chapter 6 give the values for these upper limits shown in Table 9-1.

If we could assume these upper limits to be a measure of the actual variation $T_{\text{ex}}(k)$, we would expect T_{ex} to increase toward later members of the Balmer series. However, if we use $T_{\text{ex}}(\tau_0)$ derived from $I_{\lambda_0}(\mu,0)$ to obtain T_{ex} from several lines at the same $\tau_{\alpha r}$, thus evaluate $T_{\text{ex}}(k)$ empirically, we apparently find indications of a decrease in T_{ex} toward later series members. A definitive investigation of $T_{\text{ex}}(k)$ must await further theoretical work, and a more detailed analysis of relative center-limb observations in the lines based on a more correct form than that of Eqs. (9-5) or (9-8). We are hardly justified in embarking here on the latter before carrying out the former.

2. Comment on the Use of Limb-Darkening Observations of the Line Profile to Infer $S_L(\tau_{\alpha r})$ and/or $\tau(\Delta\lambda)$. Once it has been established that over some part of the line profile S_L is independent of $\Delta\lambda$, that part of the observed line profile may be combined with a known $S_L(\tau_0)$ to specify $\tau(\Delta\lambda)$. Conversely, an observed line profile may be combined with a known function $\tau(\Delta\lambda)$ to specify $S_L(\tau_0)$. If one starts with no a priori knowledge either of $S_L(\tau_0)$ or

Table 9-1

h	500 km	1100 km	1300 km
$10^{-4}T_e$	0.615	0.74	0.90
$\tau_{\alpha r}$	60	20	5–10
b_2	3.0	12	38
$T_{\text{ex}} >$:			
Hα	4700	4050	3600
Hβ	5000	4600	4300
Hγ	5100	4750	4500
Hδ	5150	4850	4650

of $\tau(\Delta\lambda)$, wishing to perform a wholly empirical analysis, further assumption must be introduced.

If one assumes that he is analyzing a spherically symmetric atmosphere containing no macroscopic velocity fields, he may try to replace an a priori knowledge of $S_L(\tau_0)$ by an empirical function derived from limb-darkening observations. We have

$$I_\lambda(\mu,0) = \int_0^\infty [S_L(\tau_0) + r_\lambda S_C(r_0\tau_0)](d\tau_\lambda/\mu)e^{-(1+r_\lambda)(\tau_\lambda/\mu)} \qquad (9\text{-}26)$$

Consider points on the profile of a strong line for which $S_L \gg r_\lambda S_C$. If it is possible to define corresponding points, $\Delta\lambda_1$ and $\Delta\lambda_2$, on profiles obtained at different μ such that for all τ_0, $\tau_{\lambda_1}/\mu_1 = \tau_{\lambda_2}/\mu_2$, then we should observe $I_{\lambda_1}(\mu_1,0) = I_{\lambda_2}(\mu_2,0)$. Set

$$\tau_{\lambda_i}/\mu = N_{2r}(\tau_0)\,\frac{\pi\epsilon^2}{m_e c} f_{2k}\lambda_0 \left[\frac{M_a}{2\pi k T_e}\right]^{1/2} \frac{x_i}{\mu_i} \exp\left[-\left(\frac{\Delta\lambda_i}{\Delta\lambda_D}\right)^2\right] \qquad (9\text{-}27)$$

Thus x_i represents the ratio of actual to Doppler absorption coefficient at $\Delta\lambda_i$. M_a and m_e are, respectively, the mass of atom and electron. If we consider two such points of equal intensity, $I_{\lambda_i}(\mu_i,0)$, we obtain from Eq. (9-27) an expression for $\Delta\lambda_D$, viz.,

$$\Delta\lambda_D = \left\{\frac{(\Delta\lambda_2)^2 - (\Delta\lambda_1)^2}{\ln \mu_1/\mu_2 + \ln x_2/x_1}\right\}^{1/2} \qquad (9\text{-}28)$$

If we consider the Doppler core of a line, Eq. (9-28) with $x_i = 1$ gives us an estimate of $\Delta\lambda_D$. If by mistake we go outside the Doppler core, $x_2/x_1 > 1$ and the neglect of this term will give an overestimate of $\Delta\lambda_D$.

In Fig. 9-3, we have plotted de Jager's limb-darkening observations for Hα, Hβ, and Hγ, for $\Delta\lambda = 0, 0.2, 0.4, 0.6$ A. Applying Eq. (9-28) with $x_i = 1$, by starting with $I_{\lambda_1}(1,0)$ and seeking the same intensity at the next larger $\Delta\lambda$, we obtain the values for $\Delta\lambda_D$ given in Table 9-2.

If we take these results literally, thus accepting as valid the assumptions underlying them, we obtain both internal contradiction among the results for Hα − Hγ, and disagreement with the results from Chapter 6 and from Section 9-IIA1. The computed $\Delta\lambda_D$ suggest $T_k \sim 6000°$ in the effective region of origin of the central core of Hα at the center of the disk, and $T_k \sim 1.5 \times 10^4$ for the corresponding parts of Hβ and Hγ. Moreover, $\Delta\lambda_D$ increases downward, from all lines.

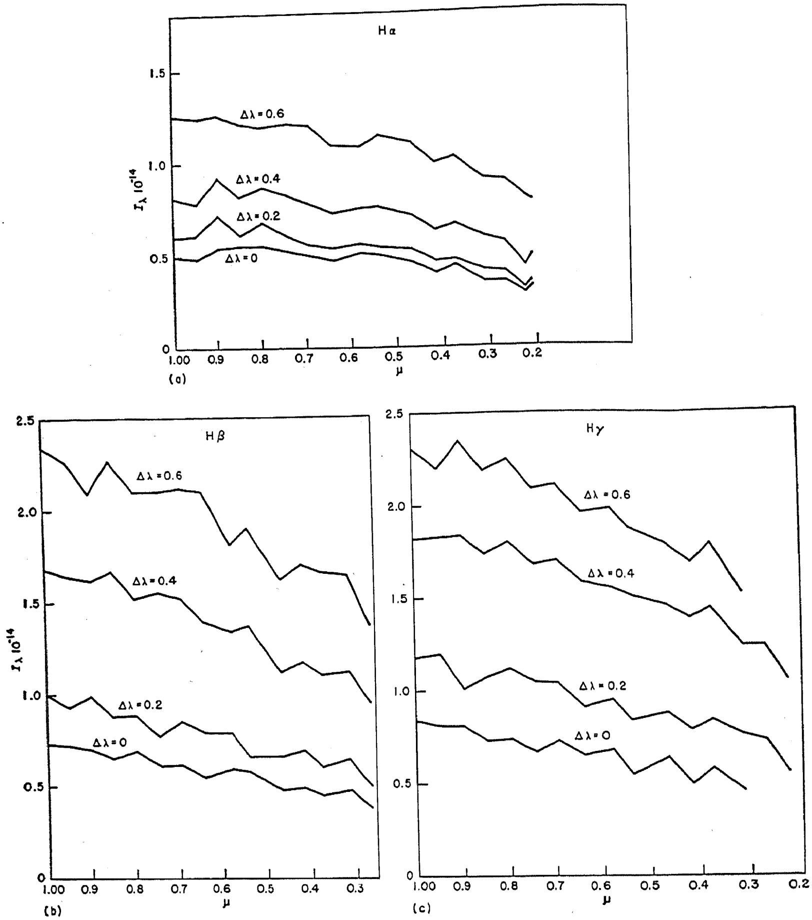

Fig. 9-3. De Jager's limb-darkening observations.

Table 9-2

	$\Delta\lambda_1 = 0$ $\Delta\lambda_2 = 0.2$	$\Delta\lambda_1 = 0.2$ $\Delta\lambda_2 = 0.4$	$\Delta\lambda_1 = 0.4$ $\Delta\lambda_2 = 0.6$	Thermal value
Hα	0.22	0.38	0.42	$0.281\ (10^{-4}T_k)^{1/2}$
Hβ	0.25	0.31	0.50	$0.208\ (10^{-4}T_k)^{1/2}$
Hγ	0.22	0.31	0.52	$0.186\ (10^{-4}T_k)^{1/2}$

We have already remarked on the cause of the discrepancy for Hα—the likelihood, based on a comparison of theoretical prediction and the results from Chapter 6, that the line is formed in a region of rapidly changing Ly-α opacity and strongly influenced by inhomogeneities toward the limb. Thus none of the assumptions underlying the derived $\Delta\lambda_D$, save those of a frequency-independent S_L for $\Delta\lambda \lesssim 0.4$, and small $r_\lambda S_C$, are trustworthy.

For Hβ and Hγ, it cannot be immediately excluded that the observational scatter combines with departure from spherical symmetry to suggest $T_k \sim 1.5 \times 10^4$ rather than the value $T_k \lesssim 1 \times 10^4$ obtained from the analysis of an assumed spherically symmetric atmosphere in Chapter 6. It is not possible, however, to accept an increase in $\Delta\lambda_D$ downward. There is no question, on the basis of the analysis of Chapter 6, but that T_k—even a mean value averaged over an inhomogeneous atmosphere—decreases downward in the region $20 \gtrsim \tau_{\alpha r} \gtrsim 7$. We also saw that no significant macroscopic motions are required to explain the observed emission gradient. We note, however, that in the interval $\Delta\lambda \sim 0.4$ to 0.6 we are certainly leaving the Doppler core, thus require non-trivial values of x_i, and a decrease in the derived values of $\Delta\lambda_D$ in this interval. To analyse the data in this region, we require not only values of x_i but a reconsideration of the frequency dependence of S_L. Thus, we must defer a detailed consideration of these results until such time as a consideration of the Balmer lines in the combined Doppler and Stark cores has been completed. (On this point see note 9-1 in Appendix II.)

This method of inter-comparison of profiles of a given line at differing μ is the only approach to analysis of the line profile having theoretical justification. In our earlier analysis (Athay and Thomas, 1955), we presented an approach based on the assumption of a common T_{ex}, and attempted to show the assumption led to a contradiction. Goldberg (1958), Goldberg, Mohler, and Mueller (1958), and Unno (1959a, 1959b) have applied this method of an assumed common T_{ex} to two lines having a common lower level (Ca$^+$, H, and K), or to several lines from a multiplet, without investigating its validity. We wish to emphasize that the method *should not* be applied without investigating the question of a common T_{ex}. We comment in Section 9-III on the procedure as applied to Ca$^+$ H and K.

In this earlier analysis of ours, we again restricted our attention to an assumed Doppler core. Then the procedure was: (1) choose the center of one line as reference, and determine the number of Doppler half-widths required to reduce the absorption coefficient from its value at the center of each earlier line to that at the center of the reference line; (2) arbitrarily choose T_k, thus fixing $\Delta\lambda_D$. These two steps determine a point on each of the earlier lines, from which we obtain T_{ex} by $I_\lambda(1,0) = B_{\lambda_0}(T_{ex})$. Plot the T_{ex} so-determined versus the assumed T_k. For each Balmer line there will be a graph consisting of several lines, one corresponding to each of the earlier lines. If there is indeed a common T_{ex}, the several lines on the graph should intersect at T_{ex} corresponding to the center of the reference line. We reproduce in Fig. 9-4 our results for Hγ, Hδ, H8, H10.

Essentially, these results reconfirm the results reached earlier in this chapter. There is a scatter in intersection of the lines on a given graph, thus suggesting the assumption of a common T_{ex} to be

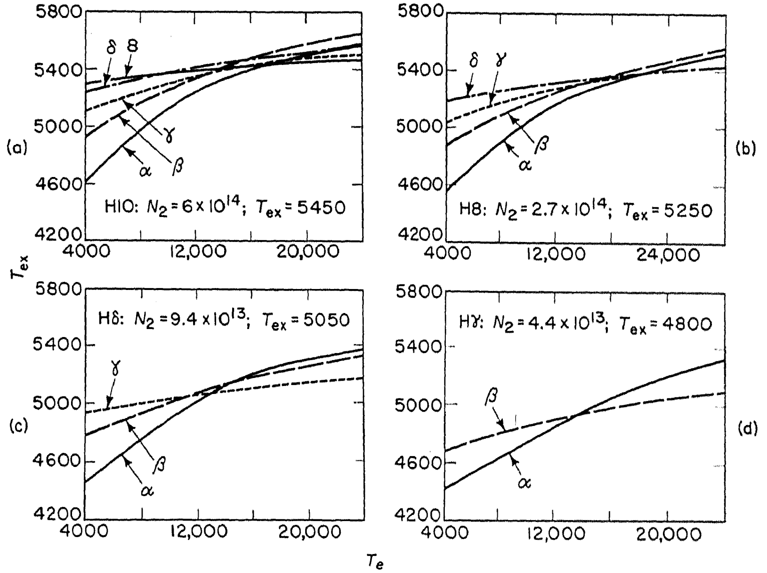

Fig. 9-4. A test of the assumption $T_{ex} = T_e$ from Balmer line profiles at the center of the disk: (a) center of H10 as reference, $T_{ex} = 5450$ and $\tau = 1$ for $N_2 = 6 \times 10^{14}$; (b) center of H8 as reference; (c) center of Hδ as reference; (d) center of Hγ as reference. [From *Astrophys. J.* 127, 102 (1958).]

invalid, but the data are not adequate to really substantiate this conclusion. The values of T_{kin} near the intersection region are essentially the same as those found for Hβ and Hγ by the method discussed first in this section, lying between 1×10^4 and 2×10^4. Our conclusions, and the suggested direction of further work, are the same as already mentioned, viz.: (1) more detailed consideration of the dependence $T_{\text{ex}}(k)$, for which we require further cross sections; (2) a consideration of S_L—and of course a_{2k}—in the Doppler-Stark core; and (3) more detailed observational material, particularly of the high-resolution variety.

B. Limb Observations of the Early Balmer Lines

Equation (9-2) gives the emergent intensity to be expected from a strip of the solar atmosphere, viewed tangentially, of vanishingly small height. Any actual observation covers a non-zero height range, owing either to the exposure time for the case of eclipse observations or to the effect of seeing for out-of-eclipse observations. Thus the observed emission represents a height integration, and is given by

$$E_\lambda(h) = \int_0^\infty \int_0^{\tau_\lambda(h)} S_\lambda(\tau_\lambda', h')\mathcal{S}(h')e^{-\tau_\lambda'}\, d\tau_\lambda'\, dh' \qquad (9\text{-}29)$$

where $\mathcal{S}(h')$ is the "seeing" function. In the case of slitless eclipse observations, we replace $\mathcal{S}(h')$ by an integral over h' ranging from h to ∞. For slit observations at an eclipse, we have an effective upper limit to the integration over h', fixed by a combination of slit width and seeing. For extra-eclipse observation, there exists the seeing problem at both upper and lower limits on h'. Thus, it is extremely difficult to specify with any certainty the atmospheric region to which the observations apply. The exception lies in the case mentioned at the beginning of the chapter, eclipse observations covering the whole chromosphere above the moon's limb and having sufficient height resolution to permit accurate differencing. Such data do not presently exist; we hope to obtain them at the 19?? solar eclipse.

We illustrate the problem of interpretation by considering the oversimplified case of a constant source function, a seeing function that can be represented as giving a uniform integration over a height range h_1, and an optical thickness varying exponentially with height. Under these assumptions, Eq. (9-29) integrates to give

$$E_\lambda = S_\lambda \gamma^{-1}[\gamma h_1 - E_1(z_\lambda) + E_1(C_\lambda)] \qquad (9\text{-}30)$$

where

$$\tau_\lambda = \tau_0 \varphi_\lambda e^{-\gamma h} = C_\lambda e^{-\gamma h}; \qquad z_\lambda = \tau_\lambda(h_1) \qquad (9\text{-}31)$$

We compute φ_λ by assuming only Doppler plus natural broadening to occur, the relations

$$\varphi_\lambda = H_0 + aH_1; \qquad a = \Delta\lambda_N/\Delta_{\lambda D} \qquad (9\text{-}32)$$

and Harris' tables (1948) to evaluate H_0 and H_1 from $\Delta\lambda/\Delta\lambda_D$. We compute the profile, using the constants for Hα: $\Delta\lambda_N = 6.46 \times 10^{-4}$ and $\Delta\lambda_D = 0.281(10^{-4}T_e)^{1/2}$. In Fig. 9-5(a), we plot the computed profiles of E_λ, normalized to unity at the line center, as functions of $\Delta\lambda/\Delta\lambda_D$ for several values of γh_1 and τ_0 as parameters. Figure 9-5(b) shows a typical profile observed at such a height that the double-peak characteristic of lower heights does not appear. Figure 9-5(c) shows the profiles of Fig. 9-5(a) in terms of $\Delta\lambda$, $\Delta\lambda_D$ having been chosen such as to make the normalized value of E_λ agree with the value 0.4 for the observed profile in Fig. 9-5(b) at $\Delta\lambda = 0.9$. It is clear that an interpretation of the observed profile in terms of one of the several alternatives permits a wide range in τ_0, even if the parameter γh_1 is well-fixed. Usually, however, we require also a value for γh_1 to be determined from the data. Thus, rather than determining an atmospheric model from such observations, we can usually only ask whether the observations are in general accord with a model determined otherwise. This point has been stressed by Zirker (1956), in connection with attempts to match eclipse profiles observed by Redman (cf. Section 9-III).

The profiles actually observed are incompatible with the assumption of a constant source function throughout the region of line formation. Figure 9-6 reproduces typical observations (after correction for scattered light) of extra-eclipse line profiles (E. v. P.

Fig. 9-5. (a) Computed profiles for constant scale height γ^{-1} for optical thickness; seeing function $\equiv$ integration over height range h_1. (b) Observed profile for Hα at sufficiently great height that double peak is absent. (Courtesy E. v. P. Smith, Sacremento Peak Observatory.) (c) Profiles of part (a) matching E_λ at $\Delta\lambda = 0.9$ A.

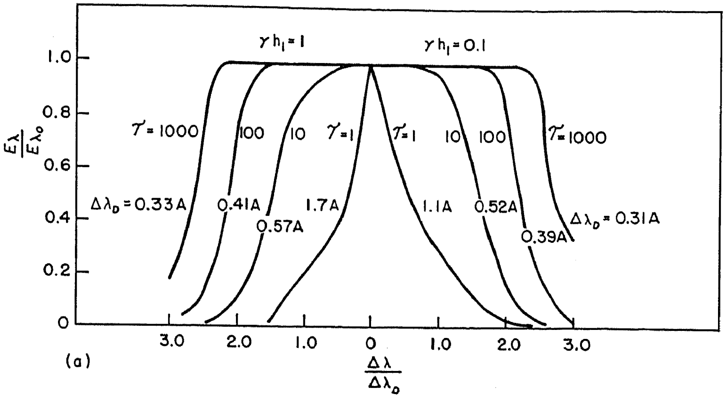
$\gamma h_1 = 1$
$\gamma h_1 = 0.1$
$\tau = 1000$
100
10
$\tau = 1$
$\tau = 1$
10
100
$\tau = 1000$
$\Delta\lambda_D = 0.33$A
0.41A
0.57A
1.7A
1.1A
0.52A
0.39A
$\Delta\lambda_D = 0.31$A
$\frac{E_\lambda}{E_{\lambda_0}}$
1.0
0.8
0.6
0.4
0.2
0
3.0
2.0
1.0
0
1.0
2.0
3.0
$\frac{\Delta\lambda}{\Delta\lambda_D}$

(a)

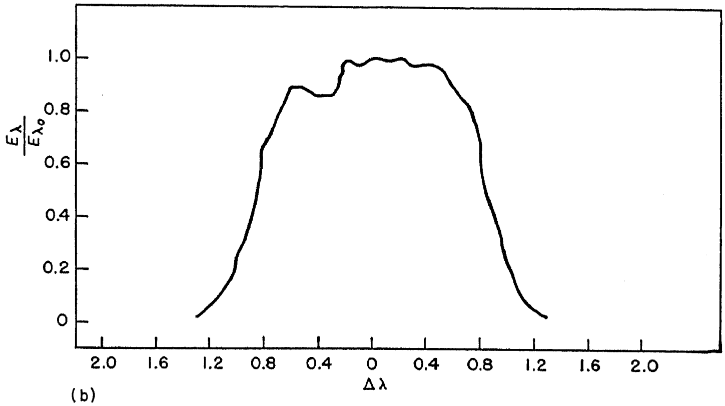
$\frac{E_\lambda}{E_{\lambda_0}}$
1.0
0.8
0.6
0.4
0.2
0
2.0
1.6
1.2
0.8
0.4
0
0.4
0.8
1.2
1.6
2.0
$\Delta\lambda$

(b)

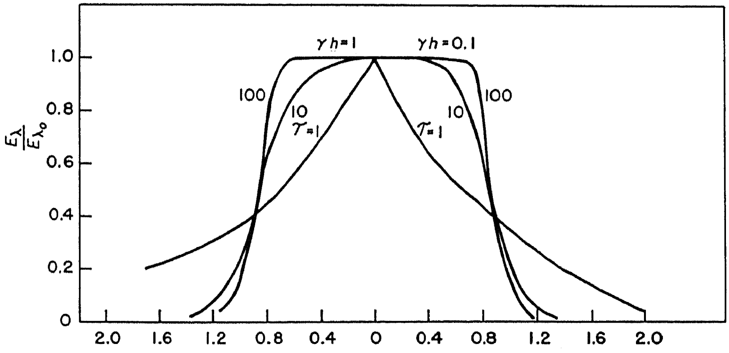
$\gamma h = 1$
$\gamma h = 0.1$
100
10
$\tau = 1$
10
$\tau = 1$
100
$\frac{E_\lambda}{E_{\lambda_0}}$
1.0
0.8
0.6
0.4
0.2
0
2.0
1.6
1.2
0.8
0.4
0
0.4
0.8
1.2
1.6
2.0
$\Delta\lambda$

(c)

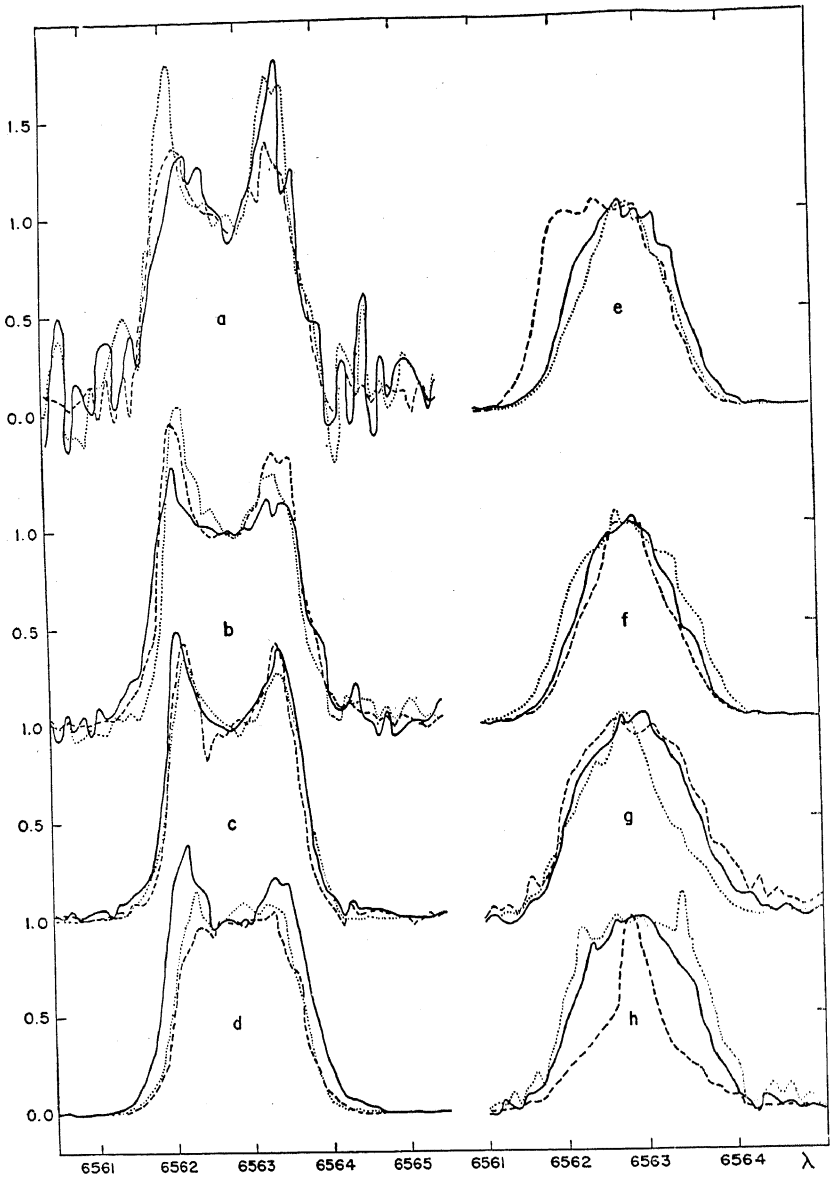

Fig. 9-6. Chromospheric profiles at increasing relative heights: (a) arbitrarily set at 0 km; (b) 1900 km; (c) 3600 km; (d) 5000 km; (e) 6400 km; (f) 9500 km; (g) 10,200 km; (h) 12,500 km. Narrow profile in *h* is that of a prominence. [From E. v. P. Smith, *Astrophys. J.* **126**, 529 (1957).]

Smith, 1957). Other examples are found in the work of Keenan (1932), de Jager (1952), Krat and Krat (1955), Clube (1958), and Kanonovich (1958); in the investigations of spicules in the high chromosphere, Michard (1959) and Athay (1958); and in eclipse observations, Redman (1942) and Redman and Suemoto (1954) together with Redman's largely unpublished 1952 eclipse data. These results, save de Jager's and Clube's, agree in the general trend exhibited by Fig. 9-6, viz.: double-peaked profiles in the low chromosphere, with the peaks decreasing in relative amplitude at greater heights, finally reaching the single peak. De Jager and Clube concluded that these double peaks, observed in uncorrected data, represented the effects of scattered light. The other investigations, however, agree in their reality, even after proper correction for scattered light. Thus, we must conclude that the source function varies over the region of line formation. Whether this variation has its source in the general outward decrease predicted in our theoretical results, or whether it arises from an inhomogeneous atmosphere, cannot be decided on an a priori basis. We require a detailed analysis of the

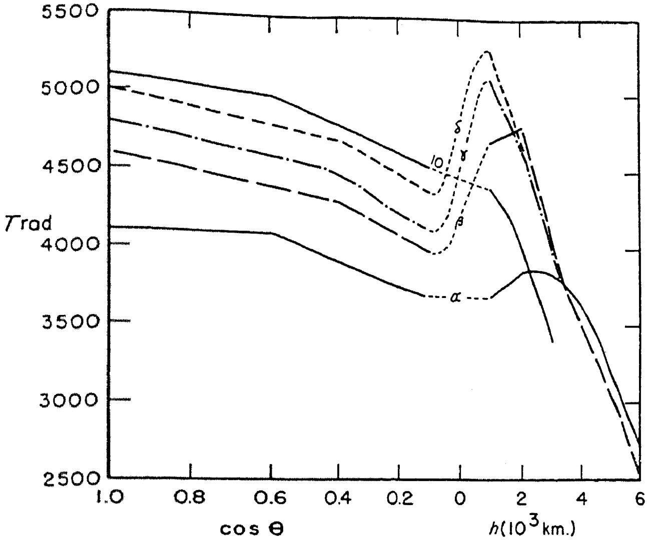

Fig. 9-7. $T_{\rm rad}$ determined from central intensities across the disk and in the chromosphere. [From *Astrophys. J.* **127**, 98 (1958).]

prediction on the basis of each alternative, and a detailed comparison with observations having good height resolution.

At the time of this writing, we believe that the combined uncertainties of region of origin for the observed line profiles, relative S_L for $H\alpha - H\delta$, and structure of the chromosphere for $h \gtrsim 1500$ km argue against presenting here what could only be an uncertain analysis of these data. We only caution against any analysis based on the assumption of a constant source function, and note that the methodology of a more correct analysis lies explicit in our development thus far. The first point of analysis must lie in a resolution of the factors producing the double peaks in the low chromosphere; the balance of outward decrease of S_L in the regions locally opaque in the Lyman lines against the effect of decreased Lyman opacity. Superficially, as noted in Chapter 4, the double-peaked appearance in the low chromosphere is exactly what we would expect on the basis of our theory for an atmosphere locally opaque in the Lyman lines. The rise to the "peak" would correspond to the inward increase of S_L; and the presence of the peak, to increasing transparency of the atmosphere; thus τ_λ(tangential) ~ 1 at the peak. In consequence, we should be able to combine these results with theoretical prediction to map out $\tau_{\alpha,\text{tang}}(h, \Delta\lambda)$. The directness of this approach must be modified by the influence of Lyman opacity, thus an investigation in terms of a source-function of the form of Eq. (9-15) with a more careful quantitative investigation of the relative importance of scattering and Lyman terms than we presented in Section 9-IIA1a. Also, the relative behavior and properties of the spicule and interspicular components with respect to S_L and $\tau(\Delta\lambda)$ must be included. Work is in progress on these points, as well as on the problem of better-defined observational material, within the NBS-HAO-SacPeak group.

Reference should be made to the attempts at analysis of such extra-eclipse profiles by Kononovich ($H\alpha - H\delta$, 1958) and Clube ($H\alpha$, 1958). We do not discuss these analyses in detail here because each makes assumptions which, on the basis of the theory developed in Chapter 4, vitiates the analysis. Clube assumes a constant source function throughout the region of line formation. Kononovich considers a source function compounded of two terms; one, representing coherently scattered photospheric radiation, thus with a position-dependence given by $\exp(-\tau_r \sec \theta)$; the other, frequency-independent, represented by a term which is effectively assumed constant in depth under the method of analysis used. There is also the same problem of a proper treatment of the seeing correction, mentioned above, and emphasized in Zirker's analysis. It can be shown that these effects lead to an underestimate of the Balmer opacity, which is the direction of their results relative to ours in Chapter 6 and in our earlier work on the later Balmer lines. The difference is about two orders of magnitude for n_2 near 500 km, so it is not insignificant.

Finally, as one piece of empirical evidence on this question of the effect of Lyman opacity on source function in the Balmer lines, we may summarize a result from our earlier analysis of these lines. The 1952 eclipse data provide values of $E = \int E_\lambda \, d\lambda$ for Hα − Hδ and H10 (cf. Appendix) determined from slitless observations. We estimate $\int I_\lambda \, d\lambda$ by computing $E \, d \ln E/dh$ from these data, assuming these two quantities to be equal. Then, we use extra-eclipse observations of the profiles of Hα − Hδ (Athay and Smith, 1956) to estimate the ratio $I_{\lambda_0} \left(\int I_\lambda \;\; d\lambda \right)^{-1}$ for these lines. These ratios are 0.55, 0.92, 1.26, and 1.67 for Hα − Hδ, showing no strong change with height. Combining these data, we obtain an estimate of I_{λ_0} for each of these lines at several heights above the limb. All the numerical factors entering are only roughly determined, and systematic effects are not at all unlikely. Nonetheless, the results show marked limb brightening for Hβ − Hδ, marginal limb brightening for Hα, and only a monotonic limb darkening for H10.

We reproduce the results of our original discussion in Fig. 9-7, where we plot $T_{\rm rad}$ ($\equiv T_{\rm ex}$ in the discussion of Section 9-IIA1) for both disk and limb observations.

In our original discussion, we arbitrarily reduced all eclipse intensities by a factor 2 for the reason discussed in Chapter 6. If we remove the factor 2 correction, all values of $T_{\rm rad}$ above the limb increase, by about 500° near the maximum and somewhat less at greater heights. Thus, there is support for our conclusion reached in the disk study of Hα that near $\tau_{\alpha r} \sim$ 1–3 we have entered the region where departure from detailed balance in the Lyman lines induces a rise in S_L(Balmer). Since $\tau_{\alpha t \rm ang}/\tau_{\alpha r} \sim 50$, the induced limb-brightening should begin to disappear about at Hδ; its observed presence at Hδ but complete absence at H10 lies in rough agreement with the above value of $\tau_{\alpha r}$ where we noted its effect. In this earlier work, we conjectured that the change in Lyman opacity might underlie the observed limb brightening, but we had not the supporting evidence of the discussion in Section 9-IIA1. At that time, we did not have the theoretical prediction of $I_{\lambda_0}(1,0)$ for Hα with which to compare the observations. Thus, we might rephrase our conclusion to state that these results on the disk analysis of Hα now support our earlier-obtained conclusions on limb brightening for Hβ − Hδ.

We have ignored the influence of the spicule structure, which in Section 9-IIA1 we invoked to explain the limb darkening in Hα. So long as the optical thickness of these spicules lies between about 1 and 10 in $\tau(\mathrm{H}\alpha)$, we do not change the qualitative nature of our results. Also, we note that our scanning slit embraces an area on the limb which must include both spicule and interspicular regions, based on the spicule statistics discussed earlier in Chapter 3.

We again emphasize that we regard this discussion of the early Balmer lines as most incomplete, but we do believe that we have outlined the methodology required to extend both the theoretical structure for the analysis, and the analysis proper of more complete data.

C. Eclipse Observations of the "Later" Balmer Lines: H10–H30

Since we expect moderate or small self-absorption in the later Balmer lines, we use Eq. (9-1), which gives for the total emission per unit solid angle in the line H_k observed with a slitless system:

$$E_{k2}(h) = \frac{A_{k2}h\nu_{k2}}{4\pi} \int_{-\infty}^{+\infty} j_\nu \, d\nu \int_h^\infty dx \int_{-\infty}^{+\infty} n_k e^{-\tau_\nu} \, dy \qquad (9\text{-}33)$$

Introducing the modified Boltzmann-Saha Eq. (4-3), we rewrite Eq. (9-33) as

$$E_{k2}(h) = C_1 A_{k2} k^2 h\nu_{k2}$$
$$\times \int_{-\infty}^{+\infty} j_\nu \, d\nu \int_h^\infty dx \int n_e n_p T_e^{-3/2} b_k e^{\chi_k} e^{-\tau_\nu} \, dy \qquad (9\text{-}34)$$

We also write the corresponding expression for the emission per unit frequency at the head of the Balmer free-bound continuum as

$$E_{3640}\,d\nu = (Kh/8)\int_h^\infty dx \int_{-\infty}^{+\infty} n_e n_p T_e^{-3/2} e^{-\tau_\nu}\,dy \qquad (9\text{-}35)$$

We have already discussed the inherent ambiguity in solution resulting from the restricted nature of the data, thus the necessity of limiting the range of possible solution by other considerations. We proceed, then, to establish such limits.

Although we have in earlier chapters laid much foundation for the belief that the chromosphere is actually in a non-LTE state, much of the early substance for this conclusion came from a consideration of these later Balmer lines. Thus, in the following development, we attempt to avoid prejudging the state of the chromosphere but to develop an independent check on the conclusions reached in preceding chapters. Such an approach is particularly important in view of the critical discussion of the validity of our approach to the analysis of these later Balmer lines, and the conclusions drawn from these treatments (cf. van de Hulst, 1953, for a good summary on this point; de Jager's more recent summary, 1959, does not consider the problem). We particularly wish to consider the various analyses of these later Balmer lines in the light of the more explicit theoretical understanding we now profess to have. Such an approach is of interest not simply as a matter of history, but to stress the conceptual evolution of thinking on the problem with the hope of possible wider application to the general stellar atmospheres.

1. Character of the Solutions of Equation (9-34) That Are Compatible with Various Empirical Data. First, we ask whether the data are compatible with a solution that neglects both self-absorption and departures from local thermodynamic equilibrium. If we neglect both these effects, then b_k and τ_ν drop out of Eq. (9-34), and τ_ν from Eq. (9-35), leaving the right sides of the two equations to differ only by the factor $\exp(X_k)$ and a numerical constant. From the data in Chapter 2, $d \ln E_{k2}/dh \equiv \beta_k$ appears to be constant with height for $k \gtrsim 13$. For $10 < k < 13$, β_k decreases with decreasing height for $h < 1000$ km, but appears to be constant for $h \gtrsim 1000$ km. For the free-bound data, $\beta_\infty \sim$ constant appears satisfactory above about 500 km. In Fig. 9-8(b) we plot β_k versus k for the Balmer lines observed at four eclipses. We note that β_k approaches β_∞ asymptotically, but differs significantly and systematically from it for $k \lesssim 25$. Either we must attribute

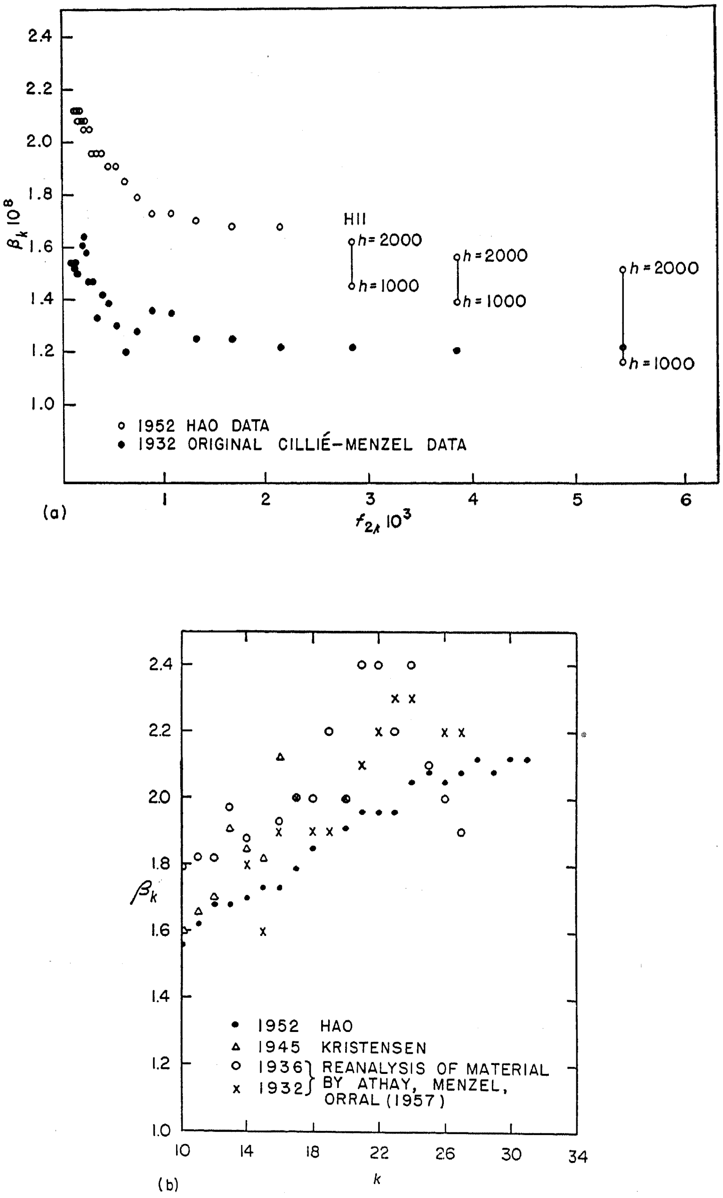

Fig. 9-8. Logarithmic emission gradient $-\beta_k$ for the Balmer lines H10 to H30.

this behavior of the β_k to the term $\exp(X_k)$, or we must conclude that at least one of the quantities b_k and $\exp(-\tau_\nu)$ cannot be neglected.

If the effect arises from $\exp(X_k)$, we must have

$$\beta_\infty - \beta_k = -X_k(d \ln T_e/dh) \tag{9-36}$$

This alternative is unsatisfactory for two reasons.† First, we note that a plot of β_k versus k^{-2} should be linear under this alternative. Figure 9-9 illustrates the departure from this expectation. Second, considering the 1952 data, we note that the numerical value of $\Delta\beta$ ranges from $\sim + 0.5 \times 10^{-8}$ at H12 to $\sim + 0.1 \times 10^{-8}$ cm^{-1} at

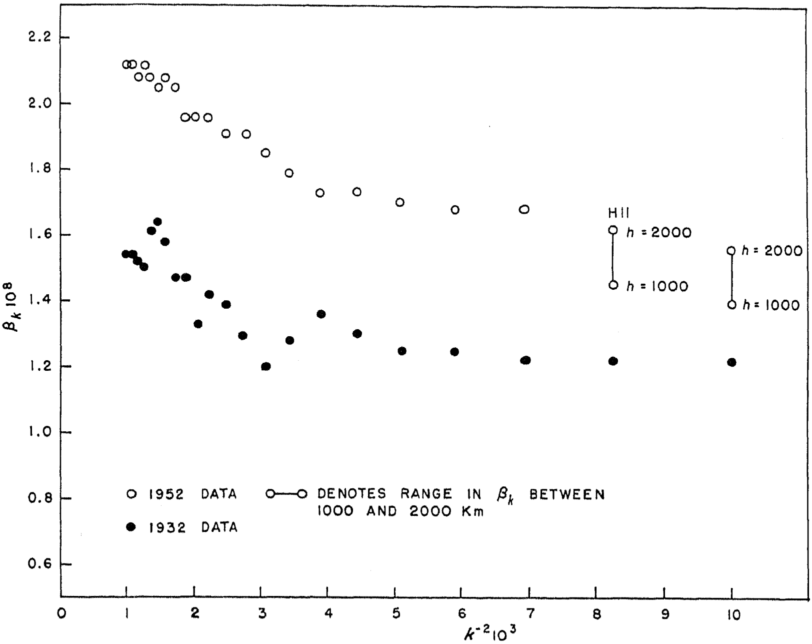

Fig. 9-9. Logarithmic emission gradient—β_k for the Balmer lines H10 to H30.

---

† For such numerical considerations as this, we restrict our attention to the 1952 data. Our arguments were originally developed on the basis of the 1932 data (Thomas, 1950a, 1950b), and were criticized as reflecting overanalysis of the data, so we planned the more extensive 1952 program to remedy this possible defect.

H30. Thus, were the differential values of β_k to originate from X_k, T_e must *decrease outward* over the whole height range up to about 2500 km, and at such a rate that T_e halves in less than 1000 km. (Since, even for $T_e = 5000°$, $X_k < 0.3$ for $k > 10$.) Such a result is incompatible with any other information on the chromosphere.

Thus we conclude that it is not permitted to neglect both b_k and exp $(-\tau_\nu)$ in analyzing the later Balmer lines. This conclusion rests on what we may call the first characteristic of the departure of the emission in the Balmer lines from that expected from a thin atmosphere in LTE, viz., a lesser height gradient for line emission than for free-bound emission in the Balmer continuum.

If it could be assumed that only one of the factors b_k or exp $(-\tau_\nu)$ were significant, the analysis could be simplified very considerably. We now show that the data require the presence of both factors in the analysis.

Consider the effect of self-absorption. The first attempt at empirical analysis of departures from LTE in the chromosphere, by Cillié and Menzel (1937), rests upon the assumption of negligible self-absorption in all the later Balmer lines. Although their analysis is inadequate in several respects, particularly their discussion of the expected theoretical values for the b_k as indicated in Chapter 4, its results have been often quoted and have been adopted by van de Hulst (1953) as proving that self-absorption effects are indeed absent. Thus a summary of the analysis and its deficiencies is useful for orientation.

Setting $\tau_\nu = 0$ in Eqs. (9-34) and (9-35), we see that the observed constant slope, β_k, for log E_{k2} versus height implies that the occupation number, n_k, varies with height as exp $(-\beta_k)$; so we obtain:

$$E_{k2}(h) = C_2 A_{k2} k^2 h\nu \beta_k^{-3/2} \{n_e n_p T_e^{-3/2} b_k e^{X_k}\}_h \tag{9-37}$$

$$E_{3640}(h) = C_3 \beta_\infty^{-3/2} \{n_e n_p T_e^{-3/2}\}_h \tag{9-38}$$

The observed quantities, E_{k2} and E_{3640}, together with the known numerical values of C_2 and C_3, permit an empirical determination of the quantity b_k exp (X_k) from Eqs. (9-37) and (9-38). From the 1932 eclipse data, Cillié and Menzel obtained values of this quantity, which lay between 0.1 and 1.0 for b_3 to b_{20}, and were about 1 for

$k > 20$. Since $\exp(X_k) > 1$, these results imply $b_k < 1$. The direction of this empirical inequality on b_k agreed with the theoretical calculations carried out by Cillié and Menzel, under the assumption of a pure capture spectrum. The numerical agreement was, however, not good, computed b_k always lying below the observed, with the difference about a factor of 2 at H20.

The actual numerical disagreement is worse than found by Cillié and Menzel; for they used in their analysis the total emission observed at λ3640. One must, however, separate out the actual Balmer free-bound emission from the electron-scattered photospheric continuum, thus raise Cillié and Menzel's empirical b_k by the ratio of total emission to Balmer emission. On the basis of an assumed 35,000° value for T_e, we estimated a correction of about a factor of 2 for these 1932 results (Thomas, 1948, 1950; cf. also Zanstra, 1950). Our 1952 data would suggest a correction factor 1.3 to 1.6 rather than 2.

The systematic nature of this discrepancy between the empirical and theoretical results of Cillié and Menzel attests to a real difficulty in the analysis. Cillié and Menzel recognized this situation, and placed the blame on the theoretical values, conjecturing that some unknown source of excitation from the lower to the higher levels must be the explanation but not investigating the problem further. From our discussion in Chapter 4, we recognize that the additional excitation mechanism is radiation from the chromosphere itself in the Balmer and Lyman lines, and collisions, particularly from adjacent levels. Indeed, the existence of an appreciable self-absorption effect is equivalent to stating the importance of excitation by chromospheric radiation in the Balmer lines. On the other hand, van de Hulst—differing vigorously with our then-current attempts to draw attention to the importance of the self-absorption effects—considered only the ratio b_{10}/b_{25}, and found good agreement between the Cillié-Menzel empirical values and their theoretical ones. He ignored the discrepancy in absolute values, also the numerical error in the use of the total observed emission at λ3640. In discussing non-LTE effects, one should pay careful heed to this analysis by Cillié and Menzel, particularly to its subsequent use and misuse, as an object lesson. Both absolute and relative effects must be considered. It is simply unfortunate that in Cillié and Menzel's treatment an inadequate discussion of observational data was combined with an incomplete theoretical analysis to give a superficial agreement.

Thus, on the basis of the Cillié-Menzel 1932 *data*, we recognize a second characteristic of the departure of the observed emission from that expected from the thin, LTE atmosphere, viz., *too low* an emission in the line relative to that in the free-bound continuum. Quite apart from inconsistencies in the Cillié-Menzel non-equilibrium calculations, we reject their *interpretation* of the effect as coming from non-equilibrium effects *alone*. For, we must either assume that self-absorption is so small as to be negligible or it is not. If it is negligible, then the results of Chapter 4 demonstrate $T_{\text{ex}} < T_e$, $b_k > 1$ for either kind of source function, collisional or photoelectric (cf. Figs. 4-3 and 4.5). For the photoelectric source function, we can obtain $T_{\text{ex}} > T_e$, $b_k < 1$ but only in regions of significant opacity (Fig. 4-5). Thus, granted the validity of the results of Chapter 4, we must admit the presence of self-absorption effects whenever the empirical b_k obtained from Eqs. (9-37) and (9-38), uncorrected for self-absorption, are less than unity. Such a conclusion accords with what we would expect from the values of n_2 determined in Chapter 6.

The 1952 data show the same results. We present these data in Table 9-3, uncorrected for the ratio β_∞/β_k. The value of this ratio is given in the first column of the table; the value of X_k, for two different values of T_e, in the last two columns. If it be assumed that there is no self-absorption, hence that the β effect comes wholly from non-equilibrium effects plus the effect of a height gradient in T_e, then the value given in the first column must be subtracted from the tabular entries. In such a case we would obtain, for these empirical values neglecting self-absorption, $b_k < 1$ up to somewhere just below 2400 km. For $k \gtrsim 20$ to 25 the scatter in the data becomes too large for any very definite conclusion.

Thus, we conclude that self-absorption effects must be included when analyzing the latter Balmer lines, at least for lines up to H20 to H25. The effect can be presented in an alternative way by contrasting the observed Balmer decrement with that expected theoretically from a thin, LTE atmosphere. Figure 9-10(a) illustrates the effect in the 1932 data; Fig. 9-10(b), in the 1952 data. For comparison, we plot also the theoretical decrement with $X_k = 0$, corresponding to infinite T_e, which is thus a lower limit on the dec-

Table 9-3. log $[(b_k e^{X_k}\mathrm{ABS})\,(\beta_\infty/\beta_k)^{3/2}]$

k	3/2 log β_∞/β_k	h, km										X_k	
		530	750	960	1180	1390	1610	1820	2040	2260	2400	5000°	35,000°
10	0.30–0.22	−0.27	−0.27	−0.16	+0.01	+0.13	+0.16	+0.18	+0.16	+0.17	+0.36	0.31	0.04
11	0.27–0.20	−0.25	−0.22	−0.12	+0.03	+0.13	+0.18	+0.17	+0.01	+0.13	+0.35	0.26	0.04
12	0.17	−0.14	−0.13	−0.05	+0.10	+0.14	+0.20	+0.14	+0.14	+0.26	+0.38	0.22	0.03
13	0.17	−0.05	−0.06	+0.03	+0.16	+0.19	+0.21	+0.11	+0.37	+0.19	+0.46	0.19	0.03
14	0.16	−0.02	+0.02	+0.06	+0.17	+0.23	+0.25	+0.09	+0.34	+0.26	+0.47	0.16	0.02
15	0.15	−0.06	−0.08	−0.02	+0.11	+0.16	+0.21	+0.03	+0.21	+0.08	+0.42	0.14	0.02
16	0.15	−0.06	−0.02	+0.04	+0.16	+0.17	+0.21	+0.03	+0.20	+0.06	—	0.12	—
17	1.13	−0.08	−0.03	+0.03	+0.16	+0.18	+0.18	+0.04	+0.24	+0.12	+0.40	0.11	0.02
18	0.11	−0.07	−0.06	−0.02	+0.17	+0.15	+0.10	0.00	+0.13	+0.10	+0.23	0.10	0.01
19	0.09	−0.02	0.00	+0.02	+0.18	+0.25	+0.27	−0.01	+0.19	+0.08	+0.34	0.09	0.01
20	0.09	−0.02	+0.01	+0.01	+0.17	+0.22	+0.05	+0.26	+0.10	+0.05	+0.30	0.08	0.01
21	0.07	+0.06	+0.08	−0.06	+0.22	+0.20	+0.14	+0.19	+0.07	+0.07	+0.31	—	—
22	0.07	−0.03	−0.01	−0.09	+0.18	+0.15	+0.09	+0.23	+0.09	+0.03	+0.26	—	—
23	0.07	−0.01	0.00	−0.12	+0.11	+0.16	+0.09	+0.13	+0.07	+0.07	+0.33	—	—
24	0.04	0.00	−0.01	−0.10	+0.10	+0.10	+0.01	+0.09	+0.03	+0.05	+0.26	—	—
25	0.03	+0.08	+0.03	−0.14	+0.12	+0.12	0.00	−0.01	+0.02	+0.03	+0.09	0.05	—
26	0.04	−0.03	−0.02	−0.16	+0.09	+0.13	+0.02	0.00	+0.04	−0.04	+0.26	—	—
27	0.03	−0.01	−0.05	−0.07	+0.02	+0.12	−0.03	−0.04	+0.02	+0.04	+0.15	—	—
28	0.02	+0.11	+0.02	−0.11	+0.01	+0.11	−0.01	0.00	−0.02	+0.01	+0.33	—	—
29	0.03	−0.06	−0.04	−0.23	0.00	−0.01	−0.05	−0.14	−0.02	+0.06	+0.21	—	—
30	0.02	+0.32	+0.21	−0.04	+0.11	+0.14	+0.09	−0.02	+0.09	+0.15	+0.33	0.03	—
31	0.02	−0.14	−0.07	−0.25	−0.08	+0.07	−0.11	−0.14	−0.06	—	+0.24	—	—

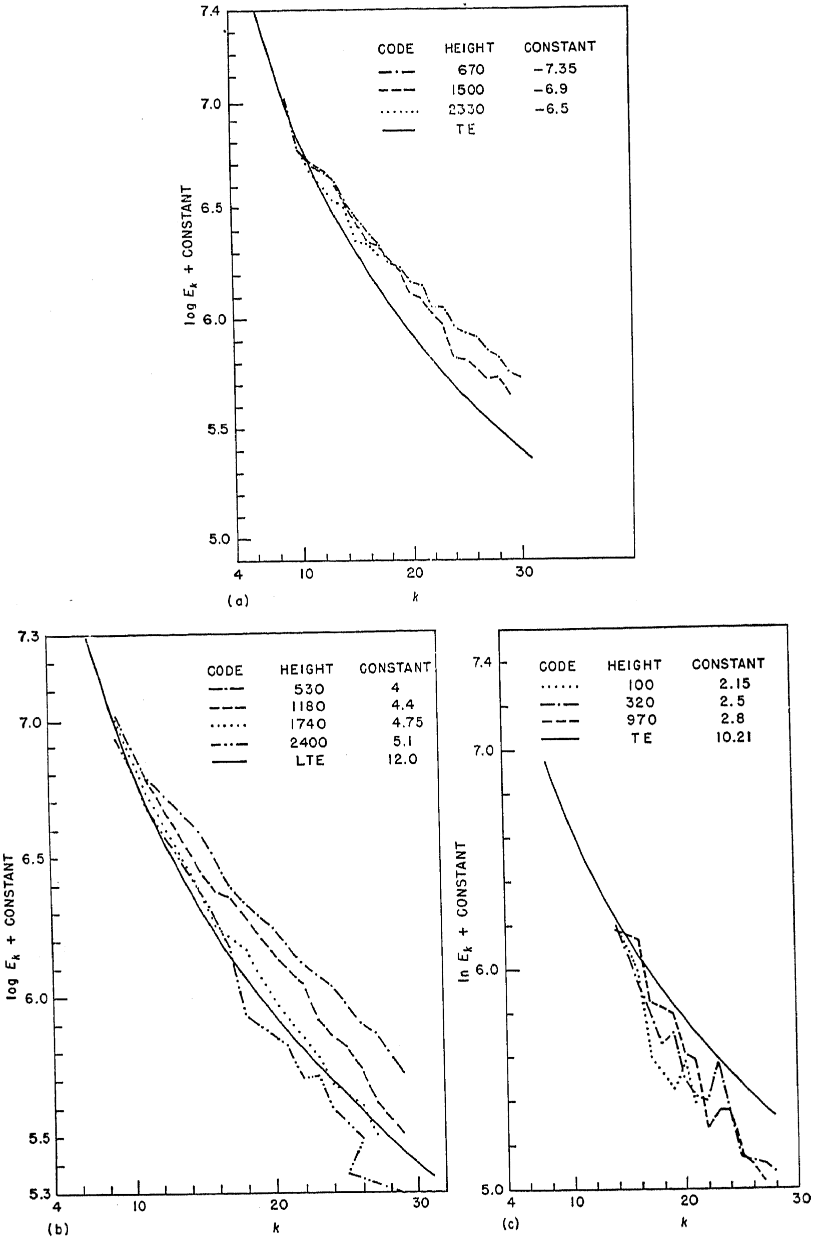

Fig. 9-10. (a) Cillié-Menzel 1932 Balmer decrement; (b) HAO 1952 Balmer decrement; (c) HAO 1952 Paschen decrement.

rement. The flatter decrement in the observed data at the lower heights, and the gradual increase with height of this observed decrement, illustrate graphically the self-absorption effect. It was this difference between observed and theoretical decrements which formed the basis for our first assessment of the importance of self-absorption (Thomas, 1949, 1950).

The 1952 data show, at greater heights, an effect not present in the 1932 data. The empirical decrement becomes steeper than the lower limit on the theoretical one. Comparing the size of this differential steepness with $\Delta_k \ln X_k$ in Table 9-3, we recognize that we can draw no completely certain inference that the empirical decrement exceeds the theoretical one for a thin atmosphere in LTE, unless we can be certain $T_e \gtrsim 1 \times 10^4$. However, taking into account the developments in previous chapters, we would indeed accept T_e to be sufficiently great that the term exp (X_k) cannot be responsible for the steepening of the decrement at these greater heights. Then, we would conclude that the data require $b_k > b_k + \Delta$, at least for $h \gtrsim 2000$ km.

There is one final bit of evidence coming from the uncertain observations of the Paschen lines described in Chapter 2. In Fig. 9-10(c), we compare theoretical lower limit with observed decrement for these lines. From our results in Chapter 6, we expect self-absorption effects to be negligible for the Paschen lines, and indeed we observe in Fig. 9-10(c) that the empirical decrement is the larger by a considerable amount, even at the lower heights. Thus, these data—recognizing their unreliability but noting the systematic nature of the effect—argue for the conclusion $b_k > b_k + \Delta$, even at these lower heights. Thus, again, the empirical evidence for a self-absorption effect in the Balmer lines, and for departures from LTE is strong.

Summarizing these comments on the character of the solution for the occupation numbers—or the b_k—permitted by the empirical data, we see that we can neither assume LTE nor neglect self-absorption. Therefore the data are insufficiently complete for a wholly empirical solution, and we must add auxiliary conditions. We have also seen that the over-all empirical behavior of the data—height gradient of the line emission relative to that of the continuum, magnitude of the line emission relative to that of the continuum—accords with expectation from the non-LTE analysis of Chapter 4 and the results on self-absorption to be expected from the population of the Balmer ground state found in Chapter 6. Therefore, we consider it legitimate to draw upon the results of Chapter 4, and of Chapter 6, to provide auxiliary conditions required for the analysis. In essence, we ask for an approximation scheme to be used in the analysis of the data, which emphasizes at each stage the physical ideas developed in Chapter 4. Given such a scheme, we can summarize the work that has been done thus far on these later Balmer lines in terms of the degree to which it may represent physical reality.

2. An Approximation Scheme for the Analysis of the Later Balmer Lines, Based upon the Background of Chapter 4 and Its Subsequent Application. We actually have two problems to solve: how to treat the difference in behavior of n_2 and n_k; and how to take into account effects of non-spherical symmetry in chromospheric structure. Since the data are inadequate for a unique, wholly empirical solution to even the first of these problems, a scheme of successive approximation will refer both to differential variation of n_2 and n_k and to the introduction of atmospheric inhomogeneity. We ask first into an approximation scheme in a spherically symmetric atmosphere, then the influence of departures from such symmetry. Empirical analyses of the later Balmer lines have thus far considered only the spherically symmetric atmosphere.

a. Approximation Scheme in a Spherically Symmetric Atmosphere. There are two extremes from which to start an approximation scheme: either by considering the depth dependence of some kind of mean source function for the Balmer lines to be primary, and the variation from line to line to be secondary; or, the converse. In a wholly opaque atmosphere, one obtains as the first approximation under these two schemes, respectively, the depth dependence of a k-independent S_L, or the k dependence of a depth-independent S_L. From the analysis of Chapter 4, and its application to the early Balmer lines in Section 9-IIA, we conclude that the former extreme lies much closer to reality than does the latter. It would be useful to obtain independent confirmation of these conclusions from the later Balmer lines, but this does not appear feasible with the data presently available. We note that eclipse observations in these later Balmer lines refer to an atmosphere of finite opacity, with the opacity varying with k. Thus, the assumption of a k-independent S_L does not require that a k dependence in the observed emission imply a

depth variation of S_L; nor does the assumption of a depth-independent S_L require that a k dependence in the observed emission imply a k dependence in S_L. In consequence, we adopt the approximation scheme suggested by the theoretical development of Chapter 4, and its application in Section 9-IIA.

(*i*) *Zero-Order Approximation: No Variation of the Source Function through the Chromosphere.* Making reference to Eqs. (9-11) and (9-21) and Fig. 4-5, we see that this approximation corresponds to one of two atmospheric regions: either (1) $\tau_{\alpha r}$ is so large that $S_L(\mathrm{H}\alpha)$ is constant, also $b_k \exp(X_k)/b_3 \exp(X_3)$ is constant in height; or (2) the opacity is so small that there is no variation of the Balmer radiation field either in lines or continuum. Alternative (2) would make the analysis wholly determinate; for the self-absorption term would be negligible. Our arguments in section 1 show this alternative to be inapplicable to the chromosphere. Alternative (1) requires $\tau_{\alpha r} \gtrsim 10^3$ and $d \ln(n_k/n_3)/dh = 0 = \gamma_3 - \gamma_k$. The latter of these conditions would be satisfied by $b_k \propto q(h)p(k) \exp(-X_k)$, which is the *qualitative* form of variation established for b_2 in Chapter 4, and which would be the form for the other b_k if no terms were important in $\mathcal{F}_{U1}$ and $\mathcal{R}$ (Section A, this chapter) save F_{U1}, F_{U2} and if $E_1(-x) = x^{-1} \exp(-x)$ for all X_k, Y_k of interest. The difference in *quantitative* form lies in $q(h)$ generally being dependent upon k, and in the violation of the conditions just stated. Moreover, $b_k \exp(X_k)$ must approach 1 at the series limit. Thus, we would require $q(h)$ to be constant. But since we have from our analysis in Chapter 4 that $b_2 \propto X_2^{-1} \exp(-X_2)$, we cannot simultaneously preserve $S_L(\mathrm{H}\alpha)$ constant and $b_k \exp(X_k)/b_3 \exp(X_3)$ constant, with constant $q(h)$, unless T_e remains constant. Thus, we require an isothermal atmospheric region. Because we have both a constant Hα radiation field and constant T_e, n_2, all the n_k, and the Balmer continuum vary with height in the same way, depending only upon $n_e n_p$, and this variation is as $\exp(-\beta_\infty h)$.

This zero-order approximation permits a determinate solution by reducing the variation of all occupation numbers to the same function. Thus, we obtain $\gamma_k = \gamma_\infty$, n_2, and n_k.

(*ii*) *First-Order Approximation: Source Function May Vary through Atmosphere Only as a Result of Variation of b_2. $dS_L/dr \neq 0$, but $\Delta_k d \ln(b_k e^{X_k})/dr = 0$ for $k > 2$.* This first-order approximation differs from that discussed in connection with the early Balmer lines, where first-order referred to a permitted variation of S_L with radiation field but not with T_e. The second condition above would be satisfied by the same form for b_k discussed above, $q(h)p(k)\exp(-X_k)$; and for the reasons discussed, we require $q(h) =$ constant. However, because S_L may vary with b_2 we need not require the atmosphere to be isothermal. We have $\gamma_2 \neq \gamma_k = \gamma_\infty = \beta_\infty$. Thus, this first-order approximation requires $b_k \exp(X_k)$ to be independent of T_e and radiation field, for $k > 2$. Actually, since we apply the analysis only to the later Balmer lines, we need the restriction only for $k \gtrsim 12$. By applying the approximation to the later Balmer lines, we are in effect attributing the differential values of β_k to self-absorption. Note that the approximation does not prohibit variation in S_L, in $b_k \exp(X_k)$, nor in T_{ex}, from line to line; it requires only that the ratio of each of the first two of these quantities for any pair of levels, $k \gtrsim 12$, be depth-independent.

This first-order approximation permits a determinate solution by reducing the height gradient of the late Balmer occupation numbers to a single parameter, which is measured by the height gradient of the Balmer continuum. The resulting solution gives n_2, n_k, γ_2 and also S_L in addition to the value $\gamma_k = \gamma_\infty$.

(*iii*) *Second-Order Approximation: Source Function Variation through Atmosphere May Result from Variation of* b_k *as Well as of* b_2. $dS_L/dr \neq 0$; $\Delta_k d \ln(b_k \exp(X_k))/dr \neq 0$; $\gamma_2 \neq \gamma_k \neq \gamma_\infty$. This approximation corresponds to variation of Balmer radiation field and T_e through the atmosphere, together with a permitted differential dependence of $S_L(k)$ and b_k upon them. Analysis under such an approximation is indeterminate, from presently existing data. Exploration of its possibilities from a complete basis requires starting with an assumed chromospheric model, computing the variation of S_L and b_k, and comparing them with the observed emission. Such a complete application of this second-order approximation does not seem presently feasible, until better and more complete theoretical discussions of $S_L(k)$ and b_k have been performed and until the effects of inhomogeneities and their actual distribution have been more carefully explored.

Analyses of the later Balmer lines that have thus far been reported fall generally under the zero-order approximation in that generally a constant S_L has been assumed, but the remainder of the analysis generally does not maintain consistency with the requirements associated with constant S_L. Several analyses have come close to the first- and second-order schemes. All have treated an assumed spherically symmetric atmosphere. We summarize these analyses, according to the approximation scheme, after commenting on the effects of departure from spherical symmetry.

b. Effect on the Approximation Scheme of Departures from Spherical Symmetry. (*i*) *Zero Order.* The approximation corresponds to an isothermal atmospheric region analysed, and to either negligible self-absorption or to $\tau_{\alpha r} \gtrsim 10^3$ so that the radiation field in Hα is constant. The space variation of n_2, n_k, and Balmer continuum are the same, varying as $n_e n_p$. Thus, the differential variation of the β_k results from self-absorption effects. A choice between interpreting the value of β_∞ as a height gradient for $n_e n_p$, or as a height gradient for an effective volume along the line of sight where $n_e n_p$ is large enough to provide observable emission, is the same for Balmer emission and absorption.

(*ii*) *First Order.* The height variation of the integrated number of emitting atoms along the line of sight again has the same value as that for the Balmer continuum—the differential values of the β_k have been ascribed to self-absorption effects. Thus, the choice between gradient of n_k and of emitting volume is again the same as that for the Balmer continuum. However, since $\gamma_2 \neq \gamma_\infty$ is permitted under the approximation—the relation between them to be fixed by the analysis of the data—a differential effect of inhomogeneity may be permitted between n_2 and n_k.

The effects of two kinds of inhomogeneities must be distinguished, as in our discussion of the early Balmer lines in Section 9-IIA; those where no change in the condition of detailed balance in the Lyman lines occurs across the boundary of the inhomogeneity, and those where such a change occurs. In the former, n_2 has somewhat less sensitivity to variations in T_e than do n_k or the free-bound continuum—$T_e^{-1/2}$ versus $T_e^{-3/2}$, both varying as $n_e n_p$ [recalling that $b_2 \propto X_2^{-1} \exp(-X_2)$]. Thus the major variation in n_2, n_k, and Balmer free-bound emission will come from the change in the factor $n_e n_p$ associated with a change in ionization of hydrogen induced by the change in T_e. From the background of Chapters 4 and 6, we would estimate that this situation covers inhomogeneities where T_e does not exceed $2 - 3 \times 10^4$ °K. For $T_e \gtrsim 8000°$, the change in $n_e n_p$ with hydrogen ionization ceases to predominate over the $T_e^{-3/2}$ term.

Under such situations, variations in emitting properties are nearly, but not quite, reflected by variation in absorbing properties, with the difference being the factor T_e.

If across the border of an inhomogeneity we pass to a region where detailed balance in the Lyman lines fails, n_2 drops by the factor $(1 + \delta_{21}/F_{22})$ in addition to whatever the change arising from $n_e n_p T_e^{-1/2}$. Thus, the effect of this type inhomogeneity is relatively larger on n_2 than on n_k or on Balmer free-bound emission.

(*iii*) *Second Order.* The essential change over the first-order conditions lies in the possible variation of $b_k \exp(X_k)$ with T_e and radiation field. The limitations on an estimate of the direction and size of this effect are precisely those discussed in connection with the dependence of S_L on k for the early Balmer lines. As in that discussion, we can only conclude that a proper assessment of the effect must await more detailed knowledge of the cross sections and NRB linking adjoining upper levels.

(*iv*) *Rough Approximation for Assessing Effect of Departures from Spherical Symmetry.* We see from the foregoing that inhomogeneities are felt *roughly* similarly in variation of emission and absorption property. For $T_e \lesssim 8000°$ under chromospheric conditions, the large variation accompanies fluctuation in $n_e n_p$ and is the same for emission and absorption. For $8000° \lesssim T_e \lesssim 2$ to 3×10^4, variations in T_e assume more importance, the fluctuation in absorption properties being less by a factor T_e. For higher T_e, fluctuation in absorption property is greater, coming from fluctuation in effect of Lyman-line NRB on n_2.

We further recognize that the region covered well by observations of the later Balmer lines and the Balmer continuum extends $500 \text{ km} \lesssim h \lesssim 2500 \text{ km}$. From the analysis in preceding chapters, T_e increases from about 6000° at the lower limit of this range, to 2 to 6×10^4°K in at least parts of the atmosphere in the upper part of the range. Above 4000 to 5000 km, the Balmer emission lies concentrated in the spicules, which occupy at most a few per cent of the surface.

Thus, in a rough approximation, we might try to represent the combined effects of density gradient and growth of inhomogeneity by dividing β_∞ into two parts: ${}_1\beta_\infty$, representing $d \ln(n_e n_p T_e^{-3/2})/dh$ in the treatment of an assumed spherically-symmetric atmosphere; and ${}_2\beta_\infty$, representing an upward decrease in the "effective" volume emitting the Balmer continuum along the line of sight. Corresponding to the first-order approximation in a spherically-symmetric atmosphere, we would treat $d\ln(n_k)/dh$ in the same way, with n_k replaced by these same β values. We would set $d\ln N_{2,\mathrm{rad}}/dh = -\gamma_2$ and $d\ln N_{2,\mathrm{tang}}/dh = -\gamma_2 - {}_2\beta_\infty$. N_2, with appropriate subscript, denotes integrated values of n_2. After summarizing the analyses performed under the assumption of spherical symmetry, we consider briefly this rough modification to obtain a rough estimate of the effect of departure from spherical symmetry.

3. Summary of Analyses of Later Balmer Lines Under the Assumption of a Spherically Symmetric Chromosphere. We rewrite Eq. (9-34) as

$$E_{k2}(h) = C_1 A_{k2} k^2 h\nu_{k2} (n_e n_p T_e^{-3/2} b_k e^{X_k})_{h,y=0} \gamma_k^{-3/2} \text{ (ABS)} \qquad (9\text{-}39)$$

where

$$\text{(ABS)} = (2\pi R_\odot)^{-1/2} \gamma_k^{3/2} \int_{-\infty}^{\infty} j_\nu \, d\nu \int_h^\infty dx \int_{-\infty}^{\infty} \rho(x,y) e^{-\tau_\nu} \, dy$$

$$= F(\gamma_2, \gamma_k, n_2\alpha_{2k}) \qquad (9\text{-}40)$$

$$\rho(x,y) = (n_e n_p T_e^{-3/2} b_k e^{X_k})_{x,y} (n_e n_p T_e^{-3/2} b_k e^{X_k})^{-1}{}_{h,y=0} \qquad (9\text{-}41)$$

If n_k varies as $\exp(-\gamma_k h)$, the quantity (ABS) is the self-absorption correction, (ABS) ≤ 1, with equality holding for $\tau_\nu = 0$.

The first attempt to analyse the later Balmer lines, that by Cillié and Menzel (1937) already discussed in Section 9-IIC1, set (ABS) = 1, assumed n_k to vary as $\exp(-\gamma_\infty)$, and focused attention on $b_k \exp(X_k)$. We have already discussed our objections to this analysis. Here, we only remark that interpreted in terms of our approximation scheme, the Cillié-Menzel analysis rests on the basic assumption that zero- and first-order effects may be neglected relative to those of second order. Our initial analysis (Thomas, 1949, 1950) represented a first attempt at a self-consistent approximation scheme. Subsequently, other reanalyses of this 1932 data have appeared, and we have analyzed the newer material obtained at 1952. We summarize these analyses according to the order of the approximation implied, and any further assumptions introduced.

a. Zero-Order Analyses. (*i*) *Thomas* (*1949*, *1950*). In this reanalysis of the Cillié-Menzel 1932 data, the following additional assumptions are introduced: n_k varies as $\exp(-\gamma_k h)$; the absorption coefficient is wholly Doppler; $b_k \exp(X_k)$ *decreases* monotonically to its value 1 at the series limit.

The zero-order condition gives $\gamma_2 = \gamma_k$ and $b_k \exp(X_k)$ is independent of position. With these conditions, Eq. (9-40) integrates to

$$(\mathrm{ABS}) = \sum_{m=0}^{\infty} (-1)^m (N_2 \alpha'_{2k})^m [m!(1+m)^{5/2}]^{-1} \tag{9-42}$$

where

$$N_2 = n_2(h)\gamma^{-1/2}(2\pi R_\odot)^{1/2} \tag{9-43}$$

is the number of second-quantum hydrogen atoms along the line of sight, and

$$\alpha'_{2k} = (\pi\epsilon^2/mc) f_{2k} \lambda_0 (m_{\mathrm{H}}/2\pi k T_e)^{1/2} \tag{9-44}$$

is the absorption coefficient at the line center.

The Balmer decrement, defined by

$$\Delta_j \ln E_{k2} = \ln E_{k2} - \ln E_{k+j,2} \tag{9-45}$$

and evaluated from Eq. (9-39), depends only upon $N_2(h)$ and the constant factors $b_k \exp(X_k)$. The assumption that $b_k \exp(X_k)$ decreases toward the series limit ensures that a computation of Balmer decrement from Eq. (9-45), based on using $b_k \exp(X_k) = 1$ will be a lower limit to the correct value. Thus, if we use such a computed value to compare with the observed value of the decrement and compute the required self-absorption, we will underestimate N_2.

A limited part of the 1932 data was analyzed by this procedure, each pair of lines giving one value of N_2. Table 9-4 shows the results. To compute N_2 from the value $N_2\alpha_{2,30}$ derived directly from the data, some value of T_e is required. The value $T_e = 35{,}000°$ was chosen; any other value simply changes N_2 by the square root of the T_e ratio.

Before commenting on these results, we summarize the extension of this work by Matsushima.

Table 9-4. Thomas Analysis: 1932 Data

Height, km	670		1500		2330		3170
$N_2\alpha'_{2,30}$	0.90		0.19		0.08		0.05
$10^{-16}N_2$	2.4		$0.5\underline{2}$		$0.2\underline{1}$		$0.1\underline{3}$
$10^8\gamma_2$		1.9		1.1		0.5	

(*ii*) *Matsushima* (*1955*). In the first part of his analysis of the Cillié-Menzel 1932 data, Matsushima followed the above procedure of inferring values of $N_2\alpha'_{2k}$ from pairs of lines. A slight difference was introduced in procedure, by the assumption that $b_k = 1$ and including the actual value of $\exp(X_k)$. Analysis of the 1932 data was carried out for $T_e = 6000°$ and for 35,000°. Reference should be made to Matsushima's Table 2 for the detailed results from 40 pairs of lines at between 1 and 4 heights each. The scatter for individual lines is large. The mean values are summarized in Table 9-5, rows 2 to 5. Also included, rows 6 and 7, are a set of results obtained by Matsushima from using a theoretical set of b_k, computed by us (Thomas, 1949) in an attempt to place an upper limit on b_k for $T_e = 35{,}000°$ and $n_e = 2 \times 10^{11}$. Matsushima used these values of b_k, which are

Table 9-5. Matsushima Analysis: 1932 Data

Height, km	670		1500		2330		3170
$10^{-16}N_2(6000°, b_k = 1)$	0.85		0.42		0.22		0.11
$10^8\gamma_2$		0.85		0.78		0.86	
$10^{-16}N_2(35{,}000°, b_k = 1)$	1.97		0.91		0.44		0.22
$10^8\gamma_2$		0.92		0.91		0.80	
$10^{-16}N_2(35{,}000°$, upper limit $b_k)$	2.22		1.09		0.54		0.28
$10^8\gamma_2$		0.86		0.65		0.78	
$10^{-16}N_2(35{,}000°$, b_k by iteration$)$	2.5		$0.7 < () < 1.4$		—		—
q	$\sim+4$		$\sim+1$		—		—

k	10	13	15	20	25	30
b_k	4.7	3.9	3.6	3.0	2.8	2.6

to correct the observed Balmer decrement before applying the above analysis to determine N_2.

Matsushima also tested the data for any significant correlation with k, after removing self-absorption, to see if any b_k effect could be detected empirically. Noting that the general form of the $b_k(k)$ dependence resembles

$$\log b_k = p + q/k \tag{9-46}$$

he attempted a differential correction scheme by defining

$$\varphi_k = [\log E_{k2} - C(h)]_0 - \log [A_{k2}(k^2 - 4)] - \log (\text{ABS})_0 \tag{9-47}$$

and fitting by least squares the expression resulting by applying Eq. (9-47) to Eq. (9-39), using Eq. (9-46), viz.,

$$\varphi_k = (\Delta C + p) + q/k + k^{-2}(X_1/2.3) + [\Delta \log(\mathrm{ABS})/\Delta(N_2\alpha_{2k})]\Delta(N_2\alpha_{2k}) \qquad (9\text{-}48)$$

$C(h)$ is that part of Eq. (9-39) independent of k. $(\mathrm{ABS})_0$ is some initial approximate value of (ABS). The solution is by iteration, until the differential corrections become of the order of their probable errors. Matsushima found the procedure reasonably convergent at $h = 670$ km. At 1500 km the behavior of the φ_k was such that a series of differential corrections fixed only a range for N_2. For greater heights, the results were unreliable. Lines 8 and 9 of Table 9-5 give the results.

Three comments may be made on our investigations of the 1932 data. First, within the framework of the assumptions characterizing the zero-order analysis and the added assumption on the form of the absorption coefficient, the mean N_2 values for a given height do not vary more than about a factor of 2 over the various kinds of solutions and values of T_e. The conversion from N_2(tang) to N_2(rad) is about a factor of 60, which leads to $\tau_{\alpha r} \sim 90$ at the lowest height, 670 km. It is of interest that this value lies reasonably close to the value $\tau_{\alpha r} \sim 40$ found at this height from the model based on the continuum in Chapter 6. The value found by Cillié and Menzel from their original analysis (1935) of their 1932 material, but using the early Balmer lines, was $\tau_{\alpha r} \sim 1$ at height 0 in the chromosphere. Thus, these re-analyses of the 1932 material suggested a change of some 2 orders of magnitude in the Balmer opacity of the chromosphere.

Second, the values of γ_2 show only small variation from one solution to another. All save the first entry in Table 9-4 lie well below the value of β_∞, by something near a factor of 2. The results in Table 9-4 represent an analysis of only a small part of the data, with the first two alternatives in Table 9-5 representing the more complete analysis. No well-defined height variation can be ascribed to γ_2 from these results. In our first discussion of the results in Table 9-4 (Thomas, 1950), we attempted to use the γ_2 values to infer dT_e/dh. The results of Matsushima's more detailed analysis showed these first results to lack sufficient accuracy for such an attempt. Our discussion here of the implications of the zero-order analysis shows that the attempt was also unjustified theoretically, from a consistency standpoint. Thus, its results should be rejected on two accounts.

Third, these two results—$\tau_{\alpha r} \sim 10^2$ at the lower height range of the analysis, and γ_2 very significantly different from β_∞—show that the data are not in accord with the assumptions underlying the zero-order approximation. Both the value of $\tau_{\alpha r}$ judged in relation to Fig. 4-5, and γ_2 relative to β_∞, imply that we must include the effect of variable S_L. Thus, while the results are interesting, we must proceed at least to the first-order approximation before we can trust them. Before doing so, we summarize other applications of this zero-order approximation to check these conclusions.

(*iii*) *Matsushima* (*1955*). The logic of this analysis of the High Altitude Observatory 1952 data follows that of the analysis of the 1932 data, except that no approach setting $b_k = 1$ was tried, and the relation of Eq. (9-46) was replaced by a linear relation

$$\log b_k = s + tk \tag{9-49}$$

Table 9-6 summarizes the results. The series member following the height is the "earliest" Balmer line used at that height. The results roughly fit the following relations:

$$\log N_2 = 16.37 + 0.5 \log (T_e/5040) - 0.58 \times 10^{-8}h \tag{9-50}$$

$$\log b_k - \log b_{k+\Delta} = 0.022\Delta \tag{9-51}$$

Thus, both in absolute value of N_2, hence $\tau_{\alpha r}$, and of γ_2 relative to β_∞, the 1952 results agree with the 1932 results. The absolute values of γ differ, however, in the two sets of data, as already indicated by the material in Fig. 9-8.

(*iv*) *Kawaguchi* (*1952*). In his reanalysis of the Cillié-Menzel 1932 data, Kawaguchi contends that our analysis in (i) through (iii) above rests upon the assumption that the Balmer lines arise from a capture spectrum, and that he is able to interpret the observations equally well by a combination of *coherent* scattering and cascade. In place of either Eq. (9-1) or (9-2) he adopts the form

$$I_\nu(h) = \int_0^{\tau_{\nu\max}(h)} J_\nu e^{-\tau_\nu}\, d\tau_\nu + (A_{k2}h\nu_0/4\pi) \int_0^{\tau_{\nu\max}(h)} (n_k j_\nu/n_2\alpha_\nu) e^{-\tau_\nu}\, d\tau_\nu \tag{9-52}$$

Table 9-6. Matsushima Analysis: 1952 Data

h	$N_2\alpha_{30} \pm \epsilon$	$t \pm \epsilon$	h	$N_2\alpha_{30} \pm \epsilon$	$t \pm \epsilon$
530(H15)	1.19 0.10	−0.021 0.015	1930(H9)	0.16 0.01	−0.027 0.007
750(H13)	0.83 0.47	+0.024 0.11	2040(H9)	0.12 0.01	−0.019 0.006
960(H12)	0.54 0.04	−0.028 0.010	2150(H9)	0.06 0.01	−0.008 0.004
1180(H11)	0.41 0.05	−0.023 0.014	2260(H9)	0.06 0.01	−0.006 0.006
1390(H11)	0.45 0.04	−0.029 0.011	2400(H9)	0.09 0.01	−0.014 0.006
1610(H10)	0.22 0.02	−0.023 0.009	3060(H9)	0.04 0.01	−0.013 0.007
1820(H9)	0.19 0.04	−0.023 0.018	3180(H9)	0.04 0.01	−0.032 0.018

where $J_\nu(h)$ is the mean intensity of ν-radiation at height h. He assumes J_ν and $n_k j_\nu / n_2 \alpha_\nu$ to be independent of position, and so removes them from the integral. Stimulated emissions are neglected in the definition of τ_ν. He introduces the assumption $\tau_{\nu\max} \propto \exp(-\gamma h)$ so that the expression for E_{k2} becomes

$$E_{k2}(h_0) = \int_{-\infty}^{\infty} d\nu \left[J_\nu + \frac{A_{k2} h\nu_0}{4\pi} \frac{n_k j_\nu}{n_2 \alpha_\nu} \right] \int_0^{\tau_{\nu\max}(h_0)} (1 - e^{-\tau_{\nu\max}}) \frac{d\tau_{\nu\max}}{\tau_{\nu\max}} \tag{9-53}$$

but then, introducing

$$\Delta(t_{\max}) = \left[\int_{-\infty}^{\infty} (1 - e^{-\tau_{\nu\max}})\, d\nu \right] \Big/ (1 - e^{-t_{\max}}) \tag{9-54}$$

he asserts Eq. (9-53) becomes

$$E_{k2} = \Delta[t_{\max}(h_0)] \left[J_\nu + \frac{A_{k2} h\nu_0}{4\pi} \frac{n_k j_\nu}{n_2 \alpha \nu} \right] \int_0^{\tau_{\max}(h_0)} (1 - e^{-t_{\max}}) \frac{dt_{\max}}{t_{\max}} \tag{9-55}$$

where $t_{\max}$ is $\tau_{\nu\max}$ at the line center. Assuming a form for the absorption coefficient—Kawaguchi assumes it to be Doppler—$\Delta(t_{\max})$ and the remaining integral in Eq. (9-55) may be evaluated as functions of $t_{\max}(h_0)$. Then, the data may be used to obtain $t_{\max}(h_0)$.

It is unfortunate that Kawaguchi's analysis does not do what he thinks it does. First, Eq. (9-52) is incorrect, since it counts the scattered emission twice, once in J_ν and once in $n_k A_{k2}$. (Simply consider the case of LTE and detailed balance.) Second, his treatment of J_ν—removing it from the integral sign in passing from (9-53) to (9-55)—makes it a treatment of non-coherent rather than coherent scattering. Thus, his treatment is simply that of a source function which is frequency-independent and constant through the atmosphere, exactly the case treated by us with which Kawaguchi takes issue. (If the development in Chapter 4 is recalled, our treatment is not at all based on the assumption of a capture spectrum.) Finally, we have been unable to understand how $\Delta(t_{\max})$ can be removed from the integral in passing from Eq. (9-53) to (9-55), and so would question the derived N_2 values. The interesting nature of Kawaguchi's result is his assertion that his results agree numerically with ours. Since the basic physical assumptions are identical, we should expect this result were it not for the questionable algebraic simplification introduced in the self-absorption calculation. Unfortunately, we are unable to obtain numerical consistency between Kawaguchi's tabulated results, and so can only leave the question open.

(*v*) *Böhm-Vitense* (*1955*). Reanalysis of the Cillié-Menzel 1932 data, for a constant source-function, Eq. (9-2) gives for the integrated emission in the line

$$I_{k2}(h) = S_{k2} \int_{-\infty}^{\infty} (1 - e^{-\tau_{\nu\max}})\, d\nu \qquad (9\text{-}56)$$

so that the total emission above a given height is

$$E_{k2}(h) = S_{k2} \int_{h}^{\infty} dx \int_{-\infty}^{\infty} (1 - e^{-\tau_{\nu\max}})\, d\nu \qquad (9\text{-}57)$$

Böhm-Vitense applied Eq. (9-56) to the analysis of the 1932 data, remarking that she uses this equation rather than (9-57) because preliminary investigation using (9-57) showed S_{k2} and γ_2 to be variable with height. We simply note that this remark implies an unwarranted belief in the generality of the results obtained, for the same assumptions underlie both (9-56) and (9-57). So long as S_{k2} is independent of k, Eq. (9-56) *appears* to depend upon only one parameter, $N_2(h)$, while (9-57) depends upon both $N_2(h)$ and γ_2. This apparent difference is of course illusory, having been reached only by integrating Eq. (9-2) over τ_ν by assuming $\gamma_2 = \gamma_k$, i.e., S_{k2} to be independent of position. Any departure of γ_2 from γ_k, derived from an analysis of Eq. (9-56) or (9-57), simply indicates the non-validity of both equations.

Böhm-Vitense applied van de Held's (1931) curve of growth computed from Eq. (9-56), which gives $I_{k2}/S_{k2}\Delta\nu_D$ as a function of $N_2\alpha_0\Delta\nu_D$, to analyze the data.† Van de Held's computations refer to an absorption coefficient compounded of Doppler and natural broadening, thus involve the damping coefficient as a parameter.

---

† It should be noted that the Cillié-Menzel data fall into two parts: λλ3200 to 5300, observed with an ultraviolet prism, and λλ3900 to 6800, with a plane grating. Böhm-Vitense arbitrarily corrects the ultraviolet data by a factor 2, leaving unchanged the grating material. The differencing process to form I_{k2} from E_{k2} involves differences of grating and ultraviolet data for the early Balmer lines, and it is to reduce scatter in these differences that the correction was made.

Böhm-Vitense makes no mention of her assumption on a value for this last parameter; but it appears from her work that she neglected it, and assumed pure Doppler broadening, which she assumes to be a compound of thermal broadening at 4200° and a factor two greater turbulent broadening, leading to an equivalent kinetic temperature of some 17,000°.

The results give $N_2(h)$ and $S_{k2}(h)$, the height variation of the latter being systematic and non-trivial, and that of the former lying below β_∞. These directly obtained results are not given in the paper, only those obtained after a further correction procedure. The correction consists of forcing agreement between the S_{k2} values obtained directly from the above-type analysis and those obtained in her earlier analysis of the early hydrogen lines (cf. Section 9-IIA). The resulting values of N_2 are as follows:

h, km[a]	255	1085	1915	2750	3585
log N_2	15.41	14.92	14.43	14.00	13.37

[a] In summarizing Böhm-Vitense's work, we use throughout the Cillié-Menzel height scale on which the original data are based, for simplicity of comparison with other analyses of these data. Böhm-Vitense points out that the Cillié-Menzel height scale has a zero point based on measures in the continuum at λ3100, while more contemporary work usually rests on measures in the visual region. Thus, she suggests that the Cillié-Menzel zero point lies higher than one based on the visual region, and arbitrarily adopts the interval between successive exposures, 830 km, as the correction.

The corresponding value of γ_2 is 1.3×10^{-8} cm^{-1}. Thus the N_2 values are about an order of magnitude smaller than those in (i) through (v) above.

Although the discrepancy in N_2 value between this and the analyses above based upon the zero-order approximation is hardly trivial, there is little point in discussing its possible origin in detail; for the results from each of these analyses show that the assumption of constant S_L is invalid. We note only that the Böhm-Vitense analysis attempts to strengthen the basis for the results by combining both early and late Balmer lines, whereas the preceding analyses dealt only with the later lines. Because Böhm-Vitense attempted to force her discussion of the early Balmer lines into the framework of $S_L = B_{\lambda_0}(T_e)$, it is hard to say, a priori, whether this combination of early and later lines gives greater or lesser reliability to the derived value of N_2. If it is allowed to compare 1952 and 1932 chromospheres, we can only note that her value for $\tau_{\alpha r}$ at 500 km is about a factor of 4 less than that in Chapter 6, while the other analyses give about 50 percent greater than that from the continuum model.

(*vi*) *Zirker (1956)*. This analysis by Zirker of the 1952 High Altitude Observatory data contains implicitly the assumption of constant S_L through the explicit assumption that $\gamma_2 = \gamma_k$, but he allows γ to depend upon height through the relation

$$10^8\gamma = 2.38 - 0.207h\ (10^3\ \text{km}) \tag{9-58}$$

The development of this height variation for γ proceeds as an extension of Zirker's analysis of the metallic spectrum of the chromosphere (cf. Section 9-III). In essence, it results from a trial-and-error approach, starting from the assumption that self-absorption is small by the time the intensity in a given line reaches the threshold sensitivity of the spectrograms. Analysis of the data under this condition on γ leads to the following values for the tangential optical depths at 500 km:

Line	H9	H12	H22	H31
$\tau_{0,\text{tang}}$(500 km)	25	10	1	0.5

These values give $1.2 \times 10^{16}(10^{-4}T_e)^{1/2}$ for N_2(tang) at 500 km, and applying Eq. (9-58) leads to $\tau_{\alpha r} \sim 50$, in very close agreement with the value in Chapter 6. The value of γ_2 is, however, somewhat greater than that in Chapter 6.

This model for the analysis demonstrates how wide is the range of assumption on the behavior of γ which gives roughly the same $\tau_{\alpha r}$ in the region 500 to 1000 km. As in the other analyses under this first-order approximation, the derived $\tau_{\alpha r}$ is such as to vitiate the possibility that S_L can indeed be constant. By contrast with the other first-order analyses, which give derived γ_2 appreciably less than $\gamma_k = \beta_\infty$, Zirker's approach has "built in" to it the condition that $\gamma_2 = \gamma_k$. We return later to comment on the $b_k \exp(X_k)$ this analysis would predict, in comparison with those from the first- and second-order analyses and from the other zero-order analyses. These values reflect this variation in result on $\gamma_2 - \gamma_k$. Here, we note only the utility of the auxiliary theoretical conditions on the kind of behavior to be expected for S_L for the Balmer lines, when assessing the consistency and reliability of the various empirical analyses.

b. First-Order Analysis. Only one analysis has been conducted under the first-order approximation (Athay and Thomas, 1955). We follow the algebraic approach of our original zero-order analysis, except that we permit $\gamma_2 \neq \gamma_k$, still holding $\gamma_k = \gamma_\infty = \beta_\infty$. Then Eq. (9-42) is replaced by

$$(\mathrm{ABS}) = \sum_{m=0}^{\infty} \left\{ (-N_2\alpha'_{2k})^m \, [2^m m!(1 + mr^{-1})(1 + m)^{1/2}]^{-1} \times \sum_{j=0}^{m/2} \frac{m!}{(2j)!\,(m - 2j)!} I_{r,2j} \right\} \tag{9-59}$$

where

$$I_{r,l} = 2(r/\pi)^{1/2} \int_0^\infty e^{-r^2t^2} \left[2/\sqrt{\pi} \int_0^t e^{-s^2}\, ds \right]^l dt \tag{9-60}$$

and

$$r = \gamma_k/\gamma_2 = \gamma_\infty/\gamma_2 \tag{9-61}$$

In our zero-order analysis, we worked with the Balmer decrement at a given height, ascribing the departure of the decrement from that of a thin atmosphere in LTE wholly to self-absorption effects. Thus we ignored the decrement in $b_k \exp(X_k)$ at a given height, in the first approximation, later making attempts to correct for it. In this first-order analysis, we attempt to exploit its primary characteristic, the allowed departure of γ_2 from γ_k but the constancy of γ_k for $k > 2$. That is, we work with the decrement in β_k, in the slope of $\log E_{k2}$, rather than in $\log E_{k2}$ itself. Thus, differentiating Eq. (9-39) under the assumption that E_{k2} varies as $\exp(-\beta_k h)$ and that n_k varies as $\exp(-\gamma_\infty h)$, we obtain

$$-\beta_k = -\gamma_\infty + \gamma_2(N_2\alpha'_{2k})\, C_1 \left\{ 1 - \sum_1^\infty d_i(N_2\alpha'_{2k})^i \right\} \tag{9-62}$$

The last term represents the change in β_k arising from self-absorption, and is of the form [also compare with Fig. 9-8(a)]

$$\gamma_\infty - \beta_k = aZe^{-Z} + \sum_{j=3}^\infty a_j Z^j \tag{9-63}$$

where the a_j are small and $Z \propto N_2\alpha_{2k}$. If the value of γ_2 is sufficiently small, we see how the observed behavior of β_k could occur, and result mainly from the self-absorption effect. That is, β_k would be essentially constant with height except for large values of Z, and would show significant variation with k. We have, of course, not proved anything; the physical question is still what part of the observed variation of β_k with k belongs to this self-absorption effect and what part to a differential height gradient of $b_k \exp(X_k)$. All we have done is to demonstrate that the predicted behavior of β_k under the first-order approximation is qualitatively the same as the observed.

For a quantitative investigation using the β_k, we note that because γ_2/γ_∞ is independent of k, the only k-dependent terms on the right side of Eq. (9-63) are the α'_{2k}. Thus, the right side is equivalent to a power series in the α'_{2k} or, alternatively, in the f_{2k} since the variation in λ_{2k} for $k \gtrsim 10$ is negligible. Thus, we fit the observed β_k to a power series in f_{2k} by least squares. Comparing the empirically determined coefficients to those computed algebraically from Eq. (9-62), we infer r. Both results are given in Table 9-7.

The point of the two empirical representations follows from the fact that an expansion about $f_{2k} = 0$ weights the larger values of f_{2k} disproportionately in the determination of the coefficients of the higher powers of f_{2k}. Thus, we prefer the expansion about $f = 2 \times 10^{-3}$, which corresponds to $k = 12$. The residuals from least-squares representations out to the third, fourth, and fifth powers of f_{2k} indicate that representation beyond f^4 is not justified by the data.

Table 9-7. Representations of $\beta_k (k > 10)$

Empirical Representations

Expansion about $f_{2k} = 0$:

$$\beta_k = 2.17 - 1.59Z(1 - Z + 0.363Z^2 - 0.021Z^3);\ Z = 405f_{2k}$$

Expansion about $f_{2k} = 2 \times 10^{-3}$:

$$\beta_k = 2.23 - 1.48Z(1 - Z + 0.438Z^2 - 0.067Z^3);\ Z = 662f_{2k}$$

Theoretical Representations

r	$10^8\gamma_2$	β_k	
1	2.20	$2.20 - 2.09Z(1 - Z + 0.676Z^2 - 0.240Z^3 + 0.0555Z^4)$;	$Z = 0.186N_{2\alpha}'$
2	1.10	$2.20 - 1.90Z(1 - Z + 0.579Z^2 - 0.157Z^3)$;	$Z = 0.137N_{2\alpha}'$
3	0.71	$2.20 - 1.65Z(1 - Z + 0.531Z^2 + 0.024Z^3 - 0.267Z^4)$;	$Z = 0.114N_{2\alpha}'$
4	0.55	$2.20 - 1.54Z(1 - Z + 0.447Z^2 + 0.119Z^3 - 0.274Z^4)$;	$Z = 0.101N_{2\alpha}'$
5	0.44	$2.20 - 1.41Z(1 - Z + 0.361Z^2 + 0.189Z^3)$;	$Z = 0.092N_{2\alpha}'$

We find good agreement between coefficients of Z in the empirical and theoretical expansions in the range $3.5 \lesssim r \lesssim 4.5$. The coefficients of Z^3 differ in sign between theoretical and empirical representations; but since we carry no higher terms than Z^3 in the empirical representation, this term in Z^3 must represent the effect of all remaining terms. Thus it should lie intermediate to the third and fourth terms in the theoretical expansion, since they change sign, and it does. Thus the results suggested by Table 9-7 are

$$0.49 \lesssim 10^8\gamma_2 \lesssim 0.63 \tag{9-64}$$

$$N_2\alpha'_{2k} \sim 6 \times 10^3 f_{2k} \pm 50 \text{ percent} \rightarrow N_2 \sim 1.5 \times 10^{16}(10^{-4}T_e)^{1/2}$$

As in our zero-order calculations, we have assumed that Doppler broadening is wholly thermal. Thus T_e, rather than some kind of "turbulence" parameter, appears in the absorption coefficient. Since the height variation of the β_k is not determinate from the data, it is difficult to specify the height at which the derived value of N_2 applies. However, since γ_2 corresponds to a scale height of some 2000 km, while the data themselves are fixed in the height range 500 to 2500 km, a choice of the mid-point, 1500 km, introduces an uncertainty of only $e^{1/2}$ in N_2. These results suggest several comments.

First, we note that again the values of N_2 and $\tau_{\alpha r}$ at 500 km do not change much under the change in analysis. The derived value of N_2 at 1500 km is higher by a factor of about three than our zero-order results, but agrees with our zero-order results at 500 km to well within their scatter of about a factor of two. These factors should be compared with those between 100 and 20 by which these results exceed the early results of Cillié and Menzel, and the recent results of Clube and Kononovich, based upon a zero-order approximation applied to the early Balmer lines.

Second, the results of the various analyses differ more seriously in the value of γ_2, both within the zero-order and between zero- and first-order approximations. Even with a good determination of N_2 at 500 km, precise values of $\gamma_2 - \gamma_k$ and of γ_2 are critical for a good empirical determination of the sign of non-LTE effects, of chromospheric structure, and of line formation. $\gamma_2 - \gamma_k$ determines the variation of S_L. γ_2 determines the self-absorption effect in the region 1000 to 2000 km, where the questions of departures from spherical symmetry and from local opacity in the Lyman lines become serious. A comparison of the values of $b_k \exp(X_k)$ inferred from the analyses illustrates these points. We compare first-order and zero-order analyses as representing a wide range in γ_2 and $\gamma_2 - \gamma_k$.

If we set, in conformity with the results (9-64) and the empirical expansion about $f_{2k} = 2 \times 10^{-3}$ for β_k,

$$Z = 660 f_{2k} \exp[-0.55(h - 1500 \text{ km}) \times 10^{-3}] \qquad (9\text{-}65)$$

and use this height variation of Z to integrate the empirical expansion for β_k, we obtain

$$\ln E_{k2} = \ln C_k - 2.20 \times 10^{-8} h - 2.70 Z(1 - 0.5Z + 0.146Z^2 - 0.0168Z^3) \qquad (9\text{-}66)$$

We adjust the constant C_k to force agreement with the observed E_{k2} at 1500 km. Comparing Eqs. (9-66) and (9-39), we see that

$$\Delta_k \log[b_k \exp(X_k)] = \Delta_k \log C_k - \Delta_k \log[A_{k2}(k^2 - 4)] \qquad (9\text{-}67)$$

The derived values of $b_k \exp(X_k)$ are in Table 9-8.

Table 9-8. Values of $b_k \exp(X_k)$ from First-Order Analysis

Lines	$\Delta_k \log C_k$	$\Delta_k \log[b_k \exp(X_k)]$
H11, H29	2.27	1.01
H15, H29	1.42	0.56
H20, H29	0.82	0.34

The values of b_k demanded by Table 9-8 are quite large compared with what we would estimate from the results of Chapter 4, incomplete as those results are and even noting that our first-order analysis requires $b_k \exp(X_k)$ to be constant over the height range 500 to 2500 km. Even for $b_{29} \sim 1$, Table 9-8 requires $b_9 \sim 10$. By contrast, the zero-order analyses lead to smaller values. Zirker's analysis, which differs the greatest in γ_2 from our first-order analysis, requires only $b_9 \sim 1.5$. Matsushima's analysis, whose γ_2 lies intermediate to the first-order and Zirker values, gives $b_9 \sim 3$.

The relative values of these empirical b_k focus attention on the extreme sensitivity of an empirical determination of the non-LTE state of the chromosphere to the values of γ_2 and $\gamma_2 - \gamma_k$. This is, indeed, the basis of our approximation scheme. To see directly the origin of this differential behavior, and of variation in the inferred values of N_2, compared the behavior of I_λ, E_λ, or $\int E_\lambda \, d\lambda$ treated by two sets of differing analyses: one set compares results of a treatment holding S_L constant with results based on a proper inclusion of its outward decrease; the other set compares results from an analysis based on an underestimate of γ_2 with an analysis using a correct value.

(*i*) *Constant S_L versus Variable S_L.* We write Eq. (9-2) in the form

$$I_\lambda = \int_0^{\tau_\lambda(\max)} S_\lambda e^{-\tau_\lambda} \, d\lambda = \bar{S}_\lambda \{1 - \exp[-\tau_\lambda(\max)]\} \qquad (9\text{-}68)$$

If we do not assume S_λ constant, $\bar{S}_\lambda$ represents some kind of mean. If we consider a height where $\tau(\max)$ is very large, then $\bar{S}_\lambda \sim S_\lambda$ $(\tau_\lambda \sim 1)$ and remains reasonably constant as we observe at greater heights until $\tau(\max)$ drops to a value near unity; thereafter $\bar{S}_\lambda$ decreases monotonically (with the exception of some effect such as a change from detailed to non-detailed balance in the Lyman lines). Thus, if we require that S_L keep the same constant value at the greater heights, we will overestimate the value of the integral. If we compare the predicted value to the observed value of I_λ, holding to this constant value of S_L, and evaluate $\tau_\lambda(\max)$, we will underestimate $\tau_\lambda(\max)$. The underestimate will be the greater, the greater the height. Thus, we will overestimate γ_2, in addition to underestimating $\tau_\lambda(\max)$. This same result will hold for an analysis of E_λ and $\int E_\lambda \, d\lambda$, with the differential effect at greater heights being intensified by the integration.

(*ii*) *Underestimate of γ_2 versus Correct Value.* Integrate Eq. (9-68) to form $E_\lambda/4\pi$. If we assume too small a γ_2, we overestimate $\tau_\lambda(\max)$ at each height, thus overestimate the integral. However, we also overestimate the outward decrease of S_λ through the quantity $\gamma_2 - \gamma_k$; and this underestimate of S_λ is the more important until τ_λ is so small that $\exp(-\tau) \sim 1 - \tau$, when the two effects cancel. Thus, the net result is an underestimate of the integral. Applying the computation to analyze an observed E_λ leads to an overestimate of S_λ. Since our estimate of $b_2 \exp(X_2)$ is also too great at greater heights, the overestimate of S_λ leads to an overestimate of $b_k \exp(X_k)$.

Thus, we expect that the correct values of γ_2 and $\gamma_2 - \gamma_k$ lie intermediate to the results of zero-order and first-order analyses, since the former rests on the assumption of constant S_L, and the latter underestimates γ_2 by ascribing the whole of the differential β_k effect to self-absorption. If we had an empirical method to fix γ_k, we could expect to obtain a wholly empirical intermediate solution, corresponding to a second-order approximation. Lacking the Paschen data, where the observed β_k should closely approximate the γ_k because of negligible self-absorption, we are forced to defer further wholly empirical analysis to the next successful eclipse. We illustrate the problems posed in trying to make any kind of successful, wholly empirical, choice of an intermediate solution on the basis of presently available data by comparing representations of E_{k2} by the first-order analysis and the most extreme zero-order analysis, that by Zirker. Figure 9-11 simply reproduces Fig. 22 of Zirker's thesis; Fig. 9-12 is our earlier work on the first-order approximation (Fig. 3, Athay and Thomas, 1955). It is clear that no wholly empirical choice can be made between the two representations. Thus, we must add the theoretical considerations already outlined. Before doing this, we summarize an approach to a second-order analysis by C. Pecker.

c. Second-Order Analysis. From the preceding, we see that an extension of our analysis beyond the first-order approximation without adding new kinds of data requires a completion of the theory for S_{2k}, viz., a specification of the change in S_{2k} to be expected under a change in k and in thermodynamic parameters of the atmosphere. Our theoretical development of $b_2(\tau_{\alpha r}, T_e)$ permits a check of the first-order analysis for consistency, by intercomparing the derived γ_2 with a γ_2 constructed from the theoretical $b_2[\tau_{\alpha r}(h)]$ combined with values of the height-gradient of $n_e n_p T_e^{-1/2}$ obtained by some independent procedure. We can also ask whether the derived values of $b_k \exp(X_k)$ "look" reasonable, noting that the derived values of $b_k \exp(X_k)$ are quite sensitive to the values of γ_2 and $\gamma_2 - \gamma_k$. However, neither the results of the consistency check nor of the "look" provide an unambiguous scheme of iterative correction, at least until we have the theoretical structure for S_{2k}.

A procedure suggested by C. Pecker and J.-C. Pecker (1956),

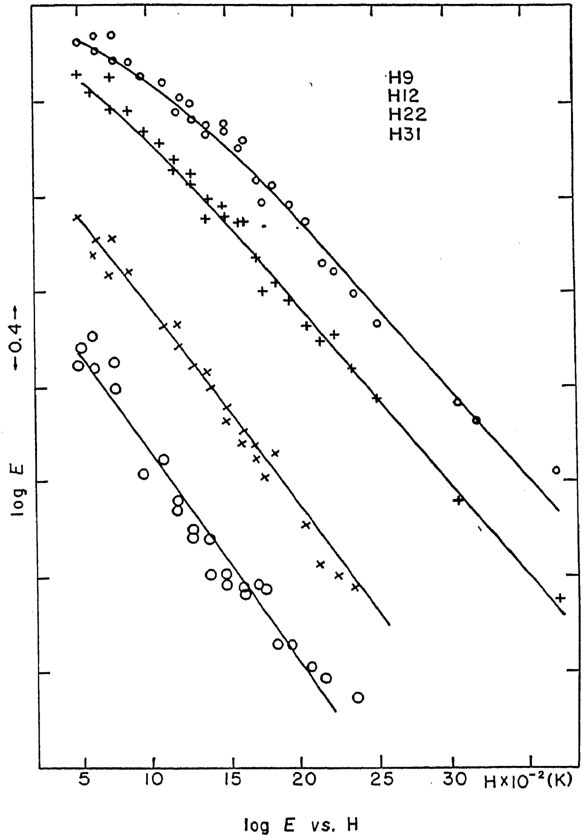

Fig. 9-11. Representation of Zirker's results.

further developed and applied by C. Pecker (unpublished results communicated to us), has an iterative character aimed at a completely self-consistent approximation scheme, using only presently available data on the Balmer lines. The basic iterative procedure depends upon an extrapolation of the value of b_2 from a derived set, b_k, which terminates at some $k > 2$. For this reason, the method cannot be used with confidence until we have the above-mentioned complete theoretical structure for S_{2k}; in practice, we believe that the iterative procedure is not as sensitive as would be desirable. We wish, now, to separate clearly a discussion of these two intrinsic limitations of the method from a commentary on the results derived to date from the

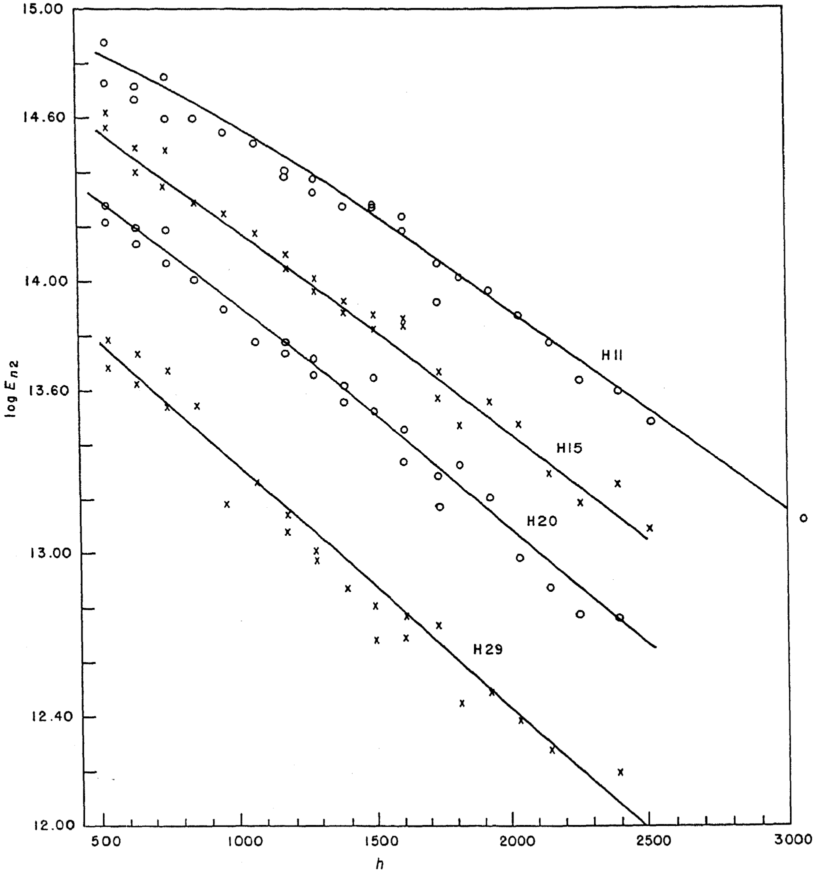

Fig. 9-12. Representation of first-order-analysis results.

analysis. These results represent an application of the method under assumptions that correspond to our zero- and first-order approximations, thus suffer from the same limitations of the analyses already described, but these limitations reflect the stage to which the analysis has been carried rather than any inherent limitations on the method.

The analysis proceeds according to the following scheme, which we cast in terms of the algebraic structure used in this monograph, rather than in terms of the formally-equivalent but slightly different approach of Mrs. Pecker. In Eq. (9-40), arbitrarily select a value of

n_2 at height h, and also assume values for γ_2 and γ_k. These values determine a numerical value for (ABS). With this value for (ABS), enter Eq. (9-39) with the observed E_{k2} and the assumed γ_k to determine $[n_e n_p T_e^{-3/2} b_k \exp(X_k)]$, thus n_k. The non-LTE Boltzmann-Saha equation gives

$$\log b_2/b_k = \log n_2/n_k + \log k^2/4 - X_{2k} \ln 10 \qquad (9\text{-}69)$$

An assumed model, $T_e(h)$, for the chromosphere gives X_{2k}, thus a value for b_2/b_k, from the assumed n_2 and the derived n_k. One plots b_2/b_k versus k for as many lines as he can analyze, then extrapolates the relation to $k = 2$. If he obtains at $k = 2$ the value $b_2/b_k = 1$, he considers the original assumed value of n_2 to be correct; if not, he iterates until the condition is satisfied. Carrying out this analysis at several heights gives $n_2(h)$, $n_k(h)$—thus more correct values of γ_2 and γ_k than those assumed. With these values, one repeats the iteration. Finally, unless one assumes that he had a correct chromospheric model, $T_e(h)$, he uses the results to estimate a better model, and repeats the iteration. Thus, there are two, possibly three stages of iteration involved: for n_2, for γ_2 and γ_k, and possibly for T_e. The success of the iteration at each stage depends upon the ability to decide, uniquely, compatibility between a given set of b_k, $k > 2$, and a value of b_2.

From this summary of the methodology of the analysis, the basis is clear for our assertion that its successful application requires a complete theoretical structure for S_{k2}—or b_k, $k > 2$. Our belief that the iteration scheme is not as sensitive as would be desired, even given the complete theoretical structure for S_{k2}, comes from the observation that the analysis under any stage of approximation still rests upon the comparison of $\Delta_k b_k$ with b_2, a second-order approximation effect. For example, in a first-order approximation we suppress any height gradient of b_k, $k > 2$, which is a second-order effect, in order to get a first approximation to the value of n_2 and its height gradient, which are, respectively, zero- and first-order effects. Thus this first-order approximation requires that several values of n_2—those at the several heights covered by the data—be compatible with the same $\Delta_k b_k$; in other words, that there be no unique b_2 compatible with a given set of b_k. We know that this requirement is invalid, but it is invalid to second order; hence the determination of a first-order effect by its departure from validity does not seem a sensitive method.

We illustrate the difficulties by Fig. 9-13, which shows a plot of log b_2/b_k for two extreme values of the radiation field in Hα, represented by values 1 and 0 for the parameter W_{23} described in Chapter 4, but the same value of T_e. It is difficult to see how one could decide that each of the two curve segments, ending for even as small a k as 3, does indeed extrapolate to $b_2/b_k = 1$ at $k = 2$. The same kind of indeterminacy accompanies a bad guess on T_e. We have seen

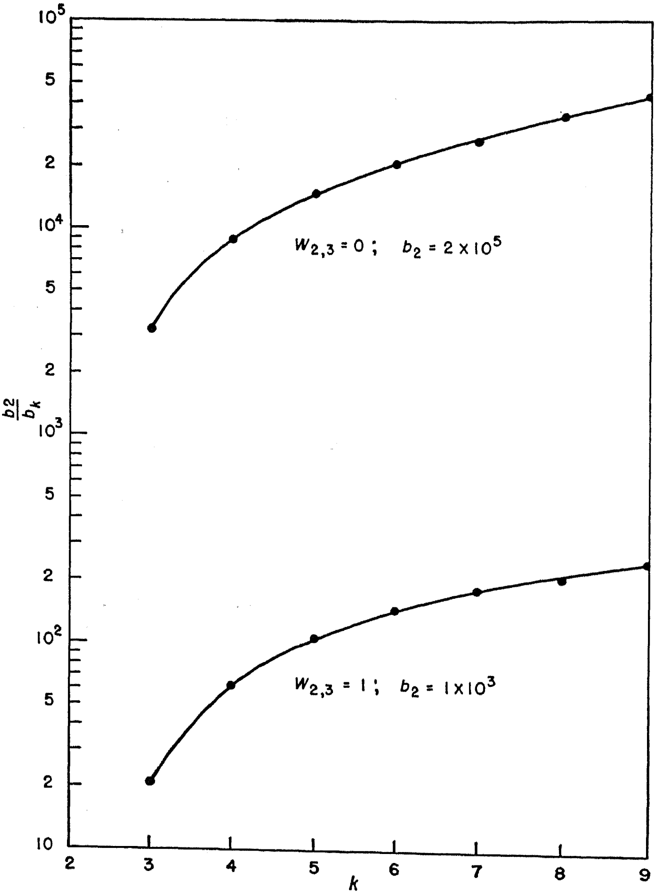

Fig. 9-13. Sensitivity of b_2/b_k to Hα radiation under constant T_e = 35,000°.

that the factor $\exp(X_2)$ drops out of the expression for n_2 when the correct expression for b_2 is used. Thus, there is a wide range in T_e over which a comparison of correct sets of b_j and n_j in Eq. (9-69) will show large shifts along the log b_2/b_k axis with comparatively small accompanying change in the value of n_2.

I am much indebted to Mrs. Pecker for extended discussion on these points, and on the accompanying background in Chapters 4 and 6. It now seems to us that the most promising approach to an iterative analysis is a combination of the behavior of $n_e n_p T_e^{-3/2}$, inferred either from Balmer lines near the series limit or from the Balmer continuum, with a theoretical $b_2(\tau_{\alpha r})$, determining $\tau_{\alpha r}$ from n_2 and γ_2. This leaves free the multiplicative factor T_e entering n_2, thus the factor $d \ln T_e/dh$ entering γ_2. In a spherically symmetric atmosphere, we can then attempt to use the sensitivity of the derived $b_k \exp(X_k)$ to γ_2 in order to estimate $d \ln T_e/dh$, once we have a more complete theory for S_{k2} and b_k for the higher k. Alternatively, we can add other information on $T_e(h)$, such as in Chapter 6, and attempt to combine all this material to investigate departures from spherical symmetry.

Finally, we should comment on one important aspect which has been neglected in all the other analyses, but which Mrs. Pecker has included—the departure of the absorption coefficient from a wholly Doppler profile. She finds the following:

Hα – Hδ: mainly Doppler, natural broadening must be included for $n_2 \gtrsim 10^6$.

H9–H15: Dopper and Stark contributions roughly equal.

H18–H31: mainly Stark.

(In these computations, she has essentially used the Pannekoek approximation to the Holtzmark representation of the Stark effect.) From Eq. (4-49), we see that this means that we should use an absorption coefficient of the form

$$\alpha_{2k}{}^{i} = \# \left\{ \sum_m f_m \int_{-\infty}^{\infty} \exp[-(x - \beta/y_m)^2] \, W(\beta) \, d\beta + f_0 \exp(-x^2) \right\} \quad (9\text{-}70)$$

while the form used in the zero- and first-order analyses described is

$$\alpha_{2k}{}^{ii} = \# \left\{ \sum_m f_m + f_0 \right\} \exp(-x^2) \quad (9\text{-}71)$$

We note that $\int W(\beta)\,d\beta = 1$ and $(\Sigma f_m + f_0) = f_{2k}$. The Pannekoek approximation simply corresponds to "spreading" the Stark components f_m over the whole λ region between the separate components, rather than locating them at definite $\Delta\lambda_m$. To a considerable extent, the Doppler smearing lessens the contrast between the literal, and Pannekoek approximate, application of the Holtzmark representation.

If we consider constant S_L, and an extreme Pannekoek-type approximation where we take a constant value of α_{2k} between $\pm\Delta\lambda_k$, we can see the direction of the effect of a neglect of Stark broadening on the inferred N_2 values. Under these two assumptions, and the assumption that n_2 varies as $\exp(-\gamma_2 h)$, the expression for E_{k2} becomes

$$E_{k2} = S_{2k} 2\Delta\lambda_k (N_2\alpha'_{2k}/\gamma_2)[1 - N_2\alpha'_{2k}/4 + (N_2\alpha'_{2k})^2/18 \cdots] \quad (9\text{-}72)$$

We recognize that adding the Stark effect leaves invariant the integral $\int \alpha_{2k}(\lambda)\,d\lambda$. Thus, a comparison of results including only Doppler effect and including Doppler plus Stark effect is equivalent to comparison of two results which include only Stark effect but with different values for $\Delta\lambda_k$, holding constant the product $(\alpha'_{2k}\Delta\lambda_k)$. If the result neglecting Stark effect be represented by Eq. (9-72), and if the addition of Stark effect increases $\Delta\lambda_k$, and decreases α'_{2k}, by a factor s, then Eq. (9-72) with s^{-n} applied to the terms in the second bracket represents the result of Doppler plus Stark effect. The net result is a decrease of the self-absorption effect, for a given N_2, when the Stark effect is added. Thus, if one tries to interpret a given numerical effect in E_{k2} as coming from self-absorption, he will derive a *greater* value of N_2 when he includes Stark effect than when he neglects it. Thus, our zero- and first-order results should be lower limits on N_2, from this effect.

The results of Mrs. Pecker's preliminary calculations differ from ours in the predicted direction, but the size of the difference is very large. She has analyzed the data at 2000 km and at 3000 km, starting both from the zero-order case $\gamma_2 = \gamma_k$, and from an attempt at a first-order iteration starting with $\gamma_2 = 0.5\gamma_k$. The results are preliminary, but suggest very large N_2 at 2000 km, and that $\gamma_2 \sim \gamma_k$ is more consistent than $\gamma_2 \sim 0.5\,\gamma_k$. Because the iterative method weights so heavily the earlier lines, her analysis has been carried out for heights greater than those to which data on the later Balmer lines restrict our analysis. Since the effects of inhomogeneities are presumably greater at the greater heights, it is difficult to assess properly those preliminary results, except to note that their trend is toward higher values of N_2(tangential). (On this point see note 9-2 in Appendix II.)

4. Rough Estimate of Effect of Departure from Spherical Symmetry on Results of Analysis of Later Balmer Lines. Consider the rough approximation suggested in the last part of Section 9-IIC2b, viz., splitting β_∞ into two parts, one referring to gradient of $(n_e n_p T_e^{-3/2})$ and one to gradient of effective emitting region. We can see that an attempt to set an upper limit by attributing all of β_∞ to the last effect would indeed be an upper limit. $\beta_\infty = 2.2 \times 10^{-8}$ cm^{-1}, and under this situation would refer to the relative *linear* dimension along the line of sight, not the total area. Thus, if we assume that the atmosphere is roughly spherically symmetric near 1000 km height, the relative emitting area would have dropped to about 0.1 percent at 2500-km height, where emission in the later Balmer lines and Balmer continuum has dropped below threshold. From Chapter 3, we see that the spicules, which produce the Balmer emission above about 4000 to 5000 km, occupy somewhat greater a fractional area than this 0.1 percent. Thus, the inference is strong that at lower heights, the relative area of effective Balmer emission is at least as large as that occupied by spicules above 4000 to 5000 km.

On this basis, and in the zero-order approximation, we see that there is only small change in the value of n_2 in the effective emitting regions for $h \leq 1500$ km. Only the value of N_2(tang) enters in computing the self-absorption effect, so the value obtained in the spherically symmetric case carries over unchanged. The value of n_2 derived from N_2 simply increases by the reciprocal of the relative linear dimension of the emitting region, or about a factor of three at 1500 km. Since we have attributed all of β_∞ to the gradient in dimension of effective emitting region, and required absorption and emission to come from this same region, γ_2 will be $-[\beta_\infty - \gamma_2$ (spherical-symmetry result)$] < 0$. That is, n_2 increases upward, and we again find the zero-order analysis inconsistent in the sense of giving an outward-decreasing, rather than constant, source function. The value of $\tau_{\alpha r}$ in the emitting region is, in consequence, indeterminate.

We find essentially the same behavior in the first-order approximation, so long as we hold to the requirements that regions of emission and absorption coincide and that these regions are essentially homogeneous in n_k; viz., all of β_∞ represents a gradient of dimension of emitting region. We note that an outward-decreasing source function and a very large increase in $\tau_{\alpha r}$ are still quite compatible, for the important dimension in fixing S_L is the optical depth to the nearest surface. Just as discussed in our analysis of the early Balmer lines and the effects of departure from spherical symmetry there, the nearest surface becomes the lateral boundary of the emitting region rather than its "top."

Thus, just as in the process of developing a completely self-consistent second-order analysis for the case of spherical symmetry, we find our analysis for the non-spherically symmetric atmosphere limited by the extent to which our theoretical analysis of the behavior of the source function has been carried. We have shown that in the spherically symmetric case an extension of the first-order analysis to the second order requires an extension of the theory for $S_{k2}(\tau_{\alpha r})$ to that for $S_{k2}(k, \tau_{\alpha r})$, then an iterative analysis for $\tau_{\alpha r}(h)$ from $\tau_{\alpha \mathrm{tang}}(h)$. In the non-spherically symmetric case, we now recognize that even a first-order analysis requires an extension of the theory for $S_{k2}(\tau_{\alpha r})$ to one for $S_{k2}[\tau_\alpha(\Theta)]$, then an iteration for $\tau_{\alpha \mathrm{tang}}(h)$ *and* $\tau_\alpha(\Theta)$. [By $\tau_\alpha(\Theta)$, we denote the non-spherically symmetric character of τ_α.] Thus, further empirical analysis from the hydrogen lines of the atmospheric region where departure from spherical symmetry becomes important must be deferred to the investigation of the behavior of the source function in a non-spherically symmetric atmosphere.

D. Summary of Analysis of Hydrogen Lines Relative to the Structure of the Lower Chromosphere

Such a summary is best constructed by intercomparison of results derived from analysis of the hydrogen lines with those derived from analysis of the hydrogen continuum in Chapter 6. Since hydrogen dominates in abundance and in total mass, and since its influence in the energy balance predominates until the beginning of the "second" stable region at some $T_e \gtrsim 2 \times 10^4$°K, this combined information from the hydrogen spectrum is critical in specifying the thermodynamic structure of the initial, gradual rise in T_e in the lower chromosphere.

The initial analysis of the continuum, Table 6-6, gives a structure according with hydrostatic equilibrium to the accuracy of the observations over the range 500 km $\lesssim h \lesssim$ 1000 km. Thus, both this initial analysis, and the final one of Table 6-10 forcing exact agreement with hydrostatic equilibrium, give the same results on chromospheric structure and state of excitation over this height interval. As noted in Chapter 6, the H^- emission measures n_1, while the Balmer free-bound emission measures $n_e n_p T_e^{-3/2}$, thus the two combine to measure the excitation term. Our theoretical approach relates b_1, T_e, $\tau_{\alpha r}$ and permits a determination of $T_e(h)$ from the excitation term; then n_1, T_e combine to permit the check on hydrostatic equilibrium. In this region of the atmosphere, $b_1 \cong b_2$; thus the consistency of inferred behavior of n_2 measures the consistency of our approach to n_1 and the derived structure of the atmosphere.

The continuum results in both Tables 6-6 and 6-10 give n_2 (500 km) $\sim 2 \times 10^6$, and $\gamma_\infty > \gamma_2 \sim 1.7 \times 10^{-8}$ over the interval 500 km $\lesssim h \lesssim$ 1000 km. Our analyses of the line spectrum, conducted from a quite independent viewpoint except in using the theory as a guide in establishing an approximation scheme, give agreement with these results from the continuum to all orders of approximation. There is about a factor-of-two scatter around the value for n_2(500 km). The scatter in γ_2 is greater, but all those analyses that do not explicitly force equality of the derived γ_2 and γ_k show $\gamma_2 < \gamma_\infty$. Finally, analysis of observations of Hβ–Hδ at the center of the disk support this value of γ_2 and its relation to γ_∞. The theoretical prediction of $T_{ex}(\tau_{\alpha r})$ for Hα reproduces semi-quantitatively the empirical $T_{ex}(\tau_{\alpha r})$ derived from Hβ–Hδ by neglecting the k-dependence of T_{ex}. These center-of-the-disk observations of Hβ–Hδ span the range of $\tau_{\alpha r}$ over the interval 500 km. $\lesssim h \lesssim$ 1000 km, if we accept the derived values of n_2(500 km) and γ_2.

We interpret the self-consistency of these four sets of material—eclipse observations of hydrogen continuum, eclipse observations of hydrogen lines, disk observations of hydrogen lines, theory for b_1, b_2, and Balmer source function—to imply that a spherically symmetric model lying very close to that of Table 6-10 is a good over-all representation of the chromosphere in the range 500 km $\lesssim h \lesssim$ 1000 km. At the same time, we do not wish to underemphasize the need for more careful determination of the behavior of the Balmer continuum near 500 km, of the Stark contribution to the absorption coefficient and its effect upon the analysis of the later Balmer lines, and of the k-dependence of S_{k2} to ensure that these uncertain effects do not modify the conclusion just reached. We also recall that in this determination of properties for $h \lesssim 1000$ km, we have removed the contribution to the observations from the region $h \gtrsim 1000$ km by essentially treating the latter region as spherically symmetric. Errors arising from this procedure must ultimately be checked by iteration on the basis of the model for the region $h > 1000$ km, but our rough analysis in the preceeding section suggests that there will be no essential change in $n_2(500 \text{ km})$ and γ_2.

We saw in Chapter 6 that the greatest uncertainty in extending the chromospheric model to $h \gtrsim 1000$ km, through the steep rise in T_e, lies in the value at which T_e stops its abrupt rise. We have already discussed in Section 6-IIIA3 the various alternatives on conditions at the top of this rise, and their influence on the solution at lower heights through alteration of Balmer and Lyman opacity calculations. Analysis of the hydrogen lines has added only two definite pieces of information: one, that for most of the chromosphere, $\tau_{\alpha r} \sim 1$ corresponds to $\tau_{\mathrm{Ly}\,\alpha} \sim 1 \times 10^3$, where detailed balance in Ly-α no longer holds; the other, that some non-homogeneous structure exists at these heights such that small parts of the chromosphere have sufficient Lyman opacity to satisfy detailed balance in Ly-α. However, this information characterizes a region located only as being some 2 to 3 scale heights in n_2 above the last reasonably reliable value of $\tau_{\alpha r}$ in Table 6-10, and does not give information on the details of the abrupt rise in T_e. Although a major part of the eclipse data on the Balmer lines refers to heights at which the abrupt rise in T_e has presumably occurred, we have seen that uncertainty in separating γ_k from β_k empirically, and in evaluating the k-dependence of S_{k2} theoretically, precludes drawing any reliable conclusion on $T_e(h)$ from the present state of data and theory. Thus, for empirical determination of the state of the chromosphere above the rise in T_e, we must turn to the helium observations.

Another approach to determining T_e through the region of the abrupt rise lies in the stability considerations of Chapter 5. However, as we saw there, a definite—rather than range of—result requires a specification of height variation of non-radiative energy input. We have implicitly introduced the required information on non-radiative input in the region covered by Table 6-10 through the use of an empirical value for $d \ln(n_e n_p T_e^{-3/2})/dh \equiv -\gamma_\infty$ and the condition of hydrostatic equilibrium. We see demonstrated in these results the limitation on the use of the stability calculations; viz., they place only an upper bound on the T_e within which a stable solution may be found. The steep gradient may set in at lower T_e, depending on dynamic and energetic conditions in the particular atmosphere. We might extend the model across the abrupt rise in T_e to greater heights simply by continuing to apply these two assumptions. Indeed, if there were no evidence for inhomogeneity, we should have no empirical reason to question the continued application to $h \sim 2500$ km of a roughly constant value for γ_∞; and we could interpret the emission at λ4700 as electron scattering to check the validity of hydrostatic equilibrium (cf. Pottasch, 1960). However, there is nothing in such a model to introduce the departure from spherical symmetry implied by the Hα observations (viz, regions of higher Ly-α opacity, thus presumably lower gradients in T_e) unless we can show that some kind of structural instability occurs in this region where, over a few hundred kilometers, we pass from the condition of detailed balance in the Lyman contiuum to a condition requiring an abrupt rise in T_e.

This implication from the Hα observations combines with the character of the non-radiative energy source implicit in the model for $h \lesssim 1000$ km to suggest a relation between non-radiative energy source and departure from spherical symmetry. The non-spherically symmetric structure above the abrupt rise in T_e may reflect an instability arising in the transition region. Alternatively, it may reflect the presence of a non-radiative energy source which, although of small total mass compared with the low chromosphere, becomes observable at greater heights because of differential density and excitation gradients. Note that the density of the chromosphere drops by a factor of $\sim 10^2$ between 500 km and the region of abrupt rise in T_e, or a factor of $\sim 10^4$ between 0 km and this rise. Thus we do not require much differential gradient to provide an observable difference at $h \gtrsim 1000$ km. We note that the non-radiative source implicit in the model for $h \lesssim 1000$ km cannot, because of hydrostatic equilibrium, contribute significantly to the momentum balance. Because it must contribute to the energy balance, its velocity field must be super-thermal. Thus, its mass must indeed be negligible compared to that of the low chromosphere. Consequently, and pending a quantitative investigation of the instability possibility, I prefer to consider the departure from spherical symmetry at the greater heights as reflecting the increasing observability of the non-radiative energy supply. This is essentially the spicule model of a few years back (Thomas, 1948); which still seems attractive because it is a non-radiative energy system which we know exists in the chromosphere.

We note that the spicule model effectively requires either a three-component structure or a continuous lateral variation in T_e; for it consists of a superthermic jet of material heating the surrounding atmosphere by lateral diffusion of jet atoms. The "hottest" region of the atmosphere should be adjacent to the spicule, with T_e decreasing to regions midway between adjacent spicules. The original model (Thomas, 1948, 1950) treated cold spicules because of the "jet" model. Unfortunately, the situation is still what it was 10 years ago as regards an empirical inference of properties of spicules in the region $h \lesssim 2000$ to 3000 km, and will remain so until we can sort out the relative contribution to the emission from interspicular and spicular material. We have discussed the inference from hydrogen; that from helium and the radio data, together with more elaborate models of the possible inhomogeneity, lie in other chapters. We summarize in the balance of this chapter what has been done thus far on the analysis of the metallic spectrum of the chromosphere. From a theoretical standpoint, the methodology of the non-LTE approach has almost been developed to the point where we might try to extend it to a hydrodynamic problem, rather than simply analysing hydrostatic situations, and the spicule problem offers a good choice for the first application.

III. Summary of Analysis of the Metallic Spectrum of the Chromosphere

Essentially nothing has been done to date in the way of explicitly applying the non-LTE methodology thus far developed to interpretation of the metallic spectrum. Attempts at discussion of the implication of the self-reversed emission cores of Ca^+ H and K form the exceptions (Miyamoto, 1947, et seq.; Jefferies and Thomas, 1959, 1960). Primarily, the reason is that until the developments of the last few years on equivalent two- and three-level approximations to the source function, the non-LTE computations have been wholly numerical treatments of 10- and 15-level atoms, including all the levels below some principal quantum number, and representing the radiation field parametrically. Such solutions are extremely laborious, and generally do not give simple, direct physical insight. Attempts to simplify the numerical solutions by picking out "major" terms have usually proceeded via consideration of absolute rates, and are not always physically meaningful, as we have emphasized in discussing the formulation in terms of net rates. Now, however, the introduction of the equivalent two-level approach to the general spectral line, and the resulting simplified solution of the transfer problem, developed in terms of net rates as outlined in Chapter 4 and briefly discussed in the present chapter for the Balmer lines, promises more insight. The development of an algebraic methodology seems possible, both for functional form of the source function and for solution of the transfer equation to determine depth variation of the source function. Speculation on the course of such development is pointless here; we note only that it has not reached the stage where we can apply it, or summarize its application to the metals, in this monograph, except for the preliminary discussion of Ca^+ H and K.

Those empirical analyses of the metallic spectrum of the chromosphere which have thus far been reported must be described as exploratory. They correspond to a zero-order analysis, in terms of the approximation scheme we developed for hydrogen, viz., no variation of source function over the atmospheric region analysed. The analysis by Böhm-Vitense (1955) of the 1932 eclipse data and that by Zirker (1956, 1958) of the 1952 eclipse data represent the most complete such studies. Although these two analyses treat different material, and differ in methodology of approach under the zero-order approximation, their results lead to the same two broad general conclusions. First, there are sufficiently large self-absorption effects in the metallic spectrum of the chromosphere that their neglect will lead to erroneous conclusion on differential excitation effects. An immediate corollary of this result is the conclusion that the effect of the chromosphere is not at all negligible in the formation of many line profiles observed in the disk Fraunhofer spectrum, even for some lines of Rowland intensity < 10. Second, the source function for these lines is not $B_\nu(T_e)$, and a non-LTE treatment of the lines must be performed if one is to interpret their behavior to

Table 9-9. Heights of Formation of Fraunhofer-Line Centers: Zirker Analysis

Element	λ	H_1, km	Rowland intensity	T_{ex}, °K
0	7772.0	4×10^2	2	5200
	7774.2	7	2	5300
	7775.4	8	1	5400
Na	5890.0	3	30	3850
	5895.9	2	20	3850
Mg	3829.4	6	10	3850
	3832.3	4	15	3750
	3838.3	6	25	3750
	5167.3	—	15	3950
	5172.7	2	20	3900
	5183.6	3	30	3800
Al	3944.0	—	15	4050
	3961.5	3	20	4000
Ca	4226.7	3	20	3350
Ca^+	3968.5	2×10^3	700	3950
	8498.1	6×10^2	12	4050
	8542.1	9	16	3700
	8662.1	9	15	3800
Ti^+	3361.2	2	8	4600
	3372.8	7	5	4500
	3380.3	2	3	4850
	3383.7	4	3	4900
	3394.6	2	3	5000
	3491.1	2	5	5150
	4294.1	1	5	4400
	4395.0	2	3	4550
	4443.8	1	5	4450
	4468.5	2	5	4450
	4501.3	1	5	4700
Cr^+	3368.1	8×10^2	5	4700
	3408.8	5	3	5100
	3421.3	5	4	5100
	3422.7	5	4	4700
	3433.3	4	3	5000
Mn^+	3442.0	7	6	4650
	3460.3	4	4	4750
	3474.1	3	2	4800
Fe	3859.9	4	20	4200
	3886.3	6	15	4200
Sr^+	4077.7	6	8	4000
	4215.5	5	7	4000

infer abundance or atmospheric structure. The nature of these conclusions, and their apparent invariance under method of analysis and degree of completeness of data, are identical to the corresponding results obtained in preliminary, zero-order analyses of the hydrogen spectrum.

As an over-all characterization of these two broad results, we reproduce in Table 9-9 Zirker's conclusions from analysis of the 1952 data on the height corresponding to $\tau_0(\text{radial}) \sim 1$ for lines of a number of neutral and ionized metals (Zirker, 1958, Table 8). Included in this table are T_{rad} from the Utrecht Atlas for each line, together with the (disk) Rowland intensity of the line. These values of T_{rad} for $h > 500$ km lie, without exception, significantly below the values of T_e in our model of Chapter 6; thus they show the expected kind of non-LTE results. In Section 9-IIIA we summarize the methodology of these two zero-order treatments of the metallic spectrum of the chromosphere.

Given an arbitrary line observed in the disk spectrum, but not necessarily included in an analysis of eclipse observations, one asks whether a non-LTE approach must be used to analyse it. Such non-LTE effects may be introduced because parts of its core are chromospheric in origin, or because S_L departs from $B_\nu(T_e)$ from effects not dependent upon the chromospheric rise in T_e. (Such effects as would characterize the Balmer lines, for example.) An attempt to answer this question wholly empirically has been initiated by Pecker, and we include a summary of it in Section 9-IIIA.

Finally, in Section 9-IIIB, we comment on the interpretation of the Ca^+ H and K lines, where the beginnings of a systematic attempt to apply the non-LTE theoretical structure have been made.

A. Summary of Wholly Empirical Analysis of the Metallic Spectrum

1. The Chromospheric Spectrum, Zero-Order Analyses. From Eq. (9-57), we see that the assumptions of a constant source function, a spherically symmetric atmosphere, and a wholly Doppler-broadened absorption coefficient with constant $\Delta\lambda_D$ makes the quantity $E(h)/S_L\ \Delta\lambda_D \equiv \exists$ depend only upon $\tau_0(h) = \alpha_0 N_L(h)$. N_L is the number of atoms in the lower state along the tangential line of sight. Both Böhm-Vitense and Zirker make these three assumptions. Thus, the function $\exists(h)$ depends upon three constant parameters—$S_L\ \Delta\lambda_D$, $\Delta\lambda_D$, $N_L(h_1)$—and the function $\gamma(h)$. A rigorous application of the zero-order analysis would involve only two constant parameters, since S_L would be fixed by the residual intensity in the line observed on the disk. However, these analyses seek to determine mean quantities at each height, and an approximation to the height variation of the mean; so $S_L \Delta\lambda_D$ is retained as a free parameter. Then, just as in the case of hydrogen, there are two methods to determine the parameters: analyzing the height variation of a single line, after specifying $\gamma(h)$ from other considerations; and analyzing jointly several lines of one ion at a particular height, introducing additional assumptions to specify the variation of S_L and N_L from line to line. Böhm-Vitense follows the second alternative; Zirker, the first.

a. Böhm-Vitense Analysis (1955). Böhm-Vitense introduces three additional assumptions: $\gamma(h)$ is independent of h, and is the same for all lines of a given ion; T_{ex} (which she calls the radiation temperature T_S) is the same for all lines of a given ion; there exists a single excitation temperature T_A for a particular ion, which relates occupation numbers of excited levels to total concentration of the ion through a Boltzmann distribution. The combined assumptions of constant S_L and $\gamma(h)$ the same for all lines of a particular ion require T_A to be independent of height, of course. Indeed, this set of assumptions can never rigorously be satisfied except under an LTE state in an isothermal chromosphere. One should, however, simply regard the introduction of this set of temperature parameters as a device to give a zero-order-approximation solution, which can then be investigated for consistency. The only cause for concern lies in taking literally any of the temperature parameters as actually giving T_e. Unfortunately, such a literal approach is not unusual. As we emphasized in discussing hydrogen, one should regard the value of such zero-order analyses as lying chiefly in providing a rough preliminary measure of the distribution of absorbing material.

These assumptions permit a curve-of-growth type analysis to obtain n_i/U_i, T_A, T_S, γ, and $\Delta\lambda_D$ for each ion at each height covered by the data. U_i is the partition function for the ion, and Böhm-Vitense simply uses the value of T_A to estimate its value. The analysis treates lines of FeI and TiII, using the Cillié-Menzel 1932 eclipse data. As regards details of the procedure, we need note only that in performing the analysis, T_S is set equal to T_A and a choice of "best" values for T_S comes from requiring the various multiplets to combine to define a single curve of growth. Introducing the assumption that, under conditions in the chromospheric height range studied, the metals are virtually all in the singly-ionized state, and adopting abundance ratios log H : Ti = 7.38 and log Fe : Ti = 2.35, Böhm-Vitense obtains values for the concentrations of H and FeII. We summarize these results in Table 9-10.

From her results on n_2 for hydrogen, which we have discussed earlier, Böhm-Vitense obtains n_e by applying the Boltzmann-Saha equation under the assumptions that the temperature parameter entering it is the excitation temperature of the Balmer lines, $T_A(n_2)$, and that $n_e = n_p$. With this value of n_e, and the above values of concentrations of H, FeI, FeII, she obtains ionization temperatures for hydrogen and iron from the Saha equation. These values are also summarized in Table 9-10. We defer comment until after summarizing Zirker's analysis.

Table 9-10. Summary of Böhm-Vitense Analysis of Metals: 1932 Data (Cillié-Menzel height scale; add 830 km for Böhm-Vitense scale)

h, km	log (FeI)	log (TiII)	log (H)	log n_e	T_A (FeI)	T_A (TiII)	T_i(Fe)	T_i(H)
−160	—	5.92	13.30	—	—	4300°	—	—
670	5.70	5.52	12.90	11.15	3800°	4000°	4890°	5930°
1500	4.95	5.18	12.56	10.74	3800°	3800°	4860°	5600°

b. Zirker Analysis (1956, 1958). Zirker's analysis of the 1952 eclipse data rests on an empirical determination of $\gamma(h)$. His starting point is an attempt to check Houtgast's suggested (1953) correlation of observed logarithmic emission gradient, β, with ionization potential of the ion—β decreasing with increasing ionization potential. Houtgast's correlation was based essentially on H, HeI, HeII, and the metals taken as a group. Zirker finds that no such correlation exists within the metals; rather, that β correlates with strength of the line and, for some lines with a common lower level, β decreases with increasing $\tilde{\omega}f$ value. As we saw in our discussion of hydrogen, such a behavior of β suggests that at least part of the differential variation results from a self-absorption effect. Zirker investigates the extreme assumption that all the differential variation of β over all lines of the singly ionized and neutral metals observed is a self-absorption effect. He picks an intensity (which he sets at 12.00 for log E), near the plate limit, determines β for each line at the height in the atmosphere where log E for the line reaches this intensity, and plots this β versus this height for all lines taken together. We reproduce his results in Fig. 9-14. Although there is a considerable scatter in the data, it is hard to disentangle any systematic effect. In consequence, Zirker draws a mean curve through the points on this relation, and assumes that it is $\gamma(h)$ for all lines of the metals, neutral and singly ionized. The relation is

$$\begin{aligned} 10^8\gamma(h) &= 1.12 + 0.10s + 0.005s^2 + 0.003s^3 + 0.0012s^4 \\ s &= 7 - h, \text{ in } 10^3 \text{ km} \end{aligned} \tag{9-73}$$

With this $\gamma(h)$, theoretical curves $\exists(h)$ as functions of the parameters $S_L\ \Delta\lambda_D$ and τ_0 (500 km) can be computed, and the values of these parameters determined for each line from the observations,

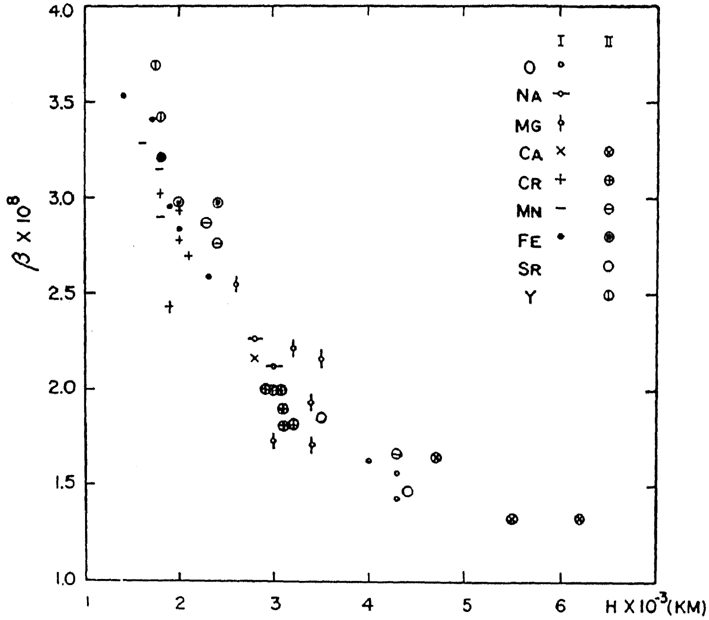

Fig. 9-14. Emission gradients of neutral (I) and singly ionized (II) metals at the height H where the line intensities fall to the plate limit (log E = 12.00). [From J. B. Zirker, *Astrophys. J.* 127, 680 (1958).]

$E(h)$. Because the analysis covers all heights simultaneously, S_L (and T_{ex}, Vitense's T_S) are forced to constant values; however, no assumption need be introduced on T_A. One can ask whether a T_A exists by attempting to fit a Boltzmann distribution over the lines in a given transition array; Zirker finds that most of the lines of a transition array can be combined with a reasonably constant T_A.

Zirker's original analysis (1956) applied the methodology based on the use of Eq. (9-73) only to the ionized metals. He noted that the assumptions of negligible gradients in T_A, partition function, and degree of ionization lead to the conclusion that $\gamma(h)$ is the actual logarithmic density gradient in the chromosphere, since the metals are mainly singly ionized and no height gradient in abundance is to be expected. His results for the ionized metals are of a different sort than those obtained by Böhm-Vitense; for he obtains a value of T_{ex}(or T_S) for each line, but does not give concentrations of TiII because of lack of confidence in absolute f values. His main emphasis lies on the value of τ_0(500 km) for each line; these values are quoted in Table 9-9. The range of values found for T_{ex} is interesting, to compare with Böhm-Vitense's results and the general methodology. We have the following as examples:

λ	3361	3373	3394	3504	3456	4444	4274
T_{ex}	6300	5900	6600	7400	5900	5200	4800

Zirker notes that an uncertainty in log τ_0 of 0.5 corresponds to a factor 2 in the derived S_L, or something like 900° in T_{ex} for a line at λ3500 and 2300° at λ8500. Thus, although we can attach no great significance to random differences in T_{ex}, the scatter in the above values is sufficiently large to emphasize the difficulty in direct physical interpretation of T_{ex}.

As mentioned, Zirker finds that a reasonable representation of most of the lines in a given transition array can be accomplished with a reasonably-constant value of T_A. For the $(d^2s - d^2p)$ transition array of TiII, he finds $T_A \sim 6100° \pm 1000°$. Again, the value differs non-trivially from that of Böhm-Vitense, but the significant result is probably that both lie below the value of T_e determined in Chapter 6.

The above reasoning on $\gamma(h)$ should fail for the neutral metals, consequently a different $\gamma(h)$ should be required, and Zirker adopted other procedures, which we summarize from the standpoint of the sensitivity of the results to the particular form of $\gamma(h)$ assumed. We note, however, that the results in Fig. 9-14, if taken only by themselves, suggest no clear-cut distinction between neutral and singly ionized lines; we return to this point below.

By looking for correlations between β and $\bar{\omega}f$, Zirker demonstrates that many lines of FeI have β values affected by self-absorption. (This result lies in contrast to that by Böhm-Vitense, who concludes that almost all lines are emitted in optically thin layers, so uses the observed β as γ. Since she does not list lines analysed, nor individual result, we could not compare detailed conclusions. We note only the much better height resolution of the 1952 data, hence the more sensitively determined β values.) Zirker finds 12 lines, sharing the common ground term a^3F, which show a particularly well-defined correlation between β and $\bar{\omega}f$. He analyzes these lines by two methods: one, that used by us for hydrogen, where one investigates the change of β with theoretical strength of the line (Section 9-II3C), thus hold γ constant; the other, based on a rapid decrease of γ with height, similar to the relation of Eq. (73). For the line λ4064 of a $^3F - Y^3F^\circ$, the results of the two approaches are as follows (τ_0 measured tangentially):

	$\tau_0(500)$	$\tau_0(1000)$	$\tau_0(1500)$	$\gamma(500)$	$\gamma(1000)$	$\gamma(1500)$
Constant γ	14	2.2	0.35	—	3.68	—
Variable γ	34	0.65	0.14	12.7	3.4	3.0

Thus, just as in the case of hydrogen, we have a variation of a factor of two to three in τ_0 and in occupation number resulting from the adopted relation between β and γ. As a rough average, the FeI concentration at 600 km is 1×10^7.

c. Over-All Commentary on Results of Zero-Order Analysis. Just as in the case of hydrogen, we emphasize two characteristics of these zero-order-approximation studies, and note the limitation of the analysis coming from the assumption of spherical symmetry. First, the most we can expect is a rough, preliminary estimate of distribution of material. A greater refinement requires a self-consistent specification of the relation between the several β_i and γ_j, which requires building into the analysis some non-LTE structure on the one hand, and resolving the effect of departures from spherical symmetry on the other. Second, the analyses give by themselves essentially no direct information on the distribution of T_e. By contrast with the case of the Balmer lines of hydrogen, this situation does not result because S_L is to first order independent of T_e, but because the empirical analyses have not even progressed to the stage of asking upon what S_L depends. These analyses are characterized by wholly arbitrary assumptions on the relations between the various temperature parameters introduced and their variation from line to line. The relations between these parameters, and their dependence upon T_e and n_e, must be built into the analysis.

Zirker's discussion makes somewhat more explicit the implication of an assumed relation between T_{ex} and T_A, the conclusion following essentially from the same standpoint as his criticism of our original use of the H^- data to determine T_e rather than n_H. His analysis covers both FeI and FeII. The FeI lines are resonance lines; those of FeII are transitions between two excited levels. Then, as a function of an assumed T_A for the lower level of the FeII transition, Zirker computes the total concentration of FeII from the occupation number of the lower level as derived from the empirical analysis. From the FeII and FeI concentrations, he computes an ionization temperature, T_i, using a value for n_e from the continuum data. At 500 km, he obtains the results shown in Table 9-11.

Since T_i is defined by $b_1 \exp \chi_1/kT_e = \exp \chi_1/kT_i$, the variation in T_i corresponds to the variation in b_1, which refers to the ground state of FeI. Thus, we see that an assumed relation between T_A(FeII) and T_i is completely equivalent to specifying the abundance of Fe, if Fe is mainly in the FeII state. In these particular results, we note that the abundances adopted by Böhm-Vitense, combined with ours on n_H from Chapter 6, would give T_A some 2000° less than T_i. We do not stress the numerical value of this result, because of uncertainty on f values and in the numerical analysis. We only note that once again a non-trivial difference between the various temperature parameters arises whenever self-consistency is

Table 9-11. Zirker Computation of T (ionization) for FeI FeII as $f(T_A)$

T_A	log (FeII)	T_i
4000°	7.96	5000°
5000°	7.26	4600°
6000°	6.79	4400°
7000°	6.46	4200°

sought and the structure of the empirical solution does not force their equality.

Within these factors of two to three that are introduced into the analysis by uncertainty on a proper treatment of excitation effects, we see that the Böhm-Vitense and Zirker results are in good agreement on the metallic-ion concentrations for $h \lesssim 1500$ km. This is particularly true if Böhm-Vitense's suggested shift of about 800 km in the zero point of the Cillié-Menzel height scale be adopted. As in the case of hydrogen, such agreement between different analyses of different material between different epochs lends confidence to the general results illustrated in Table 9-9 on the mass distribution for $h \lesssim 1500$ km and on the contribution of the chromosphere to disk profiles. We note that there is considerable disagreement on the derived γ values, both between the Böhm-Vitense and Zirker analyses, and within the various alternative approaches discussed by Zirker (Böhm-Vitense does not allow a range of possibilities for the variation of γ, by the nature of the assumptions she makes beyond those of constant S_L). Such variation of γ values, their consequences and implications, again mimics the behavior found for hydrogen.

We return now to the question of an interpretation of the relation (9-73), with the apparent implication of Fig. 9-14 that the relation is valid for both ionized and neutral ions. Although the scatter is large, there is no obvious systematic discrepancy between lines from neutral and ionized ions. We also note that the β for the OI infrared triplet accord well with the relation. The independent determination of the γ for the a^3F-associated lines of FeI discussed above gives values lying systematically low. Zirker's attempt to fit the Balmer lines with variable γ (Section 9-II3C) gives values also lying systematically lower than those from Eq. (9-73), until heights $h \gtrsim 5000$ km:

Height, km	500	1000	1500	2000	3000	4000	5000
γ (Balmer)	2.28	2.17	2.07	1.96	1.76	1.55	1.34
γ, Eq. (9-73)	4.94	4.11	3.41	2.87	2.10	1.64	1.38

Consider first the kind of relation expected between gradients of neutral, M, and singly ionized, M^+, metals, which we can try to estimate from the Boltzmann-Saha equation for the ground state of the neutral metal. Since both neutral metal and hydrogen Balmer lines (in the region of detailed balance in the Lyman lines) have photo-ionization-dominated S_L, we might use our analysis of b_2 for hydrogen as a rough kind of guide to the expected behavior of b_1 for the neutral metal. Thus, we might expect

$$n_1(M) = C_1 n(M^+) n_e T_e^{-3/2} b_1 e^{\chi_1} U_{M^+}^{-1} \sim C_2 n(M^+) n_e T_e^{-1/2} U_{M^+}^{-1} \quad (9\text{-}74)$$

from Eq. (4-48) for hydrogen. The constant C_2 incorporates the term in $Y_1 \exp(Y_1)$. Thus, we should expect the gradients of neutral and ionized metals to differ by the gradient of $n_e T_e^{-1/2}$ and of the partition function (plus whatever else our approximation may have omitted, of course). If the relation (9-73) is valid in the region $h \lesssim 1000$ km where our analysis of Chapter 6 gives what we consider to be reliable results, and if the metallic spectrum originates in the atmospheric region producing the hydrogen spectrum, then we should expect an appreciable difference between neutral and ionized metals because the gradient of $n_e T_e^{-1/2}$ is not negligible in this region. (Between 500 and 1000 km, $d \ln n_e T_e^{-1/2}/dh \sim -0.9 \times 10^{-8}$.) The exception would occur if we could prove that the partition function decreases outward at nearly the same rate.

Consider next the identification of the gradient of the ionized metals with the density gradient. Again for this region $h \lesssim 1000$ km, we note that the γ predicted from Eq. (9-73) lie significantly below the density gradient determined in Chapter 6. However, noting that this is a region of increasing T_e, that the opacity in the resonance lines of the ionized metals is large, and that S_L for the resonance lines of the ionized metals is of the collision-dominated type, this relation between γ and density gradient is not unexpected. Consider the resonance line of the ionized metal originating in one of the excited states, k, involved in the line which was analyzed. We can write, for the S_L of this resonance line,

$$S_L(k, 1) \sim C_\lambda n_k/n_1 \sim C_\lambda n_k/n_{M^+} \quad (9\text{-}75)$$

thus

$$d \ln n_k/dh \sim d \ln n_{M^+}/dh + d \ln S_L(k, 1)/dh \quad (9\text{-}76)$$

So long as there is sufficient opacity in the center of this resonance line, $d \ln S_L/dh > 0$ in a region of rising T_e (cf. our discussion in Chapter 4); thus the left side of Eq. (9-76) should be numerically smaller than the first term on the right side, which is the direction of the differential effect we are trying to interpret.

From the results of these two paragraphs, we could understand an empirical relation in the region $h \lesssim 1000$ km that showed emission gradients of the resonance lines of neutral metals and of subordinate lines of ionized metals scattering around the true density gradient, the neutral metals lying systematically high in gradient and the ionized metals systematically low. As already remarked, we do not observe such systematic scatter. We also note, however, that the empirical values underlying the construction of $\gamma(h)$ in Fig. 9-14 and Eq. (9-73) only refer to the region $h \gtrsim 1000$ km, because of the manner of construction of the relation. The empirical points are not really significant until $h \gtrsim 1500$ km, and actually begin to define a curve only for $h \gtrsim 2000$ km. Thus, the relation of Eq. (9-73) really defines the behavior of γ only in the region where the question of nonspherically symmetric structure has become critical. Its use in the region $h \lesssim 1000$ km is at best an extrapolation.

Because Eq. (9-73) appears to refer to neutral and ionized metals impartially, because earlier results in the monograph suggest $T_e \gtrsim 2 \times 10^4$—possibly reaching 3 to 5×10^4—over a significant fraction of the chromosphere for $h \gtrsim 1200$ km, and because we recognize the presence of cooler regions imbedded in these hot regions, the obvious temptation is to regard $\gamma(h)$ as characterizing the gradient in relative size of the cooler regions. In this way, we avoid the difficulty of no systematic difference between gradients of neutral and ionized metals. One difficulty in this simple intepretation lies in the difference between γ(Balmer) and γ[Eq. (73)]. A second difficulty lies in the apparent indication that T_e in the spicules above 5000 km has about the same values as in the "hot" component below 4000 to 5000 km, while significant Balmer and Ca^+ emission occurs in the spicules. Thus, we cannot simply interpret all the emission underlying the construction of Fig. 9-14 as arising from one "component" of the chromosphere. We must investigate in some detail the metallic emission and absorption expected from the several regions, on a non-LTE basis. Then, we will be in a position to properly utilize the several kinds of data on γ and absolute intensities. Here, we wish only to re-emphasize the point made in a preliminary superficial study of the Wolf-Rayet atmosphere a few years back (Thomas, 1949); viz., the conditions for the simultaneous presence of several stages of ionization and excitation have as yet been too little explored. We note the degree of T_e sensitivity of the ionization of a neutral metal, illustrated by Eq. (9-74), by comparison with the LTE result, as one example.

2. Pecker's Approach to the Disk Metallic Spectrum. The development of the non-LTE approach outlined in Chapter 4 was originally motivated by application to those atmospheric regions having significant non-radiative energy supply. Clearly, however, many of the non-LTE effects discussed can be introduced simply by anisotropy of radiation field, associated with low optical depths. The classical treatment of the source function of a resonance line as arising wholly in coherent scattering is an obvious example. Generally, however, analysis of disk spectra of sun and stars by curve-of-growth methods, and more detailed analysis of line profiles on the solar disk, proceed under the twin assumptions of (1) *LTE*, to interrelate occupation numbers through the Boltzmann and Boltzmann-Saha equations; and (2) *pure absorption*, setting $S_L = S_C = B_\nu(T_e)$. Our developments thus far would lead us to question the validity of both these assumptions, even for weak lines, until they had been explicitly investigated. In principle, such an investigation is straightforward. In practice, the difficulties which we have already outlined exist—stemming primarily from lack of cross sections and f values.

Pecker has attempted to develop a methodology to assess whether such non-LTE effects actually exist in the disk spectra of weak lines, from wholly empirical considerations, thus to establish a guide for more detailed work combining theoretical and empirical approaches. In two short notes (1957a, 1957b), he has outlined, and given preliminary results of analyses from considerations of line profiles and of a curve-of-growth approach. More extensive results by himself and collaborators have been presented verbally (Liege Conference, 1959) and will be in print by the time this monograph appears [Pecker (1959a, 1959b)].

The principle of the line-profile approach is simply that of comparing $T_{ex}(\tau_C)$ determined from several multiplets using observed solar line profiles. The assumption of LTE permits $\tau_0(\tau_C)$ to be computed. We reproduce as Fig. 9-15 his preliminary results from TiI. From these results, he concludes that significant departures from LTE exist for $\tau_C \tilde{<} 1$; and that the effect diminishes as the lower level of the transition occurs higher in the term diagram. In addition to these conclusions, we note with considerable interest

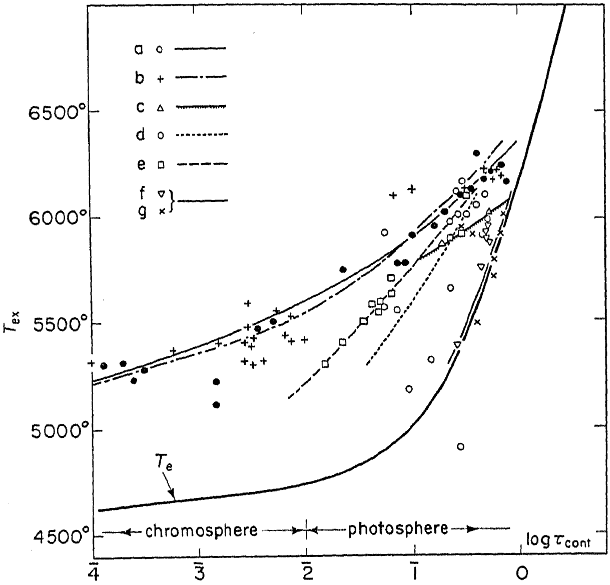

Fig. 9-15. [From J-C. Pecker, *Compt. rend.* 245, 501 (1957).]

that $T_{ex} > T_e$. What Pecker infers from his analysis is of course S_ν(total), equal to the second term on the right of Eq. (4-95), and not directly S_L. However, for lines with $r_0 \lesssim 10^{-1}$ in this region of outward-decreasing T_e, S_{ν_0} is essentially S_L if we observe $T_{ex} > T_e$. This is the direction we would expect for a resonance line of a neutral metal like TiI. In a rough sort of a way, lines from higher levels might be expected to be even more photo-ionization-dominated because both χ_{LU} and χ_L are even smaller (cf. our original discussion in Chapter 4 of the three classes of lines), until the electron-collision terms completely dominante all scattering terms, and S_L becomes $B_\nu(T_e)$. This is however speculation—it is simply illustrative of the guide that such analyses as Pecker's may be in indicating where the theory may make progress.

Pecker's curve-of-growth approach rests on the point that we emphasized by our sample calculations of $S_L(\tau_0)$ in Chapter 4; viz., the profile of an absorption line often depends as much or more upon non-LTE effects as it does upon $T_e(\tau_\nu)$. In the conventional approach to a curve-of-growth analysis, with $S_L = B_\nu(T_e)$, the integral over the line profile to determine total absorption depends only upon $T_e(\tau_\nu)$; and several multiplets are superposed to form a curve of growth, determining relative concentrations from the Boltzmann-Saha equation with $b_k = 1$. Pecker notes, from his results reproduced in Fig. 9-15, that there should be a different curve of growth for at least each multiplet. That is, in the general case, one must consider $T_{\text{ex}}(\tau_\nu)$; T_{ex} may vary from one line to another, even more from one multiplet to another. Pecker then uses his observation that non-LTE effects appear to decrease with increased excitation of the lower level to introduce an approximation procedure very close to our first-order approximation. That is, he assumes that an initial approximation finds S_L differing from $B_\nu(T_e)$ by $b_k \neq 1$ for the lower term of the transition only, thus the correction to S_L is the same factor for all lines within a multiplet. One can attempt to improve this approximation by iteration and requiring some kind of smooth trend of the b_k with excitation. He can also attempt to require consistency with an analysis of the kind in the preceding paragraph. Pecker's preliminary results suggest alterations by as much as a factor of 4 in abundances determined by these curve-of-growth methods.

These results, preliminary though they may be, emphasize once more the necessity for a complete re-examination of the analytical structure underlying the analysis of stellar spectra. Our first results emphasized the problems associated with the chromospheric contribution to any line. A simple extension of the theoretical work suggests that many of the same difficulties may arise even when the line is mainly formed outside the chromosphere. Pecker's preliminary results suggest that there are also strong, wholly empirical, reasons for questioning the conventional approach. One clearly requires, then, simultaneous attempts to extend the theoretical structure to weak lines, more extensive results on cross sections and f values, and more detailed observational results on weak lines, particularly their center-limb variation on the solar disk. We have mentioned in Chapter 4 our hopes that the first two aspects may be attacked through joint programs now underway. The Sacramento Peak Observatory has commenced a program of photoelectric photometric reproduction of the Utrecht Atlas at a number of positions across the solar disk. From this, and specific, high-resolution, investigations of individual lines, we hope that adequate material for detailed analysis may ultimately be avialable.

B. Comment on the Ca^+ H and K lines

1. Over-All Characteristics of the Approach. We have used the observed form of the profiles of the Ca^+ H and K lines in Chapter 4 as an a priori exhibit attesting simultaneously the presence of a non-trivial rise in T_e in the low chromosphere, and the verification of the general form of a collision-dominated S_L predicted for a resonance line. The same general conclusion could have been based on the observed form of the Mg^+ lines at λ2800, which again typify the collision-dominated S_L, and on the observed form of Ly-α of hydrogen, which typifies the intermediate class of S_L. All these lines exhibit self-reversed emission cores; the Ly-α differ from the Ca^+ and Mg^+ lines in having the emission core rise above the intensity in the adjacent continuum. The significant aspect of any theory of these lines is the possibility of interpreting the observed line profile to fix in more detail the atmospheric structure. Thus, although the general form of all these lines with respect to the self-reversed cores is the same, the details of these cores and of the differential behavior must be analysed.

We emphasize that the combination of a thermally redistributed radiation field in the line with collisional excitation to fix intensities in the core of the line is not novel to our recent systematic attempts to discuss these lines. (In this section, "our" refers to the series of papers entitled *The Source-Function in a Non-Equilibrium Atmosphere*, by J. T. Jefferies and Thomas.) It is implicit in the reformulation of the non-LTE equations of statistical equilibrium to include collisions, discussed in Chapter 4 (Giovanelli, 1948, et seq., Thomas, 1948, et seq.). The earliest explicit application to Ca^+ of which we are aware is that by Miyamoto (1947; 1953; 1954a, b, c, d, e; 1955; 1958). However, the emphasis in Miyamoto's work lies on the emission peak arising from a combined effect of assumed noncoherent scattering in the core and assumed coherent scattering in the wings. No attempt is made to discuss the character of the emission core in terms of either absolute value or gradient of T_e in the chromosphere; the amplitude of the K_2 emission peak is taken to be fixed by the value of T_e at the photosphere-chromosphere boundary. Miyamoto has also discussed hydrogen Ly-α from this same standpoint (1951, 1953, 1954), as have Giovanelli (1949), Jefferies (1953), Giovanelli and Jefferies (1954), and Athay and Thomas (1957).

These discussions of Ly-α include consideration of a chromospheric value of T_e in the region of the core formation, but not of the gradient of T_e. In essence, these investigations of Ca$^+$ and Ly-α treat isothermal atmospheres in the region of the K_2, K_3 core formation, and the equivalent of a one-point quadrature when non-coherence has been introduced into the scattering. Thus, the interrelation between the scale of the radiative diffusion and the scale of T_e variation has been suppressed.

We wish to emphasize the characteristics, and particularly the presently existing limitations, of our attempt to extend the analytical framework for interpreting these lines. We have tried to explicitly compute the frequency-dependence of S_L, then to obtain explicit algebraic expressions for the factors entering $B_\nu(T_{\text{ex}})$, and finally to introduce a quadrature scheme on the scattering term that can be explicitly used to relate diffusion and T_e gradient scales. Our results on the frequency-dependence begin to become quite uncertain in just that region of the profile where an analysis ignoring T_e gradient would place the K_2 peak. Our computations on $B_\nu(T_{\text{ex}})$ rest, at the moment, on a two-level atom. The extension of these discussions by the "equivalent two-level atom" developed in Eqs. (4-85)–(4-87) are at this writing only rudimentary. Finally, we have thus far investigated in detail only the third approximation to the quadrature, and a Doppler absorption coefficient, which carries us essentially through the Doppler core. Thus, practically, an extension of the quadrature and an inclusion of the damping wings are completely bound up with an extension of the region over which we have explicit results on the ν variation of S_L.

Finally, before summarizing the approach to these emission cores thus far developed, it should be remarked that the work by the several authors mentioned above, incomplete as it is, seems most often to have been ignored or overlooked. Compare the discussions of the chromospheric model by McMath et al. coming from an initial analysis of high-dispersion observations, summarized in earlier sections of this chapter. Compare also the various discussions of the Wilson-Bappu observations of the separation of the emission wings of Ca$^+$, where the line profiles are variously treated as though they are formed in optically thin layers, $S_L = B_\nu(T_e)$, and it is assumed that the only parameter influencing the position of the emission wings is the profile of the absorption coefficient (Wilson, 1957;

Hoyle and Wilson, 1958; de Jager, 1958; Kraft, 1958; Schatzman, 1958). Even when the necessity to treat the core as being formed in a thick atmosphere is stressed (Goldberg, 1957), the same critical analysis is not applied to the behavior of S_L which the scattering term alone would introduce. For example, it is assumed that S_L (or T_{ex}) must be the same for the H and K lines at a given point in the atmosphere because the energy-level separation is small (Goldberg, Mohler, and Mueller, 1959). Yet note, from Chapter 4 (or any of the other treatments which include scattering), that for large r_0 and an isothermal atmosphere, $S_L = S_L(\tau_0; \epsilon)$. Since the inelastic cross sections for H and K are presumably in the ratios of their f values, ϵ will be the same for the two lines. Then, at a given point in the atmosphere, τ_0 will differ by a factor of 2 for the two lines; so S_L will differ by whatever amount corresponds to a change in τ_0 by the factor of 2, the amount being a function of τ_0. (On this point see note 9-3 in Appendix II.)

2. Summary of Preliminary Results on Ca$^+$ H and K. What we want to stress is the comparative behavior of the emission core in an atmosphere where the line core is formed in an isothermal region, and in an atmosphere where the range of optical depth covered by the line core ($0 \lesssim \tau_0 \lesssim 10^4$) spans a non-trivial range in T_e. For this purpose, we consider a T_e distribution given by Eq. (4-93), with $A = c = 0 = \beta$ corresponding to the isothermal chromosphere. We note that $r_0 \sim 10^{-8}$ for Ca$^+$ H and K, and $\epsilon \sim 10^{-16}n_e$ for $f_{12} = 1 = \bar{Q}_{12}$. Jefferies's computations give $\bar{Q}_{12} \sim 10$ (1954), more recent work by van Regemorter and Seaton give about a factor of five higher (private communication). We summarize the Jefferies and Thomas (1960) analysis.

Consider the isothermal case. Then Eqs. (4-94) and (4-95) and the discussion in Chapter 4 centered on the case $r_0 = 0 = c = A$ gives

Line center: $$S_L(\tau_0 \sim 0) \sim S_1\epsilon^{1/2} \tag{9-77}$$

S_L(max) occurs at $\tau_0 \sim k_3^{-1} \sim (0.1\ \epsilon^{1/2})^{-1}$

or

$$\Delta\lambda/\Delta\lambda_D \sim (2.3\text{–}0.5 \ln \epsilon)^{1/2} \tag{9-78}$$

of size $S_L(\max) \sim S_1$. That is, the important characteristics are that the amplitude of the emission maximum is $B_\nu(T_e)$ in the chromosphere, and the ratio of values at line center to maximum is about $\epsilon^{1/2}$. Thus, the observed K_2 maximum of about 10 percent of the continuum would, if the isothermal case actually applied, require $T_e \sim 4300°$ at $\tau_0 \sim k_3^{-1}$, and a central intensity of something like 10^{-3} the continuum. This is the essence of Miyamoto's result (1954e). As already emphasized, we see that the essential physics of the K_2, K_3 transition is fixed by the diffusion parameter k_3. The eventual fall from the K_2 maximum is fixed entirely by the temperature profile in the atmosphere, and effects of T_e gradient and diffusion are completely uncoupled. (Up to the extent of our neglect of the ν dependence of S_L and the damping wings outside the Doppler core.)

In the actual solar atmosphere, we note that we have in Chapter 6 set the region of T_e(min) at somewhere $10^{-2} < \tau_5 \overset{\sim}{<} 10^{-5}$; and we have a region of abrupt T_e rise near $\tau_{\mathrm{Ly-C}} \sim 1$ to 10^2. Thus in the region of T_e(min), $10^6 \overset{\sim}{<} \tau_0(\mathrm{Ca}^+$, H and K) $\overset{\sim}{<} 10^3$. For an H : Ca abundance of about 10^5, and assuming Ca mainly singly ionized, we estimate $\tau_0(\mathrm{Ca}^+) \sim 1$ to 10^2 in the region of the abrupt rise in T_e. This estimate is in reasonable agreement with Zirker's estimate, quoted in Section 9-IIIA, of 2000 km as the height of $\tau_0 \sim 1$ for these lines. (These estimates refer to the non-spicular regions.) Thus, the rise from T_e(min) would suggest that for "average" regions of the solar atmosphere we should consider values $10^{-6} \sim c \sim 10^{-3}$, and $A \sim 20$ if $S_1 \sim B_\nu(4750°)$. In the region of the jump, $1 \gtrsim c \gtrsim 10^{-2}$, and $A \sim 10^3$ for the same S_1, would be suggested. These results from Chapter 6 would suggest that we must consider a region where $c > k_3$, and where c may indeed be quite large. Actually, we should probably consider a distribution of T_e of the form

$$B_\nu(T_e) = S_1(1 + A_1 e^{-c_1\tau_0} + A_2 e^{-c_2\tau_0}) \tag{9-79}$$

which leads, for the case r_0 very small, and neglecting β,

$$S_L = S_1 \frac{\epsilon}{\epsilon + \eta} \left\{ 1 + A_1\sigma_1(e^{-c_1\tau_0} + \Sigma L_j e^{-k_j\tau_0}) \right. \\ \left. + A_2\sigma_2(e^{-c_2\tau_0} + \Sigma L_j e^{-k_j\tau_0}) + \frac{\eta B^*}{\epsilon S_1}(1 + \Sigma L_j e^{-k_j\tau_0}) \right\} \tag{9-80}$$

$$\left\{A_1\sigma_1 + A_2\sigma_2 + \frac{\eta B^*}{\epsilon S_1}\right\}\left\{\sum \frac{L_j}{1 - k_j/x_i} + 1\right\}$$
$$= -\left\{1 + \frac{A_1\sigma_1 c_1/x_i}{1 - c_1/x_i} + \frac{A_2\sigma_2 c_2/x_i}{1 - c_2/x_i}\right\} \quad (9\text{-}81)$$

and the σ_i, s_i are defined as in Eq. (4-113), etc.

Such a situation includes the case $c > k_3$ as a possibility, and we see that the $A_i\sigma_i$ may have values numerically much less than A_i. For example, we have the following values of σ for various values of $(\epsilon + \eta)$ and c:

c	10^{-5}	10^{-3}	10^{-2}
$\epsilon + \eta = 4 \times 10^{-5}$	1.0008	−0.440	+0.00517
$\epsilon + \eta = 10^{-6}$	1.010	−0.00977	$+1.05 \times 10^{-4}$

We picked the values of $\epsilon + \eta$ as corresponding, respectively, to Ly-α and to a lower limit for Ca$^+$ on the basis of the figures given above. Under these conditions, we can drop the ratio of $S_L(\max)/S_L(\tau_0 \sim 1)$ from $\gtrsim 10^2$ to $\lesssim 5$ as c increases from 10^{-5} to 10^{-2}, for $A \sim 10^3$. Likewise, $S_L(\max)$ drops from a value near $B_\nu(T_e)$ to up to several orders of magnitude below $B_\nu(T_e)$. The actual values, however, depend upon the particular values of the parameters.

Further discussion is, at this point, unwarranted by the theoretical analysis thus far performed. We see that there is a hope, from a detailed analysis of the line profile, paying particular attention to the three parameters $S_L(\max)$, $S_L(\max)/S_L(\tau_0 \sim 1)$, $\Delta\lambda(\max)/\Delta\lambda_D$, to further fix the conditions *within and near* the regions of rise in T_e. Further, we have hopes that we may use the differential behavior of the Ca$^+$ profiles over plages, sunspots, and the normal disk to fix the characteristics of the T_e structure and distribution of opacity in these regions. (cf. E. v. P. Smith, 1960; in addition to the discussion by Jefferies and Thomas, 1960). Particularly, we hope that we may use the combined behavior of Ca$^+$, the Mg$^+$ lines, and Ly-α over the disk as a whole to add information on the behavior of the T_e gradient in the region of the steep rise, noting that we might expect Ly-α, Mg$^+$, Ca$^+$ to form a sequence of decreasing opacity at given height. Thus, we obtain a range of c values from these lines. Such efforts are currently in progress as part of the *source function* series cited.

Finally, we note relative to our classification scheme of source functions, that the collision dominance and photo-ionization dominance must be considered in terms of the ratio $\eta B^*/\epsilon B_\nu \sigma_1$, from Eqs. (4-111) and (9-80), which increases the range of situations over which ηB^* must be considered.

3. Comment on Ly-α Emission Core Relative to That of Ca$^+$ H or K. The comment echoes that made for Ca$^+$; viz., one cannot neglect the T_e gradient when trying to interpret the Ly-α profile in terms of atmospheric structure. The details underlying it are, however, more readily seen for Ly-α because of our detailed discussion of the behavior of hydrogen in various parts of the atmosphere. From our discussions in Section 6-IIIA3 and Section 9-IIA1 we have already estimated that the transition from detailed balance to non-detailed balance in Ly-α occurs in a region of rapid rise in T_e, near $\tau_0(\text{Ly-}\alpha) \sim 10^3$. We have already mentioned in Chapter 4 that Ly-α falls into the intermediate category of S_L, with the relative importance of the collisional and photoionizational terms being strong functions of Lyman opacity and T_e. Indeed, the values of b_1, b_2 found in our discussion of the ionization equilibrium of hydrogen—Eqs. (4-41) through (4-48) and Pottasch and Thomas (1959)—under conditions of detailed balance in the Lyman lines, together with the discussions in Chapters 6 and 9 just mentioned, illustrate this behavior in detail. In the three regions defined in Eqs. (4-41) through (4-48), we have (in the notation used there):

Region 1: high local opacity in Lyman continuum:

$$S_L \sim B_\nu(T_e)(1 + M) \tag{9-82}$$

Region 2: transfer problem in Lyman continuum critical:

$$S_L \sim (1 + \Delta)B^* \tag{9-83}$$

Region 3: $P \ll 1$:

$$S_L \sim \epsilon B_\nu(T_e)/\eta \tag{9-84}$$

In the discussion in Chapter 4, we did not prove that the conditions for Region 3 were attained while detailed balance in the Lyman lines still holds. If detailed balance fails, we multiply the expression for region 3 by the factor $(1 + \eta^{-1}(\text{NRB})_{1,2})^{-1}$, thus enter the region where the transfer problem in the lines must be solved. Then, we simply proceed via Eq. (4-90) and the various solutions already discussed. Thus, not only the details of the behavior of S_L depend upon the distribution of T_e, as in the case of Ca^+; but also the character of S_L according to our classification scheme, which differs from the case of Ca^+.

This conclusion can be supported from observations of Ly-α itself, in the same manner as we concluded from $S_L(\tau_0 \sim 0)$ or $S_L(\max)$ of Ca^+ that the isothermal-atmosphere case was inadequate. Values of ϵ, η, and B^* can be computed from Eqs. (4-89) through (4-91), and have, indeed, already been used in discussions in the earlier sections cited above. The greatest uncertainty arises from the value of Y_1—the intensity in the Lyman continuum—which enters linearly in η and exponentially in B^*. The uncertainty arises because $\tau \sim 1$ at the head of the Lyman continuum comes in the vicinity of the steep rise, as we saw in Chapter 6. From the results in Table 6-10 and the accompanying discussion, we would estimate $6000° \lesssim T_{\text{rad}}(\nu = \nu_1) \lesssim 7000°$, $22 \lesssim Y_1 \lesssim 26$; so the uncertainty in η is small but that in B^* is an order of magnitude. We have (see note 9-4 in Appendix II)

$$\epsilon \sim 1 \times 10^{-6}(10^{-11}n_e) \text{ for } 1 \lesssim 10^{-4}T_e \lesssim 4$$

$$\eta \sim 4 \times 10^{-5}$$

$$B^* \sim (2h\nu^3/c^2)(e^{-16} \text{ to } e^{-20})$$

Thus $\epsilon < \eta$, and for $T_e \gtrsim 2 \times 10^4$, $\epsilon B_\nu > \eta B^*$. For the isothermal case, we have the same kind of result as given by Eqs. (9-77) and (9-78) for Ca^+, with the change occassioned by $\eta > \epsilon$ rather than $\epsilon > \eta$, viz.,

$$S_L(\tau_0 \sim 0) \sim (\epsilon S_1/\eta)\, \eta^{1/2} \tag{9-85}$$

$$S_L(\max) \sim \epsilon S_1/\eta \tag{9-86}$$

The various values of T_{rad} observed for Ly-α seem to be converging on a "mean" value near 7500° in some kind of an average over the central core. If this value corresponds to $S_L(\max)$, then even if $n_e = 10^{10}$, $T_e \lesssim 1.2 \times 10^4$; if to $S_L(\tau_0 \sim 1)$, $T_e \lesssim 2.5 \times 10^4$. And, the ratio $S_L(\max)/S_L(\tau_0 \sim 1) \sim 10^2$. This combination of values is completely incompatible with the results in Chapter 6, and variations on the model in subsequent chapters. Thus, we again conclude that we must discuss a solution of $S_L(\tau_0)$ that covers such a range of conditions as to permit a coupling between terms describing the gradient in T_e and those describing the radiative diffusion. (On this point see note 9-5 in Appendix II.)

As a second comment on Ly-α, we want to emphasize the distinction between the basis upon which we have here concluded that the T_e gradient must enter critically in an interpretation of the Ly-α profile, and the basis for a similar conclusion by Goldberg (1954), which we have criticised (Athay and Thomas, 1956). Goldberg bases his conclusion wholly upon the observed narrow profile of Ly-α, a total width of the order 1A separating regions where $T_{\text{rad}} \lesssim 4600°$. Goldberg's detailed conclusion is considerably more extreme; for he asserts that the Ly-α data require a model of the Woolley-Allen prototype, viz., T_e constant with height from the top of the photosphere to about 4000 km (with a value $\sim$ 4600°) rising to about 6000° at 6000 km, and thereafter rising abruptly to coronal values. On the Woolley-Allen kind of model, which Goldberg supports, hydrogen is about half-ionized at the 6000° level.

The fundamental difference between the basis for our conclusions and that used by Goldberg lies in our explicit attempt to relate T_{ex} to the thermodynamic and opacity structure of the chromosphere, and Goldberg's implicit identification of T_{ex} with T_e. Although he defines the source function used in his discussion as $B_\nu(T_{\text{ex}})$, it is, of course, a truism to say that a sharp profile requires a gradient of T_{ex}; so he implicitly identifies T_{ex} with T_e, and both with T_{ion} of hydrogen, in discussing the relation between line profile and the Woolley-Allen model. We want to emphasize this point here very strongly; for the literature is becoming increasingly characterized by discussions that start out in terms of an attempt to allow for non-LTE effects by expressing results in terms of T_{ex}, T_{ion}, etc., then implicitly identifying either these quantities with the value of T_e or their gradient with the gradient of T_e. Although in many cases the gradient of T_{ex} does have the same sign as that of T_e, this is not at all generally true as we have demonstrated in our discussion of $S_L(\tau_0;\, \epsilon,\, \eta,\, B^*,\, c)$. In the particular case of Ly-α, the expressions (9-82) through (9-84) are particularly useful to ponder over when asking the implications of a narrow profile.

Further discussion of Ly-α should consist of a detailed analysis of a high-resolution (to something near 0.01 A) profile; we must defer this discussion for no such data are available to us. (On this point see note 9-5 in Appendix II.)

CHAPTER 10

Summary Comments on the Chromospheric Model

R. N. THOMAS AND R. GRANT ATHAY

In this monograph we have discussed the current state of two parallel investigations: a development of an analytical methodology for the treatment of a gaseous atmosphere in a spectroscopically steady, but not necessarily LTE, state, and an analysis of observational data to infer the thermodynamic state of the solar chromosphere. As outlined in the introductory chapter, this parallel treatment reflects an attempt to test the assertion that non-LTE effects are of major consequence in interpreting stellar line spectra, by applying this methodology to the particular case of the solar chromosphere where the classical approach to stellar atmospheres has led to seeming anomalies. Thus a summary of the preceeding nine chapters has two aspects to consider: (1) the stage of sophistication reached in the development of the analytical methodology, and (2) the over-all model that has thus far emerged for the solar chromosphere.

We have, in Chapter 4, already gone into considerable detail on the state of development of the non-LTE methodology, its present limitations in terms of unknown cross sections and unexplored analytical development, and the most promising directions of current investigations. In succeeding chapters, we have again re-emphasized each of these points in making specific application of the general methodology. Any kind of further detailed summary of the state of development of the methodology would seem redundant. We only note, in an over-all way, that the severest limitations on the theory thus far developed, consequently the immediate directions for extension, are fourfold.

1. We have neglected terms contributed by the divergence of the velocity field in setting up the equations of statistical equilibrium.

The neglect is likely to be of most consequence in regions of sharp gradients in thermodynamic variables.

2. We have not investigated the frequency dependence of the source function outside the Doppler core of a line, and its relation to the order of the Gaussian quadrature used in the solution to the transfer equation. The same is true with regard to the proper inclusion of Stark broadening, particularly for the higher Balmer lines.

3. We must ask how far the "equivalent-two-level-atom" approach may be pushed in delineating the terms that are most influential in S_L for an arbitrary line. This question is particularly important in asking about non-LTE effects in the weaker Fraunhofer lines, thus in extending the theoretical background to encompass the great bulk of lines treated in conventional analyses of solar and stellar spectra to obtain relative abundances of elements.

4. We must investigate the solution of the non-LTE problem in a non-spherically symmetric atmosphere, which emphasizes even further the problem of the coupling between radiative diffusion and thermal gradient terms stressed in Chapter 9. Such a solution must also underlie a proper treatment of spicules and prominences.

Our attention in the remainder of this summary chapter focuses upon the chromospheric model. In the detailed discussions accompanying the analysis of each of the individual kinds of data, we have tried carefully to distinguish between uncertainty in derived characteristics of the model arising from incompleteness in analytical methodology, and that arising from incompleteness of data. Such a distinction automatically highlights any properties of the model that depend only slightly upon the non-LTE effects. In this summary chapter, we want to draw together the various characteristics of the model, implied by the several kinds of data, into one overall picture, again emphasizing the uncertain aspects in terms of either weakness of methodology, or incompleteness of data, or both. We emphasize four aspects: (1) distribution of T_e and mass, (2) distribution of absorbing material, (3) deviations from spherical symmetry, and (4) the question of energy supply. With regard to the last, we emphasize that we have not tried, in this monograph, to identify the non-radiative energy supply, only to establish whatever requirements were indicated by the analysis. We have adopted this attitude because, on the one hand, we do not feel that the properties of the possible systems of non-radiative energy supply have as yet been sufficiently well established, either empirically or theoretically. On the other hand, we do not feel that computations of the net radiative emission have as yet been carried out in sufficient detail to balance radiative output against non-radiative input. We believe that the approach developed in Chapter 4 via the NRB and illustrated in several places in the monograph offers the best solution to the latter problem.

We summarize the model according to regions of increasing height in the chromosphere, each region being characterized by some physical property of the region or aspect of the analysis.

$-500\text{ km} \lesssim h \lesssim +500\text{ km}; \qquad 0.02 \gtrsim \tau_5 \gtrsim 10^{-5}; \qquad \tau_{\text{LyC}} \gtrsim 10^4$

This is the region of the sharp solar limb, as observed in the optical spectrum. In this region, the distribution of T_e is virtually unknown to the accuracy we require. We can be certain of two conclusions only. First, $T_e(\text{min}) \lesssim 4750°$, and occurs somewhere within this region. Second, at the top of the region, $T_e \sim 6100°$. Thus, the significant aspect of the thermal structure that we are able to establish is a minimal rise of some 1500° above the value that would result in the absence of a non-radiative energy input. In consequence, the non-radiative energy supply must already be significant at these heights. To say how significant, we require proper solutions of the transfer equation, using correct values of the relevant source functions, to provide accurate values of the NRB for all spectral regions where radiative dissipation is likely to be of importance.

From our summary in Chapter 6, it is evident that the various analyses of disk observations of strong lines to suggest inhomogeneities in T_e within this region are largely inconclusive, as attested both by their neglect of non-LTE effects and the contradictory results among the several analyses.

The uncertainty in mass distribution essentially reflects that in T_e, since our theory for b_1 of hydrogen in this region shows it to be order-of-magnitude unity. The concentration of hydrogen at the top of the region seems fairly well fixed at $\sim 1 \times 10^{14}$. In the same way, the uncertainty in the distribution of opacity reflects the uncertainty in T_e—directly, for the singly ionized metals; and indirectly, through the uncertainty in n_e and n_i, for the neutral metals.

To fix more precisely the thermodynamic structure of this region, two kinds of investigations are needed. On the one hand, data with good height resolution in the Balmer and Paschen continua throughout the entire height range would permit the kind of analysis discussed in Chapter 6. On the other hand, an extension of the non-LTE theory to the Doppler cores of subordinate lines of the singly ionized metals, and outside the cores of the resonance lines, will permit the use of high-resolution disk data to cover this region. Use of the neutral metals is less promising, for the reasons discussed in Chapter 9.

The use of the CN emission bands may clarify some aspects of the structure in this region (Pecker and Athay, 1955; D. V. Thomas, 1958). At heights of 0, 50, and 400 km (but with large uncertainty in these height determinations), D. V. Thomas obtains rotational temperatures for the $\lambda 3883$ band of $\sim$7500°, $\sim$5000°, and $\sim$4500°, respectively, after making rather crude corrections for self-absorption under the assumption of LTE. On the other hand, Pecker and Athay assume that self-absorption is negligible and obtain an outward increase in rotation temperature, starting from a value of $\sim$4500° at $h = 100$ km. While Thomas's data are considerably superior to those used by Pecker and Athay, and while he rather clearly demonstrates that there is an observable effect from self-absorption, his rotation temperature of 7500° cannot be accepted without extreme reservation. Such a value for the rotation temperature can occur only if there exists either a radiation temperature or kinetic temperature of equal or greater magnitude. No evidence for either such temperature exists.

The absolute intensities in the CN bands provide a further argument against the 7500° value. Pecker and Athay found, on the basis of our earlier model (Athay, Menzel, Pecker, Thomas, 1955), a predicted intensity falling below the observed intensity by a factor of 20. Because of the low dissociation energy of CN, a value of $T_e \sim$ 7500° near $h = 0$ would result in almost complete dissociation, and a much larger discrepancy between predicted and observed intensities. It seems to us more likely that the rotation temperature lies nearer 4500° at $h \sim 0$. The problem must be re-analyzed, with serious thought given to possible influence of non-LTE effects.

Because of the uncertainty in height to which D. V. Thomas's work applies, and because of the large probable errors in the rotation temperatures obtained by Pecker and Athay, it is difficult to say much from comparison of these results on rotation temperatures of

CN with T_e from the model of Chapter 6. Particularly, this is true, because of the uncertainty in the T_e model in this region $-500 < h < +500$. We emphasize only the possibility that further analysis of CN, including the possibility of non-LTE populations in the rotational electronic states—and possibly departure from spherical symmetry in these atmospheric regions—may give important information on this height range.

500 km $\lesssim h \lesssim$ 1000 km.; $10^4 \gtrsim \tau_{\text{LyC}} \gtrsim 10$; $10^2 \gtrsim \tau_{\text{H}\alpha} \gtrsim 10$

In this region, under the assumption of spherical symmetry, T_e is well-determined, increasing from ~6100° to a value near 8000°, where it rises very rapidly to something in excess of 2×10^4 in the next atmospheric region. The value near 8000° is not well-determined, primarily for two reasons. First, we need a good description of the behavior of the state of the material through the region of abrupt rise and immediately above it, in order to tie down the optical opacities upon which the theory depends. Second, the existing non-LTE theory *may* require significant correction in the vicinity of such abrupt rises in T_e and attendant changes in density. There seems little question, however, that in the region 1000 to 1200 km, T_e and its height gradient reach such values that a very steep rise occurs.

The most significant aspect of this required abrupt rise in T_e is its occurrence in an analysis of data carried out under the assumption of a spherically symmetric atmosphere, and in precisely the height range where emission from helium first appears. This result is the really significant modification by the present analysis over the results of our preliminary analysis of a few years back. The major analytical modification introducing this change is a proper treatment of the ionization of hydrogen in this region of large Lyman continuous opacity. In the preliminary analysis, we simply assumed $b_1 = 1$. The effect of $b_1 \neq 1$ is a very considerable steepening of the gradient of T_e everywhere in the region 500 to 1000 km, leading to the conclusion of an abrupt rise near 1200 to 1000 km.

The greatest uncertainty on the values of T_e below the region of abrupt rise lies in the assumption of spherical symmetry—whether there may not be in fact a significant horizontal gradient in T_e. If, for example, the spicule system is one of superthermic jets traversing this region, and if the spacing of the spicules is large compared with their diameter, we should expect horizontal gradients in T_e over the interspicular region. Within the spicule itself, T_e would be strongly coupled to the dynamical state of the spicule, so should differ from T_e in the surrounding atmosphere. We are currently investigating the properties of such a configuration. If, on the other hand, the mechanical energy source is distributed more or less homogeneously through the atmosphere, and its own *structure* is not a major perturbation on the thermodynamic state of the ambient atmosphere, we might expect a more uniform horizontal distribution of T_e.

We might hope to explore a differential behavior of the metallic lines to investigate such a possible horizontal gradient in T_e. Zirker's attempt along these lines (1956) indicates the ambiguities arising in the absence of a satisfactory knowledge of non-LTE effects. Thus, just as in the question of using disk spectra to supplement the analysis of the next-lower atmospheric region, the primary problem to be overcome lies in extending the non-LTE methodology to, and determining the necessary cross sections for, the whole range of subordinate metallic lines, particularly those of the singly ionized configurations.

We might expect that the result showing hydrostatic equilibrium to be satisfied to the accuracy of the data would give some clue to the question of possible inhomogeneity in this region. The fact that our earlier, preliminary analysis reached the same conclusion on the adequacy of hydrostatic equilibrium, yet gave a considerably different distribution of T_e, does not in itself indicate the results on hydrostatic equilibrium to be insensitive to atmospheric structure. As already emphasized, the continuum data by themselves essentially fix only the distribution of $n_e n_p T_e^{-3/2}$ and of n_{H}, the last of which provides the test of hydrostatic equilibrium. Only by adding the theoretical relation $b_1(T_e,\tau_{\alpha r})$ can we infer a distribution of T_e from these two sets of parameters; the change in distribution of T_e in the two analyses reflects the use of this theory for b_1 to replace the assumption $b_1 = 1$. Thus, the validity of the condition of hydrostatic equilibrium does give information on homogeneity of atmospheric structure. It states that there is no significantly large momentum supply in the atmosphere, for $h \lesssim 1000$ km. In particular, the non-radiative energy supply, whatever it is, can contribute only negligibly to the momentum balance of the atmosphere. If we were to look for such a non-radiative energy supply in the form of a system of macroscopic mass motion, the velocities associated with the system must be superthermic. The condition of negligible momentum supply thus would require the mass in the system to be small relative to that of the atmosphere as a whole. Thus, the presence of such a system would give only negligibly small inhomogeneity, for $h \lesssim 1000$ km.

1200 to 1500 km $\lesssim h \lesssim 4000$ km; $\tau_{\mathrm{LyC}} \lesssim 10$; $\tau_{\mathrm{Ly}\alpha} \lesssim 10^3$ to 10^4

As we have already stated, the greatest uncertainty lies in the transition from the preceding region to this one; the next greatest lies in the gradient of T_e within this region. Until the distribution of T_e in the region above the abrupt rise has been fixed, one cannot describe the distribution within, and just preceding, the transition region because of the strong opacity effects within the hydrogen Lyman region. Thus, the procedure is an iterative one, requiring as the next step a reasonably good model above the abrupt rise, then a return to a re-analysis of the region immediately preceding and in the abrupt rise. The He spectrum, as analysed in Chapter 7, provides at present our only quantitative results on T_e in the region above the rise. The analysis of HeI suggests $T_e \sim 4$ to 5×10^4 in the interspicular component, with no indication that presently available data will give a value for the gradient of T_e from the methodology that has been used. A refinement of this determination of T_e awaits the completion of the wholly self-consistent treatment of the NRB for HeI, discussed in Chapter 7. With the results of this solution available, one may ask again into the possibility of obtaining the gradient of T_e.

We have made no direct evaluation of T_e within the spicular component other than the rough estimates from the radio data. The *presumption* is, that T_e lies below the upper limit of some 11,000° set by stability arguments. It would appear that a determination of T_e within the spicular component must await the development of an approach to treating the spectroscopic state of whatever kind of an aerodynamic configuration the spicule represents.

A direct determination of conditions within and near the rise, as well as the gradient of T_e in this atmospheric region above the rise, may result from current attempts at the analysis of the Ca^+, Mg^+, and Ly-α of hydrogen self-reversed emission cores. An analysis of the Ca^+ material is also of particular interest with respect to the possibility of more directly determining the details of the inhomogeneous structure in this height range 1200 to 4000 km. We have already commented on this possibility for the use of the early Balmer lines, in Chapter 9. That is, we note that the emission from the spicules in the next height range, $h \gtrsim 4000$ km, consists essentially of lines from He, Ca^+, and the early Balmer lines, and that the thermal structure of the spicules in this height range presumably lies close to that of the He-emitting component at $h \lesssim 4000$ km. We also obtain Balmer and Ca^+ emission from the non-He-emitting component at the lower heights. Thus, a theoretical discussion of the expected emission from the "hot" and "cold," and possibly "diffuse" and "dense" components may clarify the inhomogeneous structure. In this connection, as we have already emphasized in describing the spicule observations above 4000 km in Chapter 3, it is not at all clear that the spectroscopic state can be treated wholly removed from considerations of the aerodynamic (including of course hydromagnetic) configuration.

The most important structural question to be clarified in this atmospheric region [and this also bears heavily on the question of the non-radiative energy source(s)] is that of the significance of the cooler component. Do we identify it with the spicules observed at $h \gtrsim 4000$ km? If so, do the spicules extend downward into the regions $h \lesssim 1200$ km, having the character of supersonic jets, as we suggested several years ago [Thomas (1948a, 1950c)]? Or, do the spicules somehow originate in the region of abrupt rise in T_e, reflecting the radiative instability of this region? We recall that our original suggestion (Athay and Thomas, 1956) on the onset of the abrupt rise in T_e associated with the instability was offered as an alternative to Parker's suggestion (1953) that the instability resulted in a collapse of material to a configuration of higher density, possibly associated with formation of a prominence. If we could show that such a collapse might occur in at least part of the material, and result in an outward acceleration either directly or by coupling with some other phenomenon, we might have a possible origin for the spicules in this region of instability. We would then have a natural division into two chromospheric components according to the reaction of the material to the onset of instability; either an abrupt rise in T_e and a quasi-static configuration, or a collapse to increased density and an outward acceleration. These remarks are wholly speculative, intended only to focus attention on the apparently-simultaneous onset of inhomogeneity and abrupt rise in T_e. We also note, of course, that the apparent onset of inhomogeneity may simply reflect a rapid drop in density of the interspicular medium, thus an increased *relative* mass in the spicule component. Such a drop in density must accompany the abrupt rise in T_e, unless justification for an outward increase in pressure is introduced. These alternatives on the kinematic configuration of the spicules, and their relation to the non-helium-emitting regions below $h \gtrsim 4000$ km, must be investigated in detail.

$h \gtrsim 4000$ km

The observational characteristic defining this region is the concentration in spicules of all line emission found in the visible spectrum—with the exception of that from highly ionized metals, which is usually associated with the corona. Our fixing the boundary of this region at $h \sim 4000$ km is somewhat arbitrary. From the discussion in Chapters 2 and 3 based on Dunn's extensive observations, one can only say that the region probably does not extend as low as 3000 km and rarely begins above 4000 km. Although it has occasionally been asserted that the structure of the spicules differs when viewed in different lines—thus raising the possibility of a less-simple division than spicular and interspicular regions—our own observations summarized in Chapter 3 lead us to conclude that there is no observable difference in the spicule structure observed in H, He, and Ca^+.

There are two aspects to a characterization of the thermal structure of this region: T_e within the spicules, and the relative T_e between spicular and interspicular material. In a rough way, the similarity of emission from spicules and from what we have identified as the He-emitting regions at $h \lesssim 3000$ to 4000 km leads us to infer a similar thermal structure for these two regions. We have summarized in Chapter 3 the direct attempts to infer T_e in the spicules, which lead to the same conclusion, that $T_e \approx 4$ to 5×10^4 °K. Without detailed observations of the coronal-line emission with good height resolution, or without observations in the "rocket" ultraviolet, we cannot proceed to a direct quantitative evaluation of T_e in the interspicular medium. Our summary in Chapter 2 suggests that the emission from FeXI extends as low as 7000 to 8000 km, much lower than previously accepted; we would only raise the question whether, indeed, it extends to the boundary of this region $h \gtrsim 4000$ km. These are the only quantitative data available.

For completeness we should note here that the question as to whether the self-reversed profiles of strong lines refer only to the emitting region and not to the enveloping medium is not completely settled. The viewpoint we have adopted in Chapter 4 and Chapter 9 would interpret these self-reversed cores as coming wholly from the regions of low optical depth at the outer boundary of the emitting regions—i.e., the spicules in the present instance. Michard (1959) argues that the asymmetry of the self-reversed cores suggests that, on the contrary, a better first approximation is to choose a constant source function within the spicule and attribute the self-reversed cores to the enveloping medium. He is then led to a Woltjer-type model (1954) of 'hot' spicules in a 'cold' medium. It is our conjecture—hope is maybe a better word—that when the source-function theory is extended to the case of an atmosphere with differential velocity gradients, such an asymmetry will result. (See further note on this point in Appendix II.) If we adopt Michard's arguments, we are left with the choice as to whether 'hot' or 'cold' refer to excitation or to actual electron temperature. We have difficulty reconciling the former alternative with the direction of change in T_{ex} found in Chapter 9—we would, rather, expect a higher T_{ex} in the interspicular medium. In the latter case, it is hard for us to understand the lack of emission in some line mimicking the spectrum found at lower heights, which spans the range in T_e from $\sim$5000° to 4 to 5 $\times 10^4$. From the standpoint of physical continuity, it is hard to see how the great mass of material would show a minimum of T_e in this region. That is, we have established that the He-emitting component occupies most of the area, at $h \lesssim 4000$ km, and has $T_e \sim 4$ to 5×10^4. In the corona, most of the material has T_e lying above this value. Thus, were the interspicular material cold relative to the spicular, T_e must show this minimum, at heights in the 4000 to 6000 km range. Very candidly, these arguments for a cold interspicular medium seem to us mainly holdovers from the main thesis of the Woolley-Allen model, viz., that T_e in the great mass of the chromospheric material must remain low up to heights $h \sim 6000$ km. Our discussion of the ionization equilibrium of hydrogen removes the physical basis upon which the model was based. Our analysis of the continuum to obtain the general character of the T_e gradient in the low chromosphere destroys the empirical basis for any such maintainance of a photospheric T_e to any significant height. Our analysis of the He spectrum in Chapter 7 presents evidence for the much higher values of T_e in a predominant portion of the chromosphere at quite low heights. We therefore find it difficult to support any belief that the interspicular medium above $h \sim 4000$ km has a T_e lying below the value characterizing the "helium" plateau, and thus a lesser T_e than in the spicule. We would however emphasize that we recognize the burden of the proof to lie on the source-function theory, extended to the case of differential velocity fields, to meet Michard's points on the observed asymmetric self-reversed cores.

The distribution of mass and opacity in both spicular and interspicular media are even less certain than that of T_e. Mainly, the uncertainty centers about the dynamic structure of the spicules, and their relation to the general coronal structure. Two sample calculations illustrate the point. In both, we use the general result that the material density in the spicule seems to be reasonably well fixed at $n_{\mathrm{H}} \sim n_p \sim 10^{11}$ at heights of 4000 to 6000 km.

First, we note that although spicules occupy less than 1 percent of the solar surface, their contribution to the coronal structure still remains to be properly assessed. The outward proton flux in spicules is $A_S N_S n_p V$. From Chapters 3 and 7, we take for the 4000-km level the values: spicule area, $A_S \sim 3 \times 10^{15}$ cm^2; number of spicules, $N_S \sim 5 \times 10^4$; $n_p \sim 2 \times 10^{11}$; $V \sim 30$ km sec^{-1}. Thus, the outward proton flux at this level is $\sim 10^{38}$ protons sec^{-1}. The total number of protons in the corona is of order $\sim 10^{42}$; thus they could be entirely replaced by protons from spicules in about 3 hours. We have computed only the outward-moving component; spicule observations show that about half of the spicules eventually move downward, indicating that much of this material returns directly to the chromosphere. Nonetheless, the role of spicules in the coronal mass balance must be investigated.

Second, in discussing the region $h \lesssim 4000$ km, we have summarized the choice between spicules as phenomena arising near the 1500-km level, where material densities are of the order 10^{11} to 10^{12}, and spicules as phenomena arising at lower regions, where material densities are much higher. If, for example, spicules originate below the base of the chromosphere, where $n_{\mathrm{H}} \sim 10^{16}$, we must find some mechanism permitting a density decrease by a factor 10^5 to reach $n_{\mathrm{H}} \sim 10^{11}$ at the 4000-km level. Either the spicule volume must expand by a factor 10^5, or all but a fraction 10^{-5} of the atoms must be lost by diffusion.

These two computations illustrate the intimate relation between the problems of origin and structure of the spicule, and the relation of the spicule to the mass balance of the upper chromosphere, lower corona. A third illustration arises when we ask into the details of the transition from the value $T_e \lesssim 11{,}000°$ characterizing the non-helium-emitting regions below $h \sim 4000$ km to the value $T_e \sim 4$ to 5×10^4 characterizing the spicules for $h \gtrsim 4000$ km. The transition is either induced by some dynamic property of the spicule which requires a rise in T_e at these heights, or by a heating of the spicule associated with its passage through the atmosphere (the same diffusion mechanism by which spicule atoms may heat the atmosphere, if V is superthermic). Again, the problem has as yet not been investigated; its solution must give information on both mass and energy balance between spicule and atmosphere.

Thus, this monograph closes on a note characterizing our first inquiry into non-LTE effects in the chromosphere some years ago—the relation between spicules and chromospheric structure, indeed—between spicules and the structure of the whole outer solar atmosphere. It must be admitted that we have not made a great deal of progress on the answer to this particular physical question. Indeed, we have not even resolved satisfactorily the basic assumption from which we started those early investigations—that spicules are the non-radiative energy supply for the chromosphere. We have made progress in developing an analytical methodology which will help answer these questions. We have determined considerably more satisfactorily the thermodynamic state of the atmosphere enveloping the spicules, for $h \lesssim 4000$ km. We have linked the spicules to the question of the steep T_e gradient in the low chromosphere, but have been unable to specify whether this link arises from the spicules as the non-radiative energy source producing the T_e gradient, or whether the spicules originate in some association with the jump in T_e climaxing this steep T_e gradient. We would only emphasize that, although the corona manifests itself as a more sweeping phenomenon than the chromosphere, and the prominences as more spectacular phenomena than the spicules, we believe the key to the structure of the outer solar atmosphere, including the corona, lies in the combination chromosphere-spicules, even though we do not know which is the cause and which is the effect.

Appendix I

R. Grant Athay

I. Continuum at λ4700

At each point in a slitless spectrogram the intensity of the continuum results from the contribution of all the overlapping monochromatic images. Each such image is a ring of light, of which the moon's limb fixes the inner boundary, and the radial extent of the corona fixes the outer boundary. Thus, each point on the spectrogram receives light from both sides of the sun as well as from numerous images of one side of the sun. The different solar images correspond to different wavelengths and different heights above the limb with the scale set by the observed size of the solar image on the spectrum. Thus we may express the total continuum intensity at λ4700 as

$$E_T = \int_h^\infty \int_{-\infty}^\infty \mathcal{E}_E \, dy \, dx(\lambda) + \int_{h'}^\infty \int_{-\infty}^\infty \mathcal{E}_w \, dy \, dx'(\lambda) \qquad \text{(A-1)}$$

where subscripts E, W refer to east and west limbs of the sun. In practice, we may introduce some simplifications. Certainly points more than a solar diameter above the limb contribute little. In our spectrogram, a solar diameter corresponds to a difference in wavelength of about 150 A, over which range neither $\mathcal{E}_\lambda$ nor E_λ varies significantly at λ4700. Thus, we may safely ignore the wavelength dependence in Eq. (A-1).

In order to reduce errors arising from local film irregularities, the continuum intensities were also measured at λ4400 and λ4100, and corrected by a constant factor to give best agreement with the intensities at λ4700. The three sets of data were accordant at all heights, and the averages of the three intensities at each height were taken as the final data.

To use the continuum data at λ4700 we must separate the contributions from the two limbs of the sun. The telluric absorption bands in the infrared regions of the spectrum furnish a straightforward means for accomplishing such separation. These bands, which appear as absorption rings, affect the emission from only one side of the sun at a given point on the spectrum. Figure A-1(a) represents a microdensitometer tracing through the O_2 band at $\lambda 7596$. The intensities in this band are measurable over the height range from about 3000 to 48,000 km relative to one limb of the sun. At these heights, electron scattering is the source of the continuum (cf. Chapter 5). In consequence, E_E/E_W is independent of wavelength and a value of E_E/E_W determined at $\lambda 7596$ may be used at $\lambda 4700$ without danger of systematic error.

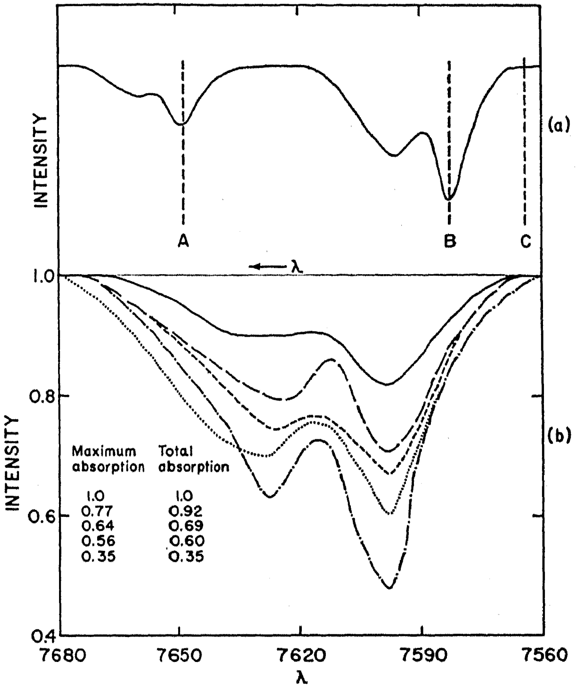

Fig. A-1. The terrestrial O_2 band at $\lambda 7596$ showing (a) the difference in the absorption at the two limbs of the sun and (b) the band profile at several heights.

At each wavelength in the band let k be the percentage terrestrial atmospheric absorption. Now, if we replot a tracing of the continuum on a scale such that the maximum is equal to unity, on both sides of the absorption bands, we have the equations

$$kE_W + E_E = E_a \tag{A-2}$$

$$E_W + kE_E = E_b \tag{A-3}$$

$$E_W + E_E = 1 \tag{A-4}$$

which yield the solution

$$E_E/E_W = (1 - E_b)/(1 - E_a) \tag{A-5}$$

In theory, the measurements of E_a and E_b require corrections for lack of resolving power, for incomplete absorption away from the band head, and for finite width of the coronal source.

Figure A-1(b) exhibits band profiles for one limb of the sun at five heights between 3000 and 46,000 km. At four of these heights, including the two extremes, the band profiles show the same ratio between absorption at the band head and integrated absorption. The one exception shows an obvious defect in one side of the band that accounts for the discrepancy and lies in the opposite sense from that expected from the effect of a change in resolving power. We

Table A-1. Continuum Intensities[a] λ4700

Height, km	log $(E_E + E_W)$	E_E/E_W	log E_E	Height, km	log $(E_E + E_W)$	E_E/E_W	log E_E
−120	3.44	—	3.44	1,980	1.69	—	1.57
−10	3.28	—	3.28	2,250	1.64	—	1.51
100	2.72	—	2.72	2,520	1.68	—	1.55
310	2.12	—	2.09	3,060	1.58	2.60	1.43
530	1.91	—	1.85	3,870	1.61	2.47	1.46
640	1.87	—	1.80	4,680	1.55	—	1.38
750	1.76	—	1.69	5,400	1.58	1.90	1.40
850	1.80	—	1.72	6,300	1.58	1.59	1.37
960	1.76	—	1.67	22,500	1.54	1.03	1.25
1,070	1.75	—	1.66	28,400	1.40	0.92	1.08
1,180	1.73	—	1.63	39,100	1.48	0.80	1.13
1,280	1.65	—	1.54	45,300	1.48	0.83	1.14
1,390	1.69	—	1.58	46,100	1.51	0.72	1.13
1,500	1.67	—	1.56	46,900	1.56	0.63	1.15
1,610	1.61	—	1.49	47,700	1.60	0.64	1.19
1,750	1.64	—	1.52	48,500	1.60	0.61	1.18

[a] Intensities are in ergs $\sec^{-1}$ frequency^{-1} from a slice of chromosphere and corona 1 cm wide.

conclude, therefore, that for our purposes the absorption at the band head is proportional to the integrated absorption, and we may use E_a and E_b to separate the contribution from the two limbs of the sun without further correction. E_E is tabulated in Table A-1.

II. Balmer Continuum and Line Data for a Normal Chromospheric Region

Data tabulated in Tables A-2 through A-12 are fully explained in Chapter 2.

Table A-2. Balmer Continuum Intensities[a] ($\log_{10} E$)

	λ			
Height, km	3640	3600	3550	3500
−10	2.57	—	—	—
40	2.64	—	—	—
80	2.57	—	—	—
100	2.65	2.74	2.80	2.80
150	2.39	—	—	—
190	2.52	—	—	—
260	2.56	—	—	—
300	2.48	—	—	—
530	2.42	2.38	2.40	2.31
640	2.26	2.33	2.08	—
750	2.24	2.22	2.18	2.02
850	2.04	2.24	2.25	1.92
960	2.03	2.01	1.94	1.82
1070	1.80	1.65	1.58	1.64
1180	1.75	1.67	1.62	1.62
1280	1.59	1.51	1.46	1.51
1390	1.51	1.44	1.41	1.40
1500	1.44	1.43	1.43	1.41
1610	1.39	1.43	1.37	1.35
1730	1.26	1.20	1.21	1.17
1820	1.18	1.25	1.19	1.19
1930	1.18	1.17	1.13	1.20
2040	0.96	1.07	1.00	0.98
2150	0.88	0.93	0.81	—
2260	0.78	0.88	0.72	0.71
2400	0.52	0.70	—	—

[a] Intensities are in ergs $\sec^{-1}$ frequency^{-1} for a slice of chromosphere 1 cm wide.

Table A-3. Balmer-Line Intensities ($\log_{10} E_k - 10$)

Line	Height, km													
	100	530	640	750	850	960	1070	1180	1280	1390	1500	1610	1730	1820
Hα	—	—	—	—	—	5.76	—	5.81	5.62	—	5.63	5.59	—	—
Hβ	—	5.68	5.75	5.62	5.69	5.62	5.55	5.66	5.52	5.52	5.45	5.36	5.38	—
Hγ	—	5.66	5.68	5.62	5.63	5.52	5.50	5.56	5.44	5.37	5.31	5.27	5.20	—
Hδ	—	5.51	5.55	5.47	5.42	5.35	—	5.36	5.21	5.11	5.02	5.04	5.04	—
H8[a]	5.27	5.27	5.07	5.12	5.08	5.03	5.00	4.84	4.85	4.79	4.80	4.74	4.63	4.63
H9	—	5.01	4.88	4.86	4.80	4.73	4.72	4.62	4.58	4.51	4.53	4.46	4.25	4.47
H10	5.04	4.90	4.77	4.75	4.69	4.63	4.59	4.50	4.44	4.40	4.36	4.32	4.12	4.15
H11	4.99	4.80	4.70	4.67	4.60	4.55	4.51	4.40	4.36	4.28	4.28	4.22	4.00	4.02
H12[b]	4.97	4.80	4.68	4.66	4.59	4.51	4.46	4.36	4.30	4.18	4.17	4.13	3.91	3.88
H13[b]	4.98	4.78	4.64	4.62	4.54	4.48	4.46	4.31	4.22	4.14	4.10	4.03	3.80	3.74
H14	4.86	4.71	4.58	4.60	4.45	4.41	4.34	4.22	4.07	4.06	3.95	3.97	3.72	3.62
H15	4.69	4.58	4.44	4.41	4.29	4.25	4.18	4.07	3.99	3.91	3.85	3.85	3.63	3.48
H16	4.64	4.49	4.36	4.39	4.20	4.22	4.08	3.98	3.97	3.83	3.80	3.77	3.54	3.39
H17	4.57	4.40	4.28	4.30	4.17	4.13	4.03	3.96	3.85	3.76	3.67	3.65	3.47	3.32
H18	4.43	4.35	4.22	4.20	4.07	4.01	3.93	3.90	3.76	3.66	3.65	3.50	3.42	3.21
H19[b]	4.45	4.31	4.20	4.19	4.11	3.98	3.92	3.84	3.73	3.69	3.61	3.60	3.32	3.13
H20	4.42	4.26	4.17	4.13	4.01	3.90	3.78	3.76	3.69	3.59	3.59	3.40	3.23	3.33
H21	4.37	4.27	4.17	4.15	4.01	3.77	3.75	3.75	3.61	3.51	3.50	3.34	3.15	3.20
H22	4.35	4.12	4.02	3.99	3.91	3.68	3.68	3.65	3.60	3.47	3.33	3.23	3.11	3.18
H23	4.27	4.08	3.97	3.94	3.80	3.59	3.57	3.52	3.40	3.35	3.22	3.17	3.04	3.02
H24	4.25	4.05	3.93	3.88	3.78	3.56	3.51	3.45	3.32	3.24	3.19	3.04	2.93	2.93
H25[b]	4.26	4.05	3.89	3.86	3.75	3.46	3.47	3.43	3.32	3.19	3.10	2.97	2.90	2.77
H26	—	3.90	3.81	3.76	3.69	3.39	3.39	3.34	3.26	3.16	3.03	2.94	2.85	2.73
H27	4.18	3.87	3.78	3.68	3.65	3.43	3.35	3.21	3.15	3.10	2.96	2.83	2.76	2.64
H28[b]	4.29	3.94	3.87	3.70	3.71	3.34	3.35	3.16	3.16	3.04	2.91	2.81	2.79	2.63
H29	—	3.73	3.67	3.60	3.54	3.18	3.26	3.11	3.00	2.88	2.74	2.73	2.76	2.45
H30[a]	—	4.05	3.88	3.80	3.71	3.32	3.36	3.17	3.21	2.98	2.80	2.82	2.75	2.52
H31	—	3.57	3.58	3.48	—	3.07	3.14	2.94	2.82	2.73	2.63	2.58	2.60	2.36

Height, km														
1930	2040	2150	2260	2400	2520	3060	3180	3720	3870	4680	5490	6300	$\beta' \times 10^5$ 2000 km	$\beta' \times 10^5$ Max. ht.
5.67	—	—	5.65	—	5.49	5.44	—	—	5.11	4.80	4.27	3.82	0.35	1.30
5.32	—	—	5.22	—	5.15	4.74	—	—	4.25	—	3.08	2.64	0.87	1.60
5.12	—	—	4.98	—	4.78	4.54	—	—	3.94	3.23	2.53	—	1.20	1.80
4.85	—	—	4.70	—	4.49	4.20	—	—	3.60	2.94	2.42	—	1.36	1.80
4.55	4.46	4.44	4.38	4.44	4.09	3.74	3.79	3.44	—	—	—	—	1.39	1.39
4.20	4.12	3.96	3.92	3.83	3.70	3.38	3.30	3.08	—	—	—	—	1.51	1.51
3.97	3.95	3.85	3.80	3.73	3.55	3.24	3.22	2.92	—	—	—	—	1.56	1.56
3.97	3.88	3.78	3.64	3.60	3.49	3.12	3.00	2.82	—	—	—	—	1.62	1.62
3.81	3.70	3.63	3.66	3.52	3.38	2.97	2.90	2.55	—	—	—	—	1.68	1.68
3.79	3.82	3.50	3.48	3.49	3.25	2.88	2.84	—	—	—	—	—	1.68	1.68
3.61	3.69	3.57	3.45	3.40	3.20	—	—	—	—	—	—	—	1.70	1.70
3.56	3.48	3.30	3.19	3.27	3.10	—	—	—	—	—	—	—	1.73	1.73
3.50	3.38	3.20	3.09	—	3.07	—	—	—	—	—	—	—	1.73	1.73
3.46	3.34	3.04	3.06	3.08	2.92	—	—	—	—	—	—	—	1.79	1.79
3.33	3.16	2.94	2.97	2.84	2.78	—	—	—	—	—	—	—	1.85	1.85
3.33	3.15	2.95	2.88	2.88	2.66	—	—	—	—	—	—	—	1.91	1.91
3.21	2.99	2.88	2.78	2.77	—	—	—	—	—	—	—	—	1.91	1.91
3.11	2.90	2.73	2.74	2.72	—	—	—	—	—	—	—	—	1.96	1.96
—	2.86	2.70	2.64	2.61	—	—	—	—	—	—	—	—	1.96	1.96
2.86	2.78	2.70	2.62	2.62	—	—	—	—	—	—	—	—	1.96	1.96
2.81	2.69	2.58	2.55	2.50	—	—	—	—	—	—	—	—	2.05	2.05
2.76	2.62	2.56	2.47	2.27	—	—	—	—	—	—	—	—	2.08	2.08
2.72	2.59	2.52	2.35	2.39	—	—	—	—	—	—	—	—	2.05	2.05
2.65	2.52	2.35	2.38	2.23	—	—	—	—	—	—	—	—	2.08	2.08
2.60	2.43	2.42	2.30	2.36	—	—	—	—	—	—	—	—	2.12	2.12
2.49	2.39	2.28	2.31	2.20	—	—	—	—	—	—	—	—	2.08	2.08
2.60	2.45	2.38	2.35	2.27	—	—	—	—	—	—	—	—	2.12	2.12
2.37	2.26	2.22	—	2.14	—	—	—	—	—	—	—	—	2.12	2.12

---

[a] Strong blends.
[b] Weak blends.

Table A-4. Paschen-Line Intensities ($\log_{10} E_k - 10$)

Line	Height, km						
	100	320	530	640	750	850	960
H14	4.16	3.91	3.74	3.68	3.60	3.56	3.53
H16	4.05	—	3.64	3.56	3.47	3.37	3.29
H17	3.66	3.49	3.63	3.17	3.24	3.16	3.26
H18	3.72	3.37	3.33	3.15	3.11	—	3.24
H19	3.52	3.42	3.20	2.96	2.79	—	3.21
H20	3.64	3.21	3.03	—	—	—	3.03
H21	3.44	3.13	3.01	—	—	—	3.00
H22	—	3.11	—	—	—	—	2.69
H23	—	3.29	—	—	—	—	2.77
H24	—	—	—	—	—	—	2.77
H25	—	2.86	—	—	—	—	2.57
H26	—	—	—	—	—	—	2.52
H27	—	2.83	—	—	—	—	2.45
H28	—	2.79	—	—	—	—	—

Table A-[illegible]. Helium Line Intensities[a] ($\log_{10} E - 10$)

Line	δ	Height, km 420	530	640	750	850	960	1070	1180	1290	1390	1500	1610	1730	1820
7065	6.6	—	4.62	4.61	4.51	4.46	4.45	4.44	4.45	4.40	4.26	4.30	4.23	4.18	—
4713	160	3.19	3.21	3.17	3.18	3.19	3.08	3.03	3.01	2.96	2.95	2.96	2.87	2.81	2.70
4121	630	—	3.15	2.80	2.60	2.73	2.66	2.57	2.58	2.39	2.50	2.37	2.43	2.17	—
5876	1	—	5.39	5.37	5.29	5.34	5.32	5.27	5.21	5.34	5.26	5.11	5.10	4.95	—
4472	12	—	4.31	4.30	4.18	4.29	4.16	4.12	4.14	4.13	4.01	3.97	3.97	3.99	—
4026	48	—	3.86	3.79	3.67	3.69	3.55	3.54	3.55	3.52	3.48	3.36	3.39	3.37	—
3820	100	—	3.64	—	3.66	3.52	3.37	—	3.26	3.00	3.14	3.21	3.14	3.05	—
5016	160	—	3.28	3.16	3.20	3.19	3.15	3.09	2.99	2.97	2.96	2.92	2.90	2.91	—
3965	180	—	3.07	2.93	2.95	2.97	2.93	3.01	2.83	2.81	2.90	2.76	2.72	2.74	—
6678	36	—	3.90	3.90	3.84	3.79	3.64	3.64	3.78	3.47	3.49	3.41	3.26	3.46	—
4922	210	—	3.17	3.09	3.10	3.04	2.96	2.92	2.90	2.83	2.84	2.77	2.77	2.67	—
4388	300	—	3.03	2.91	2.67	2.75	2.74	2.74	2.69	2.49	2.57	2.45	2.42	2.55	—
4009	660	—	2.94	2.77	2.39	2.46	2.37	2.40	2.41	2.27	2.35	2.09	2.06	2.02	—
4686		2.90	2.53	2.51	2.55	2.51	2.44	2.59	2.35	2.40	2.44	2.39	2.37	2.34	2.25

Height, km 1950	2040	2150	2260	2400	2520	2630	2900	3060	3170	3710	3870	4680	5490	6300
4.10	—	—	4.10	—	3.88	—	—	3.69	—	—	3.20	2.82	2.42	—
2.73	2.61	2.69	2.65	2.43	2.38	2.35	2.19	2.02	2.24	2.12	—	—	—	—
2.23	—	—	2.01	—	1.92	—	—	—	—	—	—	—	—	—
4.94	—	—	4.71	—	4.71	—	—	4.35	—	—	4.14	—	2.89	2.60
3.93	—	—	3.74	—	3.83	—	—	3.35	—	—	2.76	2.47	—	—
3.19	—	—	3.10	—	3.08	—	—	2.75	—	—	2.15	—	—	—
2.95	—	—	—	—	—	—	—	—	—	—	—	—	—	—
2.75	—	—	2.53	—	2.51	—	—	—	—	—	—	—	—	—
2.73	—	—	2.55	—	2.55	—	—	2.27	—	—	—	—	—	—
3.36	—	—	3.28	—	3.08	—	—	2.89	—	—	2.38	2.25	—	—
2.60	—	—	2.50	—	2.36	—	—	—	—	—	—	—	—	—
2.35	—	—	2.27	—	2.12	—	—	—	—	—	—	—	—	—
—	—	—	—	—	—	—	—	—	—	—	—	—	—	—
2.15	2.19	—	2.10	1.99	—	1.92	1.76	—	—	—	—	—	—	—

[a] For λ3889, which is blended with H8, $\delta \simeq 10$.

Table A-6a. Metal Line Intensities ($\mathrm{Log}_{10}\,E\ -10$)

λ	Ion	Height, km																$\beta' \times 10^8$
		100	530	640	750	850	960	1070	1180	1280	1390	1500	1610	1750	1980	2250	2520	
3361	Ti^+, Sc^+	5.02	4.58	3.90	4.42	4.29	—	3.92	3.83	3.81	3.66	3.61	3.68	3.45	—	—	—	1.9
3368	Cr^+	4.54	4.29	4.06	4.21	3.99	3.84	3.84	3.86	3.84	3.71	3.71	3.67	3.41	—	—	2.94	1.4
3373	Ti^+	4.98	4.65	4.47	4.55	—	4.20	4.16	—	—	4.10	4.09	4.04	3.68	—	—	3.39	1.5
3380	Ti^+	4.47	4.30	4.67	3.93	3.75	3.81	3.73	3.85	3.60	3.49	3.42	3.36	3.11	—	—	2.64	1.9
3384	Ti^+	4.92	4.61	4.25	4.49	4.36	4.11	4.15	4.18	—	4.06	3.99	4.02	3.62	—	—	2.25	1.6
3358	Ti^+	4.97	4.35	—	4.22	4.16	3.67	3.95	3.80	3.74	3.64	3.60	3.49	3.25	—	—	2.81	1.7
3394	Ti^+	4.72	4.37	4.09	4.00	3.99	3.72	3.88	3.85	3.72	3.52	3.58	3.46	3.31	—	—	2.77	1.8
3409	Cr^+	4.54	4.20	3.87	4.05	4.05	3.69	3.50	3.60	3.45	3.36	3.23	3.30	2.90	—	—	2.68	1.9
3415	Ni	4.28	3.76	3.31	3.15	3.17	3.15	2.96	2.93	2.80	2.64	2.59	2.58	2.00	—	—	1.84	2.4
3421	Cr^+	4.54	3.90	3.81	4.00	3.69	3.70	3.52	3.60	3.70	3.38	3.20	3.14	2.91	—	—	2.67	1.8
3422	Cr^+	4.74	4.26	3.82	4.02	3.85	3.74	3.56	3.55	3.54	3.48	3.38	3.34	3.09	—	—	2.68	1.8
3433	Cr^+	4.72	4.36	3.88	3.94	3.70	3.64	3.57	3.68	3.42	3.34	3.28	3.30	3.05	—	—	2.63	2.0
3438	Mn^+, Zr^+	—	—	—	3.07	3.11	3.01	2.95	2.71	2.94	3.00	2.37	2.30	—	—	—	—	—
3442	Mn^+	4.59	4.15	4.01	4.12	3.99	3.70	—	3.69	3.61	3.53	3.61	3.45	3.20	—	—	2.87	1.7
3444	Ti^+	4.61	4.12	3.76	3.88	3.84	3.59	3.49	3.31	3.38	3.15	3.05	—	2.74	—	—	2.29	2.3
3446	Ni^+	4.36	3.57	3.25	3.05	3.11	3.05	2.84	2.74	2.66	2.51	2.52	2.26	2.17	—	—	—	2.8
3456	Ti^+	4.51	3.73	3.13	3.72	3.74	3.03	3.02	2.99	2.87	2.63	2.47	2.33	2.25	—	—	—	2.9
3460	Mn^+	4.68	4.18	3.99	3.90	3.75	3.85	3.67	3.58	3.56	3.38	3.36	3.14	3.03	—	—	2.59	2.0
3461	Mn^+, Ti^+	4.64	4.15	3.76	3.86	3.75	3.59	3.53	3.38	3.36	3.13	3.10	2.89	2.70	—	—	2.43	2.2
3474	Mn^+	4.54	4.30	3.94	4.08	4.01	3.77	3.69	3.54	3.60	3.34	3.39	3.25	3.16	—	—	2.74	2.0
3475	Fe	4.64	4.08	3.59	3.47	3.62	3.04	2.90	2.87	2.71	2.77	2.77	2.61	2.30	—	—	—	—
3477	Ti^+	4.67	4.37	3.92	4.19	4.08	3.50	3.10	3.28	3.05	3.16	3.10	2.90	2.71	—	—	—	2.6
3479	Zr^+	4.80	—	3.21	—	3.19	2.76	—	—	—	—	—	—	—	—	—	—	—
3481	Zr^+	4.43	3.76	3.08	—	3.23	2.86	2.91	2.43	—	—	—	—	—	—	—	—	—
3483	Mn^+	4.74	4.21	3.85	3.74	3.67	3.33	3.26	3.36	3.11	3.12	3.15	3.10	2.83	—	—	—	2.9
3489	Mn^+	4.76	4.15	3.82	4.30	3.80	3.34	3.32	3.32	3.20	3.27	3.19	3.24	2.98	—	—	—	2.8
3491	Fe, Ti^+	4.41	4.38	3.79	4.18	4.00	3.64	3.40	3.28	3.21	3.25	3.12	3.05	2.77	—	—	—	2.4
3493	Ni	4.65	4.08	3.69	3.63	3.27	3.12	3.07	3.06	2.75	3.01	2.81	2.83	2.49	—	—	—	2.8
3505	Ti^+	4.91	4.34	4.13	4.18	3.88	3.43	3.35	3.32	3.25	3.21	3.18	3.12	2.85	—	—	—	2.8
3511	Ti^+	4.90	4.37	4.15	3.71	3.68	3.46	3.28	3.34	3.15	—	3.09	2.93	2.79	—	—	—	2.9
3515	Ni	4.62	3.96	—	3.50	3.36	3.14	2.97	2.95	2.79	2.66	—	2.40	2.35	—	—	—	—
3520	Ti^+	4.74	4.03	3.58	3.52	3.30	3.11	2.92	3.01	2.72	2.76	2.82	—	—	—	—	—	—
3524	Ni	4.91	4.07	3.61	3.48	3.66	3.22	2.96	3.06	2.86	2.84	2.80	2.70	2.59	—	—	—	—

3535	Ti$^+$	4.87	4.33	3.91	3.93	3.67	3.35	3.29	3.23	3.00	3.07	3.07	2.90	2.84	—	—	—	—
3545	V$^+$	4.61	3.96	3.47	3.20	3.36	3.01	2.90	2.78	2.56	2.62	2.75	2.58	—	—	—	—	—
3556	V$^+$	4.75	4.25	3.61	3.81	3.27	3.22	2.97	3.06	2.80	2.73	2.74	2.57	2.41	—	—	—	—
3558	Sc$^+$	4.64	4.16	3.61	3.50	3.71	3.20	3.01	3.12	2.77	2.93	2.77	2.61	—	—	—	—	3.1
3568	Sc$^+$	—	4.05	3.55	3.74	3.53	3.14	3.05	3.26	2.90	2.69	2.86	—	—	—	—	—	2.9
3570	Fe	4.62	4.14	3.77	3.65	—	3.39	3.27	—	3.16	2.92	2.99	2.85	2.71	—	—	—	2.7
3576	Sc$^+$	4.69	4.30	3.54	4.14	3.88	3.48	—	—	3.27	2.91	3.00	2.81	2.64	—	—	—	3.0
3579	Cr$^+$	—	4.04	—	3.70	3.61	3.15	3.12	—	3.13	2.74	2.85	2.77	2.40	—	—	—	2.6
3581	Fe	4.68	4.31	3.66	4.18	3.94	3.59	3.46	—	3.36	3.18	3.04	3.02	2.86	—	—	—	2.7
3596	Ti$^+$	4.13	3.91	3.49	—	—	3.15	2.87	—	2.81	2.83	2.80	2.41	2.41	—	—	—	2.6
3609	Fe	—	3.94	3.55	3.39	3.39	3.05	3.16	—	3.06	2.81	2.82	2.63	2.60	—	—	—	2.3
3614	Sc$^+$	4.57	3.29	—	—	3.54	3.62	3.41	—	3.40	3.24	3.10	3.02	2.94	—	—	—	2.4
3625	Ti$^+$	4.52	4.03	3.62	3.40	3.31	3.42	3.05	—	3.08	2.67	2.79	2.68	2.51	—	—	—	—
3641	Ti$^+$	4.61	4.18	3.59	3.62	3.43	3.43	3.28	—	3.12	2.94	2.94	2.78	2.53	—	—	—	2.8
3643	Sc$^+$	4.65	4.29	3.57	3.56	3.66	3.81	3.33	—	3.20	2.88	3.10	2.72	2.67	—	—	—	2.8
3645	Sc$^+$	4.56	4.01	3.70	3.56	—	2.98	2.90	—	2.99	2.74	2.71	—	—	—	—	—	3.3
3648	Fe	4.58	4.11	3.40	3.69	3.32	3.35	3.17	—	3.15	—	—	2.74	2.55	—	—	—	2.7
3685	Ti$^+$	4.92	4.91	3.87	3.83	4.30	3.95	4.19	—	4.34	4.07	—	4.01	3.49	—	—	—	1.9
3709	Fe	—	—	4.24	2.98	2.88	2.91	2.60	2.64	2.49	2.47	—	—	—	—	—	—	3.0
3710	Y$^+$	4.64	4.14	4.69	3.42	3.32	3.16	3.00	2.94	2.83	2.54	2.46	2.32	—	—	—	—	3.7
3720	Fe	4.57	4.30	4.74	3.64	3.68	3.68	3.58	3.67	3.83	3.34	3.21	3.15	—	—	—	—	2.3
3742	Ti$^+$	4.74	4.21	4.69	3.28	3.60	3.44	3.22	3.20	3.46	2.88	2.81	2.77	2.64	—	—	—	3.1
3746	Fe	4.86	4.28	4.82	3.67	3.77	3.58	3.45	3.51	3.47	3.19	3.05	3.05	2.75	—	—	—	2.9
3748	Ti$^+$. Fe	4.72	4.12	4.75	3.52	—	3.23	3.33	3.36	3.22	3.21	2.68	2.86	—	—	—	—	3.0
3759	Ti$^+$	5.16	4.91	—	—	—	—	3.96	3.22	4.09	3.56	3.98	3.87	3.42	—	—	—	2.2
3761	Ti$^+$	5.14	4.84	5.09	3.97	4.00	3.76	3.97	3.90	3.86	3.70	3.09	3.83	—	—	—	—	2.3
3764	Fe	4.79	4.02	3.45	3.54	3.42	3.19	3.04	3.08	2.93	2.91	2.72	2.71	—	—	—	—	3.1
3767	Fe	4.73	3.87	3.56	3.12	3.18	3.07	2.81	2.78	2.81	—	2.60	2.64	—	—	—	—	3.2
3774	Y$^+$	4.64	4.14	4.62	3.12	3.14	2.99	2.78	2.81	2.85	2.54	2.54	2.49	—	—	—	—	3.4
3789	Y$^+$	4.84	3.90	3.40	2.99	2.97	2.86	2.60	—	2.38	—	—	—	—	—	—	—	4.5
3795	Fe	—	—	4.37	3.05	—	2.88	—	—	—	—	—	—	—	—	—	—	—
3799	Fe	—	—	4.46	3.28	3.06	3.12	2.95	2.90	2.85	—	—	2.71	—	—	—	—	2.2
3813	Ti$^+$	4.92	—	4.54	2.82	2.93	2.93	2.70	2.63	—	2.54	2.63	—	—	—	—	—	1.9
3814	Ti$^+$	4.91	—	4.37	—	2.94	2.84	2.63	2.55	2.53	2.47	2.33	—	—	—	—	—	2.3
3816	Fe	4.90	4.07	4.61	3.27	3.36	3.32	3.03	2.98	3.04	2.73	2.78	2.74	—	—	—	—	3.4
3820	Fe	—	—	4.82	3.45	3.63	3.32	3.28	3.41	2.98	2.99	3.08	—	2.41	—	—	—	2.9
3824	Fe	—	4.04	3.59	3.31	3.42	3.32	3.09	3.10	2.98	2.58	2.80	2.70	—	—	—	—	3.0

Table A-6a. (*Continued*)

λ	Ion	Height, km																$\beta' \times 10$
		100	530	640	750	850	960	1070	1180	1280	1390	1500	1610	1750	1980	2250	2520	
3826	Fe	—	4.09	4.60	3.23	3.51	3.39	3.07	3.20	3.15	2.87	2.74	2.96	2.41	—	—	—	2.8
3827	Fe	4.90	3.95	4.86	2.97	3.29	3.25	2.87	2.73	2.77	2.57	2.31	2.65	2.50	—	—	—	3.5
3829	Mg	4.09	4.20	3.77	3.84	—	3.62	—	3.48	3.98	—	3.24	3.35	3.25	—	—	—	1.7
3832	Mg	4.60	4.51	3.95	3.94	4.12	3.85	3.77	3.36	—	—	3.82	3.76	3.67	—	—	—	1.9
3838	Mg	4.56	4.50	3.95	3.99	4.20	3.98	3.78	3.74	3.98	—	3.91	3.87	3.63	—	—	—	1.7
3850	Fe	—	3.62	2.86	3.32	2.94	2.63	2.52	—	—	—	—	—	—	—	—	—	3.7
3856	Fe	—	4.09	3.45	3.79	3.62	3.46	3.19	3.29	3.22	—	2.66	2.92	2.73	—	—	—	2.9
3860	Fe	—	4.29	3.60	3.83	4.13	3.69	3.47	3.74	3.85	—	3.27	3.41	3.13	—	—	—	1.9
3865	Fe	—	3.54	2.77	3.31	2.96	2.62	2.41	2.40	2.15	—	—	—	—	—	—	—	3.3
3879	Fe	4.25	4.16	3.59	3.80	3.67	3.37	3.19	3.18	2.95	—	2.58	2.99	2.65	—	—	—	2.5
3886	Fe	4.49	4.24	—	—	—	3.62	3.49	—	3.44	—	—	3.35	—	—	—	—	1.8
3944	Al	—	3.68	3.48	3.41	3.36	3.12	3.12	3.06	2.76	2.82	2.58	2.24	2.38	—	—	—	2.6
3962	Al	—	3.73	3.72	3.73	3.63	3.39	3.48	3.36	3.16	3.10	3.10	2.71	2.74	—	—	—	2.1
3983	Y$^+$	—	3.40	3.18	2.98	2.76	—	—	—	—	—	—	—	—	—	—	—	4.6
4005	Fe	—	3.37	3.20	3.03	2.84	2.52	2.59	2.47	2.12	—	—	—	—	—	—	—	3.5
4031	Mn	—	3.67	3.56	3.36	3.28	3.03	3.07	2.97	2.56	2.46	2.37	2.23	—	—	—	—	3.2
4033	Mn	—	3.56	3.41	3.36	3.14	2.81	2.93	2.67	—	2.44	2.41	—	—	—	—	—	2.9
4034	Mn	—	3.52	3.45	3.30	3.02	2.82	2.78	2.73	2.39	2.25	2.26	—	—	—	—	—	3.3
4046	Fe	—	3.84	3.79	3.70	3.57	3.29	3.28	3.22	2.95	2.85	2.88	2.69	2.51	—	—	—	2.6
4064	Fe	—	3.73	3.62	3.43	3.37	3.07	3.09	2.95	2.73	2.66	2.57	2.41	2.23	—	—	—	2.8
4072	Fe	—	3.70	3.60	3.44	3.31	3.11	3.04	2.87	2.65	3.53	2.44	2.31	2.26	—	—	—	3.0
4078	Sr$^+$	—	4.39	4.35	4.32	4.26	4.10	4.15	4.03	3.96	4.00	3.92	3.76	3.67	3.51	3.29	—	1.5
4144	Fe	—	3.65	3.42	3.19	3.09	2.98	2.97	2.73	—	—	—	—	—	—	—	—	2.9
4164	Ti$^+$	—	3.55	3.32	2.95	2.97	2.77	2.70	—	—	—	—	—	—	—	—	—	—
4199	Fe	—	3.37	3.26	2.99	2.87	2.78	2.58	—	—	—	—	—	—	—	—	—	—
4202	Fe	—	3.42	3.21	3.00	2.94	2.66	2.62	—	—	—	—	—	—	—	—	—	3.5
4215	Sr$^+$	—	4.24	4.30	4.22	4.21	4.15	3.95	3.89	3.72	3.78	3.65	3.61	3.43	—	—	—	1.9
4227	Ca	—	3.98	4.12	3.93	3.87	3.76	3.66	3.57	3.46	3.43	3.20	3.10	2.91	—	—	—	2.2
4233	Fe$^+$	—	3.86	3.79	3.52	3.41	3.29	2.98	3.00	2.78	2.66	2.69	2.50	2.37	—	—	—	3.0
4236	Fe	—	3.31	3.15	2.71	2.70	—	2.24	—	—	—	—	—	—	—	—	—	4.6
4247	Sc$^+$	—	4.06	4.02	3.93	3.87	3.74	3.52	3.47	3.39	3.28	3.09	3.00	2.77	—	—	—	2.5
4251	Fe	—	3.55	3.35	3.02	3.00	2.69	2.51	2.31	—	—	—	—	—	—	—	—	—
4254	Cr	—	3.77	3.81	3.62	3.58	3.44	3.19	3.10	2.91	2.92	2.79	2.64	2.38	—	—	—	2.7
4260	Fe	—	3.59	3.41	3.10	3.00	2.84	2.66	—	—	—	—	—	—	—	—	—	4.0

4272	Fe	—	3.73	3.65	3.33	3.09	3.03	2.87	2.81	2.70	2.71	2.50	2.27	—	—	—	—	3.0
4275	Cr	—	3.80	3.80	3.54	3.52	3.36	3.08	2.99	2.87	2.72	2.64	2.48	2.35	—	—	—	2.9
4290	Cr, Ti^+	—	4.07	4.02	3.75	3.69	3.46	3.31	3.18	3.00	3.05	2.89	2.59	2.50	—	—	—	—
4294	Ti^+	—	3.77	3.78	3.60	3.49	3.26	3.19	3.03	2.90	2.87	2.78	2.64	2.47	—	—	—	2.6
4300	Ti^+	—	4.05	3.93	3.73	3.65	3.43	3.28	3.19	3.12	3.07	3.00	2.71	2.57	—	—	—	2.7
4321	Ti^+, Sc^+	—	3.75	3.76	3.43	3.30	3.10	2.91	2.80	2.77	2.49	2.54	2.48	—	—	—	—	—
4325	Fe, Sc^+	—	3.94	3.85	3.64	3.55	3.36	3.17	3.11	2.99	2.91	2.83	2.69	2.44	—	—	—	2.7
4383	Fe	—	3.84	3.83	3.69	3.66	3.43	3.31	3.25	3.12	2.92	2.78	2.61	2.72	—	—	—	2.6
4395	Ti^+	—	4.05	4.05	3.88	3.86	3.60	3.57	3.54	3.29	3.26	3.18	2.94	2.90	—	—	—	2.4
4405	Fe	—	3.66	3.56	3.30	3.24	3.05	2.96	2.88	2.73	2.59	—	—	—	—	—	—	2.8
4444	Ti^+	—	3.97	3.96	3.87	3.77	3.62	3.47	3.43	3.21	3.16	3.04	2.91	3.02	—	—	—	2.4
4450	Ti^+	—	3.59	3.36	2.98	2.99	2.83	2.90	2.90	2.63	2.34	2.14	—	—	—	—	—	2.9
4468	T^+	—	4.00	3.91	3.80	3.74	3.53	3.49	3.35	3.29	3.15	3.10	2.84	2.97	—	—	—	2.2
4501	Ti^+	—	3.95	3.90	3.71	3.68	3.44	3.39	3.32	3.16	3.02	3.02	—	2.57	—	—	—	2.5
4508	Fe^+	—	3.32	3.16	2.62	2.62	2.65	—	—	—	—	—	—	—	—	—	—	4.0
4515	Fe^+	—	3.32	3.06	2.78	2.80	2.65	—	—	—	—	—	—	—	—	—	—	3.5
4520	Fe^+	—	3.34	2.99	2.75	2.64	2.68	—	—	—	—	—	—	—	—	—	—	3.6
4534	Ti^+, Fe^+	—	4.07	3.95	3.79	3.73	3.58	3.45	3.41	3.23	3.06	2.95	2.83	2.54	—	—	—	—
4549	Ti^+	—	4.13	3.95	3.85	3.87	3.57	3.47	3.42	3.29	3.12	3.06	2.96	2.63	—	—	—	2.6
4554	Ba^+	—	4.14	3.98	3.93	3.88	3.66	3.58	3.52	3.31	3.16	3.05	2.82	2.50	—	—	—	2.9
4559	Cr^+	—	3.37	3.33	3.04	2.97	2.83	2.79	2.64	2.62	—	—	2.19	—	—	—	—	2.5
4561	Ti^+	—	3.94	3.82	3.60	3.60	3.37	3.26	3.22	3.13	2.96	2.85	2.69	—	—	—	—	2.6
4572	Ti^+	—	4.02	3.89	3.74	3.74	3.55	3.41	3.33	3.20	3.12	2.99	2.86	2.60	—	—	—	2.5
4584	Fe^+	—	3.84	3.72	3.48	3.45	3.15	3.01	2.95	2.87	—	2.49	2.30	—	—	—	—	3.2
5018	Fe^+	—	4.20	4.01	4.06	3.81	3.63	3.63	3.30	3.19	3.27	2.96	2.90	2.68	—	—	—	2.9
5167	Mg	—	—	4.11	4.01	4.02	3.70	3.70	3.57	3.38	3.33	3.15	2.96	2.87	2.74	2.36	—	2.6
5169	Fe^+	—	—	4.17	4.03	3.98	3.79	3.67	3.59	3.30	3.26	3.10	2.84	2.69	2.53	2.16	—	3.0
5173	Mg	—	—	4.34	4.20	4.23	4.18	4.00	4.04	3.86	3.76	3.73	3.47	3.40	3.17	2.93	—	2.2
5184	Mg	—	—	4.44	4.26	4.28	4.39	4.12	4.21	4.06	3.99	3.85	3.70	3.66	3.44	3.17	—	2.2
5189	Ti^+	—	—	3.23	3.18	3.08	—	2.94	2.86	2.60	2.72	—	—	—	—	—	—	1.8
5198	Fe^+	—	—	2.99	2.85	2.71	—	2.51	2.60	2.30	—	—	—	—	—	—	—	2.1
5205	Cr	—	—	3.27	3.13	3.04	2.81	2.76	2.74	—	—	—	—	—	—	—	—	2.4
5206	Cr	—	—	3.51	3.37	3.26	3.05	2.90	2.90	2.68	2.49	—	—	—	—	—	—	3.0
5208	Cr	—	—	3.56	3.39	3.30	3.11	2.90	2.96	2.69	2.66	—	—	—	—	—	—	2.8
5233	Fe	—	—	2.75	2.72	2.65	2.50	2.35	2.46	—	—	—	—	—	—	—	—	—
5235	Fe^+	—	—	3.07	2.92	2.85	2.62	2.62	2.57	—	—	—	—	—	—	—	—	2.2
5890	Na	—	4.12	—	4.05	3.95	3.91	3.84	3.81	3.65	3.64	3.45	3.30	3.19	3.01	2.50	2.54	2.1
5895	Na	—	4.15	4.14	4.06	3.90	3.85	3.64	3.71	3.51	3.45	3.21	3.15	3.03	2.81	2.54	—	2.3

Table A-6b. Oxygen and Ca^+ Line Intensities ($\log_{10} E - 10$)

λ	Ion	Height, km																					$\beta' \times 10^8$
		100	530	640	750	850	960	1070	1180	1280	1390	1500	1610	1750	1980	2250	2520	3060	3870	4680	5490	6300	
7772	0	4.99	—	4.52	4.56	—	4.23	—	4.12	3.98	3.83	3.82	3.71	—	3.55	3.59	—	2.91	2.30	—	—	—	1.6
7774	0	4.94	—	4.34	4.41	—	4.10	—	3.99	—	3.76	—	—	—	3.46	3.44	—	2.67	—	—	—	—	1.6
7775	0	4.73	4.23	4.30	4.24	—	3.94	—	3.83	—	—	—	—	—	3.53	—	3.13	—	—	—	—	—	1.4
8498	Ca^+	5.37	4.22	—	—	—	4.56	—	4.36	4.45	4.25	3.99	3.96	—	3.90	3.80	3.71	3.02	2.45	0.03	—	—	1.7
8542	Ca^+	5.50	4.21	—	—	—	—	—	—	—	4.73	4.75	4.52	—	4.38	4.40	4.23	—	3.29	0.80	—	—	1.3
8662	Ca^+	5.07	4.80	4.73	4.77	—	4.50	—	4.45	4.51	4.49	4.31	4.31	—	4.09	4.16	3.76	3.46	2.84	2.36	—	—	1.3
3968	Ca^+	—	—	6.12	—	—	—	6.01	—	—	—	5.81	—	5.81	—	—	—	5.39	5.21	—	4.66	—	0.7

III. Continuum and Line Data for the 1952 Active Region of Chromosphere

The tabulation of data in Tables A-7 through A-12 are explained in Chapter 3 and Section I of the Appendix.

Table A-7. Continuum Intensities, λ4700[a]

Height, km	log $(E_E + E_W)$	E_W/E_E	log E_W	Height, km	log $(E_E + E_W)$	E_W/E_E	log E_W
400	1.91	>10	1.91	4,590	1.77	3.0	1.65
510	1.84	>10	1.84	5,400	1.77	2.6	1.63
620	1.79	>10	1.79	11,600	1.76	2.1	1.59
810	1.80	>10	1.76	22,300	1.60	2.0	1.42
1,620	1.80	~7	1.74	28,200	1.69	1.4	1.46
2,160	1.78	5.5	1.71	44,400	1.70	0.7	1.32
2,970	1.76	6.2	1.68	45,200	1.67	0.7	1.29
3,780	1.78	4.8	1.68	46,000	1.71	0.7	1.33

[a] Intensities are in ergs sec^{-1} $frequency^{-1}$ for a 1-cm-wide slice of chromosphere and corona.

Table A-8. Balmer Lines (log E − 10)

	Height, km									
Line	290	400	510	620	810	1350	1620	2160	4590	$\beta' \times 10^8$
Hα	—	6.12	5.98	6.11	—	—	5.96	5.76	5.33	0.45
Hβ	—	6.01	5.97	6.04	—	—	5.80	5.52	5.19	0.45
Hγ	—	5.87	5.78	5.83	—	—	5.64	5.40	5.04	0.46
H8	5.60	—	5.18	—	5.25	5.11	5.10	—	—	—
H9	5.39	—	4.98	—	5.01	4.83	4.64	—	—	0.8
H10	5.25	—	4.85	—	4.86	4.61	4.47	—	—	0.8
H11	5.06	—	4.76	—	4.61	4.50	4.38	—	—	0.8
H12	5.07	—	4.73	—	4.55	4.45	4.32	—	—	0.8
H13	5.01	—	4.65	—	4.58	4.40	4.28	—	—	0.8
H14	4.87	—	4.55	—	4.49	4.26	4.08	—	—	0.9
H15	4.70	—	4.48	—	4.29	4.13	4.01	—	—	0.9
H16	4.56	—	4.38	—	4.19	4.03	3.96	—	—	0.9
H17	4.46	—	4.27	—	4.13	3.90	3.82	—	—	0.9
H18	4.40	—	4.19	—	3.98	3.80	3.74	—	—	0.9
H19	4.35	—	4.25	—	3.93	3.75	3.65	—	—	0.9
H20	4.25	—	4.10	—	3.79	3.71	3.70	—	—	1.0
H21	4.18	—	4.03	—	3.85	3.61	3.56	—	—	1.0
H22	—	—	3.96	—	3.70	3.53	3.46	—	—	1.0
H23	—	—	3.95	—	3.69	—	3.30	—	—	1.3
H24	—	—	3.77	—	3.59	—	3.21	—	—	1.2
H25	—	—	3.78	—	3.57	—	3.13	—	—	1.3
H26	—	—	3.71	—	3.47	—	3.11	—	—	1.2
H27	—	—	3.60	—	3.32	—	2.98	—	—	1.3
H28	—	—	3.54	—	—	—	—	—	—	—

Table A-9. Paschen Lines (log E − 10)

	Height, km										
Line	180	290	400	510	810	1620	2160	2970	3780	4590	$\beta' \times 10^8$
H14	3.90	3.82	3.70	3.48	3.54	3.32	3.17	2.97	2.69	2.53	0.65
H16	3.79	3.73	3.46	3.43	3.48	3.12	2.97	2.79	2.43	2.30	0.67
H17	—	3.55	3.26	3.44	3.26	3.15	2.87	2.61	2.34	—	0.74
H18	—	3.49	—	3.11	3.05	3.01	2.82	2.55	—	—	0.74
H19	—	3.34	—	—	3.13	2.90	2.68	2.50	—	—	0.76
H20	—	—	—	—	3.11	2.80	2.61	2.44	—	—	0.74
H21	—	—	—	—	2.79	—	2.53	—	—	—	—
H22	—	—	—	—	2.61	—	2.40	—	—	—	—
H23	—	—	—	—	2.49	—	2.47	—	—	—	—
H24	—	—	—	—	—	—	2.20	—	—	—	—
H25	—	—	—	—	—	—	2.11	—	—	—	—

Table A-10. Helium Lines (log E −10)

Series	Line	Height, km											$\beta' \times 10^8$
		290	400	510	620	810	1620	2160	2970	3780	4590	5400	
2^3p-k^3s	3-7065	4.99	4.85	4.69	4.66	4.81	4.49	4.43	4.23	4.00	3.85	3.64	0.55
	4-4713	—	3.60	3.59	3.56	3.57	3.39	3.39	3.17	2.84	—	—	0.57
	5-4121	—	3.19	3.19	3.12	3.21	2.90	—	—	—	—	—	0.55
2^3p-k^3d	3-5876	—	5.85	5.64	—	5.63	5.51	5.28	—	—	4.75	—	0.55
	4-4471	—	4.75	4.63	4.84	—	4.60	4.48	—	—	4.00	—	0.46
	5-4026	—	4.27	4.16	4.17	4.23	3.97	—	3.62	3.40	—	2.97	0.60
2^1s-3^1p	3-5016	—	4.10	4.07	3.85	3.82	3.88	3.75	3.52	3.22	—	2.84	0.60
2^1p-3^1s	3-7281	3.53	3.38	3.34	3.32	3.38	3.14	3.01	2.84	2.66	2.37	2.27	0.55
2^1p-k^1d	3-6678	4.74	4.58	4.42	4.47	4.50	4.32	4.16	4.02	3.80	3.67	3.36	0.51
	4-4922	—	3.89	3.89	3.84	3.66	3.63	3.53	3.18	2.94	—	2.52	0.62
	5-4388	—	3.63	3.55	3.48	3.54	3.31	3.22	2.88	—	—	—	0.58
	7-4009	—	3.09	2.95	2.99	2.86	2.87	—	—	—	—	—	0.42
3-4(HeII)	4686	—	3.30	3.30	3.28	3.33	3.11	3.12	2.90	2.56	—	—	0.45

Table A-11. Metal Lines (log E − 10)

		Height (km)								
λ	Ion	400	510	620	810	1620	2160	2970	3780	$\beta' \times 10^8$
4227	Cr	4.19	4.12	4.00	4.02	3.40	—	—	—	1.5
4290	Cr	3.76	3.72	3.61	3.58	2.98	—	—	—	1.3
4275	Cr	3.68	3.63	3.52	3.42	3.00	—	—	—	1.3
4254	Cr	3.71	3.73	3.56	3.52	3.08	—	—	—	1.3
5169[a]	Fe	4.24	4.18	4.04	3.44	3.46	3.14	2.49	—	1.4
4384	Fe	3.93	3.81	3.71	3.75	3.20	2.96	—	—	1.3
4272	Fe	3.50	3.60	3.29	3.25	2.76	—	—	—	1.4
4072	Fe	3.57	3.47	3.36	3.24	2.90	—	—	—	1.3
4064	Fe	3.69	3.61	3.48	3.35	2.97	—	—	—	1.3
4046	Fe	3.88	3.74	3.72	3.63	3.16	—	—	—	1.3
5018	Fe^+	4.14	4.15	4.06	3.83	3.52	3.08	2.87	—	1.3
4924	Fe^+	4.07	3.99	3.93	3.62	3.28	2.89	2.56	—	1.5
4584	Fe^+	3.64	3.61	3.38	3.01	—	—	—	—	—
4233	Fe^+	3.78	3.63	3.48	3.58	2.93	—	—	—	—
5184	Mg	4.46	4.61	4.43	3.58	3.98	3.49	3.41	—	1.0
5173	Mg	4.25	4.45	4.17	3.49	3.92	3.56	3.13	—	1.1
5167[b]	Mg	3.92	3.91	3.82	3.26	3.37	3.26	2.62	—	1.2
4034	Mn	3.37	3.15	3.11	2.99	—	—	—	—	—
4033	Mn	3.39	3.33	3.27	3.08	—	—	—	—	1.8
4031	Mn	3.51	3.48	3.35	3.19	2.58	—	—	—	1.8
4247	Sc^+	3.96	3.87	3.74	3.90	3.19	—	—	—	1.4
4215	Sr^+	4.42	4.35	4.22	—	3.69	3.57	3.03	2.64	1.2
4078	Sr^+	4.58	4.41	4.35	4.37	3.86	3.71	3.33	2.82	1.1
4395	Ti^+	3.88	3.89	3.74	3.81	3.22	—	—	—	1.4
4300	Ti^+	3.74	3.70	3.63	3.54	2.99	—	—	—	1.4
4294	Ti^+	3.54	3.51	3.41	3.27	2.79	—	—	—	1.4

[a] Blend with Fe^+.

[b] Blend with Fe.

Table A-12. Oxygen Lines (log E -10)

Line	Height, km											$\beta' \times 10^8$
	290	400	510	620	810	1620	2160	2970	3780	4590	5400	
7775	4.29	4.12	4.04	4.02	4.07	3.60	3.44	3.22	2.98	2.66	2.50	0.75
7774	4.38	4.16	4.16	4.13	4.08	3.87	3.59	3.45	3.14	2.77	2.56	0.75
7772	4.47	4.29	4.35	4.24	4.30	3.95	3.72	3.57	3.29	2.92	2.81	0.75

Appendix II: Chapter Notes

Chapter 4

1. The significance of these two sets of computations, and those in Table 4-3 for a thick atmosphere, comparing the effect of ignoring and including collisional excitation from levels other than the lowest, seems to be largely overlooked in the literature (cf., e.g., de Jager, 1959.) The smallness of the change in the b_k indicates that for the chromospheric range of n_e, T_e, and radiation field, excitation out of the second level comes essentially only by radiative processes. Only if a considerable increase in n_e, or a considerable drop in radiation field, occurs might we expect collisional excitation from the second level to be of importance for hydrogen. Thus, on the one hand, the original discussion underlying Table 4-3 suggested that an increase in n_e of something like a factor 50 would be required, but uncertainty in cross sections makes the factor uncertain. On the other hand, when considering the "dilute" radiation field in such objects as planetary nebulae, neglect of collisional excitation from the second level can be serious. Thus, in the original discussion underlying Table 4-3, we have criticized as physically unrealistic case B of the Planetary Nebulae series treated by Menzel and coworkers; for its assumptions of detailed balance in the Lyman lines, no Balmer radiation field, and neglect of Balmer collisional excitations leaves no exit from the second level. Again, this point seems to have been overlooked, except in the recent work by Pottasch (1960*b*).

Chapter 6

1. We do not here go into the problem of the various discrepancies reported in the literature for local departures of the empirically inferred absorption coefficient from the value given by H^- alone. Pierce and Waddell discuss some of these problems in the visual region. Conclusions on the requirement of an additional opacity source in the ultraviolet region, beginning at about λ4000,

do not seem at this time to be in complete agreement on either requirement or interpretation for an additional opacity source. We simply note the presence of these uncertainties.

2. Pagel has kindly communicated, in advance of publication (*Astrophys. J.*, in 1961, in two papers), the results of a current attempt to tie down more definitely the distribution $T_e(h)$ in the region at the limb and up to about 500 km. To the material discussed here he has added other eclipse data, particularly that by Kristenson from the 1954 eclipse, which has a very fine height resolution in just the atmospheric region where the HAO material is scanty. Pagel attempts to delineate the range of model permitted by these data, concluding that the most likely result on T_e (min) is a value 4300° ± 100° near $\tau_{5000} \sim 0.007$, provided that there exists no significant departure of the H^-:H ratio from the Saha equation value in this atmospheric region.

Chapter 9

1. A very interesting investigation by J-C. Pecker and J. Lefevre has been reported at the Varenna Symposium, and kindly communicated to us in advance of publication, bearing on this question of separating non-LTE effects from effects arising from departure from spherical symmetry of the atmosphere. In the cited investigation of the empirical source functions of the early Balmer lines, by Athay and Thomas (1958), we found that the separate curves $T_{ex}(\tau$, or $N_2)$ determined for each line from limb-darkening data, did not lie parallel (cf. Fig. 4 of the paper). We discussed these results from the standpoint of the question of whether or not T_{ex} could be assumed to be the same for all lines—noting, but not investigating, that effects of the absence of spherical symmetry had been neglected. Lefevre and Pecker have attempted to push further the empirical investigations of non-LTE effects in the metallic lines (summarized in Section 9-IIIA2) in progress at Meudon, and have found precisely the same effect for these metallic lines that we found for the Balmer lines. They have, however, attempted a quantitative interpretation of the effect in terms of departures from spherical symmetry; the interpretation leads to a preliminary estimate of the size of the "elements." Their results suggest that a reanalysis of the material on the early Balmer lines might be profitable, along the lines adopted by them for discussing the metallic lines.

2. The sensitivity of the method of analysis followed by Mrs. Pecker to the initially assumed model, $T_e(h)$, should be explicitly emphasized. The numerical results of her initial calculations, leading to the large values mentioned in Chapter 9, were based on our 1955 model, obtained from the continuum analysis. She emphasized to us that when a model having a steeper gradient in T_e was adopted, the derived values of N_2 dropped, thus suggesting that our 1955 model had the wrong T_e gradient if these various results on $N_2(h)$ were to be reconciled. And, indeed, our revised model in Chapter 6 gives precisely this direction of change in gradient of T_e. I emphasize again that the revision of the model results from a coherent theory for b_1 and b_2, with the theory emphasizing and clearly pointing out just where this sensitivity of b_2 to T_e lies. But I also emphasize that this "coherent theory" was developed later, in a region where our original "insight" told us that large optical opacity made such a theory unnecessary because non-LTE effects would be negligibly small. Only because of several clear-cut contradictions, such as that just mentioned above by Mrs. Pecker and that stressed earlier by Zirker, resulting from looking at an analysis of the data from alternate directions and requiring the same result, were we forced into the rediscussion of the theory. I stress this point here, because while we certainly need more data, it is not at all clear to me that we have exhausted the clarification of insight that is still possible from existing data, particularly on the metals, and also on hydrogen in the nonhomogeneous regions of the chromosphere.

3. I would emphasize here that this conclusion on the source function for Ca^+ H and K comes from treating each line as if it came from a two-level atom, neglecting the coupling between the two upper levels. This neglect of coupling between two levels, whose separation is so minute, is not at all consistent with the assumptions made at the outset of the original numerical calculations on hydrogen: that a Boltzmann population (thus, equality of the b_k) would be maintained among the substates of a given principal quantum number by the effect of collisions. Thus, both these approaches, applied severally to Ca^+ and to hydrogen, cannot be right; and I would think that the error lies in too literal an extension of the two-level atom results, in being flushed with the enthusiasm of having

such a nice algebraic result to work with. The situation emphasizes the need to extend the discussion of the effect of additional levels, possibly along the lines of the "equivalent two-level atom" proposed in Chapter 4 and illustrated in Chapter 9, as a means of retaining the direct insight permitted by this algebraic development of the two-level atom. Jefferies has kindly communicated to us in advance of publication (*Astrophys. J.*, November, 1960) an approach alternate to the "equivalent two-level atom" arising from this interlocking of levels, which he has applied to the Ca^+ problem, and in which he finds that S_L should be taken to be the same for H and K.

4. Because the rocket observational data now provide at least good estimates of the flux in the Lyman continuum, it may be useful to sketch at this point precisely what we can say, from this monograph, on the Lyman continuum. The source function is:

$$S_\nu[\text{Ly-C}] = (2h\nu^3/c^2)\left\{b_1 \exp\left[h\nu/kT_e\right] - 1\right\}^{-1}$$

and in a rough way, the emergent intensity is S_ν at $\tau_\nu \sim 1$. From Table 6-10, we see that $\tau_\nu \sim 1$ at the head of the Lyman continuum comes just in the region where the model is uncertain. If, however, we take the values in Tables 6-10 and 6-6 literally, we may estimate I_ν. Correcting Eq. (6-43) by the quantity Ш given by equation (6-51), we obtain an expression for $b_1 \exp X_1$ (X_1 is $h\nu/kT_e$ at the head of the Lyman continuum)

$$b_1 e^{X_1} = \frac{1.05(10^{-12})}{4.15(10^{-16})}(1 + \Delta)\, 10^{-4} T_e e^{X_{12}}$$

$$\left\{\frac{2R(1 + \Delta)^{-1} + 1}{2R(1 + \Delta)^{-1}\left[1 - \dfrac{\exp\,(-\tau_1\sqrt{3\Lambda}}{1 + \sqrt{\Lambda}}\right] + 1}\right\} \simeq 0.77(1 + \Delta)\,T_e e^{X_{12}}$$

Tables 6-10 and 6-6 suggest $T_e \sim 9000°$ and $\Delta \sim 0.5$ near $\tau \sim 1$. Thus we obtain $b_1 \exp X_1 \sim 5.0 \times 10^9$. As discussed in Chapter 6, the solution in Table 6-10 must ultimately be revised once we obtain a method with which to compute the variation of Lyman continuous opacity across the abrupt rise in T_e. This effect will be a lowering of T_e at $\tau \sim 1$. For $T_e = 8500°$ and $8000°$, we obtain values 1×10^{10} and 2.3×10^{10} for $b_1 \exp X_1$. In a paper on the interpretation of the NRL rocket observations in the Lyman region, presented at the September 1960 Meudon colloquim sponsored by IAU Commission 29a, to be published in full in *Astrophys. J.* in 1961, and kindly communicated to us in advance of publication, D. C. Morton and K. G. Widing give a value of 6900° ± ~200° for T_{ex} at the head of the Lyman continuum. *Note:* $b_1 \exp X_1 \equiv \exp (h\nu_1/kT_{ex})$. This value corresponds to $b_1 \exp X_1 \sim 8 \times 10^9$ with an uncertainty of a factor of 2. Thus the prediction, from Table 6-10, of the Lyman continuum intensity is quite satisfactory at the present stage of sophistication of model and observations.

5. In connection with Ly-α, we should remark again on the paper by Morton and Widing cited in the last note. The observations show that if one ascribes a very narrow central core to a geocoronal effect, the ratio of central intensity in Ly-α to peak intensity is about 0.7. In an isothermal atmosphere, we see, from Eqs. (9-85) and (9-86), that the ratio would be $\eta^{\frac{1}{2}}$, or less than 1 per cent. Thus, Ly-α observations suggest very strongly, as discussed in Chapter 9, that the central core is formed very much in the middle of a rise in T_e. Morton and Widing find, indeed, that, in the notation of Chapters 4 and 9, a value of $c \sim 0.1$–0.3 seems required. Plage values for c are higher. Their analysis suggests, further, that T_e lies in the range 7×10^4–1×10^5 in the region of formation of the core; with slightly lower values holding for plages. The simple two-level atom, with constant value for ϵ, $\Delta\lambda_D$ etc., predicts too steep a falloff in the extremities of the core relative to observations. Morton and Widing have very kindly furnished Jefferies and myself with results on their investigations at each stage of the analysis so that we could have the pleasure of working along with them to see just how well the simple two-level atom theory, with constant parameters, represented the data. It seems very clear to all of us that these presently existing observations on Ly-α are already quite adequate to force us to go to numerical treatments, allowing ϵ, $\Delta\lambda_D$, etc., to vary through the region of core formation. In particular, the simple one-term exponential representation of $T_e[\tau_0]$ clearly gives too steep a variation of T_e, both for the above-mentioned effect on the wings, and for the model from Table 6-10. Thus, two things should be emphasized here.

First, the two-level atom, using constant values for the parameters, has been very useful in pointing out the kind of physical effects for which we must look, e.g., properties of the self-reversed emission core in terms of a temperature gradient, separation of the peaks in their relation to velocity fields or temperature gradients, and distinction between collision-dominated and photoionization-dominated) (or some other indirect process) lines. Indeed, we have probably not yet exhausted the use of the two-level atom in getting rough physical pictures.

Second, when it comes to detailed application of the theory to high-quality data, both the two-level atom approach and the use of constant values for the parameters must be refined. The thing one must keep in mind is the definition of high-quality data. All this theory refers to the central regions of spectral lines. For years, many astronomers have argued that the problems of observing these central regions are so bad that if the interpretation depends on good observational data here one had best forget such sophistication of interpretation. Consequently, it is very encouraging to see the observational data forcing not only a detailed theory for the central parts of these lines, but a second-order approach.

Chapter 10

1. Reference should be made here to the preliminary treatment of such a problem for the Ca^+ H and K lines by Miyamoto (1958), although he refers to a semi-infinite atmosphere while we require a treatment for differential motions in a cylindrical column for Hα. However, this consideration of the asymmetric self-reversed core in Hα focuses attention on what probably should be a fifth direction of extension of source function work in addition to the four listed at the beginning of this chapter, viz: the question of the source function and the transfer problem in an atmosphere with differential systematic velocities. Pecker and Thomas have presented a critical summary of some of the problems connected with such an extension at the Varenna Symposium on Aerodynamical Problems in Stellar Atmospheres (proceedings to be published in 1961).

Bibliography*

Adams, W. S., and Burwell, C. G., 1915, *Astrophys. J.*, **41**, 116.

Allen, C. W., 1955, *Astrophysical Quantities*, London, Athlone.

Allen, C. W., and Asaad, A. S., 1955, *Monthly Notices Roy. Astron. Soc.*, **115**, 571.

Aller, L. H., 1941, *Astrophys. J.*, **93**, 236, PPGN XIV.

Aller, L. H., 1953, *The Atmospheres of the Sun and Stars*, p. 248, New York, Ronald.

Aller, L. H., Baker, J. G., and Menzel, D. H., 1939, *Astrophys. J.*, **89**, 587, PPGN VI.

Aller, L. H., Baker, J. G., and Menzel, D. H., 1939, *Astrophys. J.*, **90**, 601, PPGN VIII.

Aller, L. H., and Menzel, D. H., 1945, *Astrophys. J.*, **102**, 239, PPGN XVIII.

Athay, R. G., 1958a, *Ann. astrophys.*, **21**, 98.

Athay, R. G., 1958b, *IAU Symposium No. 9: Radio Astronomy*, R. N. Bracewell (ed.), Stanford University Press.

Athay, R. G., 1958c, *Astrophys. J.*, **128**, 447.

Athay, R. G., 1959a, *Astrophys. J.*, **129**, 164.

Athay, R. G., 1959b, *Observatory*, **79**, 12.

Athay, R. G., 1960a, *Ann. astrophys.*, **23**, 250.

Athay, R. G., 1960b *Astrophys. J.*, **131**, 705.

Athay, R. G., Billing, D. E., Evans, J. W., and Roberts, W. O., 1954, *Astrophys. J.*, **120**, 94.

Athay, R. G., Evans, J. W., and Roberts, W. O., 1953, *Observatory*, **73**, 244.

Athay, R. G., and Johnson H. E., 1959, *Astrophys. J.*, **131**, 413.

Athay, R. G., and Menzel, D. H., 1956, *Astrophys. J.*, **123**, 285.

Athay, R. G., Menzel, D. H., and Orrall, F. Q., 1957, *Smithsonian Contributions to Astrophysics*, **2**, 35.

Athay, R. G., Menzel, D. H., Pecker, J-C., and Thomas, R. N., 1955, *Astrophys. J.*, Suppl. **1**, 505, TSOSA V.

Athay, R. G., and Roberts, W. O., 1955, *Astrophys. J.*, **121**, 231.

Athay, R. G., and Smith, E. v. P., 1956, *Solar Research Memorandum*, 17 Sept., Sacremento Peak Observatory.

Athay, R. G., and Thomas, R. N., 1956a, *Astrophys. J.*, **123**, 299.

Athay, R. G., and Thomas, R. N., 1956b, *Astrophys. J.*, **123**, 309.

Athay, R. G., and Thomas, R. N., 1956c, *Astrophys. J.*, **124**, 586.

Athay, R. G., and Thomas, R. N., 1957a, *Astrophys. J.*, **125**, 788.

---

* The following abbreviations refer to several series of papers treating non-LTE phenomena, which are designated by the series number in the bibliography for ease of reference to follow developments within each series: PPGN, Physical Processes in Gaseous Nebulae; SPTS, Superthermic Phenomena in Stellar Atmospheres; TSOSA, Thermodynamic Structure of the Outer Solar Atmosphere; SFNEA, Source Function in a Non-Equilibrim Atmosphere.

Athay, R. G., and Thomas, R. N., 1957b, *Astrophys. J.*, **125**, 804.

Athay, R. G., and Thomas, R. N., 1958, *Astrophys. J.*, **127**, 96.

Athay, R. G., and Zirin, H., 1957, *Astron. J.*, **62**, 137.

Baker, J. G., and Menzel, D. H., 1938, *Astrophys. J.*, **88**, 52, PPGN III.

Baker, J. G., Menzel, D. H., and Aller, L. H., 1938, *Astrophys. J.*, **88**, 422, PPGN V.

Baker, J. G., Aller, L. H., and Menzel, D. H., 1939, *Astrophys. J.*, **90**, 271, PPGN VII.

Bates, D. R., and Damgaard, A., 1949, *Phil Trans. Roy. Soc. London*, **A242**, 101.

Bates, D. R., Fundaminsky, A., Leech, J. E., and Massey, H. S. W., 1950, *Phil. Trans. Roy. Soc. London*, **A243**, 93.

Biermann, L., 1946, *Naturwiss.*, **33**, 118.

Biermann, L., 1948, *Z. Astrophys.*, **25**, 161.

Blackwell, D. E., Dewhirst, D. W., and Dollfus, A., 1957, *Nature*, **180**, 211.

Blum, E. J., Denisse, F. J., and Steinberg, J. L., 1952, *Ann. astrophys.*, **15**, 184.

Böhm, K. H., 1954, *Z. Astrophys.*, **35**, 179.

Böhm-Vitense, E., 1953, *Z. Astrophys.*, **32**, 135.

Böhm-Vitense, E., 1954, *Z. Astrophys.*, **34**, 200.

Böhm-Vitense, E., 1955, *Z. Astrophys.*, **36**, 145.

Branscomb, L. M., and Smith, S. J., 1955, *Phys. Rev.*, **98**, 1028.

Bugoslavskaya, E. J., 1946, *Astron. Zhur.*, **23**, 4.

Christiansen, N. W., and Warburton, J. A., 1955, *Australian J. Phys.*, **8**, 474.

Chandrasekhar, S., 1934, *Monthly Notices Roy. Astron. Soc.*, **94**, 16.

Chandrasekhar, S., 1945, *Astrophys. J.*, **101**, 328.

Chandrasekhar, S., 1945, *Astrophys. J.*, **102**, 223, 395.

Chandrasekhar, S., 1958, *Astrophys. J.*, **128**, 633.

Chandrasekhar, S., and Breen, F. H., 1946, *Astrophys. J.*, **104**, 430.

Cillié, G. G., and Menzel, D. H., 1935, *Harvard Observatory Circ. No. 410.*

Clube, S. V. M., 1958, *Monthly Notices Roy. Astron. Soc.*, **118**, 18.

Coates, R. J., 1958, *Astrophys. J.*, **128**, 83.

Covington, A. E., and Broten, N. W., 1954, *Astrophys. J.*, **119**, 569.

Davidson, C. R., and Stratton, F. J. M., 1927, *Mem. Roy. Astron. Soc.*, **64**.

De Jager, C., 1952, *Recherche Astron. Observatory Utrecht*, **13** (No. 1).

De Jager, C., 1954a, *Proc. Conf. Stellar Atmospheres*, M. H. Wrubel (ed.), p. 108, Indiana University Press.

De Jager, C., 1954b, *Nature*, **173**, 680.

De Jager, C., 1957a, *Bull. Astron. Inst. Netherlands*, **13**, 133.

De Jager, C., 1957b, *Bull. Astron. Inst. Netherlands*, **13**, 275.

De Jager, C., 1958, *Mem. soc. roy. sci. Liège*, ser. IV, 20, 172.

De Jager, C., 1959, *Handbuch der Physik*, Vol. 52, p. 80, Berlin, Springer.

De Jager, C., and De Groot, C., 1957, *Bull. Astron. Inst. Netherlands*, **14**, 21.

De Jager, C., and Pecker, J-C., 1951, *Compt. rend.*, **232**, 1645.

Dizer, M., 1952, *Compt. rend.*, **235**, 1016.

Dunn, R. B., 1956, *Astron. J.*, **61**, 3.

Dunn, R. B., 1959, *Astrophys. J.*, **130**, 972.

Edlen, B., 1942, *Z. Astrophys.*, **22**, 30.

Edlen, B., 1954, *Monthly Notices Roy. Astron. Soc.*, **114**, 700.

Elwert, G., 1954, *Z. Naturforsch.*, **9a**, 637.

Evans, J. W., 1955, Paper read at Solar Symposium, Troy meetings of AAS.

Frenkiel, F. N., and Schwarzschild, M., 1952, *Astrophys. J.*, **116**, 422.

Fite, W. L., and Brackmann, R. T., 1958, *Phys. Rev.*, **112**, 1141, 1151.

Fite, W. L., Stebbings, R. F., and Brackmann, R. T., 1959, *Phys. Rev.*, **116**, 356.

Garstang, R. G., 1955, *Vistas in Astronomy*, A. Beer (ed.), Vol. I, p. 268, London, Pergamon.

Giovanelli, R. G., 1948, *Australian J. Sci. Research*, **1**, 275, 289, 305, 360.

Giovanelli, R. G., 1949a, *Monthly Notices Roy. Astron. Soc.*, **109**, 298.

Giovanelli, R. G., 1949b, *Monthly Notices Roy. Astron. Soc.*, **109**, 372.

Goldberg, L., 1939a, *Astrophys. J.*, **89**, 673.

Goldberg, L., 1939b, *Astrophys. J.*, **90**, 414.

Goldberg, L., 1941, *Astrophys. J.*, **93**, 244, PPGN XV.

Goldberg, L., 1957, *Astrophys. J.*, **126**, 318.

Goldberg, L., 1958, *Astrophys. J.*, **127**, 308.

Goldberg, L., and Mohler, O. C., and Mueller, E. A., 1959, *Astrophys. J.*, **129**, 119.

Gollnow, H., Ten Bruggencate, P., Günther, S., and Strohmeier, W., 1949, *Z. Astrophys.*, **26**, 51.

Hachenberg, O., Furstenberg, F., and Prinzler, H., 1956, *Z. Astrophys.*, **39**, 232.

Haddock, F. T., 1957, *IAU Symposium No. 4 Radio Astronomy*, H. C. van de Hulst (ed.), London, Cambridge University Press.

Hagen, J. P., 1951, *Astrophys. J.*, **113**, 547.

Hagen, J. P., 1954, *J. Geophys. Research*, **59**, 158.

Harris, D. L., 1948, *Astrophys. J.*, **108**, 112.

Hebb, M. H., and Menzel, D. H., 1940, *Astrophys. J.*, **92**, 408, PPGN X.

Hemmindinger, H., 1939, Thesis, Princeton University.

Henyey, L. G., 1940, *Proc. Natl. Acad. Sci. U. S.*, **26**, 50.

Houtgast, J., 1953, *Proc. Conveg. Volta*, Rome Acad. Nat. Lincei.

Houtgast, J., 1957, *Recherche Astron. Observatory Utrecht*, 13 (No. 3).

Howard, R., 1959, *Abstr. AAS Meetings*, Rochester, N. Y.

Hoyle, F., 1949, *Recent Researches in Solar Physics*, London, Cambridge University Press.

Hoyle, F., and Wilson, O. C., 1958, *Astrophys J.*, **128**, 604.

Hylleraas, E. A., 1937, *Z. Physik*, **106**, 395.

Huang, S. S., 1948, *Astrophys. J.*, **108**, 354.

Janssen, J., 1896, *Ann. Obs. Paris* (*Meudon*), **1**.

Jefferies, J. T., 1953, *Australian J. Phys.*, **6**, 22.

Jefferies, J. T., 1954, *Australian J. Phys.*, **6**, 22.

Jefferies, J. T., 1955, *Australian J. Phys.*, **8**, 335.

Jefferies J. T., and Giovanelli, R. G., 1954, *Australian J. Phys.*, **7**, 574.

Jefferies, J. T., and Giovanelli, R. G., 1955, *Australian J. Phys.*, **8**, 335.

Jefferies, J. T., and Orrall, F. Q., 1958, *Astrophys. J.*, **127**, 714.

Jefferies, J. T., and Thomas, R. N., 1958, *Astrophys. J.*, **127**, 667, SFNEA II.

Jefferies, J. T., and Thomas, R. N., 1959, *Astrophys. J.*, **129**, 401, SFNEA III.

Jefferies, J. T., and Thomas R. N., 1960, *Astrophys. J.*, **131**, 695, SFNEA V.

Johnson, F. S., Malitson, H. H., Purcell, J. D., and Tousey, R., 1958, *Astrophys. J.*, **127**, 80.

Kawaguchi, I., 1951, *Publ. Astron. Soc. Japan*, **3**, 171.

Keenan, P. C., 1932, *Astrophys. J.*, 75, 277; also *Astrophys. J.*, **76**, 134.

Kiepenheuer, K. O., 1953, *The Sun*, G. P. Kuiper (ed.), University of Chicago Press.

Kononovich, E., 1958, *Bect. Moscow Univ.*, No. 4, (ser. Math., Mech., Astron., Phys., Chem.).

Kononovich, E. W., and Shklovsky, I. S., 1957, *Astron. Zhur.*, **35**, 37.

Krat, V. A., and Krat, T. V., 1955, *Izvest. Glavnoi Astron. Obs. Pulkova*, **19**, 1.

Kristensen, H., 1955, *Stockholm Obs. Ann.*, **18** (No. 5).

Labs, D., 1957, *Sitzber. heidelberg. Akad. Wiss. Symposium uber Prob. Spektralphotometrie*, Heidelberg, Springer.

Layzer, D., 1954, *Monthly Notices Roy. Astron. Soc.*, **114**, 693.

Layzer, D., 1956, *Astrophys. J.*, **124**, 664.

Leighton, R., 1959, *Astron. J.*, **61**, 8.

Lippincott, S. L., 1956, *Astron. J.*, **61**, 8.

Lippincott, S. L., 1957, *Smithsonian Contributions to Astrophysics*, **2**, 15.

Lyot, B., and Dollfus, A., 1953, *Compt. rend.*, **237**, 855.

McCrea, W. H., 1929, *Monthly Notices Roy. Astron. Soc.*, **89**, 718.

McMath, R. R., Mohler, O. C., Pierce, A. K., and Goldberg, L., 1956, *Astrophys. J.*, **124**, 1.

Makarova, E. A., 1957, *Astron. Zhur.*, **34**, 539.

Martyn, D. F., 1948, *Proc. Roy. Soc. London*, **A193**, 44.

Massey, H. S. W., 1955, *Vistas in Astronomy*, A. Beer (ed.), Vol. 1, p. 277, London, Permagon.

Massey, H. S. W., 1956a, *Handbuch der Physik*, Vol. 36, p. 307, Berlin, Springer.

Massey, H. S. W., 1956b, *Revs. Mod. Phys.*, **28**, 199.

Massey, H. W. W., and Burhop, E. H. S., 1952, *Electronic and Ionic Impact Phenomena*, Oxford, Clarendon Press.

Massey, H. S. W., and Mohr, C. R. O., 1931, *Proc. Roy. Soc. London*, **A227**, 38.

Massey, H. S. W., and Moiseiwitsch, B. L., 1954, *Proc. Roy. Soc. London*, **A227**, 38.

Matsushima, S., 1952, *Astrophys. J.*, **115**, 544, SPSA VII.

Matsushima, S., 1955, *Astrophys. J.*, **1**, 479, TSOSA III.

Menzel, D. H., 1931a, *Popular Astron.*, **39**, 16.

Menzel, D. H., 1931b, *Publ. Lick Obs.*, **17**, Part 1.

Menzel, D. H., 1937, *Astrophys. J.*, **85**, 330, PPGN I.

Menzel, D. H., and Aller, L. H., 1941, *Astrophys. J.*, **93**, 195, PPGN XII.

Menzel, D. H., and Aller, L. H., 1941, *Astrophys. J.*, **94**, 30, PPGN XVI.

Menzel, D. H., and Aller, L. H., 1941, *Astrophys. J.*, **94**, 436, PPGN XVII.

Menzel, D. H., Aller, L. H., and Baker, J. G., 1938, *Astrophys. J.*, **88**, 313, PPGN IV.

Menzel, D. H., Aller, L. H., and Hebb, M. H., 1941, *Astrophys. J.*, **93**, 230, PPGN XIII.

Menzel, D. H., and Baker, J. G., 1937, *Astrophys. J.*, **86,** 70, PPGN II.

Menzel, D. H., and Cillié, G. G., 1937, *Astrophys. J.*, **85,** 88.

Menzel, D. H., and Pekeris, C. L., 1935, *Monthly Notices Roy. Astron. Soc.*, **96,** 77.

Michard, M., 1956, *Ann. astrophys.*, **19,** 1.

Michard, M., 1959, *Ann. astrophys.*, **22,** 547.

Milne, E. A., 1930, *Handbuch der Astrophysik*, Vol. 3, Chap. ii, Berlin, Springer.

Minnaert, M., 1953, *The Sun*, G. P. Kuiper (ed.), p. 88, University of Chicago Press.

Minnett, H. C., and Labrum, N. R., 1950, *Australian J. Sci. Research*, **3,** 60.

Mitchell, S. S., 1947, *Astrophys. J.*, **105,** 1.

Miyamoto, S., 1947a, *Mem. Astrophys.* (Japan), **1,** 8.

Miyamoto, S., 1947b, *Mem. College Sci. Kyoto Univ.*, **25,** 31.

Miyamoto, S., 1953, *Z. Astrophys.*, **31,** 282.

Miyamoto, S., 1954a, *Publ. Astron. Soc. Japan*, **5,** 142.

Miyamoto, S., 1954b, *Publ. Astron. Soc. Japan*, **6,** 103.

Miyamoto, S., 1954c, *Publ. Astron. Soc. Japan*, **6,** 140.

Miyamoto, S., 1954d, *Publ. Astron. Soc. Japan*, **6,** 150.

Miyamoto, S., 1954e, *Publ. Astron. Soc. Japan*, **6,** 196.

Miyamoto, S., 1955, *Publ. Astron. Soc. Japan*, **7,** 27.

Miyamoto, S., 1958, *Publ. Astron. Soc. Japan*, **9,** 146.

Mohler, O. C., 1951, *Monthly Notices Roy. Astron. Soc.*, **111,** 630.

Mohler, O. C., Pierce, A. K., McMath, R. R., and Goldberg, L., 1950, *Photometeric Atlas of the Near Infra-Red Solar Spectrum*, University of Michigan Press.

Mohler, O. C., and Goldberg, L., 1956, *Astrophys. J.*, **124,** 13.

Neven, L., and De Jager, C., 1954, *Bull. Astron. Inst. Netherlands*, **12,** 103.

Pagel, B. E. J., 1955, *Monthly Notices Roy. Astron. Soc.*, **115,** 493.

Pagel, B. E. J., 1956, *Monthly Notices Roy. Astron. Soc.*, **116,** 608.

Pagel, B. E. J., 1957, *Astrophys. J.*, **125,** 298.

Pagel, B. E. J., 1959, *Proc. Uccle Conference*, p. 28.

Pannekoek, A., 1930, *Monthly Notices Roy. Astron. Soc.*, **91,** 139.

Pannekoek, A., and Minnaert, M., 1928, *Verhandel. Akad. Wetenschap. Amsterdam*, **14,** (No. 2).

Parker, E. N., 1953, *Astrophys. J.*, **117,** 431.

Parker, J. M., 1957, *Astron. J.*, **62,** 29.

Pecker, C., Billings, D. E., and Roberts, W. O., 1954, *Compt. rend.*, **238,** 1101.

Pecker, C., and Pecker, J-C., 1956, *Compt. rend.*, **242,** 994, 1130.

Pecker, J-C., 1957a, *Compt. rend.*, **245,** 499.

Pecker, J-C., 1957b, *Compt. rend.*, **245,** 639.

Pecker, J-C., 1959a, *Ann. astrophys.*, **22,** 499.

Pecker, J-C., 1959b, *Proc. Uccle Conference*.

Pecker, J-C., and Athay, R. G., 1955, *Astrophys. J.*, **121,** 391.

Peyturaux, R., 1952, *Ann. astrophys.*, **15,** 302.

Piddington, J. H., 1954, *Astrophys. J.*, **119,** 531.

Piddington, J. H., 1956, *Phys. Rev.*, **101,** 9.

Pierce, A. K., 1954, *Astrophys. J.*, **119**, 312.

Pierce, A. K., and Waddell, J. H., 1960, *Monthly Notices Roy. Astron. Soc.*, in press.

Pottasch, S. R., 1960, *Astrophys. J.*, **131**, 68.

Pottasch, S. R., and Thomas, R. N., 1959, *Astrophys. J.*, **130**, 941.

Pottasch, S. R., and Thomas, R. N., 1960, *Astrophys. J.*, **132**, **195**, TSOSA VI.

Redman, R. O., 1942, *Monthly Notices Roy. Astron. Soc.*, **102**, 134.

Redman, R. O., 1942, *Monthly Notices Roy. Astron. Soc.*, **102**, 140.

Redman, R. O., 1955, *Vistas in Astronomy*, A. Beer (ed.), London, Pergamon.

Redman, R. O., and Suemento, Z., 1954, *Monthly Notices Roy. Astron. Soc.*, **114**, 524.

Rense, W., 1958, Private communication.

Richardson, R. S., and Schwarzschild, M., 1950, *Astrophys. J.*, **111**, 351.

Roberts, W. O., 1945, *Astrophys. J.*, **101**, 136.

Roberts, W. O., Brenton, V. K., Shapley, M. B., and Kopal, Z., 1949, *Publ. Astron. Soc. Pacific*, **61**, 1960.

Rohrlich, F., 1956, *Astrophys. J.*, **123**, 521.

Rösch, J., 1955, *Compt. rend.*, **240**, 1630.

Rösch, J., 1946, *Compt. rend.*, **243**, 478.

Rosseland, S., 1926, *Astrophys. J.*, **63**, 218.

Rosseland, S., 1929, *Monthly Notices Roy. Astron. Soc.* **89**, 49.

Rush, J. H., and Roberts, W. O., 1954, *Australian J. Phys.*, **7**, 230.

Schatzman, E., 1949a, *Compt. rend.*, **228**, 738.

Schatzman, E., 1949b, *Ann. astrophys.*, **12**, 203.

Schatzman, E., 1953, *Bull. Acad. Roy. Belg.*, **39**, 960.

Schatzman, E., 1954, *Bull. Acad. Roy. Belg.*, **40**, 139.

Schatzman, E., 1958, *Contrib. inst. astrophys. Paris*, ser. A, No. 234.

Schirmer, H., 1950, *Z. Astrophys.*, **27**, 132.

Schwarzschild, M., 1948, *Astrophys. J.*, **107**, 1.

Schwarzschild, M., Rogerson, J. B., and Evans, J. W., 1958, *Astrophys. J.*, **63**, 54.

Schwarschild, M., and Schwarzschild, B., 1959, *Sci. American*, **201**, 52.

Seaton, M. J., 1958, *Revs. Mod Phys.*, **30**, 979.

Secchi, P. S., 1877, *Le Soleil*, Paris, Gauthier-Villars.

Shklovsky, I. S., and Kononovitch, E. W., 1958, *Russ. Astron. J.*, **35**, 37.

Shortley, G. H., Aller, L. H., Baker, J. G., and Menzel, D. H., 1941, *Astrophys. J.*, **93**, 168, PPGN XI.

Shortley, G. H., and Menzel, D. H., 1940, *Astrophys. J.*, **91**, 307, PPGN IX.

Smith, E. v. P., 1957, *Astrophys. J.*, **126**, 529.

Smith, E. v. P., 1960, *Astrophys. J.*, **132**, 202.

Smith, H., 1957, *Astron. J.*, **62**, 33.

Smith, S. J., and Burch, D. S., 1959, *Phys. Rev.*, **116**, 1125.

Strömgren, B., 1935, *Z. Astrophys.*, **10**, 237.

Struve, O., and Elvey, C. T., 1934, *Astrophys. J.*, **79**, 409.

Ten Bruggencate, P., Grotian, W., Von der Pahlen, E., 1938, *Z. Astrophys.*, **16**, 51.

Ten Bruggencate, P., and Müller, H., 1942, *Z. Astrophys.*, **21**, 198.

Thackeray, A. D., 1937, *Monthly Notices Roy. Astron. Soc.*, **97**, 672.

Thiessen, G., 1955, *Z. Astrophys.*, **35**, 237.

Thomas, D. V., 1958, *Monthly Notices Roy. Astron. Soc.*, **118**, 458.

Thomas, R. N., 1947a, *Astron. J.*, **52**, 158.

Thomas, R. N., 1947b, *Astrophys. J.*, **106**, 482.

Thomas, R. N., 1948a, *Astrophys. J.*, **108**, 130, SPSA I.

Thomas, R. N., 1948b, *Astrophys. J.*, **108**, 142, SPSA II.

Thomas, R. N., 1949a, *Astrophys. J.*, **109**, 480, SPSA III.

Thomas, R. N., 1949b, *Astrophys. J.*, **109**, 500, SPSA IV.

Thomas, R. N., 1949c, *Astrophys. J.*, **110**, 12, SPSA V.

Thomas, R. N., 1950a, *Astrophys. J.*, **111**, 165, TSOSA I.

Thomas, R. N., 1950b, *Astrophys. J.*, **112**, 337, TSOSA II.

Thomas, R. N., 1950c, *Astrophys. J.*, **112**, 343, SPSA VI.

Thomas, R. N., 1952, *Astrophys. J.*, **115**, 550, SPSA VIII.

Thomas, R. N., 1954a, *Solar Dept. Harvard College Observatory, Sci. Rept. No.* 16, 29 Jan.

Thomas, R. N., 1954b, *Bull. Acad. Roy. Belg.*, **40**, 621.

Thomas, R. N., 1957, *Astrophys. J.*, **125**, 260, SF NEA I.

Thomas, R. N., 1960, *Astrophys. J.*, **131**, 429, SF NEA IV.

Thomas, R. N., and Athay, R. G., 1956, *IAU Symposium No. 4: Radio Astronomy*, H. C. van de Hulst (ed.), Cambridge University Press.

Thomas, R. N., and Whitney, C., 1953, *Astron. J.*, **58**, 235.

Thompson, G. I., 1958, *Observatory*, **78**, 170.

Trumpler, R. J., and Weaver, H. F., 1953, *Statistical Astronomy*, Berkley, University of California Press.

Uberoi, M. S., 1955, *Astrophys. J.*, **122**, 466.

Uccle Conference on the Empirical Determination of Stellar Photospheric Structure, De Jager, C., and Neven, L. (eds.), *Comm. Obs. Roy. Belg.*, No. 157.

Underhill, A. B., 1950, *Publ. Dominion Astrophys. Observatory, Victoria, B. C.*, **8**, 385.

Underhill, A. B., and Waddell, J. H., 1959, *Natl. Bur. Standards Circ.* 603.

Unno, W., 1959a, *Astrophys. J.*, **129**, 375.

Unno, W., 1959b, *Astrophys. J.*, **129**, 388.

Unsöld, A., 1955, *Physik Sternatmospharen*, 2nd ed., Berlin, Springer.

Unsöld, A., 1930, *Z. Astrophys.*, **1**, 138.

Van de Hulst, H. C., 1953, *The Sun*, G. P. Kuiper (ed.), University of Chicago Press.

Voigt, H. H., 1956, *Z. Astrophys*, **40**, 157.

Vyazanitsyn, V. P., 1951, *Izvest. Glavnoi Astron. Obs. Pulkova*, **18**, 19.

Vyazanitsyn, V. P., 1952, *Iznest. Glavoni Astron. Obs. Pulkova*, **19**, 40.

Whitney, C., 1955, *Ann. astrophys.*, **18**, 375.

Whitney, C., 1956, *Ann. astrophys.*, **19**, 34, 142.

Wildt, R., 1939, *Astrophys. J.*, **89**, 295.

Wildt, R., 1947, *Astrophys. J.*, **105**, 36.

Wilson, O. C., 1957, *Astrophys. J.*, **126**, 525.

Wilson, O. C., and Bappu, M. K. V., 1957, *Astrophys. J.*, **125**, 661.

Woltjer, L., 1954, *Bull. Astron. Inst. Netherlands*, **12**, 165.

Woolley, R. v. d. R., and Allen, C. W., 1948, *Monthly Notices Roy. Astron. Soc.*, **108**, 292.

Woolley, R. v. d. R., and Allen, C. W., 1950, *Monthly Notices Roy. Astron. Soc.*, **110**, 358.

Wurm, K., 1948, *Z. Astrophys.*, **25**, 109.

Zanstra, H., 1950, *Proc. Koninkl. Ned. Akad. Wetenschap.*, 53, 1289.

Zirin, H., 1956, *Astrophys. J.*, 123, 536.

Zirker, J., 1956, Thesis, Harvard University; *High Altitude Observatory Tech. Rept.* 10, October.

Zirker, J., 1958, *Astrophys. J.*, **127**, 680.

Zirker, J., 1959, *Astrophys. J.*, **129**, 424.

Zirker, J., 1960, *Astrophys. J.*, **131**, 684.

Index

Absorption:
  effect in obscuring spicules, 66; in spicules, 71–77; in Balmer series, 98, 103, 203, 217, 310 et seq. (Section 9–II); effect in chromospheric energy balance, 144, 162–167; Lyman opacity of H, 203, 205, 217; in helium, 229, 233, 240; at radio wavelengths, 262; in metals, 354.
Absorption coefficient:
  Doppler core, 106; Stark effect, 106, 345, 377; at radio wavelengths, 262
Acoustic noise: 15.
Astronomical turbulence:
  basis for an introduction, 10, 11, 19; in low chromosphere, 10, 11; energy dissipation from, 11; interpretation of, 11; in upper chromosphere, 253

b_k:
  (*see* Thermodynamic equilibrium, local)
Balmer lines:
  chromospheric, 26, 31, 32, 37, 38, 392, 401; scale heights, 39, 40, 52, 54, 56, 392, 401; profiles in spicules, 68–77; opacity in, (*see* Opacity); ratio of $H\alpha$ D_3, 74–75; role in chromospheric energy balance, 159–163; in active region, 256; early, 381 et seq.; later, 310 et seq.
Balmer series opacity:
  (*see* Absorption)

Ca II lines:
  profiles in spicules, 68–77; possible broadening in spicules by magnetic field, 76, 77; source function for, 368, 407
Chromosphere anomaly:
  defined, 14; negated, 207
Chromospheric models: 35, 44
  theoretical, 147 et seq. (Chapter 5); from continuum, Chapter 6; in helium emitting region, 241; empirical, 252, 268 (et seq. Chapter 8), Chapter 10
Chromospheric observations:
  eclipse, 25; extra-eclipse, 26
Chromospheric structure:
  (*see* Spherical symmetry, departures from); large scale, 26, 45–49; small scale, 26, 46, 49–57, 269, 270 (*see* Spicules); spicules (*see* Spicules); "hot spots" or "active regions," 46–49, 254–260; temporal variations, 51–57
CN:
  chromospheric, 42, 379, 380; scale heights, 43
Conduction, thermal: 143, 148
Continuum emission:
  λ4700, 35, 36, 56, 57, 194, 204, 229, 388–391, 400; electron scattering, 35, 194, 204, 245; H^-, 35, 194, 204, 243; Paschen, 35, 194, 204, 243; Balmer, 37, 38, 152, 194, 204, 391; free-free, 35, 194, 204; coronal, 56, 168; free-bound, 145, 168, 229; Rayleigh scattering, 194, 204
Convection: 17, 143, 189
Coronal emission:
  extra-eclipse observations, 26; eclipse observations, 42, 46, 47, 169; scale heights, 43, 44; base of, 43, 169; yellow line, 47; role in chromospheric excitation, 232, 233, 234

Density gradients:
  hydrogen, 203, 217; metals, 262
Detailed balance:
  defined, 80; in Lyman lines of H,

  97, 99; departures from in Lyman lines, 221, 285; departures from in He I resonance lines, 237–242

Eclipse, total solar:
  1870, 25; **1893,** 25; **1926,** 25; **1927,** 31; **1932,** 28, 31, 46, 48, 49, 52–57, 259; **1936,** 28, 31, 46, 48, 49, 51, 52–57, 259; **1940,** 31; **1941,** 30, 31, 52, 53, 54; **1945,** 29, 32, 52, 53, 54; **1952,** 30, 32 et seq.
Eddington approximation to transfer equation 125
Emission scale height:
  (*see* scale height)
Energy balance, chromospheric: page 4, et seq. (Chapter 1)
  input, 142, 143, 146, 147, 155; output, 142–146, 150, 169; H^-, 150–153; H, 151–155, 162, 163, 166, 167; He I, 151, 153, 167; He II, 151, 153, 163–167; other, 151, 153, 155, 166, 168
Equations of statistical equilibrium:
  symbolic form, 7–9; general, 90; three-level atom, 99, 120
Equivalent two-level atom:
  defined, 122; applied to H Balmer lines, 285, 287; extensions of, 377

Flares: 46, 47, 293

Granulation, photospheric: 57, 187–191

H^-:
  importance in chromospheric energy balance, 150–153, 159; chromospheric emission, Chapter 6
Helium:
  chromospheric, 40–42, 229–238, 395, 401; scale heights, 40–42, 52, 56, 395, 401; profiles in spicules, 68–77; ratio of D_3: $H\alpha$, 74, 75; importance in chromospheric energy balance, 151, 153, 167; excitation, 229–242; b_k's, 230–238, 255; model atom, 236; NRB, 237–242
Hydrogen:
  importance in chromospheric energy balance, 151–155, 166; stability of emission, 159–163; Lyman opacity, 203, 205, 217; Balmer series (*see* Balmer lines); chromospheric opacity (*see* Absorption)
Hydrostatic equilibrium:
  empirical results, 207, 253, 271, 381; used in model, 212, 216
Hydromagnetic effects:
  (*see* Magnetic fields)

Ionized helium:
  chromospheric, 40–42; scale heights, 41, 42, 52, 56; importance in chromospheric energy balance, 151, 153, 155; stability of emission, 163–167

Line profiles:
  spicules, 26; chromosphere, 30; (*see* Self-reversed line profiles)
Local thermodynamic equilibrium (LTE):
  (*see* Thermodynamic equilibrium, local)
Lyman-α of hydrogen: 162, 163, 166, 373, 409

Magnetic fields:
  hydromagnetic effects, 23; correlation with emission, 46; in spicules, 75–77
Metal lines, other:
  chromospheric, 26, 42, 352 et seq., 396–400, 403, 404; scale heights, 42, 52, 56, 396–400, 403, 404; absence in spicule spectra, 74

Net collisional rate: 85
Net radiative bracket
  defined, 121; influence on source function, 123, 124; evaluation of, 133, et seq.; free-bound continuum, 139–140 145, 152, 162; role in chromospheric energy balance, 144–146, 157, 160–167; use in iteration on b_2(H), 198–201; He I, 237–242
Net radiative rate 83, 133
Non-LTE:
  defined, 18 (*see also* Thermodynamic equilibrium, local)

Opacity:
  spicules, 71–77; in chromosphere (*see* Absorption)

Paschen lines:

chromospheric, 33, 38, 47, 394, 401; scale height, 40, 394, 401; in active region, 256

Photosphere

minimum temperature, 10, 17, 170, 171, 378; temperature in upper, 173 et seq.; accuracy of T_e from limb darkening, 179; narrow-band filter data, 181, 224, 225, 406

Plages: 46, 47, 77, 293

Radiation temperature, T_r:

defined, 82

Radiative instability:

defined and discussed, Chapter 5; providing upper limit on T_e, 220, 351; possible connection with spicules, 383; (*see* stability)

Radio-noise, chromospheric: 26, 261, 263

effects of departures from spherical symmetry on, 263, 266, 268, 269; apparent temperature of sun, 263, 268; limb-brightening, 264

Resonance lines:

hydrogen, (*see* Lyman-α); ionized helium, 164, 166, 168; helium, 167, 233, 237–242

Saha equation:

non-LTE form, 80; deviations from, for H, under conditions of large Lyman opacity, 94, 104, 105; deviations from for He II, 159; deviations from for He I, 230, 231, 232

Scale heights:

defined, 1; emission vs. density, 3, 4; differential between elements 4; chromospheric, 28, 29, 51, 57, Appendix I

Self-reversed line profiles:

source-function theory of, Chapter 4; limb observations in Hα, 306; in spicules, 385

Source function

defined, 96; frequency dependence, 109; functional dependence, 116, 119, 123, 125; Milne-Stromgren, 116; types, 118, 126, 128, 130; resonance vs. subordinate lines, 123; depth dependence of, 126, 128, 130; non-LTE in visual continuum, 183–187; at radio wavelengths, 262; for early Balmer lines, 283 et seq., 296; non-LTE in Lyman continuum, 408; approximation scheme for analysis of H, 320 et. seq.; for Ca II, H and K, 368, 407

Spectrograph, chromospheric:

slitless, 27, 28, 31, 32; moving-plate, 27; jumping-film, 28; slit, 30, 31, 32

Spectroheliogram 26, 46

Spherical symmetry, departures from:

chromosphere, 1, 15–18, 45, 156, 169, 233, 234, 242 et seq. (Chapters 7 and 8), 277, 288, 323, 347, 382, 383; photosphere, 187–193

Spicules:

defined, 1; importance in chromospheric models, 12, 15, 246, 252, 253, 259, 269, 270, 380, 383, 386; line profiles in, 26; structure, 26, 49–51, 57–77; motion, 26, 58, 61, 253, 380, 386; lifetimes, 58, 59; numbers, 59, 60, 62–68; line profiles, 68–77; temperature, 72–77, 253; density, 73, 253; origin of, 386, 387; importance of in corona, 386

Stability, thermal:

introduced, 143, 148, chapter 5; criterion, 147; H^-, 152; hydrogen, 152, 159–163; He II, 163–167

Superthermic jets 12, 15, 352, 380, 383

Temperature minimum:

(*see* Photosphere)

Thermal instability of chromospheric radiation·

(*see* stability)

Thermodynamic equilibrium, local (LTE):

defined, 2, 7; departures from defined, 18; in the continuum, 35, 183–187; departures from in spicules, 74; b_k defined, 80; methodology, Chapter 4; importance of departures from in chromospheric energy balance and temperature structure, 158, 159–167; applied to chromosphere, chapters 6, 7, 9; in H^-, 183–187;

in hydrogen, Chapters 4, 6, 9; 158; in HeII, 159; in He I, 230, 231, 232; in metals, 381; in photosphere, 365–367

Thick atmosphere:
  defined, 95; solution for hydrogen, 97

Thin atmosphere:
  defined, 92; solution for hydrogen, 93, 95

Transport problems:
  mechanical vs. radiative, 18 et seq.

Turbulence:
  (*see* Astronomical turbulence)

Velocity fields:
  in stellar atmospheres, page 6 et seq.; chromospheric, 57, 143; spicule (*see* Spicules); effect on line profiles, 385, 410

W_{jk}:
  defined, 82; use summarized, 134

X_k:
  defined, 83

Y_k:
  defined, 83